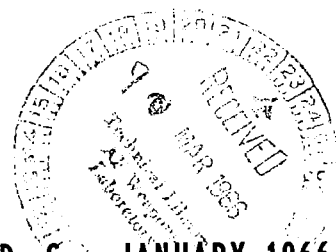# NASA CONTRACTOR REPORT

NASA CR-352

NASA CR-352

METEOROLOGICAL INTERPRETATION OF NIMBUS HIGH RESOLUTION INFRARED (HRIR) DATA

by William K. Widger, Jr., James C. Barnes,
Earl S. Merritt, and Robert B. Smith

NATIONAL AERONAUTICS AND SPACE ADMINISTRATION - WASHINGTON, D. C. - JANUARY 1966

NASA CR-352

METEOROLOGICAL INTERPRETATION OF NIMBUS HIGH RESOLUTION

INFRARED (HRIR) DATA

By William K. Widger, Jr., James C. Barnes,
Earl S. Merritt, and Robert B. Smith

FOREWORD

This report by the ARACON Geophysics Co., a division of Allied Research Associates, Inc., Concord, Massachusetts, describes and discusses the meteorological interpretation of the Nimbus I HRIR data. These analyses were performed for the Laboratory for Atmospheric and Biological Sciences (formerly, the Aeronomy and Meteorology Division), Goddard Space Flight Center, National Aeronautics and Space Administration. The work was begun under Contract No. NAS 5-3253, and continued under Contract No. NAS 5-9554.

The report has been prepared with the objective of providing both operational and research meteorologists, especially those with synoptic interests, with guidance as to the use of the HRIR data. It is applicable to the use of the data whether obtained from the global data acquisition facilities or from local readout using the so-called DRIR system (a proposed modification of the APT ground receiving equipment).

Several of the studies were possible only because the required data were made available significantly sooner than is normal from such sources as the TIROS project, the National Weather Records Center, the Nimbus project, and those members of ARACON stationed at GSFC.

The authors wish to acknowledge the significant suggestions of several members of ARACON Geophysics Co., especially Dr. R. Wexler and Messrs. Roland Boucher, C. W. C. Rogers, and P. E. Sherr. The illustrative material was prepared by Messrs. Walter Smith and James Pike.

Credits for individual sections of this report are primarily attributable as follows:

Mr. Barnes	Sections 6 and 7
Mr. Merritt	Section 8
Mr. R. Smith	Section 10, Appendices A and B
Dr. Widger	Sections 1, 2, 3, 4, 5, 9, 11, Appendix B

Since several of the conclusions discussed in the Final Report of Contract No. NAS 5-9554 were derived from, substantiated by, and/or illustrated by case studies which were presented in the Preliminary Scientific Report under the contract* (denoted as Ref. 56 in the Final Report) and not republished in the Final Report, these studies have now been reprinted as an additional appendix (see Appendix C).

In Appendix C, the mesoscale cases for western North America and for the eastern United States were the result of joint studies by Mr. Robert Smith and Dr. Widger. The remaining case studies were prepared by Dr. Widger.

---

* Widger, W. K., Jr., and R. B. Smith, 1965: <u>Preliminary Results from a Meteorological Evaluation of Nimbus I HRIR Data</u>, Preliminary Scientific Report, Contract No. NAS 5-9554, ARACON Geophysics Co.

ABSTRACT

This report provides both operational and research meteorologists, especially those with synoptic interests, with guidance in the use of the Nimbus High Resolution Infrared Radiometer (HRIR) data. After a brief review of the characteristics of the HRIR system and its data, suggested techniques for the rectification and transfer of the data are described.

Summarized conclusions as to the meteorological interpretation of the data show that, after due regard to the problems of reliable detection in the HRIR of low cloud, most of the principles developed for TIROS cloud picture interpretation can be applied to the HRIR data. Studies of HRIR data have demonstrated that: (1) measurements can be made of relative cloud height, which often cannot be reliably estimated from the TIROS pictures; (2) these measurements reveal significant details of cloud vortex structure and other synoptic patterns that are masked in the TIROS pictures; and (3) over sparse data areas, the HRIR can be used to provide an approximate synoptic analysis, or can be used to improve analyses initially prepared from other types of data.

These conclusions are substantiated by several case studies including a Eurasian blocking situation, two Antarctic case studies, two tropical case studies, and two convective situations over the eastern United States.

The appendices discuss some of the quantitative aspects of the reflected solar and emitted thermal radiation sensed by the HRIR during daylight operation, and demonstrate some of the gains that could be achieved by rectified presentations of the HRIR data.

TABLE OF CONTENTS

LIST OF FIGURES

LIST OF FIGURES(cont)

LIST OF FIGURES (cont)

LIST OF FIGURES(cont)

LIST OF FIGURES (cont)

LIST OF FIGURES (cont)

LIST OF TABLES

1. INTRODUCTION

This report has been prepared with the objective of providing both operational and research meteorologists, especially those whose interests are along synoptic lines,* with guidance in the interpretation and application of data from the Nimbus High Resolution Infrared Radiometer (HRIR). It has been prepared on the basis of a number of case studies which used Nimbus I HRIR data as a principal data source. Several of these case studies will be found in Sections 5 to 11 of this report; the others in Section 4 of Reference 56.

The report first describes the principal features of the HRIR system, and those characteristics of the radiometer and its data with which the users of the data should be familiar. Included here is a discussion of those characteristics of the Nimbus I HRIR data which may be expected to differ from those to be available from subsequent satellites.

Following these descriptions, the report summarizes the general principles and techniques that have been found applicable to the HRIR data. The final sections of the report, which are its most extensive parts, are devoted to case studies which served as the basis for, and illustrate, these principles and techniques.

---

* Those whose interests are more directly with the physical nature of the data, and their physical parameters, will in general find Reference 43 more applicable to their requirements. They may, however, be interested in the material developed in Appendix A on the relative radiation sources and the interpretation of daylight HRIR data.

2. CHARACTERISTICS OF THE HRIR SYSTEM AND ITS DATA

2.1 The Basis of HRIR Observations

Like all satellite radiometry, HRIR observations depend on radiated electro-magnetic energy from earth, cloud, and atmosphere. The amount of radiation emitted is related to:

1. The temperature, with greater amounts of radiation emitted at higher temperatures.

2. The nature or emissivity of the radiating surface. The emissivity is the ratio of the energy actually emitted to that emitted by a perfect radiator (or "blackbody") at the same temperature. For the earth's surface and most clouds of reasonable thickness, except cirrus, the emissivity at HRIR wavelengths appears to be very close to unity and its variations from unity apparently can be neglected for most operational meteorological purposes.

The amount of the emitted radiation reaching the satellite sensor depends both on that emitted from the surface being viewed, and the amount of absorption and re-emission in the atmosphere above the viewed surface. Because tropospheric temperatures normally decrease with altitude, these atmospheric effects normally lead to a slight reduction in the energy reaching the sensor, and so in the apparent temperature of the surface. In the region near 3.7 microns where HRIR operates, atmospheric absorption is relatively small, as verified by the fact that boundaries between areas with only small temperature differences (lakes and rivers, as compared to adjacent land areas) are often visible in the HRIR data. Tests from aircraft of a modified HRIR system suggest net atmospheric absorption equivalent to a 5°C decrease in apparent blackbody temperature over a moist, subtropical ocean area, and to a 2°C decrease over mid-latitude low to middle clouds.[43]

The HRIR data provide information with regard to:

1. Cloud cover, cloud patterns, and areas without cloud. HRIR does this particularly well at night, when the present satellite TV cameras cannot provide data. Useful but far less quantitative data on clouds and cloud cover can also be provided if the HRIR sensor is operated during daylight portions of the orbits, but here the data and their interpretation are complicated by the sensing of reflected sunlight as well as emitted infrared radiation. These matters are discussed in more detail later.

2. At night, relative or approximate temperatures of cloud tops, from which relative or approximate cloud top heights can be inferred. Because of the reflected sunlight sensed during daylight, useful information on these matters is primarily limited to night observations.

3. For clear areas, relative or approximate temperatures of the ground, or of the oceans and major lakes. Again, HRIR provides useful measurements of these types only at night.

The ground surface is normally at a higher temperature than are the tops of clouds. Accordingly, to a first approximation, areas observed to have relatively warm temperatures are likely to be clear (exceptions exist in polar regions and for fog and low clouds, as will be discussed later). Areas with colder temperatures are likely to be cloud covered, except for some polar and mountainous regions. Areas of abrupt temperature gradients in the HRIR data can usually be assumed to indicate the boundaries between clear and cloudy areas, or between areas with high and low clouds, except where boundaries between land and water bodies are observed in clear areas. These latter can usually be identified from geographical considerations.

Because tropospheric temperatures usually decrease with height, the colder the temperature the higher the cloud tops. If the HRIR night data are available in a quantitative form, and if radiosonde data are available for the area (or even climatological values of average upper air temperatures, preferably for the area and season of interest), the approximate height of cloud tops can be deduced from the cloud top temperature.

In practice, there are, of course, other effects which complicate application of these principles. Of these, atmospheric absorption appears, as mentioned above, to be of relatively minor significance. Some of the others will be summarized below, with more detailed discussions and examples in subsequent portions of this report.

2. 1. 1 Effects of Scattered or Broken Clouds

The instantaneous field of view of the HRIR sensor has a characteristic dimension of a few miles. With scattered to broken clouds in the field of view, the energy reaching the sensor comes in part from the warmer earth and in part from the colder clouds; the resulting radiometer reading is thus a value between that for clear skies and that for an overcast at the level of the partial cloud cover. Thus, a partial cloud cover with tops at 15,000 feet might appear the same to the

radiometer as an overcast with tops at perhaps 8,000 feet. The coverage can usually only be resolved from other types of data. Synoptic climatological considerations or rapid, small scale variations in the HRIR temperature as the sensor scans across such an area may provide cloud cover clues. As is so often the case with all types of satellite data, the integration of satellite and available conventional information leads to the best interpretation.

2.1.2 Thin Clouds

In the case of thin clouds, part of the infrared energy reaching the satellite sensor originates at the earth's surface, or from a lower cloud deck, and is able to penetrate the thin clouds without being completely absorbed. Since the lower levels are normally warmer and so produce more energy, the net effect is an HRIR value representative of cloud tops at a lower height than they actually are; i.e., the same effect as that of a partial cloud cover.

2.1.3 Identification of Low Clouds

The lower the cloud tops, the less the difference in temperature between cloud covered and clear areas (or between the cloud tops and the surface). With low clouds and a stable, isothermal atmosphere in the lower levels, there would be no difference; with a low level inversion (such as is common over arctic areas in winter) and clouds above the inversion, the cloud tops may be warmer than the surface.

The HRIR data, after some smoothing, appear to have a residual error in their temperature readings of at least $\pm 2^{\circ}$C. Accordingly, it may be difficult or impossible, when only HRIR data are available, to reliably detect clouds with tops below as much as 4,000 feet above the terrain for normal lapse rates; with a low level inversion present, the layer of uncertainty may be about 4,000 feet plus the depth of the inversion layer. This is particularly true over ocean areas; over land, the presence or absence of surface features often aids in establishing whether or not a cloud cover may exist.

2. 1. 4 Daylight Data

Although HRIR was designed primarily for operation at night, it has been at
times used under daylight conditions and, in the absence of TV cloud pictures, can
provide useful data not otherwise available. Because of the spectral interval used
(3. 5 to 4. 1 microns), however, the sensor responds to reflected solar radiation
as well as to emitted infrared energy. In these wavelengths, the amount of radiant
energy from these two sources is of the same order of magnitude. The combination
of the two sources of energy may make quantitative interpretation virtually impossible,
and often complicates qualitative interpretation. Some quantitative aspects of
these relationships are investigated in Appendix A.

Solar reflectivity tends to increase with increasing cloud thickness, but
above some point the rate of increase becomes small. [16] On the other hand, increas-
ing cloud thickness normally is associated with increasing cloud top height, colder
cloud top temperatures, and lesser emitted radiation. As a consequence, reasonably
thick clouds with tops at moderate altitudes will appear relatively bright (since both
reflection and emission will be comparatively high) while thick clouds with high
tops will be less prominent (high reflectivity but significantly decreased emission).
For example, in daylight HRIR data a moderately thick stratus or stratocumulus will
often appear brighter than a cumulonimbus complex, or a hurricane (see Fig. 4-7).
For similar reasons, it is often difficult in the daylight HRIR data to distinguish
clouds over land from the land surface.

A slightly more complete discussion of these basic radiometric principles
is given in Chapter 13 of Reference 55. Those readers interested in the general
physical basis of satellite radiometry may care to consult Reference 26 and the
references therein.

2. 2 The High Resolution Infrared Radiometer

Descriptions of the HRIR system have been published in several places;[17, 43, 44, 45]
it will be described here only in the detail of interest to those using the data. The
instrument is shown in Figure 2-1, with a schematic in Figure 2-2.

The HRIR radiometer is mounted on the base of the Nimbus spacecraft. It
scans by motion of a mirror set at a 45° angle on an axis of rotation parallel to
the roll axis of the satellite (parallel to the path of the satellite along its orbit). As
the mirror rotates, it causes the field of view of the radiometer to scan from one
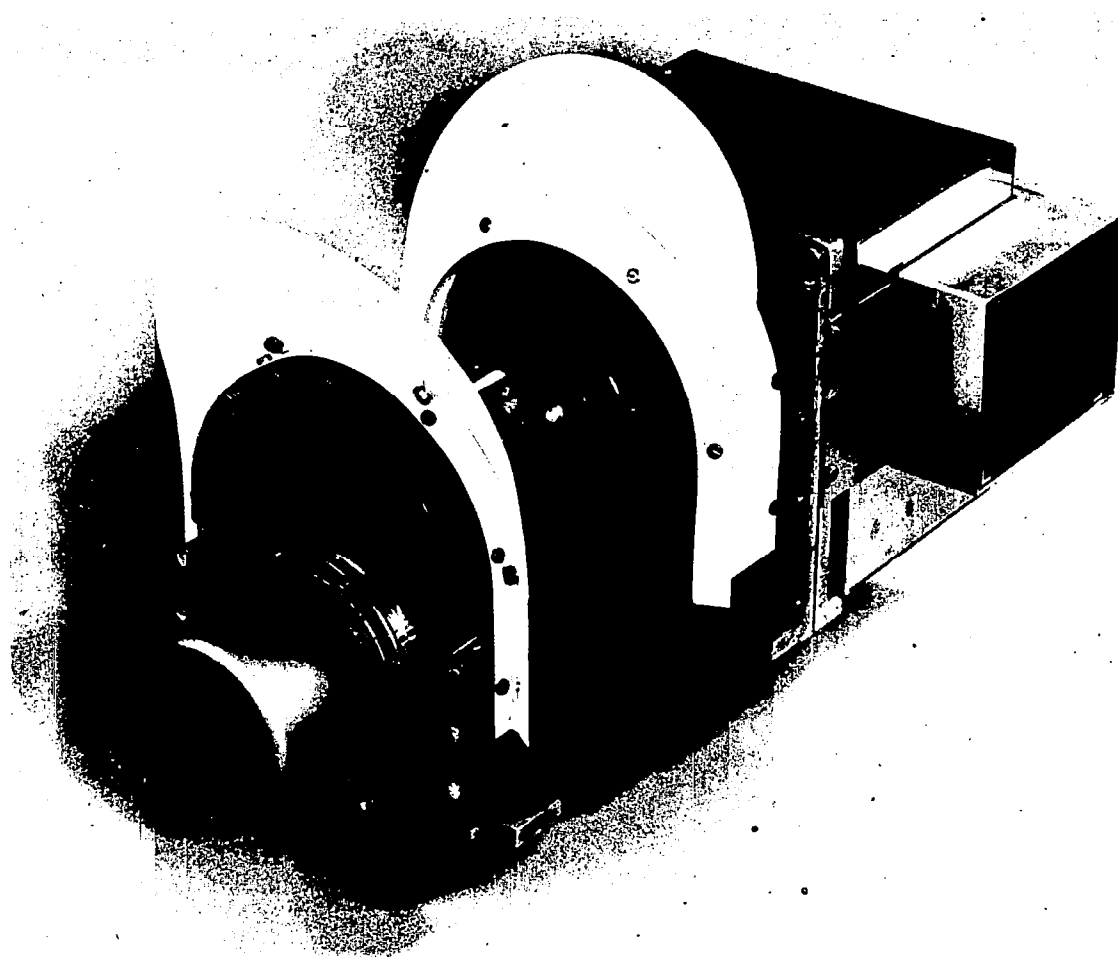
Figure 2-1   Nimbus High Resolution Infrared Radiometer
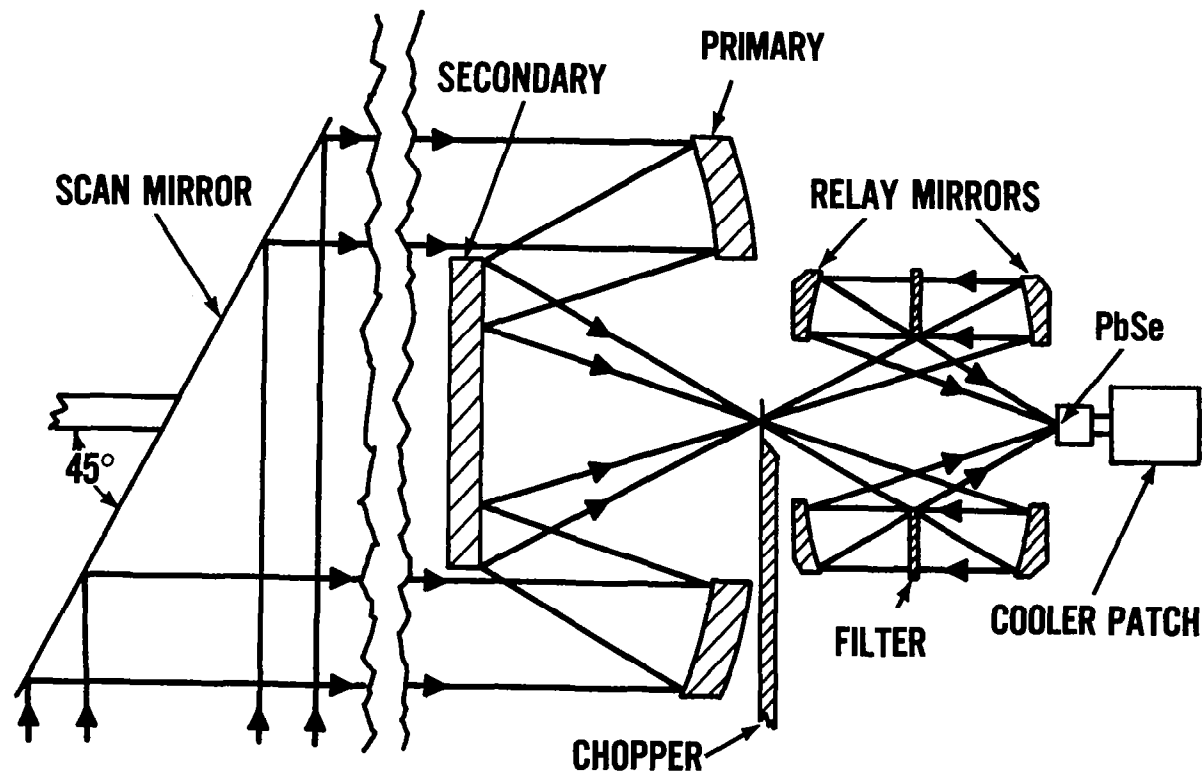
Figure 2-2   Schematic of Operation of the Nimbus High Resolution Infrared Radiometer

horizon, across the earth perpendicular to the motion of the satellite, through the sub-satellite point (assuming ideal satellite orientation), and off the second horizon. Accordingly, each scan produces observations along a relatively narrow great circle strip of the earth. This strip is oriented more or less east-west in temperate and tropical latitudes. Near the equator, the angle between a scan strip and a parallel of latitude is about 10°. This angle increases to about 30° near 60° (N or S), and to 90° at the polar extremes of each orbit (near 80^ON or S). The breadth of each individual scan strip is established by the field of view of the radiometer (see below) and the altitude of the satellite.

As the satellite advances along its orbit, successive scan strips are obtained. This combination of relatively rapid cross-track scanning along a constantly advancing scan strip is used to construct a "picture" of the earth and its clouds as seen in the infrared. The reconstructed HRIR "picture" shows an area over 2,500 miles wide, with the sub-satellite track along its center, and often extending from pole to pole.

During each rotation of the 45° mirror, the radiometer (while looking away from the earth) views a calibrating blackbody mounted below the bottom of the satellite, with the near 4^OK temperature of outer space (just above the horizons) serving as the other calibration source.

The incoming radiation is reflected by the 45° mirror through a series of focusing mirrors, a filter, and a chopper to the sensitive detector. The mirrors restrict the energy falling on the detector to a cone with an 0.5^O (7.9 milliradians) diameter, while the filter restricts the energy to that within the wavelengths between 3.5 and 4.1 microns. (For precise data on the effective spectral response of the HRIR, see Fig. 10 and Table III, page 13, of Ref. 43.)

The instantaneous field of view (or the resolution) established by the 0.5^O cone is equivalent to a diameter of about 5 nautical miles, from a nominal Nimbus altitude of 600 nautical miles, when the area observed lies directly below the satellite (7.5 km from an altitude of 930 km). When the area viewed lies about 600 miles from the subpoint, the field of view becomes approximately an ellipse of 7 x 14 nautical miles. At greater distances from the subpoint, the resolved area is, of course, even greater.

At the nominal altitude, the satellite will move forward just the width (about 5 nautical miles) of a scan line during each full revolution of the radiometer mirror. *

---

* The scan mirror rotates once every 1.3418 seconds.

Thus, there should be no overlap or underlap of the area viewed along the sub-satellite track, and a slowly increasing overlap as the nadir angle of view increases.

In the case of Nimbus I, the elliptical orbit with its low perigee on the night side led to a calculated field of view of about two nautical miles. Measurements of magnified HRIR strips (see Fig. 53 of Ref. 56) suggest the actual value (the minimum sizes of identifiable small clouds) was about three nautical miles in the direction of the scans (crosstrack). In the other dimension (parallel to the satellite track), a minimum dimension of slightly over five nautical miles was established by the characteristics of the recorder, which operated as if the design rate of satellite motion was achieved. The Nimbus I data as recorded by the photofacsimile give an impression of no subpoint underlap, although in fact it was present. Since the apogee altitude of Nimbus I was approximately that of a nominal Nimbus orbit, the resolution of the daylight HRIR data are probably rather representative of the resolution to be expected from subsequent Nimbus.

The radiant energy of the instantaneous area viewed, within the spectral response interval, is converted into electrical signals by the radiation cooled lead selenide (PbSe) detector and fed to amplifiers, rectifiers and then to a special tape recorder where the data are stored until readout, on command, when passing over a Data Acquisition Facility (DAF).

(When the proposed Direct Readout InfraRed (DRIR), or so-called HAX, capability is achieved, the signal would also be broadcast in real-time, at a specified frequency near 136 mcs, for reception and use by properly modified APT stations. This broadcast for immediate local use will be in parallel with recording for DAF readout and global use. Presumably the characteristics of the DRIR data as received and recorded at the converted APT stations will be generally comparable to those of the HRIR data as discussed in this report, although there will perhaps be some degradation in resolution and contrast. The relative characteristics of the HRIR observing system and the APT recording system make it necessary to record each entire 360° revolution of the HRIR mirror, so only about one-third of the recorded data will be of direct interest to the forecaster. DRIR should provide local stations with strips of data some 1,000 to 3,000 miles long, from each of one to three con-secutive orbits each day, as the satellite passes near the station.)

Since Nimbus is placed in a quasi-polar orbit, in theory the HRIR can view the entire earth, near local midnight, once every day with the exception of the areas midway between the subpoint traces which at low latitudes can be seen at best at excessive nadir angles and with such great foreshortening that only the

largest features can be identified. In practice, however, the location of the DAF's and the complexities of the tape recorder operation may limit observations over some areas and at times seriously delay the acquisition of data for others. These matters are discussed and illustrated in some detail in Section 5.1 of Reference 43.

For Nimbus I, the effect of these limitations was, on the average, to minimize coverage of the western hemisphere and western Europe. For subsequent Nimbus, assuming they achieve nominal orbit altitudes and nearly circular orbits, these problems should be significantly less than for Nimbus I although they may not disappear completely.

2.3 Recording of HRIR Data

Upon receipt at a DAF, or after transmission from there to the Nimbus Data Handling Facility (NDHF) at Goddard Space Flight Center, Greenbelt, Maryland, the HRIR data are recorded by a photofacsimile unit on 70 mm film. Each strip of recorded data includes the horizon-to-horizon coverage of the radiometer scan, and varies in length depending on the length of a contiguous collection and transmission of HRIR data. Some strips extend from the north to the south pole* (the Nimbus orbit is planned to provide nighttime coverage while the satellite is on the southbound half of each orbit). Where HRIR data are also taken during daylight, a strip may begin prior to reaching the north pole or continue after passing the south pole.

When prints are made from the photofacsimile negative, the data are then recorded with cold temperatures (high clouds) as white, warm temperatures (clear or low clouds) as black, and continuous intermediate tones of off-white to gray for intermediate temperatures. At night, this causes the clouds to be reproduced as white, which aids interpretation. For daylight HRIR data, this convention leads to most clouds appearing darker than the background (see Section 2.1.4). For daylight HRIR, most persons will find interpretation easier if they use a negative (reversed polarity) of the normal form of HRIR data presentation, as in Figures 2-4 and 4-7.

The photofacsimile recorder is designed to also provide a ten step gray wedge which, when operating properly, can provide semi-quantitative values of the observed radiation temperatures to an accuracy of about $\pm 10^{\circ}$C for the nighttime HRIR data (see page 93 of Ref. 43).

_____

* Because of the approximately 80°, sun-synchronous, quasi-polar orbit, the poles appear near the edge of a strip when they are observed.

Normally, as the data are being recorded, they are simultaneously geographically gridded through the use of a digital computer and an electronic signal mixer. * These latitude-longitude grid points are inscribed as adjacent black and white points to insure their visibility against either white clouds or a black clear area. The grid points are inscribed at the following intervals:

Latitude Band	Latitude Interval		Longitude Interval	
	Between Points	Between Lines of Points	Between Points	Between Lines of Points
0° - 58°, N or S	2°	10°	2°	10°
60° - 80°, N or S	2°	10°	5°	20°
82° - 88°, N or S	2°	2°	20°	20°

A grid point is also placed at the north and/or south pole. (These are illustrated in such figures as 2-4, 3-2, 4-1, 4-3, the individual strips used in the mosaics of Figs. 5-1 through 5-5, and 6-2.)

At 60°N, 30°N, 0°, 30°S, and 60°S, the latitude and the longitude (in degrees of east longitude, 0° - 359°) of a specific point near the center of the strip are printed on the film, with that point marked by an "X". When daylight HRIR data are used, it is to be noted that the computer logic (which is set for the more frequent situation of nighttime data) causes the information to be written upside-down when the strip is placed with north to the top.

The HRIR data as recorded by the photofacsimile are completely unrectified in the crosstrack (approximately east-west) dimension. Rather, the data are recorded in a quasi-cyclindrical projection established by the intersection with a plane tangent to the earth at the satellite subpoint of a line from the satellite to the point viewed, as shown in Figure 2-3. As Figure 2-3 makes obvious, this creates

---

* When the data are received in the HAX or DRIR mode, they will not be gridded. Techniques for the geographical location of these data will be published elsewhere.

Geometry of HRIR for Nimbus I Satellite at 500 Nautical Miles

	Nadir angle, degrees			
	0	45	55	60.8 (Horizon)
Distance on earth from subsatellite point, degrees of great circle arc, as shown in diagram.	0	9.07	14.74	29.2
Distance on film from subsatellite point, mm	0	17.58	21.48	23.76
Distance on film for increment of two degrees of great circle arc centered on nadir angles presented above, mm	5.34	2.06	0.87	≈ 0
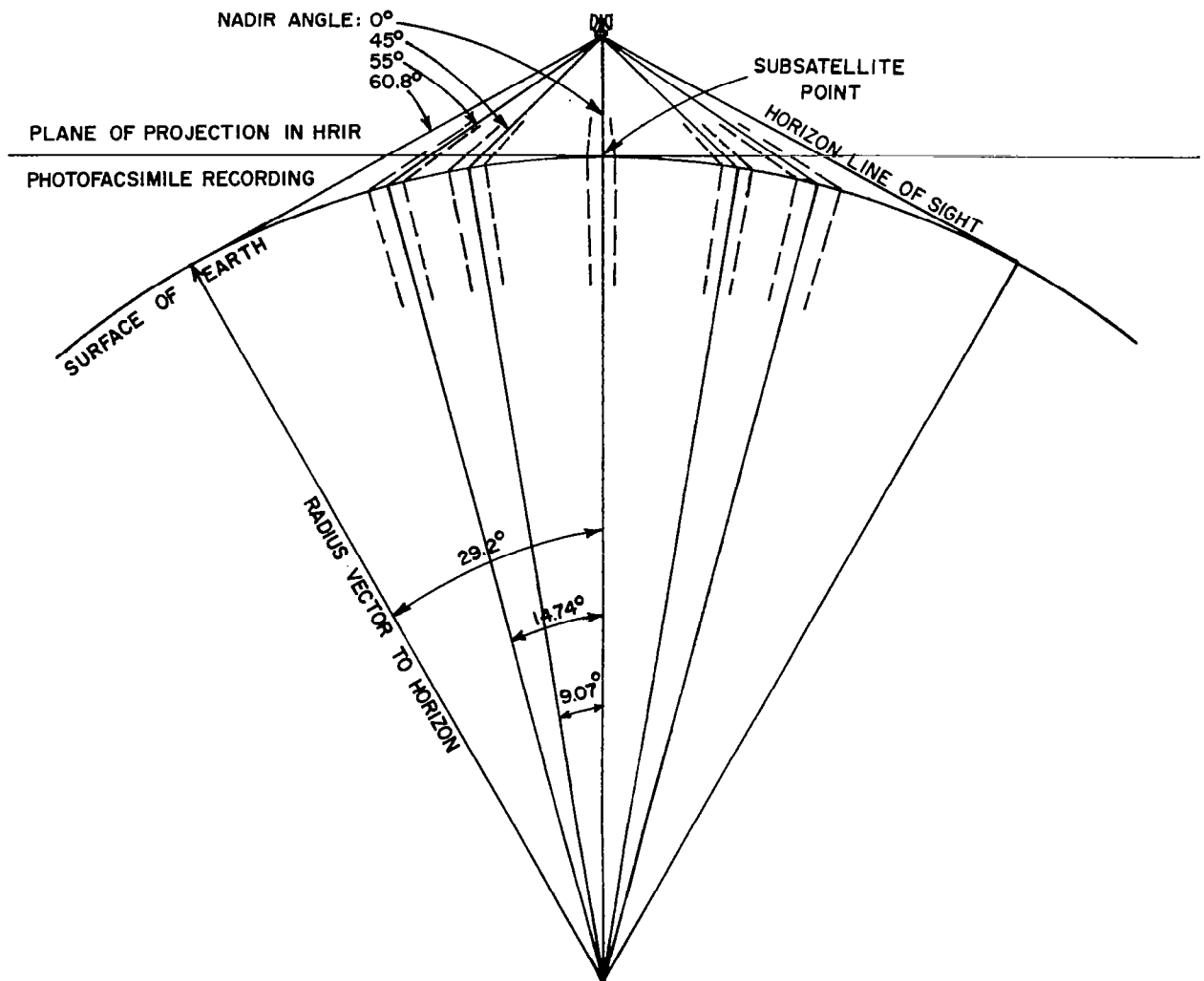
Figure 2-3   Illustration of Projection Used in HRIR Photo-Facsimile Recording

considerable distortion and foreshortening, particularly at the edges of the strips where there is extreme compression in the crosstrack (east-west) dimension.

In the Nimbus I HRIR, these effects were increased by the low perigee altitude, which led to a reverse aspect ratio (features excessively elongated in the crosstrack dimension) near the center of the strip while foreshortening distortions remained near the edges. [56]

These matters are illustrated in Figure 2-4, a Nimbus I HRIR daylight strip over the Mediterranean. When progressing from the edge of the strip toward the center, the width on the HRIR strip of a given distance in longitude increases (from Cirenaica, 33°N 22°E; to Sicily; to Sardinia; to Majorca, 39°N 3°E) in approximately the ratio 1:2:3:9, respectively.

Figure 2-4 also illustrates the degree of error more or less typical in the electronic gridding operation. By reference to Sardinia, Corsica, and the Balearic Islands (off the Spanish coast), the inscribed 40°N and 10°E grid lines are found to be about 1° too far south and too far west, respectively.

For Nimbus I HRIR data, therefore, the aspect ratio differs from unity in most parts of the photofacsimile strips, the exceptions being narrow strips located about one-quarter of the width of the film from each side. Near the center of the film, features are significantly expanded in the crosstrack dimension. This causes quasi-meridional cloud bands near the centerline of the film to appear greatly broadened. Quasi-symmetrical features and quasi-zonal cloud bands acquire a far more zonal appearance than they actually possess. It appears that the impression of a high degree of zonal banding that is obtained from a cursory scan of the Nimbus I HRIR data is largely produced by this aspect ratio factor.

This is illustrated in Figure 2-4 where the shape of Majorca is distorted and where, although the actual distance from Cape Nao (eastern Spain) to Minorca is about the same as that from Minorca to the Algerian coast, the aspect ratio appears to double the Nao-Minorca distance.

For all Nimbus HRIR data, the reverse aspect ratio or foreshortening of course exists near the strip edges, exaggerating all features in the meridional direction. This will remain until some rectification scheme is incorporated into the recording system and, even then, it seems unlikely that rectification could eliminate all these distortions, etc. At times, this foreshortening makes it difficult to be certain as to whether or not there is continuity between features near the edges of adjacent strips.

Some examples of the potential gain to be anticipated from rectification of the HRIR data are presented in Appendix B.

Figure 2-4   Nimbus I HRIR Daylight Data for Western Europe and the
              Mediterranean, Illustrating Observed Distortion and Edge
              Foreshortening

14

3. RECTIFICATION AND TRANSFER OF HRIR DATA

Normally, the HRIR data are most useful when related to or integrated with other meteorological data. It is also often desirable to relate the HRIR data to geographical features with greater precision than is possible from cursory use of the inscribed grid. Because of the unusual projection of the HRIR data, these comparisons are usually best accomplished by either superimposing the other data or features on the HRIR strips, or by transferring the HRIR data to normal maps of appropriate scale and projection.

When the HRIR data are transferred to a standard map, both geometric rectification and a method for depicting the intensity and character of the HRIR features are involved. Although these must be dealt with simultaneously in practice, for convenience of description they will be treated sequentially here.

Analysis and application of the HRIR data are nearly always aided by the mosaicing and joint use of the data from several adjacent orbits, regardless of whether this is done by mosaicing unrectified HRIR strips, or by transfer to a single map of the rectified HRIR features from several adjacent orbits.

3.1 Mosaicing of Unrectified HRIR Strips

Where adjacent strips of HRIR data are to be analyzed, and the areas of interest are primarily those poleward of some 40° to 50°, the construction of mosaics directly from the unrectified HRIR strips has been found to be a rather useful technique. Examples are shown in Figures 5-1 through 5-5 and 7-1 through 7-4, and specific procedures for constructing such mosaics are described in Section 5.1.

The advantages of such mosaics include:

1. Elimination of the labor inherent in the preparation of hand drawn, rectified nephanalyses, to be discussed below.

2. Preservation of the full resolution, gray scale, and detail of the photo-facsimile recording of the infrared data.

3. The large area, vivid panorama made available by such mosaics. In many cases, this establishes or emphasizes relationships between features which are of meteorological significance but might otherwise be overlooked.

4. Once the ten degree latitude and longitude grid lines have been traced on such a mosaic (or, better still, on a transparent overlay to avoid masking small

15

details in the mosaic), conventional weather analyses can be transferred to the "perspective" of the mosaic with relative ease and objectivity. The ease and objectivity of transferring isolines, fronts, etc., to such a mosaic is obviously greater than the transfer, from the HRIR data to a conventional map, of the irregular and often highly detailed cloud patterns in several tones of gray. Once the conventional data have been transferred to the HRIR mosaic, direct comparisons are readily possible.

The disadvantages of the use of the direct mosaics include:

1. They have not been feasible when the areas of primary interest are equatorward of about 50° unless photographic rectifications of HRIR strips can first be prepared. (For higher orbit altitudes, they should become feasible at lower latitudes.)

2. The mosaiced data are not in a form suitable for facsimile or other narrow band transmission, thus limiting their use largely to research or (for operational forecasting) to locations where the photofacsimile strips are received and the direct mosaics can be prepared.

3. At least for Nimbus I northern hemisphere cases, a false impression of perspective in the mosaics, as if the poleward areas were being viewed at a greater nadir angle than those at lower latitudes. This is, of course, not the case; along the center of each strip, the angle of view is vertical at all latitudes. It is believed this false impression may result from (a) the convergence of the meridians and possibly their apparent curvature;* and (b) the fewer brightly white areas and sharply contrasting cloud features at higher northern hemisphere latitudes.

3.2 Rectification of the Data by Transfer to Conventional Maps

When rectifying the HRIR data by hand and "eyeball" transfer to conventional maps, the geographical grid incorporated on the recorded data, while extremely valuable, still has been found inadequate for a convenient rectification. The major

---

* This curvature was not observed in the southern hemisphere mosaics and apparently results in part from the Nimbus I perigee being near the North Pole, with the North Pole appearing at a higher nadir angle than the South Pole. Furthermore, due to the lack of distinctive features at high southern latitudes, the South Pole grid point was frequently used as a match point while the North Pole was not (see Sections 5 and 7).

problem has been that of working within the $10^{\circ} \times 10^{\circ}$ "rectangles" with the 2° marks available only along the edges. The problem is increased in the east-west dimension by the change in scale due to foreshortening. In the north-south dimension, it is intensified when a 10° meridian falls near enough to the center of a strip so that, in middle and low latitudes, one side of a 10° "rectangle" is missing (see, for example, the northeast and southwest parts of Fig. 2-4).

To overcome this problem, it was found convenient to prepare a 2° average grid as a transparent overlay, with fixed latitudes and "rubber" longitudes (Fig. 3-1). Although such a grid seldom fits any strip perfectly (especially since it is desirable to match a 2° meridian line on the overlay grid to a meridian divisible by 2 on the HRIR strip), the error is seldom as great as typical gridding errors (1° to 2°) on the HRIR strips* except very near the edges where exact locations are always doubtful. ·

If increased accuracy is required, a series of a few such overlay grids for varying altitudes (and perhaps including a set with a one degree of longitude shift of the meridians along the strip centerline)could be prepared.[†]

When transferring the rectified features to standard maps, a definite problem of incompatibility between the 2° - 10° HRIR grids and the 1° - 5° - 10° grids of the standard maps was found to exist, as anticipated in Reference 54. It was found almost essential, for speed and accuracy of transfer and to minimize frustration, to provide a 2° grid for the standard maps before proceeding to the transfer. Where the same base map is used frequently but it does not seem desirable to reprint it with a 2° grid, this can be done by preparing a 2° grid in a form that can be placed under the base map and will be visible through it. If necessary, the work can be conducted on a light table.

The alternate procedure, preparation of a 5° "rubber" grid, does not appear to be feasible because of the rapid variation in scale across an HRIR strip as a consequence of foreshortening.

---

* These typical errors were determined by comparing clearly identifiable landmarks with the electronically incorporated grids.

† Current thinking suggests a similar set of "rubber" grids may be used for geographical location of the HAX (DRIR) data.
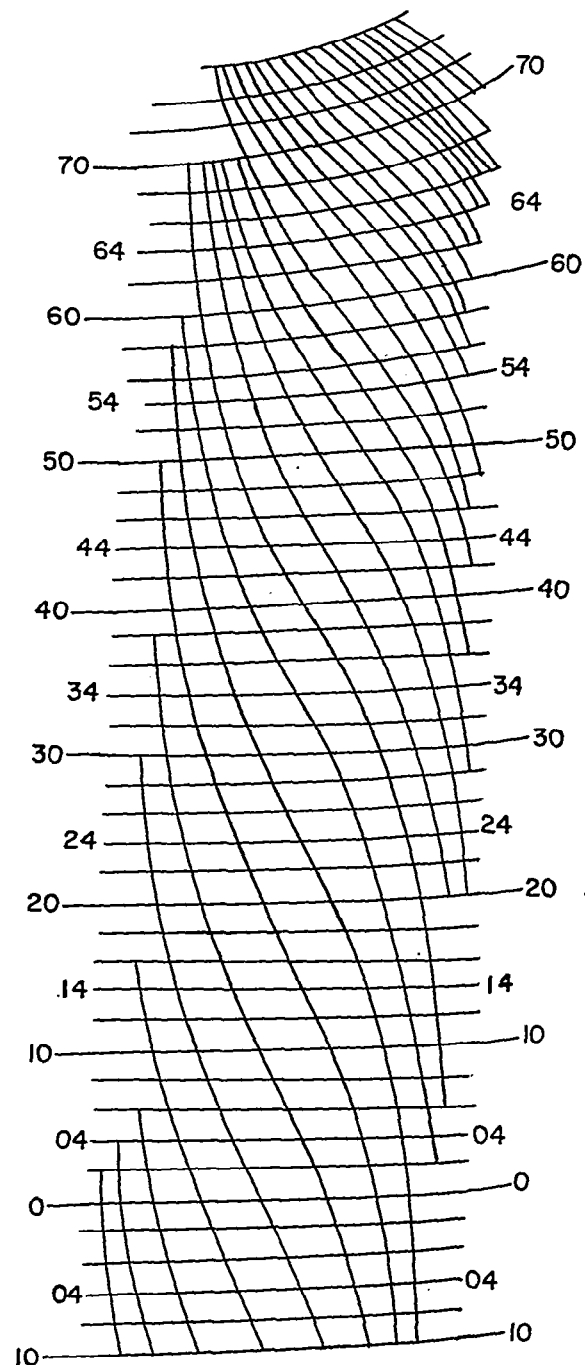
Figure 3-1   Example of a 2° Overlay Grid with "Rubber" Longitudes for use in Transfering and Rectifying HRIR Data.

3.3 Relative Temperature Depiction in Transferred Data

The variations in relative temperature shown in the photofacsimile-presented HRIR data are related to cloud top height. Accordingly, this variation is of considerably greater direct significance than the brightness in the TV cloud pictures which is the product of several factors, as discussed on pages 21-22 and 35-37 of Reference 55. These variations in cloud top temperature must be effectively depicted in the transferred data, even if only as relative temperatures. When absolute values are available, as from a calibrated gray wedge, reasonable choices of the boundaries between the areas depicted in different shades of gray can be made, retaining some degree of quantification. For very precise analysis in those cases where a calibrated gray wedge is available, there is also the possibility of converting the presentation to an isotherm analysis.

For many operational and initial research analyses, however, it is sufficient to use only a few broad categories of temperature when transferring the data. Suggested categories in this regard, and suggested conventions for use in various presentation and/or communication situations, are summarized in Table 3-1.

3.3.1 Colored Rectifications for Research or Local Operational Use

When the rectifications are to be used for research, or locally for operational analyses and forecasts, it is suggested that the data be entered on standard maps using the color conventions of the fourth column of Table 3-1. These or closely related conventions have been used with considerable success in several meteorological satellite infrared studies conducted by ARACON Geophysics Co.,[41,42] and many of the HRIR rectifications depicted by Zipatone conventions in this report were originally prepared using these color conventions.

3.3.2 Rectifications for Publication

Since color printing is usually more expensive than is merited for research reports, or is often prohibited by agency regulations or the editorial practices of most scientific journals, the color code has been converted to the Zipatone conventions of the fifth column of Table 3-1. As can be seen in Figure 3-2, and in several of the other figures in this report and in Reference 56, these conventions provide a rectified presentation which is rather analogous in tone to the original HRIR

Table 3-1

Suggested Conventions for the Transfer of HRIR Data

HRIR Brightness	Relative Temperature	Frequent Implications	Color Convention	Zipatone for Report Publication	Nephanalyses for Facsimile Transmission
White	Very cold	High clouds, polar or high level ice or snow	Blue		Cross-hatch
Off-white	Cold	Middle clouds	Green		Single-hatch
Gray	Cool	Low clouds, indefinite terrain	Red		Stipple
Black	Warm	Ocean, land, below film sensitivity, or very low clouds	Blank		Blank
Visible and identifiable landmarks		Landmarks/clear	Black; outline or shading of features	*	Heavy outline or shading of feature, "callout" pointing to feature, or mark area as "clear"
Cellular clouds		Low level convection	Stipple in appropriate color		Notation or "callout"

* or "callout" pointing to feature
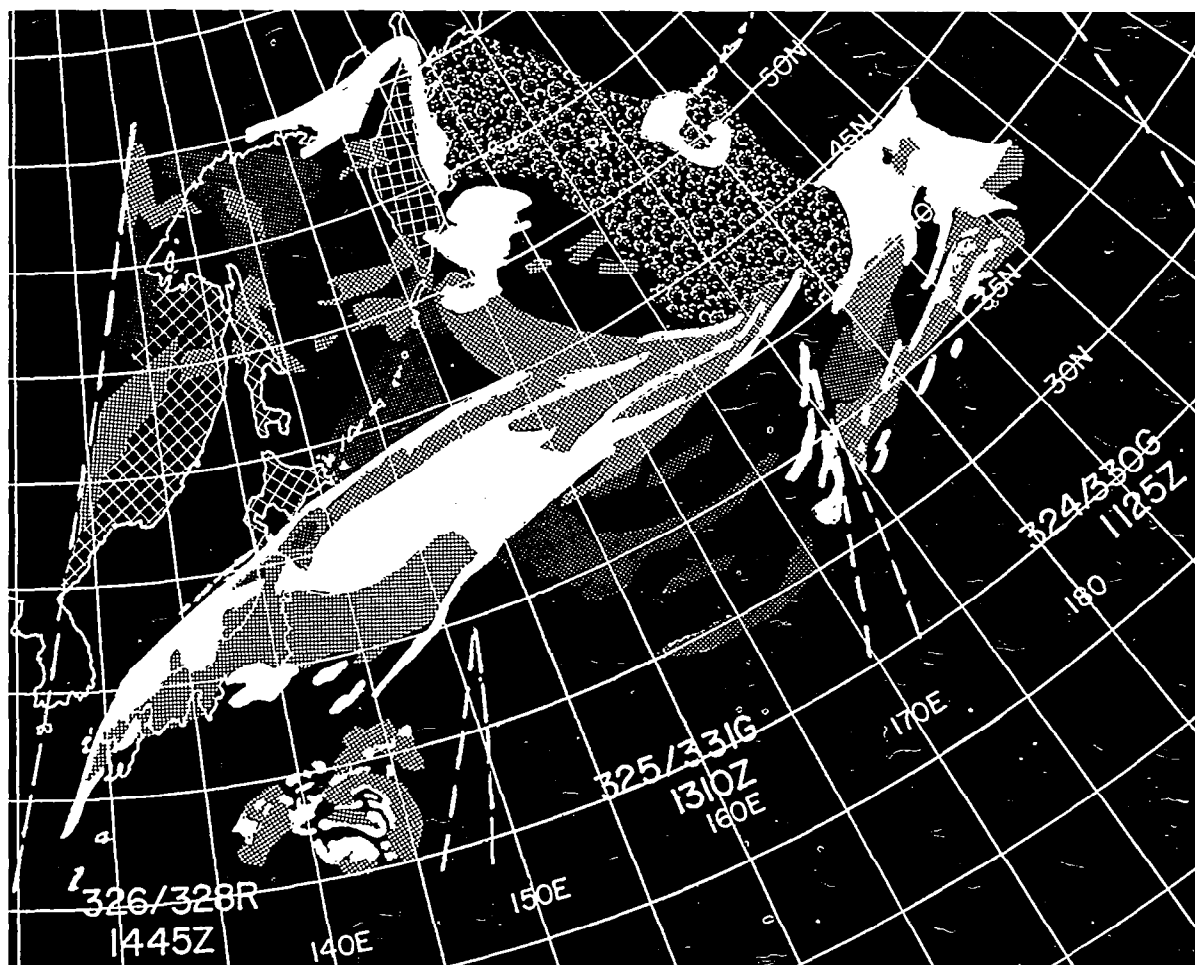
Figure 3-2   Example of an HRIR Rectified Mosaic Prepared for Publication
Using Zipatone

photofacsimiles. If good quality halftones of the unrectified HRIR data are also included in the report, the reader is provided with both the data in as good a representation as possible of their original form, and a rectified mosaic in a standard map projection.

3.3.3 Nephanalyses for Facsimile Transmission

Obviously neither the color nor the Zipatone conventions are suitable for operational facsimile transmissions, and normally operational nephanalyses will be prepared in somewhat less detail than research rectifications. Furthermore, insofar as possible, the conventions used for nephing and transmitting the HRIR should be compatible with those used for the TV data, which are given in Table 2-13, page 26, of Reference 55.

The following procedures, based on Table 2-13 of Reference 55 and the sixth column of Table 3-1 of this report, are suggested:

1. Outline the definite and indefinite boundaries of major and of unorganized cloud systems and masses, using the conventions of Table 2-13. Boundaries should be chosen so as to emphasize rather than to mask the cloud patterns and systems of known or probable synoptic significance.

2. Using the conventions in the last column of Table 3-1, indicate the brightness (or cloud top temperature) category of each area within the various boundary lines.

3. By notations in small areas left for this purpose within the areas of hatching or stippling, or by appropriate callouts and/or annotations, enter other appropriate information according to the conventions of Table 2-13 and/or other information or interpretation that may be useful to the receiving analyst or forecaster.

4. As discussed in Chapter 10 of Reference 55, and illustrated in Reference 42 operational use of the facsimile nephanalyses will be aided by:

a. Preparing the nephs on maps of the same projection and scale as those used for other facsimile-transmitted analyses, or as those prepared in the receiving weather stations. It is especially desirable that the nephs, the 500 mb analysis, and the surface analysis be compatible for use as direct overlays.

b. Where possible, combine the data for several adjacent HRIR orbits into a single nephanalysis prior to transmission.

c. Where such combination is not feasible prior to transmission, prepare the nephs so they can easily be assembled into mosaics at the receiving

points. This, of course, requires use of a common map projection and scale for contiguous areas.* In addition, the data as entered on the previously transmitted contiguous neph should be consulted and considered when preparing the neph for the next orbit. While at times a rapidly developing situation may require somewhat incompatible analyses for adjacent or overlapping areas, such cases should be relatively rare. When such apparent incompatibility is necessary, remarks should be entered on the later neph to point out the discrepancies as a source of further information to the using analyst.

Figure 3-3 provides an example of a possible facsimile nephanalysis prepared using the procedures suggested above.

---

* Except, of course, for the inevitable need of using different projections for tropical and for middle-latitude/polar areas. The nephs for the subtropical areas where the projections change should overlap from one projection to the other, rather than merely abutting.
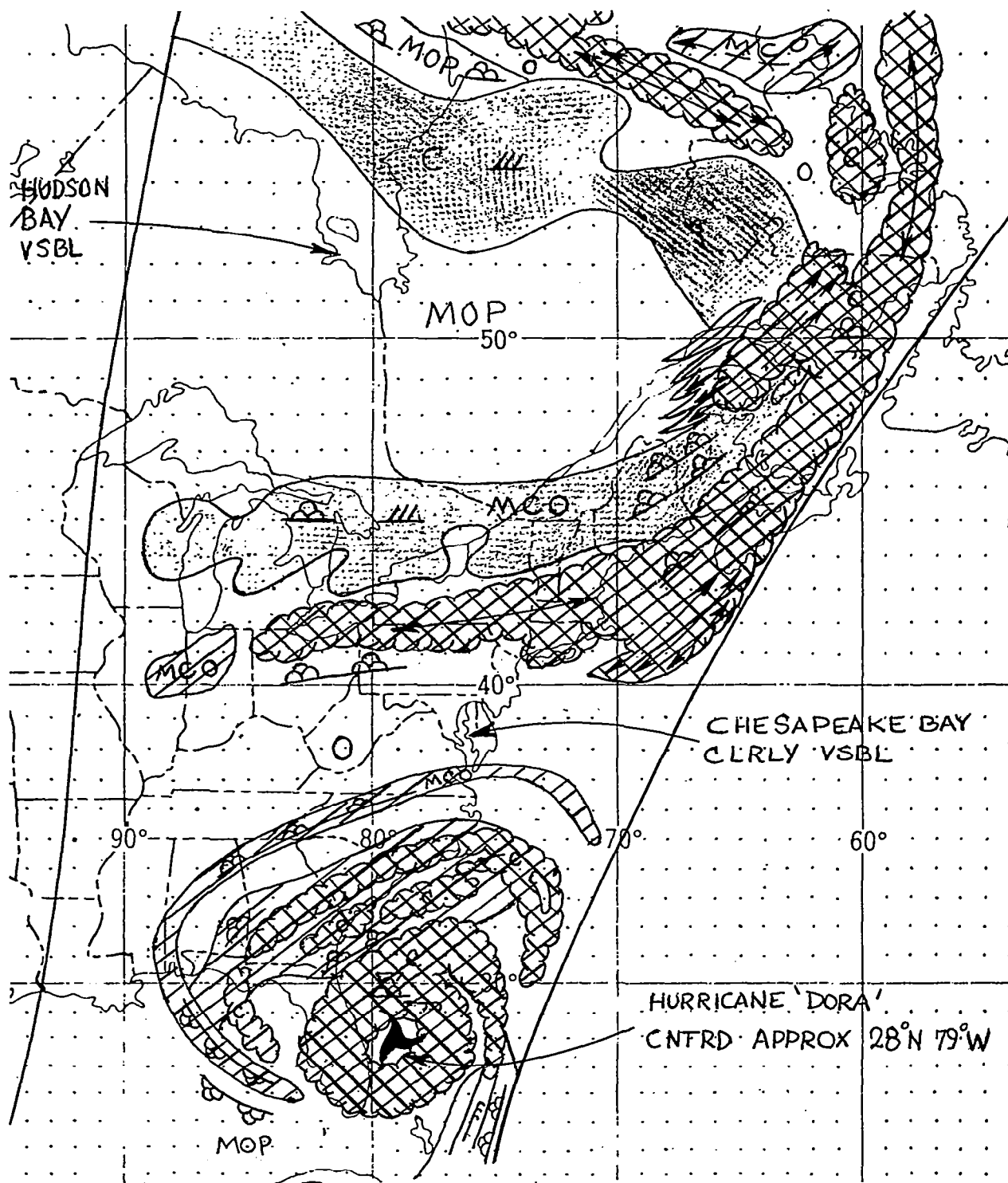
Figure 3-3   Example of an Nephanalysis in a Form Suitable for Facsimile
Transmission (Prepared from Orbit 174 of the Nimbus I HRIR;
(See Figure 4-3)

4. SUMMARIZED CONCLUSIONS AS TO THE METEOROLOGICAL INTERPRETATION OF HRIR DATA

The meteorological interpretation of the HRIR data presents no great problems to persons previously skilled in the interpretation of TIROS pictures, provided the analyst keeps in mind the fact that the visible contrasts are those of temperature and not of reflectivity. At first this requires a distinct effort because of the great resemblance between HRIR strips and many TIROS pictures, especially in the cloud features and patterns now so familiar from the TIROS pictures. Perhaps the chief new problem is the fact that low clouds, which would be among the significant features in a TIROS picture, may be only dimly visible or at times not even discernible in the HRIR data.

Otherwise, it appears that most of the principles developed for interpretation of the TIROS cloud pictures are generally valid when dealing with the HRIR data. These are discussed in Reference 55, amended as regards cloud vortex interpretation by the later findings presented in Reference 41, and as regards tropical interpretations by those in Reference 32. Vortices (Fig. 4-1), cloud patterns associated with short wave troughs (Fig. 4-2), major or active frontal bands (Figs. 4-1 and 4-3), tropical storms (Fig. 4-3), and other similar major features can usually be clearly seen and identified. In many cases, it appears that such identification is significantly aided by the relative de-emphasis of the low cloud features in the HRIR data. Even far smaller details, such as lee waves (Figs. 4-4 and 5-5, near 70°N 95°E) and billow clouds* can often be matched to AVCS or TIROS pictures taken approximately twelve hours earlier or later. Demonstration of the feasibility of analogous interpretation of the two types of data is a most significant result of our studies.

4.1 Low Cloud Detection and Identification

Because low cloud identification seems to be particularly troublesome, this and related matters will be discussed first. It has been our observation that visibility of identifiable landmarks is the only proof that an area is clear, i.e., lacks in significant low cloudiness. Otherwise, the possibility of low clouds or fog

---

* A possible case of billow clouds is included in Figure 4-5, near 39°N 281°E.

Figure 4-1   HRIR Observations of Cloud Vortices and Frontal Cloud Bands

Figure 4-2   HRIR View of a Well Developed
Short Wave Trough

Figure 4-4   Lee Waves as
              Observed in the
              HRIR (near 39°N,
              239°E)
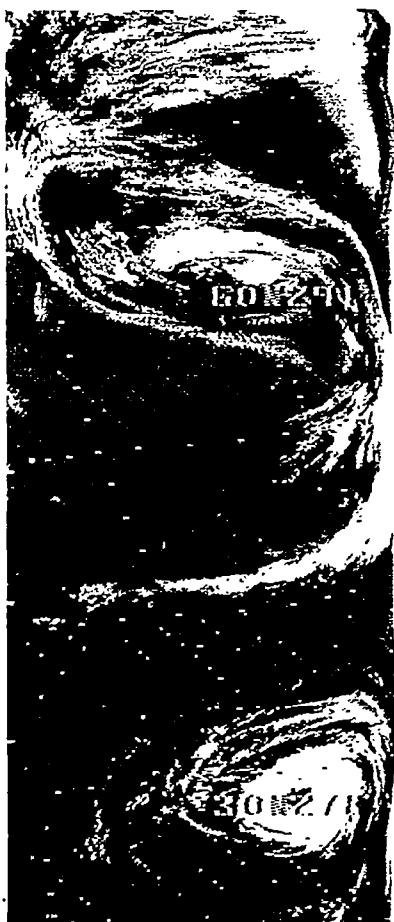
Figure 4-3   HRIR View of a
              Cloud Vortex,
              a Frontal Cloud
              Band, and a
              Hurricane

Figure 4-5   Illustration of How Clear Areas May Be Colder Than
              Those with Cloud Cover, Due to Latitudinal and Frontal
              Temperature Gradients

will always remain. Low cloud identifiability may become somewhat more reliable when standardized, high quality data presentations become available. We have found it vital when transferring the HRIR data to standard maps to outline or identify those landmarks that are visible, and to carefully inspect all warm areas to insure such landmarks are detected. Such an inspection is also performed over polar areas and high mountains, since Greenland, Antarctica, and the higher Himalayas may often otherwise be mistaken for middle-to-high clouds. In such mountainous areas as the Himalayas, there often will remain a doubt as to whether terrain-shaped white features are cold snow, high terrain, local orographic clouds, or some combination of these. The same problem often exists, of course, with TIROS pictures over mountain areas.

When attempting to differentiate areas with low clouds from possibly clear areas, the general equator-to-pole temperature gradient, and the more pronounced temperature gradients across fronts, must be considered. For example, a definitely clear area over Quebec and Labrador was noted to be significantly colder (a lighter gray) than a concurrent area of low overcast over the Ohio River valley (see Fig. 4-5, and the discussion in Section 4.5 of Ref. 56).

At the season and local time of observation of the Nimbus I HRIR, landmarks were far more visible in higher latitudes than in the tropics. With the exception of the outlines of the Antarctic continent or its ice shelves (see Sections 6 and 7) and of one series over southern South America where landmarks could be easily identified (see Fig. 65 of Ref. 56), landmarks appear more visible in the middle and high latitudes of the northern hemisphere than in comparable latitudes of the southern hemisphere. For example, the various lakes of Australia are rarely visible, while lakes and rivers over Asia and North America can frequently be seen. This perhaps resulted from the seasonal differences between the two hemispheres. Water bodies, whether oceans, lakes, or rivers, almost always appeared warmer (darker) than the adjacent land areas.

It appears that in some cases fog, or stratus formed from the lifting of fog, can be identified as untextured areas of a uniform, flat, light gray tone which often have sharp edges. Examples are shown in Figure 5-1, near 55°N 107°E and to the east thereof. Most of the cloud areas with these characteristics either coincided with or were close to stations reporting fog or a zero dewpoint depression, or were in synoptic situations where fog or stratus is likely. In such fog or stratus identification, care must be taken to insure no landmarks are visible, as,in some cases, high plateaus assume the same flat, light gray appearance except for visible and identifiable landmarks.

Although considerable further study is required, our investigation suggests that the boundaries in HRIR brightnesses noted over the oceans are cloud edges, not sharp discontinuities of sea surface temperature.

Cellular low cloud fields of the type frequently seen in TIROS pictures to the rear of cyclonic storms and cold fronts often appear in HRIR as only a general gray mass with no evidence of the cellular structure (Fig. 4-6). In other cases, however, (perhaps those cases where the clear areas between the cumulus conglomerates are larger), the cellular structure has been visible. This has been particularly true in the Antarctic Ocean, where scattered convective clouds (presumably cumulus congestus or occasionally even cumulonimbus) are frequently seen (Fig. 6-14).

The cellular patterns have also been identified in the HRIR over other oceans (Fig. 4-1, left strip), but seldom over land. With an increase in orbit altitude and a decrease in resolution, the difficulty of recognizing cellular cloud areas can be expected to increase.

As would be expected, cases have been noted where scattered cirrus (only partly filling the instantaneous field of view of the sensor) was essentially indistinguishable from a lower overcast (Fig. 4-5, over north central New England).

4. 2 Cloud Top Heights and Higher Clouds

The HRIR data have shown that cloud top heights (both relatively and absolutely) cannot be reliably estimated from TIROS or AVCS pictures alone. Brightness differences in the pictures are often insufficient and at times may even be misleading. Low stratus (only dimly visible in HRIR) may appear brighter in the TIROS pictures than large tropical cumulus masses (on the same orbit and film strip) which the HRIR data showed must extend to significant altitudes. Frontal bands (Fig. 4-5, from the middle Atlantic coast to the Great Lakes) which appeared relatively bright (and rather uniformly so) in the TIROS pictures were shown by the HRIR to be largely low to middle clouds (gray to off-white) with imbedded scattered to broken masses of clouds reaching to higher altitudes (distinctly white). These demonstrations of the unreliability of cloud top height estimates from TV pictures are in complete accord with those of Sherr,[41] who used the TIROS Channel 2 IR data in his studies.

Because of this limitation of TV pictures, plus unreliable detection of low clouds by HRIR, a multi-frequency operational observational capability would appear to be desirable. (This does not imply that either TV pictures or window IR
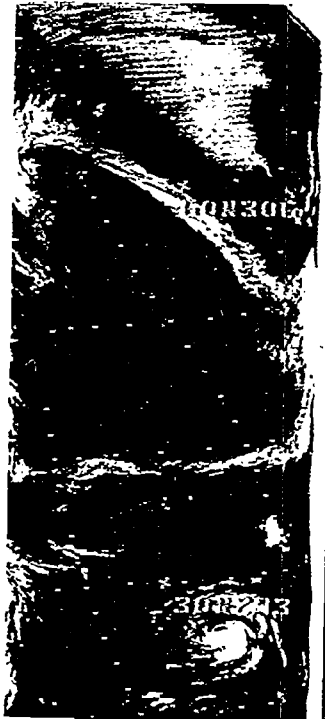
Figure 4-6   Cellular Cumulus (near 50°N, 300°E) May Appear
             as Only a General Gray Mass in the HRIR

data, alone, are not of significant operational value in the interim.) During the daylight passes, TV observations should be complemented by high resolution IR observations (ultimately in the 10μ window, since the 4μ HRIR of course provides little or no cloud height information during daylight). At night, a high resolution IR system (in either IR window) should be complemented by a starlight intensity TV camera, or some other method of observing clouds in the visible portion of the spectrum.

The success of the HRIR system suggests its scanning system and optics might be usefully applied to nighttime, starlight intensity observations of clouds in the visible spectrum. For such a use, the lead selenide detector would be replaced by an appropriate photomultiplier. Filters should not only restrict the response to the longer wavelengths of the visible spectrum (to reduce haze interference) but, insofar as possible, should also filter out the wavelengths of the principal airglow emissions. Otherwise, nighttime visible spectrum observations may be restricted to conditions of at least partial moonlight.[53] As in the case of the HRIR, it would be highly desirable for the recording system for such a sensor to provide for geometric rectification of the data presented to the user. *

Although cloud top heights often cannot be reliably inferred from the relative brightnesses of the clouds as seen in the TV pictures, on the other hand, we have found in several cases that mesoscale darker areas (or even relatively faint breaks) in large scale cloud masses as seen by TIROS often correspond to warm areas (lower cloud tops) in the HRIR data.

4.3 Relationships of Extratropical HRIR Data to Mid-Tropospheric as Compared to Frontal Analyses

These studies have tended to confirm previous findings[41,55] that the prominent extratropical cloud patterns as observed by satellites, and especially those extratropical cloud patterns shown by the HRIR data to be relatively cold and so reaching well into the middle or upper troposphere, are in general far better related to the mid-tropospheric (500 mb) flow patterns than to frontal analyses. Essentially all extratropical areas of cold clouds of significant size, as seen in the HRIR, can be satisfactorily explained in terms of areas of cyclonic vorticity or vorticity advection,

_____

* This concept would also be applicable to an HRIR sensor mounted in a cartwheel satellite, as proposed by Widger[52] and others.

or as clouds formed in such an area and subsequently advected from it. Reasonable patterns of day-to-day continuity usually present fewer problems when viewed in terms of these explanations.

While there is often a good correlation between cloud bands or areas and analyzed fronts, it can usually be noted that, in the absence of upper level support, such clouds seldom extend to significant heights. Furthermore, in many cases it appears difficult to establish a reasonable continuity, from one day to that of the next, for the frontal analyses, or for the cloud bands and areas when it is attempted to explain them and their continuity primarily on the basis of frontal concepts. Since frontal analysis is often highly subjective, [22, 37] this is not entirely unexpected.

It should not be inferred from the above that fronts do not exist, or that they are always insignificant. Rather, it would appear that their effects are more constrained to the lower levels (those where the clouds appear light gray or darker in the HRIR). A usually necessary and at times a sufficient condition for the clouds to extend to higher levels (where they appear white in the HRIR) is mid-tropospheric flow patterns which produce significant upward vertical velocities[55] at the synoptic scale, or permit them at the meso- or convective scales.

As an illustration of these matters, it may be helpful to consider the so-called "back door" cold front of New England, a front that comes in principally from the north rather than from the west. Such fronts usually are associated with significant temperature contrasts at low levels, and often there is adequate moisture in the warm air. Under classical frontal concepts, one might expect considerable weather with such fronts, but this is seldom the case. This is because they usually lack upper air support and are often under the weather suppressing influence of northwest flow aloft.

Figures 1, 2, 3, 5, and 6 of Reference 56 provide data for what is apparently the best HRIR observation of such a case (see also Fig. 4-3 and Section 11 in this report). The active weather appears to be concentrated along the eastern, north-south oriented part of the front, in association with a short wave trough over the Gulf of St. Lawrence and the Maritime Provinces. The more western or "back door" part of the front, under northwest and perhaps even slightly anti-cyclonic flow aloft, peters out with a relative lack of either high clouds or active weather, as further shown by Figures 7, 8, and 9 of Reference 56.

4.4 Types of Frontal Cloud Bands

At least three types of frontal cloud bands have been noted during these studies of the HRIR data. While they will be discussed here principally in terms of the surface and mid-tropospheric flows, it is believed that the available atmospheric moisture may in some cases also be a significant influence. Where frontal lifting is the principal available dynamic mechanism, dry air may limit cloud formation while, in other cases, moisture may be sufficient for convective instability and more extensive cloudiness to develop.

4.4.1 Frontal Bands with Only Low Level Clouds

An example of a frontal situation with clouds only in the lower atmosphere is shown in Figure 5-3, near 72°N 110°E. In such cases, the surface isobars usually indicate low level flow up the frontal surface, the front usually being analyzed as a stationary or weak warm front. There is, however, insufficient upper air support to create mid-tropospheric upward velocities and higher level clouds. The 500 mb flow is often more or less parallel to the frontal band, but there is no nearby or immediately downstream source of significant lift and mid-tropospheric cloud formation from which higher clouds or moisture can be advected along the frontal band.

In meteorological satellite TV pictures, these low level cloud bands will often appear as bright as those where clouds extend to considerably higher levels. Thus, an infrared observation is often vital to identifying these situations.

4.4.2 Low Level Frontal Cloud Bands with Higher Level Scattered-to-Broken Cloudiness

In these cases, as illustrated in Figure 5-1, near 65°N 110°E, the higher clouds often have a streaky appearance in the HRIR. The immediate surface and 500 mb flow patterns often appear much the same as in those cases which lack upper level clouds, but there is usually an upstream cyclonic vorticity maximum from which higher level clouds can be advected along and over the lower level frontal cloudiness. Some of the high level cloudiness may also be attributable to mesoscale vertical motions associated with jet stream flows[8] acting on moisture transported upward (in the upstream vertical motion area) and subsequently advected horizontally, along the lines of the hygrokinematic theory proposed some years back by Ligda.[35]

A somewhat similar cloud pattern has been observed over the Canadian Rockies of western North America when the 500 mb flow was generally parallel to the divide while the low level flow had an upslope component in relation to the large scale terrain.

4.4.3 Frontal Cloud Bands with Extensive High Level Cloudiness

In these cases, illustrated in Figure 5-2, near $54^{\circ}N$ $120^{\circ}E$ there is almost always significant upper level support in the form of a 500 mb short wave trough or vorticity maximum.

Even in these cases where the cloud band is for the most part extensive and continuous, it usually weakens to lower and more broken cloudiness when passing through a col or other area of lesser 500 mb vorticity (Figs. 5-1 and 5-2).

4.5 Cloud Vortices

Cloud vortices are well depicted in the HRIR data, and can usually be recognized without difficulty (Figs. 4-1 and 4-3). The overall shapes of the high and low cloud patterns as depicted in the HRIR are basically the same as those made so familiar by the TIROS pictures.[55] The HRIR-detected temperature variations, however, clearly reveal differences in cloud top heights which are far from obvious in the TIROS pictures (Fig. 4-1, center strip). The cloud top height distributions correspond well to those found by Sherr and Rogers,[41] using integrated analyses of TIROS cloud picture and IR data. Furthermore, the HRIR data reveal significant details (as discussed later) that are often poorly visible, if at all, in the TIROS IR data.

The sequence of ARACON studies of cloud vortex patterns, going back to the basic Boucher-Newcomb model,[7] continuing through the subsequent studies as summarized in Reference 55 and presently culminating in those reported in Reference 41, have led ARACON meteorologists to a specific hypothesis as to the mode of formation of vortex cloud patterns. The HRIR data, which became available as we were completing the studies reported in Reference 41, have assisted both in the development and substantiation of this hypothesis. The hypothesis[41] states that during the early stages of vortex formation, i.e., usually while the upper air circulation has not proceeded beyond a short wave trough, or through the early stages of occlusion, the cloud patterns are determined principally by the rather characteristic patterns

of dynamically induced vertical motions (Fig. 4-2). In later stages, as the cyclonic development leads to a closed circulation, advection and associated deformations of the clouds become of increasing importance, especially in the western portions of the system (Figs. 4-1 and 4-3). Closed circulations, and those cloud patterns formed by advection are normally first observed at lower levels and later at higher altitudes.

These developments are clearly seen in the HRIR data, but the resolution of HRIR also reveals details which may be masked or missed in the TIROS data. As an example, the high cloud spirals observed in mature cyclones, while apparently the result principally of advective processes, appear often to be modulated by mesoscale areas of varying vertical velocities (Figs. 4-1 and 4-3). In areas where the air moves poleward, the clouds often broaden and brighten, presumably due to intensified upward motion. Conversely, areas of equatorward movement are those where the clouds thin and darken, suggesting some degree of downward motion. This, of course, agrees with vorticity and thermal advection concepts since warm thermal and/or cyclonic vorticity advections most commonly exist in poleward moving air. These concepts are further discussed in Section 6.1 of Reference 55, and the references cited therein. Examples are illustrated and discussed in the case studies.

After noting these vertical velocity modulations in the HRIR data, a number of TIROS pictures of vortices were chosen at random and examined. TIROS pictures of some HRIR vortices, but taken approximately twelve hours earlier or later, were also checked. In no case were these vertical velocity modulations prominent in the TIROS pictures; in fact, they were unlikely to be noticed without a reason, such as the HRIR provided, for looking for them. In many cases, they just could not be detected; in others, they were only dimly visible. It seems likely that this type of cloud top height detail, which only an HRIR system seems likely to supply, may often be significant. In several cases, it has been possible to relate the details in the vortex cloud patterns to small short wave perturbations superimposed on cyclonic circulations (Fig. 4-3).

4.5.1 Distortions of the Short Wave Trough Cloud Patterns

The most frequent characteristic cloud pattern in the early stages of cloud vortex development is that with a crescent or comma shape which Rogers[6,41,55] has identified as indicative of a short wave trough (Figs. 4-2; 5-3, near 75°N 80°E). During these studies, it has been noted that when there is a 500 mb ridge just east of the trough, leading to an "S" shaped pattern of 500 mb contours, the

characteristic short wave trough cloud patterns may be distorted into one resembling a backwards question mark or an integral sign $(\int)$. An example is shown in Figure 5-5, near 60°N 40°E.

4.6 Clouds Outlining a High Pressure Area

During these studies, it was noted that apparently persistent cloud patterns often outlined at least the western edge of a major high pressure area, especially in the case of an Ω-block when such cloud bands conform to at least much of the western part of the Ω flow pattern (Figs. 5-1 and 5-2).

It appears that one source of these cloud patterns is a series of cloud bands or areas which are formed in areas of upward vertical velocity to the west of the high or the Ω flow. At first these clouds move eastward in a more or less normal westerly flow. When they begin to come under the influence of the high or of the Ω flow, this both reduces further eastward motion and tends to dissipate any portions of the cloud bands which do move further eastward. Thus, a series of cloud bands which moves into the western edge of a major ridge leads to the appearance of a persistent cloud outlining at least the western portion of the ridge.

A second source of the cloud band outlining such ridges is cloudiness formed in areas of significant upward motion adjacent to the western part of the ridge, as in the cutoff low typically found just west of an Ω-ridge, and subsequently advected along the flow pattern around the ridge.

In one case, it has been possible to relate the changes in such cloud bands to the partial breakdown and transformation of an Ω-block over Eurasia. It appears that similar cloud bands exist in other blocking situations, and that their patterns, movements, and changes may aid in deducing the establishment, persistence, transformation, and dissipation of Ω-blocks and other major high pressure areas. It further seems probable that a similar mechanism may occur with late spring and early summer squall lines over the eastern United States, which often appear to form in and move eastward from a trough in the Mississippi Valley, and to dissipate as they come under the influence of the Bermuda High, at times before reaching the east coast.

The case studied (see Section 5.2.5) indicated that observations at least every twelve hours are needed to really follow what is happening and to avoid interpreting the eastward movement and dissipation of a series of bands as the retrograde or fluctuating movement of a single, persistent band.

4.7 Mesoscale Observations

There appears to be a rather pronounced tendency for very white (cold) areas in the HRIR to be associated with general areas of present or very recent past precipitation. At least one exception, that of cirrus clouds, does appear to exist, however. Outside of this exception, the correlation between the white (cold) HRIR areas and areas of precipitation appears far better than the rather poor correlation found between bright TIROS clouds and concurrent precipitation.[33] More study of this relation is, of course, still desirable.

Our studies suggest that many of the bright, narrow cloud bands seen in the HRIR are, or include, jet stream cirrus bands (Fig. 4-4, near 50°N 248°E). These bands and their orientations often seem to conform to the concurrent upper level analyses. In some cases, however, these bands cut across the jet streams as analyzed, even over areas of adequate data. In such cases, they may correspond to the area of cirrus that often exists downstream from an area of confluence between two converging jet streams, as noted by Kadlec.[23, 24] Jet streams have also been noted in areas where no clues are provided by the HRIR data. Cases have also been noted where jet stream and other HRIR banded or linear clouds exhibit bends which suggest sharper curvatures in the streamlines of the wind (or the contours on upper level charts) than are normally analyzed.

As mentioned in Section 4.2, frontal bands often exhibit a texture in the HRIR, with scattered-to-broken higher clouds over a lower overcast. This texture is often in the form of mesoscale bands, generally parallel to the overall orientation of the frontal band (Figs. 3-2, 4-1 and 11-1). Sizes and spacings suggest they may be associated with the mesoscale wave-type motions of approximately 200 to 300 km wavelength, and the convection bands spaced approximately 70 km apart, that Elliott and Hovind[10] have identified in frontal zones approaching the California coast. If so, these scales of motion appear to be frequent and to be found in other parts of cyclonic vortices than along the cold or occluded front. For example, a similar scale of structure can be noted on the west side of many of the HRIR observed cloud vortices (Figs. 4-1 and 4-3). We have as yet, however, been able to study only one case where the density of conventional observations was adequate for a definitive analysis (see Section 11).

There are indications that certain more or less V-shaped cloud patterns, such as those in Figures 4-5 and 10-1, may be characteristic of certain types of squall or convective lines. After these patterns were noted on these two HRIR

orbits, patterns of the same general shape were identified in TIROS pictures of squall and convective lines. Further study will be required to determine what significance (if any) there may be to this possibly characteristic pattern, and the dynamic factors that lead to its formation. A slightly expanded discussion of these matters is given in Section 10.5.

Small details, such as lee wave clouds, are often clearly visible in the HRIR data (Figs. 4-4 and 5-5). The altitudes that lee wave clouds sometimes attain (up to 12,000 feet above the terrain[55]) may explain their visibility in the HRIR data as compared to the frequent loss of visible structure of cellular clouds of apparently similar dimensions.

Our studies indicate that medium-to-large scale details in the mesoscale features are often extremely persistent. Although the HRIR data and the TIROS TV pictures are about twelve hours apart, detailed cloud patterns can often be rather definitely related from one type of data to the other. With data at about twelve hour intervals thus available, mesoscale details can at times be traced for periods of at least twenty-four hours (see Section 7.3).

The frequency and apparent significance of the mesoscale detail available in the HRIR data raises questions as to the appropriateness of the averaging procedures required to perform objective nephanalyses as proposed by Blankenship[5] and by Maykut.[28] Such practices may be in order where only the large scale aspects of cloud cover are of concern, or where communications facilities leave little alternative. In this latter case, consideration should be given to annotating the objective nephanalysis as to significant details obliterated in the objective processing. It would appear the procedures proposed by Blankenship and developed by Maykut would reduce the resolution of the data to about that of the TIROS or MRIR Channel 2 data, so some idea of its effects can perhaps be estimated by comparing the vortex south of Kamchatka in HRIR orbits 252* and 253 (Figs. 34 and 35 of Ref. 56) with the TIROS Channel 2 data for apparently similar vortices; i.e., 3-1, 3-2 or 4-13, 4-14, 4-15 of Reference 41. Better still would be comparisons of HRIR and either TIROS VII[†] or MRIR Channel 2 data for the same systems.

---

* Orbit 252 is also included in Figure 4-1 of this report as the center strip.

† At the time of these studies, TIROS VII IR data concurrent with the Nimbus HRIR data were not yet available.

4.8 Antarctic Analysis

Two studies of a several day series of HRIR observations over the Antarctic Ocean (see Sections 6 and 7) have demonstrated that the principles developed for HRIR analysis in the northern hemisphere, as discussed in the previous sections of this report, are equally applicable in the southern hemisphere.

In most aspects, those weather systems which were observed conformed with previously published discussions of the synoptic climatology of the region. It does appear, however, that the circulation in the area just north of the Antarctic continent is more complex, and so the zonal circulation is significantly more disturbed, than is usually shown on conventional analyses of the area. Consequently, it is more appropriate to use the HRIR data to develop improved analyses for these data deficient areas than it is to attempt to use the conventional data to confirm the Antarctic area HRIR observations. The improvement possible in analyses combining the HRIR and available conventional data is discussed in Section 7.4.5 and illustrated in the revised analysis presented in Figure 7-10, which can be compared with the IAAC operational analysis in Figure 7-2a.

Because the HRIR data are most useful and most easily interpretable at night, they will be particularly valuable during the Antarctic winter months, when the extended periods of darkness permit longer periods of HRIR observations within each day. During this season, the conventional data are even more sparse than during the Antarctic summer.

Comparative studies of the HRIR and the TIROS TV data show that the cellular cloud patterns to the rear of cyclones, as seen in the HRIR, are of a larger scale than often apparently similar patterns as seen by TIROS. Usually, when the cellular patterns are seen in the TIROS pictures, the area will appear as only a solid, gray, low cloud mass in the HRIR. Accordingly, it is unlikely that the principles developed by Merritt and Rogers[30,55] for determining low level winds from such TIROS convective patterns will be applicable to HRIR data. The procedures developed for the use of the TIROS data were based on a convective cloud layer sufficiently shallow for significant changes in wind direction to be improbable; the cellular convective cloud pattern as seen in the HRIR are usually cases where the cumulus clouds appear to extend through a relatively deep layer.

Studies with the HRIR data, and with comparative TIROS and AVCS pictures, indicate that it is nearly impossible to detect cloudiness over the Antarctic continent by any present type of satellite observation. The few exceptions are usually cases where the clouds from systems off the coast can be traced for a short distance inland. It is possible to detect cloudiness over the ice pack which normally surrounds the continent, using the HRIR, providing the clouds are sufficiently high and cold. It may often be difficult to determine from the HRIR alone where the edge of the ice pack is, or exactly which areas are clouds and which are ice. In the TIROS pictures, however, the edge of the pack ice can usually be seen. Since the edge of the pack ice normally moves only slowly from day to day, this gives a reliable indication of where ice is to be expected in an HRIR observation, even if the TIROS and HRIR data were a day or so apart. Accordingly, the combination of the two types of data often gives a reliable indication of where cloudiness exists above the ice pack. (See Section 6.8.3 for a fuller discussion of these matters.)

The HRIR data are also applicable to ice surveys in the Antarctic area, since ice-free areas and "breaks" in the pack ice are often visible. In some cases, as in the vicinity of the Balleny Islands (see Section 6.8.3), the presence of, absence of, or size of such openings in the ice pack (or their changes from day to day) may be useful indications of the approximate direction of the surface wind.

4.9 Tropical Analysis

In the tropics, the principles used for TIROS picture analysis are also found to be generally applicable to the HRIR data. (These principles are discussed in Chapter 11 of Reference 55, and somewhat more recent findings are to be found in Reference 32.) Because the early stages and further development of tropical disturbances appear to be related to the extent and organization of active convective areas where cumulus extend to comparatively great heights,[32] the cloud height information that is provided by the HRIR data is at least as valuable in the tropics as at higher latitudes.

The two tropical cases studied, over the Pacific (see Sections 8 and 9), have shown that the HRIR data permit significant improvements in the conventional operational analyses, which are almost always based on an inadequate number and density of observations. Joint use of the HRIR data, and either AVCS or TIROS pictures, provides twelve hour continuity, whereas only 24 hour continuity is normally possible using either data type alone.

The HRIR data also provide previously unavailable information on small scale details of tropical cloud systems which appear to be significant to an understanding of tropical weather mechanisms. For example, the HRIR data showed (see Section 8) that the initial cloud formations associated with one upper level cyclone occurred as narrow bands of cold (high) cloud around the periphery of the cyclonic circulation. These bands appear to be related to vertical motions induced by small scale relative vorticity advections on the cyclonic side of a peripheral wind maximum.

Joint use of the HRIR and sparse conventional data has suggested that, during the period of the normal, initial, slow but progressive development of a typhoon (Wilda, 1964), the rate of development may at times have been intensified by small scale solenoidal accelerations related to several small, upper level, cold core eddies to the north of the storm (see Section 8). A similar forcing mechanism, operating on a larger scale, may have been associated with the rather rapid final development to typhoon intensity as the movements of the lower level pre-Wilda perturbation and an upper tropospheric cyclone brought the two systems into juxtaposition.

4. 10 Daytime HRIR Data

In order to use the daylight HRIR data or to compare them with TIROS or AVCS pictures, it is desirable to print the HRIR so the majority of the clouds (areas of relatively intense radiation) are white. For the daylight HRIR, where solar reflectivity usually exceeds thermal emission, this is, of course, the reverse of the most effective photographic polarity for presentation of the night HRIR data (in both cases, it is desirable for the clouds to be depicted as whiter than the background). Presentation of the clouds as white is vital to ease of interpretation, whether or not comparisons with other data are to be made. This has been noted by several groups besides ARACON which tried and often discarded attempts to work with TIROS pictures in negative form (see, for example, page 6 of Ref. 4).

Comparative analyses of daytime HRIR data and approximately concurrent TIROS pictures have left no doubt that, over the oceans, daylight HRIR would be of significant value in the absence of TV pictures. Even small details within a common cloud pattern can often be identified in both the TIROS pictures and the HRIR data (see Figs. 2-4 and 4-7; or Fig. 63 of Ref. 56).

Figure 4-7   Daylight HRIR View of the Western United States
and Eastern Pacific Ocean

In the daytime the HRIR signal is, of course, a combination of reflected sun-light and thermal emission.* In this situation, there is apparently little variation in the reflection term with cloud top height, but there is a rapid decrease in the emission term, thus causing high clouds to appear less bright in HRIR than lower clouds (Fig. 4-7, where the stratus west-southwest of Baja California is lower than much of the cloudiness to the east and southeast). This is, of course, a reversal of the usual relationship between cloud brightness and cloud top height as seen in the TIROS TV pictures, or in the nighttime HRIR. As a consequence, brightness often tends to be inversely related to significance.

Over land, the thermal emission of the relatively warm land appears to be high enough to prevent significant contrast between clouds and the land surface; it is difficult to even detect the clouds (Fig. 4-7). The value of daytime HRIR over land is highly questionable. This is because the higher temperatures and lower reflectivities of the land normally are approximately equivalent in total radiation (at the wavelengths to which the HRIR is sensitive) to the radiation resulting from the lower temperatures and higher reflectivities of the clouds.

_____

* Some of the quantitative aspects of the two sources of radiation are explored in Appendix A.

5. A EURASIAN CASE WITH PREDOMINANT BLOCKING ACTION

During the period 16-20 September 1964, the HRIR coverage of much of Eurasia was particularly good. On each of these five days, data from at least three contiguous orbits were available; on the first day, the data available were from eight contiguous orbits. Our attention was originally called to this case by the striking "backward-S" cloud band in orbit 300 (see Fig. 5-2), especially because there was no immediately obvious explanation for the cloud vortex at its southern end and the relationship of this vortex to the remainder of the band. As the analysis progressed, it became apparent that the cloud band was associated with the flow around an Ω-block, and the southern cloud vortex depicted a typical cutoff low just to the west of the blocking high.

5.1 Preparation of HRIR Mosaics

Because the data of greatest interest were primarily for latitudes poleward of $50^\circ N$, a problem considered when beginning the analysis was the handling and consistent matching of the areas of overlapping HRIR coverage. This consideration led to the construction of mosaics of the HRIR strips, as shown in Figures 5-1 through 5-5. This technique of handling high latitude HRIR data, i. e., that pole-ward of some 40 to 50°, has been found to be extremely useful. Its advantages include:

1. Elimination of the labor inherent in hand-drawn, rectified nephanalyses, such as those used in Reference 56.

2. Preservation of the full resolution and gray scale of the available photofacsimile copies of the infrared data.

3. The large area panorama made available by the mosaic.

4. The relative ease and objectivity with which conventional analyses can be transferred to the HRIR mosaic, as shown in Figures 5-1a through 5-5a; and the direct comparisons between the HRIR and other data which are then possible.

Unfortunately, similar mosaics are not feasible when the areas of interest are primarily those equatorward of about 50°, although it is likely that they could be prepared if HRIR strips in rectified form were available (see Appendix B).

In constructing the HRIR mosaics, the following procedure was used with considerable success for matching adjacent HRIR strips:

1. Find a common grid point on the two adjacent strips at 70° latitude (if either strip does not extend to 70°, use a common grid point as far poleward as possible). It is desirable that this common point be as far as possible from the edges of both of the adjacent strips.

2. Overlay this point on one strip so as to match the same point on the other.

3. Maintaining this common grid point match, match or overlay common or adjacent cloud features as close to the equatorward limit of strip overlap as the data permit. If the pole is included on both strips and is not too near the edge, it is also desirable to use it as a matching point. *

4. Adjust the overall match, along the overlapping edges of the adjacent strips, so it is optimized along the total length. In so doing, if the original common point at 70° latitude is not approximately along a line bisecting the sector of overlap of the two strips, it may help to select a new common point, at 70°, which is near the bisector.

5. Determine (approximately) the line bisecting the sector of overlap of the two strips, and trim off that part of the topmost of the two strips outside this approximate bisector. This leads to the greatest possible use of the areas of minimum foreshortening distortion in both strips.

6. Again match the strips, using a common grid point near the edge of the topmost strip along or near 70°, common cloud features near the equatorward limit of overlap, and, if feasible, the pole.

7. Adjust the overall match as necessary to achieve overall optimization.

8. Hold the strips in this finally selected position, and paste or tape them together.

Once the mosaic has been constructed, the construction of the latitude-longitude grid (using the electronically inscribed grid points) is usually rather straightforward. Poleward of 60°, it helps to first draw those meridians at 20° intervals which have been completely inscribed, and then to fill in those for the odd tens of degrees.

---

* The use of the pole was not feasible in this case because of the low perigee and consequently the high nadir angle at which it was observed. It was used in constructing the southern hemisphere mosaics in Section 7.

In using the northern hemisphere mosaics constructed as above and shown in Figures 5-1 through 5-5, it has been noted that they give a false impression of perspective, as if the poleward areas were being viewed at a greater nadir angle than those at lower latitudes. This is, of course, not the case; along the center of each strip, the angle of view is vertical at all latitudes. It is believed this false impression may result from: (1) the convergence of the meridians and probably their apparent curvature to the west;* and (2) the fewer brightly white areas and sharply contrasting cloud features at higher latitudes.

Using the latitude-longitude grid, there is no significant problem in remapping standard meteorological analyses to the "projection" of the HRIR mosaics. For this study, microfilms of NMC 500 mb analyses (which extended only to about 50^ON near 90^OE) and fronts extracted from copies of Russian 0000 GMT surface analyses were used (Figs. 5-1a through 5-5a).

5. 2 General Results

During the course of this case study, the following results of presumed general applicability were noted:

5. 2. 1 Areas of Fog or Stratus

It appears that untextured areas of a uniform, flat, light gray tone represent fog, or stratus formed from the lifting of fog. Examples include:

1. Figure 5-1, near 55^ON, between 102 and 112^OE, and the bands and areas of similar tone and texture to the east and northeast; and near 60^ON, 55^OE. It appears that much of the fog east of about 110^OE lies in the valley of the Lena River and its tributaries.

2. Figure 5-3, near 50^ON, just east of 70^OE.

3. Figure 5-4, near and north of 58^ON, 68^OE, and near 80^ON, 65^OE.

---

* Which is not duplicated in the southern hemisphere mosaics, where it was feasible to use the pole as a matchpoint.
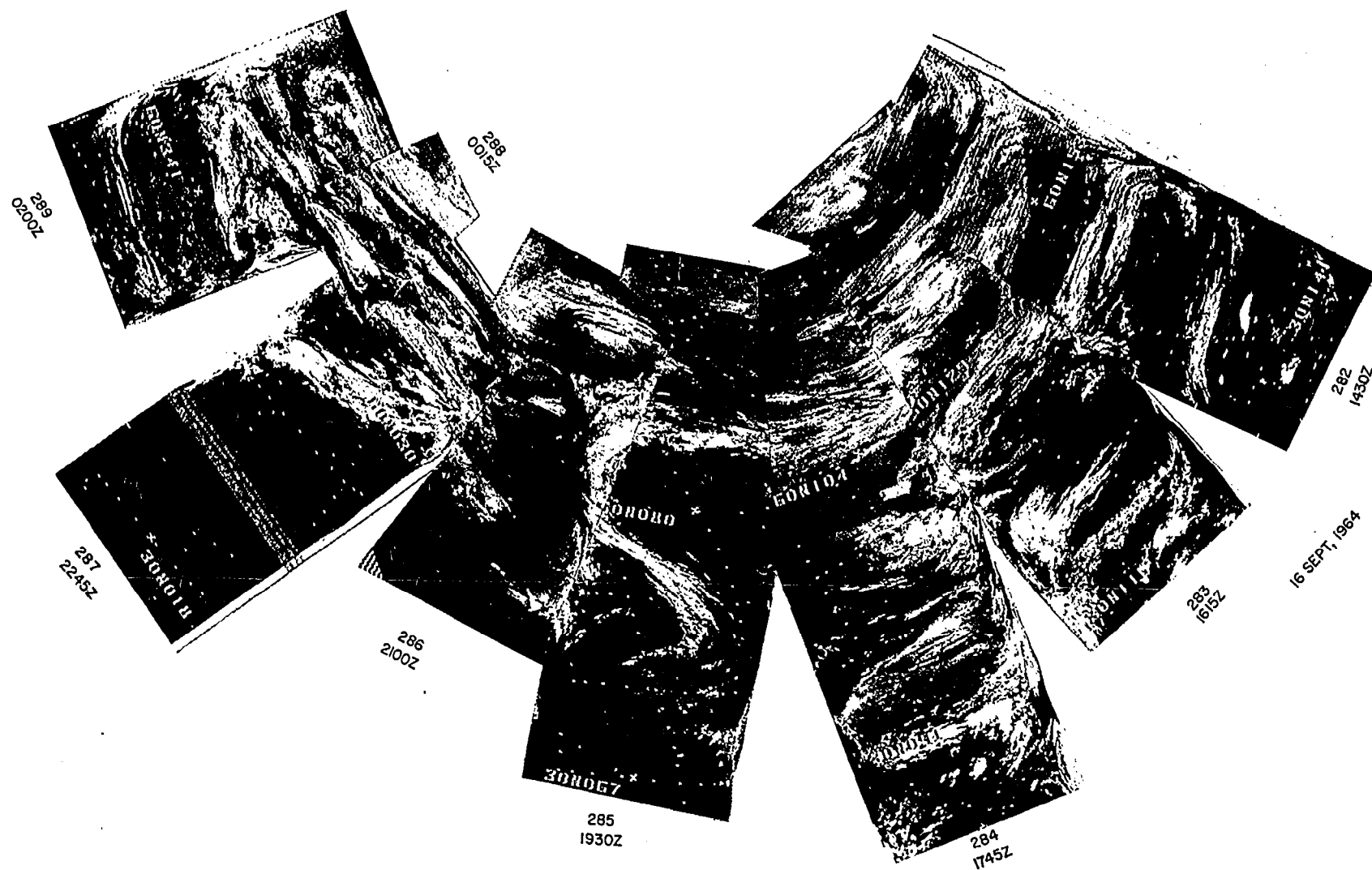
Figure 5-1   HRIR Mosaic of Eurasian Area for 16 September 1964
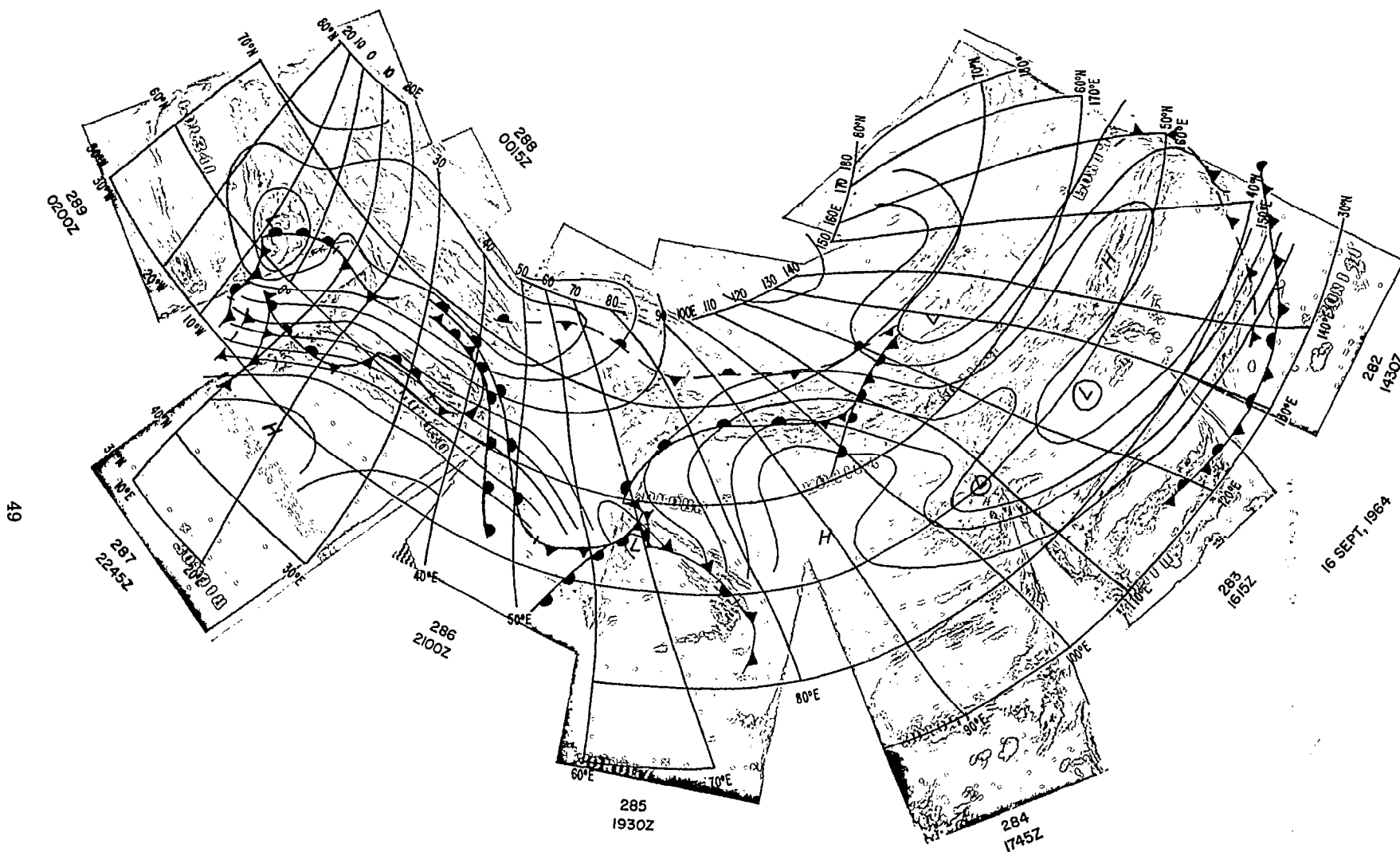
Figure 5-1a HRIR Mosaic with NMC 500 mb Analysis (0000 GMT, 17 September 1964 West of About 110°E; 1200 GMT, 16 September to the East), and Russian Frontal Analysis for 0000 GMT, 17 September 1964).
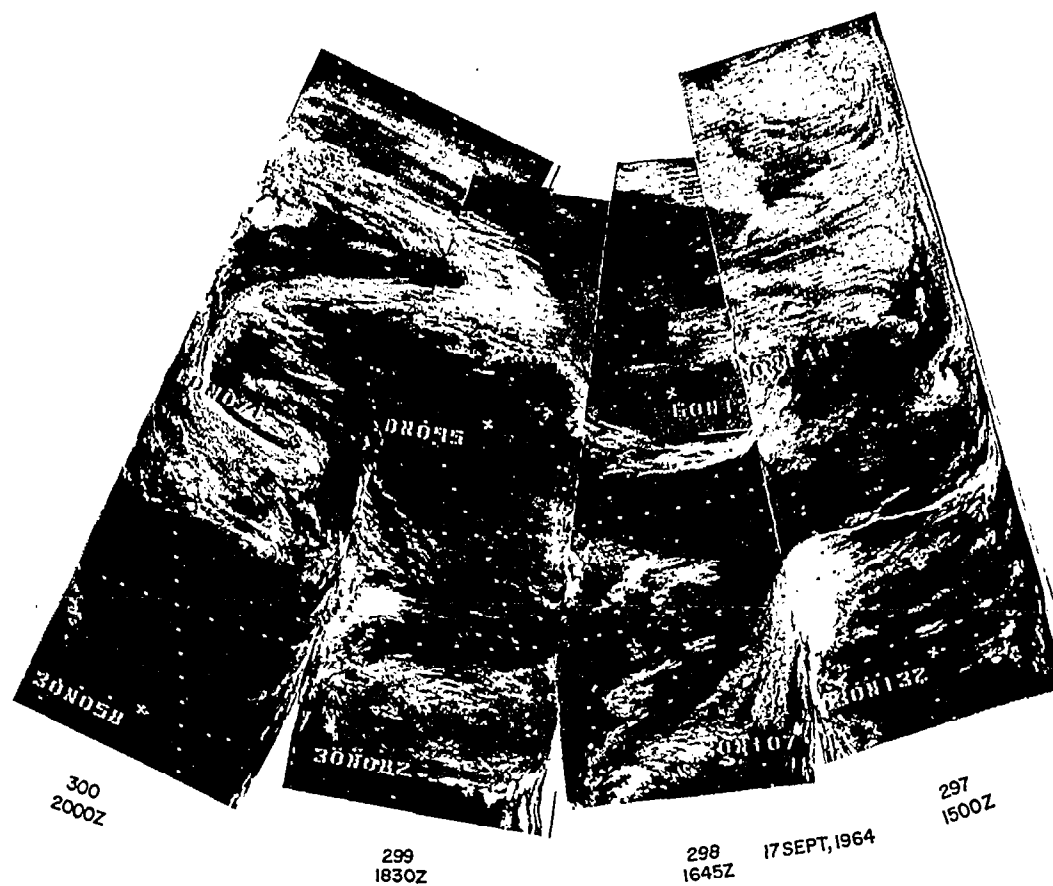
Figure 5-2   HRIR Mosaic for 17 September 1964
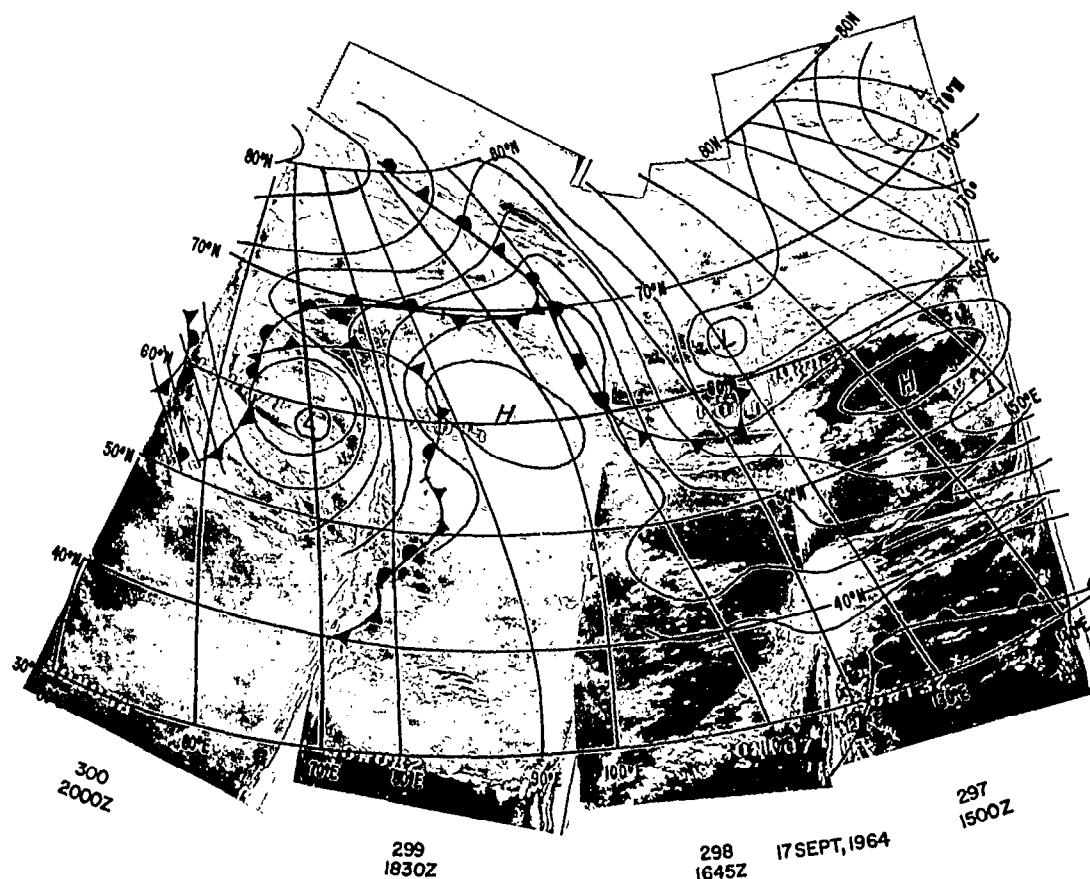
Figure 5-2 a   Mosaic with NMC 500 mb Analysis (0000 GMT, 18 September West of about 120°E; 1200 GMT, 17 September to the East), and Russian Frontal Analysis for 0000 GMT, 18 September

315
2045Z

314
1900Z

313
1715Z

18 SEPT, 1964
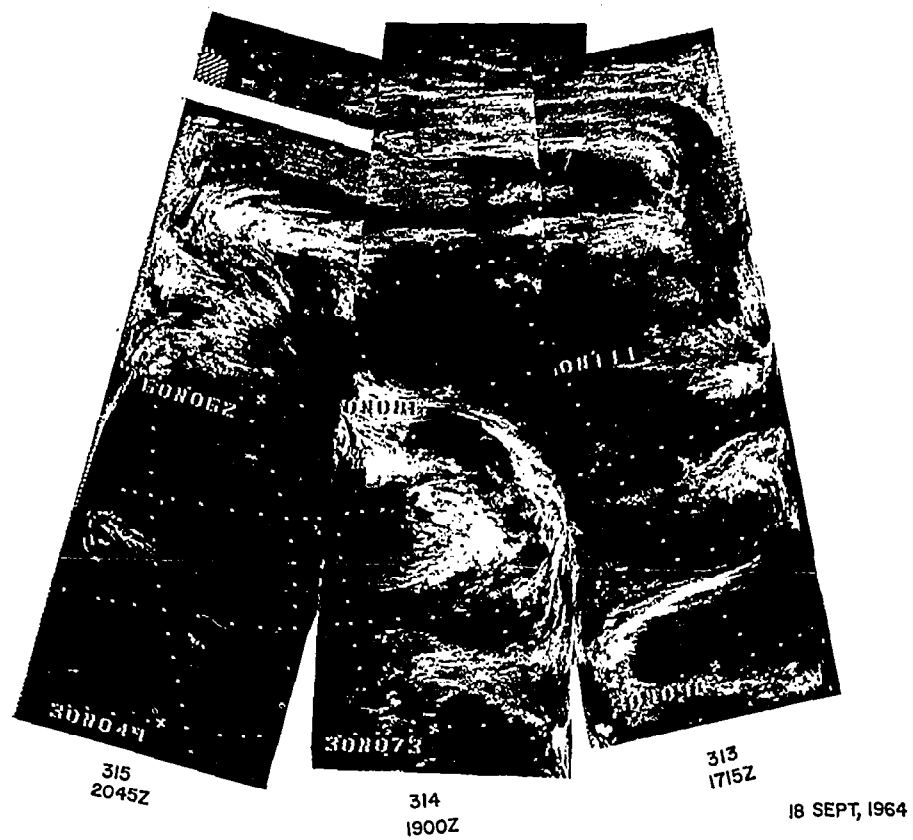
Figure 5-3   HRIR Mosaic for 18 September 1964
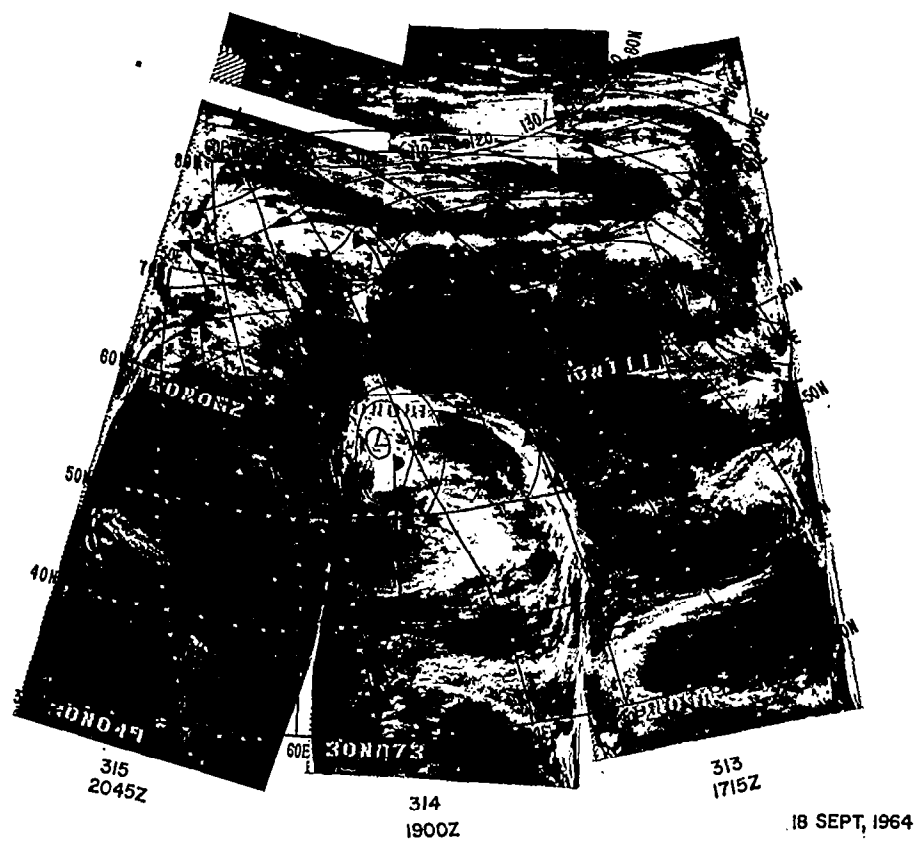
Figure 5-3 a   Mosaic with NMC 500 mb Analysis and Russian Frontal Analysis, both for 0000 GMT, 19 September 1964
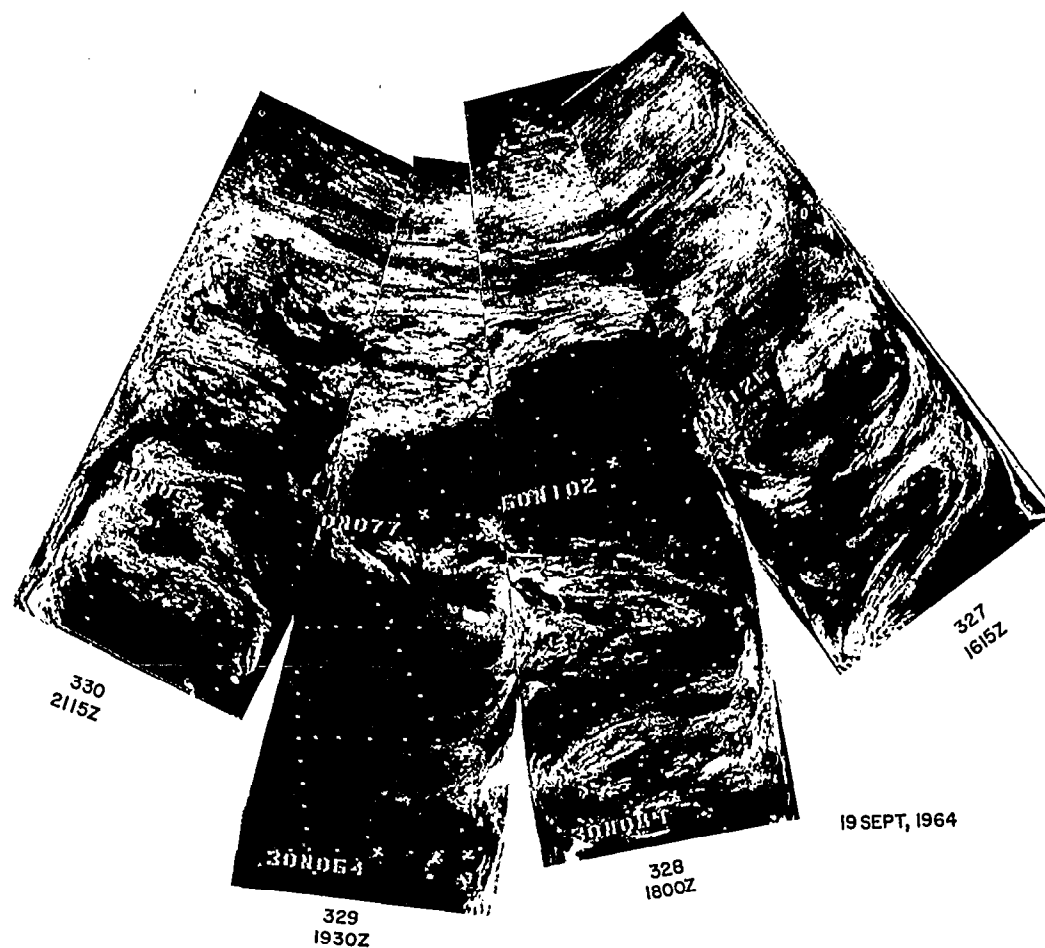
Figure 5-4   HRIR Mosaic for 19 September 1964
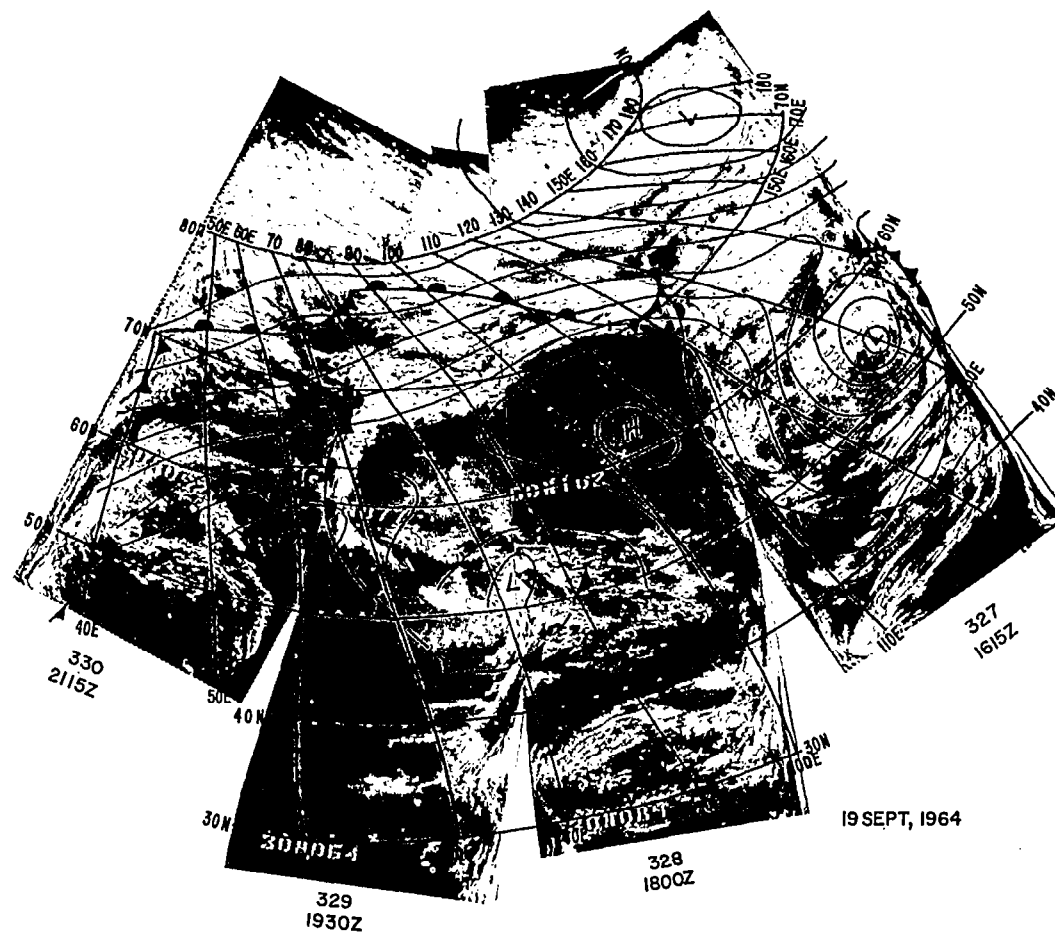
Figure 5-4 a   Mosaic with NMC 500 mb Analysis (0000 GMT, 20 September West of about 120°E; 1200 GMT 19 September to the East), and Russian Frontal Analysis for 0000 GMT, 20 September
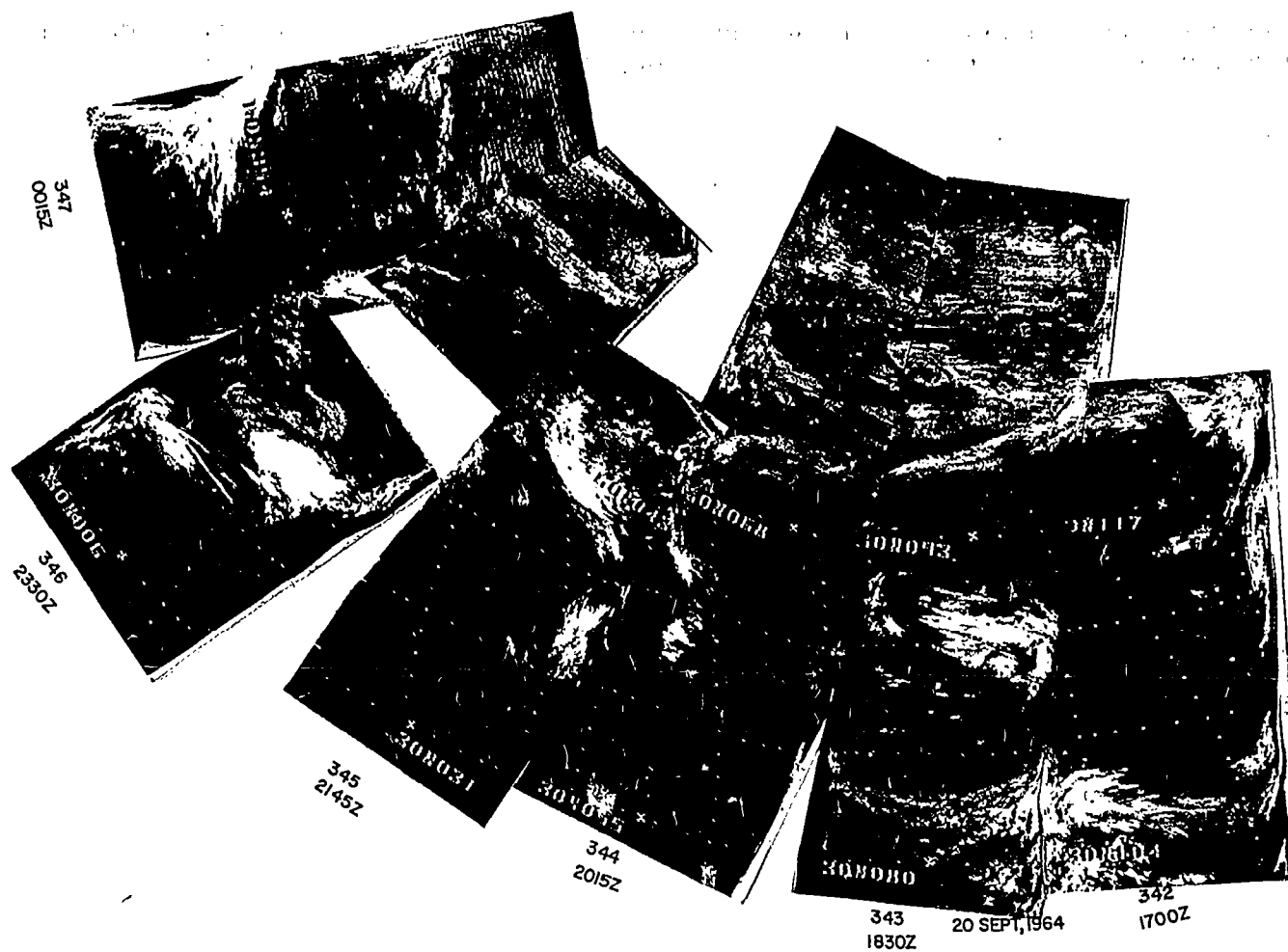
Figure 5-5   HRIR Mosaic for 20 September 1964
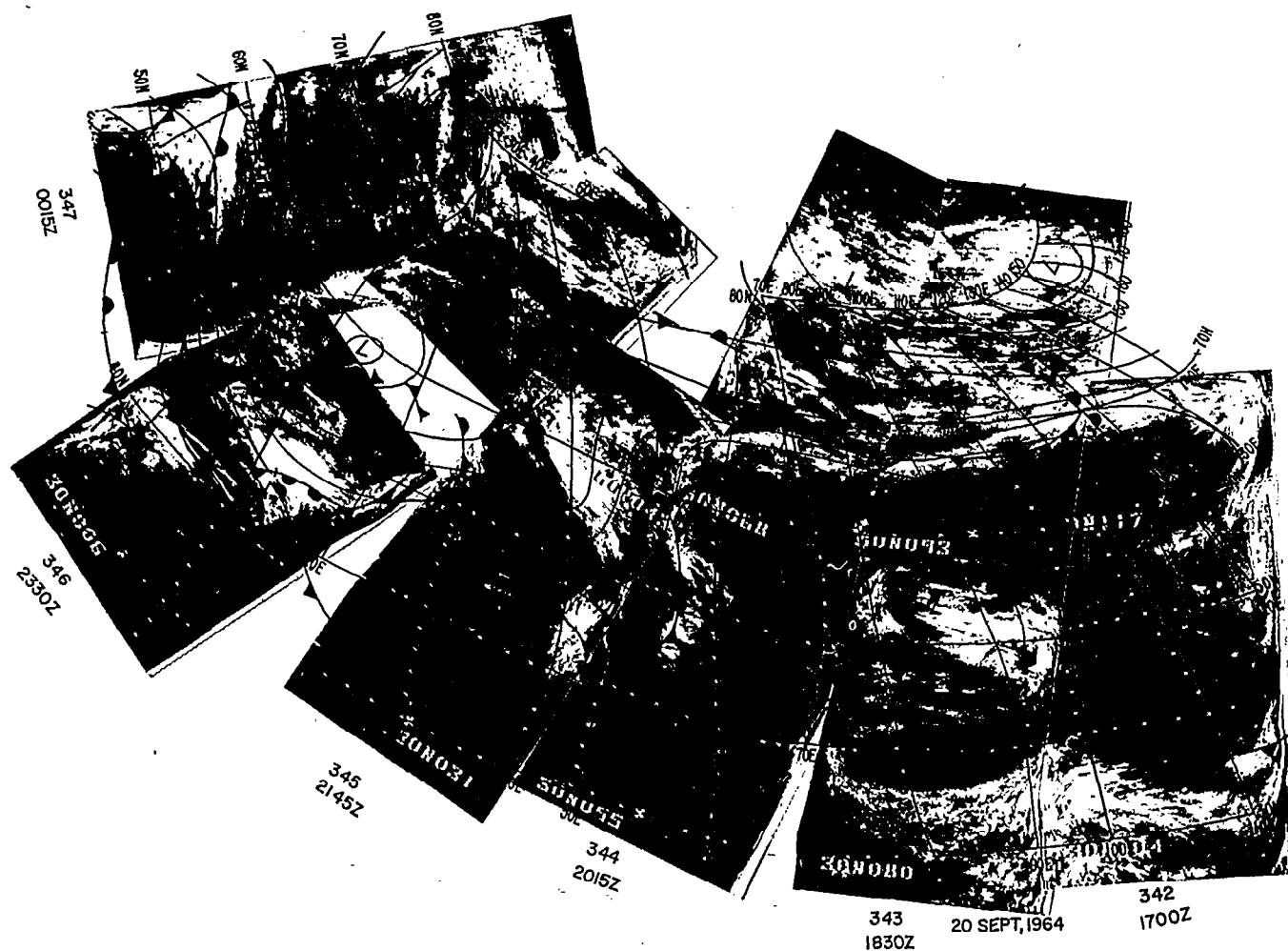
Figure 5-5 a   Mosaic with NMC 500 mb Analysis (0000 GMT, 21 September West of about 110°E; 1200 GMT 20 September to the East), and Russian Frontal Analysis for 0000 GMT, 21 September

Most of the cloud areas with the characteristics described above, in Figures 5-1 through 5-5, either coincided with or were close to stations reporting fog or a zero dewpoint depression, or were in portions of the synoptic patterns where fog or stratus is likely.

In using this finding, care must be taken to insure no landmarks are visible in such areas. For example, the area in Figure 5-1 near 35°N 90°E (the Tibetan Plateau) might be taken for fog except for the lakes that are visible. On the other hand, fog may exist in the absence of any evidence in the HRIR data; presumably, in such cases, a stable lapse rate at low levels leads to little difference in temperature between the surface and the top of the fog or stratus.[56]

5.2.2 Relationships Between HRIR Data, Mid-Tropospheric Analyses, and Surface Frontal Analyses

This case has tended to confirm previous findings[41,55,56] that the prominent cloud patterns as observed by satellites, and especially those cloud patterns shown by the HRIR data to be relatively cold and so reaching well into the middle or upper troposphere, are in general far more easily explained in terms of the mid-tropospheric (500 mb) flow patterns than by use of frontal analysis. Essentially all extratropical areas of cold clouds of significant size, as seen in the HRIR, can be satisfactorily explained in terms of areas of cyclonic vorticity or vorticity advection, or as clouds previously formed in such an area and subsequently advected from it. Furthermore, reasonable patterns of day-to-day continuity present fewer problems when viewed in terms of these explanations.

As will be discussed in the next section, there is often a good correlation between cloud bands or areas and analyzed fronts. This is illustrated in Figures 5-1a through 5-5a, where the fronts are those copied directly from the Russian surface analyses for 0000 GMT. It can be noted, however, that in the absence of upper level support, the clouds seldom extend to significant heights. Furthermore, in many cases it appears difficult to establish a reasonable continuity from the frontal analysis of one day to that of the next, or for the cloud bands and areas when it is attempted to explain them and their continuity using frontal concepts.

Since frontal analysis is often highly subjective, this is not entirely un-expected. As Jacobs-Haupt[22] has stated in connection with a case study of TIROS data over the Mediterranean: "There are eight different frontal analyses, but there are also eight different opinions. Not only the existence of fronts is often questionable or indefinite, but also their position and the kind." She illustrates this in her Figure 1, where the analyses by eight different weather services place a front (analyzed by some but not all as an occlusion) in various significantly different positions. These analyzed positions range from as far west as a Genoa-Sardinia-Bizerte line to as far east as a Graz (Austria)-Gulf of Taranto-central Libya line (some 10° of longitude difference at 40°N). Furthermore, she states that for the same synoptic hour the U. S. Weather Bureau analysis showed no fronts in the area. Similar illustrations of the variations and subjectivity of frontal analyses have been published by other investigators.[46]* During the period of this case, the NMC frontal analyses (not included) were often significantly different from those of the Russians; the Russian analyses are used here because they were the only ones available to us when the study was begun and because one might assume they would be the more accurate analyses for the area under study.

It should not be implied from the above that fronts do not exist, or that they are always insignificant. Rather, it would appear that their effects are more constrained to the lower levels (those where the clouds appear light gray or darker in the HRIR). A usually necessary and at times a sufficient condition for the clouds to extend to higher levels (where they appear white in the HRIR) is mid-tropospheric flow patterns which produce significant upward vertical velocities[55] at the synoptic scale, or permit them at the meso- or convective scales.

5. 2. 3 Frontal Cloud Bands

Three types of frontal cloud bands have been noted during this case study:
1. Those existing only in the lower atmosphere. Examples include:
> Figure 5-1; near 57°N 45°E
> Figure 5-3; from 74°N 90°E to 70°N 120°E

---

* R. J. Renard and L. C. Clarke[37] of the U. S. Navy Fleet Numerical Weather Facility reported on a recent analogous study at the January 1965 New York meetings of the American Meteorological Society.

In the cases observed during this study, the surface isobars indicate low level flow up the frontal surface but there is insufficient upper air support to create mid-tropospheric upward velocities and higher level clouds. The 500 mb flow is often more or less parallel to the frontal band, but there is no nearby, downstream source of significant mid-tropospheric cloud formation from which higher clouds or moisture can be advected along the frontal band.

It should be observed that this case study treats primarily central Eurasia, where the typical low atmospheric moisture content may limit cloud formation from primarily frontal lifting. In many other areas, the typical moisture might be sufficient for convective instability and more extensive cloudiness to develop.

It should further be noted that, in meteorological satellite TV pictures, these low level cloud band cases might well appear as bright as those where clouds extend to considerably higher levels. Such cases have been discussed in Reference 56. Unfortunately, TIROS and Nimbus AVCS data for this period, as presently available to us, were inadequate to demonstrate this point.

2. Those with low level cloudiness, and with higher level scattered-to-broken and often streaky cloudiness. Examples include:

Figure 5-1; from $68^{\circ}N$ $90^{\circ}E$ to $62^{\circ}N$ $110^{\circ}E$

Figure 5-4; from $75^{\circ}N$ $100^{\circ}E$ to $70^{\circ}N$ $120^{\circ}E$

Figure 5-5; near $68^{\circ}N$ $105^{\circ}E$

The immediate surface and 500 mb flow patterns often appear much the same as in the previous cases which lacked upper level clouds, but there is usually an upstream cyclonic vorticity maximum from which higher level clouds can be advected along and over the lower level frontal cloudiness. Some of the high level cloudiness may also be attributable to a combination of: (1) mesoscale vertical motions associated with jet stream flows,[8] and (2) the upstream upward transport and subsequent horizontal advection of moisture along the lines of the hygrokinematic theory proposed some years back by Ligda.[35]

Again, more adequate atmospheric moisture might produce greater cloudiness under otherwise synoptically similar conditions; and the problems of TV brightnesses would be the same as for low level cloudiness alone.

A somewhat similar cloud pattern has been observed over the Canadian Rockies of western North America when the 500 mb flow was generally parallel to the divide while the low level flow had an upslope component.

3. Those with extensive high level cloudiness. Examples include:

Figure 5-1; near 58°N 30°E

Figure 5-2; near 54°N 120°E

In each of these cases, and others that can be noted in Figures 5-1 through 5-5, there is significant upper level support, usually in the form of a 500 mb short wave trough or vorticity maximum.

Even in those cases where the cloud band is extensive and continuous, it weakens to lower and more broken cloudiness in passing through areas of lesser 500 mb vorticity. Note how, in Figures 5-1 and 5-2, the cloud bands just east of 60°E weaken as they cross the 500 mb col between 60° and 70°N. By the time of Figure 5-3, the area of the col is nearly clear.

5.2.4 Distortion of the Short Wave Trough Cloud Pattern

Rogers[6,41,55] has identified a characteristic crescent or comma shaped cloud pattern as indicative of a short wave trough. Several good examples of this pattern can be found in this case (Fig. 5-2, near 55°N 120°E, which was previously mentioned as a frontal area with upper level support; Figure 5-3, near 47°N 80°E and near 74°N 80°E, etc.). In Figure 5-5, the clouds associated with a 500 mb short wave trough can be found near 55°N 42°E. It is to be noted, however, that the flow around the west edge of the ridge just to east of the trough has distorted the characteristic pattern into one resembling a backwards question mark or an integral sign $(\int)$. A tendency to similar distortions can be noted in Figure 5-3 (the cloud mass near 50°N 80°E), where it is less obvious because of the clearer break along 52°N; and in Figure 5-4 (the cloud mass near 50°N 80°E), again disguised by the lesser organization of the cloudiness north of 54° N.

It is suggested that this modification of the characteristic short wave trough cloud pattern may be typical of cases where the 500 mb contours have the "S" shape of those near 60°N 45°E in Figure 5-5a. A somewhat similar cloud pattern and the related synoptic situation are also discussed in the Antarctic case study in this report (see Section 7.4.6).

5. 2. 5 Clouds Outlining, and Depicting the Transformation of, an Ω-Block

In Figure 5-1, the cloud band more or less along 70°E and then along 67°N conforms rather well to the western half of the flow pattern around the Ω-block. In Figure 5-2, nearly the entire Ω flow pattern is depicted by a more or less continuous cloud band. In Figure 5-3, although the westerlies have broken through poleward of 70°N, the Ω-block continues at lower latitudes and the cloud band along its western edge continues to conform to the flow pattern.

By the time of Figure 5-4, the breakdown has extended to south of 70°N, and the 500 mb Ω-ridge is tending to merge with the high to the west to restore a slightly more normal flow pattern. This merging of the two ridge areas (those centered near 60°E and 105°E) superficially seems to be depicted in the cloud patterns by an apparent westward displacement of the cloud band near 70°E (at 60°N, east of 70°E in Fig. 5-3, but west of 70°E in Fig. 5-4). An actual displacement, contrary to the flow at both the surface and 500 mb, is unlikely, however. (The analyzed 500 mb flow patterns, as transferred to the HRIR mosaics, are confirmed by a reasonably dense station network in that area.) Rather it appears there is a series of approximately parallel, eastward progressing cloud lines. As the merging ridges cut across the col, each line dissipates a bit further westward. With only 24-hour HRIR continuity, the superficial appearance is that of westward displacement of a semi-stationary line.

This concept is at least partially confirmed by the AVCS data for orbit 321 (see Fig. 5-8), taken about 0615 GMT on 19 September, or about halfway between the times of Figures 5-3 and 5-4. These data show cloudiness west of 65°E, between 50° and 60°N. Thus, there either must have been a second cloud band moving in from the west between Figures 5-3 and 5-4, or the less likely possibility of an irregular east-west oscillation of a single band.

In further support of this concept, a very faint broken band can be seen in Figure 5-3 extending from about 58°N 55°E to 48°N 64°E. This suggests that as the series of bands cross the western ridge, they weaken over the ridge and reintensify as they approach the longitude of the trough and col.

Still further support of these concepts is provided by, the data in Figure 5-5. By this time merging of the ridges across the col had led to a lower latitude Ω-block significantly elongated in the east-west direction. Three cloud bands can be identified which, near 60°N, are located near 40°E,50°E,and 80°E. The more western now corresponds to the western edge of the flow around the blocking high,

and as discussed in Section 5. 2. 4, is a distorted short wave trough pattern with active cloud formation in its southern half. The band near 50°E is apparently undergoing dissipation as it moves through the ridge. The band near 80°E is per- haps that which a day earlier was near 70°E; if anything, it has slightly dissipated and presumably reflects the further merging of the ridges across the col.

The above sequence of events also helps to explain the appearance of the persistence of a cloud band conforming to at least much of the western part of the Ω flow pattern. It would appear that one source of this cloud pattern is a series of bands which are formed to the west of the Ω flow and, upon reaching it, come under a regime which both reduces further eastward motion and tends to dissipate any portions of the bands that do move further eastward. A second source is cloud- iness formed in areas of significant upward motion within the cutoff low and sub- sequently advected along the Ω flow pattern.

It is suggested that similar cloud band patterns and their movements and changes may exist in other blocking situations, and may aid in deducing the establishment, persistence, transformation, and dissipation of such Ω-blocks.

5.3 Specific Discussion of Individual Days

In a case such as this, covering a five day period and sizable portions of Eurasia, there are obviously a very large number of specific features and events that could be discussed. Some of those of most probable general application have already been summarized in the previous section. In this section, we will point out some of the others, dealing with the mosaics on a day-to-day basis.

5.3.1 16 September 1964 (Fig. 5-1)

Perhaps the most significant feature as regards the development of the cloud patterns over the next 24-hours (especially the band near 60 to 70°E) is the short wave trough near 30°E. Its presence is reflected by the cloud pattern centered near 60°N 35°E. Inspection of the actual NMC 500 mb analysis for 0000 GMT, 17 September, suggests that the vorticity was more concentrated in the horizontal shear than in the rather minor curvature of the flow in this area.

Other significant features include:

1. The apparently weak cloud vortices near 60°N 5°W; 78°N 0°; 75°N 35°E; and 75°N 80°E.

2. The cloud patterns associated with the short wave trough near 50°N 100°E. While the high clouds (those mainly east of 100°E) appear poorly organized, there is a definite suggestion of a spiral pattern of lower level cumuliform clouds. The Russian surface analysis for 0000 GMT, 17 September, places a low near 44°N 98°E which the HRIR data suggest might be slightly further north. It seems likely that, this is an example, over land, of the cloud pattern associated with a short wave trough in generally northwest flow, originally identified by Rogers.[6,55] Note the resemblances between the cloud pattern in this area and that in Figure 5-17 of Reference 6 or Figure 5-12 of Reference 55.

3. Although the antecedents of the cloud band near 70°E are not known, it appears possible that it and the fog area near 55°N 57°E are influenced by the Urals, with those parts of the band north of about 55°N produced in part by upslope flow due to winds with some easterly component.

4. Note that the area of post-frontal cellular clouds near 55°N, 10° - 30°W (over the Atlantic) appears to have no counterpart over Eurasia during the period of this case.

5. Clear areas could be confirmed from landmarks in the case of Lake Baikal, the Tibetan Plateau, and in the area of Pamir (near 37°N 72°E).

One AVCS orbit (279) was available, about thirteen hours earlier than this mosaic, for the area near 10°E. Its data neither conflict with nor add significantly to the information provided by the HRIR data.

5.3.2 17 September 1964 (Fig. 5-2)

Analysis of this mosaic and the superimposed 500 mb analysis for 0000 GMT, 18 September, indicates that the vorticity maximum which 24 hours earlier was near 30°E split as it passed through the delta or exit region near 65°N 55°E. The southern portion apparently intensified the cutoff vortex near 58°N 70°E, as evidenced by the vivid cloud vortex pattern near the low center and the suggestion in the cloud pattern of at least two short wave troughs passing along the southern side of the closed low. The northern portion can be identified from the short wave trough near 75°N 105°E, and the broadened cloud band to its

east that Rogers[41] has noted as characteristic of breakaway lows (secondary development-
ments to the southeast of closed lows, the closed low in this case being that near
80°N 60°E). In confirmation, the Russian surface analysis shows the triple point
of an occlusion near 71°N 105°E.

This analysis shows that the rather striking cloud band which first drew our
attention to this case arose from the eastward advection, splitting by a delta
region, and distortion by an Ω-block and its associated cutoff low of the vorticity
maximum that was near 30°E on 16 September. Meanwhile, the cloud band that a
day earlier was near 60°E is now found between 70° to 80°E, dissipating as it comes
increasingly under the influence of the ridge.

Even the striking backwards "S" cloud band can be seen to be weaker where
it crosses the col near 65°N 63°E.

Other significant features in this mosaic include:

1. The short wave troughs and associated cloud patterns near 45°N 110°E
and near 55°N 120°E. The more northern cloud pattern is far better organized
into the characteristic form, perhaps because it is already passing through a
larger scale trough line while the more southerly system is still under basically
northwest flow.

2. The frontal wave and associated broadened and distorted cloud band near
40°N 120°E. The short wave perturbation in the 500 mb contours near this system
was introduced by the author, but is not in conflict with the plotted data on the NMC
chart.

3. Clear areas were confirmed by such landmarks as:
   The Asian coast, near 45°N 137°E.
   The Lena River, near 65°N 125°E.
   Lake Baikal, and Koso Gol to its southwest.
   Dalai Nor (49°N 117°E) and possibly Buyer Nor (48°N 118°E).
   The Tibetan Plateau and Koko Nor (37°N 100°E).
   Ubsa Nor (near 50°N 93°E).
   The Aral and Caspian Seas.

About eleven hours later than the west end of Figure 5-2, i.e., about
0715 GMT on 18 September, the AVCS cameras photographed the west edge of the
cloud system that in Figure 5-2 extends from about 48° - 60°N near 60°E (see
Fig. 5-6). The only significant common features appear to be the wave clouds near
55°N 60°E, which were just barely visible in the HRIR. It would appear they result
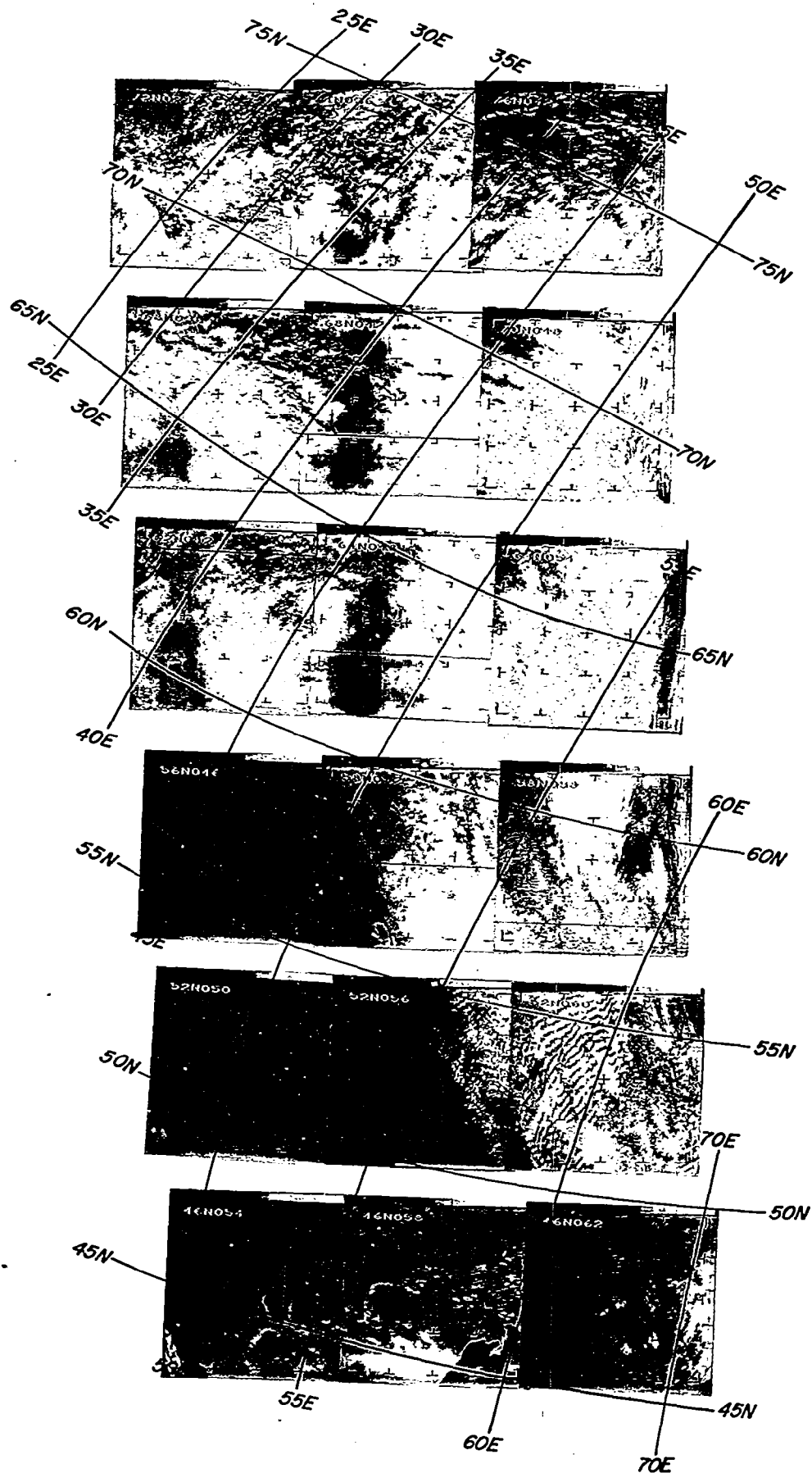
Figure 5-6   AVCS Montage for Part of Orbit 307, About 0715 GMT, 18 September 1964

from the northwest flow, which extends from the surface to at least 500 mb, over the southern Urals. From the positions of the cloud-covered areas and the Aral Sea in both the AVCS and the HRIR, it appears that not much movement took place during these eleven hours. On the other hand, during the subsequent thirteen hours most of the cloudiness in AVCS orbit 307 (Fig. 5-6) moved eastward and/or dissipated under the influence of an eastward advance of the western ridge. Accordingly, there is only limited correlation between the cloud features in Figures 5-3 and 5-6.

5.3.3 18 September 1964 (Fig. 5-3)

By the time of the 18 September HRIR mosaic, the north-south cloud band, formerly more or less along 60°E, is rather well broken up due to the merging of the ridges across the col. The triple-point cloud mass has moved rapidly eastward to near 75°N 135°E, and is connected to systems further west only by a weak, low level cloud band which lacks upper air support. Typical short wave trough cloud patterns can be seen near 45°N 80°E and near 75°N 80°E. It would appear the cloud masses near 45°N 110°E and near 53°N 115°E are also associated with short wave troughs.

Clear areas could be confirmed from the visibility of such landmarks as Lake Baikal, Koso Gol (51°N 100°E), the Lena River (near 66°N 123°E), the Enisei and Tunguska Rivers (faintly indicated near 65°N 90°E), the Aral Sea, and parts of the Caspian Sea.

Some eleven hours later, AVCS orbits 320, 321 and 322 (Figs. 5-7, 5-8, and 5-9) covered much the same area. Orbit 320 (Fig. 5-7) showed parts of the cloud band that, in Figure 5-3, was located along 90°E near 50°N, and of the short wave trough cloud pattern near 75°N 80°E, although it is very unlikely the characteristic pattern would have been identified from the AVCS data. AVCS orbit 320 does, however, show snow-covered mountains not identifiable in the HRIR (near 52°N 100°E). In AVCS orbit 321 (Fig. 5-8), the western parts of the short wave trough pattern near 45°N 80°E are easily identified. The strip also shows other cloudiness that can be seen in the HRIR, to the north-northwest of the short wave trough, and mountain snow in the area of Tien Shan (near 42°N 80°E) where the terrain is high enough to be reflected in the HRIR data. Lake Balkhash can be seen to be partly fog covered (with cumulus advected from the northwest dissipating as it comes over the fog); this corresponds to the fog area, with a hint of part of Lake Balkhash dimly visible, in the HRIR of Figure 5-3. In AVCS orbit 322 (Fig. 5-9), there is a good
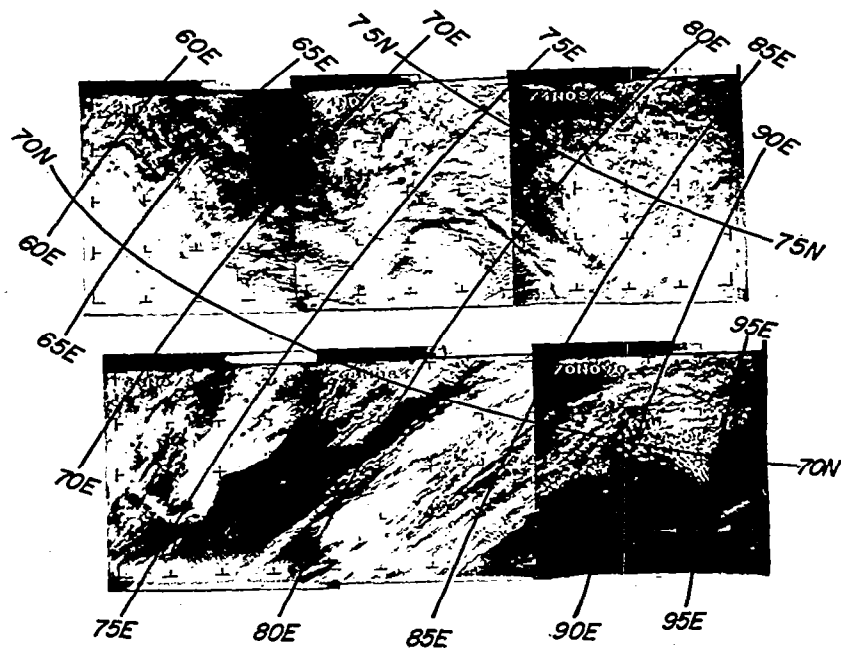
FRAME   MISSING
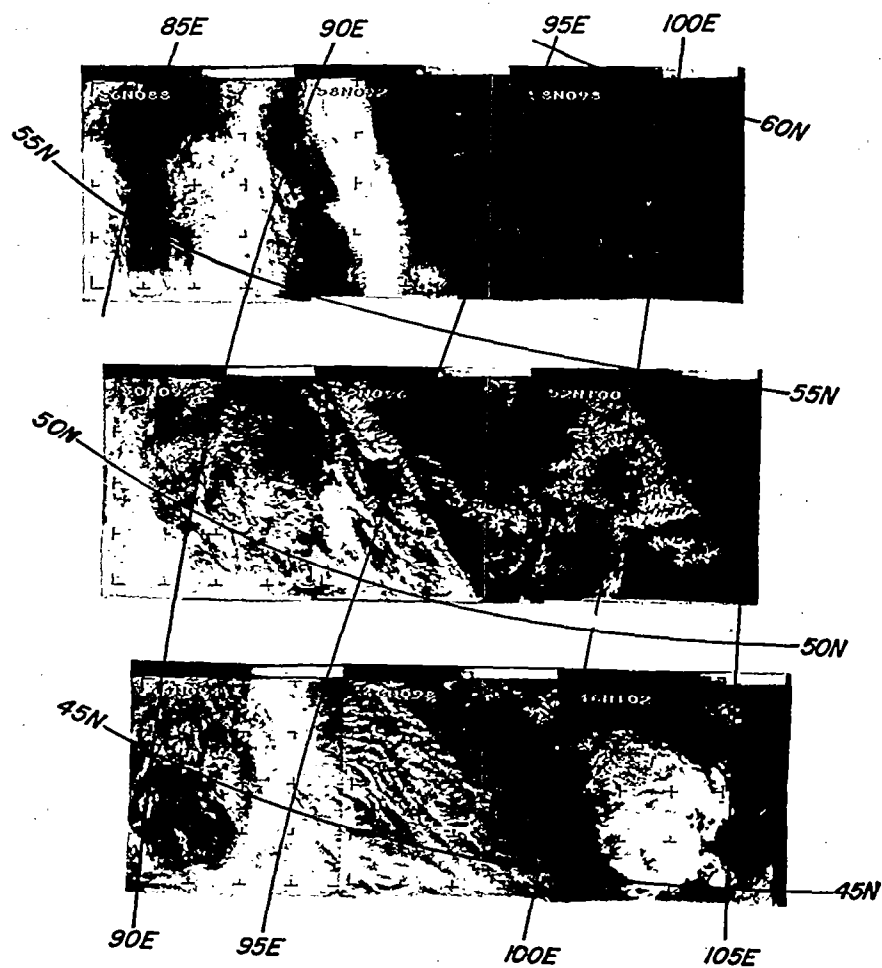
Figure 5-7   AVCS Montage for Part of Orbit 320, About 0430 GMT, 19 September 1964

68
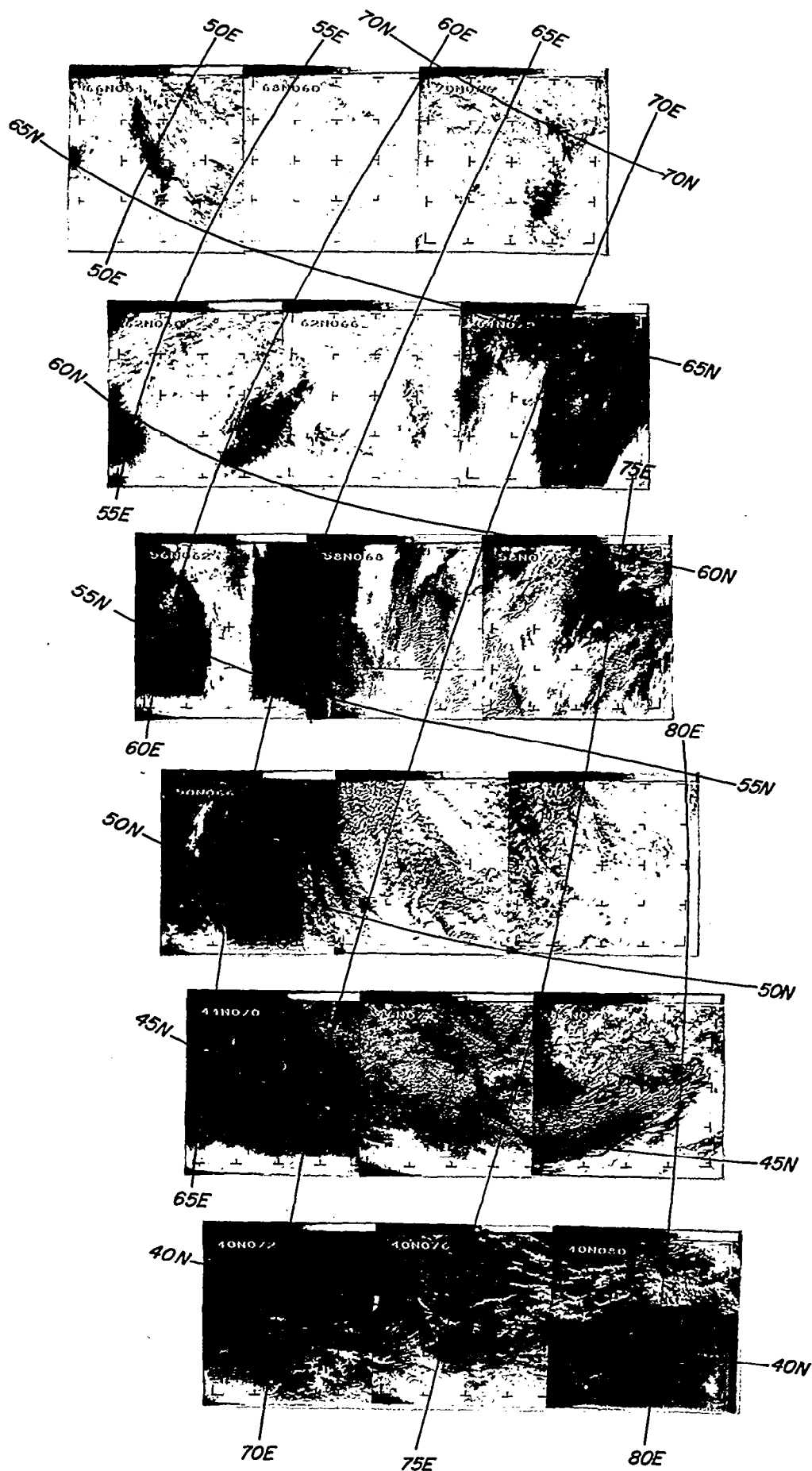
Figure 5-8 AVCS Montage for Part of Orbit 321, About 0615 GMT, 19 September 1964
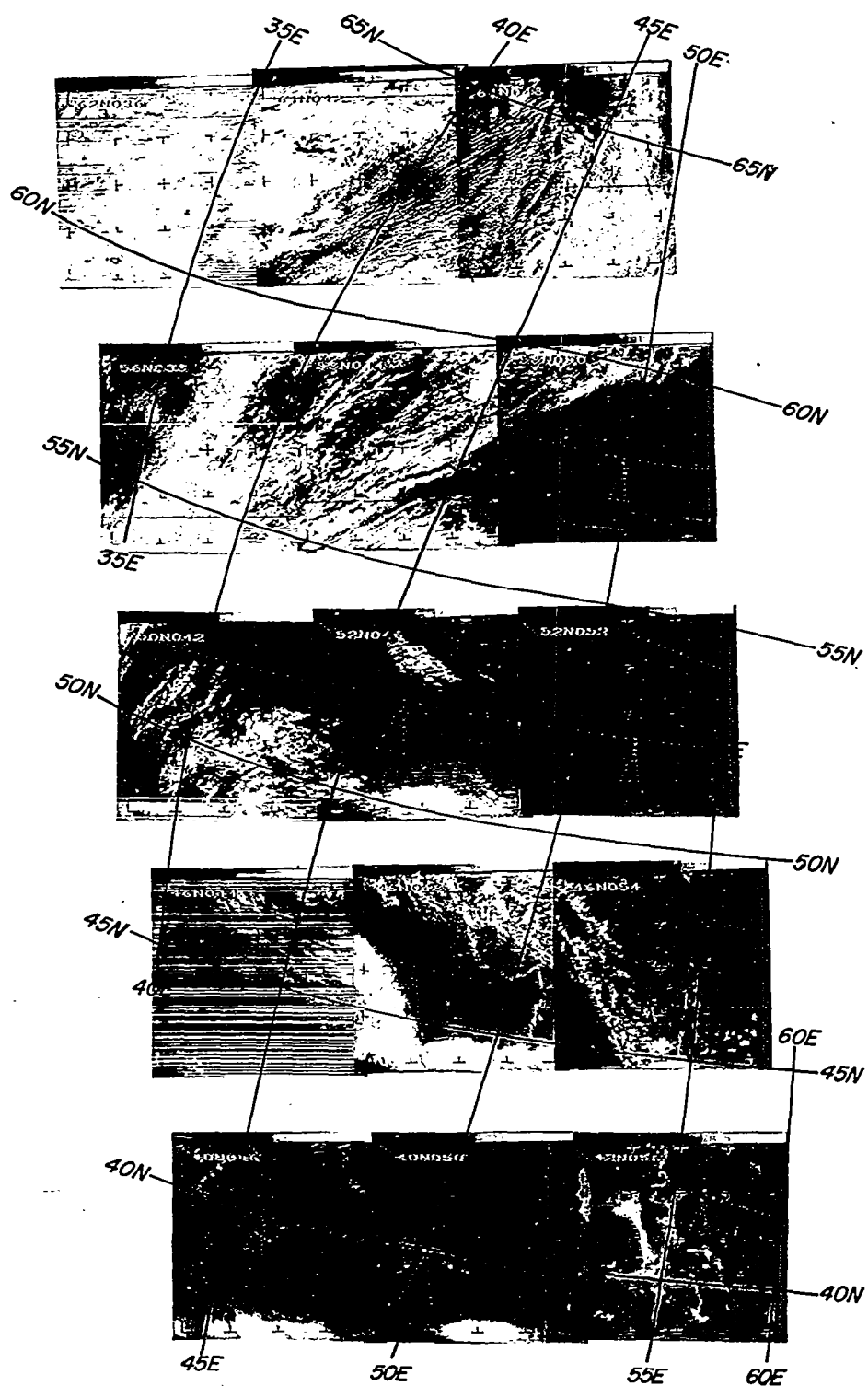
Figure 5-9   AVCS Montage for Part of Orbit 322, About 0745 GMT, 19 September 1964

correspondence to the HRIR with common features including generally clear conditions in the south (except for scattered cumuliform clouds over and near the northern Caspian), and the banded cloudiness near and northwest of 60°N 40°E.

Comparisons between the AVCS and HRIR data clearly demonstrate the deficiencies of the AVCS and the advantages of the HRIR when cloud top altitudes are of interest.

Similar relationships can be traced between the AVCS data in Figures 5-7, 5-8, and 5-9 and the HRIR of Figure 5-4, some thirteen hours later.

5.3.4 19 September 1964 (Fig. 5-4)

As the two ridges continue to merge across the col near 80°E, there is a continued progressive decrease in the cloudiness near 80°E and south of 65°N. A short wave trough cloud pattern can be seen near 50°N 80°E. The generally greater cloudiness east of about 90°E, north of 70°N, corresponds to the weak short wave trough in the northern westerlies.

Clear areas could be identified from such landmarks as the Lena and Aldan Rivers near 64°N 130°E (with the Aldan River apparently disappearing under fog or low clouds just east of 130°E), Lake Balkhash, and the northern part of the Caspian Sea.

5.3.5 20 September 1964 (Fig. 5-5)

The large number of contiguous orbits on this day makes it regrettable that this was the last day of the series (there were no Eurasian orbits the following day), and that on the previous day the HRIR did not extend significantly west of 40° E.

Significant features include:

1. The large, high cloud mass near 47°N 15°E, just east of the 500 mb trough along 10°E at a latitude where the 500 mb winds indicate a sharper short wave trough than the analyzed contours and where there are several surface reports of rain or showers.

2. The distorted short wave trough near 60°N 40°E, previously discussed.

3. A weak short wave trough and characteristic cloud pattern near 70°N 110°E.

4. The extended area of wave clouds extending along 70°N from about 90° to 110°E.

It would appear that most of these wave clouds were produced by the wind flow (which is from the west-northwest from the surface to 500 mb and increasing with altitude) over the Gory Putorana highlands in the vicinity of Gord Kamen, which extend to above 5000 feet from 68° to 70°N along 95°E. The lesser waves west of 95°E may be due to a smaller, isolated highland, extending to about 2000 feet, near 69°N 88°E. The great longitudinal extent of the wave area (some 350 miles) and the breaks in it may be related to details in the terrain east of 100°E, where mountain , and valley elevations range between 500 and 3000 feet. The surface and 500 mb charts would also suggest some possibility of the wave clouds having been induced or aided by flow over a small cold air dome.

Clear areas could be identified from such landmarks as Lake Baikal, Dalai Nor and Buyer Nor (near 48°N 118°E), the Huang Ho (Yellow River), Lake Balkhash, part of the Caspian Sea, the Black Sea, the Dnepr River, the coast of Asia Minor, the northern coast of Norway, the Baltic Sea, Sicily, Tunis and Tripoli. The Tarim Basin of Sinkiang, and its surrounding Tien Shan and Kunlun mountain ranges are clearly visible near 40°N 80°E.

A particularly intriguing landmark was a small but distinct wavy line (perhaps one degree of latitude in amplitude), running generally from southwest to northeast near 38°N 108°E. In the most detailed atlas available to us, this line would appear to correspond to a province boundary which lies more or less perpendicular to most of the rivers and so may approximate a contour, possibly a discontinuity in the land slope (Fig. 5-10). It lies very close to the Great Wall, but both the line in the HRIR and the province boundary are considerably more "wavy" than the Great Wall. No definitive explanation is presently apparent.
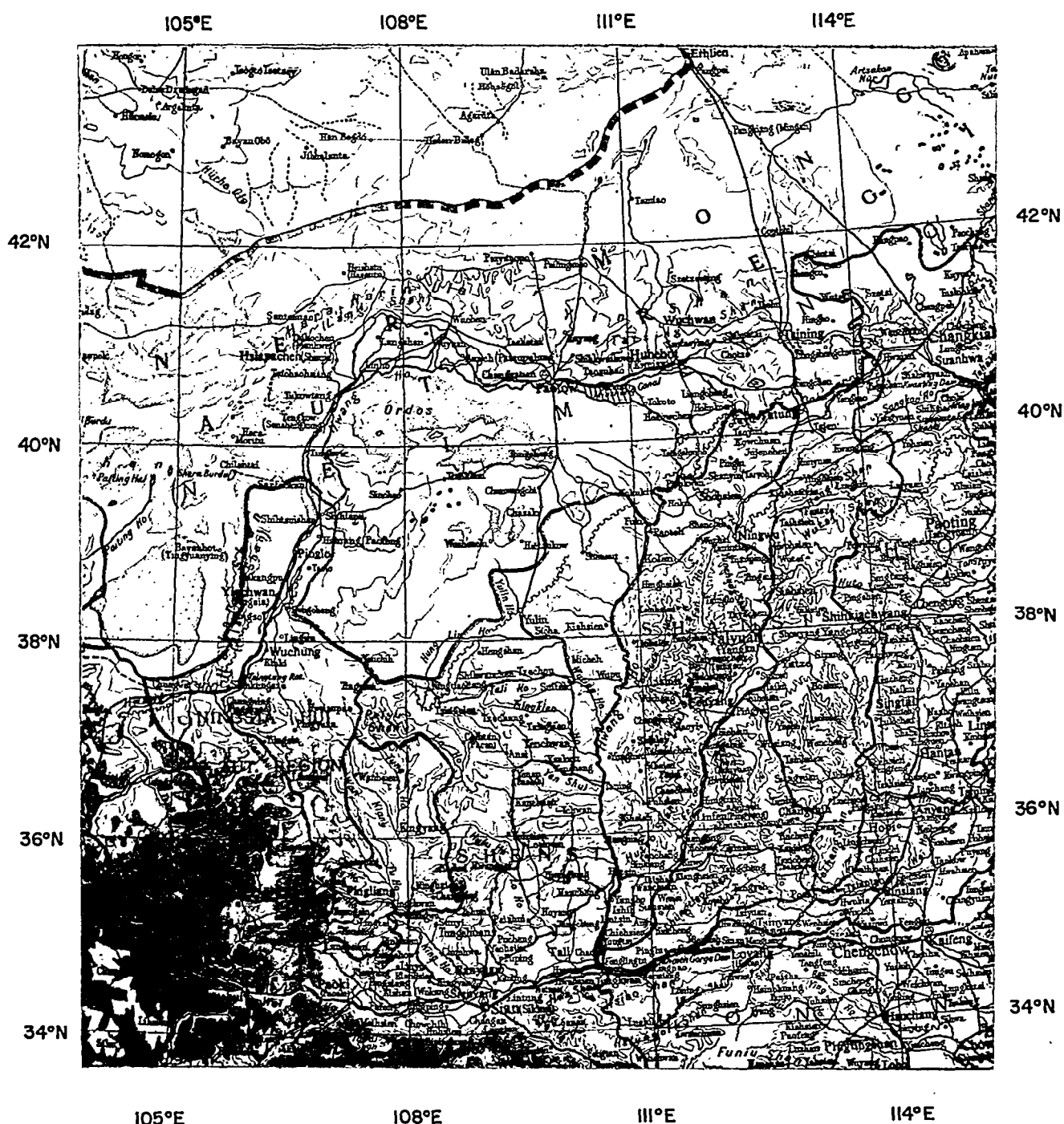
Figure 5-10   A Map of the Part of China Near 38°N, 108°E.

6. CASE STUDY OF A SOUTHERN HEMISPHERE VORTEX

6.1 Introduction

Most of the case studies in this report have been made over the northern hemisphere because of the better corroborative data there. The southern hemisphere should not be neglected, however, since there is at least an equal amount of HRIR data available for that hemisphere. In fact, the lack of conventional data over large areas of the southern hemisphere makes this region an extremely important one for satellite observation.

On Nimbus orbit 250, 14 September 1964, a vortex that appeared to be typical of a mature cyclone was seen near 60°S 180°. HRIR data were available in that area for six consecutive days, 11-16 September, permitting the development of this system to be followed. The HRIR data were rectified, using the color scheme described in Section 3.3 and the centers of the cloud formations were plotted and checked for continuity, as shown in Figure 6-1. The system moved southeastward from near Tasmania on the 11th to the Ross Sea on the 16th, with an average movement of about 450 nautical miles per day. The only conventional analyses available were those of the IAAC (International Antarctic Analysis Center) in Melbourne, and the only stations south of Australia and New Zealand available for the analyses were Campbell and Macquarie Islands, and in Antarctica, d'Urville and McMurdo (see Fig. 6-1). Because of the paucity of data, the analyses can often give little support to the satellite observations. At the 500 mb level, even the positions of the long wave troughs are often doubtful, so it is nearly impossible to detect a short wave disturbance. (The relation of the short waves to satellite observed cloudiness has been discussed by Widger, et al,[55] and by Sherr and Rogers.[41]) In most cases, a better Antarctic analysis can be provided by the satellite observations; these observations should be used where appropriate to correct the conventional analysis rather than merely attempting to show that the conventional data support the satellite data.

Time cross-sections for the above stations were available and proved to be very helpful, as previously found by Merritt[30] and others in sparse data regions. There were no Nimbus AVCS data for this area, but TIROS VIII did provide picture coverage on most days. The HRIR data were taken about 1200 GMT (during the night), while the TIROS pictures were taken nearer to 0000 GMT, or about twelve

75
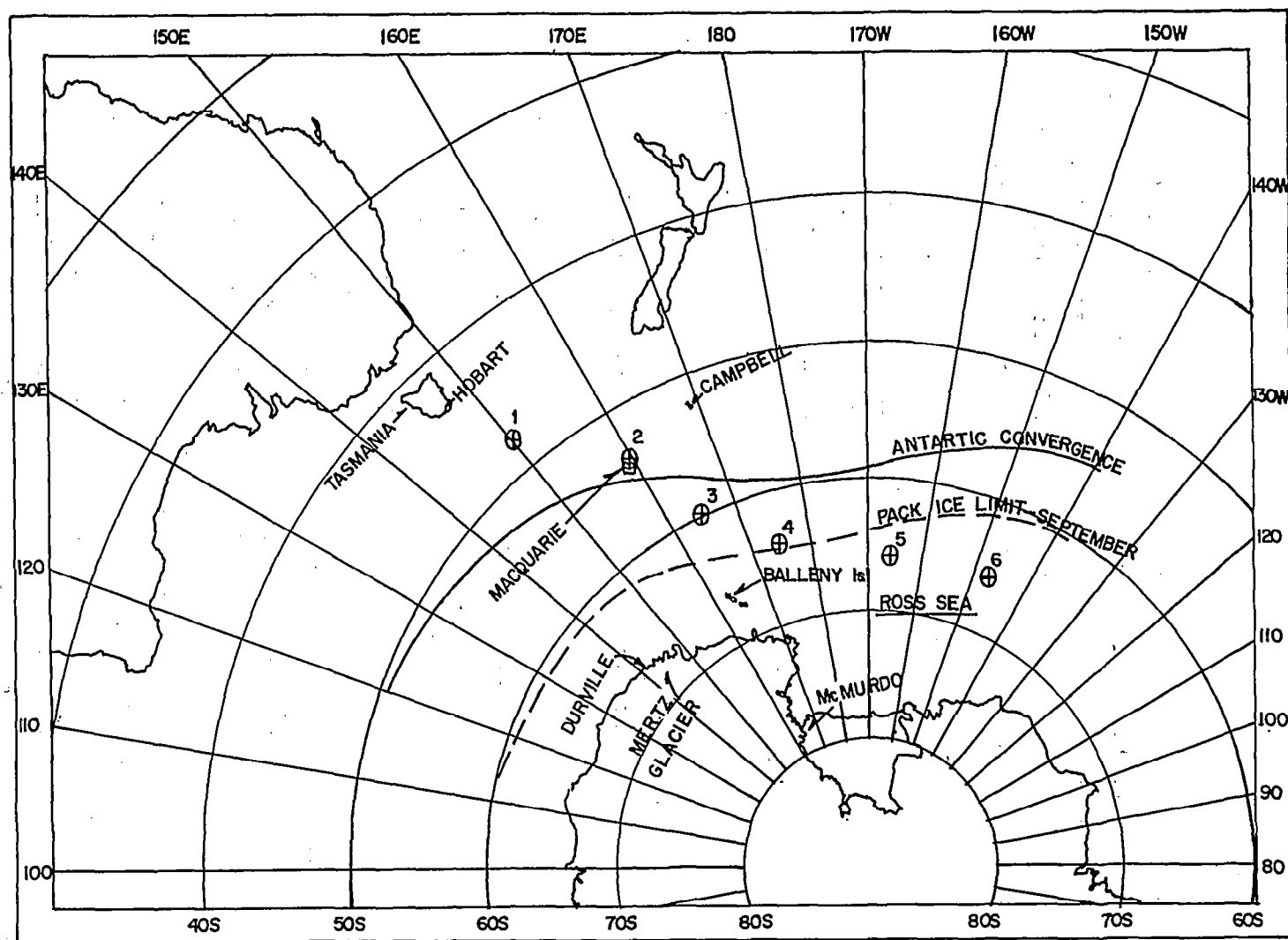
Figure 6-1   Position of Principal System at about 1200 GMT of Each Day of Study

hours earlier or later. IAAC surface charts were available for both 0000 and 1200 GMT, and upper air charts for 0000 GMT. Most of the time cross-sections were based on surface data every three hours, complete upper air data every twelve hours, and upper winds every six hours.

6.2 The First Day, 11 September 1964

Orbits 207 and 208 provided data for the first day; the HRIR strips and rectification are shown in Figure 6-2.

As in most southern hemisphere HRIR strips, the Antarctic continent is clearly seen, with the edge of the continent quite distinct in most places. The interior of the continent is an undifferentiated tone, and clouds can seldom be distinguished from the ice and snow. The pack ice around the continent can also be identified, in places, as a darker tone than the continent itself. At this time of year, the northern limit of the pack ice is about 60°S, as is shown in Figure 6-1. The pack ice will be discussed further later in this study.

In the two strips of Figure 6-2, a fairly large, high (bright) cloud mass lies along 155°E and reaches almost as far south as 50°. Although only a part of this cloud system shows on the strips, it appears to be centered near Tasmania. Based on continuity (Fig. 6-1), this cloud area, and the small but high cloud area centered near 55°S 147°E, are part of the same overall system that develops into a mature cyclone and that will be the chief feature of interest in this study. To the west of the above system is a "crescent" shaped cloud system that, in general, consists of clouds darker (not as high) than in the previously mentioned system, although there are some higher bands. A fairly large cloud mass is centered near 60°S 133°E, with much of the system appearing to be broken middle clouds (darker). A broken band appears to connect these two systems. Well to the east is an apparently mature vortex that appears to have only a narrow band of high clouds but a large amount of lower cloudiness. * Other low cloudiness covers much of the area between the somewhat higher clouds of these various features.

---

* See Section 7.2.1 for a further discussion of this vortex, which indicates that when the area east of 180° is examined, this vortex is actually a secondary system in southwest flow.

Figure 6-2   HRIR Data and Rectification of Orbits 207 and 208, about 1245 GMT, 11 September 1964

6.2.1 Early History of the System

The earlier development of the system under study can be traced fairly easily, since it took place in an area with considerable data. On the days immediately preceding 11 September, high pressure dominated Australia at the surface. However, a 500 mb short wave was moving into the region by 0000 GMT on the 9th, and was centered over southern Australia a day later. The first sign of a surface development occurred about 0000 GMT on the 10th, when a weak low appears over eastern Australia between two high cells. By 1200 GMT on the 10th, the low had moved into southeastern Australia.

The 500 mb chart for 0000 GMT on the 11th, about twelve hours before the HRIR data in Figure 6-2, shows a short wave trough, centered over southeastern Australia. (The 500 mb analyses are shown in Figs. 6-3a and 6-4a, and the surface analyses are shown in Figs. 6-3b and 6-4b.) At 0000 GMT on the 12th, twelve hours after the HRIR strip, the short wave is not so readily detectable, as a rather broad long wave trough now covers the region. However, it appears quite likely that the short wave is now centered just off the eastern coast of Australia. The time cross-section for Hobart indicates the passage of a disturbance about 1200 GMT on the 11th, which is even more apparent at the 300 mb level, where the wind went north-east at this time. This indicates that a disturbance was passing Tasmania at just about the time of the HRIR observation, agreeing well with the location of the main cloud mass.

6.2.2 Conventional Analyses

The 500 mb charts show two long wave troughs, the one mentioned above and one east of New Zealand. A ridge line was just west of New Zealand at the time of the HRIR observation, and the relatively clear area from New Zealand south-westward is under the influence of this ridge. The vortex centered near 60°S 180° is undoubtedly associated with the 500 mb closed low near the Ross Sea. A large area of cloudiness along the coast of Antarctica is in the vicinity of the 500 mb trough south of Australia, and the configurations of the remaining two cloud systems indicate that they are associated with short wave disturbances, although none are indicated on the 500 mb analyses.

The surface analyses are fairly good near Australia, but deteriorate quickly in the sub-Antarctic data void to the south. At the time of the HRIR observation,

OOOOGMT, II September 1964
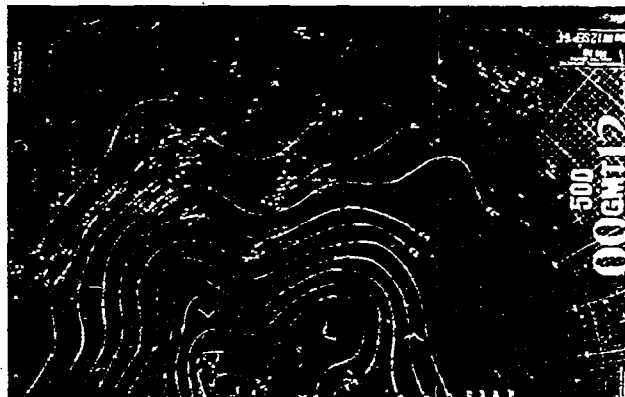
OOOOGMT, 12 September 1964
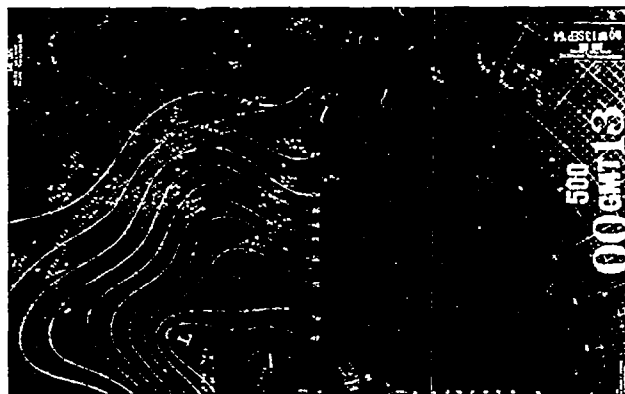
OOOOGMT, 13 September 1964

Figure 6-3 a   IAAC 500 mb Analyses for 0000 GMT, September 11, 12, and 13

1200GMT, 11 September 1964

1200GMT, 12 September 1964
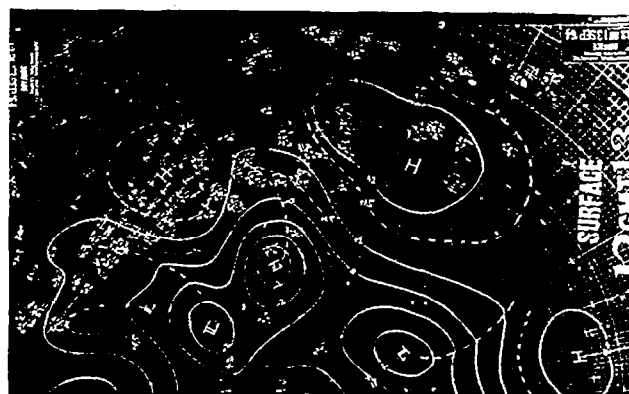
1200GMT, 13 September 1964

Figure 6-3 b   IAAC Surface Analyses for 1200 GMT, September 11, 12, and 13

OOOOGMT, 14 September 1964
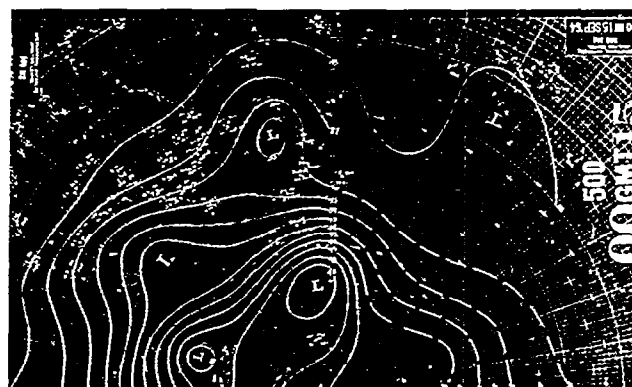
OOOOGMT, 15 September 1964

OOOOGMT, 16 September 1964

Figure 6-4 a   IAAC 500 mb Analyses for 0000 GMT, September 14, 15, and 16

1200GMT, 14 September 1964

1200GMT, 15 September 1964

1200GMT, 16 September 1964

Figure 6-4 b   IAAC Surface Analyses for 1200 GMT, September 14, 15, and 16

the analysis shows that the weak low center has moved to just east of Tasmania, but no fronts are associated with it. A low is centered near 55°S 140°E with a front extending toward southwestern Australia. The HRIR suggests there should actually be two low centers, one near 50°S 130°E and the other near 55°S 147°E. The clear area from New Zealand southward shows as a ridge at the surface, and the mature vortex can be associated with the low in the Ross Sea.

6.2.3 Comparative TIROS Data

A TIROS mosaic, taken at 0117 GMT on the 11th (Fig. 6-5), shows the vortex that was near 60°S 180° in the HRIR. In the TIROS pictures, this system has a solid appearing center with a distinct vortical band. There is an area of cellular clouds to the northwest of the center, with another more solid cloud mass still further west.

This latter cloud mass appears to be the vortical pattern centered near 50°S 130°E in the HRIR, and the small cloud to its northeast appears to be that centered near 55°S 145°E in the HRIR. While there is little variation in the brightness of the clouds in the TIROS pictures, the HRIR shows that the clouds near and west of 145°E are higher than those to the northwest of the vortex.

6.2.4 Ice Observations

The ice around Antarctica is an important feature in both the HRIR and the TIROS data. In the TIROS, the edge of the pack ice is easily distinguished, lying nearly along 60°S. However, cloudiness cannot be distinguished from the ice. In the HRIR, the gray areas near the continent are obviously pack ice. Various formations, open areas, and "breaks" can be seen, such as that in orbit 208 near 66°S 130°E (Fig. 6-2). There is a distinct formation in orbit 207, near 68°S 145°E, that appears to be thicker (brighter and hence colder) than sea ice. Maps do not indicate any extensions of the continent in this area as large as this formation, but this is near the Mertz Glacier Tongue and suggests that the tongue may be larger than shown on maps. There are some warmer (darker) areas, along the coast and near 68°S 160°E (near the Balleny Islands), that must consist of either broken ice or open water. While the edge of the pack ice is not as clearly defined in the HRIR as it is in the TIROS, cloudiness can be seen over the ice, leaving some question as to what is cloud and what is ice. For example, the
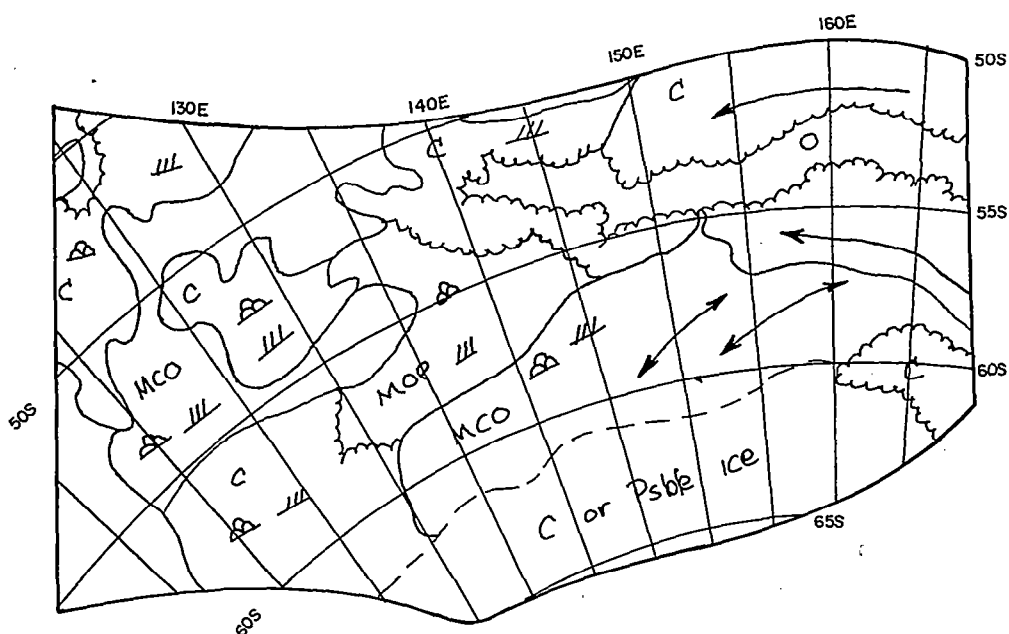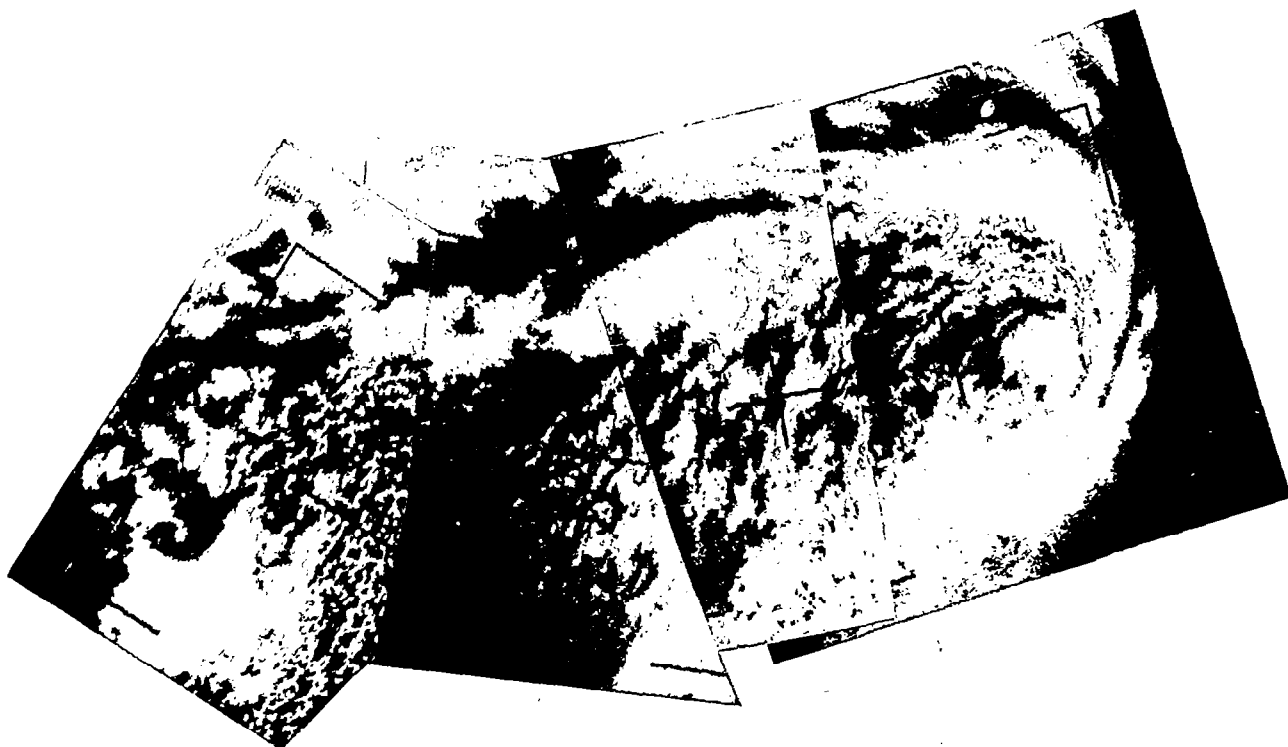
Figure 6-5   TIROS VIII Television Picture Mosaic, Orbit 3838/3836, and
Operational Nephanalysis, 0117 GMT, 11 September 1964

uniformly gray area in orbit 207, stretching from the vortex to about 67°S, has rather sharp edges in its southern section, more like what would be expected of ice than cloud. Upon closer inspection, however, it is seen that the area is connected with the cloud bands near the vortex and, as will be seen later, it moves a considerable distance in 24 hours. Therefore, it is felt that this is a cloud mass, high enough so that its temperature is considerably colder than the ice. The ice is the darker area under the cloud, with its edge visible near 62°S 160°E, in agreement with the edge of the pack ice as seen by TIROS.

6.3 The Second Day, 12 September 1964

HRIR orbits 221 and 222 and the rectification (Fig. 6-6) show the situation a day later at about 1200 GMT. The principal cloud feature is the bright, slightly vortical cloud centered near 55°S 160°E, with a frontal band stretching northward. Just south of this system is a "crescent" shaped cloud centered near 63°S 160°E, and near 55°S 125°E there is a vortex, or at least a "hooked-shaped" system. To the east of 180°, there is a large area of cellular and other lower clouds.

From continuity, the cloud system near 55°S 160°E can be established as the one that was centered near Tasmania a day earlier. It has become better organized, and is now affecting southern New Zealand. The crescent shaped cloud has moved from near 55°S 147°E to its present position, and it has also become better organized. The system that was centered near 50°S 130°E has apparently moved southwestward to its present position at 55°S 125°E. The lower cellular clouds to the east are undoubtedly in the flow associated with the mature cyclone, the center of which can no longer be seen in the HRIR strip.

6.3.1 Conventional Analyses

At 500 mb, the 0000 GMT analysis on the 13th (Fig. 6-3a), about twelve hours after the HRIR, shows that the long wave trough has progressed eastward, and that the storm system is in the northwest flow of this trough. It is almost certain from the HRIR that one or more short waves are still embedded in this flow, since the cloud system to the south also has the appearance of being associated with a second short wave. The movements of these two systems agree quite well with the 500 mb flow on the analyses. The movement of the system south of Australia indicates that the 500 mb flow there is much sharper than is

Figure 6-6   HRIR Data and Rectification of Orbits 221 and 222, about 1145 GMT, 12 September 1964

shown on the analyses. It is likely, in fact, that there is a cutoff low to the west, with the 500 mb flow having an easterly component in this area; this is the only way to account for the southwestward movement of the cloud system seen in the HRIR. The two relatively clear areas, southeast of New Zealand and south of Tasmania, are associated with the ridges shown on the analysis. The surface analysis for 1200 GMT on the 12th (Fig. 6-3b) shows a low center just northwest of Macquarie Island and another at about 60°S 120°E. The former center is placed about right according to the HRIR, but one would also expect to find a surface development under the cloud mass seen in the HRIR near 63°S 160°E.

6.3.2 Comparative TIROS Data

TIROS VIII, at 0350 GMT on the 12th (Fig. 6-7), photographed a vortex south of Australia, centered near 54°S 122°E. This is undoubtedly the vortex seen near the west edge of HRIR strip 222, but the high HRIR nadir angle makes comparison difficult. Both satellite observations indicate that the low center on the surface analysis is placed too far south. The vortical cloud band seen on the horizon in Figure 6-7 is probably the system centered near 63°S 160°E in the HRIR, with the principal system of interest being just north of the area of TIROS coverage.

6.3.3 Cross-sections

Time cross-sections provide a good indication of the movement of the system that developed over southeastern Australia. At Hobart, the pressure fell steadily from 0000 GMT on the 10th, not beginning to rise again until nearly 1200 GMT on the 12th. The wind was fairly light throughout, but went around to southeast on the 11th and shifted back to the northwest before the pressure began to rise. The weather was cloudy throughout, but with little precipitation, indicating that the system was not yet well developed and had not picked up much moisture.

The time cross-section for Macquarie Island provided excellent corroborative data, since the system, as is seen in the HRIR, passed almost directly over the island. The HRIR indicates broken (or low) cloudiness over Macquarie on the 11th, with the higher cloud system having moved into the area by 1200 GMT on the 12th. The time cross-section shows the sky going from broken to overcast after 0000 GMT on the 12th. Also, the pressure was falling, the dew point was rising, and the wind was veering from northwest to northeast, certainly indicating the approach of a

Figure 6-7   TIROS VIII Television Picture Mosaic, Orbit 3853/3852, and
Operational Nephanalysis, 0350 GMT, 12 September 1964

disturbance.   There was considerable precipitation reported at the station from
0600 GMT on the 12th until 0600 GMT on the 14th.   From the winds, it appears that
the center of the system passed nearly over the station at about 1800 GMT on the
12th, in agreement with the position in the HRIR.   The pressure at Macquarie con-
tinued to fall until 1200 GMT on the 13th, however, while the wind had become north-
west again and had increased in speed.   Apparently, the system was deepening as it
passed the station, as is to be expected from the increased circulation apparent in
the later HRIR strips.   This region near the Antarctic convergence (Fig. 6-1) is a
preferred region for cyclogenesis. [15]

   The Macquarie time cross-section also shows that a 500 mb short wave passed
the station shortly after 1200 GMT on the 12th, something not indicated on any of
the horizontal analyses.   The wind went from 310° to 350° at this time, returning
to 330° six hours later.   Another disturbance apparently passed between 0000 and
1200 GMT on the 13th, when the 500 mb wind went to 340° and the 400 mb wind went
to 030°, before both levels returned to a westerly flow.

   In orbit 221 (Fig. 6-6), varying cloud heights are apparent in the band
stretching over New Zealand, with a marked break in the clouds almost over the
island.   This could be caused by downslope motion east of the mountains of South
Island.   There is also a thin high cloud near 40°S 190°E (170°W) for which an ex-
planation is not obvious, but it may mark the northern limit of the cold air outbreak
behind the system to the east.   Pack ice can be seen in places, and cloudiness can
be seen over the ice in the Ross Sea area, but it is difficult to specifically differentiate
clouds from ice.

6.4 The Third Day, 13 September 1964

   Orbits 236 and 237 (Fig. 6-8) covered the area about 1215 GMT on
13 September.   A striking feature in 237 is the clearness of the outlines of Australia
and Tasmania.   In Figures 6-2 and 6-6, North Island of New Zealand was visible,
but not as clearly.   The only clouds discernible over Australia are in the vicinity
of Tasmania, and it is probable that the small brighter areas in southeastern
Australia are related to higher elevations and to snow cover in the Snowy Mountains.
Also the north-south temperature gradient can be observed, with northern Australia
appearing warmer (darker) than southern Australia.

   The prominent cloud feature observed in these strips is the vortex centered
near 60°S 164°E that appears to be a system reaching occlusion, but consisting
of clouds that are not very bright.   To the east, a second vortex, brighter than the
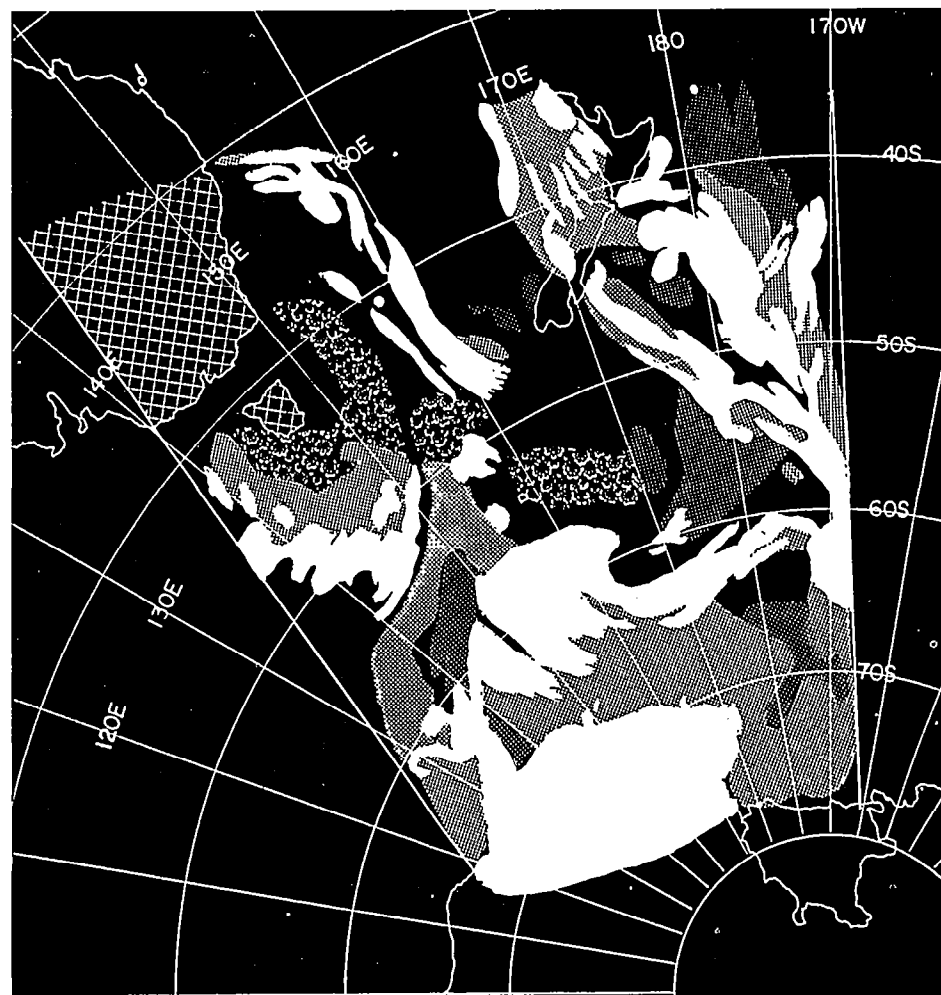
Figure 6-8   HRIR Data and Rectification of Orbits 236 and 237, about
1130 GMT, 13 September 1964

first, is centered near 60°S 175°W with a frontal band extending northward. The poor nadir angle makes it difficult to rectify the exact shape of this pattern. Some of the brightest clouds in strip 236 are located on the frontal band to the north of this second vortex. There is another frontal band off the east coast of Australia, that dries out as it reaches the continent, and an area of rather disorganized cloudiness south of eastern Australia, perhaps the remains of the system that had been centered near 58°S 125°E.

Exactly what happened during the past 24 hours is not immediately clear, but after closer inspection it appears that the two vortices in orbit 236 are the same two cloud masses that were seen the previous day. The more northerly system (in Fig. 6-6) has moved rapidly southeastward, carrying the frontal band with it, while the southerly system has moved very little while advection reorganized the clouds into a definite vortex pattern. Evidently, the circulation at mid-tropospheric levels consists of a cutoff low in the vicinity of 60°S 164°E, with a strong northwest flow northeast of the center. The cloud mass to the east is associated with a short wave in this flow and has acquired most of the energy of the overall circulation. The other system is losing its energy as it becomes advected into the closed circulation, accounting for the lower level cloud tops. Further to the north, the brighter clouds of the frontal band indicate that a development is taking place east of New Zealand. The break in the cloudiness at about 40°S is along the eastern coast of New Zealand, and again is probably the result of downslope motion.

6.4.1 Comparative TIROS Data and Conventional Analyses

Figure 6-9 shows a TIROS picture of the weaker vortex about ten hours earlier. Although the frames are rather dark, the circulation appears to be similar to that seen in the HRIR, with a fairly uniform pattern. At 500 mb (Figs. 6-3a and 6-4a), the circulation could have been drawn to be more closed off than is shown on the analyses; the rapid movement of the principal short wave can be accounted for by the strong northwesterly flow in the area of 170°E. The HRIR observations indicate that there must be a more complex surface pattern than that shown on the analysis for 1200 GMT on the 13th (Fig. 6-3b).
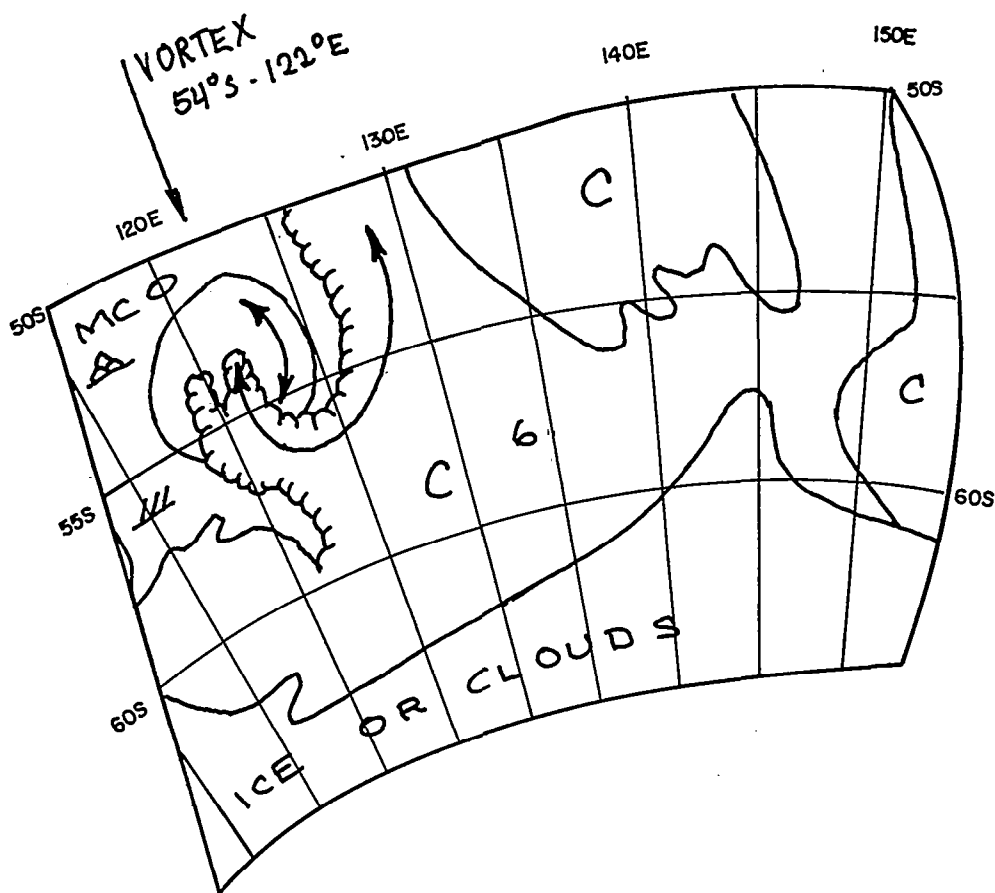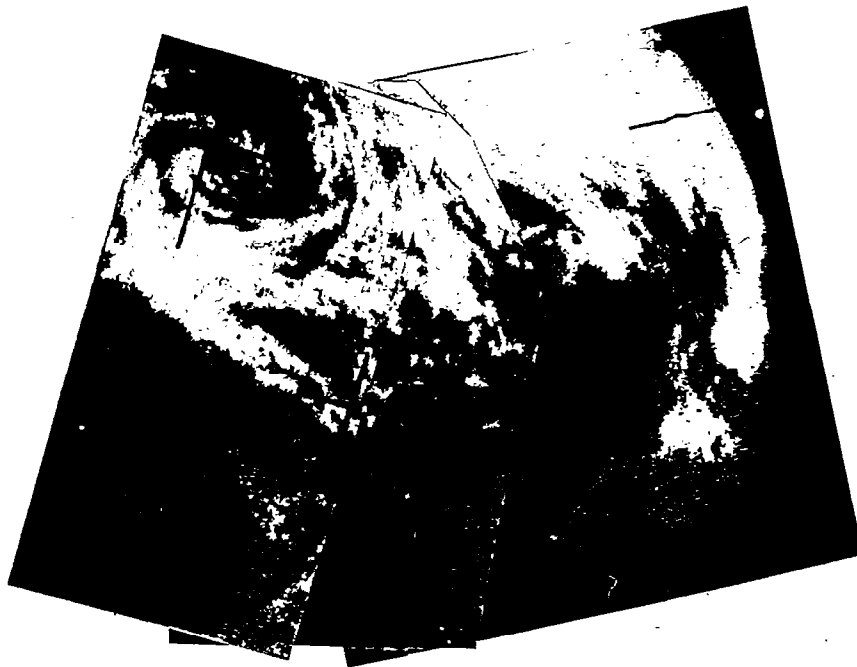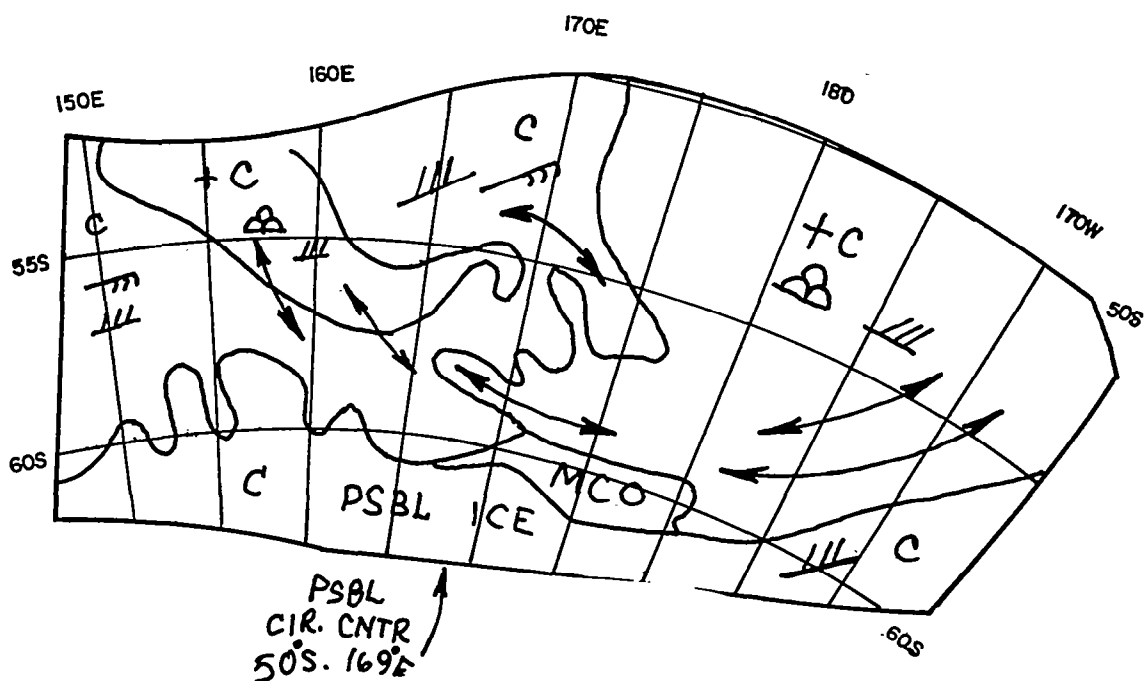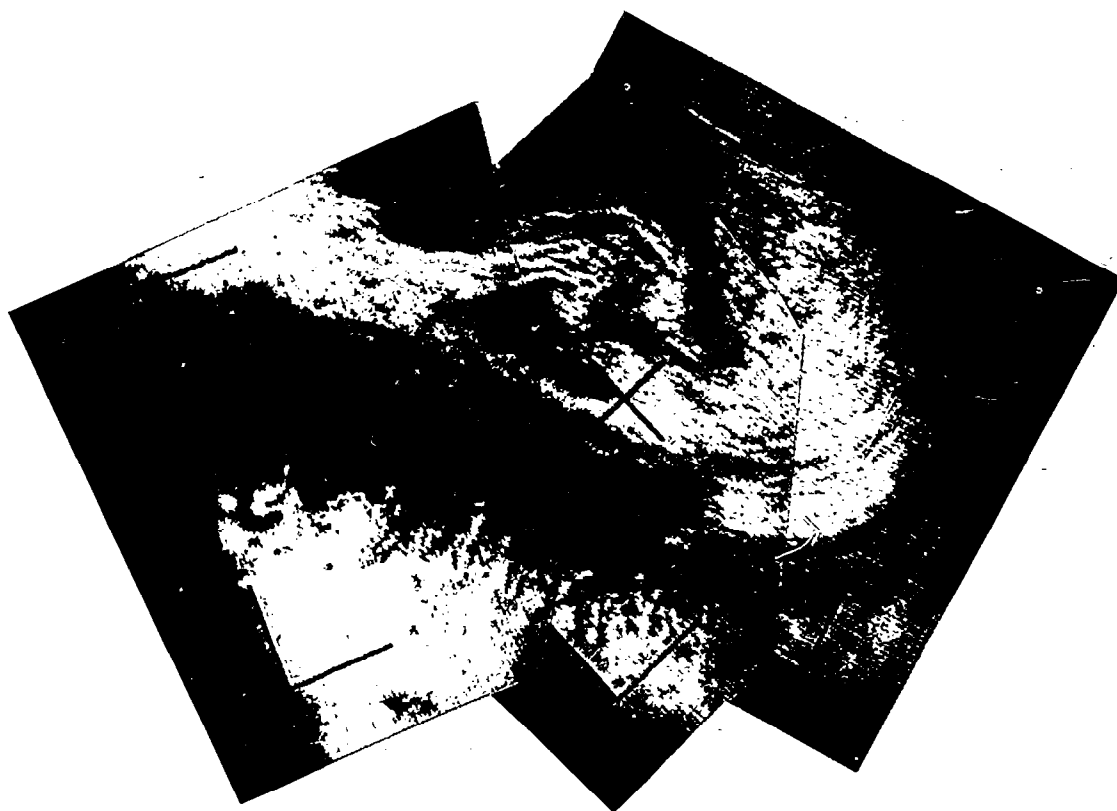
Figure 6-9   TIROS VIII Television Picture Mosaic, Orbit 3867/3865, and
Operational Nephanalysis, 0123 GMT, 13 September 1964

6. 5 The Fourth Day, 14 September 1964

Orbits 249 and 250 (Fig. 6-10) show a mature cyclone centered about
64°S 175°E, but with only surprisingly low cloudiness. Higher cloudiness is centered
to the east at about 65°S 160°W, with an area of cloudiness at different heights
stretching northward.   The mature cyclone is obviously the same system as that
seen a day earlier, now having been advected into a fully closed circulation.   More
cloudiness can now be seen in the former "clear" sector, and the area of poleward
flow appears to consist of slightly higher clouds than the area of eastward flow at
the most northerly part of the vortex.   This is analogous to the northern hemisphere
cases studied by Sherr and Rogers. [41] The higher clouds to the east must be
associated with the same short wave that was seen on the 13th, and the broad area
of cloudiness to the north indicates that development east of New Zealand is continuing.

6. 5. 1 Comparative TIROS Data

The TIROS mosaic in Figure 6-11 shows the low level cloud vortex about
twelve hours before the HRIR.   The nephanalysis (Fig. 11a) places the center of the
vortex slightly northwest (60°S 168°E) of the HRIR position (64°S 175°E), which
is in good agreement with expected movement over the time interval.   The vortex
as seen by TIROS is completely filled in, indicating that there is considerably more
very low cloudiness than is seen in the HRIR.   The cloudiness associated with the
short wave is quite probably the brighter cloudiness northeast of the vortex.

6. 5. 2 Conventional Analyses

The 500 mb analysis for 0000 GMT on the 15th (Fig. 6-4a), about fourteen
hours after the HRIR, shows a closed low in the area of the observed vortex. It is
reasonable that the closed circulation has reached to mid-tropospheric levels by the
time of the HRIR observation, but the brightness of the clouds indicates either
that they are broken or that a large part of the cloudiness is lower than the 500 mb
level.   Based on the TIROS observation, the second alternative is more likely; this
is an excellent example of the complementary character of the two types of data.
The 500 mb analysis has a suggestion of a short wave moving around the closed low
in the approximate position of the higher cloudiness, and certainly a sharper
disturbance could have been drawn in.   Another closed center is now located just

Figure 6-10   HRIR Data and Rectification of Orbits 249 and 250, about
1030 GMT, 14 September 1964

Figure 6-11   TIROS VIII Television Picture Mosaic, Orbit 3880/3878,
2255 GMT, 13 September 1964
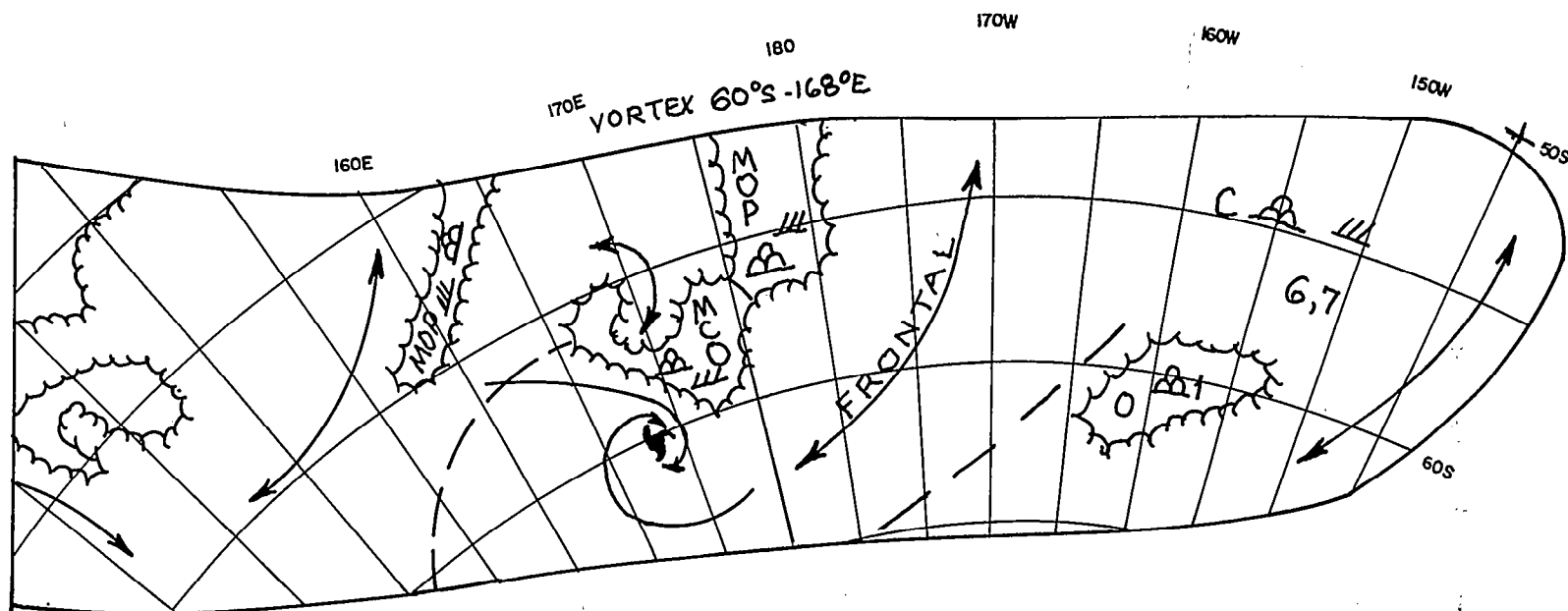
Figure 6-11a   TIROS VIII Operational Nephanalysis, Orbit 3880/3878, 2255 GMT, 13 September 1964

west of New Zealand, which may be connected with the broader cloud band just east of there in the HRIR.

The surface chart (Fig. 6-4b) shows the low center to be placed slightly west of where it should be, and less complex than it probably is. It appears from the time cross-section that a secondary cold front passed Macquarie Island at about 1200 GMT on the 14th, at which time there was a gusty wind, precipitation, and a pressure rise.

6.5.3 Cross-sections

As the system moves southward, the two Antarctic stations in these longitudes are showing signs of being influenced by the circulation. On the 13th, the pressure at d'Urville began to fall with a southeast wind; by 1200 GMT on the 14th the wind has shifted back to the southwest, but the pressure is still falling. On the 14th, the pressure at McMurdo is falling and the wind is from the east, but this station is still well south of the circulation center.

The upper winds at Macquarie Island show a remarkable increase in wind speed at the 400 to 500 mb levels at about this time. At the time of passage of the disturbance (between 0000 and 1200 GMT on the 13th), the wind was very light at the 400 mb level, being 030° at 14 knots. By 1800 GMT it had increased to 55 knots and by 0000 GMT on the 14th it had increased to 100 knots. After slacking off slightly, the wind again increased, reaching a maximum of 127 knots at 1800 GMT on the 14th. The winds at 500 mb were similar, although not quite as pronounced. At both levels, the direction of the first peak was 270 degrees and the second peak 250 degrees. In between the two maxima, the direction was 300 degrees. These wind observations indicate that a strong jet had moved over the island, but there is no jet-type cloud visible in any of the HRIR strips that could be definitely correlated with it. Macquarie Island is in the area of missing data in strip 250, so there may have been an unobserved jet cloud.

Much of the pack ice is under cloud cover in these HRIR strips (Fig. 6-10), and the "clear" areas at the Balleny Islands which were very clearly visible on several previous days cannot be seen at all. It is possible to detect some cloud cover over the continent itself, south of the vortex in orbit 250.

6.6 The Fifth Day, 15 September 1964

HRIR orbit 265 (Fig. 6-12) shows the system on the fifth day, although the coverage is not as good as on the other days. This strip shows the vortex to be centered near or east of 65°S 165°W. Due to edge foreshortening, it is difficult to tell exactly what the configuration of the vortex is, but it appears that the major part of the cloudiness is due to the short wave, since it appears quite bright in the HRIR. The old center of the vortex may be dissipating, with the short wave now being advected into a closed circulation. An area of cellular cloudiness is seen behind the vortex, with a clear area to the west. High cloudiness along 180° near 30°S indicates that a disturbance is still centered in that area, and another system is seen to the west near 60°S 160°E.

6.6.1 Comparative TIROS Data

A TIROS mosaic taken, at 0138 GMT on the 15th, is shown in Figure 6-13. The area is the same as that covered in the HRIR, and the pattern is similar to the vortex seen in the HRIR. The center of the vortex is probably the old cutoff system, and the thicker clouds to the east are probably connected with the short wave. The area which, in the HRIR, appears to be lower overcast to the north of the vortex, can be seen in the TIROS to consist of cellular cloudiness.

6.6.2 Conventional Analyses

The satellite observations indicate that the 500 mb circulation must be closed off, as shown on the 0000 GMT analysis on the 15th (Fig. 6-3b), but not on the analysis 24 hours later. A major short wave, maintained over New Zealand on the 0000 GMT analysis on the 16th, is probably connected with the clouds in that area seen in the HRIR

The surface analysis for 1200 GMT on the 15th (Fig. 6-4b) shows a low developing over New Zealand, and a system moving toward Macquarie Island. The time cross-section shows that Macquarie is now under the influence of this next system, with the wind from the northeast and the pressure falling. McMurdo now has rising pressure, indicating that the system over the Ross Sea is remaining to the north.

Figure 6-12   HRIR Data and Rectification of Orbit 265, about 1105 GMT,
15 September 1964

100

The edge of the ice pack is seen rather clearly in HRIR 265 (Fig. 6-12), with some cloudiness visible over the ice. The portion of the edge of the ice seen in the HRIR is in good agreement with the TIROS position in Figure 6-13.

6.7 The Sixth Day, 16 September 1964

Orbit 278, shown in Figure 6-14, is an excellent picture of the system on the final day of coverage. There is still an area of high cloudiness in the eastern sections, but in general the system is disorganized and apparently in the process of dissipation. There is considerable lower and cellular cloudiness in the system, and a few areas of high cloudiness are being advected around the closed circulation. The area near 58°S 145°W appears to contain a small secondary vortex. The frontal band that had been associated with the system tapers off rapidly to low cloudiness, but the disturbance that developed near New Zealand can still be seen to the north.

6.7.1 Comparative TIROS Data

TIROS (Fig. 6-15) covers a part of the system about nine hours earlier than the HRIR. From the nephanalysis, the area is the same as in the HRIR, and by inspection the two views show some remarkable similarities. The area just to the north of the 60S 211 cross mark in HRIR 278 is the same area as that seen by TIROS. Both observations appear to include the secondary vortical circulation.

6.8 Summary and Conclusions

6.8.1 Synoptic Climatology of the Area

The system under study from 11 September to 16 September 1964 followed the meridional "Tasman East" track of Alt, et al,[2] and Rastorguev and Alvarez.[36] This is "track 2" in Notes on Antarctic Forecasting.[48] Accordingly, this is the general type of system that forms over western Australia as a non-frontal depression, moves southeastward and deepens as it crosses the Antarctic convergence at about 50° to 60°S, reaches its maximum intensity in the occlusion process, and finally moves eastward and decays. The system filled in a preferred location over the eastern Ross Sea, a "principal cyclone graveyard."[48]
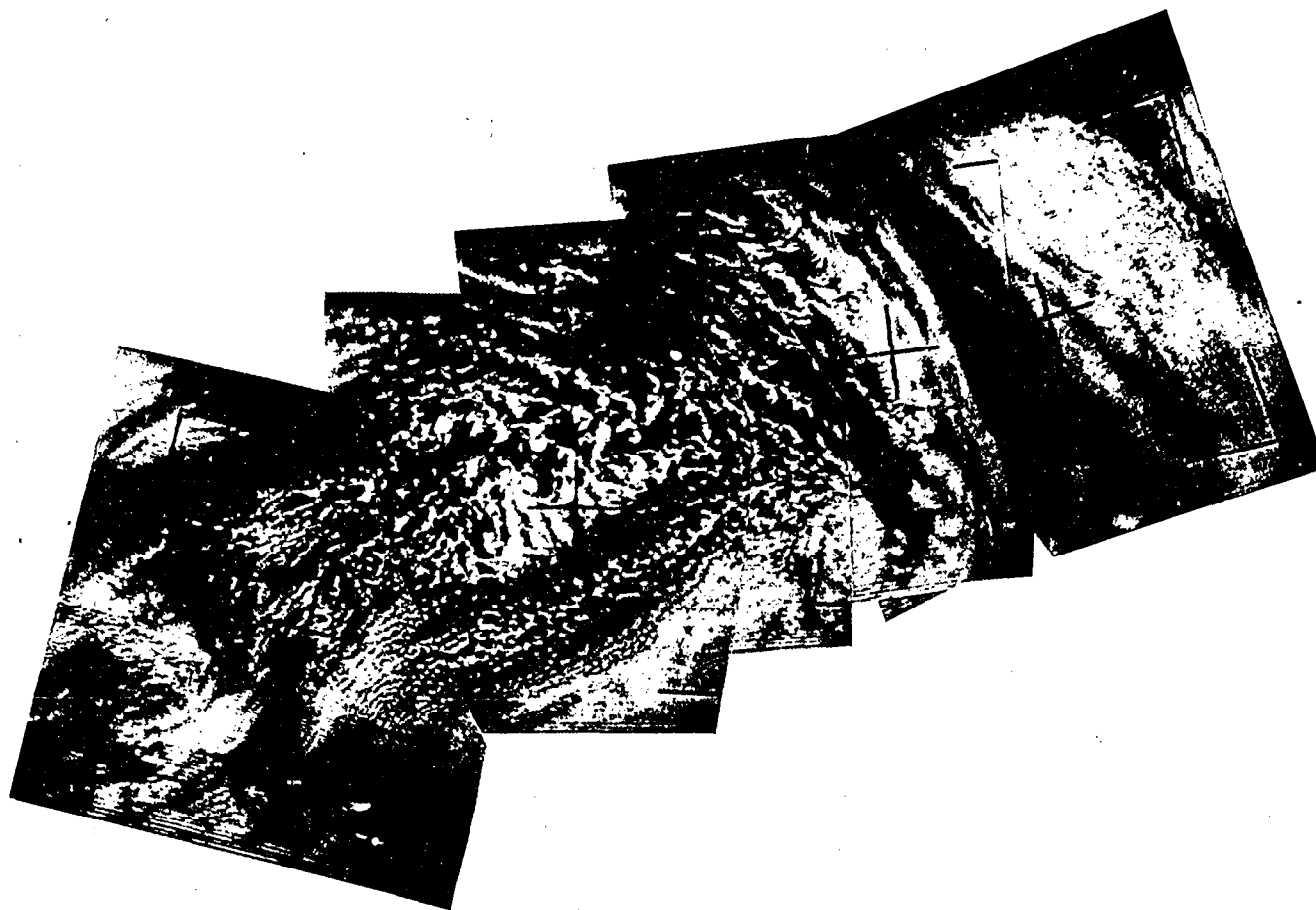
Figure 6-13   TIROS VIII Television Picture Mosaic, Orbit 3896/3894,
0138 GMT, 15 September 1964

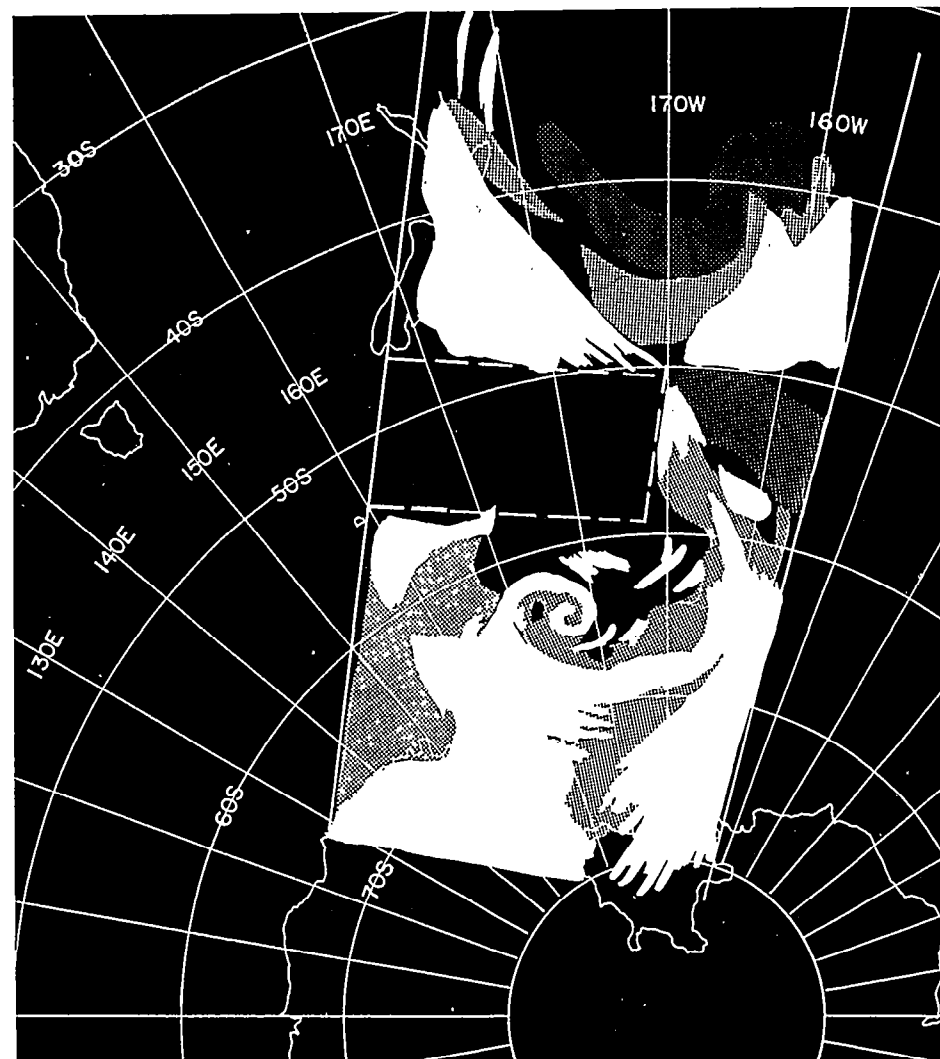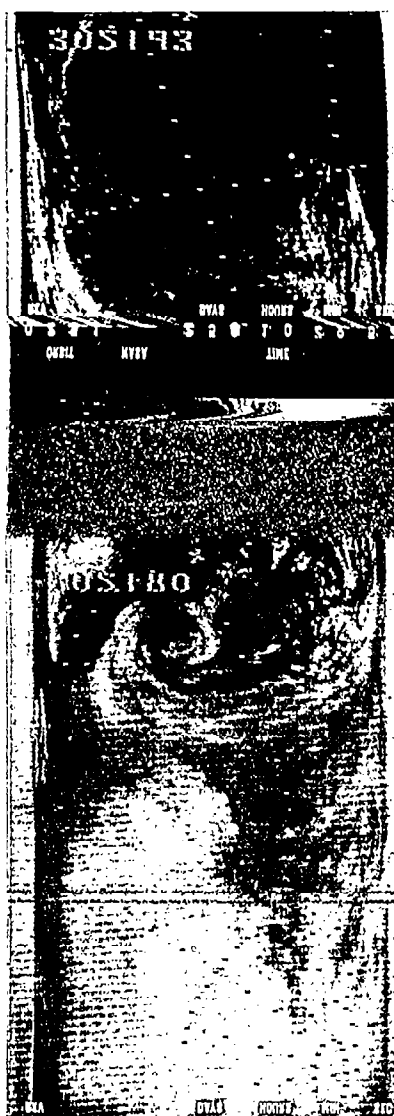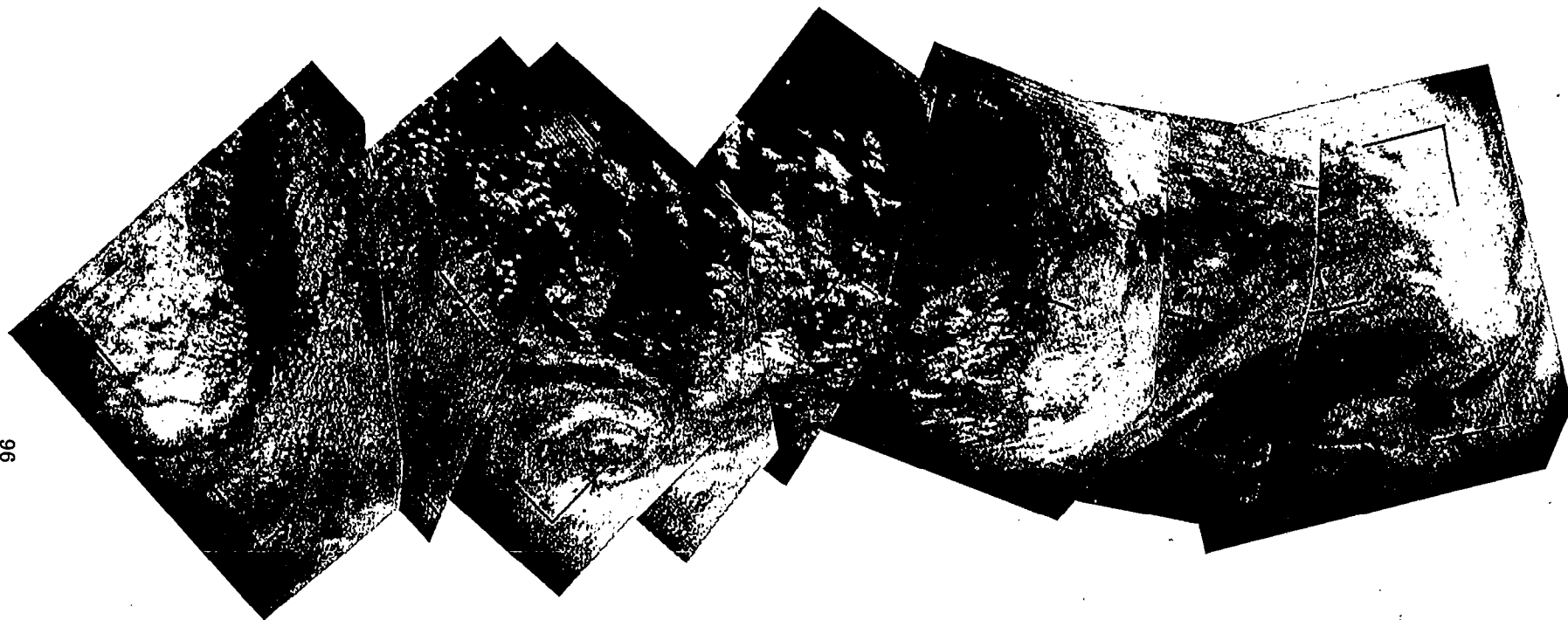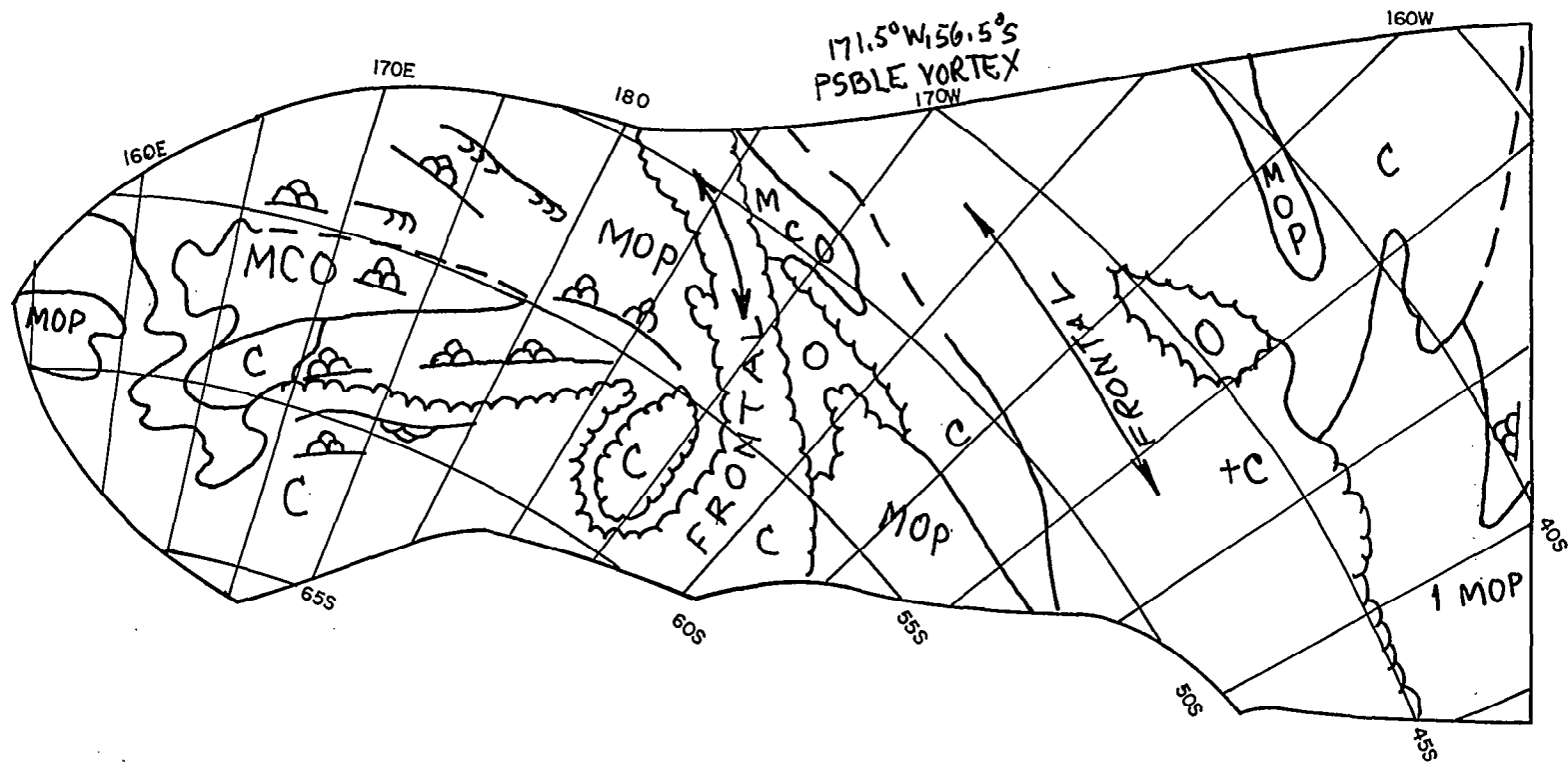Figure 6-13a   TIROS VIII Operational Nephanalysis, Orbit 3896/3894, 0138 GMT, 15 September 1964
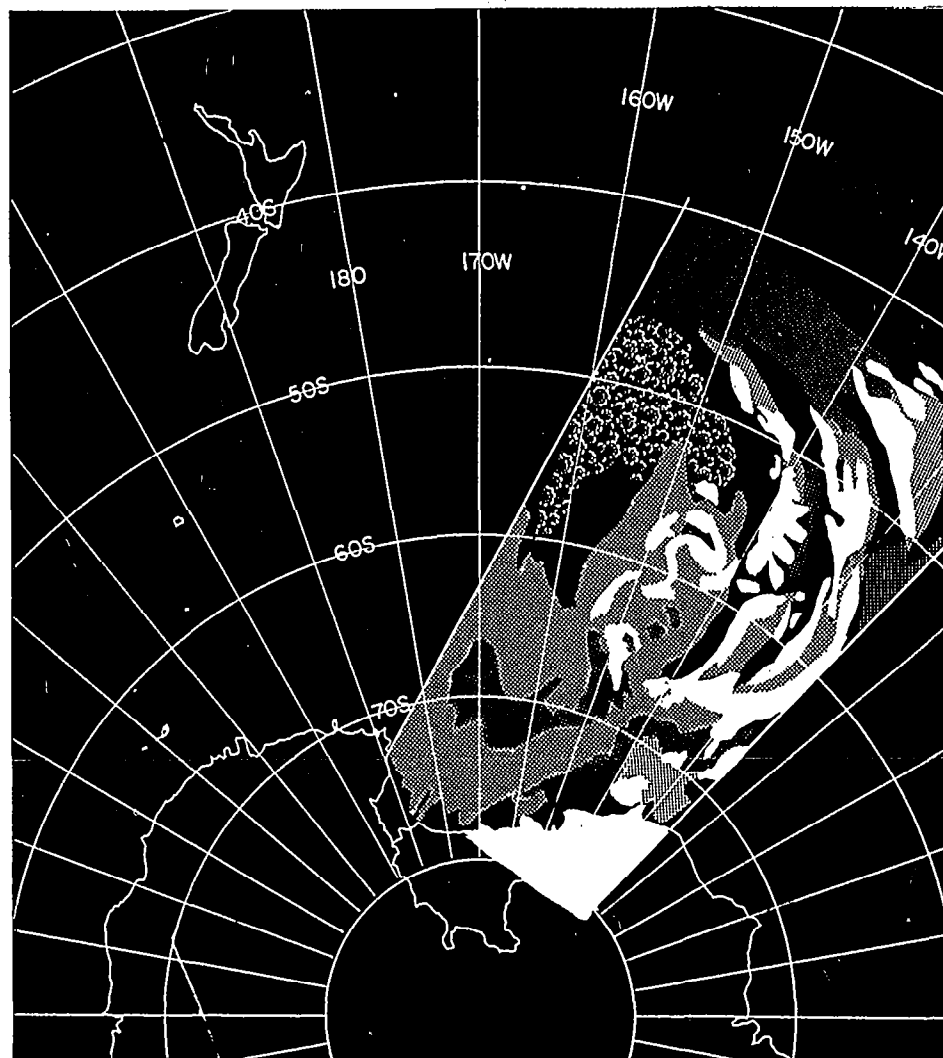
Figure 6-14   HRIR Data and Rectification of Orbit 278, about 0830 GMT,
16 September 1964
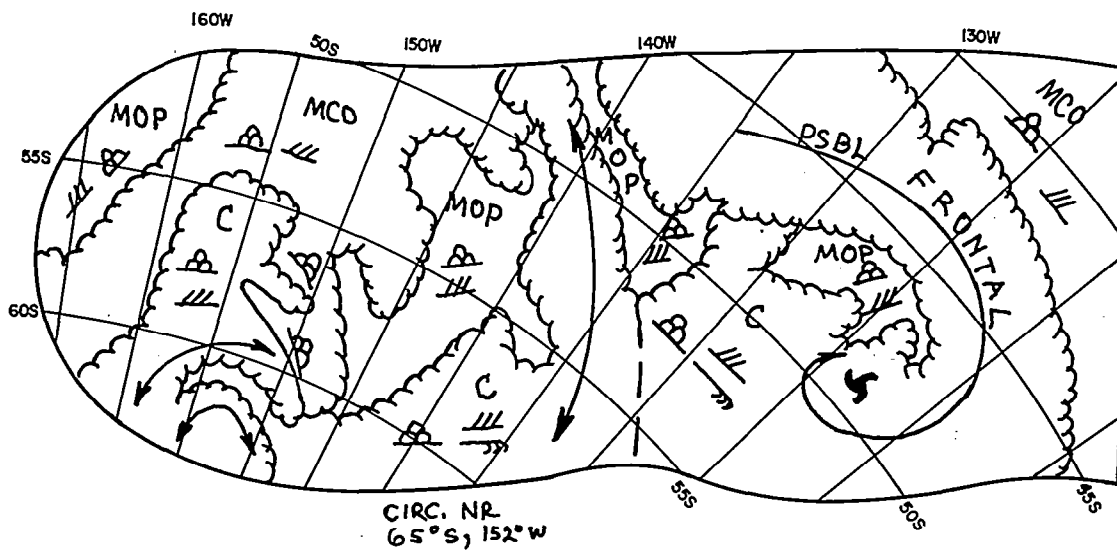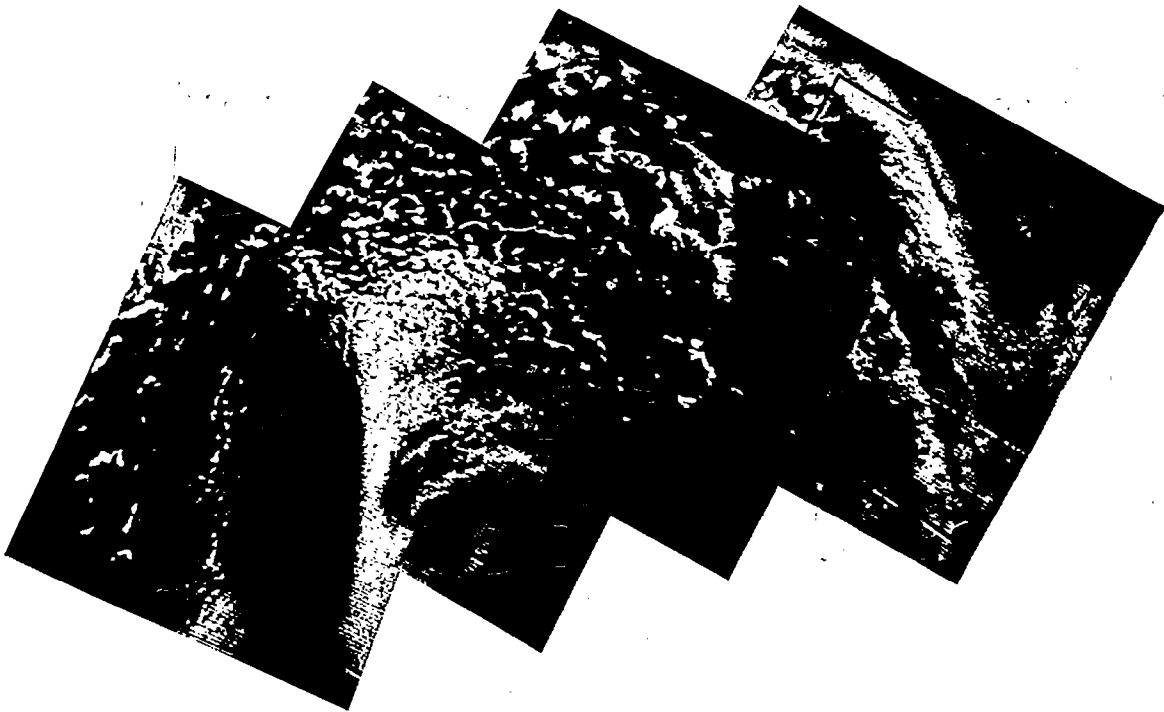
Figure 6-15   TIROS VIII Television Picture Mosaic, Orbit 3909/3907, and
Operational Nephanalysis, 2310 GMT, 15 September 1964

The development of a system of this type is explained by Karelsky,[25] who shows an area of high cyclonicity to exist from south of western Australia to southern New Zealand in winter. He also suggests that orographic barriers help development, particularly in winter, with a principal region west and south of Tasmania.

Gibbs[15] points out the importance of the strong concentration of sea surface isotherms associated with the Antarctic convergence, in the deepening of cyclones; the concentration of isotherms would act like a coastline in this case. He also says that it is likely in these developments that the fronts are the result, rather than the cause, of the depression. This seems to be true in the case studied, where the system developed in a non-frontal zone, but soon had a definite frontal system associated with it. The system followed Gibbs' model fairly well, originating as frontless vorticity, moving southward to the westerlies, ceasing to deepen when it reached the zone of lower baroclinicity south of the Antarctic convergence, moving eastward and eventually losing its identity. It is seen, then, that this system was not an unusual one in this region of the southern hemisphere, and therefore the conclusions reached in the study should be valid for other systems as well.

6.8.2 Comparisons with Previous Satellite Studies

The variability of cloud width and height, as shown by the HRIR, indicates preferential areas of upward vertical motion similar to those found by Sherr and Rogers.[41] The frontal bands also show considerable variability in the cloud heights, something not noticeable in the TIROS pictures. The small scale aspects of this variability of cloud height may be connected with mesoscale vertical motions, as described by Elliott and Hovind.[10] Cellular cloudiness (in the cold sectors of the cyclones) as seen in the HRIR appears similar to that seen in the TIROS. In some cases the formations are quite similar, for example, in Figures 6-14 and 6-15. In other cases, cells appear in the TIROS pictures where the HRIR shows only a solid low cloud mass. In such cases, only the larger cells further away from the occlusion center may be seen by the HRIR. In previous HRIR studies, Widger[56] noted that the cellular structure appeared to be more prevalent in the southern hemisphere HRIR strips than in the northern hemisphere. It may be that, during the brief life of Nimbus and due to seasonal temperature gradients, more systems reached full occlusion in the southern hemisphere than in the northern, or that the greater southern hemisphere temperature gradients, at this time of year, promoted greater development of cellular cloudiness behind the centers of occlusions.

The cellular patterns seen in the HRIR were examined to see if it was possible to estimate wind speeds in the same manner as that used by Rogers[30] for TIROS data. Because of the lack of corroborating data, it was difficult to check the actual wind speed, but the cellular areas in both the TIROS and the HRIR were examined to see if the patterns observed by Rogers existed.

Various TIROS pictures show the characteristic patterns, such as the "blown out" ellipses in Figure 6-13. In the HRIR, orbit 207 (Fig. 6-2) shows what could be called "blown-out" ellipses, but the pattern is much larger than the scale seen by TIROS. Orbit 221 (Fig. 6-6) shows quite definitely a chain-like pattern, and some blown-out ellipses. The cellular areas in the other HRIR strips show no definite patterns. It is seen, then, that it is possible to discern patterns, somewhat like those observed by Rogers, in the HRIR, but they are of a larger scale and the correlation with the TIROS patterns is not good. Usually the patterns seen in the TIROS pictures are in an area that appears solid in the HRIR, with the patterns that are seen in the HRIR being larger scale patterns. Accordingly, it is unlikely that the criteria reported by Rogers are directly applicable to the HRIR data.

In this study, there were no clouds observed that could be definitely correlated with jet streams. The strong jet observed at Macquarie Island and mentioned previously (Section 6.5.3) does not have any obvious cloud associated with it, and in most other cases it is difficult to determine exactly where the jet is because of the sparsity of data. Possibly the thin clouds along 50°S in orbit 207, along 40°S in 221, and south of 60°S 173°E in 221 are associated with jets, but the brightnesses indicate that the clouds are not too high. However, the thin bright clouds seen in orbit 236, east of 60°S 164°E and along the northern part of the vortex, would be in the approximate positions in relation to the cyclone center where jets were observed by Merritt.[30] In none of these cases could there conclusively be shown to be jet-associated clouds.

6.8.3 Ice Observations and Ice-Snow-Cloud Differentiation

Satellite observations taken over the high latitudes of the southern hemisphere present the problem of the differentiation between clouds, and ice or snow. The HRIR strips used in this study cover both the pack ice region around Antarctica and the Antarctic continent itself. The TIROS passes reach as far south as the edge of the pack ice.

In the HRIR, the Antarctic continent is seen as an undifferentiated bright region, with the edge of the continent sharply defined in most cases. This is due to the pack ice having a warmer temperature than the continent and so appearing darker; also there are many areas of either broken ice or open water along the coast that appear even darker than the pack ice. In most cases, the clouds are colder than the pack ice and appear brighter, as is seen in strip 207 (Fig. 6-2) - the clouds behind the vortex. Figures 6-6, 6-8, and 6-10 also show brighter clouds over the pack ice. Only rarely can any clouds be detected over the continent itself; in strips 208 (Fig. 6-2) and 250 (Fig. 6-10) some cloudiness can be seen over the edges of the continent.

In the TIROS pictures, the edge of the ice pack can usually be seen, appearing as bright as, or brighter than, the clouds. It can be detected by its ragged but sharply defined edge. In those TIROS pictures where ice is seen, the clouds are rarely identifiable over the pack ice, or would not have been except from continuity with clouds over the water. This is especially noticable in Figures 6-5 and 6-9.

It appears, therefore, that it is nearly impossible to detect cloudiness over the Antarctic continent by satellite observations, but it is possible to detect cloudiness over the ice pack by HRIR observations, providing the clouds are sufficiently high and cold. Since it is sometimes difficult to tell where the edge of the ice pack is in the HRIR or exactly what is cloud and what is ice, it is desirable to use both the HRIR and the TIROS observations in these areas. From the TIROS data, the edge of the pack can be determined, and (since normally the location of the edge varies only slowly from day to day) this gives a reliable indication of the extent of the ice in the HRIR observation, even if there may be a day or two difference in the times of the two observations. This can then be used to help determine whether a feature seen in the HRIR is actually cloud or ice.

Various broken-ice or ice-free areas can be seen by the HRIR in the pack ice region around Antarctica. Some of these are seen along the coast of the continent, and a striking example is that near the Balleny Islands, at 68°S 164°E. These areas can be determined by their darker gray or black appearance (signifying broken ice, as is seen at 70°S 159°E in Fig. 6-6), or by their nearly black appearance (signifying nearly ice-free areas, as is seen at 67°S 162°E in the same figure). The dark area at 78°S 162°E in strip 250 (Fig. 6-10) is McMurdo Sound.

The Balleny Islands appear slightly brighter than the surrounding ice, because of their higher terrain and snow cover. However, it is the ice-free areas to their northeast that make them stand out. In strip 207 (Fig. 6-2), the dark area

is seen, but it is partially obscured by clouds (the brighter area) that are associated with the system to the northeast. In this same strip a fairly large dark area is seen along the Antarctic coast at 70°S 160°E. In strip 221 (Fig. 6-6), the Balleny Island area is larger and is quite dark; some clear areas are still seen along the coast of the continent, but they are not so dark. It is also seen that there are actually three distinctive ice-free areas northeast of the Islands, undoubtedly due to the separate major islands of the group. (Navy Weather Plotting Chart 6836 shows the group to consist of three islands.)

In strip 236 (Fig. 6-8), the Balleny Islands area is still seen but is neither as large nor as dark as before. There are still some areas seen along the coast, but they are not very dark. In strip 250 (Fig. 6-10), although some areas along the coast can be seen, the Balleny Islands cannot be seen. In strip 265 (Fig. 6-12), a small part of the Balleny Islands ice-free area can be seen, with the rest obscured by clouds.

As an explanation of these ice-free areas, it is felt that the prevailing southerly winds have produced ice-free "leads" along the coast of the continent. The larger ice-free or broken ice areas may be in preferred regions for katabatic winds. The areas to the northeast of the Balleny Islands would be in the lee during a prevailing southwesterly wind. In strip 221 a strong southwest wind has produced a fairly large ice-free area; in 236 the system from the north is approaching, so the wind has possibly become easterly and the area decreases; in 250, no ice-free area is seen because cloudiness probably obscures the islands and the easterly wind may have pushed some ice back in; in 265, the wind has become westerly again and the ice-free area can be seen where the clouds are not obscuring it. The variations in the other areas along the Antarctic coast may also be due to variations in the wind, both large scale and local, and after sufficient data and experience in interpretation are developed, may provide additional clues as to the direction of the surface wind.

6.8.4 Conclusions

In conclusion, this southern hemisphere case study does not indicate any pronounced differences between southern hemisphere and northern hemisphere synoptic systems as observed in the HRIR. Because of the larger ocean areas in the southern hemisphere, a system such as the one studied has a chance to develop with fewer of the "obstructions" which are generally present in the northern

hemisphere. While this may allow a longer system lifetime, it does not appear to produce significant differences in the dynamic structure of the system. Larger cellular areas associated with occlusions may be more common in the southern hemisphere, but this cannot be definitely shown with the HRIR data so far available.

This case study indicates that nighttime HRIR observations can be useful in detecting cloud systems as far south as the Antarctic continent. This would be especially useful in the winter months, when the more extended darkness would permit longer periods suitable for HRIR observations. This is the season when conventional data are even more sparse than during the summer. The HRIR could also be used for ice surveys, as shown by the ice-free areas and "breaks" that are visible. With further study, the HRIR observations may provide additional clues useful in predicting cyclone movement in the Antarctic area.

A study of southern hemisphere systems over a greater region than was covered in this case study is given in Section 7.

7. A LARGER AREA SOUTHERN HEMISPHERE STUDY

7.1 Introduction

This study of the Antarctic and adjacent regions of the southern hemisphere covers a far larger area than the previous one of a specific system (Section 6), but includes the period of development of that system. It was undertaken using HRIR mosaics, which were constructed in a generally similar way to those used in the Eurasian study in Section 5. The southern hemisphere mosaics were found to be easier to construct than the northern hemisphere ones, because of the altitude of the satellite, and to a lesser extent the presence of the Antarctic continent. Since the satellite was near apogee over the high latitudes of the southern hemisphere, the South Pole appears reasonably far from the edge of practically every HRIR strip. However, the Antarctic continent obscures any clouds south of about 70°S. Therefore, it was found desirable to use the Pole as one matching point in the construction of the mosaics, with the other being initially a grid point at 60°S and ultimately the various cloud features north of the boundary of the Antarctic continent. Comparison of the Eurasian mosaics (see Section 5) with those in this section will demonstrate the differences between the two hemispheres, as previously discussed in Section 3.1. The HRIR mosaics proved to be very useful in the southern hemisphere, since they give rather complete coverage from about 40 to 70 degrees south latitude, the latitudes of maximum cyclonic activity.[19]

.Nighttime HRIR data were available over a fairly large area of the southern hemisphere for part of the period during which the vortex case in Section 6 was studied. Mosaics were constructed for four consecutive days, September 11 to 14, as shown in Figures 7-1 through 7-4. The coverage on the first three days is primarily of a common region, 40°E to 180°, while a large part of the coverage on the fourth day is more to the east. It is possible to follow some systems over the entire period.

Other satellite data available over the area during this period included some Nimbus AVCS pictures, and a considerable number of TIROS VIII pictures. As was pointed out in Section 6, conventional data are sparse in this region of the world, especially in the South Pacific where "non-existent" might be a better term to use. The IAAC 500 mb and surface analyses were again used (as in Section 6), as they provided the best corroborative data available. As in the Eurasian study

Figure 7-1   HRIR Southern Hemisphere Mosaic for 11 September 1964
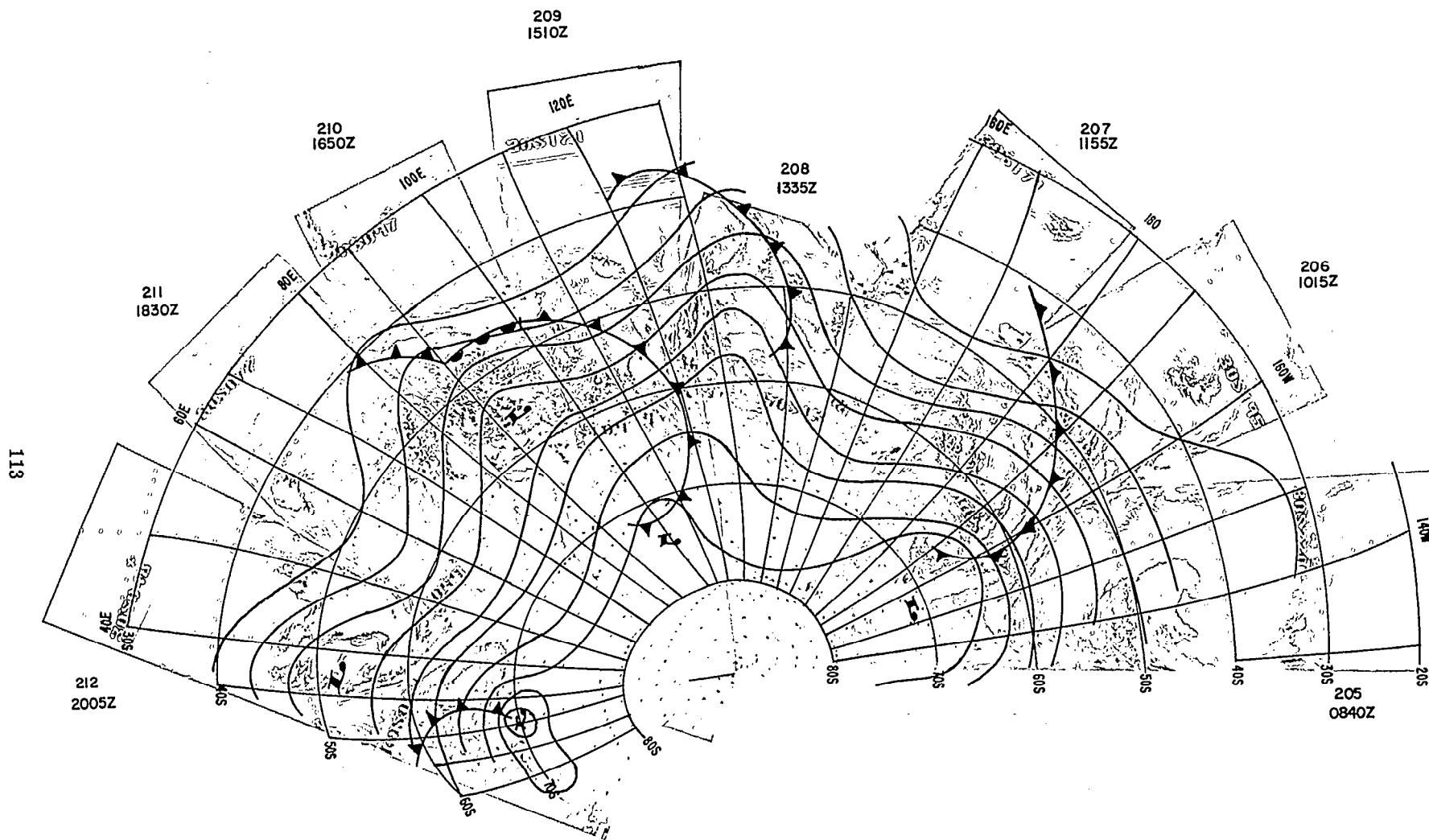
Figure 7-1 a Mosaic for 11 September, with IAAC 500 mb Analysis (0000 GMT, 12 September) and IAAC Surface Frontal Positions (1200 GMT, 11 September)

of Section 5, the analyses were drawn directly on the mosaics. The 500 mb analyses and surface fronts are shown in Figures 7-1a through 7-4a and 7-4b.

7.2 Description of Features

7.2.1 11 September

The principal cloud features of the mosaics were first examined to determine their day-to-day movements and changes. It was immediately obvious that (as in the individual strips used in Section 6) the Antarctic continent stands out vividly with the coast clearly recognizable in many places. The only other land features that are visible are Australia and southern South America.

The mosaic for the 11th (Fig. 7-1) includes strips 207 and 208, which were discussed earlier in Section 6. To the east of this area, two major systems are visible. Southeast of the vortex centered at about 60°S 180°, there is another vortical pattern centered about 68°S 175°W, with a cloud band stretching northward to nearly 40°S. It now appears that the smaller vortex, that was first thought to be a primary system based on what could be seen in strip 207 alone, is, in fact, a secondary vortex that has developed in the southwest flow behind the principal system. * The cloud band extending northward to 40° may be associated with a trough, sharper than analyzed, extending north from the large closed 500 mb circulation; the secondary vortex is probably associated with a short wave trough. Still farther east in the HRIR mosaic, there is another system centered about 45°S 140°W, probably associated with a well developed short wave, with a frontal band reaching northward to 30°.

To the west of strip 208, a frontal wave appears to be developing near 45°S 100°E (note the area of solid high cloudiness), with a large area of disorganized and lower cloudiness to the southwest. Along 45°E, there is a broad band stretching northward from the continent, with a still broader area of high cloudiness near 55°S again indicative of a development. In both cases, these developments can be associated with the trough to the west. Large areas of both solid and cellular low

---

* This is another example of the value of mosaicing of satellite data, and for including data well beyond the area of direct interest, as discussed in Section 3.

cloudiness appear in the mosaic; in places there are rather "sharp" edges (such as near 65°S 70°E and 63°S 20°E) that are similar in appearance to the areas of fog or low stratus seen in the northern hemisphere mosaics (Section 5, Fig. 5-1). Due to the lack of surface observations, it cannot be determined whether these areas are truly areas of small cellular cloudiness or fog or, in the southernmost cases, areas of pack ice. There are very few large clear areas in this mosaic except in the lower latitudes, as over Australia in strip 209.

7.2.2 12 September

On September 12 (Fig. 7-2), about 24 hours later, many features can be identified with those of the previous day. This mosaic includes strips (221 and 222) which have been discussed in Section 6. The cyclonic circulation that was centered near 68°S 175°W has moved slightly eastward, and the secondary vortex has apparently moved toward the northeast; because of a missing strip, it is difficult to find its exact location. The clouds near 68°S 170°W may be part of the secondary vortex but more likely these are clouds that have been advected around the closed circulation. Clouds extend to nearly 80°S over the Ross Sea, and there appears to be less pack ice in the Ross Sea, under the circulation there, than to both east and west. The texture of the "gray" area to the east of 130°W, with its rather sharp edge along 66°S, indicates that it must be an area of very dense pack ice; there is also pack ice to the west of 180°. Skies must be clear in both of these regions since the coast of the continent can be seen. In the Ross Sea, however, the darker tone indicates that the pack ice is less dense, possibly having been broken up by the storm. A time cross-section for McMurdo (78°S 166°E) shows that the station was under the influence of a vigorous storm. Surface winds were from the east or southeast, with sustained speeds of 30 knots or more, from 0000 GMT on the 10th until 1200 GMT on the 13th. Sustained speeds of as much as 50 knots were observed at various times during this period. (From personal experience at Ellsworth, Antarctica, in 1962, the author (Barnes) can testify to the breaking up and movement of pack ice under such winds.)

The vortical cloud pattern that had been centered near 45°S 140°W has moved about 20 degrees eastward, and has become more of a closed circulation, with much of the cloud pattern probably due to advection. What active higher cloudiness is still in the system is in the areas of poleward flow, with lower cloudiness in the eastward flow along 42°S. This is similar to patterns observed by Sherr and Rogers. [41]

115

Figure 7-2   HRIR Mosaic for 12 September 1964

Figure 7-2 a   Mosaic for 12 September, with 500 mb Analysis (0000 GMT, 13 September) and Surface Frontal Positions (1200 GMT, 12 September)
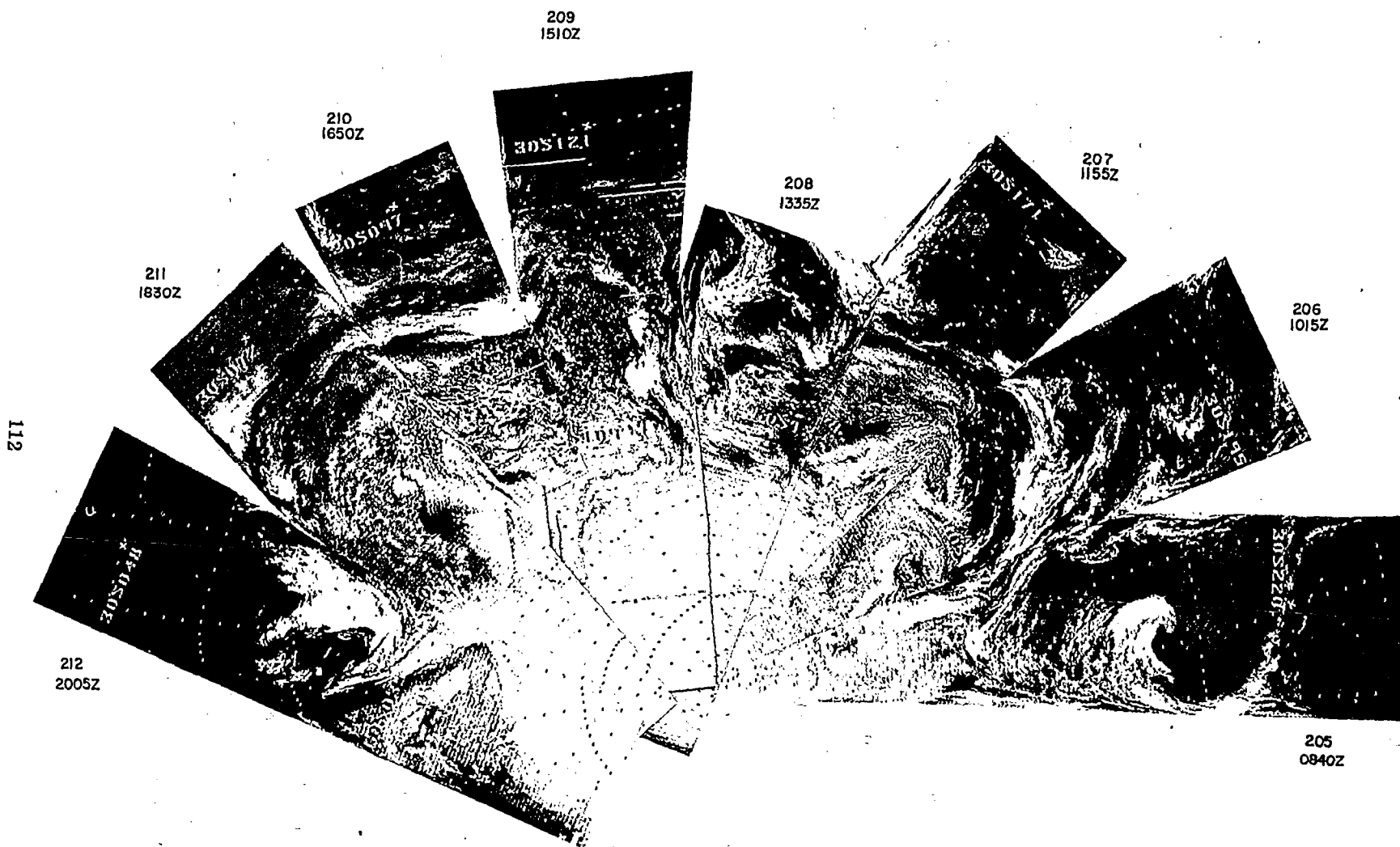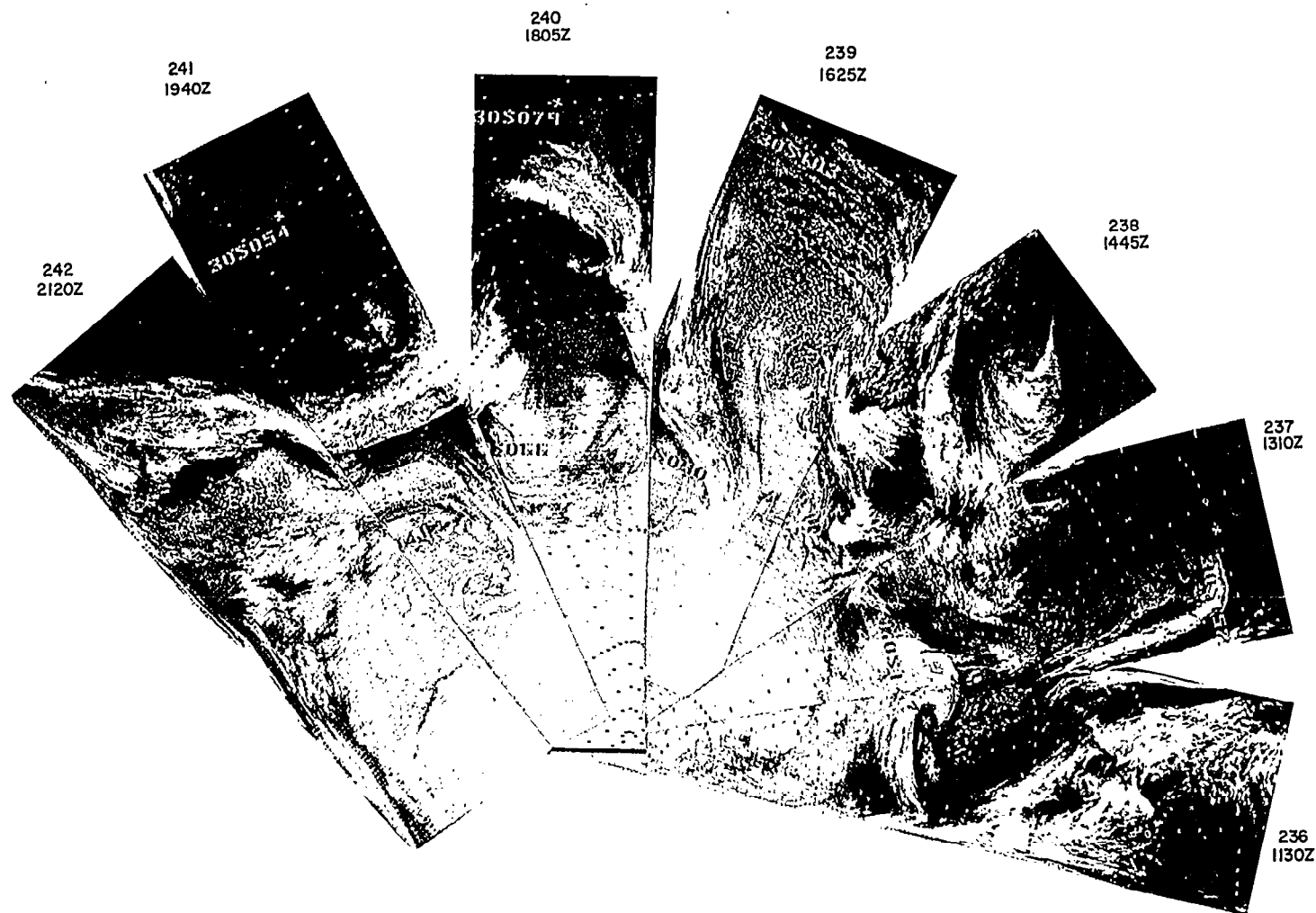
Figure 7-3   HRIR Mosaic for 13 September 1964

118
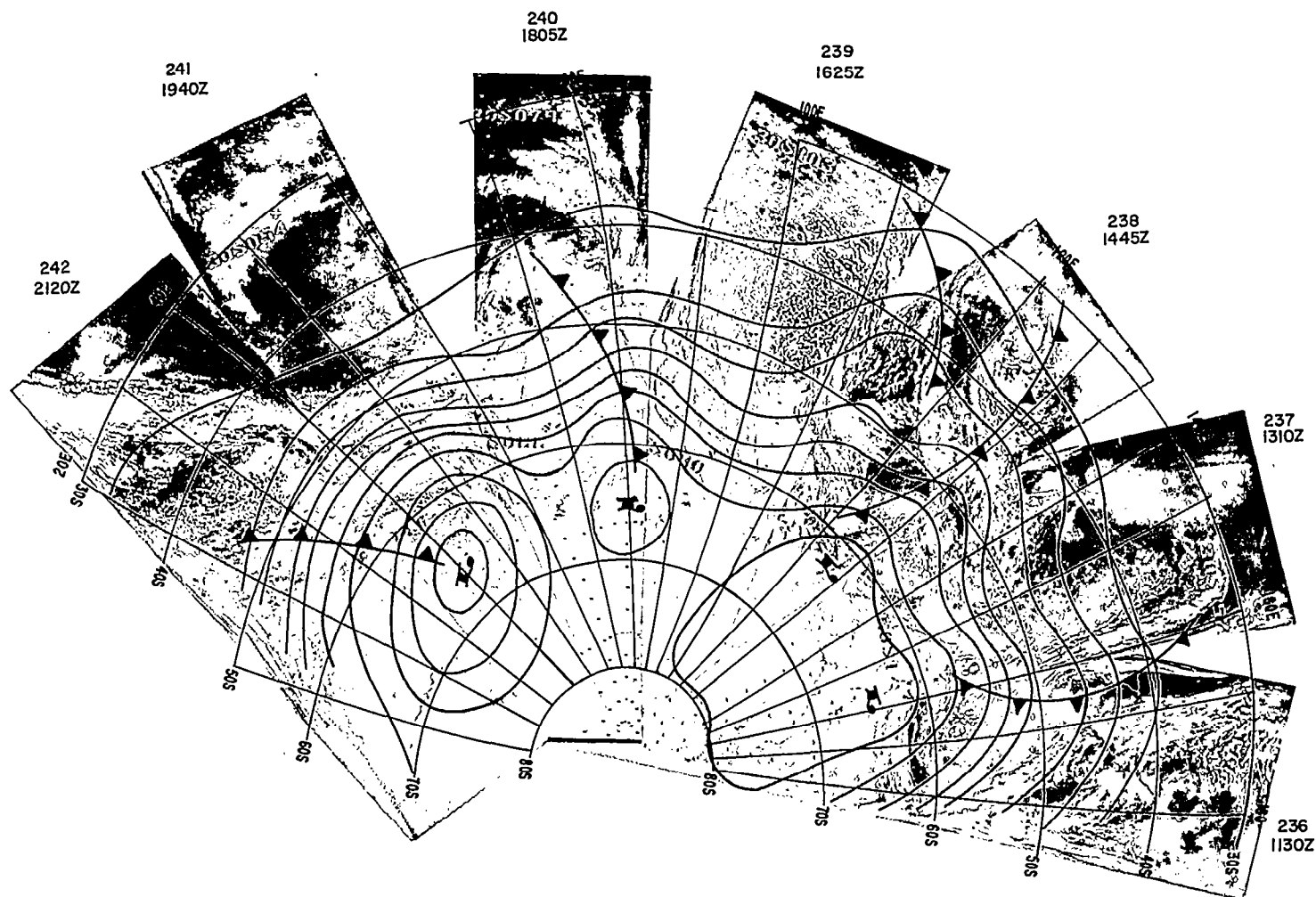
Figure 7-3 a   Mosaic for 13 September, with 500 mb Analysis (0000 GMT, 14 September) and Surface Frontal Positions (1200 GMT, 13 September

Farther east there are data from the South American area, which was not covered the day before. The Andes Cordillera is visible running north-south along 70°W, with a rather long band that is apparently cirrus running northwest to southeast across the mountains. A system with a well defined vortex, approaching the continent from the southwest, covers a broad area. (This HRIR strip was also discussed in Section 4.6.3 of Reference 56.)

In the western part of the mosaic, it is seen that the frontal wave (formerly near 55°S, 100°E), is now near 50°S 120°E and has developed into a pattern indicative of significant upper air support. The disorganized area west of 110°E is still apparent, although the clouds on its eastern side seem to be a bit more organized than before. The broad cloud band that was lying along 45°E has moved eastward about 20 degrees, and does not show the broader section that was seen on the 11th. The southern end of this band can be seen over the continent. This band has now assumed a shape that resembles an "inverted S"; a similarly shaped band was found to be associated with a blocking situation over Eurasia, as described in Section 5 of this report. In light of the similarity, this area was studied in more detail, as is discussed later (see Section 7.4.6). The low cloudiness to the east of the band has become solid, and there appears to be another area of low cloudiness or fog to the west.

7.2.3   13 September

On September 13 (Fig. 7-3), the western areas observed the previous days can again be seen, but the coverage ends at 180°. In this mosaic, strips 236 and 237 have been discussed previously (see Section 6). To the west of the system centered near 60°S 165°E, there is a large area of various cloud formations, with at best limited organization. The area of cellular cloudiness, formerly near 45°S 90°E, has moved northeastward and spread out; it appears that the cloud formation at 50°S 115°E is the same system that was centered near 50°S 100°E a day earlier. The well defined frontal wave southwest of Australia the day before is not seen as clearly, but the broad bright area that was centered near 50°S 120°E is probably now associated with the conglomeration of clouds centered just south of 50°S 135°E. Near 60°S 120°E, there now appears a bright crescent-shaped cloud, seemingly of the type that would be associated with a small short wave trough. The "inverted S" band has moved eastward to about 85°E, but no longer has as much of an "inverted S" shape as it did on the 12th. To the west, an area

not observed the previous day, there is another rather extensive area of apparent mid-tropospheric cloudiness leading northwestward from what appears to be another mature system. The band extends northwest to equatorward of 30°S, reaching the southeast coast of Africa. The well defined cloud edge (near 54°S 50°E) could be associated with a jet just poleward of the frontal wave suggested by the broader E-W cloud band. To the southwest, there are lower clouds associated with a closed and probably dissipating circulation centered near 70°S 40°E.

7.2.4 14 September

On September 14 (Fig. 7-4), the HRIR coverage is more to the east than on the 13th, but the coverage does overlap in the area from 100°E to 180°. In the overlapping region, the area near 120°E is still predominantly cellular, now reaching across southwestern Australia. The frontal bands and cloud groups ahead of the cellular area resemble the clouds of the previous day, with some fairly bright areas indicative of high clouds and upward vertical motions. In fact, the cloudiness seems to have consolidated somewhat, especially near 50°S 140°E (corresponding to the area around 50°S 130°E on the 13th). One is led to suspect an occlusion near 55°S 135°E, with a frontal wave about 10° farther north. South of this area, the cloudiness probably associated with a short wave trough has apparently moved rapidly eastward to near 60°S 145°E. The southern part of the band, which had extended to about 60°S 95°E and had just begun to show signs of a circulation the day before, has definitely acquired a vortical circulation and moved eastward to 120°E. However, the highest cloudiness in this system is still centered more to the west, near 50°S 95°E.

East of the system in strips 249 and 250, which was discussed earlier in Section 6, there is an area of cloudiness that is apparently the northern part of the cyclone that was over the Ross Sea two days earlier (although it is difficult to determine the exact movement of the system during the 48 hours). The cyclone is definitely in a very dissipated stage, with little organization in the clouds. The secondary vortex has been deformed and is probably the cloudiness near 50°S 120°W. There is no sign of the weaker vortical pattern that was seen near 45°S 120°W on the 12th; this may be due in part to the missing strip. Farther to the east, South America is seen, with the Andes again appearing along 70°W. There is a disturbance along the west coast of the continent with considerable upslope activity; most likely this is the system that was approaching the continent on the 12th, but again the missing day makes it difficult to maintain continuity. There is a rather sharp edge
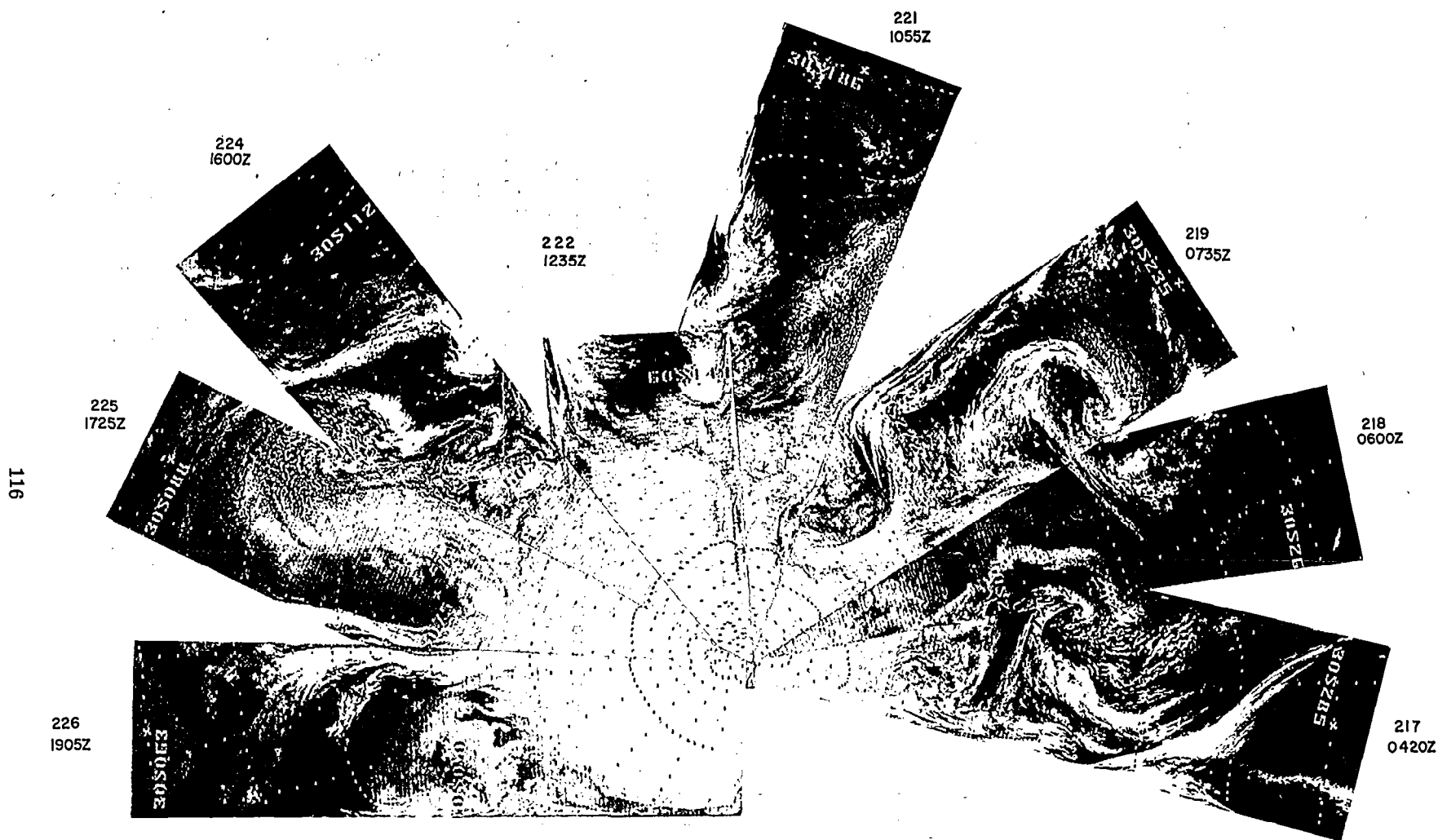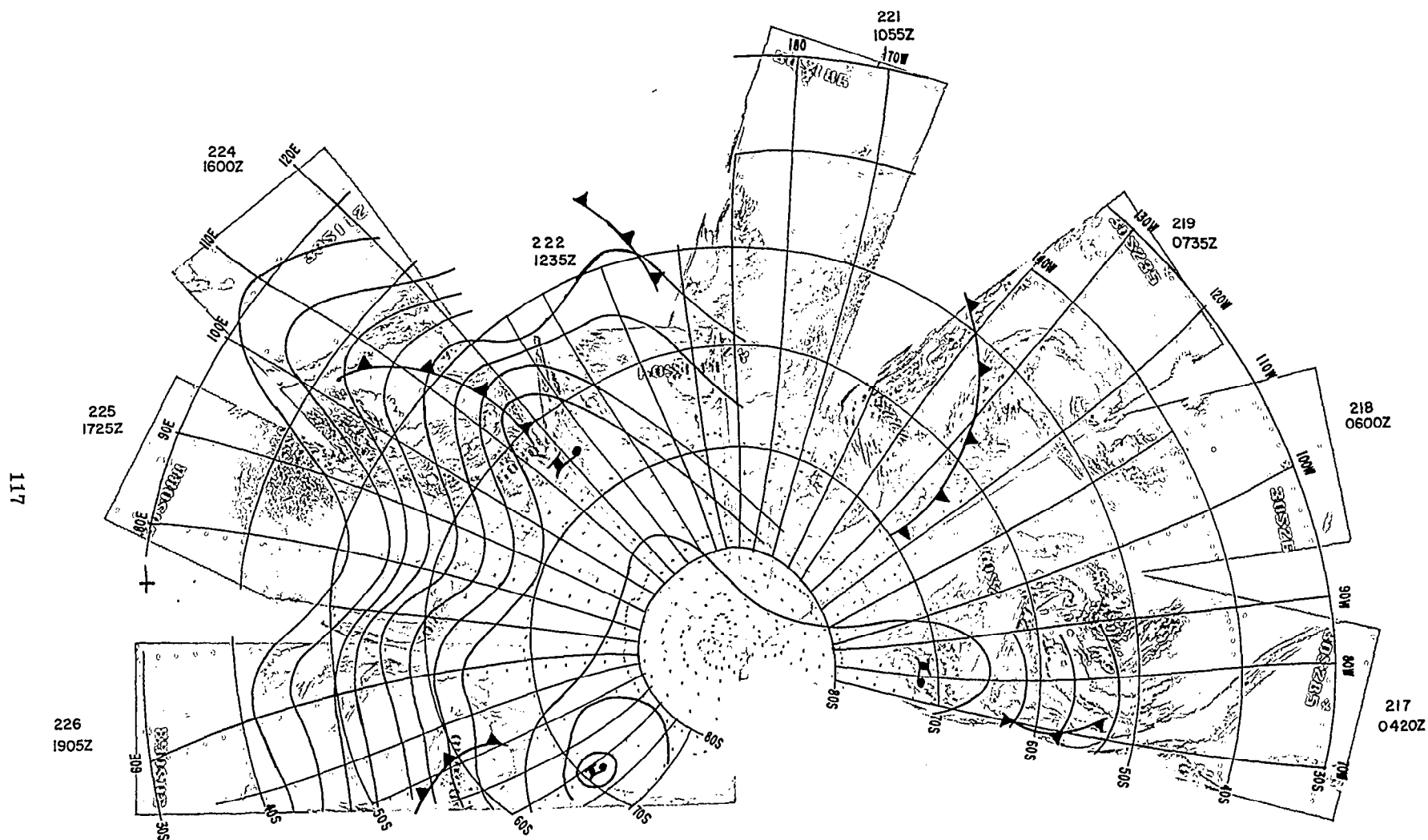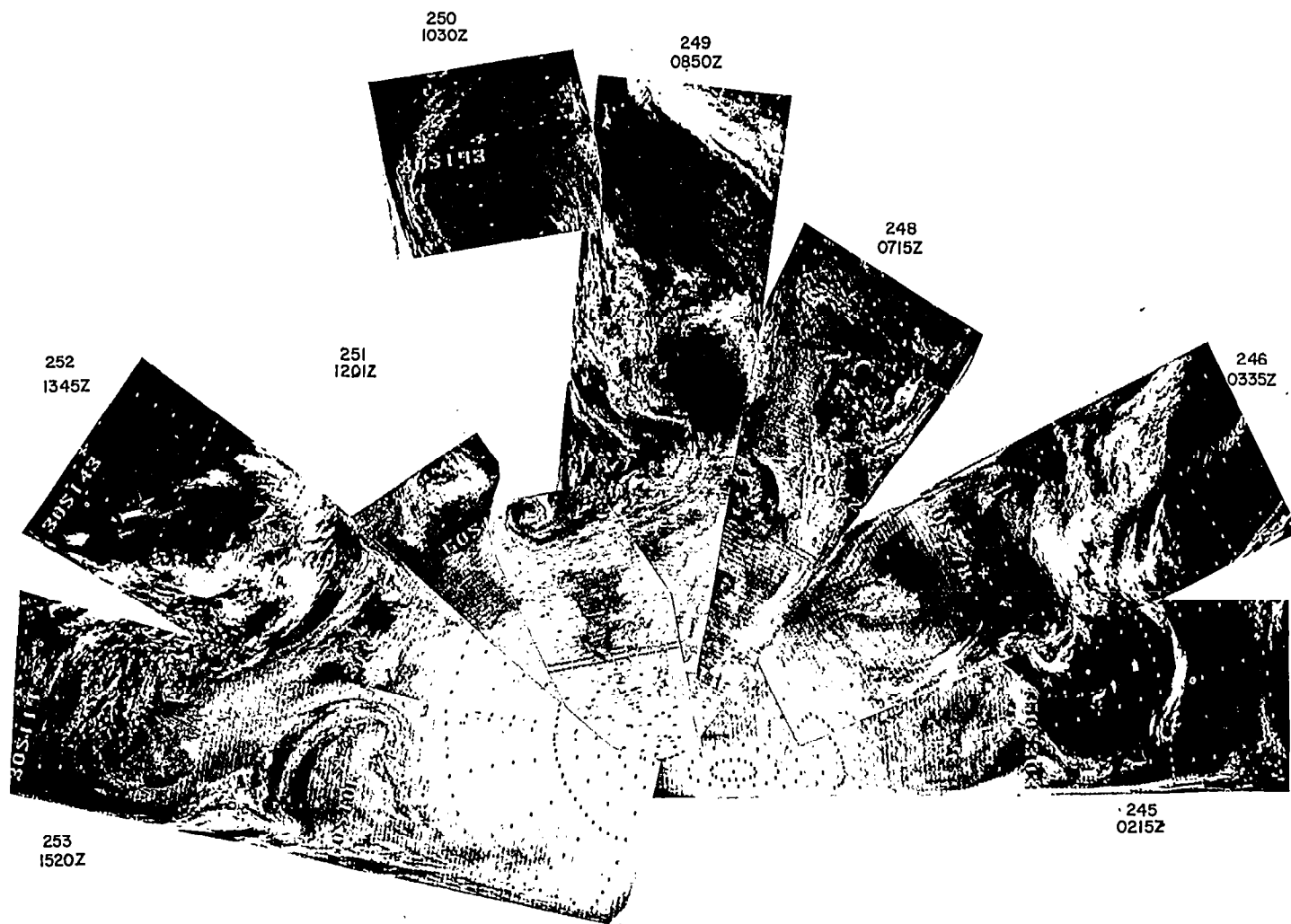
Figure 7-4   HRIR Mosaic for 14 September 1964
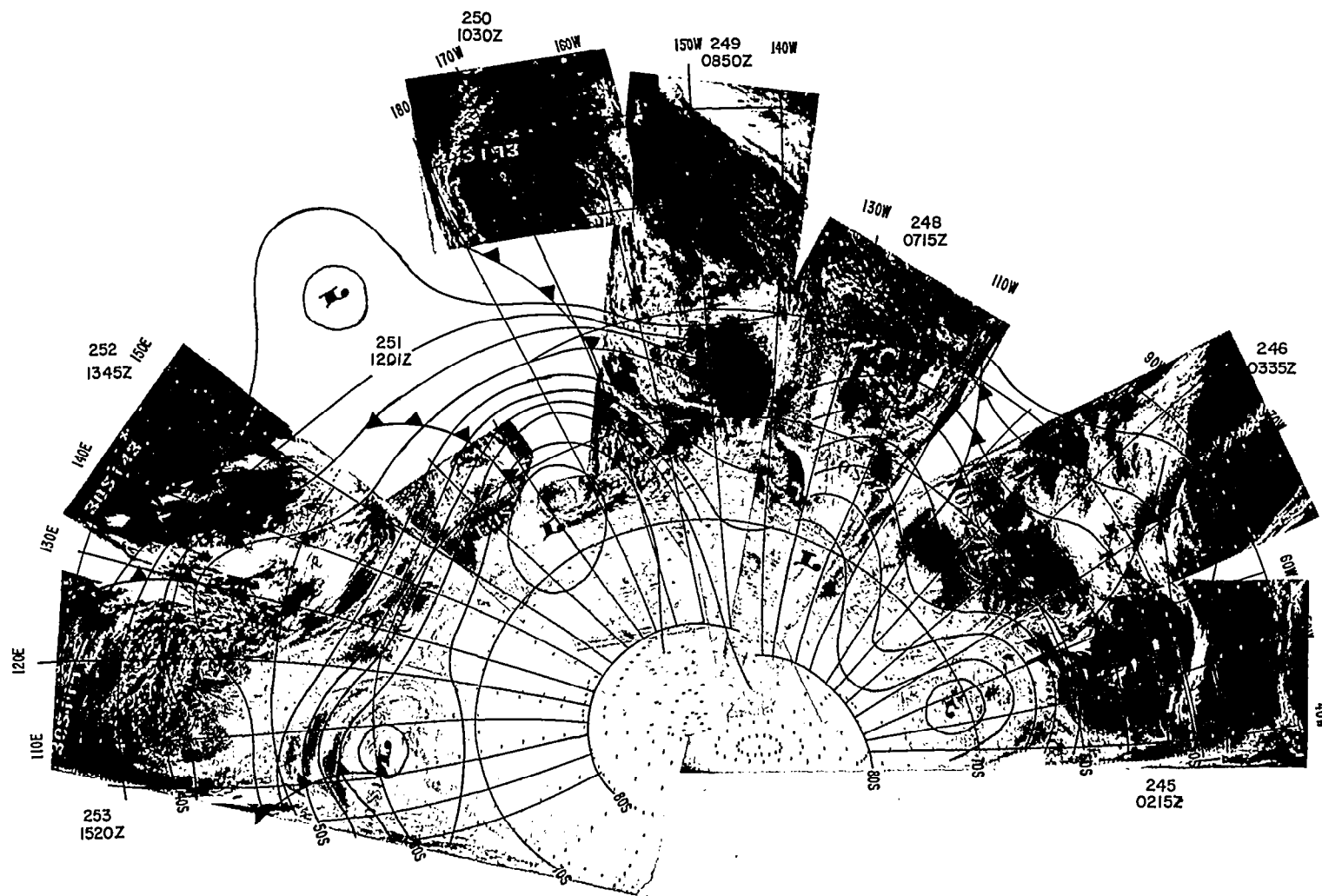
Figure 7-4 a   Mosaic for 14 September, with 500 mb Analysis (0000 GMT, 15 September) and Surface Frontal Positions (1200 GMT, 14 September)

Figure 7-4 b   Same Mosaic and Frontal Positions, but 500 mb Analysis for 0000 GMT, 14 September

123

to the principal area of cloudiness which coincides with the crest of the range, and at 45°S 72°W there are mountain waves. The cloudiness to the east of the Andes looks like a front with two waves, one over Argentina and one farther east. From the brightness of this band, however, it could also be associated with the upper level flow. There is considerable cloudiness in the region of the Antarctic (Palmer) Peninsula, but no distinct pattern can be detected.

7.3 Other Satellite Data

There was a certain amount of concurrent coverage by both the Nimbus AVCS and TIROS VIII, but these satellite data will only be mentioned briefly, since the main purpose of this report is to discuss the HRIR.

Of the AVCS pictures available, there were few that could be readily correlated with the HRIR, mainly due to the differences in resolution and fields of view. The Antarctic continent is visible in much of the AVCS data, with landmarks (such as McMurdo Sound) occasionally seen. In some cases, clouds can be detected over the continent. Figure 7-5 shows three AVCS triplets taken in the area of 45°S 120°E about ten hours earlier than the HRIR of September 14 (Fig. 7-4). The cellular pattern is seen in both, with the solid area in the southwestern part of the AVCS probably corresponding to the gray area in the HRIR. The solid appearance in the AVCS indicates that this could be fog or low stratus. Figure 7-6, taken about five minutes before Figure 7-5, shows the ice pack, with its edge near 62°S. The cloud pattern is unmistakably the same as that seen in the HRIR, near 60°S 145°E, about ten hours later (Fig. 7-4). (In the AVCS, it is at about 60°S 135°E.)

This same cloud pattern was also photographed by TIROS VIII, about two hours before the AVCS and twelve hours before the HRIR of Figure 7-4. This is shown in Figure 7-7. The nephanalysis places the position of the "comma" shaped cloud at about 58°S 135°E. This is an excellent comparison of the same cloud feature in the three different types of observation, all within a reasonably short period of time.

Although the system has moved eastward about ten degrees by the time of the HRIR observation, and has changed somewhat, the principal features remain. In the TIROS and AVCS, all of the cloud features and even the ice pack are essentially the same brightness whereas, in the HRIR, the "comma" part of the cloud and most of the east-west band appear definitely to be higher (brighter)
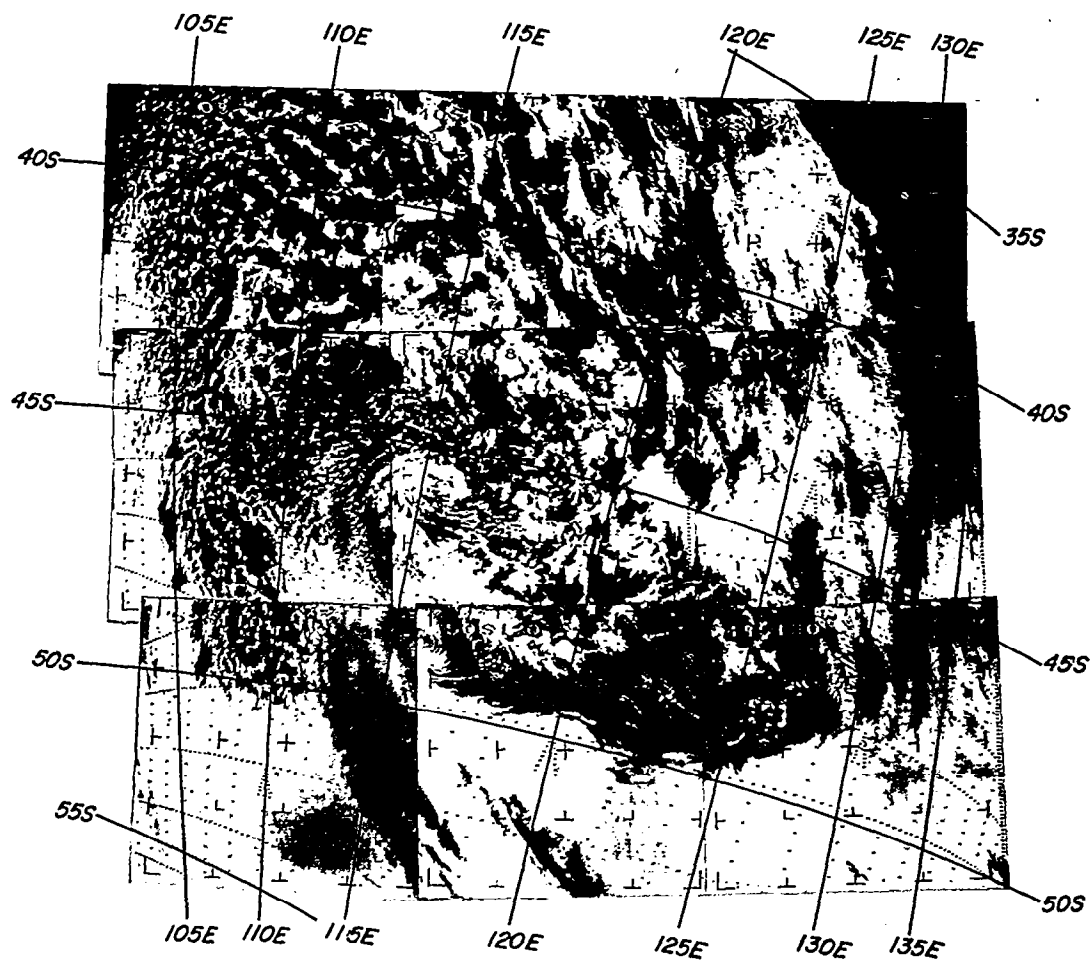
Figure 7-5   AVCS Montage for Part of Orbit 246, about 0420 GMT,
14 September 1964.   This Unrectified Mosaic Shows Some
Duplication Near the Edges because of Perspective

125
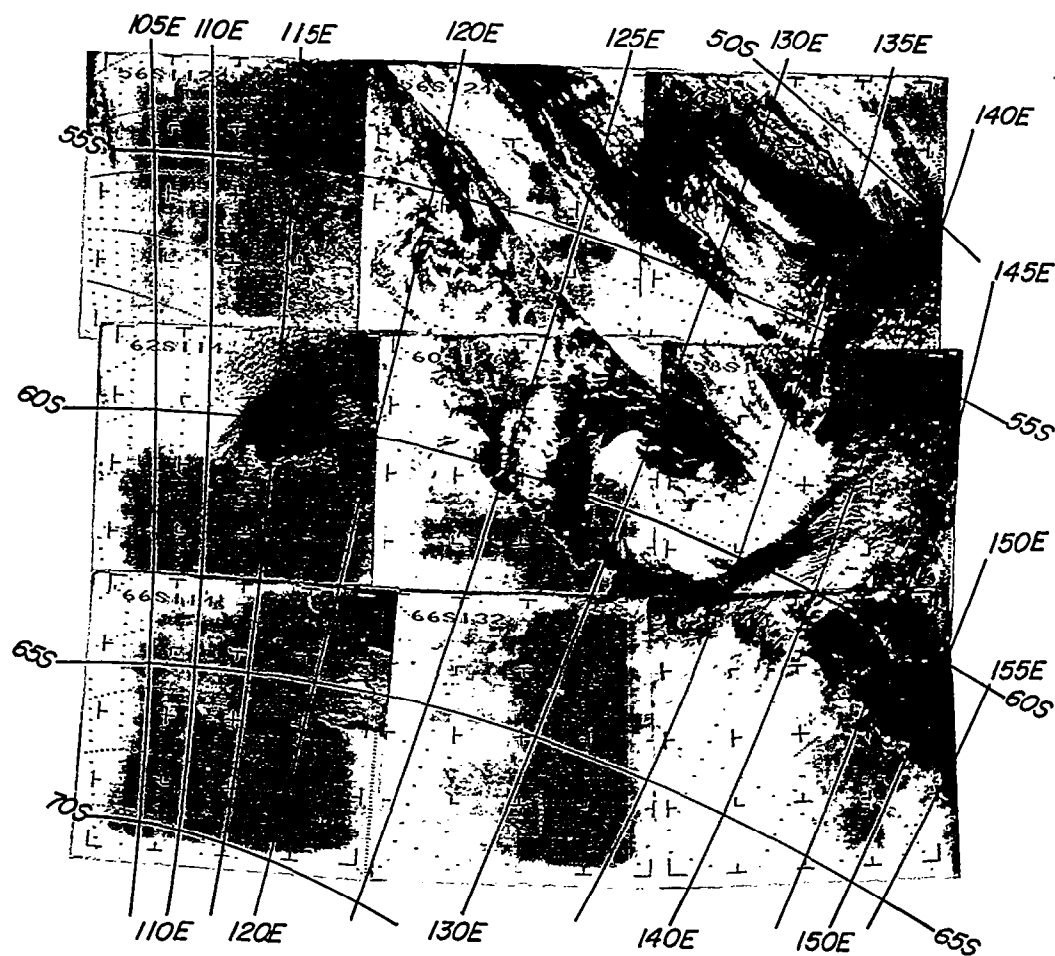
Figure 7-6　AVCS Montage for Part of Orbit 246, about 0415 GMT,
14 September 1964.　This Unrectified Mosaic Shows Some
Duplication Near the Edges because of Perspective
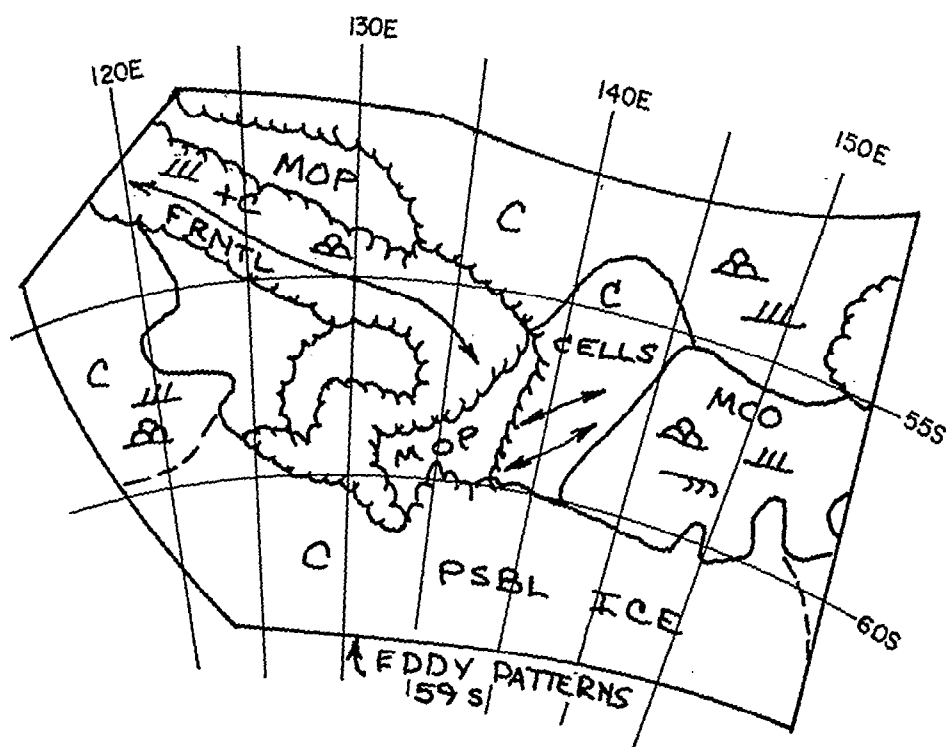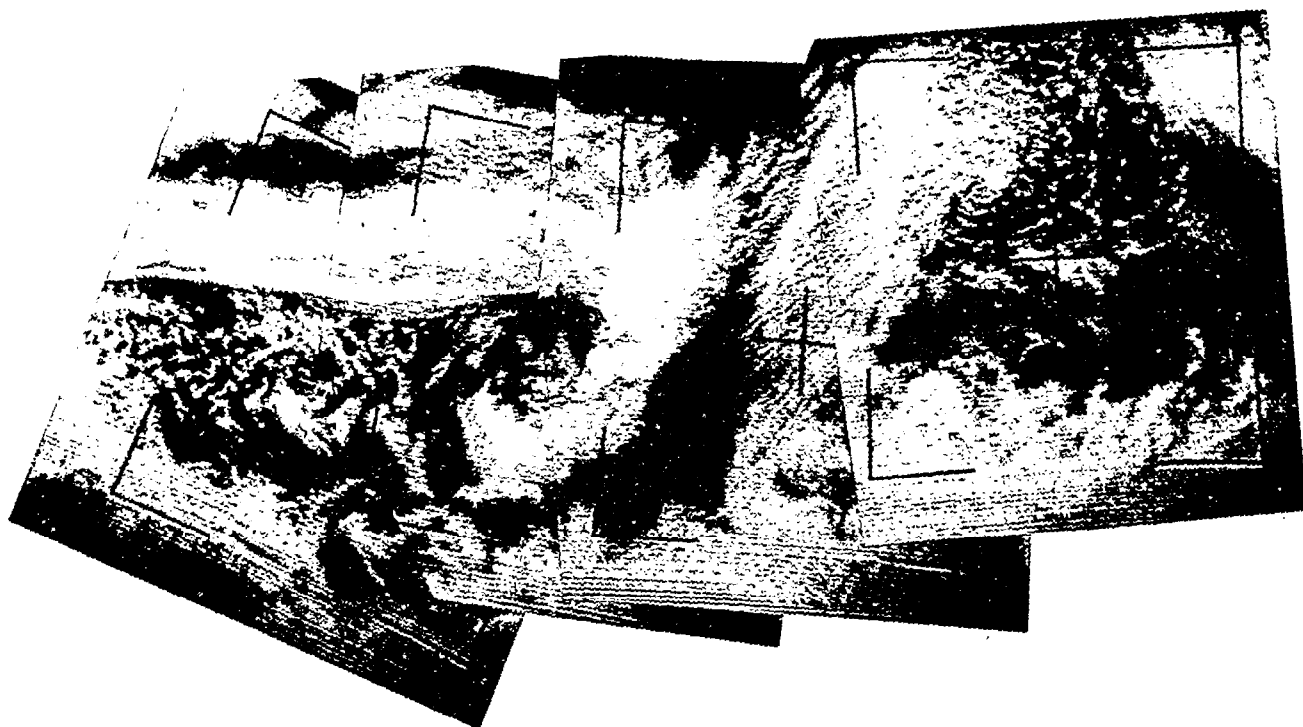
Figure 7-7   TIROS VIII Television Picture Mosaic, Orbit 3882/3880, and Operational Nephanalysis, 0224 GMT, 14 September 1964

127

than the surrounding clouds. The "comma" shape of the cloud and its brightness in the HRIR would indicate that it was associated with a mid-tropospheric short wave as described by Rogers,[6] and Widger, et al;[55] the straight band with such a sharp edge would be expected to be associated with a jet stream. The 500 mb analyses for 0000 GMT on the 14th and 0000 GMT on the 15th (Figs. 7-3a and 7-4a) support these assumptions. There are indications of a short wave in this area on the 14th, and there could easily be a short wave imbedded in the 500 mb flow on the 15th. The strong flow shown on the 15th supports the jet stream assumption, and the rapid eastward movement of the cloud feature.

There is another interesting feature in these same AVCS and HRIR data and in Figure 7-8, another TIROS view of the same region taken about one hour later than the previous TIROS pictures. This is the small clear area seen at about $60^{o}S$ $115^{o}E$ in the AVCS, $61^{o}S$ $115^{o}E$ in the TIROS, and $60^{o}S$ $125^{o}E$ in the HRIR (Fig. 7-4). The area appears larger in the HRIR than in the TV pictures. While the clear area appears to be some sort of local effect in the AVCS and TIROS, the HRIR suggests the true situation. In the HRIR (Fig. 7-4), the edge of the continent can be seen, indicating that the clear area is the northern fringe of a larger clear area; it is seen by the television cameras only where it is just off the ice. (In the AVCS and TIROS, the southern boundary of the darker area is ice, not cloud.) The clear area is probably associated with a ridge that is between the short wave moving off to the east and the approaching system to the west; these systems can be seen in both the HRIR and the TIROS (Fig. 7-8). This, then, is another example of the advantages of the HRIR near the Antarctic continent.

In many cases, continuity can be maintained over a period of twelve hours or so by using both HRIR and TIROS observations. Figure 7-9 is a TIROS mosaic of the area southwest of Australia taken about halfway between the HRIR Figures 7-2 and 7-3. The "fan" shaped cloud in the TIROS picture is probably the same cloud that is seen near $48^{o}S$ $100^{o}E$ in Figure 7-2 and $50^{o}S$ $115^{o}E$ in Figure 7-3, having maintained remarkable continuity over the period. This is also a case where the cellular structure is large enough to be seen in both the TIROS and the HRIR. There were other cases (not shown) where a fine cellular structure could be seen in the TIROS pictures in an area where the HRIR suggested a solid cover. There were also cases where the TIROS pictures showed a complete cloud cover of rather uniform brightness in the same area where the HRIR showed that there were considerable and significant differences in the heights of the clouds.
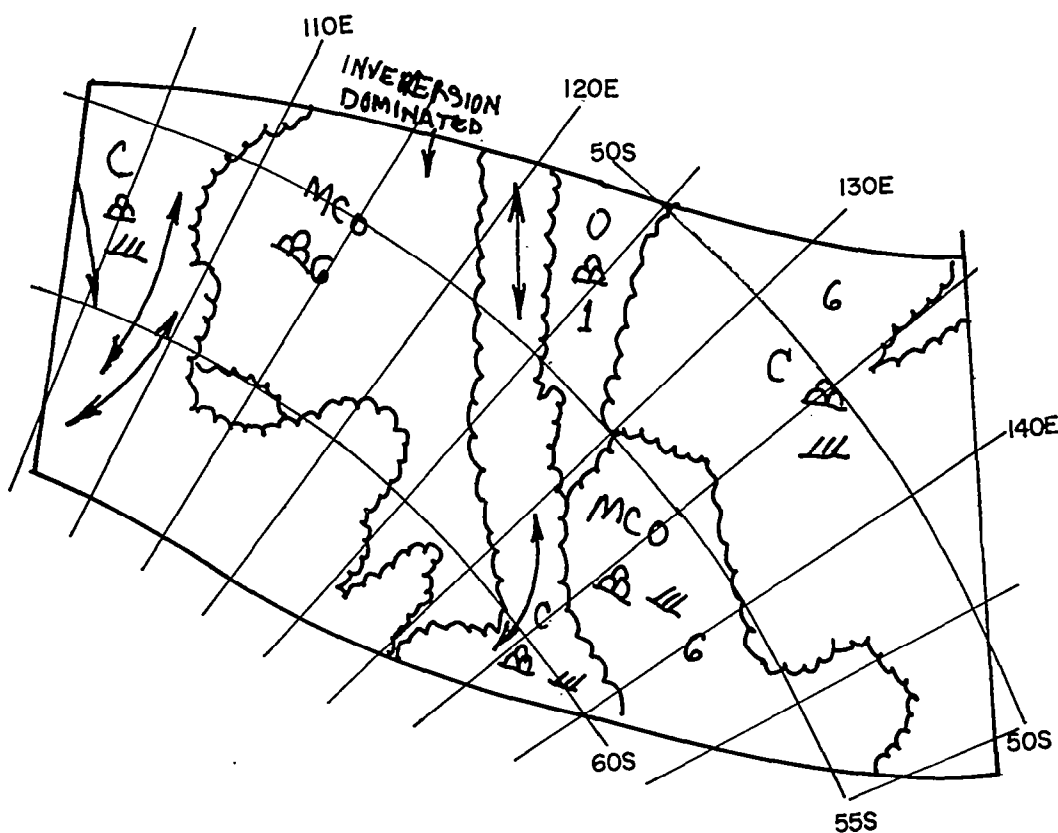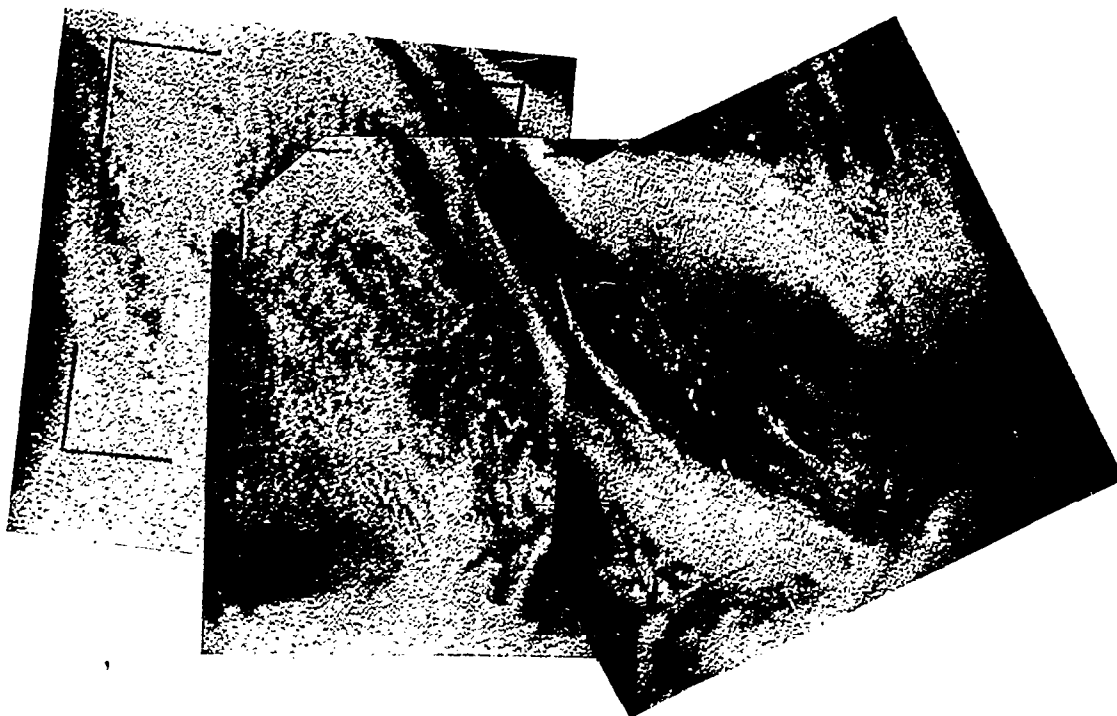
Figure 7-8   TIROS VIII Television Picture Mosaic, Orbit 3884/3882, and
Operational Nephanalysis, 0541 GMT, 14 September 1964

129
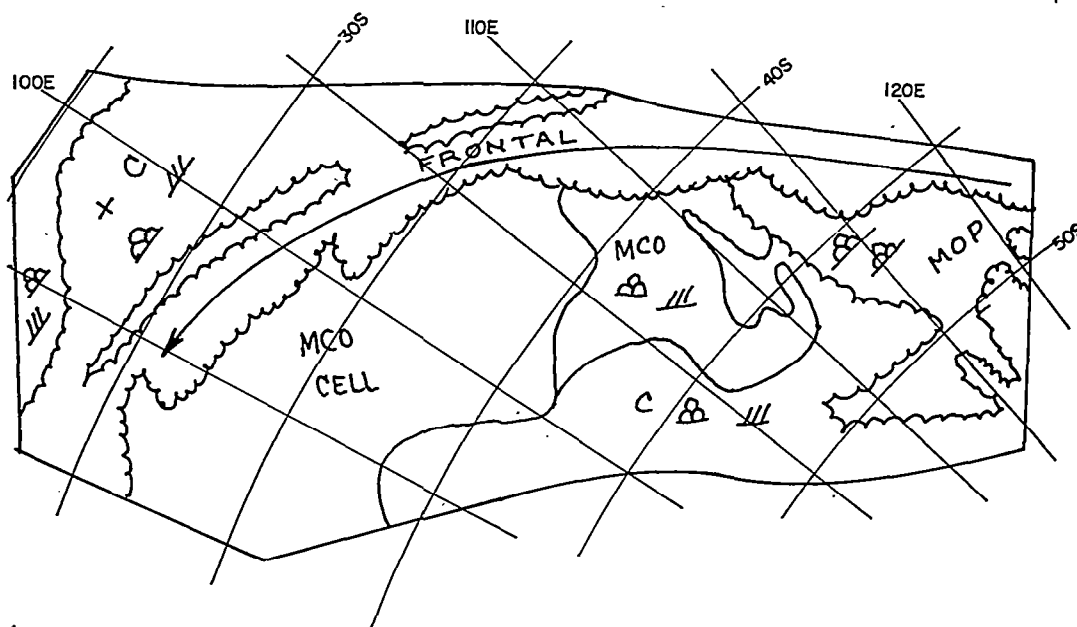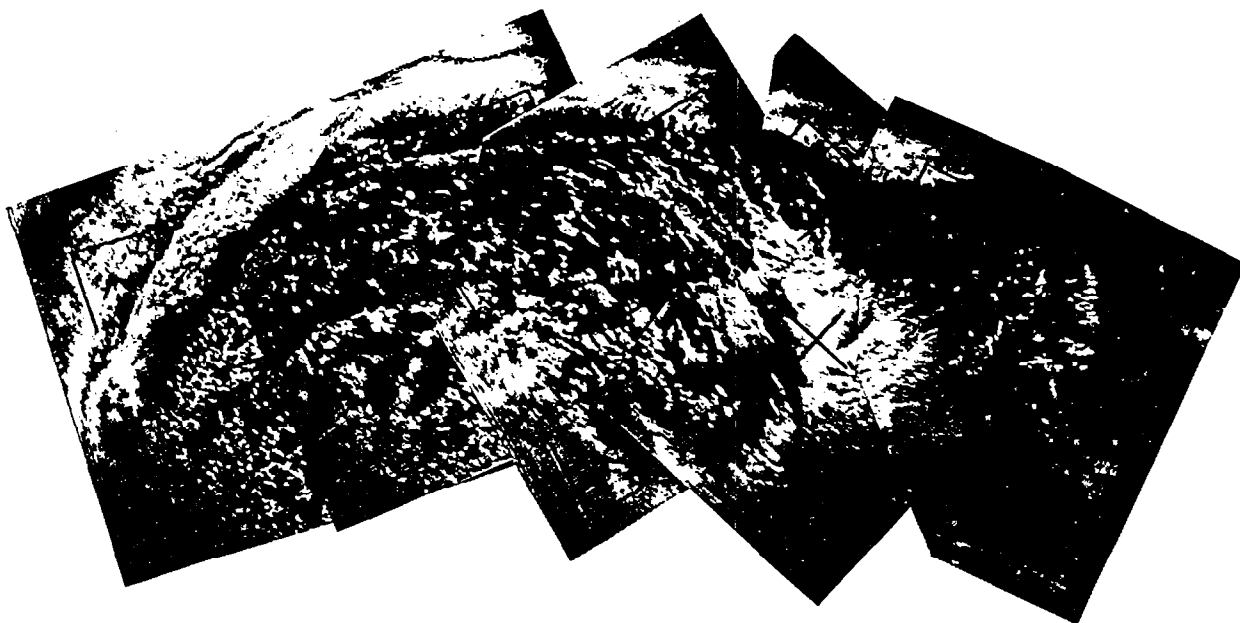
Figure 7-9   TIROS VIII Television Picture Mosaic, Orbit 3867/3865, and
Operational Nephanalysis, 0123 GMT, 13 September 1964

7.4 Comparisons Between HRIR and Conventional Analyses

Comparisons between the HRIR and the conventional analyses have not been discussed extensively because the conventional analyses, based on such sparse data, offer little additional information. As was noted in the southern hemisphere vortex study (Section 6), only the gross patterns over the sub-Antarctic can be deduced from the conventional data; such smaller atmospheric entities as short wave troughs are almost entirely lost. Only the overall patterns will be discussed here, in less detail even than in the vortex study. As was stated before, the IAAC analyses (500 mb and surface fronts) are shown as overlays to the HRIR mosaics (Figs. 7-1a to 7-4a and 7-4b). Some problem was experienced in selecting the most appropriate analysis to be used with each mosaic, since the individual strips range over periods of as much as 15 hours, and only the 0000 GMT 500 mb analyses were available. In each case, however, the 500 mb analysis for 0000 GMT of the following day seemed the most appropriate to use. The majority of the strips in each mosaic were observed after 1200 GMT, and those eastern strips that were before 1200 GMT were in a region where data were so sparse that analyses were often not drawn. Since 1200 GMT surface charts were available, these were used.

The broad patterns for each day will be discussed briefly, followed by a closer look at more interesting situations.

7.4.1 11 September

Figure 7-1a shows the 500 mb analysis for 0000 GMT, September 12, essentially a zonal pattern. The long wave troughs are generally in the areas of the most extensive cloudiness, but there are practically no indications of short wave troughs. The HRIR data indicate that the circulation near 74°S 175°W is closed at the mid-tropospheric level, with a short wave imbedded in the southwest flow. In the westernmost part of the mosaic, there is an indication of a short wave near 50°S 45°E, which is probably responsible for the broader cloud band just east of there. At the surface, some fronts are in fairly good agreement with the HRIR and some are not. The frontal wave near 45°S 95°E is shown, evidently because it was close enough to Australia for data to be available.

7.4.2 12 September

The 500 mb analysis 24 hours later is shown in Figure 7-2a, with a large part of the southern Pacific region not drawn. There is a long wave in the vicinity of South America, and two long waves in the western parts of the mosaic. Judging from the HRIR, there is a closed circulation in the Ross Sea area, and some short wave activity in the large trough near 120°E. The "inverted S" cloud formation along 70°E is on the eastern side of a trough, in a position where the contours indicate a vorticity maximum. Ahead of this trough a ridge is indicated on the analysis, but it is not as pronounced as the cloud patterns would indicate from the Eurasia study of Section 5. A ridge was also indicated on the surface analysis reaching as far south as the Antarctic continent.

7.4.3 13 September

The 500 mb analysis for 0000 GMT on the 14th (Fig. 7-3a) indicates a return to more zonal flow, especially in the region from 80° to 140°E. The circulation near 80°E is shown as closed off, with another major closed-off circulation to the west. Some short wave activity is indicated in the region south of Australia. The complete surface analysis (not shown) shows that a high (which had been centered near 80°E) has moved eastward and has retreated toward the north.

There is a low center drawn on the analysis in the area of the low level circulation near 70°S 40°E, as seen in the HRIR, but nothing is indicated on the surface in the area of the cloudiness north and east of that circulation. From these analyses, it is quite certain that the major cloud features seen by the HRIR are mid-tropospheric clouds being advected around a closed circulation that extends at least to 500 mb. (It can be noted in Figure 7-3a that the sharp edge of the cloudiness near 50°E and south of 50°S could well be in the vicinity of the 500 mb jet.) The less bright cloudiness is that associated with the surface circulation, and with an analyzed front which is probably really only a secondary cold front.

7.4.4 14 September

At 0000 GMT on the 15th (Fig. 7-4a), a small cutoff 500 mb low is moving
in the strong flow near 60°S 110°E, with a short wave well to the northeast. Both
of these are well supported by the clouds observed in the HRIR. In the South
American region, one of fairly good data, the 0000 GMT analysis on the 14th
is much closer to the time of the HRIR observation, so this analysis has been used
in Figure 7-4b. A vorticity maximum is moving around a major trough in the
area of the disturbance in the HRIR, but the trough probably should be west of its
analyzed position. The bright band east of the Andes could also be associated with
the 500 mb flow, but suggests a ridge near 65°W and a trough near 55°W. The
surface analysis shows circulations under the short waves mentioned above.

7.4.5 A Revised 500 mb Analysis, Combining HRIR and Conventional Data

To demonstrate the possibilities of improving southern hemisphere high
latitude analyses by the use of HRIR data, the 500 mb analysis shown in Figure 7-10
was prepared. Conventional data for 0000 GMT on the 13th were plotted, except
for the two easternmost stations where the observations are those of 0000 GMT on
the 12th. (One or two stations had 1200 GMT observations which would have been
nearer the time of the HRIR data, but since most stations had only 0000 GMT ob-
servations, those for 0000 GMT were used.) The analysis was drawn using the
HRIR data, without violating the conventional data; it can be compared with
Figure 7-2a, the corresponding IAAC analysis. The features observed in the HRIR
and described in earlier parts of this section were used to construct the analysis;
time cross-sections also provided an aid. The movements of the systems over the
next 24 hours followed the flow pattern rather closely, as can be seen by the
positions of the features in Figure 7-3a. While this is still only a relatively crude
analysis, it does account for the features seen in the HRIR, and obviously presents
a better and more detailed analysis than it was possible for the IAAC to prepare
from conventional data alone.

7. 4. 6 A Possible Blocking Situation

Because the "inverted S" cloud pattern seen in the HRIR (Fig. 7-2) appears similar in shape to the pattern associated with an Ω-block over Eurasia (Section 5), this situation was studied in somewhat more detail. Blocking in the southern hemisphere has been discussed by Gray,[19] Gibbs,[15] Hannay,[20] Van Loon,[50, 51] and the U. S. Navy Weather Research Facility.[48] The area of interest in this study is one of the preferred regions for blocking, and September is the season of maximum blocking activity.[51] It is felt, therefore, that the "inverted S" cloud pattern seen in the HRIR is indicative of at least a "semi-blocking" situation. The cloud is just west of a well developed ridge at the 500 mb level, with the shape of the cloud seeming to indicate a more meridional circulation than is shown on the analysis (particularly in light of the similarity to the Eurasian case (Section 5), where a comparison with adequate conventional data was possible). The area near 80°E in Figure 7-2 could be reanalyzed without violating the conventional data, as was done in Figure 7-10. At the surface, the circulation is reflected by the penetration of the subtropical high as a ridge that reaches to Antarctica. This may be due to a high having moved off the coast and having merged into the subtropical high near 70°E, on the day before, a situation similar to that discussed by Gibbs.[15] A time cross-section shows that Kerguelen Island (49°S 69°E) reached a surface pressure of 1027. 8 mb at 0600 GMT, September 12, the approximate time that the ridge, according to the HRIR, was over the station. This was the highest pressure reached at Kerguelen during the month.

The HRIR mosaics show that the cloud band that was near 70°E in Figure 7-2 moved eastward about 15 degrees per day during the following two days (Figs. 7-3 and 7-4), a slightly slower than usual rate for the sub-Antarctic region. The ridge broke down completely in the southern section, where a 500 mb short wave developed by 0000 GMT on the 15th and moved rapidly eastward. It is seen, therefore, that the situation was not a permanent "block," but rather a migrating anticyclone that could be considered a "semi-block," at least on the 12th. The "inverted S" shaped cloud seen in the HRIR was associated with the mid-tropospheric circulation around the western side of the anticyclone, and the presence of this cloud suggested that the circulation was more meridional than was shown on the 500 mb analysis.
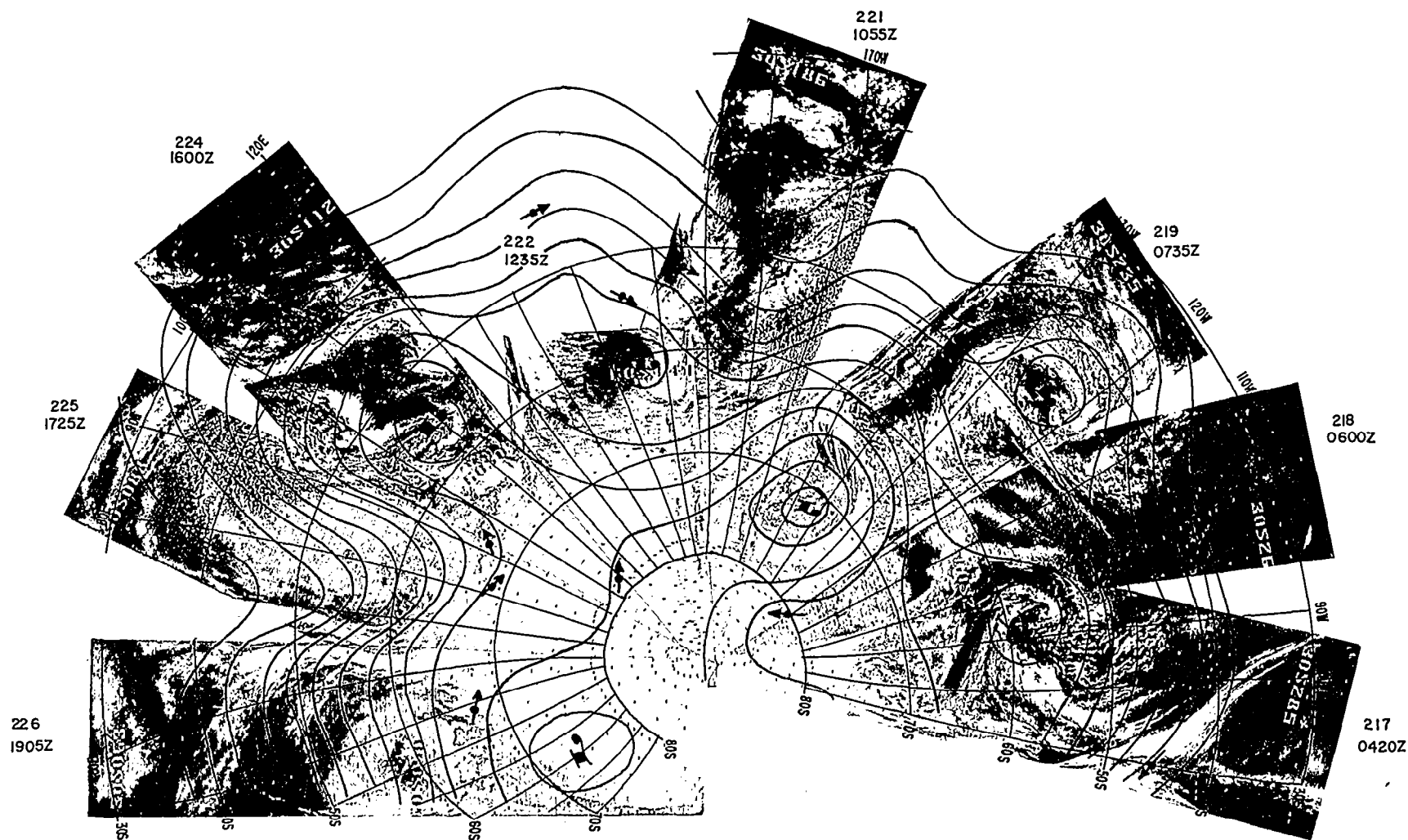
Figure 7-10   HRIR Mosaic for 12 September 1964, with 500 mb Data (0000 GMT, 13 September) West of 180°, and 500 mb Data (0000 GMT, 12 September) East of 180°.   Analysis Drawn Combining HRIR and Conventional Data

7.4.7 Secondary Vortices

The vortex centered near 60°S 175°E on September 11 (Fig. 7-1) appears to be a secondary vortex imbedded in the southwest flow behind a major mid-tropospheric circulation. The vortex is extremely well developed, and must have strong support from a short wave at the 500 mb level. Presumably analogous secondary vortices associated with short wave troughs in northwest flow (northern hemisphere) have been discussed by Nagle and Serebreney,[34] Boucher et al,[6] Widger et al,[55] and Sherr and Rogers[41] using TIROS data. Rogers[6,55] shows that the smaller vortices found in polar air in the extreme western portions of major cloud vortices and cyclonic circulations are associated with short wave upper troughs, and at the surface with a sharper trough or a minor closed low. The previous studies point out that these disturbances often develop into systems producing weather and precipitation of considerable operational significance. The capability of the HRIR to detect and follow the movement of this type of secondary development in the data-sparse Antarctic areas is clearly demonstrated in this study.

7.5 Conclusions

The following conclusions can be drawn from these southern hemisphere studies:

7.5.1 The Nimbus HRIR is capable of detecting and following the movements of weather systems over the sub-Antarctic region, a region nearly void of conventional data. The cloud top height data provided by the HRIR are of significant value in differentiating between primarily lower level circulations and the deeper mid-tropospheric circulations; this consitututes a definite advantage over satellite television observations for determining the operational significance of the system under surveillance. The development of secondary vortices, which often produce operationally significant weather, can be followed by the HRIR, and the amount of upper air support for these vortices can perhaps be inferred from the observed cloud heights.

7.5.2 The Nimbus HRIR can detect cloudiness over the Antarctic pack ice, something that satellite television observations usually cannot do (see Section 6). This ability to observe clouds as far south as the Antarctic continent itself extends the usefulness of satellite observations in Antarctic operations. The possibility of detecting the extent and density of the pack ice with HRIR observations is also demonstrated.

7.5.3 The Nimbus HRIR can provide a better insight into both the synoptics and the general circulation of the sub-Antarctic than can usually be obtained from conventional analyses. The HRIR observations indicate that the zonal circulation may often be more disturbed than is usually shown on the conventional analyses.

7.6 Recommendations

HRIR observations taken over ice and snow should be further investigated so that methods to better differentiate between clouds and ice or snow may be found. For example, experiments might be carried out using "clipped" digitized data, presenting only temperatures below a certain level, to see if they might isolate the colder clouds over the Antarctic continent itself. The results might also prove beneficial for determining cloud cover over other snow covered regions of the world. By comparing the HRIR gray scale for cases of known pack ice density, it might well be possible to determine the tenths of ice cover from the HRIR data. Finally, methods might be developed to provide improved operational forecasts of cyclone movement based significantly on the HRIR data.

8. TROPICAL ANALYSIS APPLICATIONS

8.1 Introduction

Meteorological analysis and forecasting in tropical ocean regions has always suffered from an acute deficiency of data. Fortunately for many operational interests, deleterious weather occurrences in the tropics have a somewhat smaller frequency of occurrence than in mid-latitudes, where the data deficiency is less acute. However, this lower frequency does not reduce the requirement for accurate tropical analyses, both for these areas themselves and since many aspects of numerical weather prediction for middle and high latitudes suffer from less than adequate tropical boundary information. In addition, any attempt at useful numerical prediction in the tropics will require an accurate analysis.

Meteorological satellite data, primarily photographic, from the TIROS series has permitted a new look at tropical weather systems. Some of the previous studies of meteorological satellite data in the tropics have included:

1. Analysis of an asymptote of convergence situation over the South Pacific, by Hubert. [21]

2. Analysis of perturbations over West Africa which eventually produced Atlantic hurricanes, by Merritt. [29]

3. Analysis of upper tropospheric cyclones over the Pacific, and preliminary definition of a circulation scheme for the tropics, by Sadler[39] and by Merritt. [32]

4. Analyses of tropical cyclones, over both the Atlantic and the Pacific, which have led to techniques for inferring development intensity and maximum surface winds. Merritt;[6,55] Fett;[11] Zipser;[57] and Timchalk, Hubert and Fritz[47] have all contributed in this area.

5. Reappraisal of easterly wave structure, with suggestions as to the mode of development of easterly wave or easterly perturbation phenomena, by Merritt. [31,32,55]

The most common and significant cloud features, as discussed in these TIROS-based studies, are characteristic patterns of cumuliform cloudiness and of cirriform cloudiness. The utilization of photographic data in this interpretive process requires that cloud height determinations be based on brightness and character as discussed by Conover. [9] Infrared measurements from TIROS reduce this subjectivity somewhat (Merritt[32]) but at a resolution that is frequently too great to be operationally useful. *

---

* Note, however, the results of maximum utilization of the resolution available in the TIROS IR data, as discussed in Reference 41.

The Nimbus data may well provide the beginnings of a further breakthrough in the tropical utilization of meteorological satellite data. This potential breakthrough is not so much due to the increased photographic resolution of the Advanced Vidicon Camera System (AVCS), although this is certainly useful. It is due instead to the excellent results that can be achieved using the High Resolution InfraRed data (HRIR). The success of the HRIR provides, for the first time, semi-quantitative measurements of cloud heights at a resolution approximately equal to the TIROS photographs. The value of this imagery, is, of course, not limited only to providing the vertical dimension; it also provides nighttime coverage, permitting (with complementary AVCS or APT data) tracking and analysis of important tropical weather systems at twelve hour intervals. The following four-day case study of a situation over the tropical central and western Pacific will present data and analyses demonstrating the types of tropical analysis made possible by the Nimbus HRIR imagery and the complementary AVCS and APT photographs.

8. 2 Data and Analysis

8. 2. 1 Data

The data for this study were selected from the Nimbus I HRIR Catalog.[43] Conventional data and analyses were obtained from microfilm copies of charts prepared at Anderson AFB, Guam.

AVCS photographs for 18 September and 20 September were selected from the Nimbus I User's Catalog, AVCS and APT.[1] Copies of the desired frames were provided by NASA.

8. 2. 2 Analysis Procedure

The analysis procedures used during this study included:

1. Rectification of the HRIR imagery and AVCS photographs onto charts suitable for streamline analysis, utilizing the gray scale codes suggested by Widger and Smith,[56] and discussed in Section 3. 3 of this report.

2. Transfer of plotted data, for the surface and 300 mb levels, from the analyses prepared at Anderson AFB, Guam, onto blank charts.

3. Revised streamline analyses of the data transferred in 2, using the rectified HRIR imagery and AVCS photographs as a primary source of analytical guidance.

4. Subjective comparisons between day-to-day HRIR imagery, and the related data and analyses at the surface and 300 mb.

8.3 General Synoptic Situation

The general situation for the period 16-20 September 1964, as depicted in the Guam streamline analyses at the surface and 300 mb (Fig. 8-1), was fairly normal, i.e., a series of cyclonic centers in the lower troposphere near 15°N. The upper troposphere was characterized by a second series of cyclonic centers, but these were nearer to 20° - 25°N. Anticyclonic centers or curvature persisted aloft over the lower troposphere cyclonic centers. The two features which will be followed with some detail are: (1) the lower tropospheric formation of Typhoon Wilda, which began late on 16 September near 13°N 145°E and reached typhoon intensity on 19 September; and (2) an upper tropospheric cyclonic center, located near 21°N 177°E on 16 September, which may have had a part in the final development of Wilda to typhoon intensity.

As will become apparent during the subsequent discussion, the HRIR data made possible significant improvement in the operational Guam analyses, which were inevitably based on inadequate conventional data.

8.4 HRIR-Based Analyses

8.4.1 16 September 1964

8.4.1.1 General Situation

The situation depicted in the HRIR data, orbits 281 and 282, unrectified in Figure 8-2 and rectified in Figure 8-3, shows a large cloud mass centered near 15°N 147°E, east of Guam. Comparison with the Guam surface analysis in Figure 8-1 shows no associated circulation feature in this area. Subsequent analyses, using the HRIR data, will show that a north wind at Guam was probably related to this cloud mass, which was the first phase of the Wilda development as depicted by the HRIR imagery. The second feature of note, i.e., the upper level cyclone near 21°N 177°E, appears to be related to the area of banded cloudiness near 20°N 172°E. In both cases the areas of primary interest were located near the edges of the HRIR strips, requiring considerable care in the rectifications and preventing any highly detailed depictions.
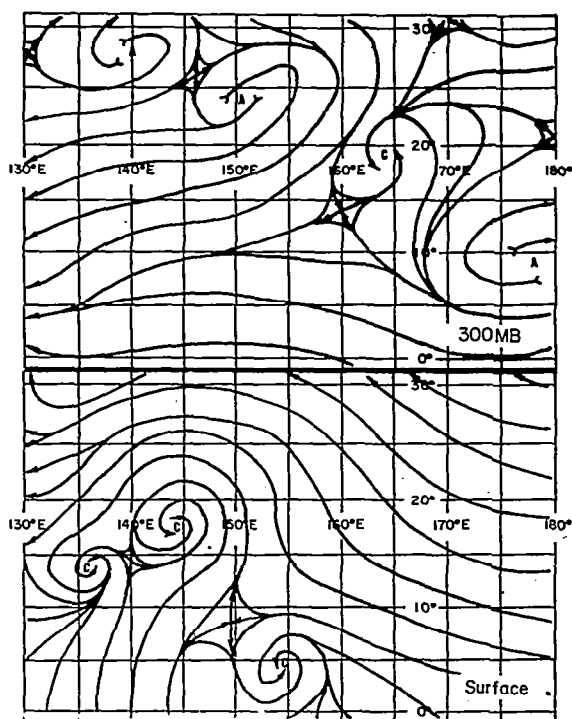
September 18, 1964 (1200 GMT)
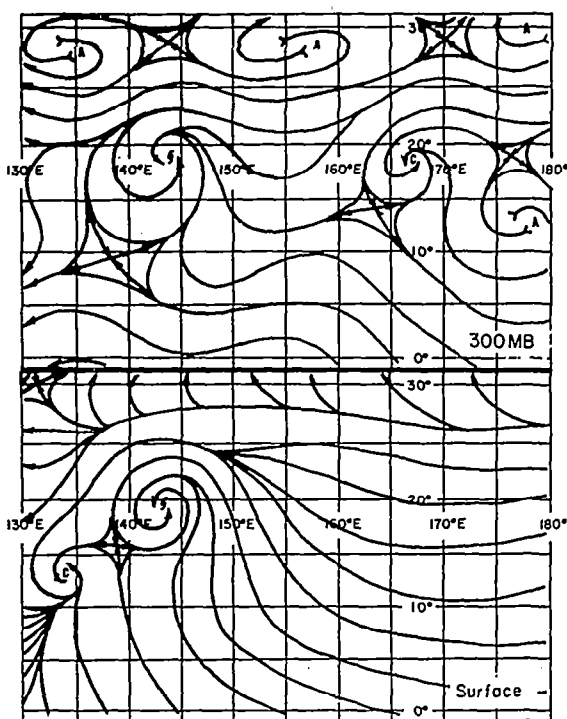
September 19, 1964 (1200 GMT)
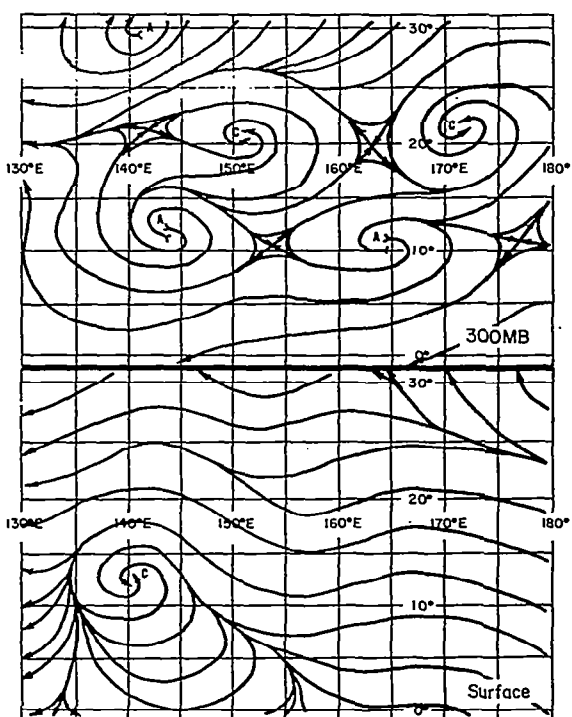
September 16, 1964 (1200 GMT)
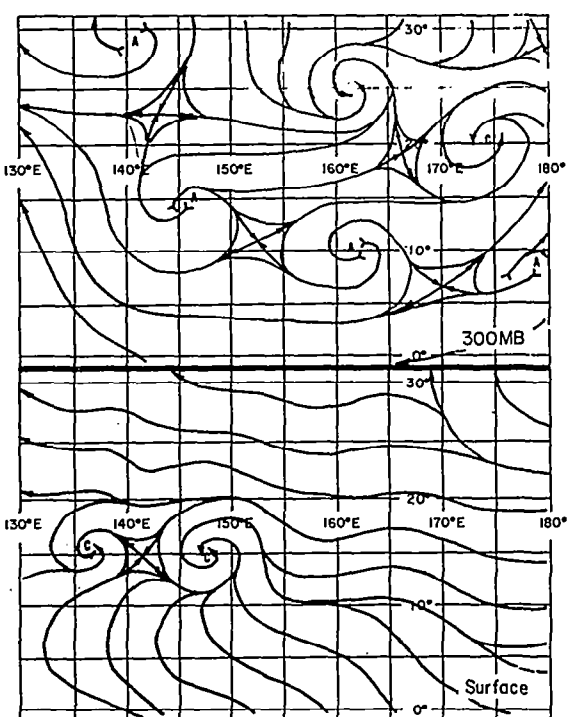
September 17, 1964 (1200 GMT)

Figure 8-1 1200 GMT Anderson AFB (Guam) Streamline Analyses

8.4.1.2 Streamline Analyses

Streamline analyses, based on a combination of the HRIR imagery and the existing conventional data, are shown in Figures 8-4 and 8-5 at the surface and 300 mb, respectively.

8.4.1.2.1 Surface

The weak cyclonic indraft inserted near 14°N 147°E is based on Guam's north surface wind and the HRIR cloud pattern. The banding which extends eastward from the main cloud mass, and then southward, appears to relate to an area of cyclonic curvature and directional convergence near 157°E. The area of cold clouds southeast of 20°N 172°E appears related to directional convergence in the lower troposphere.

8.4.1.2.2 300 mb

The 300 mb level circulation pattern is more confused, but three features are worthy of mention: (a) the weak formative anticyclonic center above the heavy cold Wilda cloud mass, centered at 14°N 147°E; (b) the small cyclonic centers near 22°N 149°E and 23°N 159°E; and (c) the cyclonic center at 20°N 170°E. The analyses of the small centers are based on continuity backward from a well defined vortex observed on 19 September, and the requirements of the peripheral streamline systems.

8.4.1.3 Meteorological Implications

Studies by Merritt[32] have shown that tropical perturbations with cloud distributions similar to the pre-Wilda system (that located near 14°N 147°E) are experiencing warming in the middle and upper troposphere, due basically to heat release by condensation processes. This heating of the middle and upper troposphere is at least partially responsible for the formation of the anticyclonic outdraft at 300 mb. Subsequent development is, in part, contingent on some acceleration of this upper level circulation. The small cyclonic centers mentioned in (b) above can function as small scale accelerators of this warm core circulation, * since

---

*   We refer here to the vertical solenoidal circulation.
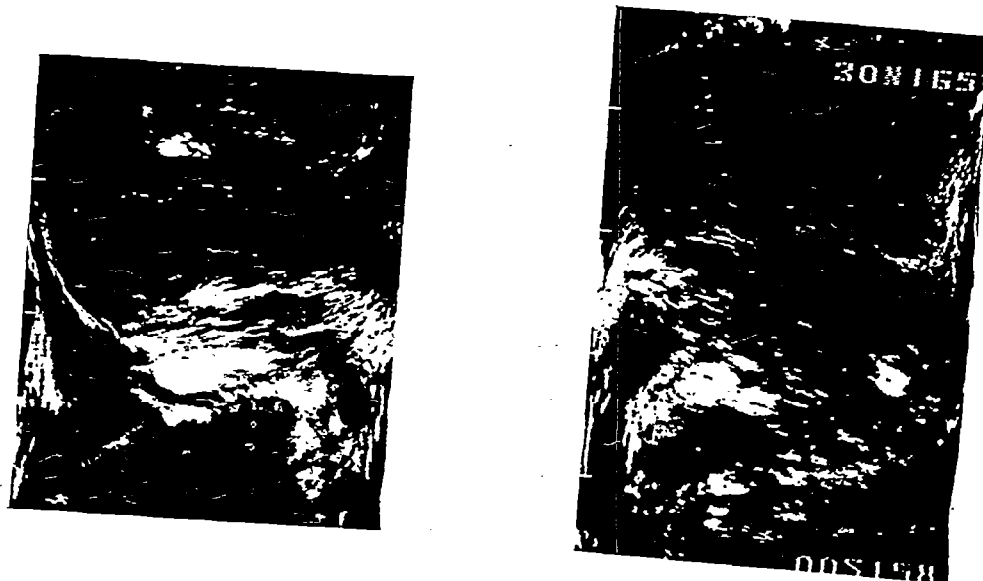
282   281

Figure 8-2   HRIR Photofacsimile Strips (Unrectified) Orbits 281 and 282, 16 September 1964

Figure 8-3   HRIR Representation (Rectified) Orbits 281 and 282, 16 September 1964

Figure 8-5   HRIR Revised 300 mb Streamline Analysis,
1200 GMT, 16 September 1964

Figure 8-4   HRIR Revised Surface Streamline Analysis,
1200 GMT, 16 September 1964

these centers are generally cold core. The third upper tropospheric circulation described in (c) of Section 8.4.1.2.2 may play a similar role.

8.4.2 17 September 1964

8.4.2.1 General

The HRIR imagery presented in Figures 8-6 and 8-7 (unrectified and rectified, respectively) show the pre-Wilda perturbation centered near 15^ON 146^OE. The overall pattern is slightly suggestive of a circulation center, but there is no clearly defined vortex. The principal feature defining the weak circulation pattern is the curved band centered at 12^ON 145^OE. The bands that were near 157^OE on 16 September appear to have a similar configuration near 152^OE. The Guam surface analysis (Fig. 8-1) shows a well defined lower tropospheric cyclonic center at about 14.5^ON 146.5^OE, based on the winds at Guam and one transient ship.

In the area of the upper tropospheric cyclone (near 21^ON 177^OE on 16 September, and now near 20^ON 171^OE), there is less defined high (cold) cloud-iness. The area of apparent clear skies (warm) between the pre-Wilda center and the upper tropospheric center has increased in amplitude and area; unfortunately, on this and the next day much of this area lies near the edges of or between two adjacent HRIR strips. The revised streamline analysis, to follow, will show that this is a reflection of the increased area and amplitude of the anticyclonic curvature at 300 mb. The cold clouds to the south, also observed on 16 September, are probably the result of low and middle level directional convergence.

8.4.2.2 Streamline Analyses

8.4.2.2.1 Surface

The revised surface streamline pattern, based on the HRIR imagery and the conventional wind observations (Fig. 8-8), clearly reveals the correspondence be-tween the curved band centered near 12^ON 145^OE and the lower tropospheric circulation. The asymptote of directional convergence in the streamline field parallels the cloud band quite readily. There is another region of low level con-vergence near 12^ON 152^OE corresponding to the clouds in that area. The lower tropospheric flow in the area of the upper cyclone is a zone of "deep easterlies," with only a slight reflection of the upper tropospheric pattern.

8. 4. 2. 2. 2 300 mb

The 300 mb circulation pattern (Fig. 8-9) has simplified somewhat from the 16th, but it still retains the same principal features. The anticyclonic outdraft over the pre-Wilda area (17°N 147°E) has increased in size. The small cyclonic centers at 27°N 147°E and 27°N 154°E have apparently moved closer together. The anticyclonic curvature of the streamlines between these small centers and the principal upper tropospheric cyclone has increased in amplitude and area as suggested by the HRIR imagery discussed in 8. 4. 2. 1. Comparison with the original Guam 300 mb analysis (Fig. 8-1) shows some rather distinct differences: (a) the location of the anticyclone over the pre-Wilda area, (b) the location of the upper tropospheric cyclone near 170°E, and (c) the large anticyclonic circulation between but somewhat to the north of these features.

8. 4. 2. 3 Meteorological Implications

The apparent increase in banding in the pre-Wilda area, particularly the broad curved band centered near 12°N 145°E, suggests the beginning of the heat concentrating mechanism pointed out by Kuo[27] and noted in studies of satellite photographs by Merritt.[32] The release of latent heat in these areas can be concentrated in the area of lowest pressure (in general the center of circulation) leading to formation of a well defined warm core. The ability of the HRIR to depict areas of high cold clouds is invaluable in interpretations of this type.

The increase in amplitude of the anticyclonic circulation separating the pre-Wilda perturbation and the upper level cyclone, suggested by the 24-hour changes in the HRIR imagery, is important in the development process of Wilda in two ways: (a) the area of clear (warm) skies is one of excess radiational cooling, thus increasing the temperature gradient between the transitional warm core perturbation and the exterior atmosphere; and (b) wave length adjustments, which will permit intensification of the principal upper tropospheric cyclone, appear to be occurring.

Figure 8-6   HRIR Photofacsimile Strips (Unrectified) Orbits 295,
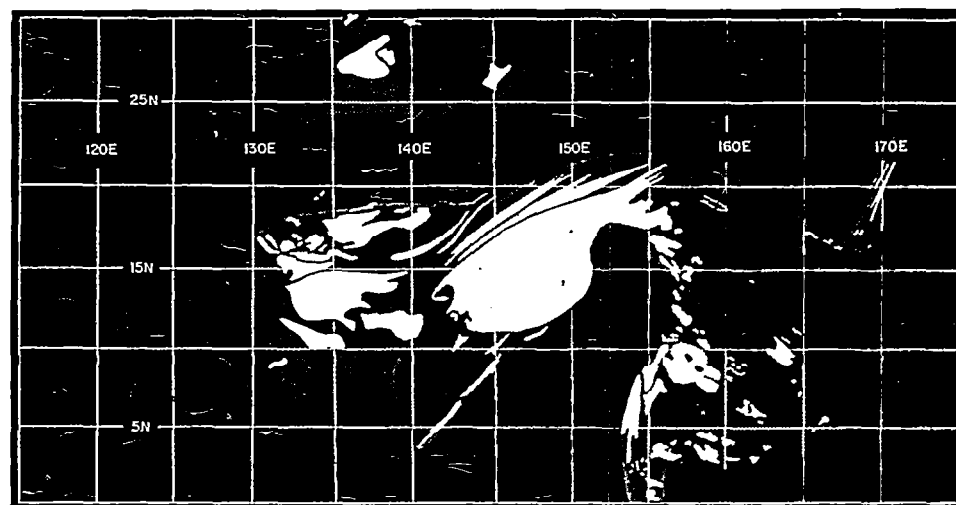296 and 297, 17 September 1964

Figure 8-7   HRIR Representation (Rectified) Orbits 295,
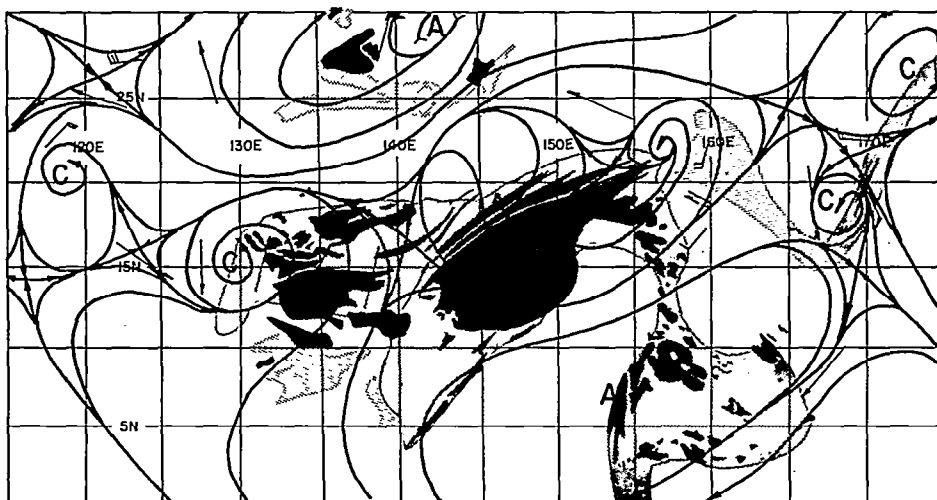296 and 297, 17 September 1964

Figure 8-9   HRIR Revised 300 mb Streamline Analysis,
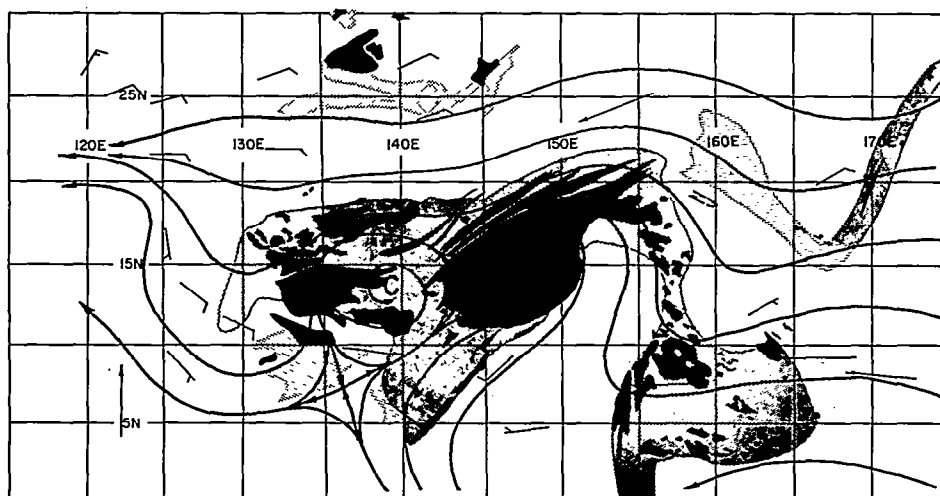1200 GMT, 17 September 1964

Figure 8-8   HRIR Revised Surface Streamline Analysis,
1200 GMT, 17 September 1964

149

8.4.3 18 September 1964

8.4.3.1 General Situation

The general situation on the 18th, as depicted first by AVCS photographs at
0200 GMT of the pre-Wilda area and at 1400 GMT by the HRIR, shows much more
organization. The AVCS mosaic (Fig. 8-10) provides some insight
into the slow rates of 12-hour changes which occur in a slowly developing tropical
perturbation. Note particularly the similarities between the HRIR imagery at
approximately 1400 GMT, 17 September, and the AVCS. The conservation of the
band,centered at $12^{O}N$ $145^{O}E$ on the 17th, is a principal feature. This band appears
to have rotated around the south side of the perturbation, and is now merging into
its southeast side.

The cloud patterns depicted by the HRIR imagery (Figs. 8-11 and 8-12)
suggest two areas of change associated with the principal analysis features:
(a) the distinct overall increase in vorticality in the pre-Wilda perturbation, and
(b) the appearance of a cyclonically curved high (cold) cloud band on the west side
of the upper tropospheric cyclone which is centered near $20^{O}N$ $163^{O}E$. The clear
area between these two systems has become smaller although the amplitude
may have increased; again its location on the HRIR strips raises some problems.

8.4.3.2 Streamline Analyses

8.4.3.2.1 Surface

The revised surface streamline analysis, prepared using both the HRIR
imagery and the conventional observations (Fig. 8-13), suggests the center of the
lower tropospheric circulation is at $16^{O} N$ $142^{O}E$. Two asymptotes of directional
convergence appear along the southwest and north sides. These are accompanied
by well marked areas of high (cold) cloud.

The lower tropospheric flow beneath the upper tropospheric cyclone at
$20^{O}N$ $163^{O}E$ still appears to resemble a "deep easterly" current. Only a very slight
cyclonic curvature hints at the existence of the upper tropospheric cyclone.
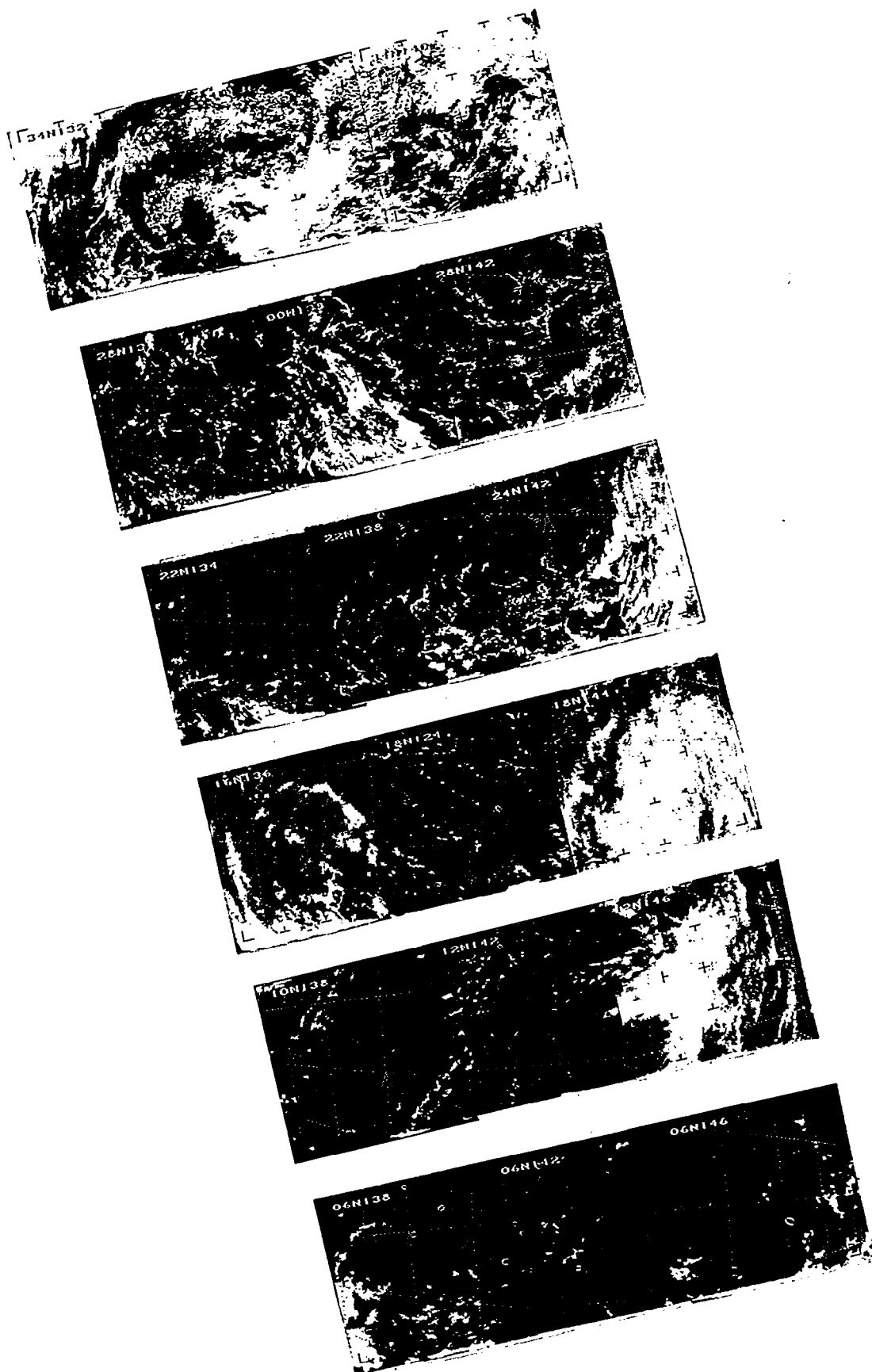
Figure 8-10   AVCS Mosaic Orbit 304, 0200 GMT,
18 September 1964

311

310

Figure 8-11   HRIR Photofacsimile Strips (Unrectified)
                Orbits 310 and 311, 18 September 1964

Figure 8-12   HRIR Representation (Rectified)
                Orbits 310 and 311, 18 September 1964
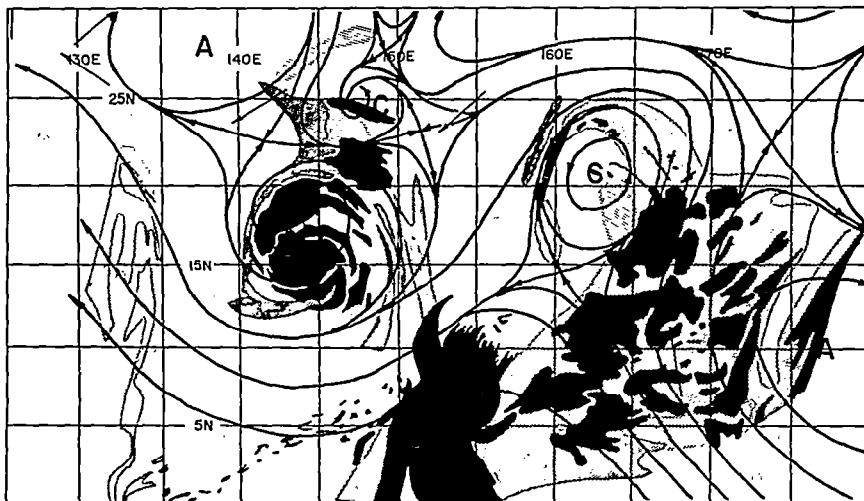
Figure 8-14   HRIR Revised 300 mb Streamline Analysis,
1200 GMT, 18 September 1964
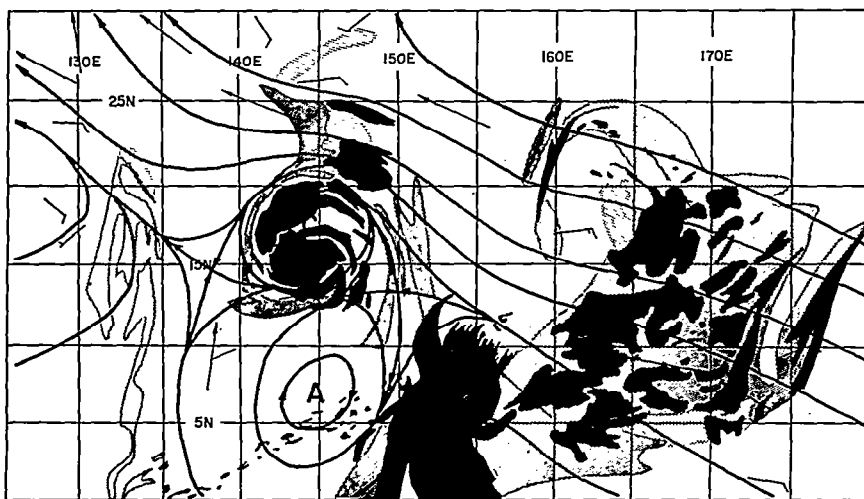
Figure 8-13   HRIR Revised Surface Streamline Analysis,
1200 GMT, 18 September 1964

8.4.3.2.2 300 mb

The 300 mb circulation (Fig. 8-14) has now evolved into two primary, and one secondary, features: (a) the principal anticyclonic outdraft over the pre-Wilda perturbation is well organized with the upper level flow parallel, but opposite in direction, to the low level flow; (b) the secondary cyclone at $25^{\circ}N$ $147^{\circ}E$, which appears to have formed from the merger of the two small cyclones; and (c) the principal cyclone near $20^{\circ}N$ $163^{\circ}E$. Comparison with the Guam analysis (Fig. 8-1) suggests that there was some considerable error in their analysis near Wilda due to a general data sparsity. The location of the cyclone at $20^{\circ}N$ $163^{\circ}E$ has been re-established by a fortunate observation from aircraft, which indicated southwest winds near $19^{\circ}N$ $166^{\circ}E$. The cold cloudiness on the south and east side of this upper level system is blending into the upper level circulation, but its cause is probably still in the middle and low troposphere.

8.4.3.3 Meteorological Implications

The increased cyclonic banding surrounding Wilda suggests further concentration of the released latent heat. The establishment of a primary high (cold) cloud band north of Wilda, at approximately $19^{\circ}N$ $144^{\circ}E$, suggests the principal area of heat input has shifted from the southeast side, as shown in the HRIR on 17 September and by the AVCS early on 18 September, to the north and northwest sides. Such a shift of the principal heat input area may relate to the observations by Merritt[55] and Zipser[57] of apparent shifts in the centers of circulation from the east to the west side of tropical cyclones at the time of upgrade in intensity from Tropical Depression to Tropical Storm. This shift is also implied from the studies of Sherman[40] regarding asymmetrical wind configurations around tropical cyclones.

The character of the cloudiness around the developing upper tropospheric cyclone, i.e., the thin, cyclonically curved band near $160^{\circ}E$ in Figure 8-11, suggests a mode of formation relating to narrow streaks of vertical motion, similar to those associated with jet streams. Inspection of data for other periods (particularly from aircraft operations through the area in 1961) indicates that narrow, jet stream-like wind zones often encircle the periphery of these upper tropospheric systems. The first appearance of significant vertical motion might well occur as a result of small scale, narrow zones of positive vorticity advection.

The appearance of such narrow high (cold) cloud zones might provide an indication of the intensification of upper level vortices over the Pacific, and possibly also the Atlantic.

8.4.4 19 September 1964

8.4.4.1 General Situation

The cloud features in the HRIR imagery for 19 September (Figs. 8-15 and 8-16) provide somewhat of a contrast to those on previous days. Wilda, centered near 17°N 143°E, has many of the characteristics of a full typhoon, i.e., an extensive, well organized high (cold) cloud shield, a sharply defined western edge to the cloud shield, well marked peripheral banding, etc. The small scale vortex near 29°N 144°E may have developed from the upper tropospheric cyclones which had been tracking north and west in that area for the past two days. The most startling change is shown by the cloud mass centered near 20°N 155°E. This is apparently the same area of clouds which first appeared on 16 September, and which finally began intensification on 18 September with the appearance of a thin curved high (cold) cloud near 160°E (Fig. 8-11). Contrary to the other upper tropospheric example analyzed in Section 9 of this report, there is no connection with the frontal-type banding to the north. However, the general relative placements of the vortices and the frontal bands in the two cases are significantly different.

8.4.4.2 Streamline Analyses

8.4.4.2.1 Surface

The surface streamline pattern (Fig. 8-17) has changed but little from 18 September. The cyclonic indraft associated with Wilda extends over a larger area, but is not basically different from the previous day. Comparisons with the Guam analysis, which was apparently based on ship and island observations, seem to indicate a slightly different location for the center of circulation. To the east of Wilda, the "deep easterly" flow continues in spite of an apparent increase in intensity of the upper tropospheric vortex.
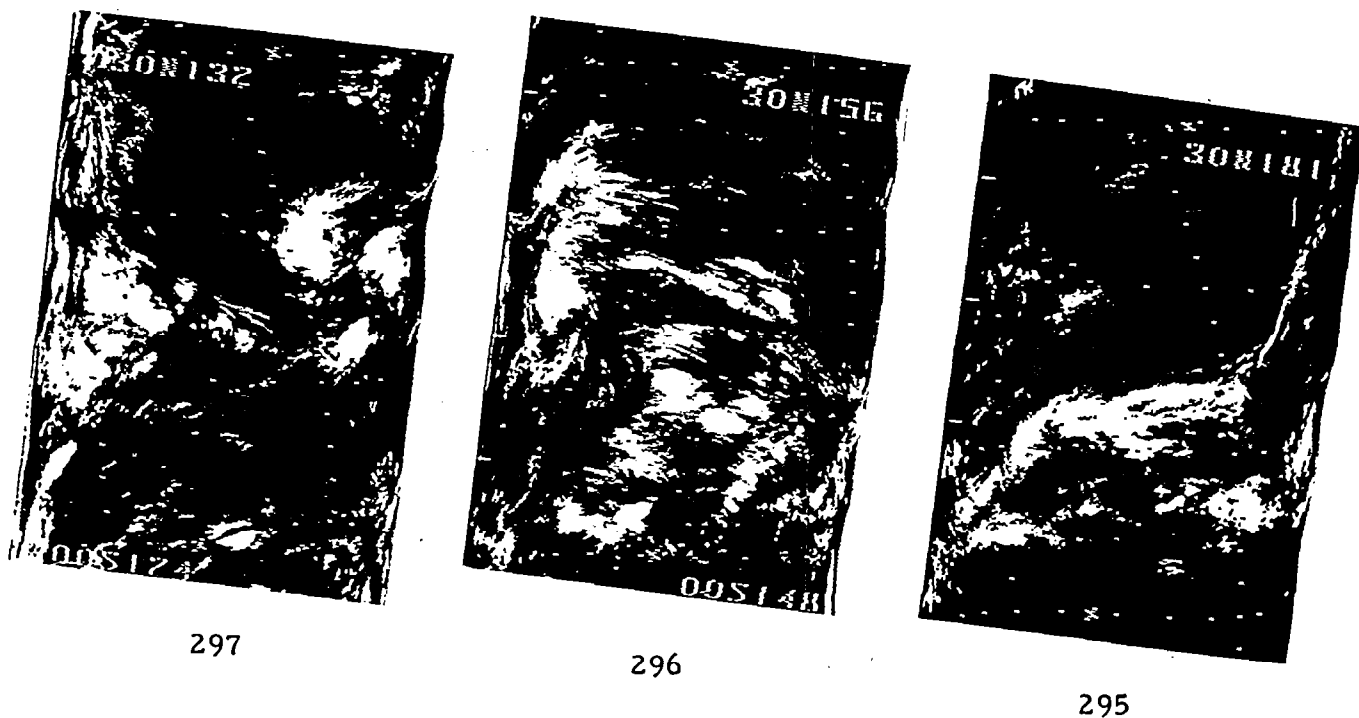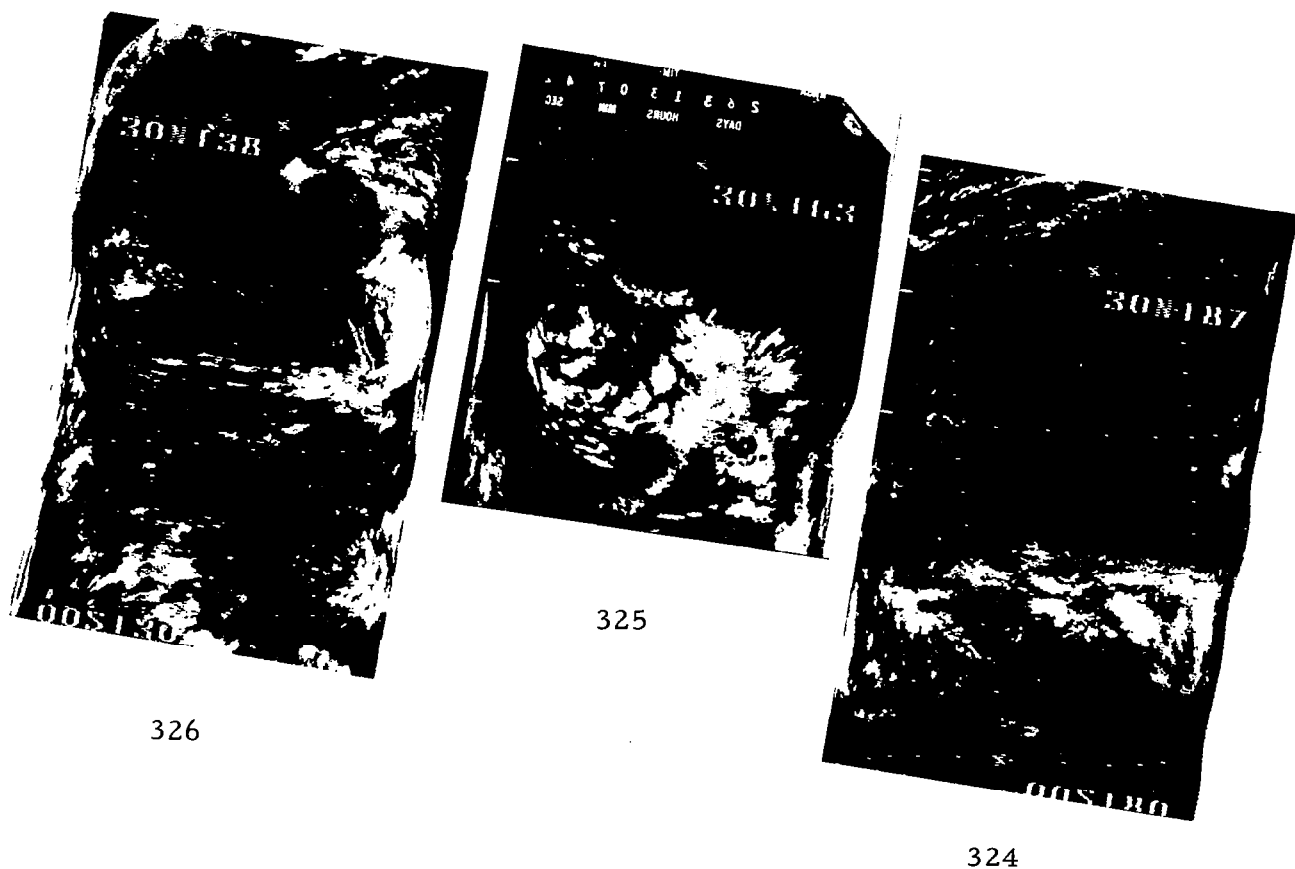
Figure 8-15   HRIR Photofacsimile Strips (Unrectified) Orbits 324,
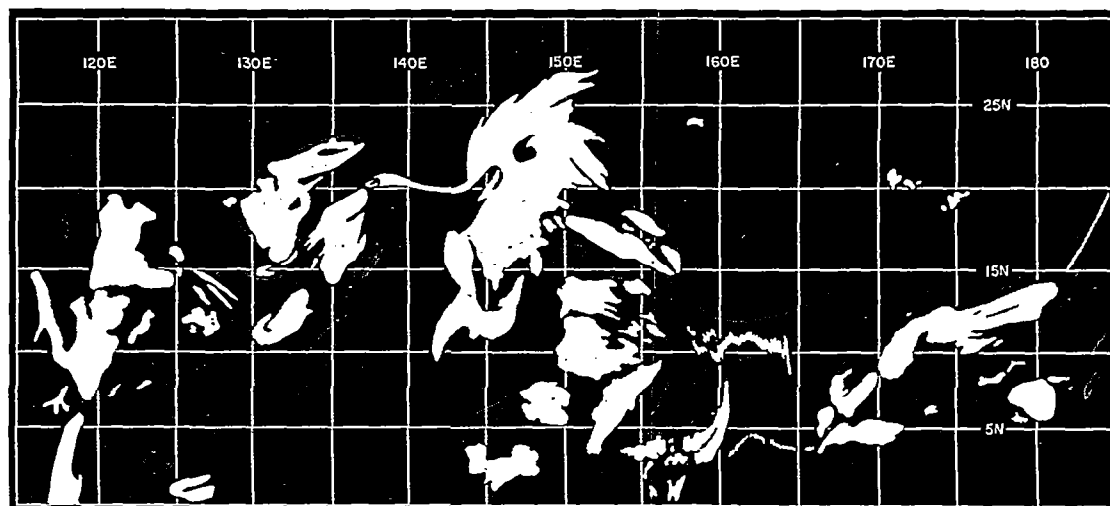325 and 326, 19 September 1964

Figure 8-16   HRIR Representation (Rectified) Orbits 324, 325 and 326,
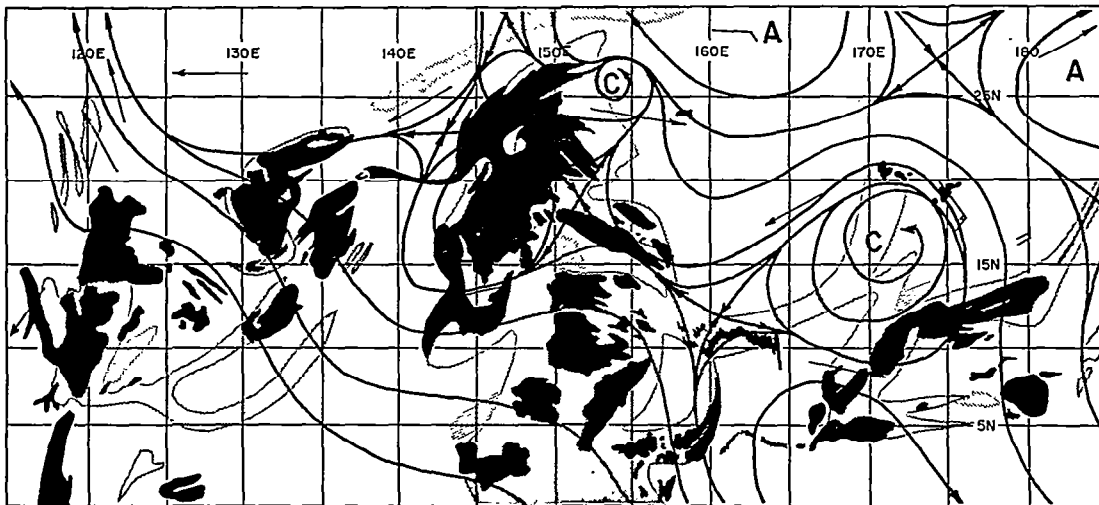19 September 1964
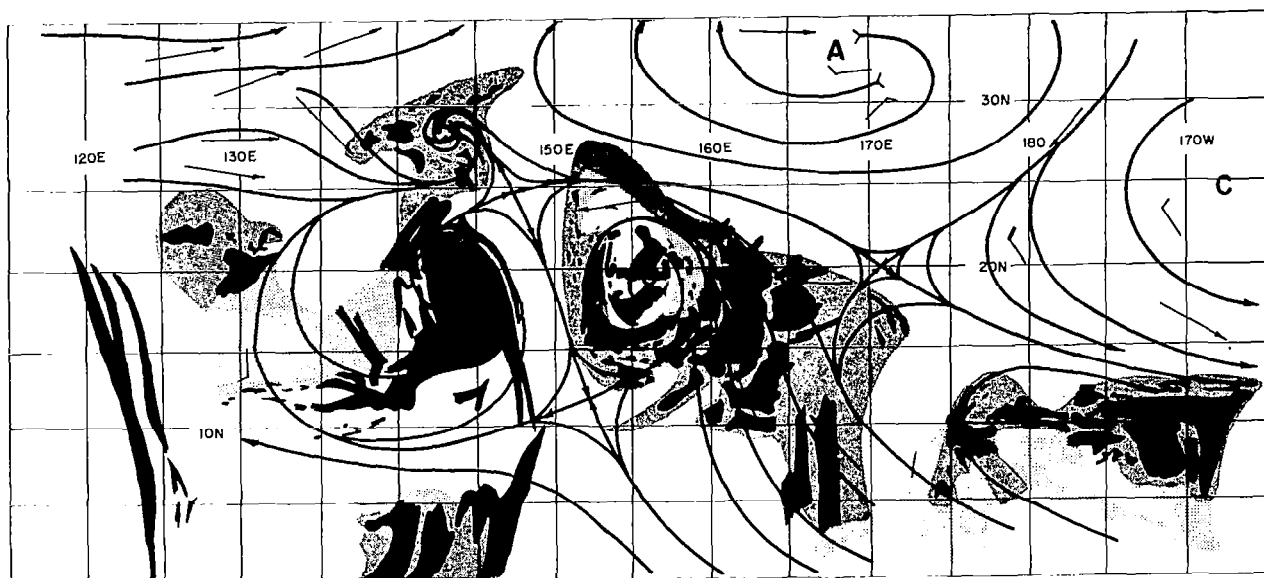
Figure 8-18   HRIR Revised 300 mb Streamline Analysis,
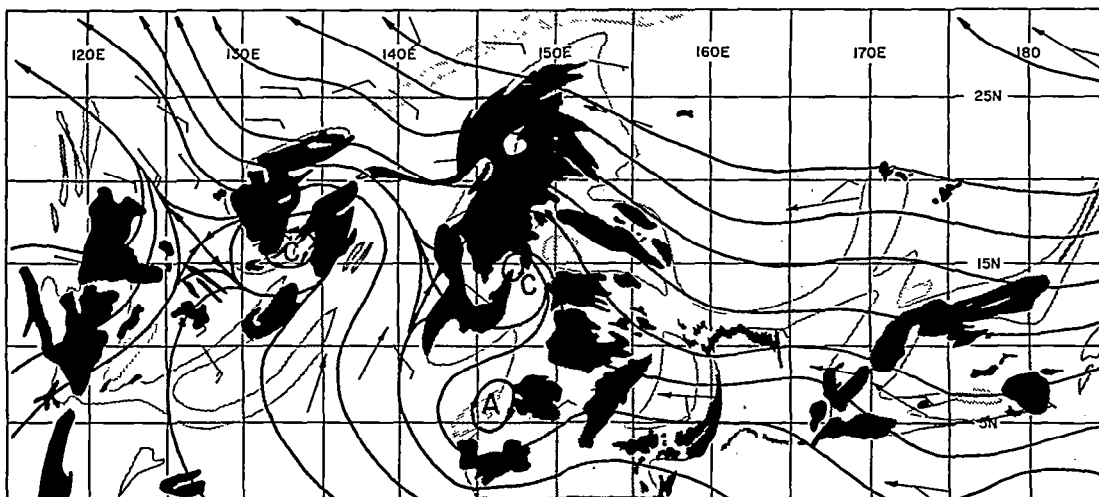1200 GMT, 19 September 1964
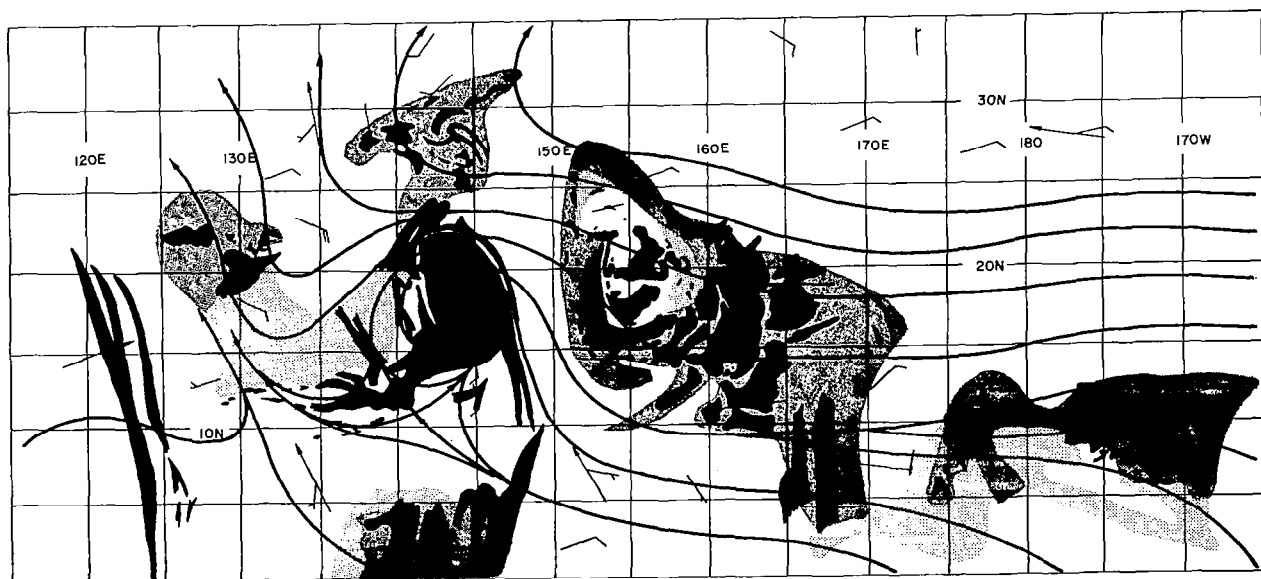
Figure 8-17   HRIR Revised Surface Streamline Analysis,
1200 GMT, 19 September 1964

8. 4. 4. 2. 2 300 mb

At 300 mb the streamline field (Fig. 8-18) is now well organized. The anticyclonic flow above Wilda occurs exactly where Guam erroneously placed a cyclonic indraft. The aircraft report of an east-northeast wind at 15^ON 141^OE should have led to a modified analysis. The streaks around the periphery of Wilda (see Fig. 8-15) indicate an outflow pattern.

The primary cyclonic center, centered near 20^ON 155^OE in both the winds and the HRIR imagery, has moved to within 500 miles of the center of Wilda. In fact, there is a marked zone of interaction, with an asymptote of directional convergence/divergence now separating the two systems. The broad area of directional convergence now existing to the east of the primary upper level cyclone continues to produce heavy (cold) cloudiness.

8. 4. 4. 3 Meteorological Implications

The final intensification of Wilda seems to follow the general development sequence proposed by Merritt.[55] The full effects of the two upper level cyclones during the final intensification of Wilda are not clear but there is certainly evidence to suggest that the nearby primary upper level cyclone may have accelerated the upper level outflow from Wilda and so intensified Wilda's warm core middle and upper tropospheric circulation. Similar external "forcing" was suggested by Riehl[38] as a means of physically connecting mid-latitude troughs to developing tropical perturbations. Since there is no reason to place the tropical upper tropospheric cold low in a different class than a mid-latitude cold trough, juxtaposition of this low could produce acceleration of the warm core circulation (through cooling of the external environment and warming within the perturbation) rather than by warming alone.

The four-day persistence of the small secondary upper tropospheric cyclones around the northern periphery of the developing Wilda perturbation suggests that these small systems may play a definite role in tropical cyclone development following establishment of a warm core in the middle and upper troposphere. Since these centers are presumably cold core, they might provide small scale solenoidal acceleration of the warm core system through increased local baroclinicity. The small scale fluctuations which are observed during tropical storm development could thus be related to these eddies. The final feature significant to the interpretation

of the meteorological situation, based on the HRIR data, is the apparent filling-in of the center and south side of the primary upper tropospheric cyclone with high (cold) clouds. Although there is no supporting data, this may be due to a broadening of the areas of positive vorticity advection on the south side. A second contributory factor, especially near the center, may be increased middle and upper tropospheric convection within the unstable air in the center of the cold core system.

8.4.5 AVCS Observation of Wilda, 20 September 1964

As a final confirmation of the Wilda development, an available ungridded AVCS mosaic for 0200 GMT, 20 September, is presented in Figure 8-19. The "eye" of the storm appears to be barely visible at the top center edge of the frame in the lower left corner. Comparison with the HRIR imagery in Figure 8-15 suggests that only slight changes have occurred in the twelve hours since the HRIR observation. For example, notice that the small scale "moat" around the periphery of the storm is clearly indicated in the HRIR imagery. The "clear" area separating Wilda from the upper tropospheric circulation to the east is, however, filled with small-scale cumulus. These would be lost in the HRIR resolution* and may well also have been present, on previous days, under the upper level anticyclonic circulation. The edge of the upper tropospheric circulation is just visible in the lower right of the AVCS mosaic.

8.4.5.1 Comparative Discussion

Comparisons between the HRIR imagery and AVCS photographs suggest that most features of significance to tropical analysis are resolved by the HRIR. In fact, the larger area of unbroken coverage provided by the HRIR in a single pictorial unit is an operational advantage, as compared to the frequent necessity to montage the AVCS to determine the overall situation before the greatest gain can be obtained from an examination of the smaller details. In any event, the nighttime HRIR data and daytime TV data (whether from AVCS or a lesser resolution system) are obviously mutually complementary and supplementary.

---

* The temperature contrasts on which HRIR observations are dependent may also be a factor.

159
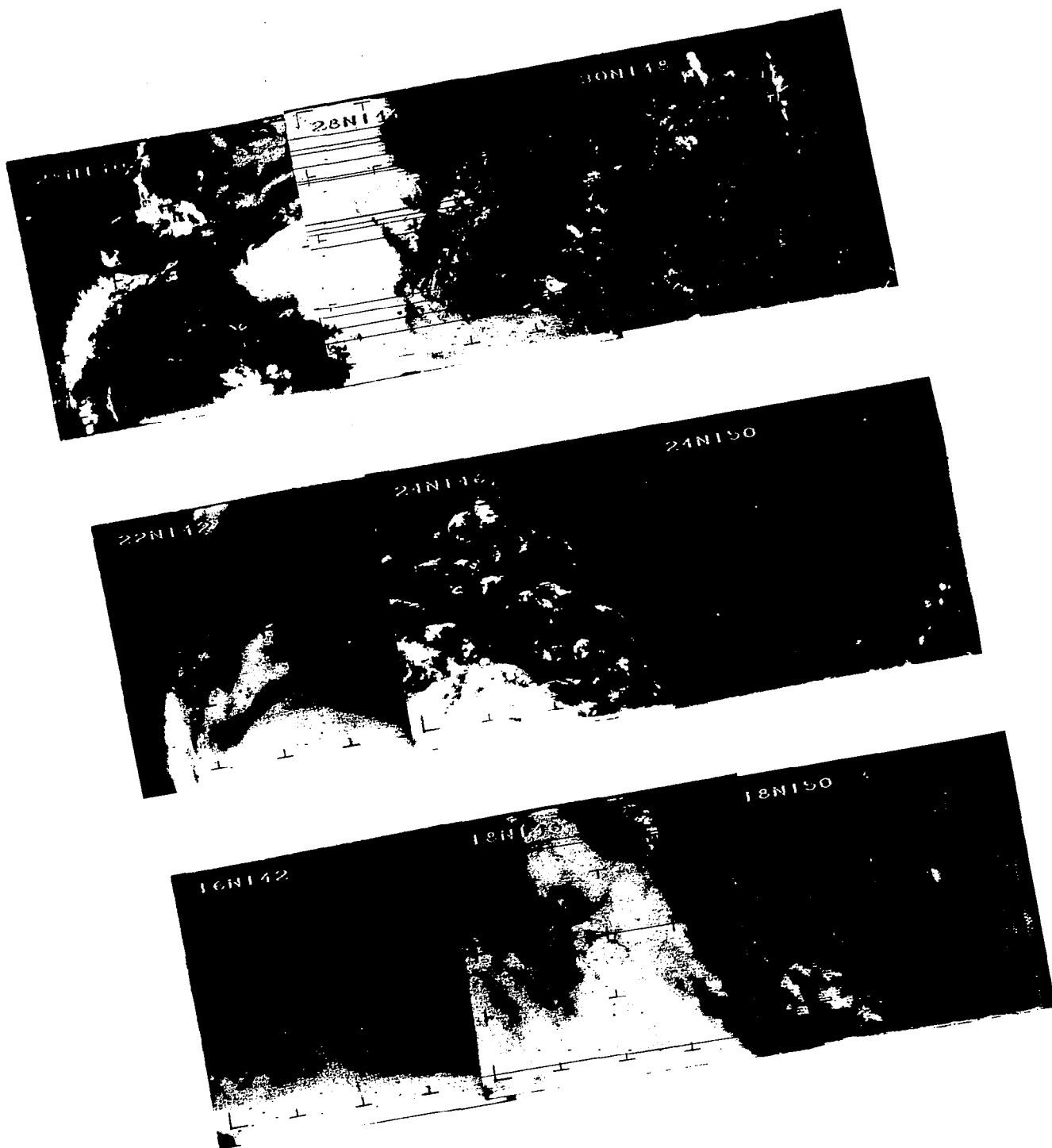
Figure 8-19   AVCS Mosaic Orbit 333, 0200 GMT,
20 September 1964 (Typhoon Wilda)

8.5 Conclusions and Recommendations

This four-day study of meteorological conditions over the central and western tropical Pacific, emphasizing the additional data provided by the HRIR imagery and to a lesser extent the AVCS photographs, suggests a potential breakthrough in tropical analysis. A vivid indication of this has been the three-dimensional view, provided by the HRIR, of the formation of an upper tropospheric tropical cyclone. These systems are very important to accurate upper air wind analyses. In addition, accurate locating of these systems may lead to more precise forecasting of the development of lower level tropical cyclones.

The formation of Wilda as observed by the HRIR seems to support the concept introduced by Merritt[55] of a convectively warmed perturbation which experiences a shift in the position of the center of apparent circulation at the time of transition from Tropical Depression to Tropical Storm intensity. This shift of the center seemed to be preceded by the peripheral banding of the perturbation becoming more intense on the north and northwest sides (Figs. 8-6 and 8-11).

The intensification of the upper tropospheric circulation, indicated by the appearance of thin jet stream-like bands (Fig. 8-16), suggests an increase in cold core baroclinicity which would be accompanied by a peripheral zone of strong, jet-like winds. Small scale vorticity advection in these areas would induce the vertical motion required to produce the banded cloudiness.

The potential of the HRIR for improved tropical analysis indicates the need for more extensive studies of the tropical zone utilizing the HRIR imagery. These studies should emphasize those periods when tropical perturbations are forming over the Pacific or Atlantic. Additional studies should utilize aircraft Doppler wind data, available from aircraft flight logs, to define the horizontal and vertical wind distribution in the area of these formative cyclones. The delays inherent in obtaining such data prevented their possible use in this study.

In summary, the HRIR imagery can obviously provide much of the data required for improved tropical analysis. The HRIR data provide a far greater amount of information pertinent to the vertical dimension aspects of an analysis than is normally or reliably available from the TIROS or Nimbus photographs. However, until resolution equivalent to that of the HRIR is available both night and day, through the use of a high resolution 10μ sensor, the TIROS or Nimbus photography provides a complementary and extremely useful data source. Even when high resolution infrared data are available during the daytime, the TV data may assist in identifying low clouds only dimly visible in the IR data.

9. AN UPPER LEVEL TROPICAL VORTEX OVER
THE CENTRAL PACIFIC

Sadler[39] has discussed upper level tropical vortices as seen by TIROS, and they have subsequently been studied by Merritt.[32]   Merritt analyzes one of these systems, as seen by the Nimbus I HRIR, in Section 8 of this report.

The HRIR recorded another of these systems on orbit 353, at about 1105 GMT on 21 September 1964, as shown in Figure 9-1.   The appearance and location immediately suggest this is one of the types of systems Sadler[39] described as typical of the mid-Pacific upper tropospheric trough.   An intriguing detail is the curved cloud band apparently connecting the tropical system to the frontal cloud band to its northwest.

It is interesting to note that the tropical system in Figure 9-1 is, in both position and appearance, about midway between what Sadler[39] denotes as cells M and N in his Figure 20 (see Fig. 9-2).   The cloud pattern in Figure 9-1 fits well with Sadler's findings that: "Those vortices located on the northeastern end of the trough, poleward of 30°N, between Hawaii and the western United States, do not have the massive cirrus shield.   Although these vortices are located over the highest surface pressure, their circulations penetrate deep into the lower layers and organize the low and middle clouds into vortex patterns which are apt to be misinterpreted, in the absence of synoptic charts, as belonging to surface storm systems."   Sadler shows an example (M in Fig. 9-2) which "could easily be mis-interpreted as belonging to a large decaying surface cyclone of the mid-latitudes."

Sadler goes on to say: "Those vortices, located along the central and western portion of the trough, equatorward of 25°N, have a massive shield of alto and cirro clouds.   Most do not exhibit a vortex pattern in the upper shield, nor do they penetrate sufficiently into the lower layers to organize the cumulus."
(See N and O in Fig. 9-2.)

In the example in Figure 9-1, centered just slightly south of 30°N, it would appear the system has acquired the high cloud shield described by Sadler, but still retains one spiral arm of what earlier may have been a distinctive vortex pattern. (Because of the gaps in the HRIR data for this area, it is impossible to establish continuity for this system.)

Conventional analyses available for this seriously data deficient area were those prepared by the Air Weather Service at Guam.   Those for the surface, 500 mb,

Figure 9-1   HRIR Observation of an Upper Level Vortex Over the Tropical North
              Pacific.   Orbit 353, about 1105 GMT, 21 September 1964
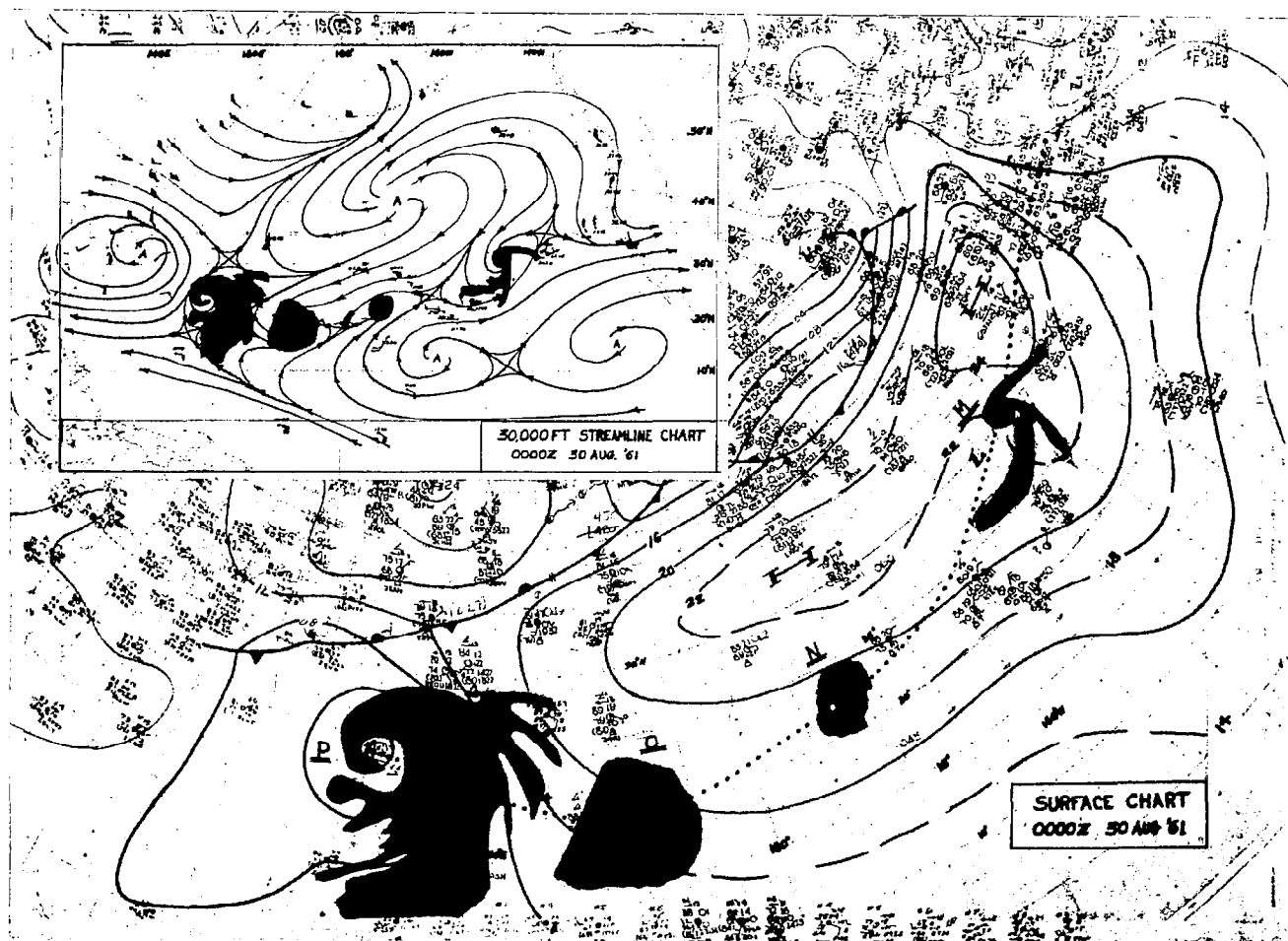
Figure 9-2   Surface Pressure Analysis and 30,000 ft Streamline Analysis for 0000 GMT,
30 August 1961.   Upper Troposphere Trough Denoted on Surface Chart by
Dotted Line.   Shaded Areas were Extracted from the Transmitted TIROS III
Nephanalyses (From Sadler, Reference 39)

and 300 mb, for 1200 GMT, 21 September, are shown as Figures 9-3, 9-4, and 9-5. The major cloud features of Figure 9-1 have been transferred, with rectification, to these analyses.

Figure 9-3 shows no surface explanation for the system near 28°N 164°W. (It does, however, suggest that some of the cloud pattern at the southwestern end of the frontal band is associated with weak surface low pressure area near 39°N 170°W.)

Figure 9-4, the 500 mb analysis, provides no definitive explanation for the tropical system, placing it at the extreme crest of a tropical trough. Inspection of the wind reports, however, especially those near 30°N 176°W and 18°N 170°W, suggests the system may have begun to penetrate down to the 500 mb level. A reanalysis using all the plotted data might place the tropical trough slightly further east and add a cyclonic circulation or trough near 25°N 172°W.

(The 500 mb anticyclone near 35°N 175°W may be associated with the rather abrupt western termination of the frontal cloud band.)

Figure 9-5, the 300 mb chart for 1200 GMT, and the 300 mb chart for twelve hours earlier (not shown) suggest the tropical cloud system results from a second, unanalyzed upper level cyclonic center located some 8° north-northeast of that shown in Figure 9-5. Such a reanalysis would fit the observed clouds without conflicting with the plotted observations at either 0000 or 1200 GMT. The existence and approximate position of the center near 20°N 170° W is substantiated by 0000 GMT data. The 0000 GMT chart does present a problem with a south-southwest wind at 29°N 170°W. This may, however, be a mean route wind, averaged over a considerable distance and more properly applicable to the area somewhat east or east-southeast of its plotted position. It is to be noted that, until 0000 GMT on 19 September, the Guam charts carried a cyclonic center in the eastern part of the analysis area and north of 25°N.

With such a reanalysis, the curved cloud band connecting the tropical system to the frontal band would then correspond well to the 300 mb flow. While an alternative would be to relate the curved connecting cloud band to the surface level anticyclonic flow, the height of most of the clouds along the band, and especially the finger of cloud extending from the frontal band south-southwest to about 32°N 170°W, suggest that relating the curved band to the upper level flow is the better explanation. There is, however, a suggestion of low clouds along the band which may be related to the lower level flow.

Without the cloud height information provided by the HRIR, an interpretation of the curved band would probably have remained completely ambiguous.
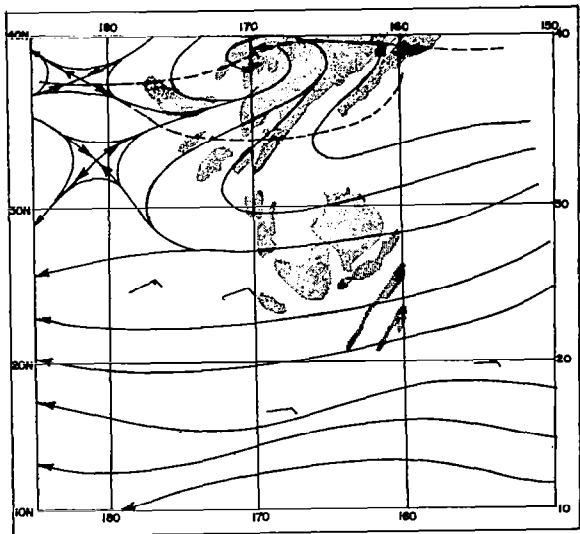
Figure 9-3 Surface Analysis for
September 21, 1964, as
Prepared by Air Weather
Service, Guam, with Rec-
tified Cloud Patterns from
Figure 9-1 Added.
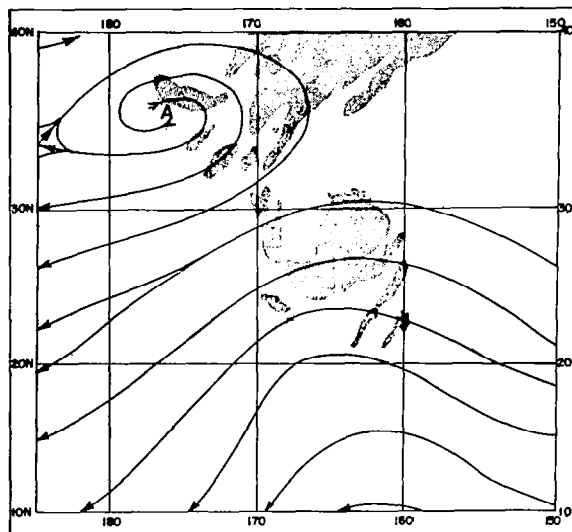
Figure 9-4 500 mb Analysis for 1200
GMT, September 21, 1964,
as Prepared by Air Wea-
ther Service, Guam, with
Rectified Cloud Patterns
from Figure 9-1 Added.
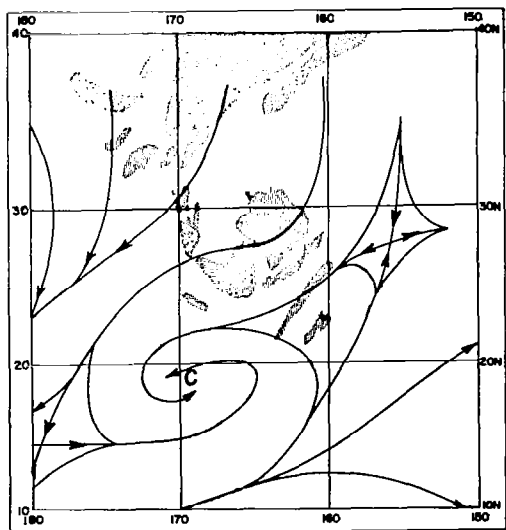
Figure 9-5 300 mb Analysis for 1200
GMT, September 21, 1964,
as Prepared by Air Wea-
ther Service, Guam, with
Rectified Cloud Patterns
from Figure 9-1 Added.

10. A CONVECTIVE CLOUD PATTERN OVER THE MIDWESTERN UNITED STATES

10. 1 Introduction

The Nimbus I HRIR film strip for orbit 306, taken at about 0600 GMT, 18 September 1964 (Fig. 10-1), shows a cloud pattern over the United States, just east of longitude 90°W, somewhat similar to the cloud pattern of orbit 335 observed two days later at about 0530 GMT, 20 September 1964. The cloud pattern for orbit 335, which was discussed in Reference 56 and can be seen in Figure 4-5, was ten to twelve degrees east of the earlier pattern in orbit 306.

The similarity extends to a large bright cloud in each strip, having a more or less similar size and shape in the two orbits. In orbit 306 the bright cloud, mostly between 38° and 40°N and 87° and 90°W, was oriented east-west and was west of the center of a "V"-shaped cloud mass (Fig. 10-1). In orbit 335, a bright cloud extended between 39° and 41°N and 76° and 78°W, had a northwest-southeast orientation,and was near the intersection of the legs of a "V"-shaped cloud mass. The bright clouds' dimensions, 100 to 180 miles, put them in the larger mesoscale range, although definitely smaller than typical synoptic scale clouds.

This case study was undertaken primarily to determine whether the bright clouds were related. The initial working hypothesis was that persistent dynamic processes might have maintained the overall pattern while translating it eastward and simultaneously moving the bright cloud slightly faster than the darker (lower) clouds.

10. 2 Available Data and Conventional Analyses

Available conventional meteorological data included:
        Six-hourly surface reports
        Twelve-hourly radiosonde reports
        Six-hourly winds aloft (incomplete)
        Surface, 700 mb and 500 mb maps at twelve-hourly intervals
        Twelve-hourly vorticity and vertical velocity maps
        Radar at 0600 GMT, 18 September 1964, for Chicago, Evansville, St. Louis, and at 0530 GMT, 20 September, for Buffalo, New York City, and Washington, D. C.

Also available were TIROS VII pictures taken at about 1825 GMT, 18 September, and 1710 GMT, 19 September.

Figure 10-1   HRIR picture of eastern North America, from orbit 306,
                at 0600 GMT, 18 September 1964

10. 2. 1 Synoptic Situation

The synoptic situation over eastern North America changed rather slowly
during the period from 18 to 20 September 1964. Figure 10-2 shows the surface
map at 0600 GMT, 18 September 1964, the time of the HRIR observation of
orbit 306. Changes from it can be inferred from the following discussion, and
from the maps in Section 4. 5 of Reference 56. At the surface, a large high
pressure area moved southeastward from the Hudson Bay region to the Maritimes
and northern New England. A weak front through the mid-Atlantic states to Michigan
was analyzed on the surface maps by 1200 GMT, 18 September (not shown), though
the basis for the analysis at that time was limited. During the rest of the period,
although this front moved slightly southward, it was essentially stationary.
Meanwhile, a cold front oriented nearly north-south moved eastward to about the
Mississippi River by 1800 GMT, 20 September, thus having little influence over
the area of chief interest during the period.

At 500 mb, a trough initially centered over Labrador intensified and moved
southeastward over the Atlantic Ocean. A closed low over the north central states
at 0000 GMT on the 18th filled, but a major short wave trough pattern associated
with this low moved eastward through the area toward New England, weakening with
time partly because it was moving into a portion of the major ridge west of the
Labrador low.

At 700 mb, the pattern was similar to that at 500 mb, with a major trough
initially over northeastern North America moving eastward over the Atlantic Ocean.
Figure 10-3 shows the map for 1200 GMT, 18 September. A significant short wave
trough persisted near Lake Michigan until 0000 GMT, 20 September, after which the
flow was dominated by the trough associated with a low over northern Canada.
Successive positions of this short wave trough have been indicated on Figure 10-3.
The Atlantic states were mostly under a weak ridge which built to a small closed
high over New England at 1200 GMT, 20 September.

Associated with the major short wave, there appeared to be two minor short
waves or vorticity maxima extending from below 700 mb to at least 500 mb. At
1200 GMT, 18 September (Fig. 10-3), the first of these was in the vicinity of
Illinois, Indiana and southern Lake Michigan. Twelve hours later it was slightly
further north, extending into southern Michigan. By 1200 GMT, 19 September, it
had moved eastward to Ohio, western Pennsylvania, Lake Erie and southern
Michigan. At 0000 GMT, 20 September, it was near but west of Buffalo, about
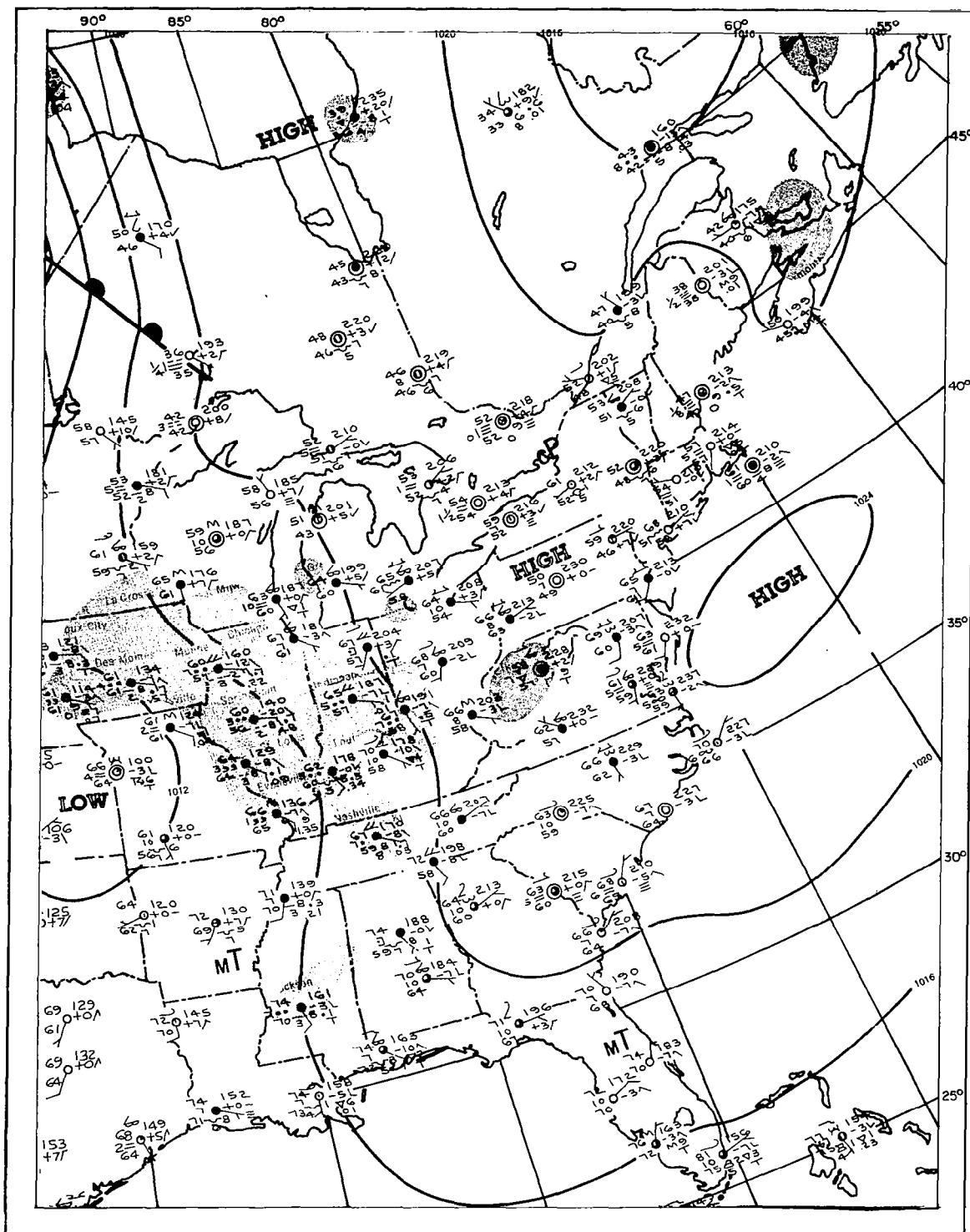
Figure 10-2   Surface weather map at 0600 GMT, 18 September 1964

Figure 10-3   700 mb map at 1200 GMT, 18 September 1964

Legend:
- ─·──·──·─ 0000 GMT, 19 SEPT 1964
- ─────── 1200 GMT, 19 SEPT 1964
- ─────── 0000 GMT, 20 SEPT 1964
- ─·─··─··─ 1200 GMT, 20 SEPT 1964

over Lake Erie. By 1200 GMT, 20 September, there was some evidence for it north of Lake Erie. This movement was, not unexpectedly, similar to that of a vorticity maximum discussed in Section 10. 3. 2 below.

The second minor short wave or vorticity maximum was in the vicinity of the Oklahoma-Arkansas border at 1200 GMT, 18 September (Fig. 10-3). By 0000 GMT, 19 September, it was in the vicinity of the Mississippi River near Arkansas and Tennessee. By 1200 GMT, 19 September, it had apparently weakened, though possibly present near the junction of the Mississippi and Ohio Rivers. By 0000 GMT, 20 September, it had weakened so much that its position was uncertain on the 700 or 500 mb flow charts; it might have been considered to have disappeared until the vorticity charts (see Section 10. 3. 2) were examined.

10. 2. 2 Raobs

Several radiosonde observations were plotted to obtain representative conditions during the period and to aid in the estimation of cloud top heights. Many of the ascents paralleled the moist adiabats starting as low as between 800 to 900 mb and extending to about 500 mb. A few inversions were noted, some frontal and some subsidence.

10. 2. 3 Winds Aloft

At the start of the period the winds aloft over eastern North America were mostly associated with the deep trough over eastern Canada and hence were predominantly from the west-northwest, at 30 to 40 knots at 700 mb. Over the midwest, winds aloft were weak southerly or southwesterly, associated with the short wave trough. A small area over the southern Mississippi Valley had stronger winds; this wind area appeared to weaken but propagate northeastward at least until 1200 GMT, 19 September 1964, almost as though associated with a large meso-system. This small area of stronger winds was probably related to the second minor short wave trough discussed in Section 10. 2. 1, and its related vorticity maximum to be discussed in Section 10. 3. 2.

10.2.4 Current Precipitation

Maps of current precipitation were prepared at six-hourly intervals from available synoptic data and surface maps (Fig. 10-4). *

Precipitation rates were mostly light. The patterns generally moved northward and eastward, but not in any marked regular progression. Precipitation was occurring over a smaller total area at the end of the period than earlier.

10.3 Results of Analyses and Interpretations

10.3.1 Current Precipitation

Areas of precipitation occurring at 0600 GMT, 18 September, are shown in Figure 10-2. Precipitation was falling over most of Iowa, Illinois, southern Indiana, and several adjacent areas as well as in central West Virginia and over a few areas near the Great Lakes. Figure 10-4 shows the subsequent patterns of the areas of precipitation. Initial northeastward movement is evident, followed by a slowdown of the northward movement over Wisconsin and Michigan.

By 0600 GMT, 19 September, precipitation was occurring south of 39°N only over the southern Appalachians and in the vicinity of Washington, D.C., where it was part of an area in which precipitation had started (or into which it had moved) in the last six hours. Subsequently, precipitation decreased and ultimately ceased to the west as the main precipitation area appeared to have moved eastward. An area of precipitation may also have moved northward along the Appalachians, to merge with that approaching from the west.

Since a study of the precipitation patterns was found insufficient to either prove or disprove continuity between the two bright clouds, maps of vorticity and vertical motion were examined.

---

* The boundaries of the precipitation areas were difficult to establish in many cases because of wide spacing between stations, and as a result, details of the precipitation patterns may have been incorrectly analyzed at times.
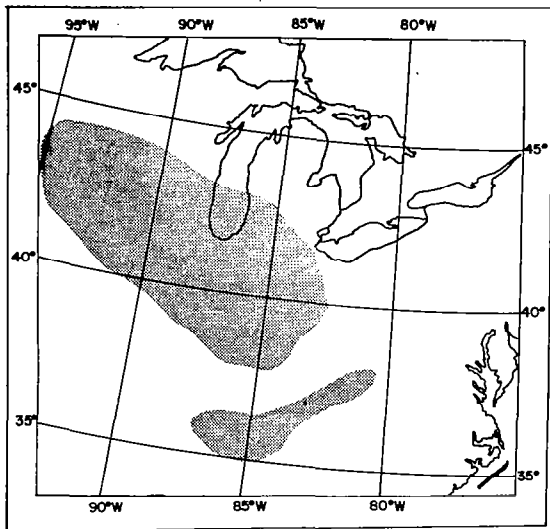
1200GMT, 18 September 1964
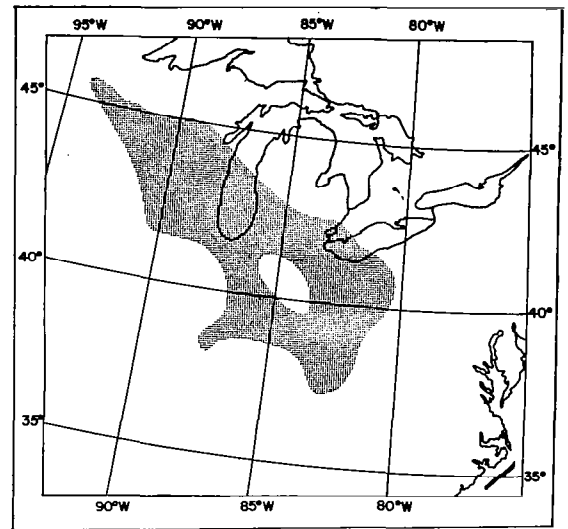
1800GMT, 18 September 1964
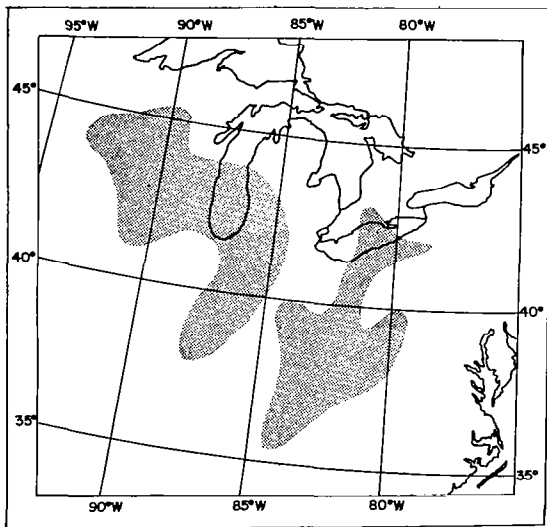
0000GMT, 19 September 1964
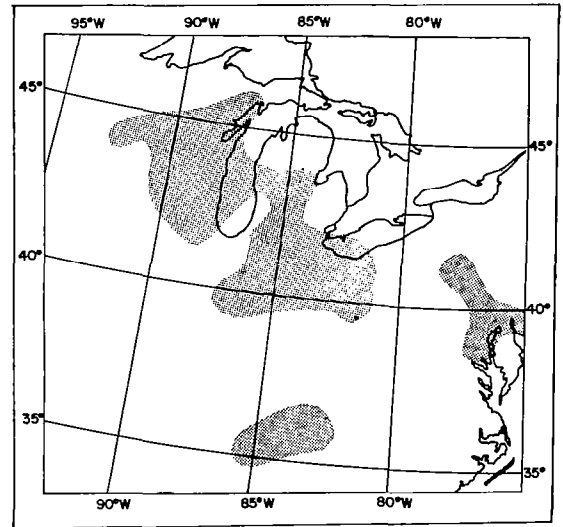
0600GMT, 19 September 1964

Figure 10-4   Current precipitation charts for 18-20 September 1964
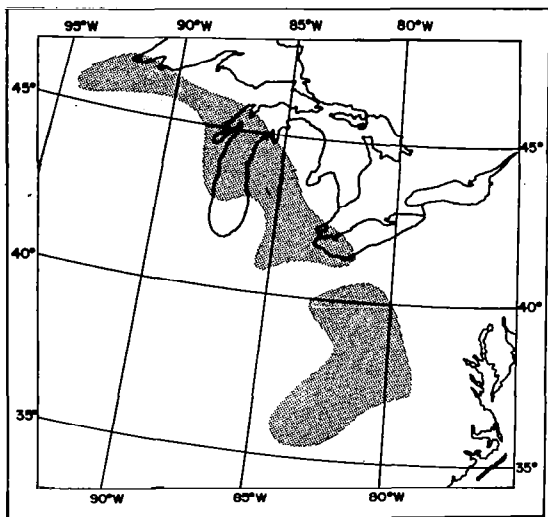
1200GMT, 19 September 1964
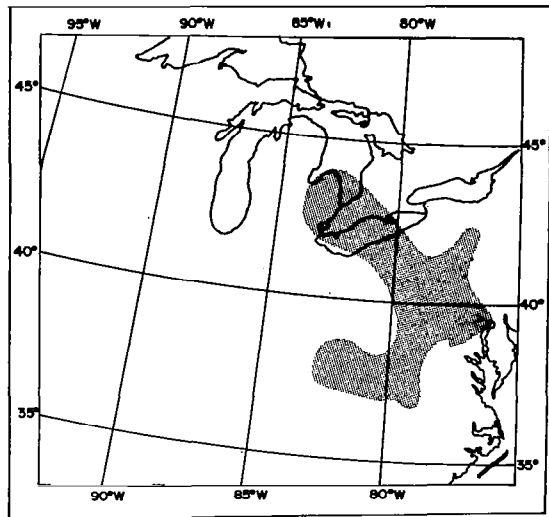
1800GMT, 19 September 1964
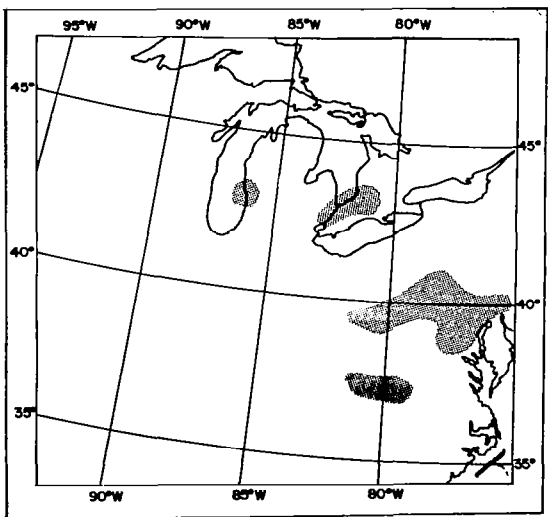
0000GMT, 20 September 1964
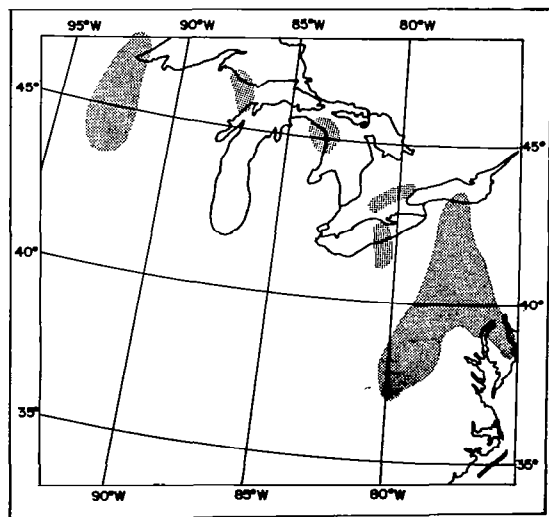
0600GMT, 20 September 1964

Figure 10-4 Continuation

177

10.3.2 Vorticity

Figure 10-5 shows the vorticity patterns at 12-hour intervals from 1200 GMT, 18 September, through 1200 GMT, 20 September. The center of the vorticity maximum which was at 41°N 94°W at 1200 GMT, 18 September, moved northeastward, then slowed down and moved eastward to just west of Buffalo by the end of the period. Figure 10-5a shows that at 1200 GMT, 18 September, the pattern of maximum vorticity had a pronounced southward extension which was probably related to the earlier mentioned area of higher winds over the southern Mississippi Valley. By 0000 GMT, 19 September, the southward extension had contracted somewhat and a pronounced southeastward extension was apparent (Fig. 10-5b). Twelve hours later the overall vorticity maximum had a definite northwest-southeast orientation, though a southward bulge of at least one of the vorticity lines remained (Fig. 10-5c). This southward bulge decreased as the whole pattern weakened and moved very slightly eastward (Figs. 10-5d and 10-5e). By the end of the period of interest, the time corresponding to HRIR orbit 335, there was still the weakened center near Buffalo with a definite extension southeastward across Pennsylvania.

10.3.3 Vertical Velocity

NMC maps of vertical velocity at twelve-hourly intervals, from 0000 GMT, 18 September, through 1200 GMT, 20 September, were examined, but were not useful in this study. The method of computation of vertical velocity used by NMC further smooths the data even beyond the smoothing for the vorticity calculations, with the result that the computed vertical motion field is seldom useful for meso-scale analyses.

Qualitatively, vertical motions could be inferred from the vorticity maps and the concurrent upper air flow patterns. Figures 10-3 and 10-5a for 1200 GMT, 18 September, show cyclonic vorticity advection southwest of Lake Michigan, and a maximum of upward vertical motion is to be expected there. Twelve hours later the vertical motion maximum would appear to be northeast of its earlier position, probably over eastern Ohio and Lake Erie. By 1200 GMT, 19 September, the 500 mb contours indicated a ridge over the vorticity maximum, so the earlier upward vertical motion pattern would be expected to have weakened greatly (Fig. 10-5c). However, another area of upward vertical motion might be
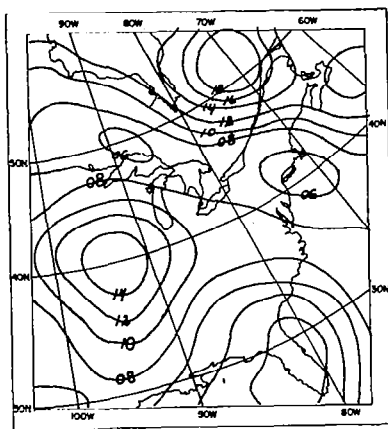
a.   1200GMT, 18 September 1964
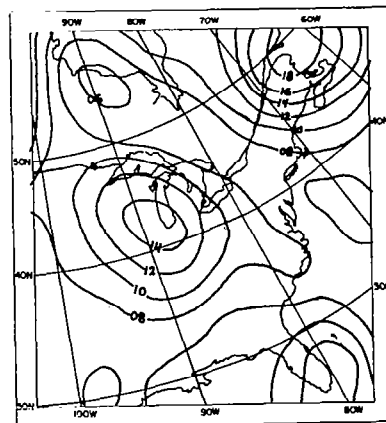
b.   0000GMT, 19 September 1964
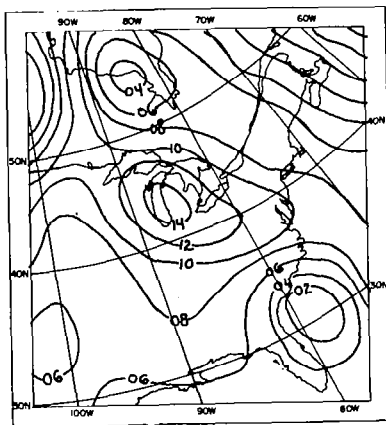
c.   1200GMT, 19 September 1964
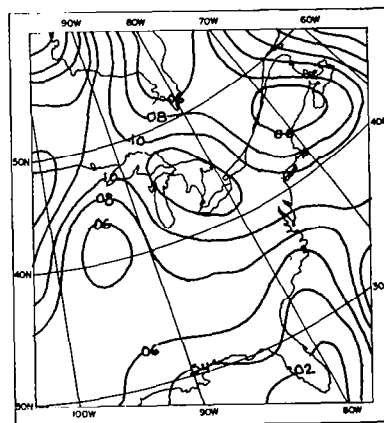
d.   0000GMT, 20 September 1964
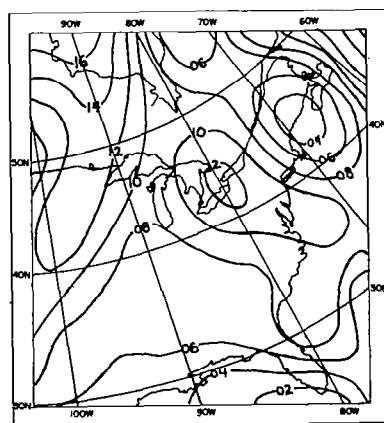
e.   1200GMT, 20 September 1964

Figure 10-5   NMC vorticity analyses for 18-20 September 1964
(units are 10^{-5} sec^{-1})

179

anticipated as forming at this time eastward of the southern vorticity bulge, in the vicinity of Tennessee and southern Kentucky. This field moved more or less eastward during the next twelve hours (Fig. 10-5d), probably moving to near the coast by 1200 GMT, 20 September (Fig. 10-5e). This tends to be confirmed by the colder (high cloud) areas in the HRIR data for orbit 335 (see Fig. 4-5).

On the basis of these vorticity and qualitative vertical motion fields, it seems probable that the first bright cloud, orbit 306, moved northeastward more or less with its associated upward vertical motion field, and dissipated or greatly weakened. The second bright cloud might be associated with the second field of upward vertical motion which moved east-northeast from the southern Mississippi Valley to the middle Atlantic coast.

10.3.4 Other Data

Radar observations at times corresponding to the HRIR pictures confirmed precipitation in the bright cloud areas of orbit 306. For orbit 335, they suggested that active precipitation was occurring south of Erie, Pennsylvania, but that the large bright cloud over portions of eastern Pennsylvania, New Jersey and Delaware was not producing much precipitation at the time of the HRIR data although it probably had been only slightly earlier (see Ref. 56).

The TIROS pictures showed an extensive cloud band over the eastern United States at about 1800 GMT on both the 18th and 19th, associated with the short wave trough and the stationary front. They were not particularly useful in this analysis, however, as estimations of variations in cloud height from them were infeasible (see Ref. 56).

10.4 Features in Nimbus I HRIR Orbit 306

In the course of the study discussed above, several interesting features were found, including:

1. There was good overall correspondence between the HRIR, a neph-analysis based on surface observations, and TIROS VII pictures (Fig. 10-6) taken on orbit 6761 about twelve hours after the HRIR observation for orbit 306. The correspondence shows in numerous ways, a few of which will be commented on below. It should also be noted, however, that the HRIR gives a very clear impression of significant variations in cloud top heights while the TIROS pictures suggest a much more uniform cloud deck.
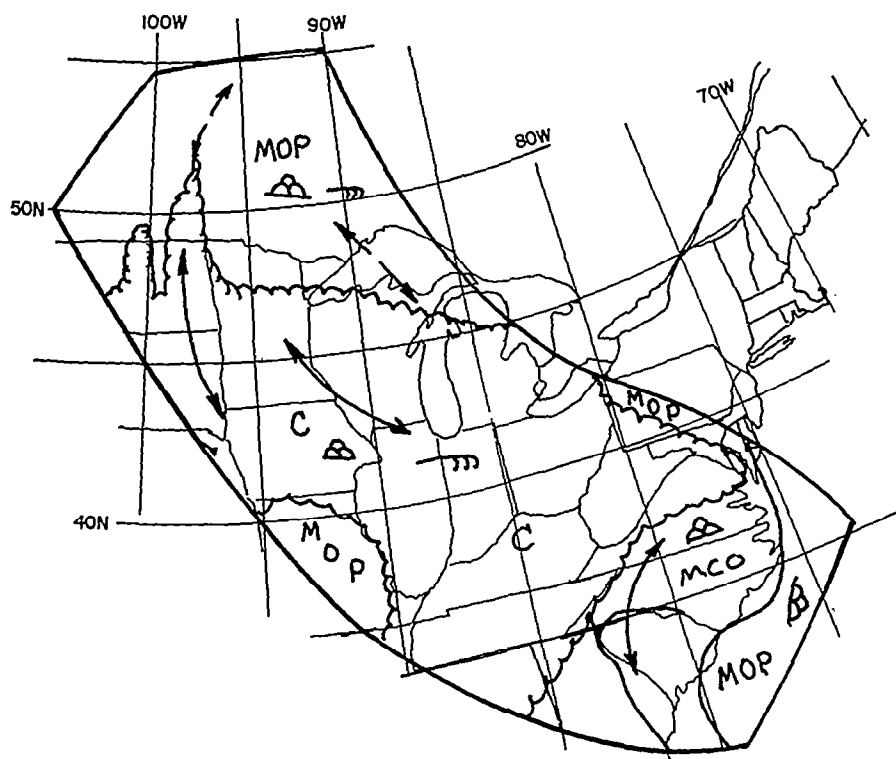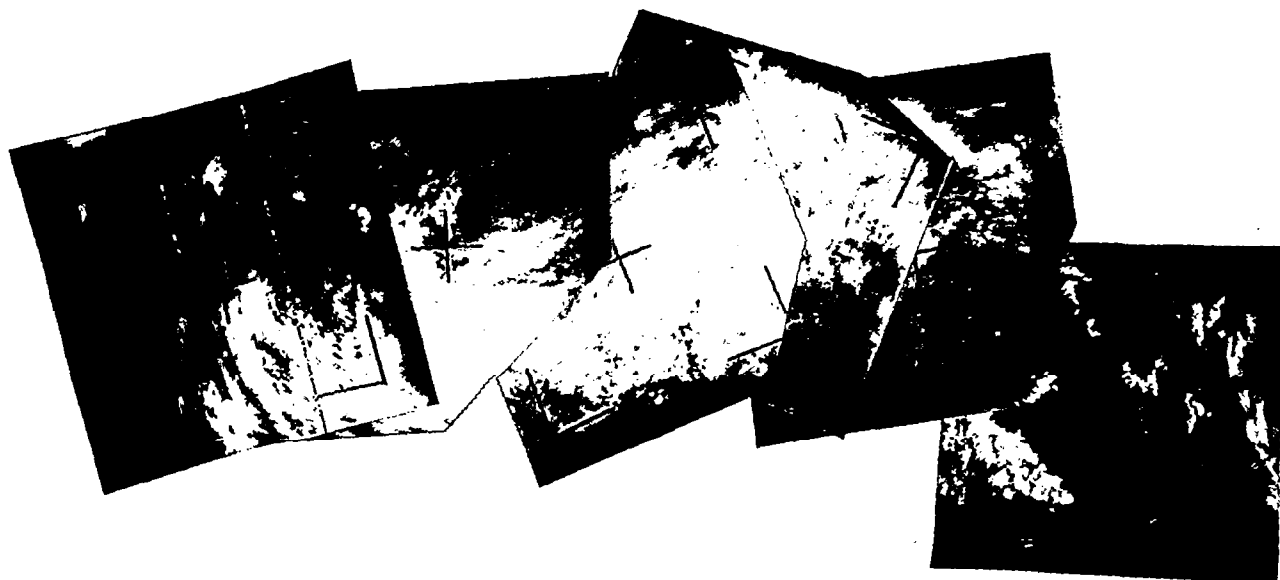
Figure 10-6   TIROS VII television picture mosaic, orbit 6763/6761, and operational nephanalysis, 1829 GMT, 18 September 1964

2. Cloud streaks (bands) were visible in both the HRIR and the TIROS near 44°N 91°W and can be related. Surface observations in the area were of thin cirrus, thin altostratus, and stratocumulus, but many stations were reporting light rain.

3. The closely spaced low cloud streets near Minneapolis, in the TIROS picture, may correspond to a gray area in the HRIR at about 45°N 94°W.

4. At about 35°N 82°W, the HRIR data includes a cloud pattern which appears similar to that in the TIROS picture. Although some details are dissimilar, the overall patterns appear to be alike.

5. The HRIR and TIROS both suggest intensified cloudiness along the Appalachians.

6. Breaks in the HRIR over the Ohio River valley (36°N 87°W) show as broken or scattered clouds in the TIROS pictures (Fig. 10-6).

7. The southern part of the "S" shaped clouds in the HRIR, near 36°N 91°W, was parallel to the 700 mb and 500 mb winds at both 0000 and 1200 GMT. The northern part of the "S" shaped cloud was approximately parallel to the 500 mb flow at both times and to the 700 mb flow at 1200 GMT, but at 0000 GMT the wind at 700 mb was light, and there was evidence of a weak cyclonic circulation in the area. On this basis and the comparative brightness of the cloud, it seems more likely to have been associated with the 500 mb than the 700 mb level. Surface observations in the area included fog, stratocumulus and cumulonimbus. Perhaps there were unobserved higher clouds above the fog and stratocumulus.

8. The thin curved band just west of the western edge of the main cloud mass in the HRIR, north of about 40°N, could be related to either the low level flow (Fig. 10-2) or the higher level flow (Fig. 10-3). The moderate brightness of much of this cloud (in a print available to us) suggests that it was composed mostly of low clouds, with a few higher tops. This interpretation is supported by surface reports in the area of fog and stratus or fractostratus, or both.

9. Lakes Ontario and Erie are visible in the HRIR. Some of the other lakes not visible and not covered by obvious cloud as observed by the HRIR may be invisible because of fog, which was reported from several stations in Michigan and Canada. Advection of fog over the lakes might be sufficient to obscure their shorelines, or all of a small lake.

10.5 Summary and Conclusions

The results of this case study can be summarized as follows: the upper air and vorticity maps suggest that the bright cloud observed by HRIR during Nimbus I orbit 306, south of Lake Michigan, moved north-northeastward and dissipated. Subsequently a new vorticity maximum or short wave trough formed in the Tennessee to West Virginia region and another cloud with a somewhat similar shape was observed on Nimbus I orbit 335 by HRIR. The precipitation patterns, although inadequate to show this alone, could be reconciled with this interpretation. Various phenomena in the HRIR picture of orbit 306, over the Mississippi Valley, correlate well with other synoptic data.

Near the conclusion of this case study, Widger noted that the V-shaped cloud patterns in HRIR orbits 306 (Fig. 10-1) and 335 (see Fig. 4-5) were not only geometrically similar to each other, but that both had much in common with a squall line cloud pattern observed by TIROS over Florida on 11 August 1963, and studied by Sherr and Wexler.[42] Bowley of ARACON subsequently compared these patterns with a series of TIROS photographs of squall and convective lines he was studying and determined that the same general V-shaped pattern, at times with a significant cloud mass between the legs of the V or somewhat over the more meridional leg, and relatively near the apex, was far from uncommon. Further study will be required to determine the significance of this apparently characteristic pattern, and the dynamic factors that lead to its formation. It is to be noted, however, that the V-shape, oriented as it usually is with the opening to the southwest, has some aspects of the comma- or crescent-shaped cloud patterns Rogers[6, 41] has identified as characteristic of short wave troughs. The chief differences are: (1) the frequently smaller size of the V-shaped pattern associated with convective situations, (2) the frequent presence of the bright cloud mass in the convective pattern, and (3) the greater relative western extension of the northern portion of the convective pattern. Since significant areas of convection often appear to require some upper air support for their development, these approximate geometric similarities may not be entirely fortuitous.

11. MESOSCALE FRONTAL STRUCTURE OVER NEW ENGLAND

Recently Elliott and Hovind[10] have studied the mesoscale structure of fronts near the coast of California. They found two characteristic scales of spacing; one of approximately 200 to 300 km, with an internal structure of convection bands spaced approximately 70 km apart.

The Nimbus I HRIR data[43] contain many frontal bands with mesoscale variations in infrared emission which appear to be of the scales found character-istic by Elliott and Hovind. After a search of these data, a frontal band which crossed New England during 8-9 September 1964 was chosen as most suitable for study to determine if the details seen in the HRIR appeared to be similar to those observed by Elliott and Hovind.

The HRIR data over New England from orbit 174, taken about 0525 GMT (0025 EST) on September 9, 1964, are shown in Figure 11-1. Figure 11-2 is the USWB surface analysis for 0100 EST on September 9, with the frontal positions for 8/1300 EST and 9/1300 EST indicated by dashed lines.

Many landmarks were visible in a differently exposed copy of Figure 11-1 (which, however, obliterated the detail in the frontal cloud band) to aid in a precise rectification. The rectification shown in Figure 11-3 was prepared by Mr. Robert B. Smith using the techniques he and Goldshlak developed.[18] Isochrones of the frontal positions, interpolated from those of Figure 11-2, have been added. An even more detailed rectification of that portion of the HRIR-observed cloud band which lay across New England is shown in Figure 11-4, with the frontal isochrones included. It can be noted that the surface frontal position over New England was approximately coincident with the northern edge of the cloud band, but that east of Maine the high clouds were well ahead of the front. Thus the eastern positions of the front were definitely katabatic, becoming progressively more anabatic to the west, a not uncommon condition.

The hourly rainfall amounts for the New England stations[49] were graphed in relation to a coordinate system moving with the front, as shown at the top of Figure 11-4. The order of the stations, from right to left, is roughly that measured from east-northeast to west-southwest parallel to the frontal isochrones. Thus the top of Figure 11-4 provides an approximation of the distribution of precipitation relative to the front and cloud band to as great a degree as is feasible from the available data. For convenience in comparisons, the 9/0030 EST points are marked on the precipitation plot for each station.

80°W

50°N

40°N

50°N

40°N

80°W
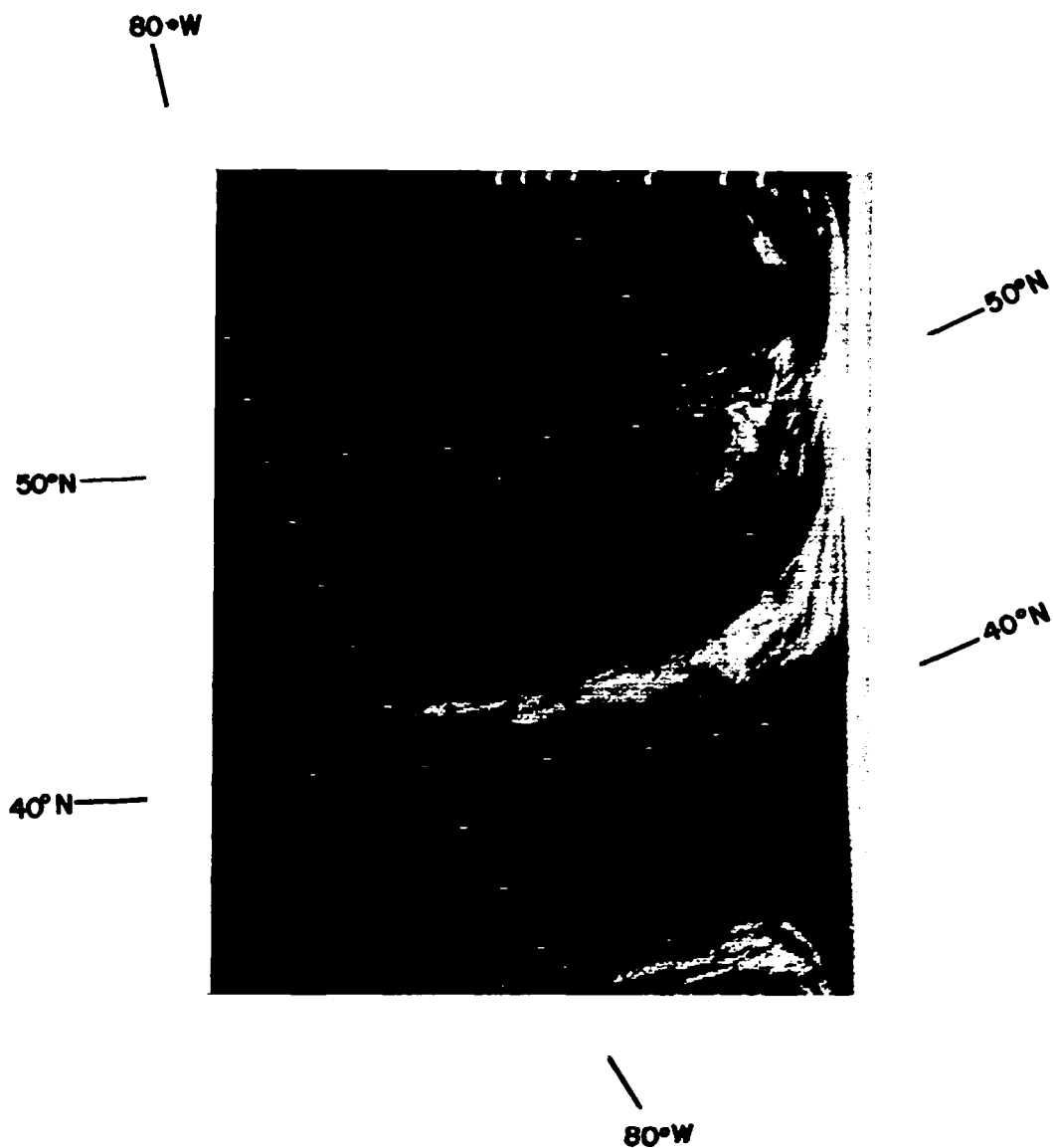
Figure 11-1   HRIR Observation of a Frontal Cloud Pattern Over New England.
A Portion of Orbit 174, about 0025 EST, September 9, 1964

Figure 11-2 Surface Synoptic Map for 0100 EST, September 9, 1964. 8/1300 and 9/1300 EST Frontal Positions are Marked by Dashed Lines.
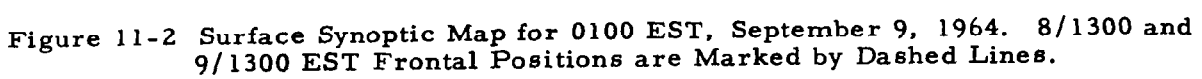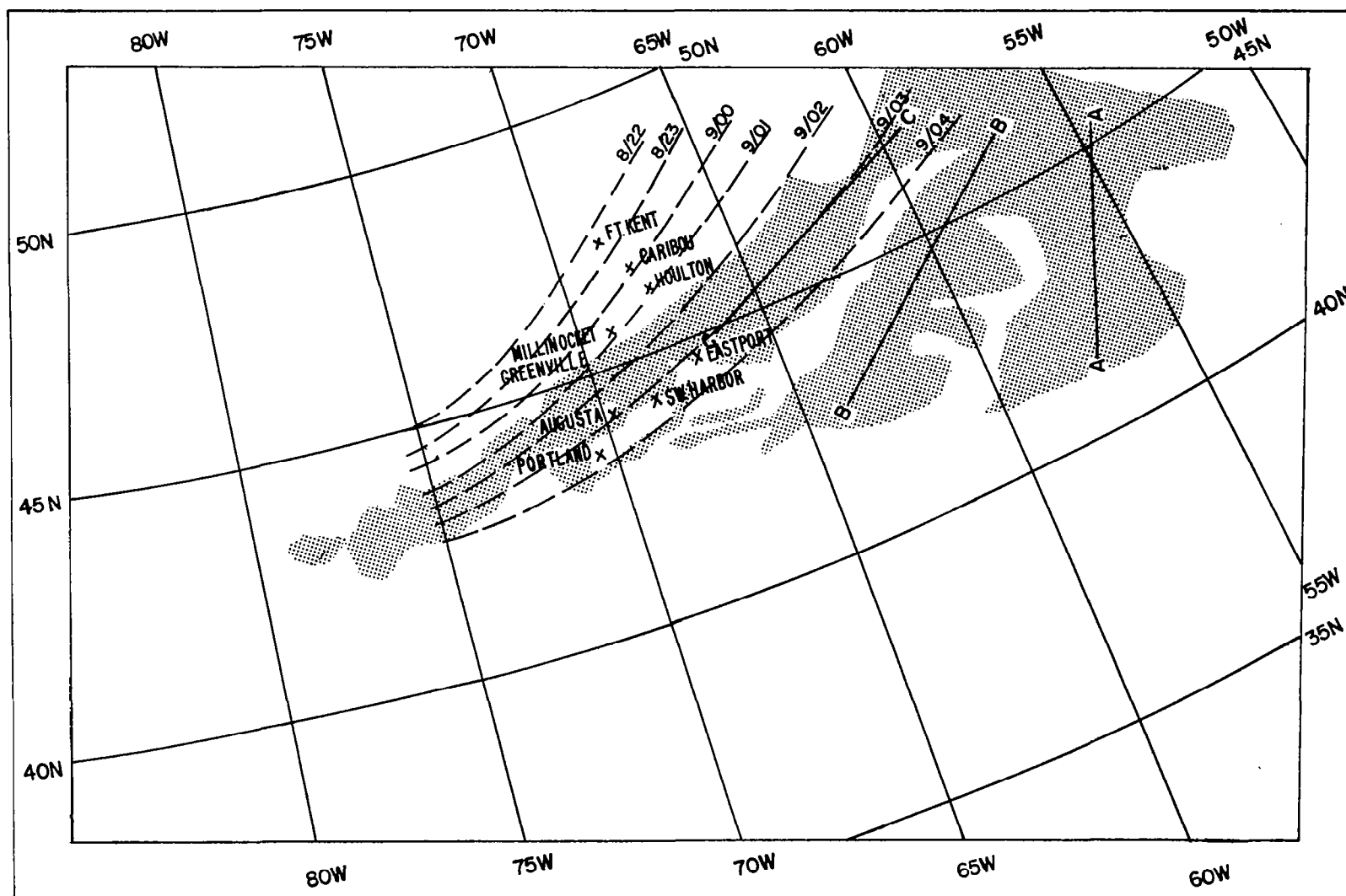
Figure 11-3   Rectification of the Cloud Pattern in Figure 11-1, with Isochrones
of Frontal Positions Labeled in EST
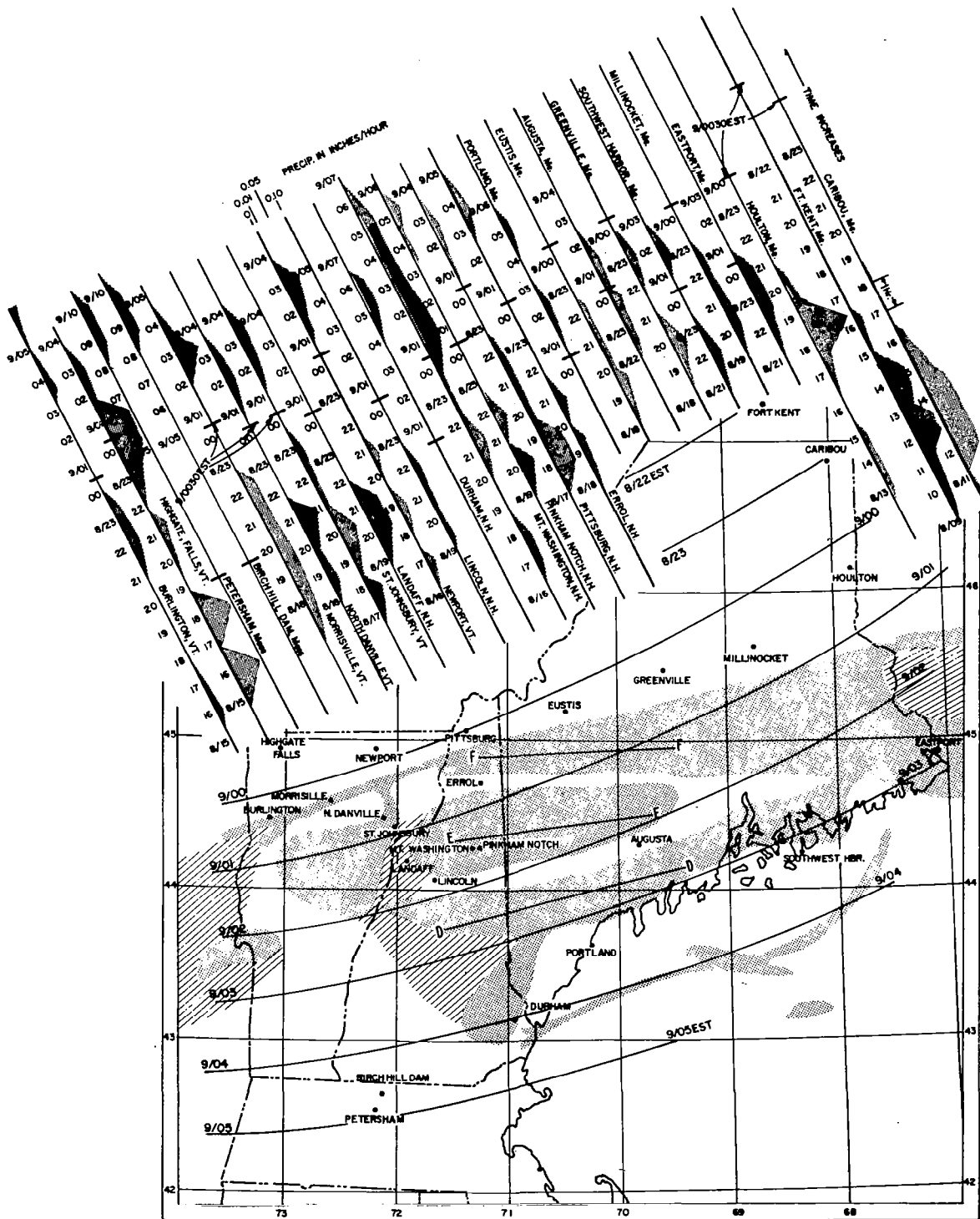
Figure 11-4   Bottom = Enlarged Rectification of the Part of the Cloud Pattern in Figures 10-1 and 10-3 Over New England, with Isochrones of Frontal Positions Labeled in EST. Locations of Stations Used in the Top Part of the Figure Are Indicated
Top = New England Precipitation data Plotted in Relation to a Coordinate System Moving with the Front. All Times Are Given in EST. Small Horizontal Bars Mark the Times of the HRIR Observation for Each Station

189

For at least eleven of the stations recording precipitation, there seems to be a reasonable correlation between the HRIR patterns of higher and lower clouds and the time sequence of precipitation and lack of measurable precipitation, although for many of the stations the intervals between the periods of precipitation are somewhat longer than would be inferred from the distances between the HRIR observed bands and the rate of frontal movement. For many of the other stations, the correlation is not unreasonable considering the small rates of precipitation generally associated with this system and the convective variations that doubtless occurred during the time period included in the top part of Figure 11-4. To the extent this case is typical, there seems reason to relate increasing whiteness in the HRIR recorded cloud bands (decreased emission and lower cloud top temperatures) with increasing probability of precipitation.

It is of further interest that the larger mesoscale bands marked AA, BB, and CC in Figure 11-3 are some 200 to 300 km apart while the lesser ones marked DD, EE, and FF in Figure 11-4 are of the order 60 km apart. It would thus appear that these mesoscale variations revealed by the HRIR data are a manifestation of the mesoscale structure reported by Elliott and Hovind.[10]

Even a cursory glance through the HRIR catalog[43] reveals that these scales of patterning are very frequently seen in the HRIR data, and that they occur in many other synoptic situations than those studied by Elliott and Hovind. They seem to be particularly frequent in cloud bands associated with stationary fronts and/or weak frontal waves (see, for example, orbit 239 near 38°N) and in the western portions of the cloud vortices associated with mature cyclonic storms (for example, the vortex near 50°N in orbit 253). Such situations will, however, be more difficult to study because they seldom undergo the rapid translations common in cold fronts.

It is further to be noted that these mesoscale patterns are far less evident, to the point where their identification becomes very highly questionable, in the TIROS pictures. This can be seen by comparing the HRIR data with the TIROS VII pictures of this same situation (Figs. 11-5 and 11-6) taken within ten hours of the time of the HRIR data. On the other hand, low cloud identification is often a serious problem in the HRIR data, making the concurrent use of both kinds of satellite sensors highly desirable.
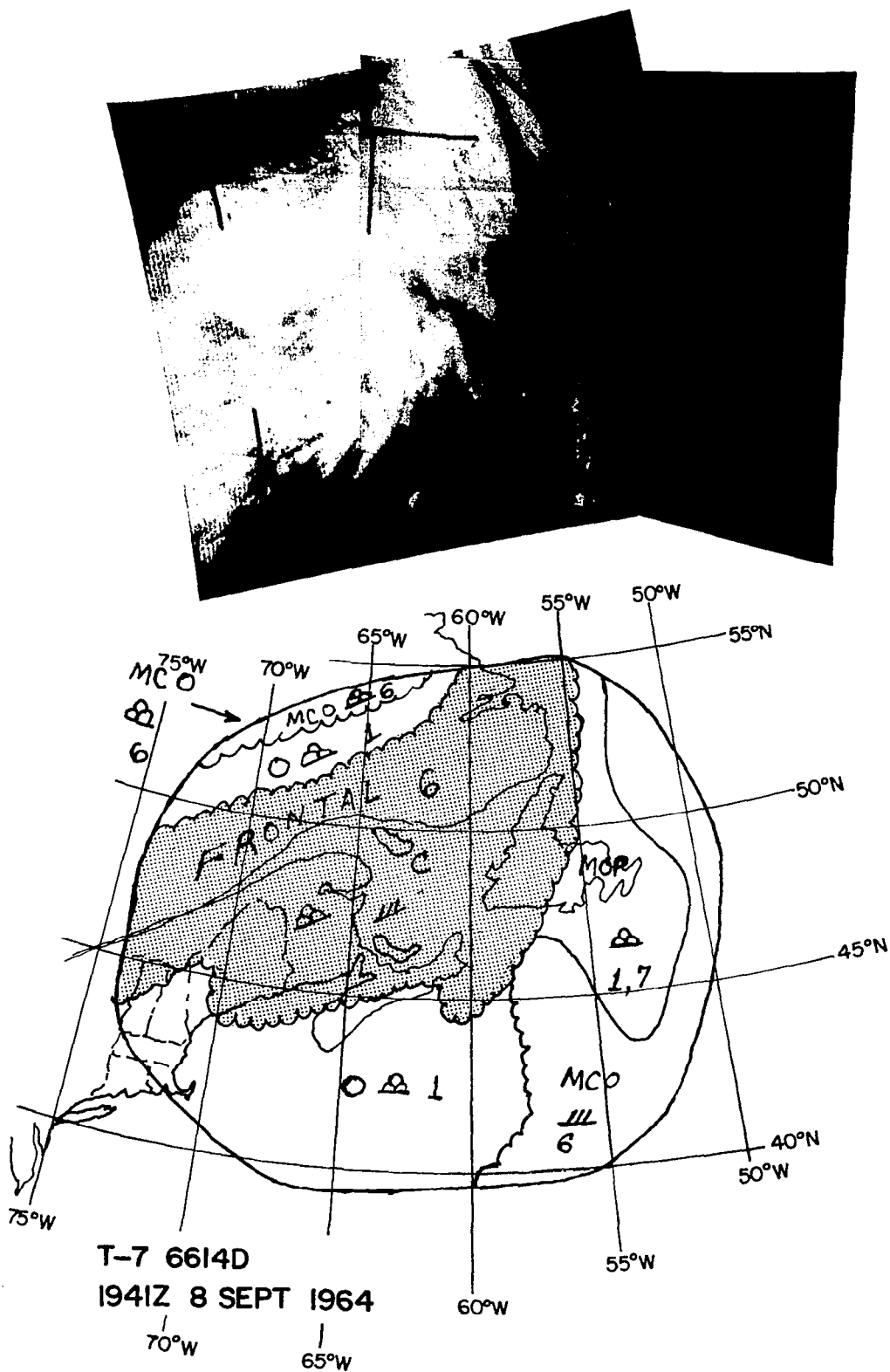
Figure 11-5 TIROS VII Mosaic and Operational Nephanalysis,
Orbit 6614 D, 1441 EST, 8 September 1964

191
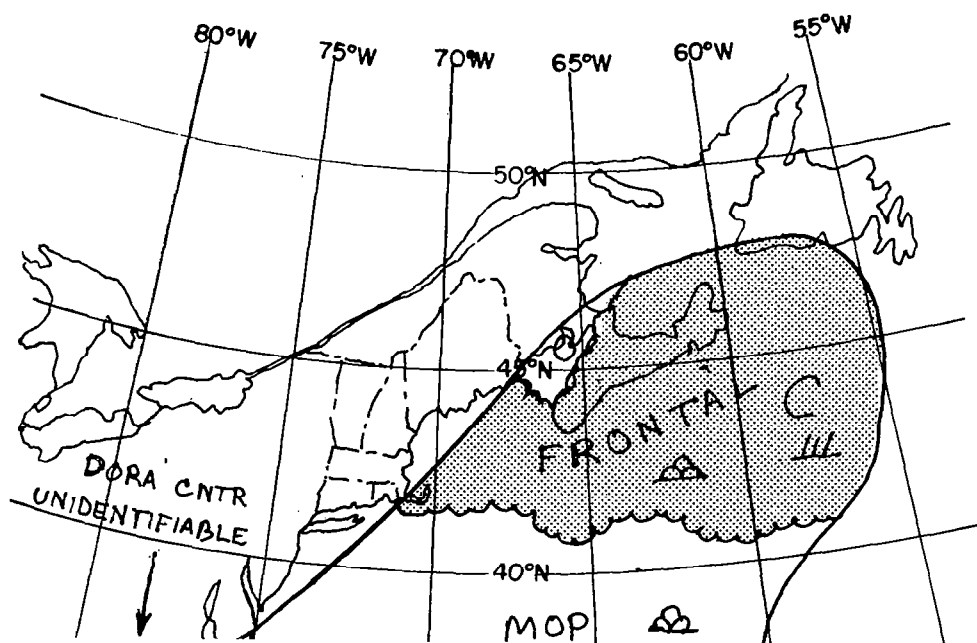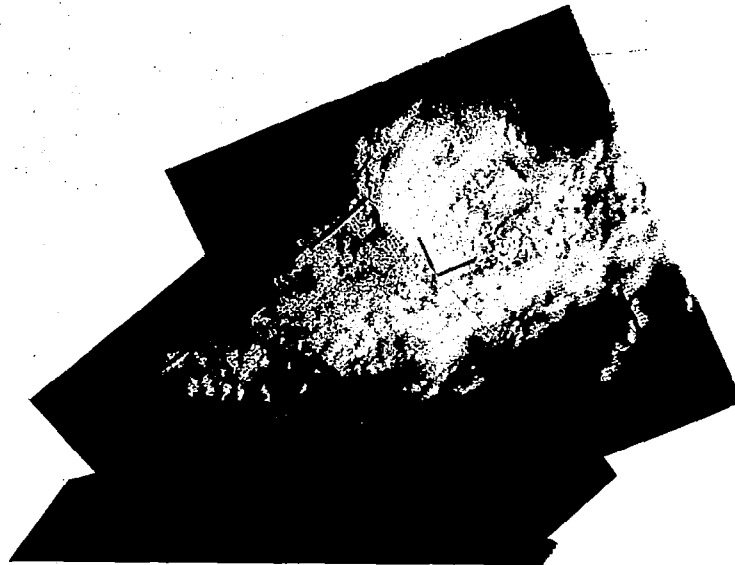
Figure 11-6 TIROS VII Mosaic and Operational Nephanalysis,
Orbit 6624 D, 0636 EST, 9 September 1964

REFERENCES

1. Aeronomy and Meteorology Division, 1965: <u>Nimbus I User's Catalog: AVCS and APT</u>, NASA, Goddard Space Flight Center.

2. Alt, J., P. Astapenko, and N. J. Ropar, 1959: "Some Aspects of the Antarctic Atmospheric Circulations in 1958," <u>IGY General Report Series No. 4</u>, National Academy of Science.

3. Bartky, C., 1965: "Theoretical Estimates of Cloud Reflection and Transmission in the Infrared," <u>Applied Optics</u>, <u>4</u>, pp. 847-852.

4. Bird, J. B., A. Morrison, and M. C. Chown, 1964: <u>World Atlas of Photography from TIROS Satellites I to IV</u>, NASA CR-98.

5. Blankenship, J. R., 1962: "An Approach to Objective Nephanalysis from an Earth-Oriented Satellite," <u>Journal of Applied Meteorology</u>, <u>1</u> (4), pp. 581-582.

6. Boucher, R. J., C. J. Bowley, E. S. Merritt, C. W. C. Rogers, P. E. Sherr, and W. K. Widger, Jr., 1963: <u>Synoptic Interpretation of Cloud Vortex Patterns as Observed by Meteorological Satellites</u>, Final Report, Contract No. Cwb-10630, ARACON Geophysics Co.

7. Boucher, R. and R. J. Newcomb, 1962: "Synoptic Interpretation of Some TIROS Vortex Patterns: A Preliminary Cyclone Model," <u>Journal of Applied Meteorology</u>, <u>1</u> (2), pp. 127-136.

8. Conover, J. H., 1959: <u>Cloud Patterns and Related Air Motions Derived by Photography</u>, Final Report, Contract No. AF 19(604)-1589, Blue Hill Meteorological Observatory, Harvard University.

9. Conover, J. H., 1962: <u>Cloud Interpretation from Satellite Altitudes</u>, Air Force Cambridge Research Laboratories, Research Note No. 81.

10. Elliott, R. D. and E. L. Hovind, 1965: "Heat, Water, and Vorticity Balance in Frontal Zones," <u>Journal of Applied Meteorology</u>, <u>4</u> (2), pp. 196-211.

11. Fett, R. W., 1964: "Aspects of Hurricane Structure: New Model Considerations Suggested by TIROS and Project Mercury Observations," <u>Monthly Weather Review</u>, <u>92</u> (2), pp. 43-60.

12   Fujita, T., 1963: A Technique for Precise Analysis for Satellite Data;
      Vol. I - Photogrammetry, Meteorological Satellite Laboratory Report
      No. 14, Meteorological Satellite Activities, U. S. Weather Bureau.

13   Gates, D. M., H. J. Keegan, J. C. Schleter, and V. R. Weidner, 1965:
      "Spectral Properties of Plants," Applied Optics, 4 (1), pp. 11-20.

14   Geophysics Research Directorate, USAF, 1960: Handbook of Geophysics,
      MacMillan Co., New York (see Chapter 16, Section 3).

15   Gibbs, W. F., 1960: "Antarctic Synoptic Analysis," Antarctic Meteorology,
      Proceedings of the Symposium Held in Melbourne, February 1959,
      Pergamon Press, New York, pp. 84-95.

16   Glaser, A. H., 1957: Meteorological Utilization of Images of the Earth's
      Surface Transmitted from a Satellite Vehicle, Final Report, Phase II,
      Contract No. AF 19(604)-1589, Blue Hill Observatory, Harvard University.

17   Goldberg, I. L., 1962: "Nimbus Radiometry," Proceedings of the Nimbus
      Program Review, NASA, GSFC, Report X-650-62-226.

18   Goldshlak, L. and R. B. Smith, 1964: Nimbus Backup Gridding: AVCS
      and HRIR, Technical Report No. 1, Contract No. NAS 5-3253, ARACON
      Geophysics Co.

19   Gray, T. I., Jr., 1960: Forecasting for Antarctic Areas (Unpublished;
      some of the concepts appear to be those presented by Gray in the discussion
      on pages 138-141 and 310-313 of Antarctic Meteorology, Proceedings of
      the Symposium Held in Melbourne, February 1959, Pergamon Press,
      New York.)

20   Hannay, A. K., 1960: "Cold Outbreaks in Southern Australia in Relation
      to Sub-Antarctic Circulations," Antarctic Meteorology, Proceedings of
      the Symposium Held in Melbourne, February 1959, Pergamon Press,
      New York, pp. 153-175.

21   Hubert, L. F., 1961: "A Subtropical Convergence Line of the South
      Pacific: A Case Study Using Meteorological Satellite Data," Journal
      of Geophysical Research, 66 (3), pp. 797-812.

22   Jacobs-Haupt, I., 1963: "TIROS Observations Over the Mediterranean and
      North Africa," Rocket and Satellite Meteorology, North-Holland Publishing
      Company, Amsterdam, pp. 322-332.

23   Kadlec, P. W., 1963: An In-Flight Study of the Relation Between Jet Stream, Cirrus, and Wind Shear Turbulence, Final Report, Contract No. Cwb-10356, Eastern Air Lines, Inc., Miami.

24   Kadlec, P. W., 1964: A Study of Flight Conditions Associated with Jet Stream Cirrus, Atmospheric Temperature Change, and Wind Shear Turbulence, Final Report, Contract No. Cwb-10674, Eastern Air Lines, Inc., Miami.

25   Karelsky, S., 1960: "The Surface Circulations Over Southern Ocean, Southern Indian Ocean, Australasia, and Southern Pacific Ocean Regions During 1957 and 1958," Antarctic Meteorology, Proceedings of the Symposium Held in Melbourne, February 1959, Pergamon Press, New York, pp. 293-310.

26   Kellogg, W. W., K. J. K. Buettner, and E. C. May, 1964: Meteorological Satellite Observation of Thermal Emission, Memorandum RM-4392-NASA, under Contract No. NASr-21(07), The RAND Corporation.

27   Kuo, H. L., 1965: "On the Formation and Intensification of Tropical Cyclones Through Latent Heat Release by Cumulus Convection," Journal of Atmospheric Sciences, 22 (1), pp. 40-63.

28   Maykut, E. S., 1964: "An Experiment in Objective Nephanalysis Using Proposed HRIR Satellite Infrared Radiation Data," Journal of Applied Meteorology, 3 (3), pp. 215-225.

29   Merritt, E. S., 1962: "TIROS-Revealed African Disturbances Related to Atlantic Hurricanes," (In Huang, T. S., E. S. Merritt, and A. H. Glaser, Meteorological Satellite Analyses), Final Report, Contract No. AF 19(604)-5582, Allied Research Associates, Inc.

30   Merritt, E. S., 1963: Fleet Applications, Meteorological Operational Satellites (Antarctic Area), Final Report, Contract No. N189(188)-56507A, ARACON Geophysics Co.

31   Merritt, E. S., 1964: "Easterly Waves and Perturbations: A Reappraisal," Journal of Applied Meteorology, 3 (4), pp. 367-382.

32   Merritt, E. S., 1965: Analysis and Forecasting Techniques Utilizing Meteorological Satellite Data, Final Report (Part A), Contract No. N189(188)-58014A, ARACON Geophysics Co.

33 Nagle, R. E., 1962: Comparison of Time Integrated Radar Detected Precipitation with Satellite Observed Cloud Patterns, Scientific Report No. 1, Contract No. AF 19(628)-284, Stanford Research Institute.

34 Nagle, R. E., and S. M. Serebreny, 1962: "Radar Precipitation Echo and Satellite Cloud Observations of a Maritime Cyclone," Journal of Applied Meteorology, 1 (3), pp. 279-295.

35 Project Staff, Dept. of Oceanography and Meteorology, 1958: Synoptic Analysis and Forecasting Applications of Radar Weather Observations, Final Report, Contract No. AF 19(604)-1564, A and M College of Texas.

36 Rastorguev, V. I., and J. Alvarez, 1958: "Description of the Antarctic Circulations Observed from April to November 1957 at the IGY Antarctic Weather Central Little America Station," IGY General Report Series No. 1, National Academy of Sciences.

37 Renard, R. J., and L. C. Clarke, 1965: Experiments in Numerical Objective Frontal Analysis, paper presented at the 45th Annual Meeting of the American Meteorological Society, New York (and subsequently submitted to the Monthly Weather Review.)

38 Riehl, H., 1963: "On the Origin and Possible Modification of Hurricanes," Science, 141 (3585), pp. 1001-1010.

39 Sadler, J. C., 1963: "Utilization of Meteorological Satellite Data in Tropical Meteorology," Rocket and Satellite Meteorology, North-Holland Publishing Company, Amsterdam, pp. 333-356. (Also published as AFCRL Research Note, AFCRL 62-829.)

40 Sherman, L., 1956: "On the Wind Asymmetry of Hurricanes," Journal of Meteorology, 13 (5), pp. 500-503.

41 Sherr, P. E., and C. W. C. Rogers, 1965: The Identification and Interpretation of Cloud Vortices Using TIROS Infrared Observation, Final Report, Contract No. Cwb-10812, ARACON Geophysics Co.

42 Sherr, P. E., and R. Wexler, 1965: Operational Use of TIROS Radiation Measurements, Final Report, Contract No. AF 19(628)-4074, ARACON Geophysics Co.

43   Staff Members, Aeronomy and Meteorology Division, 1965: Nimbus I High Resolution Radiation Data Catalog and User's Manual, Vol. 1, Photofacsimile Film Strips, NASA, Goddard Space Flight Center.

44   Stampfl, R., 1963: The Nimbus Spacecraft and Its Communication System as of September 1961, NASA Technical Note D-1422.

45   Stampfl, R., and H. Press, 1962: "Nimbus Spacecraft System," Aerospace Engineering, 21 (7), pp. 16-28.

46   Sutcliffe, R. C., 1952: "Principles of Synoptic Weather Forecasting," Quarterly Journal of the Royal Meteorological Society, 78 (337), pp. 291-320.

47   Timchalk, A., L. F. Hubert, and S. Fritz, 1965: Wind Speeds from TIROS Pictures of Storms in the Tropics, Meteorological Satellite Laboratory Report No. 33, National Weather Satellite Center, U. S. Weather Bureau.

48   U. S. Navy Weather Research Facility, 1960: Notes on Antarctic Weather Analysis and Forecasting, NWRF 16-1260-038.

49   U. S. Weather Bureau, 1964: Hourly Precipitation Data, New England, 14 (9), (for September 1964).

50   Van Loon, H., 1956: "Description of a Blocking Situation in the Central South Atlantic Ocean," NOTOS, 5 (2), pp. 117-119.

51   Van Loon, H., 1956: "Blocking Action in the Southern Hemisphere, Part I," NOTOS, 5 (3), pp. 171-178.

52   Widger, W. K., Jr., 1964: "Possible Approach to Cross-Track Radiometric Scanning from a Cartwheel Satellite," Journal of Spacecraft, 1 (4), pp. 427-429.

53   Widger, W. K., Jr., 1965: "Limitations to Nighttime Visual Observations from Satellites," Oceanography from Space, Woods Hole Oceanographic Institute, Ref. 65-10, pp. 49-50.

54   Widger, W. K., Jr., and A. H. Glaser, 1963: A Rationale for Geographic Referencing of Meteorological Satellite Data, Technical Report No. 1, Contract No. NAS 5-1204, ARACON Geophysics Co.

55   Widger, W. K., Jr., P. E. Sherr, and C. W. C. Rogers, 1964: Practical Interpretation of Meteorological Satellite Data, Final Report, Contract No. AF 19(628)-2471, ARACON Geophysics Co. (republished as Air Weather Service Technical Report 185).

56   Widger, W. K., Jr., and R. B. Smith, 1965: <u>Preliminary Results from</u>
      <u>a Meteorological Evaluation of Nimbus I HRIR Data</u>, Preliminary Scientific
      Report, Contract No. NAS 5-9554, ARACON Geophysics Co.

57   Zipser, E. J., and N. L. LaSeur, 1964: <u>Studies of TIROS Data Over the</u>
      <u>Tropical Atlantic Supplemented by Concurrent Aircraft Photography</u>, Final
      Report, Grant No. WBG 16, U. S. Weather Bureau, Florida State
      University.

APPENDIX A

QUANTITATIVE RELATIONSHIPS APPLICABLE TO

DAYTIME HRIR OBSERVATIONS*

The interpretation of daylight HRIR observations is complicated by the fact that the contribution of reflected solar radiation is normally significant in the 3.4 to 4.2μ wavelength region. The amount of the contribution depends on the solar zenith angle, and on the reflectivity of the surface. It may also depend on absorption of solar radiation, at HRIR wavelengths, by atmospheric constituents. This appendix presents calculations and a diagram which may aid in the interpretation of the daylight HRIR data. It will be assumed here that absorption by the intervening clear atmosphere is negligible in the 3.4 to 4.2μ region; this assumption is approximately valid except, perhaps, in a very hazy atmosphere.

Let the surface under view be illuminated uniformly by solar radiation of intensity $S(\lambda)$ over the wavelength interval $\Delta\lambda$. For isotropic scattering from a perfectly reflecting surface, and the sun in the zenith, the total amount of solar radiation that would be measured by the HRIR sensor is:

$$I = \frac{1}{\pi} \Sigma f S(\lambda) \qquad (1)$$

where f is the filter characteristic of the sensor over the wavelength interval, and the summation extends over the entire spectral interval where the HRIR is sensitive. The total radiation measured by the sensor for a surface of reflectivity r and emissivity ϵ is the sum of the reflected solar radiation and the emitted thermal radiation:

$$R = r I \cos Z + \epsilon B \qquad (2)$$

where Z is the solar zenith angle, and B is the effective blackbody radiation of the surface, corrected for the filter characteristics of the sensor. Since

---

* Dr. Raymond Wexler contributed significantly to the preparation of this appendix.

$\epsilon = 1 - r$ (Kirchoff's law) the equation may also be written:

$$R = r I \cos Z + (1 - r) B \qquad (3)$$

It is apparent from this equation that if the surface temperature is known, then, since B is a known function of that temperature, HRIR measurements may be used to obtain information on the reflectivities (or emissivities) at HRIR wavelength of various surfaces. On the other hand, for an assumed reflectivity, the cloud top temperature can be estimated from a daylight HRIR observation. Our present knowledge of reflectivities at wavelengths of 3.5 to 4.0μ is relatively scanty.

Table A-1 shows computations of the effective solar radiation (I) at mean solar distance from the earth and at zero solar zenith angle. Values of S (λ) were obtained from Dr. P. Gast of AFCRL and represent revisions of values which have appeared in the Handbook of Geophysics.[14] The effective spectral response values (f) were interpolated from Figure 10 and Table III, page 13 of the Nimbus I HRIR Catalog and User's Manual.[43] The computed value of I is 1.34 wm^{-2} ster^{-1}.

Reflectivities of various surfaces in the 3.4 to 4.2μ region are probably intermediate between those in the visible and a reflectivity of near zero which corresponds to those farther in the infrared. Terrestrial radiators can be considered as approximately blackbodies (r = 0, or $\epsilon = 1.0$) at wavelengths between 4 and 40μ. Thick clouds have reflectivities of 0.5 to 0.8 in the visible, whereas in the infrared (essentially 4 to 40μ) their reflectivities are near zero. One would therefore expect the reflectivities of clouds at 3.4 to 4.2μ to be near or below 20%. The reflectivities of other surfaces should be less.

Few experimental observations of reflectivities of terrestrial surfaces exist. Theoretical calculations by Bartky[3] indicate that the reflectivity at 3.5 and 4.3μ for thick water clouds is 13% for isotropic single scattering and about 37% for isotropic multiple scattering. Experimental observations (Gates et al[13]) indicate that the reflectivity of plants is about 2% in the 3.5 to 4.0μ region. The reflectivity of a water surface is also about 2%.

Figure A-1 enables one to determine reflectivity from the measured HRIR radiation (abscissa) and the temperature of the radiating surface (ordinate). *

---

* In Figure A-1, the temperatures of the observed surfaces are valid regardless of emissivity.

TOTAL RADIATION MEASURED BY HRIR SENSOR EXPRESSED AS EQUIVALENT BB TEMP (°K)
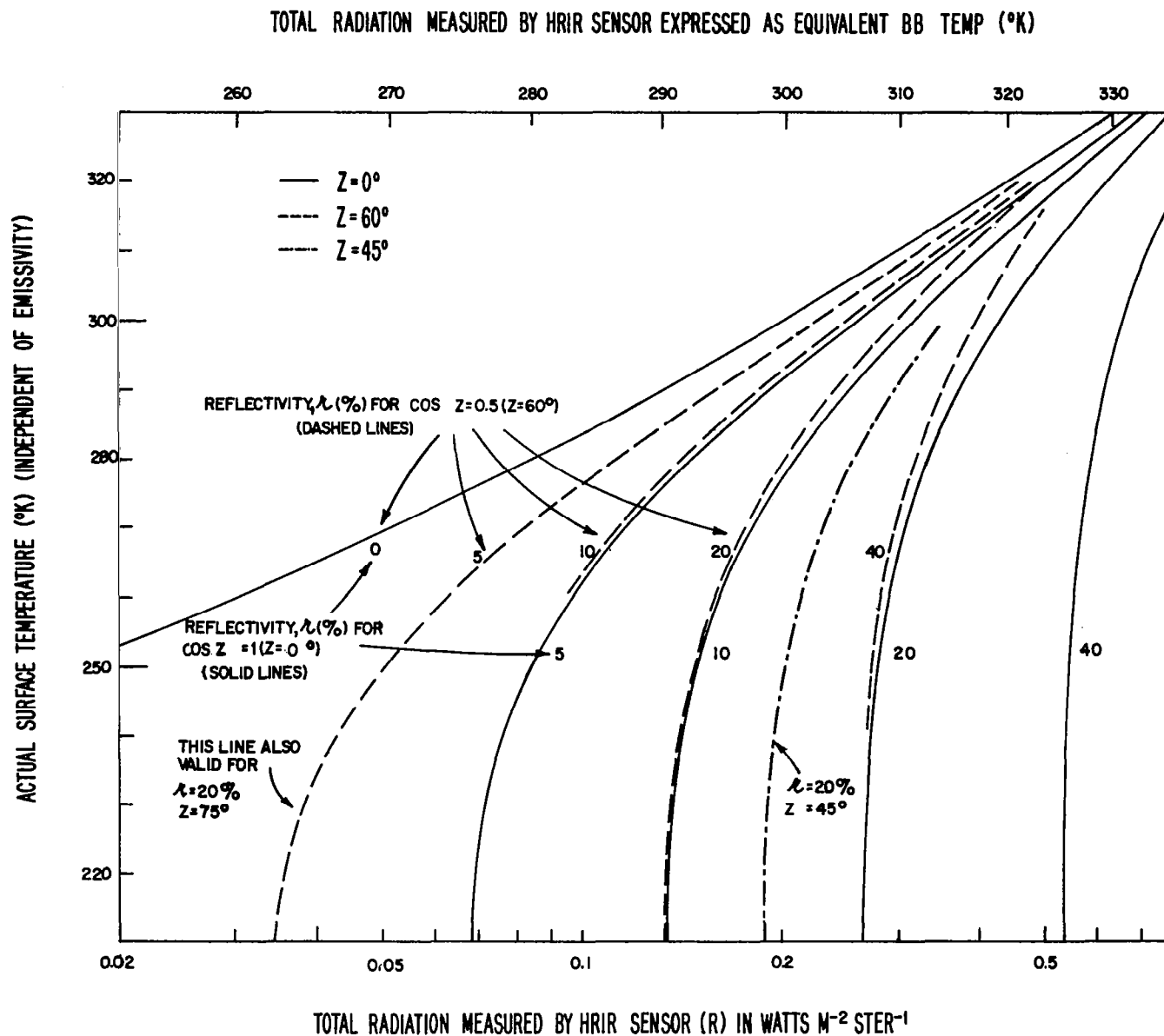
Figure A-1 Quantitative Relationships between Temperature of a Radiating Surface, Total Radiation as Measured by HRIR, and Solar Reflectivity

Table A-1. Effective Spectral Radiance of Sun at Normal Incidence
for Nimbus I HRIR Sensor

Wavelength interval $\Delta\lambda\ (\mu)$	Solar spectral irradiance $S(\lambda)$, normal to sun's rays, outside atmosphere (watts m^{-2})	Effective spectral response of sensor, f	Effective solar spectral radiance, $\frac{1}{\pi}\ f\ S(\lambda)$ watts m^{-2} sterad^{-1}
3.3 - 3.4	1.70	0.022	0.012
3.4 - 3.5	1.53	0.138	0.067
3.5 - 3.6	1.38	0.365	0.160
3.6 - 3.7	1.24	0.647	0.255
3.7 - 3.8	1.12	0.647	0.230
3.8 - 3.9	1.02	0.678	0.220
3.9 - 4.0	0.93	0.655	0.194
4.0 - 4.1	0.84	0.662	0.177
4.1 - 4.2	0.75	0.090	0.021
TOTAL			$I = 1.336$ watts m^{-2} sterad^{-1}

Lines of equal reflectivity from 0 to 40% are drawn for solar zenith angles of 0°, or cos Z = 1 (solid lines); and for solar zenith angles of 60°, or cos Z = 0.5 (dashed lines). It is seen that, for temperatures between 210° and 290° K, the solid lines (Z = 0°) for a given reflectivity, r, are very close to the dashed lines (Z = 0.5°) for a reflectivity of 2 r. Hence, for all practical purposes, the solid lines could also be considered as labelled as r/cos Z; the error in radiance would then be about 6% at 290° K, about 3% at 270° K, and less at lower temperatures. It is seen that at warm temperatures (> 300° K) the contribution of the earth's radiation becomes dominant, and little information may be obtained on reflectivities in this region.

Figure A-1 can be used for either research or operational purposes. For research, HRIR observations concurrent with measured temperatures of radiating surfaces can be used to increase the existing knowledge as to the emissivities and reflectivities of natural surfaces, including cloud tops.

For operational purposes, in the case of clouds, a reflectivity of 20% should be assumed until more accurate values are determined. * Under this assumption, the solar zenith angle (which can be computed from merely a knowledge of geographical position and time) and an HRIR measurement permit an estimate of the approximate cloud top temperature. When better values of cloud reflectivities become available, a revision of Figure A-1 will be in order to provide specific lines, at several solar zenith angles, for the best value of r for clouds.

While in principle ground surface and water surface temperatures can be estimated from Figure A-1, using the appropriate reflectivities as estimated above, the meaning and application of such a surface temperature under conditions of direct solar illumination are often questionable.

---

* For this reason, lines for r = 20% for several additional zenith angles have also been included in Figure A-1.

APPENDIX B

APPROXIMATE RECTIFICATIONS OF HRIR DATA USING

PHOTOGRAPHIC TECHNIQUES

B. 1 Introduction

The present method of recording the Nimbus I HRIR data on film strips such as those in Figures 4-1, 4-2, etc., of this report, and in Appendix C of the Nimbus I High Resolution Radiation Data Catalog and User's Manual, [43] results in various distortions, as described in Section 2.3. For many purposes (such as: determinations of cloud dimensions, shapes and orientations; cloud identification; mosaicing; comparisons with conventional data; etc.), it would be desirable to remove the foreshortening distortions near the horizons. This appendix describes and illustrates simple means by which some of this distortion can be removed photographically. While it has not been feasible in this study to obtain perfect rectifications, our intent here is: (1) to demonstrate the value of rectified data, with the hope that this may lead to consideration of rectified recording of the HRIR data from future Nimbus; and (2) to present a useful rectification technique applicable to the HRIR data from Nimbus I.

B. 2 Mechanics of Rectification

Figure 2-3 of this report shows the geometry of the projection equivalent to that used for photofacsimile recording of the HRIR data. The compression toward the horizon is evident. This compression may be counteracted by projecting the HRIR film image onto a suitably curved surface, which then represents the curvature of the surface of the earth.

To a reasonable approximation, each revolution of the HRIR mirror can be considered to scan the earth along the great circle which passes through the sub-satellite point and is perpendicular to the instantaneous velocity vector of the satellite. The length of arc from horizon to horizon is a function only of satellite height; for Nimbus I, this distance on the earth varied between about 40 and 58 degrees of great circle arc, depending on the position in orbit relative to perigee. At the horizon, the HRIR line of sight is, of course, tangent to the earth. Although each revolution of the mirror scans the earth along a great circle, the motion of the

satellite in orbit causes successive scan lines to be presented on the film strips as if the sensor had viewed a portion of a right circular cylinder. * Such a cylinder is easy to construct. Suitable projection of an HRIR film strip onto the cylinder simulates the scan geometry, and much of the distortion is thereby removed.

For the rectifications discussed and illustrated in this appendix, a semi-cyclindrical cradle was made from cardboard and used to support photographic enlarging paper. The dimensions of the cradle are not critical, and should be designed to suit the available optics. For a 90 mm, f 4.5 lens and the enlarger used (Wollensak enlarging raptar), a cradle with a 21 cm diameter and approximately 46 cm long, placed so the lowest part of the cylinder was about 60 cm from the enlarging lens, was found to be satisfactory.

Two cradles were actually constructed to these dimensions: one concave and the other convex. The geometry for the two surfaces is different, of course, but they both provide an approximate rectification by projecting the part of the image near the horizon onto those portions of the cylinder which are nearly parallel to the projection rays, thereby expanding the projected image in the direction along the scans.

The cradles were centered beneath the enlarging camera by projecting a portion of an HRIR negative onto a cradle and properly adjusting its position. For the convex surface, the enlarger height was adjusted until each horizon fell just at the edge of the cradle.

One of the problems with the setup, which could not be fully overcome, was that of depth of field (that is, attempting to keep all parts of the image in focus). Although sharp focus throughout the field of view was not achieved with the setup used, the images were adequately sharp for many purposes.

Another problem was that the length of film which could be rectified at any one time was rather small, corresponding to only 15 to 20 degrees of latitude. A different lens might have been better in this regard, but again this refinement was not vital for our purposes.

Still another problem was that of achieving proper exposure. Since the lateral images are spread over a greater length of paper than the central images, the differences in exposure had to be compensated by hand dodging; that is, manually shielding parts of the paper with an opaque surface moved between the lens and the

---

* Each great circle scanned by the HRIR being equivalent to the intersection of the cylinder and a plane perpendicular to the axis of the cylinder.

enlarging paper. Even with hand dodging, some of the images in the rectified pictures are too light toward the horizon. For the concave cradle, still another exposure problem was noted; the whole paper could not be exposed simultaneously because reflections from one side to the other tended to diffuse the image. To overcome this, black paper was laid against one side while the other was exposed. This effect is evident in the rectified images of the second case discussed below (Section B.3.2).

B.3 Results

This section illustrates and discusses three sets of rectifications which were prepared using the simple technique discussed above. *

B.3.1

The first case was a daylight strip over the Mediterranean area (orbit 207), taken on 11 September 1964. It was selected for rectification because such distinctive landmarks as Italy, the Gulf of Sidra, and Cirenaica are included toward the eastern horizon; although severely distorted in the normal HRIR recording format, they are still clearly recognizable. Figure B-1 shows enlargements of portions of the film strip, both unrectified and "rectified."

In these specific enlargements of a daylight HRIR case, the water usually appears light, because of its relatively low reflectivity compared with that of land and cloud. † The dark areas west of 10°W are produced by clouds, as are the many dark areas over northern Europe.

The right-hand side of the unrectified strip, near the horizon, shows the apparent elongation parallel to the horizon mentioned in Section 2.3. This results from foreshortening of the objects there. This effect is also apparent in the white areas near the western horizon.

---

* We are indebted to Mr. Donald Harper of Allied Research Associates, Inc., for his invaluable assistance during the preparation of these rectified photographs.

† For simplicity of processing when preparing the rectification, the prints in Figure B-1 are presented in "normal" HRIR photographic polarity rather than the reversed polarity recommended, for daylight cases, earlier in this report. The differences can be noted by comparing Figure B-1 with the same data, presented in reversed polarity, in Figure 2-4.

The rectified picture was projected onto the convex cylindrical surface. Despite such flaws as improper exposure and improper focus, the overall appearance is a great improvement over that in the unrectified picture. This is especially evident in the shapes of Italy and the Adriatic Sea, but it is also clearly noticeable in the orientation and shape of the north coast of Africa between Tunisia and Cirenaica. The shape of the Gulf of Sidra, in particular, is very much improved.

Improvement has also occurred toward the western horizon, but, because of the subject matter there (irregular cloudiness) and problems of focus and exposure, it is less obvious than toward the east. Two places where improvements can be noted are: (1) at 40°N, west of 10°W, where a pattern made by a number of white areas appeared to have the shape of an ellipse or diamond, but is more nearly circular in the rectified picture; and (2) between 46°N and 48°N, where changes in prominent white shapes are also evident.

(A few of the geographical features in the enlargements perhaps deserve mention here for their general interest. In the Sahara Desert, at indicated latitudes of 26° to 28°N between 6° and 10°E, there are lighter areas associated with the Ahaggar Plateau, which has extensive areas more than 1000 meters above sea level. Similarly, the Pyrenees Mountains at about 44°N and 0° (indicated) are lighter than surrounding terrain; presumably, with a considerable area more than 2000 meters above sea level, they are cooler than the surrounding areas. The Pyrenees are much darker than the Mediterranean Sea, however, because reflectivity from the mountains is greater than from the sea and the greater reflectivity of the mountains more than compensates for the greater thermal emission from the sea. The straight coastline of France along the Bay of Biscay shows clearly because of the whiteness of the ocean, as does the estuary of the Garonne River. The eastern portion of the English Channel appears as a whitish area at 52°N 0°; and both England and Ireland can be seen indistinctly through clouds at the upper edge of the picture. Some of the meteorological aspects of the northwestern parts of Figure B-1 were discussed in Section 4.6.1 of Reference 56.)

B. 3. 2

The second case selected for rectification was that of a striking spiral cloud pattern, at about 47°N 155°E, viewed on orbits 252 and 253 on 14 September 1964. This case is discussed in detail in Section 4.2.3 of Reference 56. Figure B-2 presents both unrectified (top) and rectified (bottom) prints, with the earlier orbit at the right and the later orbit at the left to approximate the relative geographic relationships of the two strips.
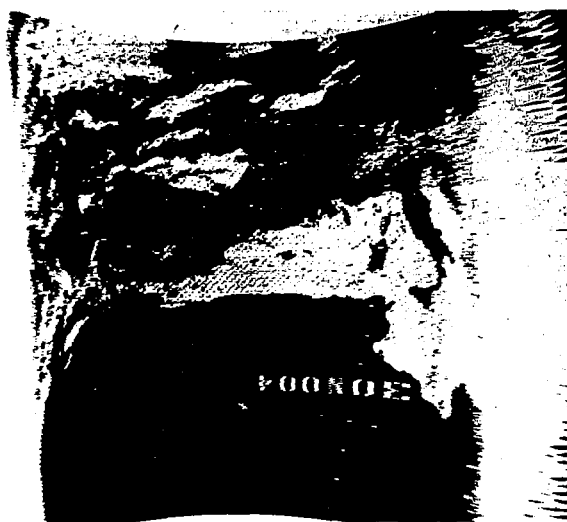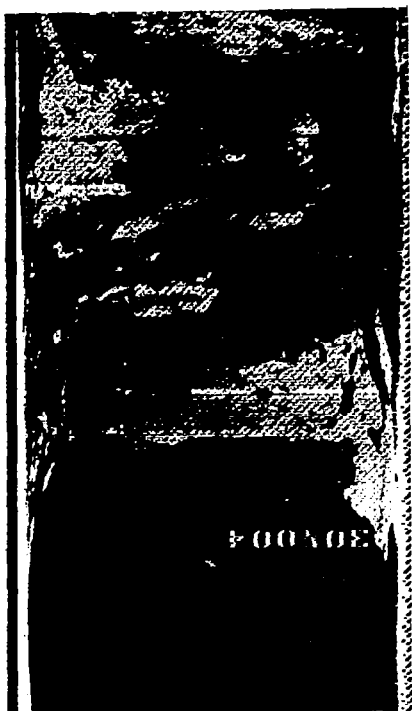
Figure B-1   Unrectified and Rectified Portion of Orbit 207

Although the rectified pictures are obviously imperfect, the improvement in the depiction of the vortex is striking. Most of the bands of the vortex can be matched from the rectified image of orbit 252 to that of 253; and a much better impression of the true shape and dimension of the vortex is provided.

The value, to the meteorologist, of the rectified image is demonstrated in this case by the fact that, from the unrectified image, there is some uncertainty as to whether the vortex has two or three bands to the west of the inner spiral band; the rectified image clearly shows three. Although synoptic meteorologists concerned only with large scale processes may have little interest in such detail, a forecaster specifically concerned with the area, or a research meteorologist, may find such information very valuable.

B.3.3

This case was included to demonstrate that: (1) from a nominal Nimbus altitude (930 km), there is enough overlap between HRIR data for successive orbits, even at the equator, to allow mosaics to be prepared; and (2) that rectification aids this technique through simplifying cloud identification, since it provides truer cloud shapes and orientations.

Along the orbits selected, the Nimbus altitude increased from about 640 km at 10°N to 730 km at 10°S. At an altitude of 640 km, the distance to the horizon is between 24 and 25 degrees of great circle arc.[12] Since successive descending nodes were also 24 to 25 degrees apart,[43] considerable overlap between successive HRIR strips must exist.

Figure B-3 shows unrectified and rectified enlargements for portions of orbit 343 (20 September 1964) on the right, and corresponding enlargements for orbit 344 on the left. The clouds in the unrectified photographs are adequate to demonstrate overlap between the successive passes, as shown by the pairs of arrows. This case is so clear-cut that rectification at first appears to add less information than in the cases discussed above. Nonetheless, after closer examination, the information gain is significant. The rectification of orbit 344 corrects the shape of the cloud on the horizon just north of 10°N, and it conforms much more closely to its shape in orbit 343. In the unrectified photographs, the cloud bands at 0 to 6°N appear to curve in opposite directions, so that their correct orientations are difficult to determine. In the rectified pictures, the orientations of the bands are nearly identical. Rough measurements of the band which reaches the equator at 56°E indicate rectification corrects its apparent orientation by about 20°.
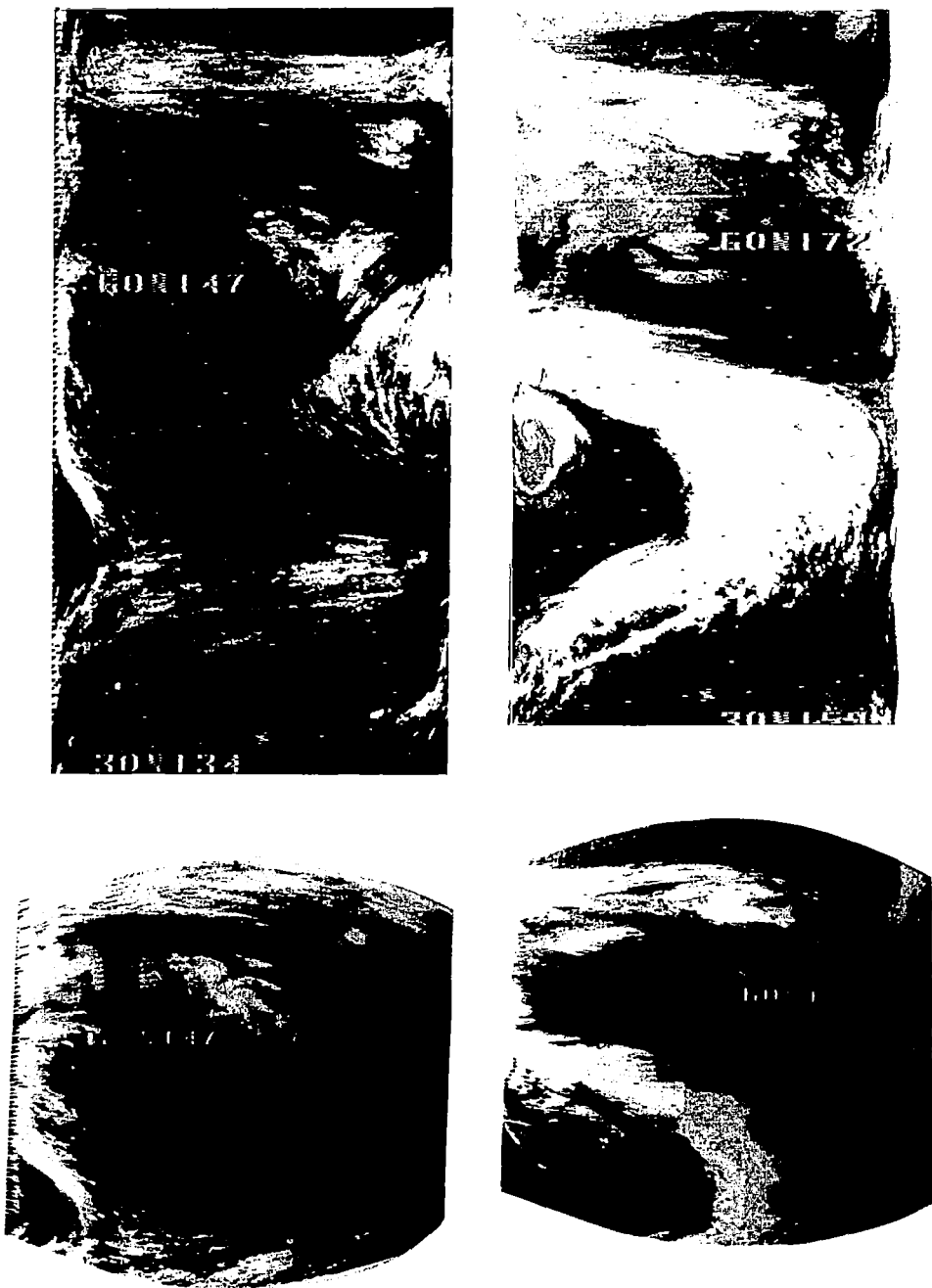
Figure B-2   Unrectified and Rectified Portions of Orbits 252 and 253

B. 4 Conclusions

Our experience with rectified HRIR images, such as those in Figures B-1, B-2, and B-3, leads us to present two suggestions, as discussed below.

B. 4. 1 The Desirability of Rectified Recording

We suggest that HRIR film strips from future satellites be rectified concurrently with their photofacsimile recording in the Nimbus ground station. This suggestion is based not only on our experience with rectified Nimbus I HRIR data as presented in Section B. 3, but also on the problems we have encountered when mosaicing or nephing unrectified HRIR film strips (see Section 3 of this report).

Modification of ground station equipments and procedures would obviously be necessary to provide such rectification. While we are not presently prepared to suggest detailed recorder designs, at least three possibilities exist:

1. An optical analog, with the film assuming a cylindrical form as it passes across the scanning plane of the recorder. This is essentially equivalent to the photographic rectification procedures described above, and does not appear to require further discussion.

2. A variable rate of recorder scan, with the rate of scan a function of the phase of rotation of the HRIR mirror. Obviously, the recorder must scan faster near the horizons as compared to its rate across the subsatellite point. It presently appears this approach would be preferable to the optical analog, but probably less attractive than the third alternative, a digital approach. Some aspects of the variable scan approach are discussed in Section B. 4. 1. 1 .

3. A digital technique, which would require only a relatively simple digital signal processor placed between the input HRIR data (which would normally come from playback of a tape recording) and the present HRIR recorder. For several reasons, including the fact it avoids the need for modifying the recorder itself, this approach seems particularly interesting. It is described in Section B. 4. 1. 2 .
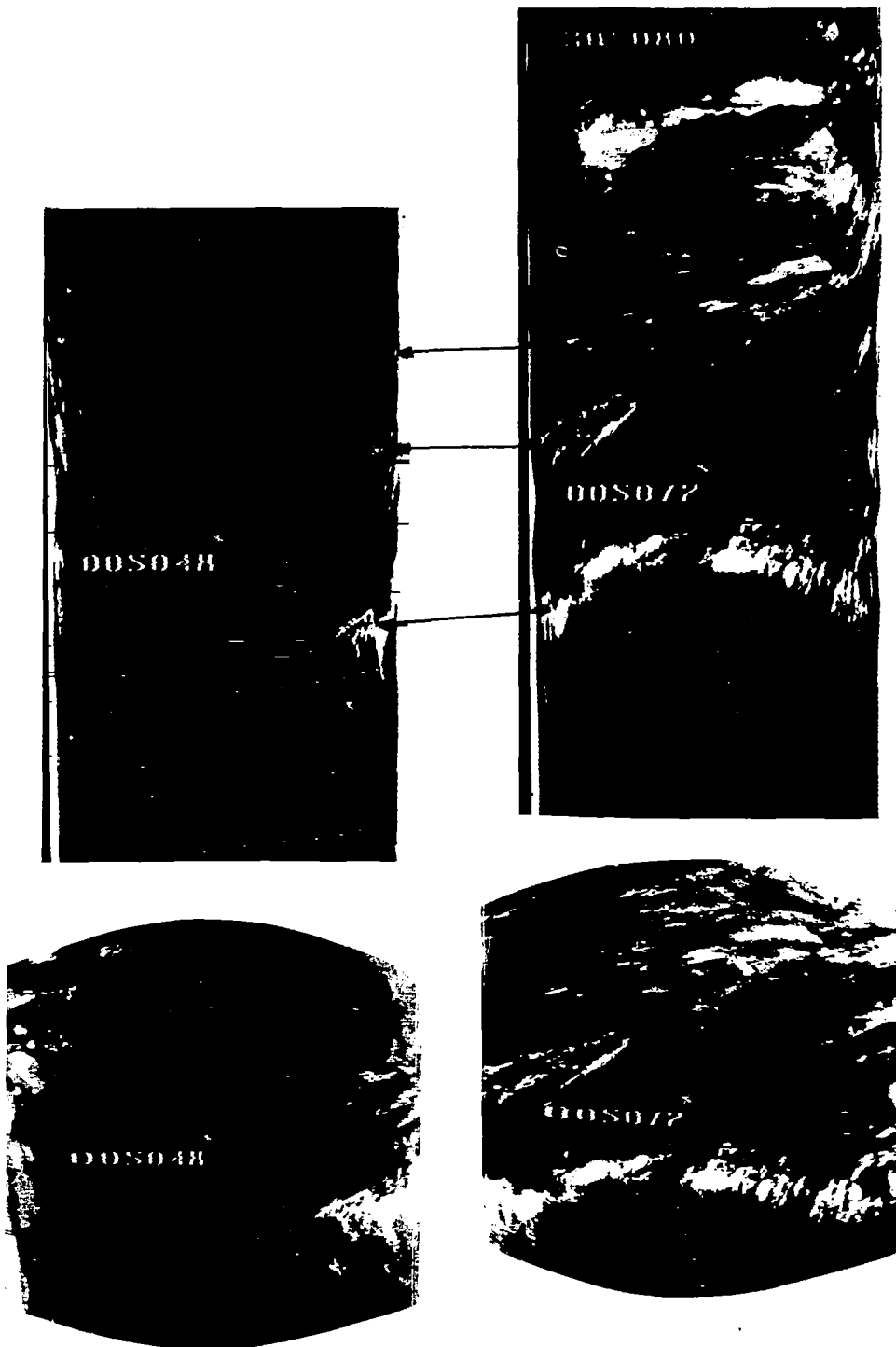
Figure B-3   Unrectified and Rectified Portions of Orbits 343 and 344

B. 4. 1. 1 Functional Relationships for the Variable Rate of Scan Approach

The required rates of a variable scan can be shown more precisely by noting, as from Widger,[52] that the HRIR observing geometry is given by:

$$B = 180^{\circ} - N - \sin^{-1}\left[\left(\frac{R + h}{R}\right) \sin N\right] , \qquad (1)$$

and $dB = MdN$,   (2)

where B = distance along the earth, measured from the subsatellite point and expressed in degrees of great circle arc,

N = nadir angle of view of the HRIR, as it scans,

R = radius of the earth,

h = altitude of the satellite,

$$M = \left[1 - \frac{\cos N}{\sqrt{\frac{R}{R + h}^{2} - \sin^{2} N}}\right] , $$

and there is a constraint that:

$$\sin^{-1}\left[\left(\frac{R + h}{R}\right) \sin N\right] \geq 90^{\circ}$$

For a flat-film recorder, the geometry of the recorder scan is given by:

$$\frac{X}{Y} = \tan \alpha \qquad (3)$$

where X = distance measured across the film, from the center line,

α = angle of rotation of the scanner, and

Y = distance from the film plane to the axis of rotation of the scanner (a constant)

From (2)

$$\frac{dB}{dX} = M \frac{dN}{dX} = M \frac{dN}{dt} \frac{dt}{dX} \qquad (4)$$

while, from (3)

$$\frac{dX}{dt} = Y \sec^2 \alpha \frac{d\alpha}{dt} \qquad (5)$$

From (4) and (5)

$$\frac{dB}{dX} = M \left(\frac{dN}{dt}\right) \left(\frac{\cos^2 \alpha}{Y}\right) \frac{dt}{d\alpha} \qquad (6)$$

For the present unrectified HRIR recorder, both $\frac{dN}{dt}$ (rate of rotation of the HRIR mirror) and $\frac{d\alpha}{dt}$ (rate of rotation of the recorder scanner) are constants; and the functional form of the unrectified projection is given by:

$$\frac{dB}{dX} = \left[1 - \frac{\cos N}{\sqrt{\frac{R}{R+h}^2 - \sin^2 N}} \right] \left(\frac{\cos^2 \alpha}{Y}\right) \left(\frac{dN}{dt}\right) \left(\frac{dt}{d\alpha}\right) \qquad (7)$$

In practice, this function is further simplified by synchronizing the HRIR scan and the recorder scan, so that $N = \alpha$, and $\left(\frac{dN}{dt}\right) = \left(\frac{d\alpha}{dt}\right)$.

For a rectified recording, $\frac{dB}{dX}$ must be a constant (the scale of the recorded data), and (6) becomes:

$$\frac{d\alpha}{dt} = \left[1 - \frac{\cos N}{\sqrt{\frac{R}{R+h}^2 - \sin^2 N}} \right] \left(\frac{\cos^2 \alpha}{Y}\right) \left(\frac{dN}{dt}\right) \left(\frac{dX}{dB}\right) , \qquad (8)$$

where $\frac{dN}{dt}$ is, of course, still a constant (the rate of rotation of the HRIR mirror).

Since, in this case, $B = kX$ (k being the scale constant), from (1) and (3):

$$Yk \tan \alpha = 180^{\circ} - N - \sin^{-1} \left[\left(\frac{R + h}{R}\right) \sin N \right] . \tag{9}$$

Thus (9) provides the relationship between α and N, and (8) and (9) are the functional form of a rectified projection on a flat film.

B. 4. 1. 2 The Digital Signal Processor Approach*

The third possibility for HRIR rectification involves the use of a relatively simple digital signal processor placed between the input data and the present HRIR photofacsimile recorder. Figure B-4 shows the basic elements of this rectification system.

The analog HRIR signal is digitized at a variable rate such that the time intervals between samplings cause distances across the film plane of the photofacsimile recorder to be proportional to great circle arc distances on the earth as scanned by the HRIR when these same samples are recorded at a constant rate. The digital samples of the HRIR signal are stored in a core memory and subsequently read out, at a constant rate, to a digital-to-analog converter (DAC). The analog output of the DAC is then fed to the facsimile recorder. (Sampling at a variable rate and recording at a constant rate, rather than the reverse, avoids crowding in one part of the scan while gaps appear in other portions.)

A simple computer routine permits the proper time intervals between digital samples, which are a function of the phase of rotation of the HRIR mirror,

---

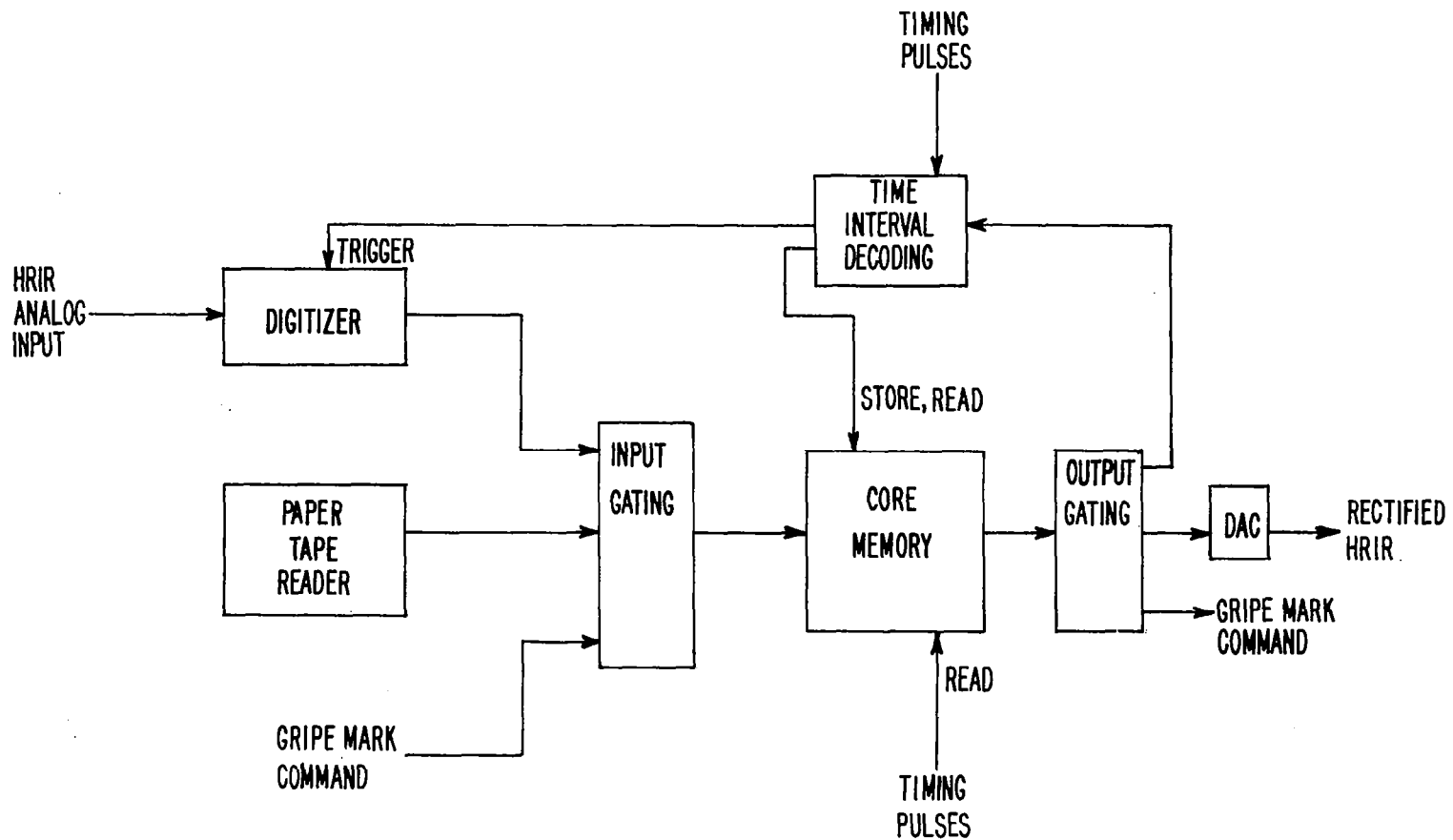* This approach was suggested by Mr. Robert Bartlett of ARACON.

Figure B-4   Block Diagram of Digital Rectification System

to be computed for any satellite height. (The functional relationships are simple transformations of those for the variable scan approach, as presented in Section B. 4. 1. 1 .) These intervals are punched on paper tape, and are entered into the core buffer from the tape reader prior to the HRIR recording run. Sufficient capacity exists in the core memory to hold: (1) these variable time interval: between samplings of the HRIR signal, which occupy word locations 1, 3, 5. ... n, n + 2 (2) the digital samples of the HRIR signal, corresponding to one facsimile recorder scan line, which occupy word locations 2, 4, 6. ... n - 1, n + 1. For synchronizing purposes, the time interval in the first word location is related to an identifiable angle of HRIR mirror rotation.

Digitizing begins when the contents of the first word location are delivered to the time interval decoder which, after the appropriate interval, triggers the digitizer and stores the digitizer output in the second memory location. Then the content of the third location is read to the time interval decoder, and so on until a full earth scan is in memory. The digital samples of the signal are then read to the DAC, at a constant rate, for recording.

Gripe mark commands are stored in a bit position, reserved in each digital sample word space, corresponding to the sample time closest to the mark time as determined by the gridding computer. Since only the gripe commands and not the grid mark video signals pass through the system, and this occurs before mixing of the grid mark into the HRIR signal, rectification of the HRIR signal does not affect the mark length. No modification of the grid mark program is needed with this rectification procedure.

The digital rectification can be achieved with minimum modification of station operations, no change in grid mark computation procedures, and without facsimile recorder modifications. It is essentially a "black box" which can be plugged in at will between the HRIR tape recorder and facsimile recorder. It has the additional advantage that only a computer input, rather than a mechanical adjust-ment, is needed for changes or variations in satellite altitude.

For either an optical analog or a variable rate of scan recorder, rectified recording with uniformity of exposure requires that the electro-optical transducer be cyclically modulated in phase with the scan; this, of course, is in addition to the non-cyclical modulations which are produced by variations in the signal from the HRIR sensor.

The costs of providing HRIR rectification should not be excessive, and, in our opinion, are fully justified by the increased ease of use of the data.

B.4.2 Other Design Considerations

Our investigations suggest that the HRIR data should be rectified out to a
distance of approximately 20° of great circle arc from the subsatellite point (nadir
angle of 56° for a 600 nautical mile orbit), but not beyond.

For a satellite at a nominal height of 600 nautical miles, successive equator
crossings (on the same side of the orbit) are approximately 27° of longitude apart.
Horizons have nadir angles of approximately 58.5°, thereby being 31.5° of great circle
arc from the subsatellite point. In theory, the HRIR on one orbit views the sub-
satellite points of adjacent orbits, even at the equator. Near the equator, however,
such points fall within the region of great foreshortening near the horizon, as dis-
cussed below.

Figure B-5 accurately illustrates the HRIR geometry of a satellite at
600 nautical miles. The diagram is generally self-explanatory, but some of the
implications do merit discussion. With increasing distance from the subsatellite
point, the rate of nadir angle change for a given rate of change of great circle arc
decreases significantly. At distances from the subsatellite point at and greater than
20°, two degree arc segments on the earth correspond to very small nadir angle
increments. * Hence, angular errors arising from any source can lead to sub-
stantial gridding errors. At 20° of arc from the subsatellite point, the elevation
angle of the satellite is only 14°. Under such circumstances, the effects of per-
spective and distance make estimates of cloud cover, type and dimensions difficult,
and perhaps even unjustified.

While the rates of change of angles and distances vary continuously, at and
beyond a distance of approximately 20° the cumulative effects make any gain from
gridding and rectification highly questionable. This forms the basis of our
recommendation to limit rectification to approximately $\pm\ 20^\circ$ of great circle arc
from the subpoint.

To provide a comparison of this recommendation with the rectifications
presented earlier (Figs. B-1, B-2, B-3), 20° of great circle arc fell either very

---

* The 20° limit is, of course, somewhat arbitrary, since an increase in fore-
   shortening occurs during all parts of the scan. Accordingly, for some purposes,
   the nadir increments corresponding to two degree of arc segments may be con-
   sidered small even closer than 20° to the subpoint.
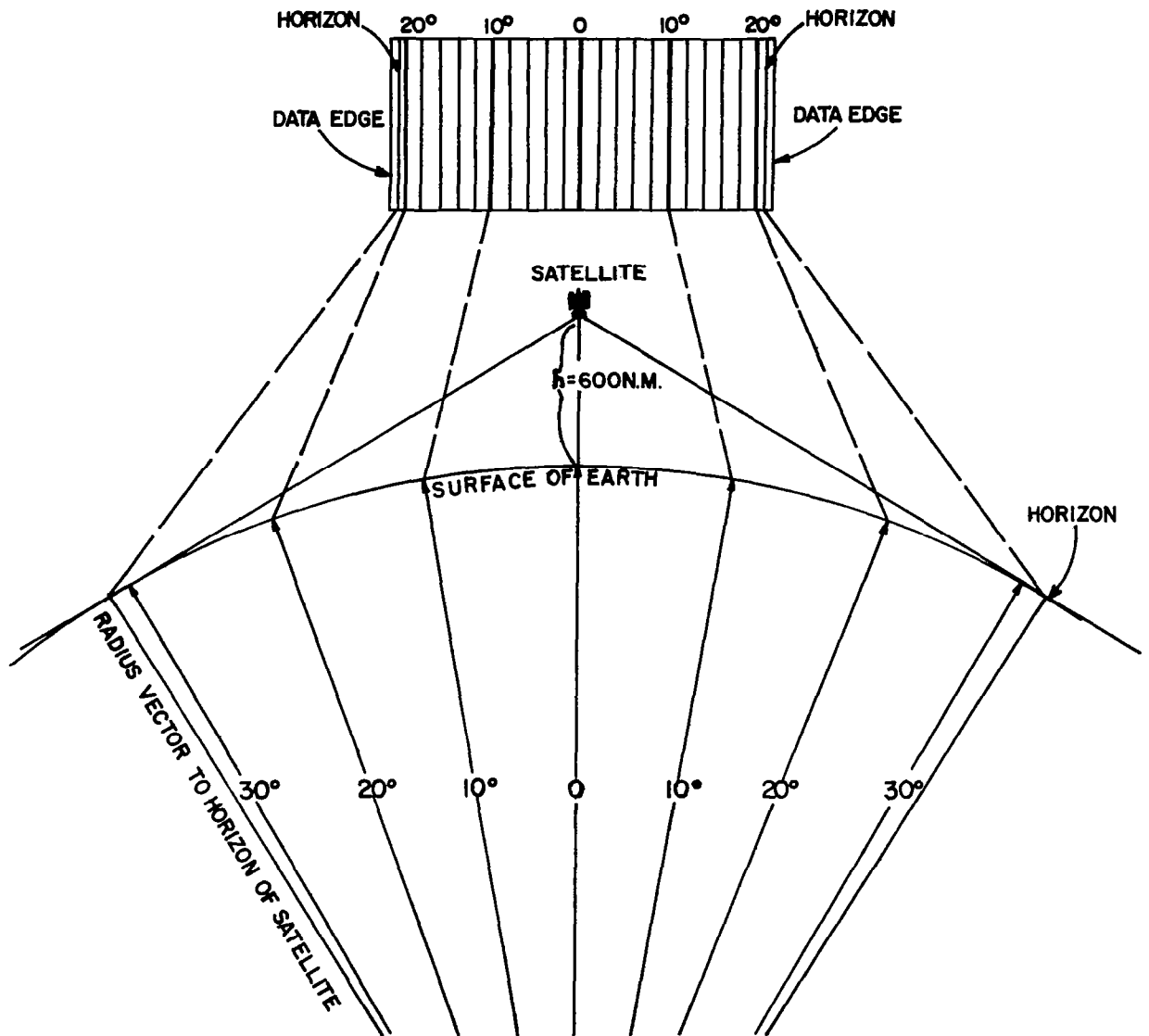
Figure B-5   Geometry of HRIR scan for a satellite at a height of 600 nautical
             miles above the surface of earth and proposed presentation
             geometry on film.   Section is in plane of a scan line

near the edge of, or beyond the limits of, these three rectifications. This was
because the Nimbus I satellite was at altitudes of less than 400 nautical miles in
all three cases. This reinforces our conclusion that rectification to approximately
20° of great circle arc would, for a satellite at 600 nautical miles, include
essentially all the significant data.

Within the width of the video presentation of the HRIR data, as presently
fixed at 54 mm by film dimensions, expansion of the scale toward the horizon can be
accomplished only by compression of the scale near the subsatellite point.
Figure B-5 also shows a possible spacing of the rectified HRIR data for increments
of two degrees of great circle arc. Approximately one millimeter of the 27 milli-
meters on each half of the video is reserved for viewing outer space above the
horizon. For a scale of 1.25 mm per degree of great circle arc, rectification
out to 20° of great circle arc from the subsatellite point requires another 25 milli-
meters. This leaves approximately one millimeter for the area between 20°
distance from the subsatellite point and the horizon.

Such compression of the data beyond 20° might seem to be treating them
in cavalier fashion. However, this is almost exactly what already happens in the
presentation format presently used for the Nimbus I data. Application of
Equation A-7 of Reference 18 shows that, for a 600 nautical mile satellite altitude,
data beyond 20° of great circle arc would be compressed into 1.1 mm on the
Nimbus I HRIR film presentation system. (The near-horizon data would appear
at a somewhat different distance from the center of the film strip, but in a favor-
able direction, since our proposed format, as illustrated in Fig. B-5, makes more
effective use of the total width of the film strip than does the present recorder when
operating with a satellite at a 600 mile altitude.)

Although the data near the subsatellite point would be presented at a
slightly reduced scale relative to those in the Nimbus I format, it has already been
pointed out above (Sections 2.3 and B.3.1) that, in the Nimbus I format, these data
have been stretched excessively in the cross-track dimension relative to the
dimension along the subsatellite track. Furthermore, enlargements can easily
be prepared from the original recordings when it becomes desirable to present
the data at an enlarged scale.

The differences in scale that would result from adoption of a rectified
presentation may make it desirable to examine whether some adjustments in the
dimensions of the individual electronically inscribed grid points would be desirable
to optimize the overall data presentation if either the optical analog or the variable

rate scan approach should be used. As mentioned above, this is not necessary in the digital signal processor approach.

The rectification considerations discussed above are also applicable, in the general sense, to MRIR data.

APPENDIX C

ADDITIONAL ILLUSTRATIVE CASE STUDIES

Several of the conclusions discussed in the preceding Final Report of Contract No. NAS 5-9554 were derived from, substantiated by, and/or illustrated by case studies which were presented in the Preliminary Scientific Report under the contract[*] and not republished in the Final Report. Accordingly, these case studies have been reprinted here as an additional appendix.

In this reprinting, several oversights and errata that remained in the Preliminary Scientific Report were corrected, and in a few places references to earlier sections of the Preliminary Scientific Report have been modified to fit the use here. No substantive scientific changes have, however, been made.

---

[*] Widger, W.K., Jr., and R.B. Smith, 1965: Preliminary Results from a Meteorological Evaluation of Nimbus I HRIR Data, Preliminary Scientific Report, Contract No. NAS 5-9554, ARACON Geophysics Company

TABLE OF CONTENTS FOR APPENDIX C

LIST OF FIGURES FOR APPENDIX C

LIST OF TABLES FOR APPENDIX C

APPENDIX C

Pages 1 through 14 have been purposely omitted.

4. ILLUSTRATIVE CASE STUDIES

The findings and conclusions discussed in the Final Report are illustrated by five case studies which used the normal nighttime HRIR data, and by three brief case studies which used daytime HRIR data.

Summary descriptions of these eight cases, and their order of presentation are as follows:

A. Nighttime Cases:

1. A four-day period over North America, with good TIROS coverage during the daylight hours. During this period, a significant cyclonic storm developed near the U.S. - Canadian border and moved into northeast Canada. On two days, hurricanes were observed near the eastern coast of the United States.

2. A three-day period, during which a cloud vortex developed in the western Pacific Ocean, within an area having relatively good radiosonde data. On the last day, the vortex included a particularly vivid spiral of high level cloudiness.

3. Another three-day period over the North Pacific, which included a frontal band extending across the central and western Pacific. During this three-day period, a wave along this front developed into a cloud vortex near the Aleutians.

4. A one day case over western North America. Cloud patterns associated with a developing frontal wave, including jet stream cirrus and an area of lee waves were present.

5. A one-day period of a cold front across the middle Atlantic states. The plentiful conventional data in this case, and the related TIROS coverage permitted a rather intensive mesoscale analysis.

B. Daylight Cases:

1. A daylight HRIR view of a short wave trough near the British Isles, with nearly concurrent TIROS data for comparison.

2. A daylight HRIR strip showing stratus and cumulonimbus cloud areas over the eastern Pacific, with a comparison to a TIROS pass over the same area.

3. A 24-hour period near Cape Horn, with two night HRIR passes and an intervening daylight HRIR observation. The daylight coverage of the HRIR is partly duplicated by a TIROS mosaic.

4.1 A Continuity Case Over North America

The period 8-12 September 1964 was one of relatively intensive HRIR and TIROS TV coverage[*] over many of the eastern and central parts of North America. During this time, a frontal wave near the United States-Canadian border developed into a mature cyclone over northeast Canada. The discussions here are merely samplings of the investigations that can be made from the composite data collected for this period. It is hoped that more intensive studies of this case can be undertaken during the remainder of this contract.

4.1.1 The HRIR Data for 9 September 1964

Orbits 174 and 175 (Fig. 1) provided rather good HRIR coverage of much of eastern North America and the central-western United States at about 0600 GMT. Our working copy of orbit 174 was at best of marginal quality (far too dark), but the key features visible are shown in the rectification (Fig. 2).[**]

The principal features in the HRIR data include: 1) a somewhat complex vortex in northeast Canada, with a cold frontal band running from it across Labrador and into the eastern United States; 2) Hurricane Dora, just east of Florida; 3) a cloud mass north of Montana, suggesting some cyclonic development just to the west, and high narrow cloud bands to the southwest of this cloud mass; 4) two small cloud masses southwest of Lake Superior, the more northern of which is somewhat suggestive of a minor short wave trough; and 5) a series of disturbed areas (probably cumulo-nimbus masses) in western Mexico for which we so far have little or no corrobora-tive data.

4.1.1.1 The Canadian Vortex

The vortex near 60°N, 70°W is composed of a number of spiralling bands. The patterns of broadening and narrowing of these bands suggest mesoscale areas of up-ward and downward vertical motions with in general northward moving air being associated with upward motion (band broadening) and vice versa. The 500 mb analysis for 1200 GMT, September 9 (Fig. 3), places a closed low in this position, as do the approximately concurrent surface analyses (not included).

---

[*] In this case, the HRIR data are compared to TIROS pictures taken approximately 12 hours both before and/or after the time of the HRIR observation.

[**] In several of the cases studied, the quality of the working copies of the HRIR data was so poor as to require obtaining copies of subsequent processing for reproduction. In such cases, the copies as reproduced herein may include features not discernible at the time of the analysis.

The complex structure (multiple cloud bands) of the Canadian vortex is believed in part to reflect the diverse origin of what now appears in the analysis as a single low pressure area extending through much of the troposphere. On September 6, the USWB surface analysis (not included) shows three lows over and just west of Hudson Bay; the 500 mb analysis has two lows, one over northeast Hudson Bay and a second to the southwest. On September 7, the surface analysis still shows three lows, now all essentially over Hudson Bay, but the 500 mb analysis shows only a single low. By the 8th, there is a single low at both levels, centered near 62°N, 75°W. Developments further to the west may also have resulted in elements of other 500 mb lows or troughs, located over northwest and southwest Canada on September 6, being drawn into the system. The structure of the bands in the HRIR data suggest at least three bands of relatively independent origin are now circulating around an approximately common center. It does not seem unreasonable to speculate that the observed cloud pattern may have originated at three separate areas of dynamic lifting which have subsequently been advected around separate cyclonic circulations and finally, as these centers merged, about a common center.

Careful comparisons of the cloud patterns in the HRIR and the 500 mb analysis (Fig. 3) show interrelationships at the mesoscale. Both the cloud vortex and the 500 mb low are elongated along the northwest-southeast axis. A perturbation in the contour labeled 540, north of the center and near 70°W, can be related to the cloud band to its west. The relatively sharp curvature of the northwestern portion of the 534 contour can perhaps be related to the cloud band near 62°N, 73°W. In both cases, the clouds are intensified just downstream from a local vorticity maximum, where dynamic lifting is to be expected. It seems reasonable to assume that, if there were a far greater density of data permitting a much more detailed analysis, one might be able to relate the other bands to other perturbations in the cyclonic circulation.

This same cloud vortex was photographed about 14 hours earlier by TIROS VII, on orbit 6612 (Figs. 4a and 4b). Comparison of the HRIR and TIROS views of this vortex leaves the impression that the same individual bands are being seen, with the southern end of the most northerly band (which in TIROS extends along Davis Strait to opposite the southern tip of Greenland) now having rotated to about the center of Baffin Island. Note that the southern tip of Greenland is visible in the HRIR strip, and if not recognized, might be interpreted as cloud.

The translation of this cloud band would have required a wind speed of slightly under 60 knots. The 500 mb geostrophic wind in Figure 3, for this area, was about 43 knots. This 25 percent discrepancy could have resulted from one or more of factors, such as 1) the end of the band being lower clouds, not visible in the poor quality HRIR strip; 2) HRIR rectification errors; and 3) 500 mb analysis errors in an area of limited data.

Figure 1. HRIR Data for Orbits 174 and 175, 9 September 1964.
(Note: In this and similar figures using unrectified HRIR strips,
the strips are placed in approximately their relative geographic
positions, with orbit number increasing from east or right to
west or left.)
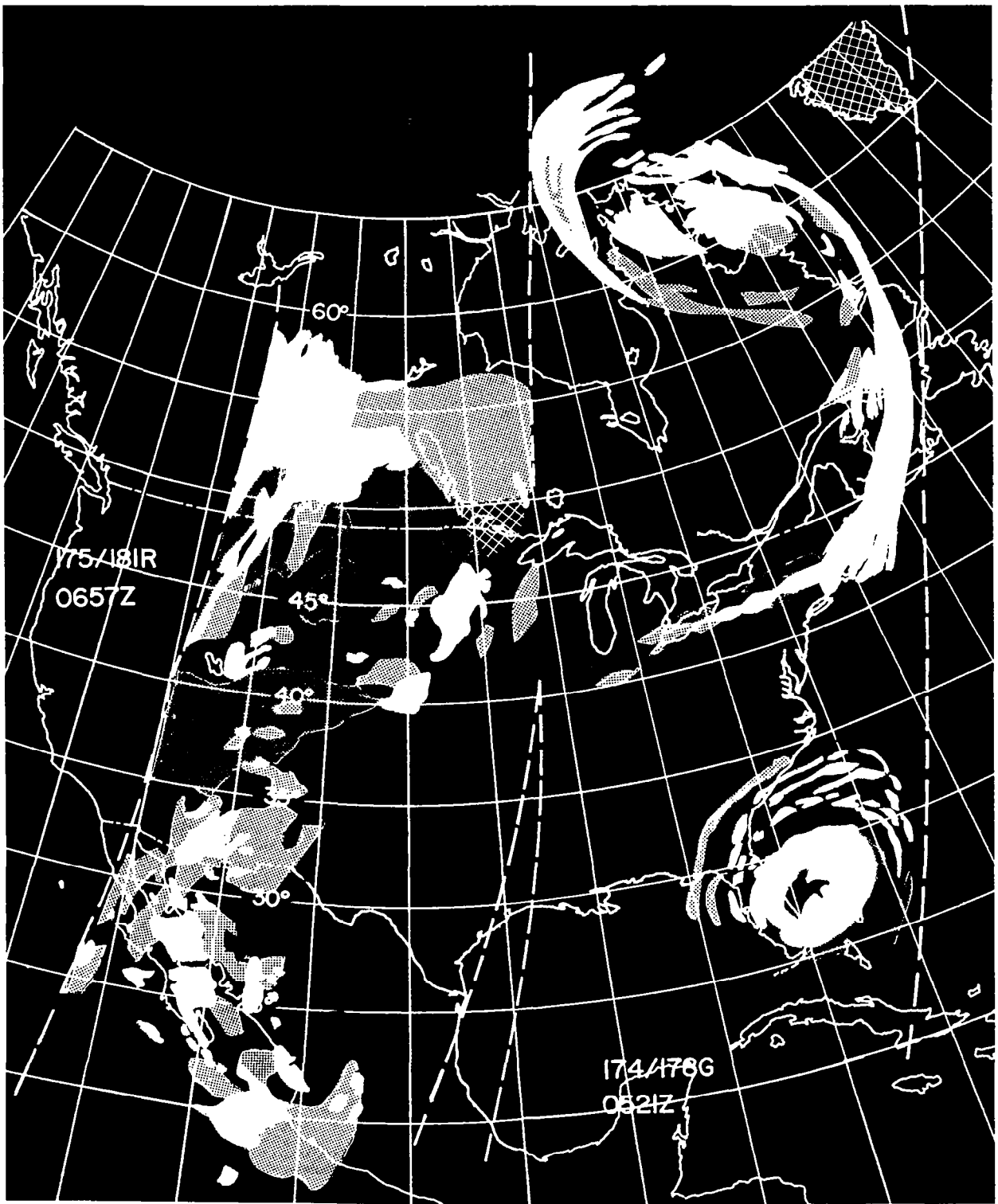
Figure 2. Rectified HRIR Data for 9 September 1964
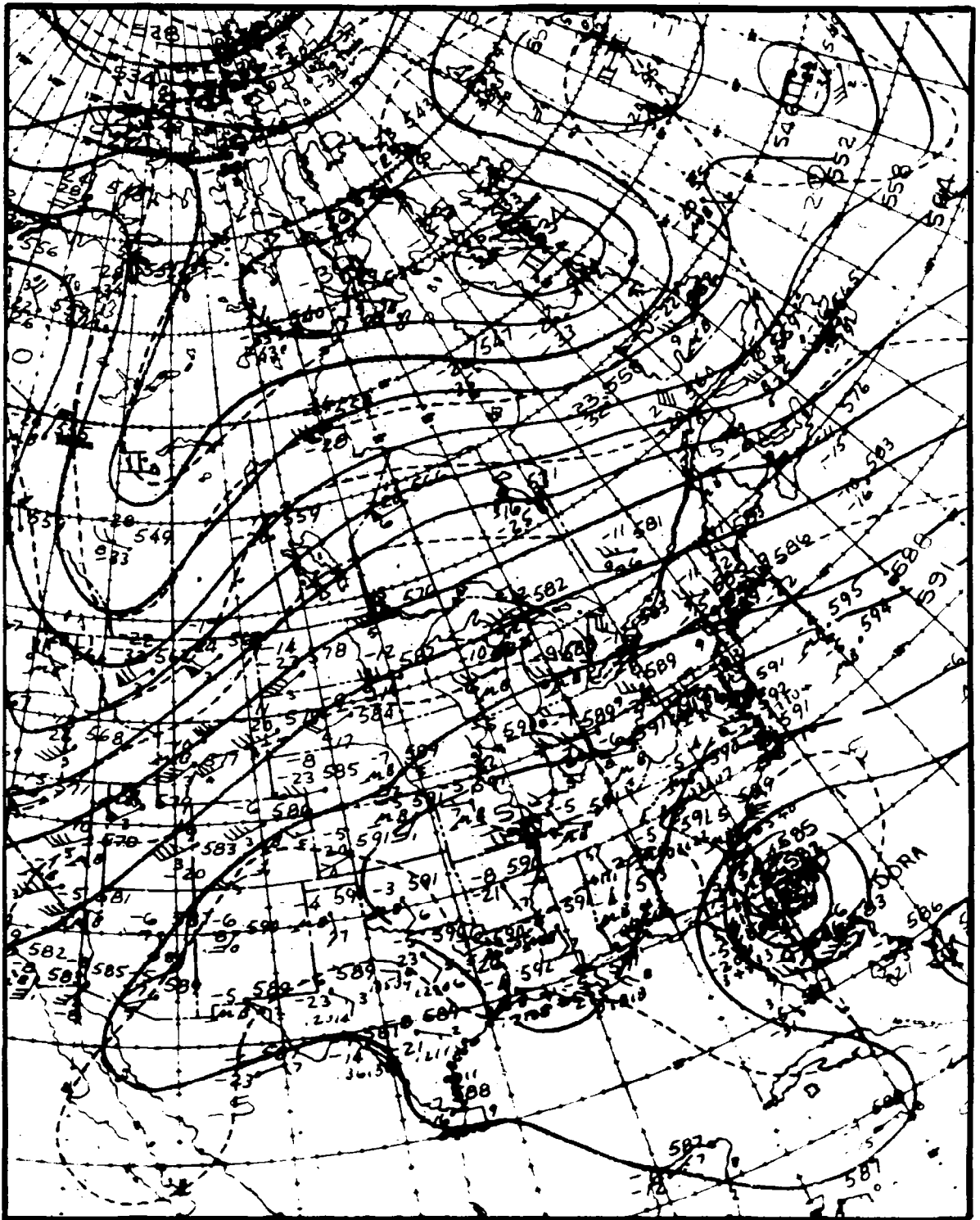
Figure 3. NMC 500 mb Analysis, 1200 UT, 9 September 1964

Although the individual cloud bands of the vortex appear identifiable in both the HRIR and the TIROS data, those in the TIROS pictures do not show the broadening and narrowing (presumably due to vertical motion patterns) which are apparent in the HRIR. It would appear that this takes place principally in the middle levels of the troposphere, which in the TIROS pictures are masked by low level cloudiness that still tends to follow the general pattern of banding.

In the TIROS pictures for September 9, only the edges of the vortex, near the horizon, can be seen and the pattern is far less obvious. Furthermore, the HRIR for September 10 (see Fig. 7) suggests either amalgamation or dissipation of many of the bands.

The cold front which extends southward from the vortex in orbit 174 was photographed by TIROS on both September 8 (Fig. 5) and September 9 (Fig. 6) as it crossed the Maritime Provinces and northern New England. This part of the cloud band, in the HRIR, is near the edge of the strip, making detailed comparison infeasible. In general, the two views are not incompatible. As has been the case with other cold front comparisons, however, the HRIR data have a more broken appearance, and indicate greater variations of cloud top altitude than the TIROS pictures suggest. Furthermore, the TIROS cloud band is about 5° of latitude across, while in the HRIR it is only about 2° across.

4.1.1.2 Hurricane Dora

The HRIR position of Hurricane Dora is completely compatible with that on the corresponding surface and 500 mb analyses. TIROS also photographed the storm on September 9 (Fig. 6). Unfortunately, it was close to the horizon in the TIROS picture, and that portion seen by TIROS at reasonable nadir angles (the eastern edge) was very near the edge of the HRIR strip. Nevertheless, there is a good correspondence between the two views of the peripheral bands to the northeast of the center. The HRIR data indicate they extend nearly as high as the central cloud mass, and cirrus characteristics are clearly visible in the TIROS picture. A comparison of the eye of the storm in the two presentations is precluded by its position in the TIROS picture.
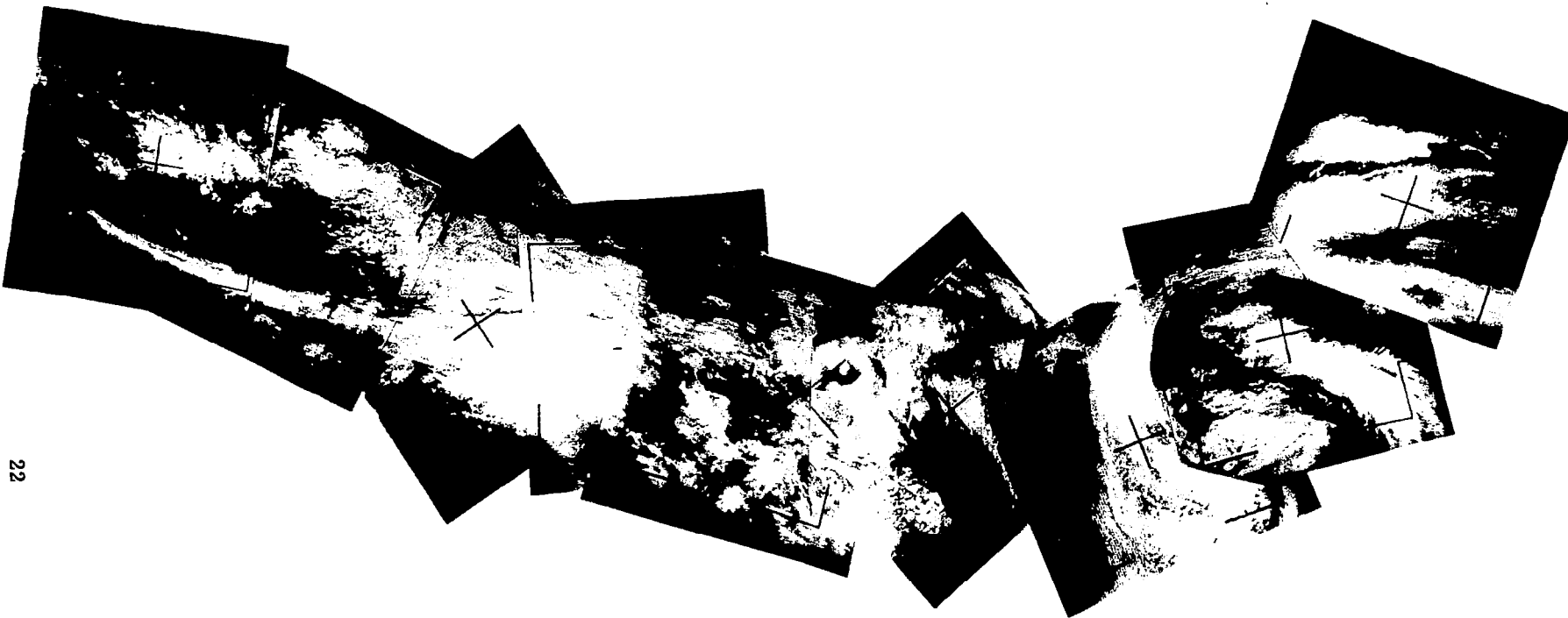
Figure 4a.   TIROS VII Television Picture Mosaic, Orbit 6614/6612
1611UT, 8 September 1964
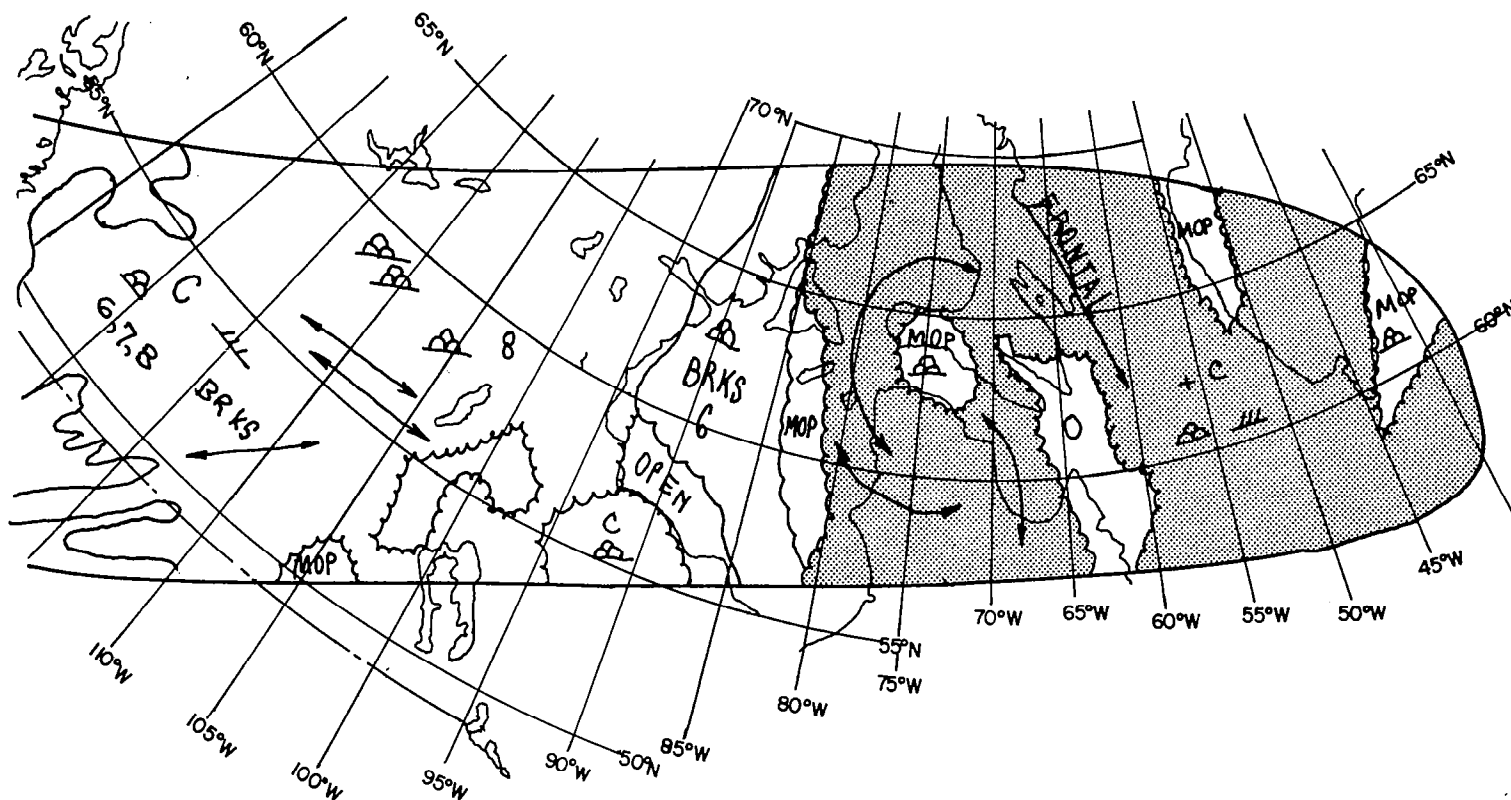
T-7 6614/6612

I6IIZ 8 SEPT 1964

Figure 4b.   TIROS VII Operational Nephanalysis, Orbit 6614/6612
1611 UT, 8 September 1964
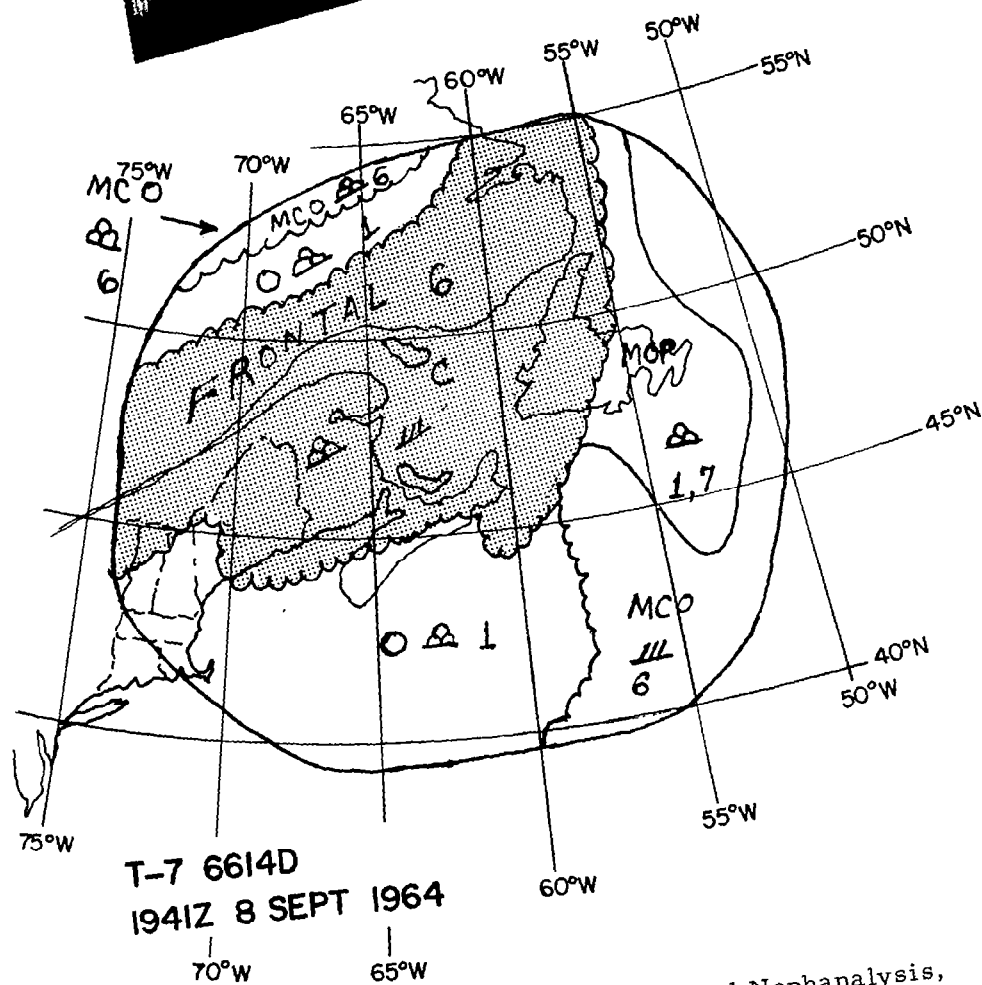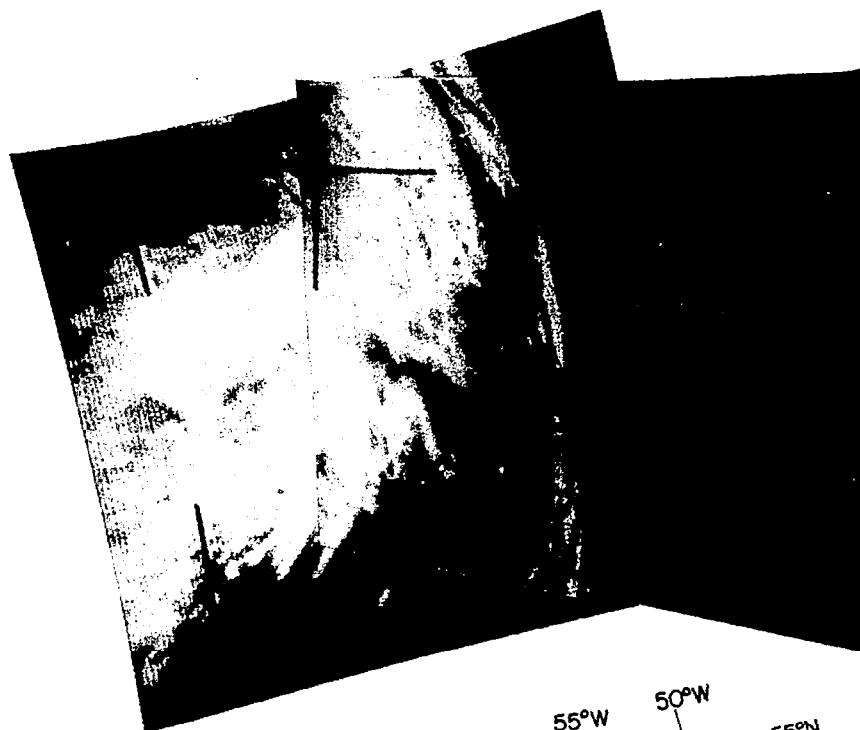
Figure 5. TIROS VII Mosaic and Operational Nephanalysis, Orbit 6614 D, 1941 UT, 8 September 1964
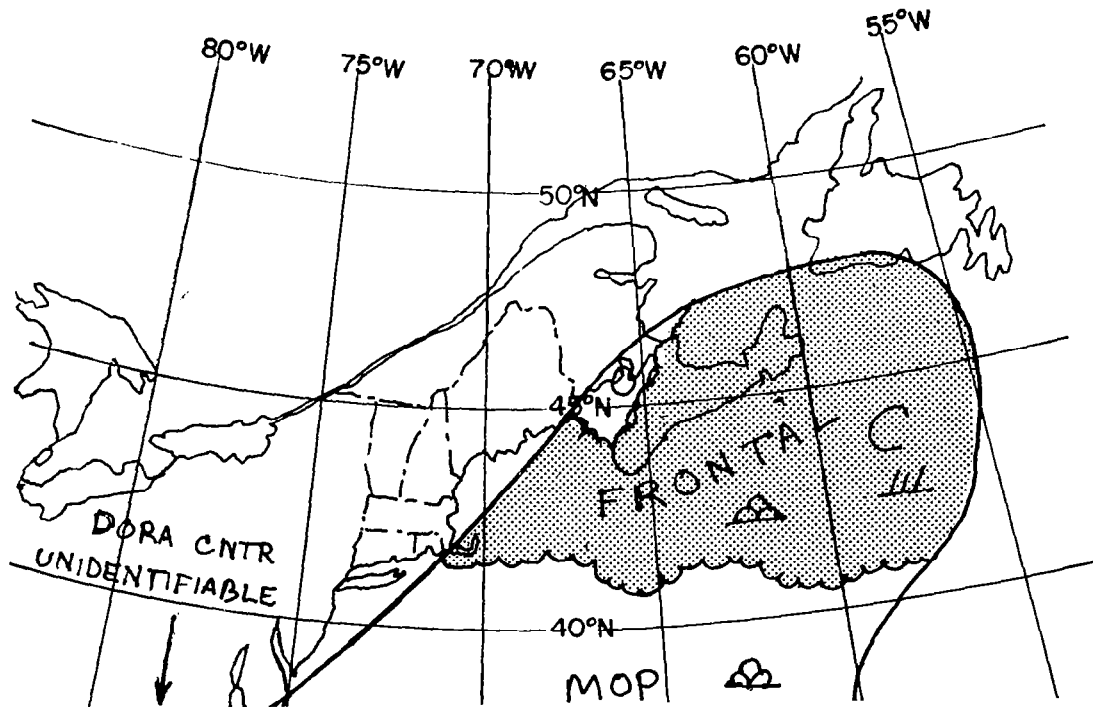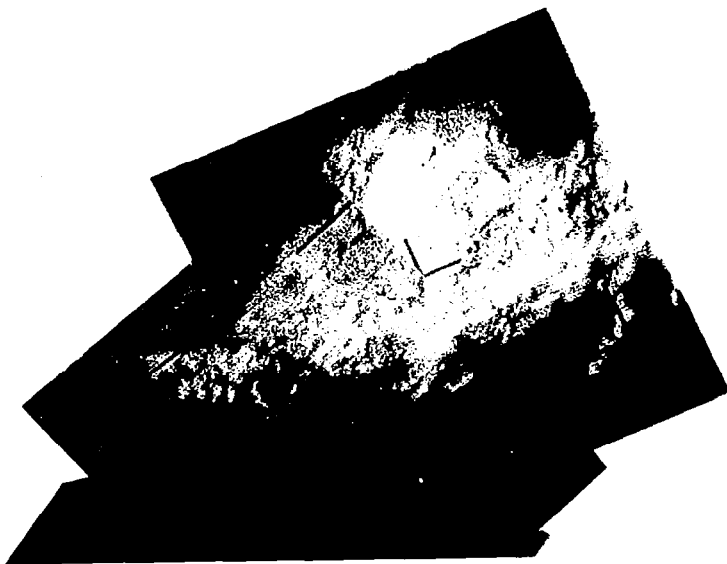
Figure 6.   TIROS VII Mosaic and Operational Nephanalysis, Orbit 6624 D,
1156 UT, 9 September 1964

4.1.1.3   The Cloud Mass North of Montana

This feature is rather well depicted in both the HRIR strip (although near the western edge and the northern limit of the data) and in the TIROS pictures for orbit 6612 (Figs. 4a and 4b). (On September 9, TIROS photographed only the northern portions of this cloud mass, north of where the HRIR data on orbit 175 started; these TIROS data are better related to their HRIR counterparts for September 10.)

This cloud mass is associated with the southerly flow at 500 mb, just east of the trough near 113°W (Fig. 3).   Comparison with the previous (0000 GMT) 500 mb chart (not included) suggests that a short wave trough is moving around the major trough, although this is not too evident from the 1200 GMT chart alone. At the time of the HRIR data for orbit 175, the surface chart (not included) carried an open front frontal wave, centered near 45°N, 105°W. Twelve hours later, this system had occluded and had moved to about the Canadian border, near 100°W.

Both the TIROS pictures (Fig. 4) and the HRIR data indicate an increase and thickening of clouds just north of the border, from about 100°W westward to about 110°W. Both sets of data also show a high southwest to northeast cirrus band across Montana. This band approximately parallels the 500 mb flow, and lies just south of the fastest 500 mb winds. The 0000 GMT and 1200 GMT 200 mb charts (not shown) have an 80 knot jet stream just northwest of the cirrus band and, like the band, slightly crossing the contours toward lower pressure. However, the 200 mb charts also show a second jet which is of somewhat higher velocity crossing Wyoming from southwest to northeast with no indication apparent in the HRIR cloud patterns.

The surface map coincident with the HRIR data suggests that most of the brighter areas in the HRIR cloud mass, except those of the jet stream cirrus band, correspond to areas with concurrent or very recent precipitation. Stations reporting precipitation include Edmonton, Fort McMurray, Island Falls, and Hudson Bay in Canada; and Bismarck, North Dakota. Well ahead of the cloud mass, the Lake of the Woods and other lakes near it could be identified in our working original of orbit 175, showing these areas to be clear.

4.1.1.4   Two Small Cloud Masses Southwest of Lake Superior

On the surface analysis, these clouds are represented only by more or less a line of cloudiness extending from Minnesota southwest into Nebraska. They are not well related to the analyzed east to west stationary front, approximately along

45°N. The 500 mb winds and analysis (Fig. 3) do, however, clearly indicate a very
weak short wave trough (influencing only the 588 contour line) near 97°W. There was
no TIROS coverage of this area on either September 8 or 9; by the time of the HRIR
data on September 10, this minor system apparently either had died out, or had been
absorbed into either the eastward moving developing disturbance to the northwest or
the front then extending southwest from it.

4.1.2   The HRIR Data for 10 September 1964

On September 10, the Nimbus HRIR data (Figs. 7 and 8) for orbits 188, 189,
and 190 provided rather good coverage of most of Canada and many parts of the
northern and western United States. The average time of observation for the three
orbits was about 0600 GMT. The 0600 GMT surface analysis for the United States
and southern Canada is shown in Figure 9; Figure 10 is the 1200 GMT 500 mb
analysis for the area of the HRIR observations.

In these HRIR data we can see the following features:

1.   The old vortex, now-located over Baffin Island, and perhaps less organized
than 24 hours ago, but still clearly visible. The location corresponds well to the
500 mb low. The brighter areas in the vortex, near 61°N, 70°W, and 65°N, 70°W,
can perhaps be related to perturbations in the 540 contour. The match in this case
is, however, far from as good as 24 hours earlier; limited data and the time discrep-
ancy may be partially responsible. A frontal band, running south-east from the
vortex, passes east of Newfoundland and then runs to the east coast of the U.S., just
south of 40°N. These frontal positions match the surface analysis reasonably well.
Both the TIROS picture for about 16 hours earlier (Fig. 6), and the HRIR strip sug-
gest an east to west weakening in portions of the front near the United States coast.
(Because the area near the United States-Canadian border, and south and central
Canada is shown in four separate TIROS mosaics, it seems better to discuss many
other aspects of the front, and other features in this area, in terms of the individual
mosaics (see Sections 4.1.2.1 through 4.1.2.4) rather than in terms of the features.)

2.   A cloud mass over and just north of the Great Lakes. Its appearance is
typical of the cloud pattern associated with a trough just developing into a closed
circulation aloft, usually with an associated occluded front. The surface analysis
(Fig. 9) shows such an occluded front, and the cold front south of it, located very
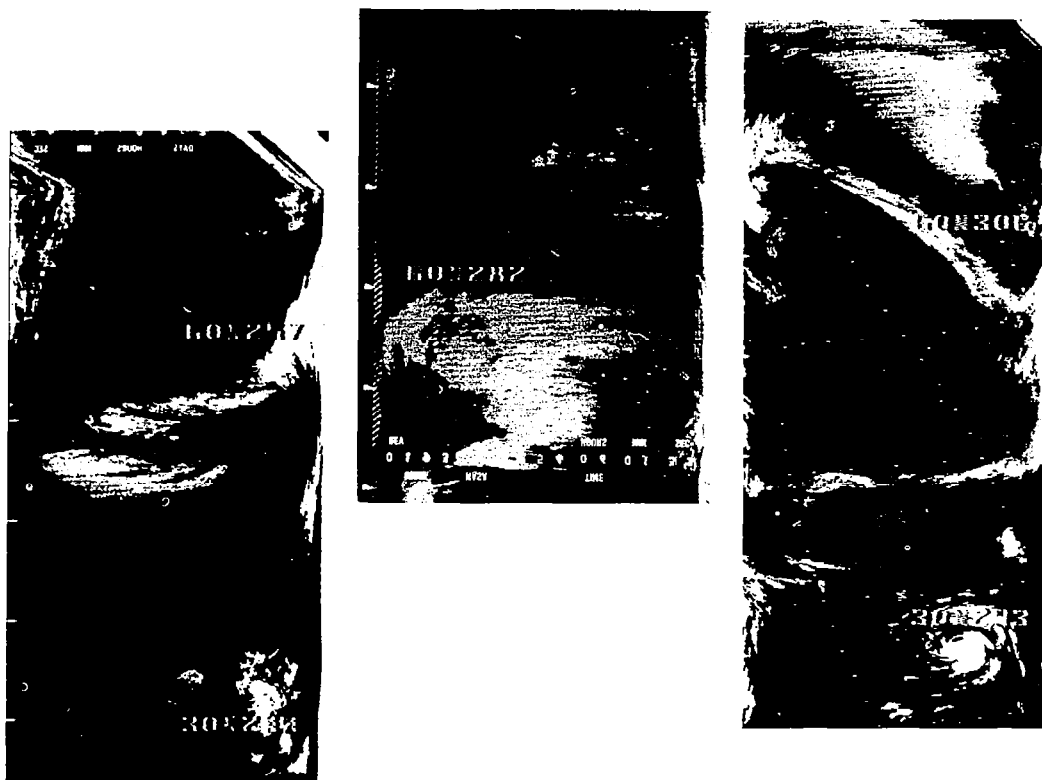
Figure 7. HRIR Data for Orbits 188, 189, 190, 10 September 1964
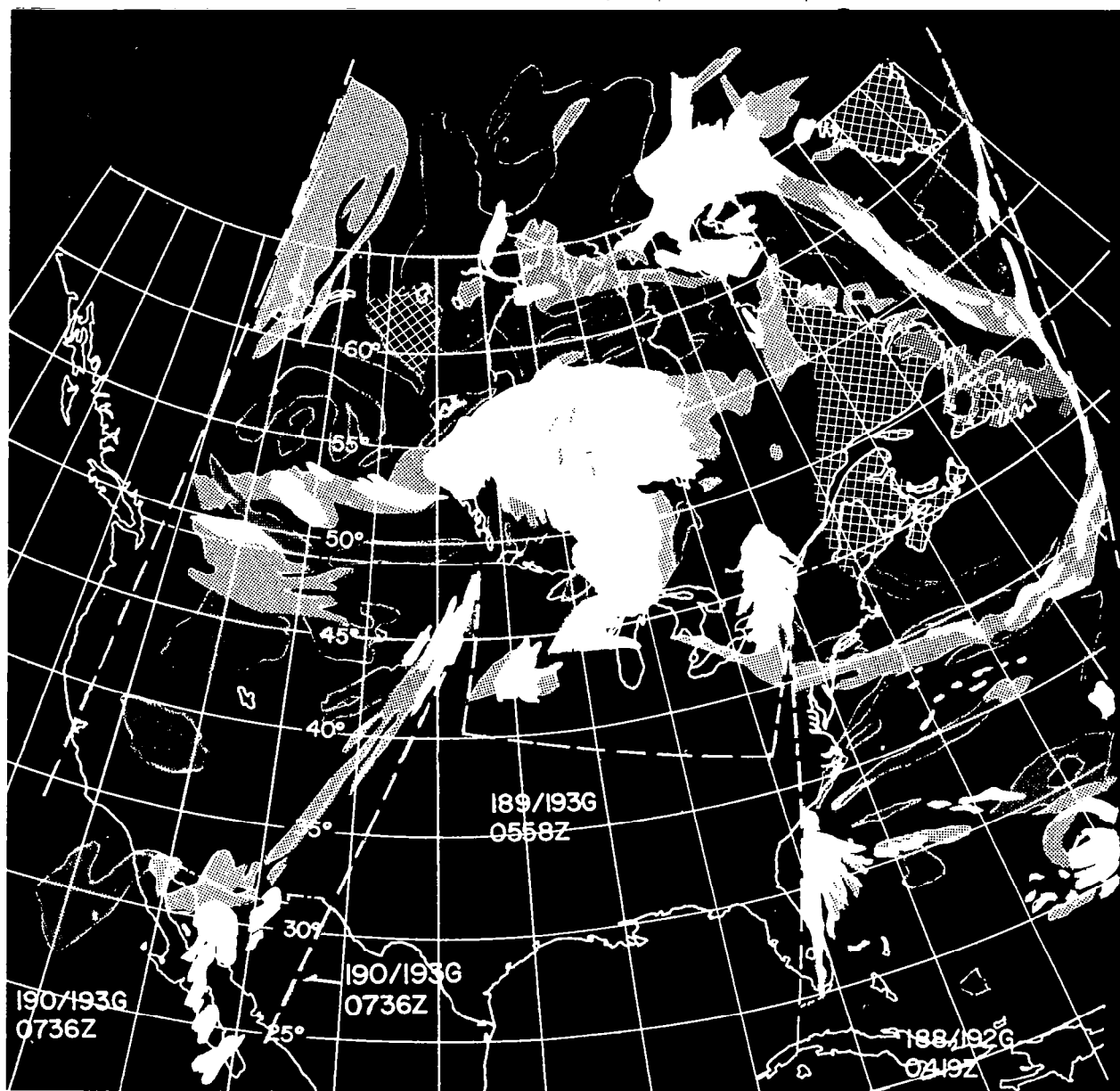
Figure 8.   Rectified HRIR Data for 10 September 1964
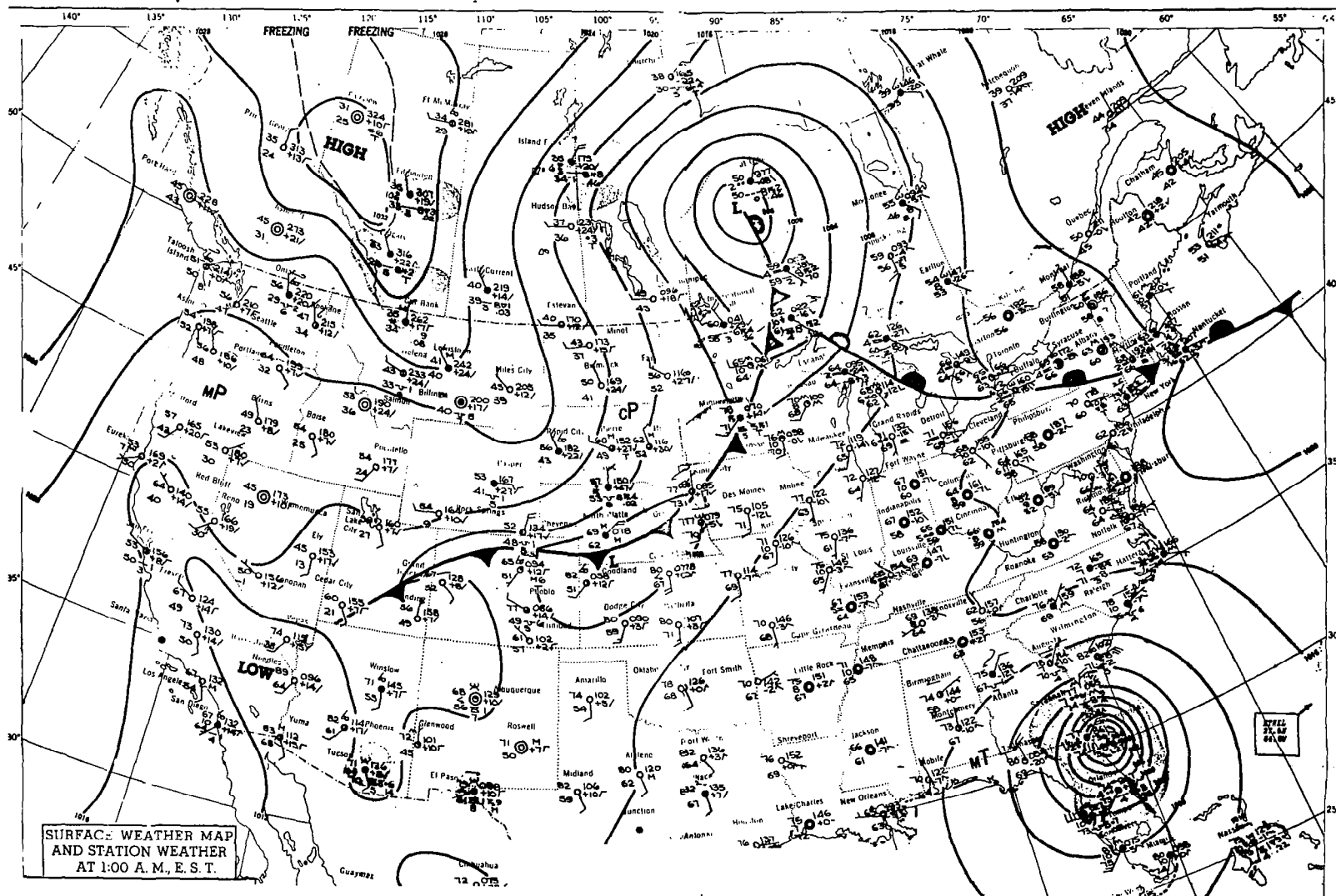
Figure 9. Surface Analysis, 0600 UT, 10 September 1964

30
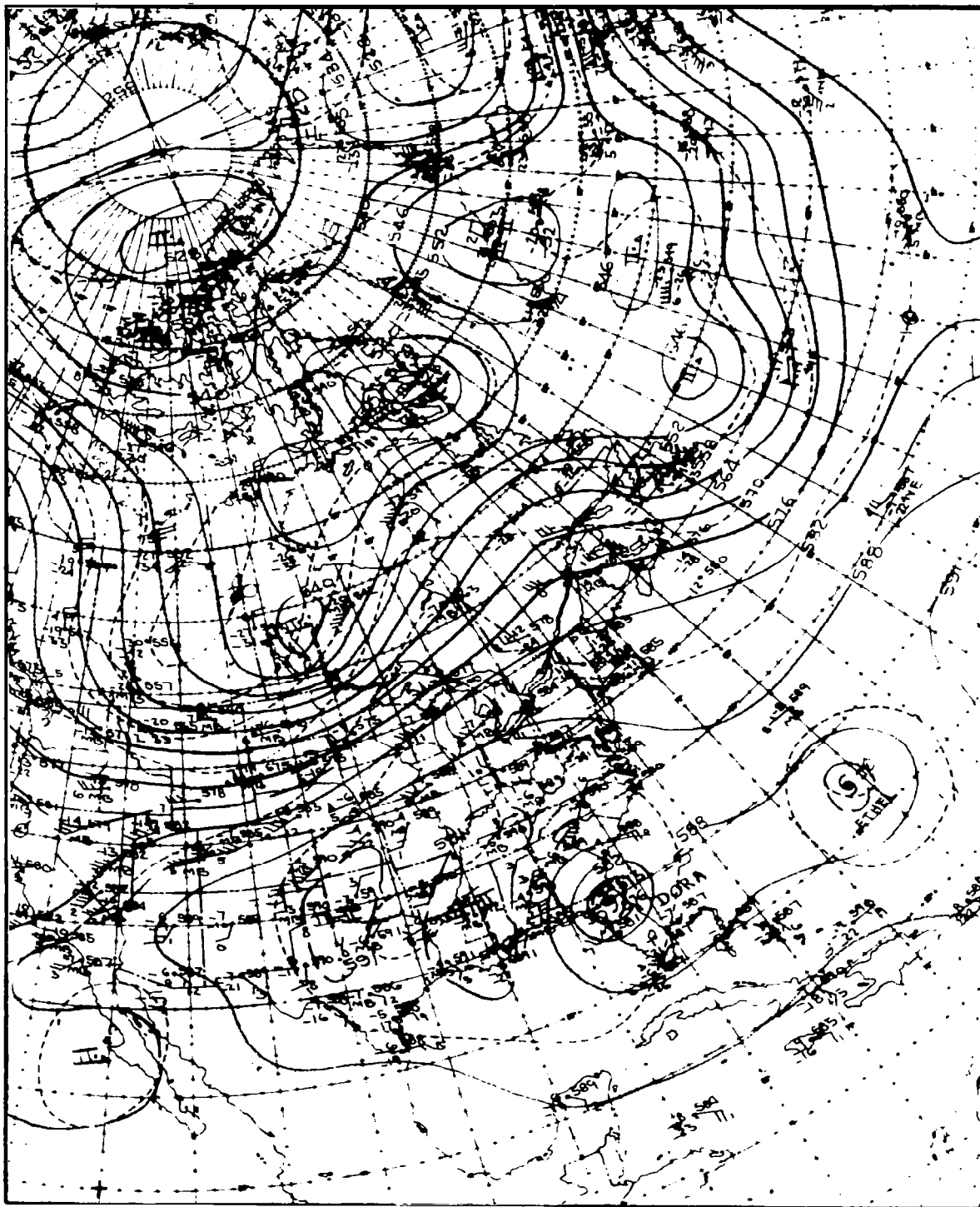
Figure 10.   NMC 500 mb Analysis, 1200 UT, 10 September 1964

nearly along the western edge of the cloud mass from north of Lake Superior to near Sioux City, Iowa. At 500 mb, the low was analyzed as closed as early as 0000 GMT, but even at 1200 GMT (Fig. 10), there are no specific wind data to positively confirm this. (The low is definitely closed at 0000 GMT on September 11.) The position of the cloud mass is typical with regard to the location of the 500 mb trough line.

3. A filmy cloud band, running south to southeast from Lake Winnipeg. Its orientation is about the same as that of a jet stream at the 200 mb level (not shown) north of the Canadian border, but as the band crosses the Dakotas it is at about a 45° angle to a second WSW-ENE jet stream. Kadlec[14] has noted that an area of cirrus often exists downstream from an area of confluence between two converging jet streams. In these cases, the cirrus extends from east of the trough line of the more northerly jet, southwest to that across the southern jet stream. These observations of Kadlec may provide an explanation of the cirrus band (or possibly area, since it is at the edge of the HRIR strip) in orbit 190.

4. Hurricane Ethel, near 25°N, 65°W. This hurricane was photographed by TIROS VII about 16 hours later (Fig. 11, where, in addition to a single frame showing the storm as a whole, a mosaic shows a slightly better view of the eastern portions of the system). The HRIR suggests a moat to the northeast of the storm which is not obvious in the TIROS picture; on the other hand, if the two types of data are combined and if drastic changes in the cloud patterns are assumed not to have occurred during the 16 hours interval , TIROS then indicates this moat must be essentially filled with low clouds, while from the HRIR alone, it might be relatively clear. The HRIR also shows a definite V-shaped indentation in the southwest part of the storm, which is far less obvious in the TIROS data. Thus the HRIR suggests high level outflows in the west to northwest and southwest quadrants of the storm which are only faintly visible in the TIROS picture. On the other hand, scattered low cloudiness to the east and southeast of Ethel, clearly visible in the TIROS data, can be seen in the HRIR only where it forms a semi-major band.

The east edge of Dora is barely visible in the orbit 188 strip, but no useful analysis is feasible.

5. Comparison of the HRIR data and the concurrent surface map (Fig. 9) shows that most of the bright (high cloud) areas of the HRIR near and over the Great Lakes, and that over Arizona, correspond to areas of precipitation. Precipitation is also occurring under the white-to-off-white cloud area over Saskatchewan and Alberta. Here, the surface and 850 mb flow patterns suggest that the clouds and precipitation are due to upslope motion east of the continental divide.
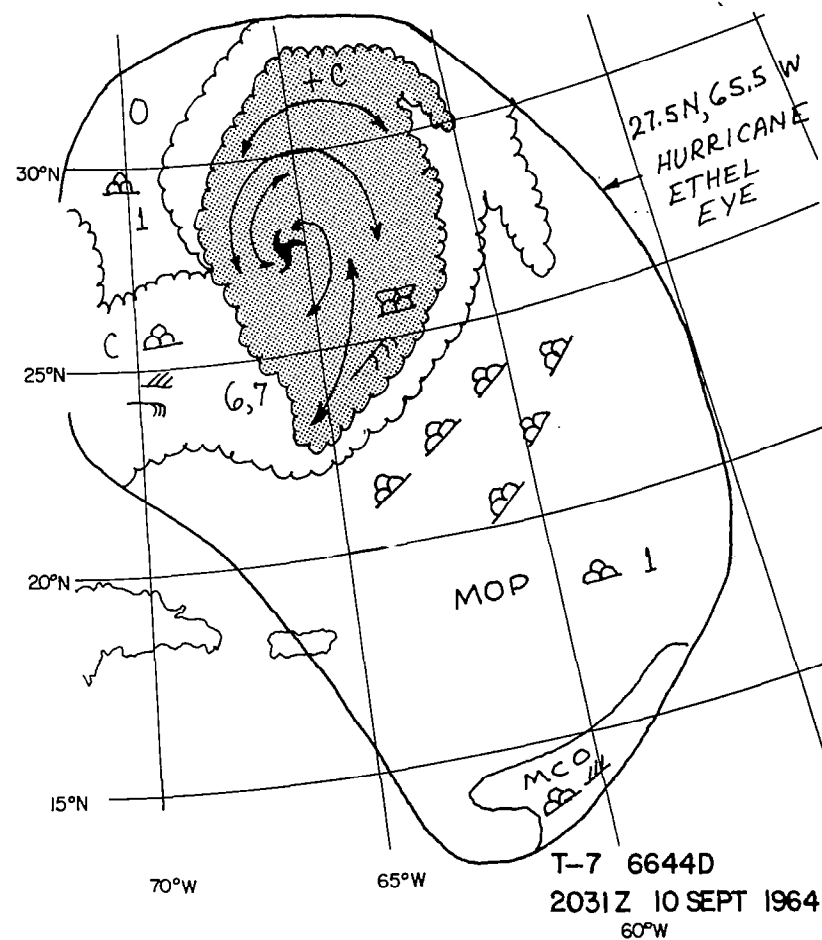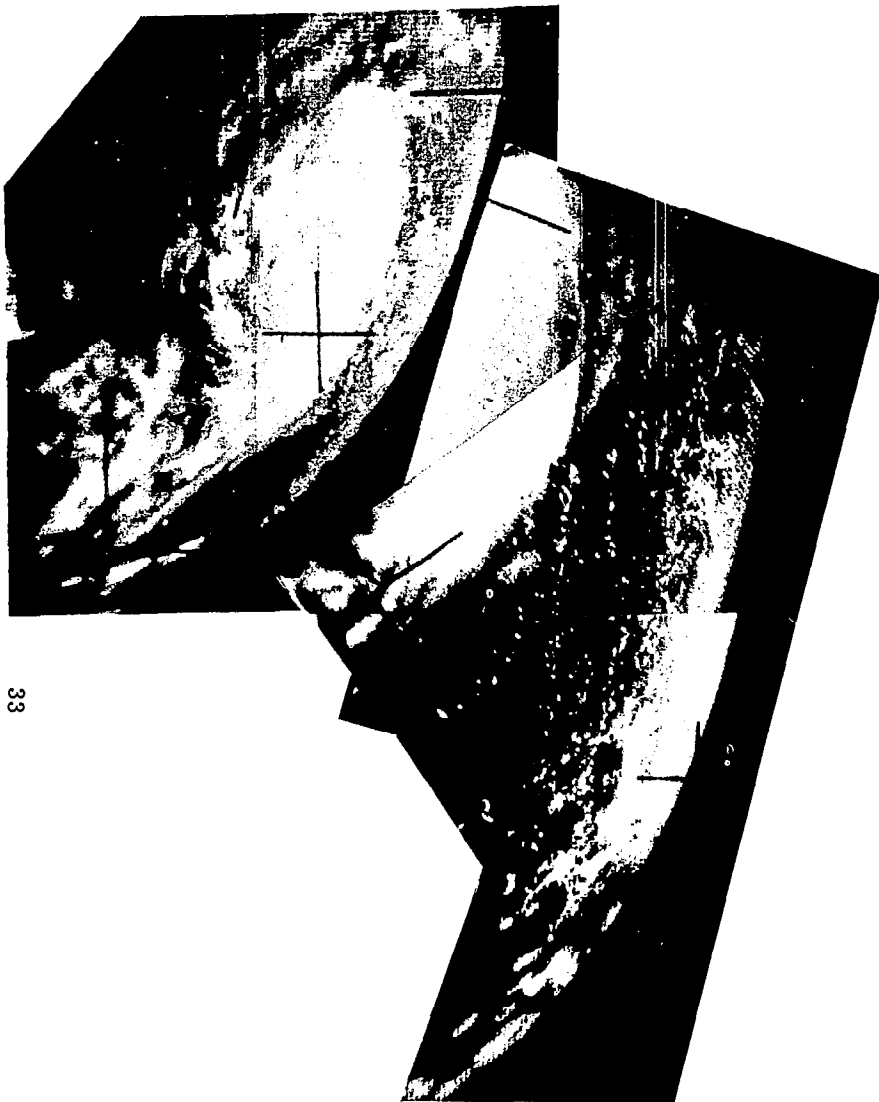
Figure 11.   TIROS VII Pictures and Operational Nephanalysis, Orbit 6644 D, 2237 UT,
10 September 1964, Showing Hurricane Ethel

6. Although the surface chart (Fig. 9) shows the cold front extending west-southwest of the Missouri River, and although this analysis is substantiated by the plotted temperatures, winds, and pressures, there is little sign of the very western end of the front in the HRIR data. There is cloudiness in this area in TIROS VII passes 6626 and 6631 on September 9 (not included). This suggests either that the frontal cloudiness is low level, or that it is primarily convective and dissipates at night. The brighter areas in the band near the east side of the orbit 190 HRIR strip, near and north of 43°N, may be associated with thunderstorm activity plotted on the surface chart at Valentine, Nebraska. Another thunderstorm area along the front, near Minneapolis, can be seen near the southwest corner of the orbit 189 HRIR strip. A cirrus plume, extending east-northeast from that cloud mass, matches the 500 mb flow.

7. Landmarks visible in the HRIR data, at least in the originals from which we worked, included:

    a. Greenland, with a definite suggestion of clouds extending over it from Davis Strait and Baffin Bay.

    b. The outline of the western shore of the Gulf of Newfoundland, showing this area to be clear.

    c. The southern California coast, which was faintly visible.

    d. Lakes in Canada, near 100°W north of 55° N.

4.1.2.1 Comparison with TIROS VII, Orbit 6629/6628

A mosaic of TIROS VII data, taken on orbit 6629/6628 about 1824 GMT, 9 September 1964, or about 12 hours before the HRIR data, is shown in Figure 12. Comparisons among Figures 7, 8 and 12 show:

1. A reasonable match of the cloud patterns over and near Newfoundland, including the clear area along the western coast of the Gulf of Newfoundland. It is to be noted, however, that the cellular cloud patterns photographed by TIROS over Newfoundland and Labrador are reproduced in the HRIR data as only a gray mass, with no significant patterning.

2. That there is also a reasonable match of the two views of the cloud patterns along the northern edge of the cloud mass near 90-100°W, and to its north and west. (Of the four TIROS mosaics in Figures 12 through 15, this one provides the

best match to the HRIR data in this area.) The (apparently middle) clouds over the northern portions of Hudson Bay, in both TIROS and the HRIR, can be related to the western extension of the 500 mb low whose center is over Baffin Island.

3.   That there are often no obvious differences, in the HRIR data, between low cellular clouds and areas of overcast low clouds.

4.   The match of a series of filmy bands over northwest Canada, suggesting some weather system still further west.

5.   A heavy cloud mass east of Newfoundland which the conventional analyses indicate to be a development along the cold front in that area.

4.1.2.2   Comparison with TIROS VII Orbit 6629/6629

The mosaic of TIROS VII, orbit 6629/6629, data in Figure 13 is for 1957 GMT on September 9, or about ten hours earlier than the HRIR data. Comparisons with Figures 7 and 8 show:

1.   A reasonable match 1) of the clouds associated with the cold front east of New England,   2) of the broken appearance of the front along its western end, and 3) of the clear area to the rear of the front, with only a few patches of scattered clouds. The HRIR data verify that these are low clouds.

2.   A good match to the northern part of the cloud mass, near $90-100^{\circ}$W, and to the more broken and lower clouds to both the east and the west of this cloud mass.

4.1.2.3   Comparison with TIROS VII, Orbit 6644/6642

The TIROS mosaic for this orbit (Fig. 14) is for 1706 GMT on September 10, or about 11 hours after the HRIR data of Figures 7 and 8. Comparisons show:

1.   The reasonable match of the cloud bands between Newfoundland and Greenland (note the tip of Greenland is just visible in the mosaic).

2.   A hint in the TIROS mosaic, near the horizon and 70°W, of the hook shaped cloud pattern in the HRIR data associated with the old vortex over Baffin Island.

3.   The match of the cloud patterns at the very north of the cloud mass over southern Hudson Bay, and of the lower clouds between it and the vortex clouds. (Note the eastward movement of this cloud mass in TIROS as compared to its location in the HRIR data.)

Figure 12a. TIROS VII Television Picture Mosaic, Orbit 6629/6628
1824 UT, 9 September 1964

T-7 6629/6628

1824Z 9 SEPT 1964

Figure 12b. TIROS VII Operational Nephanalysis, Orbit 6629/6628
1824 UT, 9 September 1964
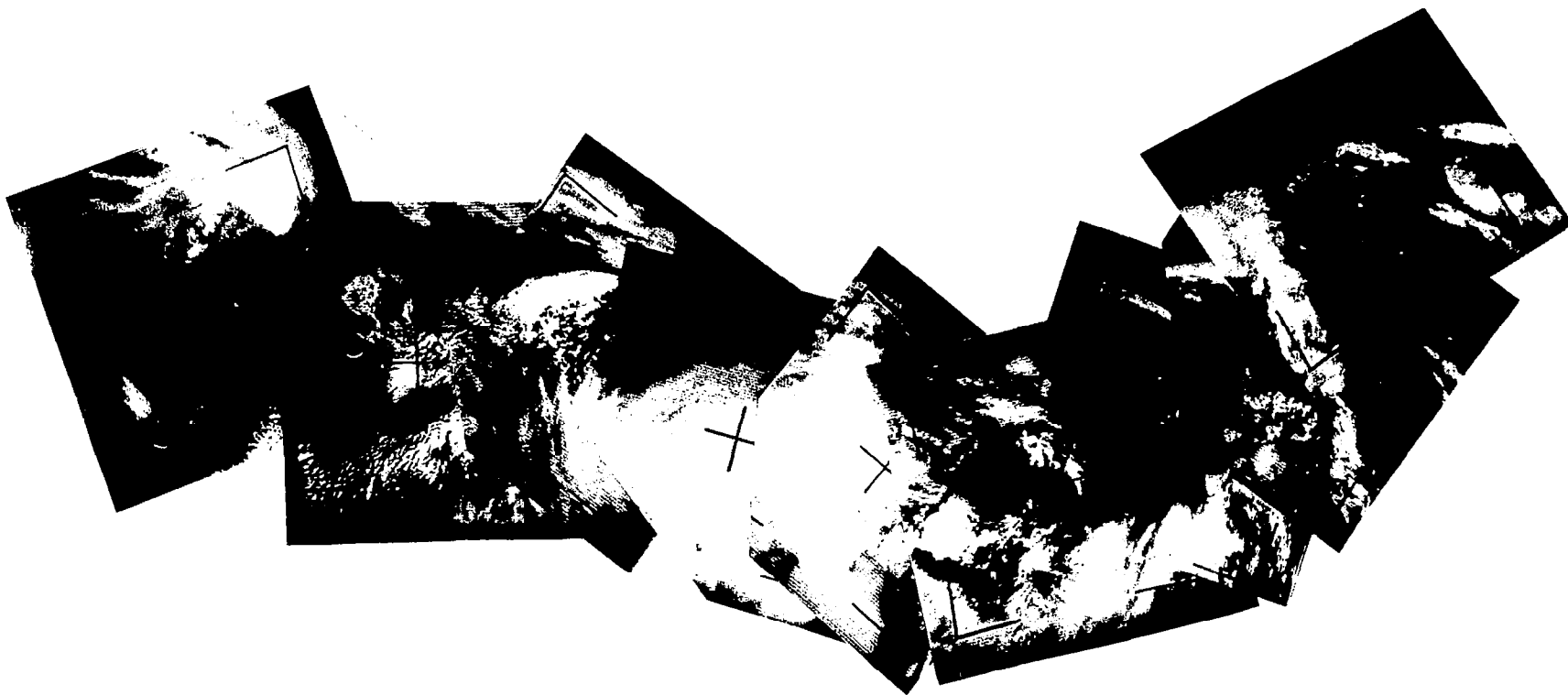
Figure 13a. TIROS VII Television Picture Mosaic, Orbit
6629/6629, 1957 UT, 9 September 1964
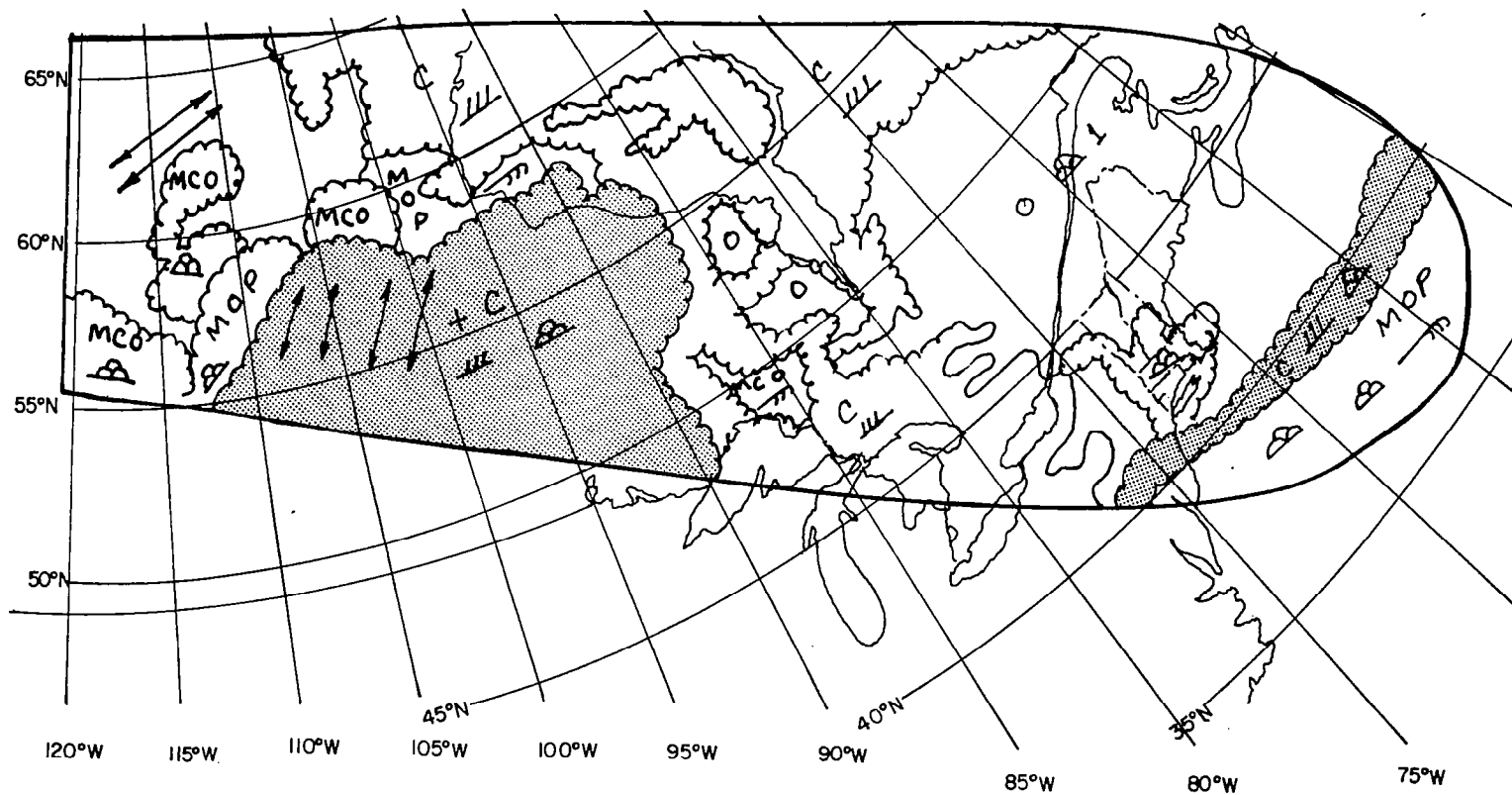
T–7 6629/6629
1957Z 9 SEPT 1964   Figure 13b.   TIROS VII Operational Nephanalysis, Orbit 6629/6629,
1957 UT, 9 September 1964

Figure 14a.   TIROS VII Television Picture Mosaic, Orbit 6644/6642,
1706 UT, 10 September 1964

T-7 6644/6642

1706Z 10 SEPT 1964

Figure 14b. TIROS VII Operational Nephanalysis, Orbit 6644/6642,
1706 UT, 10 September 1964

4.1.2.4 Comparison with TIROS VII, Orbit 6644/6643

These TIROS data, shown in Figure 15, are for 1846 GMT, about 13 hours after the HRIR data. When compared to Figures 7 and 8, it is obvious that:

1. There is, in spite of the time difference, a good match with regard to the cloud band and the clear-to-scattered area south of Newfoundland. Consideration must, of course, be given to the eastward movement of the systems during the 13-hour period.

2. The breaks and cellular patches in the TIROS pictures, near 55°N, 90°W, can be related to warmer (lower cloud) areas in the HRIR data.

3. The broken clouds to the west of 100°W in the TIROS pictures are compatible with the HRIR data.

The TIROS data suggest particularly heavy cloudiness just east of James Bay. As suggested by the subsequent HRIR data, and as shown in the surface charts (for September 11), the triple point of the occlusion was near or just south of the southern boundary of this TIROS pass, at about the longitude of this heavy cloudiness.

4.1.3 The HRIR Data for 11 September 1964

On the next day, there was only a single HRIR pass over this area (orbit 203) at about 0500 GMT. This is shown in Figures 16 and 17. Figure 18 is the 500 mb analysis for 1200 GMT on the 11th. Although the surface analysis in Figure 19 is for 1800 GMT, about 13 hours after the HRIR, it provides better coverage of the HRIR area than that available for 0600 GMT; furthermore, it is approximately concurrent with two TIROS mosaics that will be discussed.

In this HRIR strip we can identify:

1. Greenland, appearing generally clear except for clouds over the northeastern part of the portion observed by the HRIR.

2. The old vortex, still over Baffin Island, and its frontal band over Baffin Bay and the eastern part of the Davis Strait. At 500 mb, this old vortex is reflected only as a northerly extension of a closed circulation over northern Quebec. The primary circulation in this region is now associated with the storm that a day earlier was northwest of the Great Lakes. Southwest of the front, much of Davis Strait is covered with low cloud, some of which does have a cellular appearance.

3. The storm previously north of the Great Lakes, now appearing in the HRIR as a vortex centered near 57°N, 75°W. This corresponds well to the 500 mb low (Fig. 18), especially when the movement of the center at 500 mb between 0000 GMT and 1200 GMT is considered. The hook shaped bright (high cloud) area near the edge of the strip leaves no doubt that a closed circulation now exists in the mid-troposphere. The surface map (Fig. 19) shows precipitation under the bright cloud area of the hook. Much of Quebec east and south of the vortex center is covered with low clouds. There is a suggestion of cloud streets near 55°N, 68°W.

4. The frontal band extending southeast and south from the vortex, broadening very significantly over the western Gulf of Newfoundland, and definitely suggesting a triple point development. This is confirmed by the surface analyses (Fig. 19), which also shows precipitation generally associated with the brighter cloud areas. With only the HRIR data available, an analyst would have every reason to place a short wave in the 500 mb flow over New Brunswick. Rather surprisingly, there is only limited evidence for such a short wave in the 500 mb winds or analysis for 1200 GMT, September 11; or for 0000 GMT, September 12. Possibly, it was suppressed by the presence of the 500 mb ridge just east of Newfoundland. There was, however, a short wave in the 0000 GMT, September 11, 500 mb chart, between Sault Ste. Marie and Maniwaki. By 1200 GMT on September 11, the 500 mb wind at Caribou had increased to 60 knots from the west. A short wave was analyzed in the 700 mb contours, just east of Caribou.

As mentioned in Section 4.1.2.4, the TIROS data for orbit 6643, about ten hours earlier (Fig. 15) included the very northern part of the broadened cloud band associated with the triple point of the occlusion.

5. The western coast of the Bay of Fundy, detectable in the working original of the HRIR.

4.1.3.1 Comparison with TIROS VII, Orbit 6661/6657

The TIROS mosaic shown in Figure 20 was taken about 12-1/2 hours after the HRIR data. It indicates that during that interval the cloud mass associated with the triple point has moved about 400 miles to the northeast of its position on the HRIR. Unfortunately, only parts of the vortex over Labrador were within the limits of the TIROS coverage, but the positions of the center are compatible. Comparison of the two views indicates that much more of the clouds, east and south of the center, are low clouds than would probably have been deduced from the TIROS pictures alone;

Figure 15a. TIROS VII Television Picture Mosaic, Orbit 6644/6643, 1846 UT, 10 September 1964
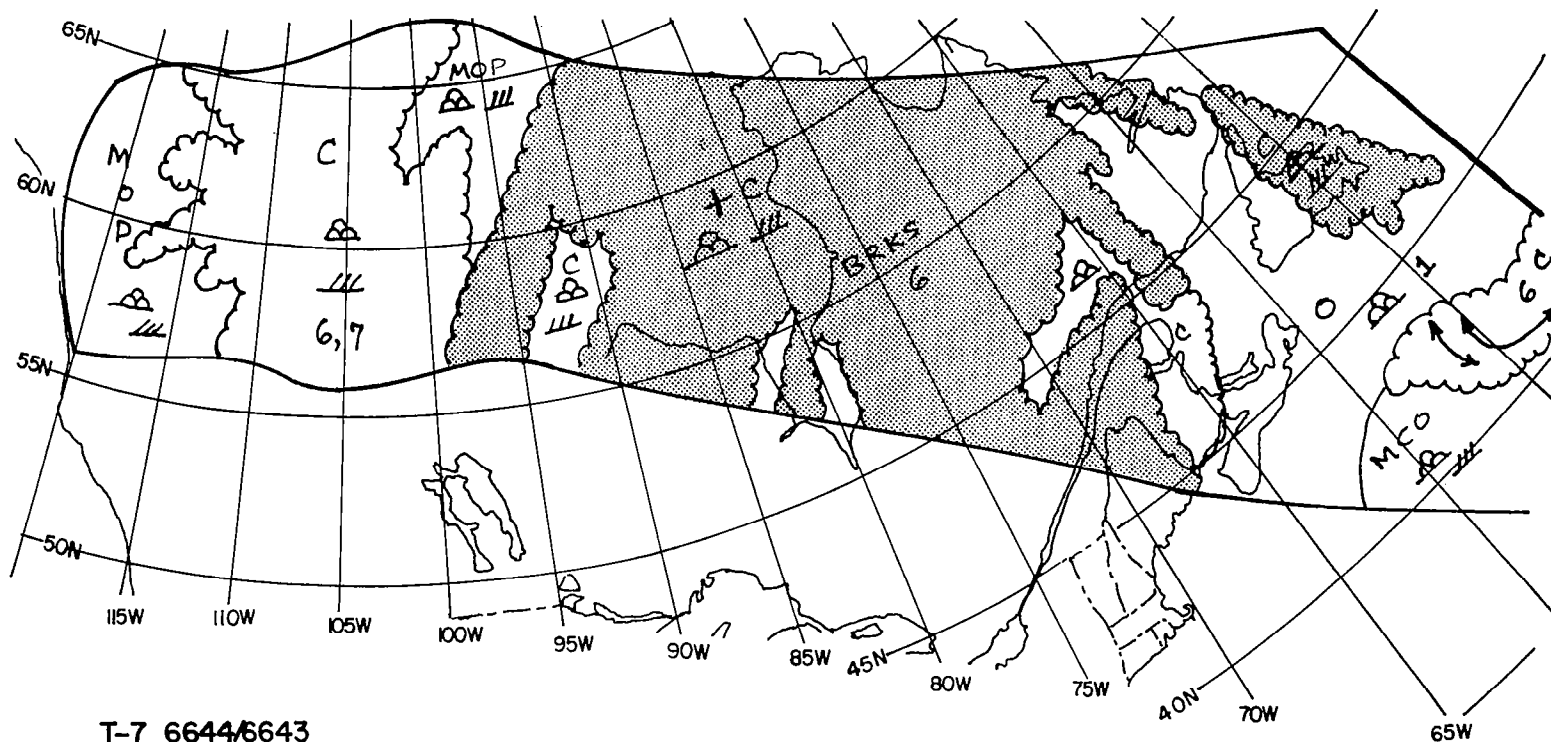
T-7 6644/6643

1846Z 10 SEPT 1964

Figure 15b.   TIROS VII Operational Nephanalysis, Orbit 6644/6643,
1846 UT, 10 September 1964

Figure 16. HRIR Data for Orbit 203, 0500 UT, 11 September 1964

Figure 17. Rectified HRIR Data for Orbit 203, 11 September 1964
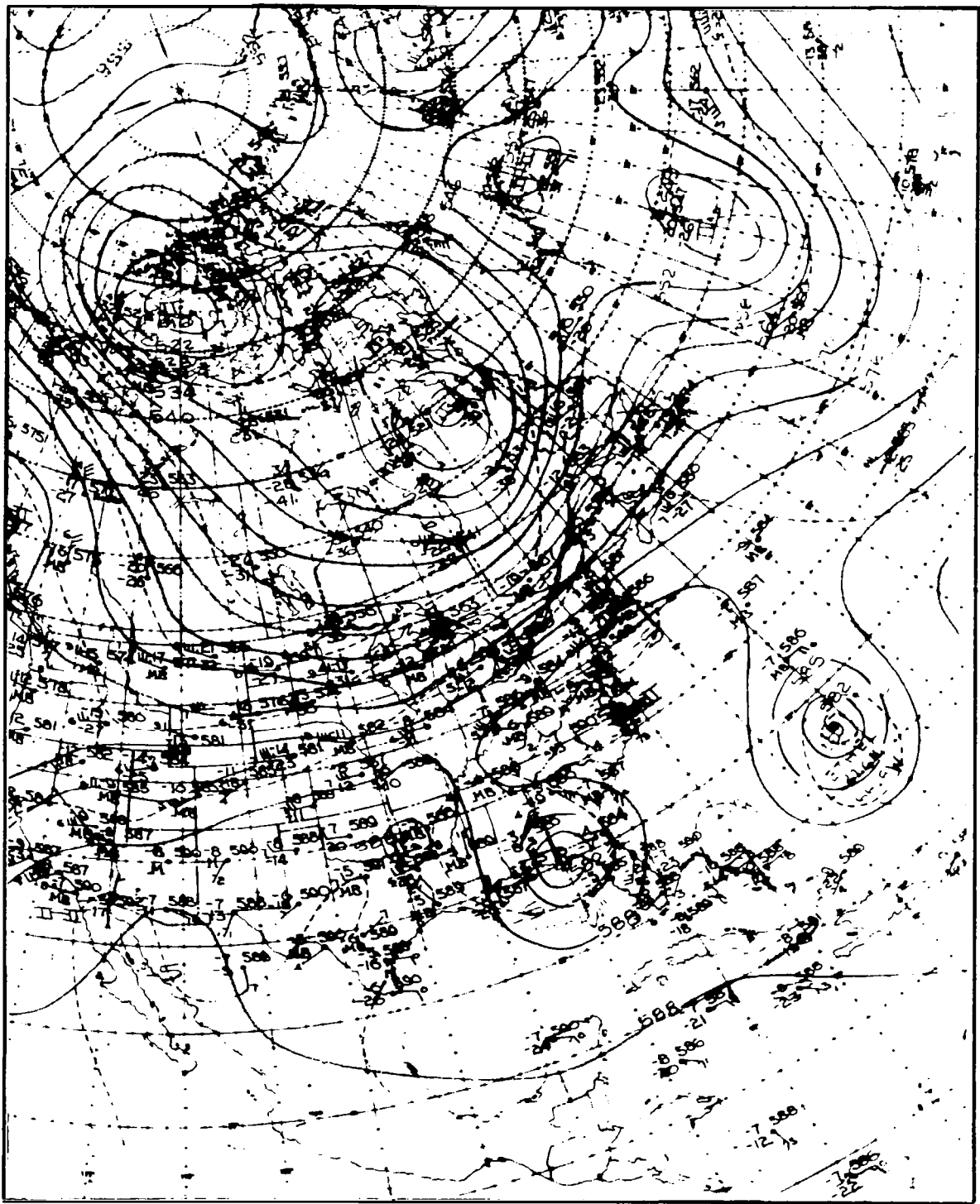
Figure 18.   NMC 500 mb Analysis, 1200 UT, 11 September 1964
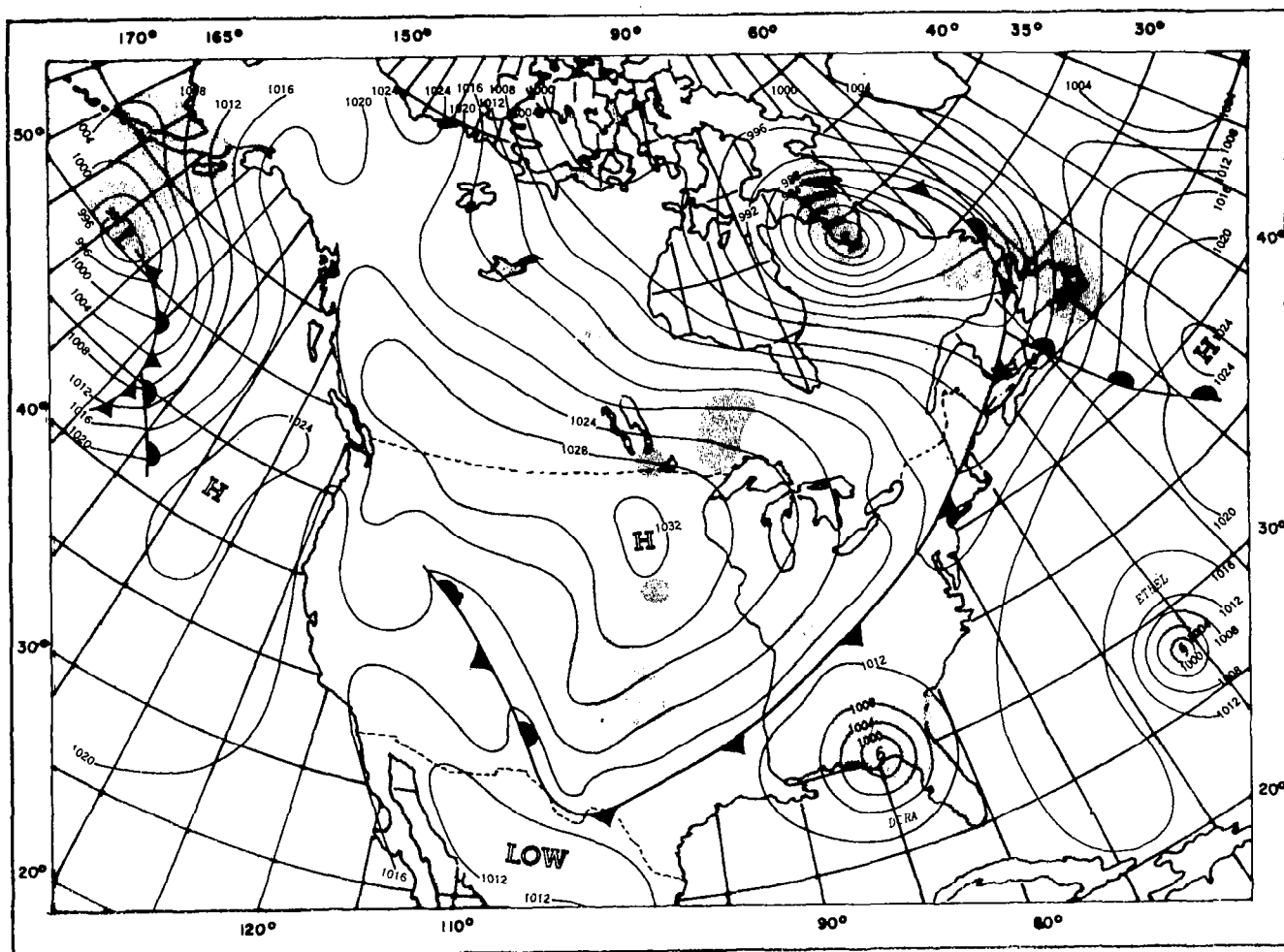
Figure 19. Surface Analysis, 1800 UT, 11 September 1964

in fact, most of the clouds in the TIROS mosaic west of 70°W are probably low clouds. For example, it seems reasonable to associate the obviously low clouds in the HRIR near 55°N, 75°W with the overcast in the TIROS mosaic near 58°N, 72°W. In the area near 55°N, 65°W , the TIROS data show considerably more detail as to cloud streets and cellular clouds than can be inferred from the HRIR.

'4.1.3.2   Comparison with TIROS VII, Orbit 6659/6658

These TIROS pictures, taken about 14 hours after HRIR orbit 203, are shown in Figure 21. Over eastern North America, Figure 21 is for the most part just south-west of the coverage of TIROS orbit 6657 (Fig. 20), with only a slight overlap. Accordingly, only the northeastern portions of Figure 21 show features in HRIR orbit 203 (Figs. 16 and 17), and then only those in the southwest parts of the HRIR. The TIROS mosaic in Figure 21 will also be found to be applicable to the HRIR data for September 12, (Figs. 22 and 23).

Comparable views of parts of the frontal band over the St. Lawrence River valley, and of the cellular cloud areas northwest of the front, can be found in both types of data. Perhaps one of the most interesting common features is the area of cloud streets just northwest of the frontal band in TIROS . In the HRIR, they appear almost to be a low cloud broadening of the band (along its northern edge west of 70°W) but the line structure could be seen in the working original.

4.1.4   The HRIR Data for 12 September 1964

The three HRIR orbits available for this final day of the series (Figs. 22 and 23) are chiefly of interest for: 1) the further continuity they provide with regard to the cyclone and front over eastern Canada, and 2) the data in orbit 217 for Hurricane Ethel. The 500 mb analysis for 1200 GMT is given in Figure 24. Again, the 1800 GMT surface map (Fig. 25) was the best for the areas of chief interest, as well as for approximating the time of the TIROS data.
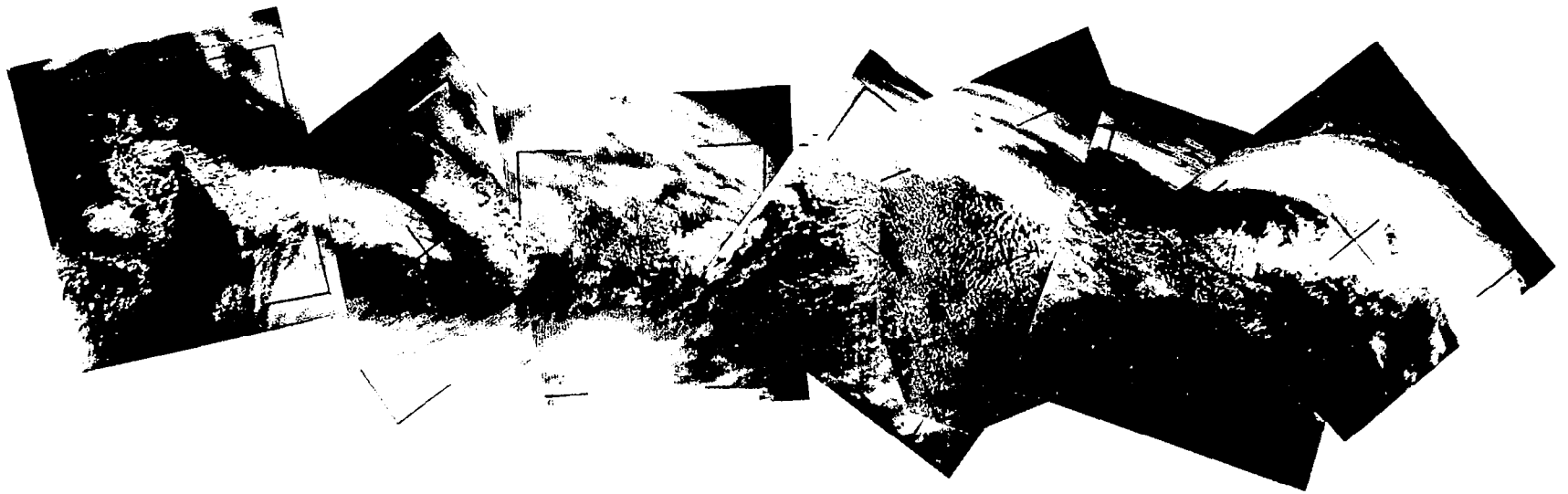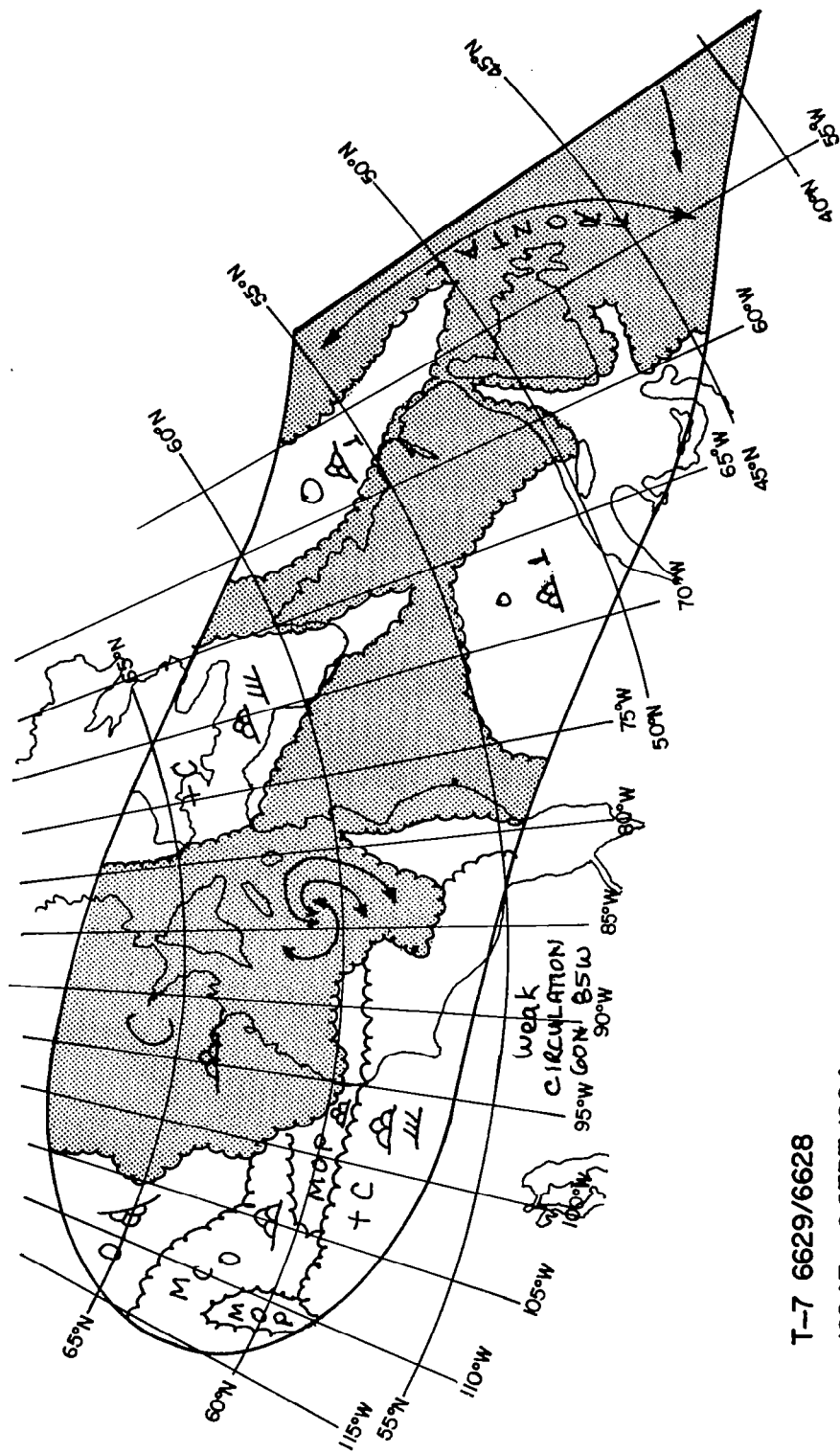
Figure 20a. TIROS VII Television Picture Mosaic, Orbit 6661/6657,
1732 UT, 11 September 1964

51

T-7 6661/6657
1732Z 11 SEPT 1964

Figure 20b. TIROS VII Operational Nephanalysis, Orbit 6661/6657,
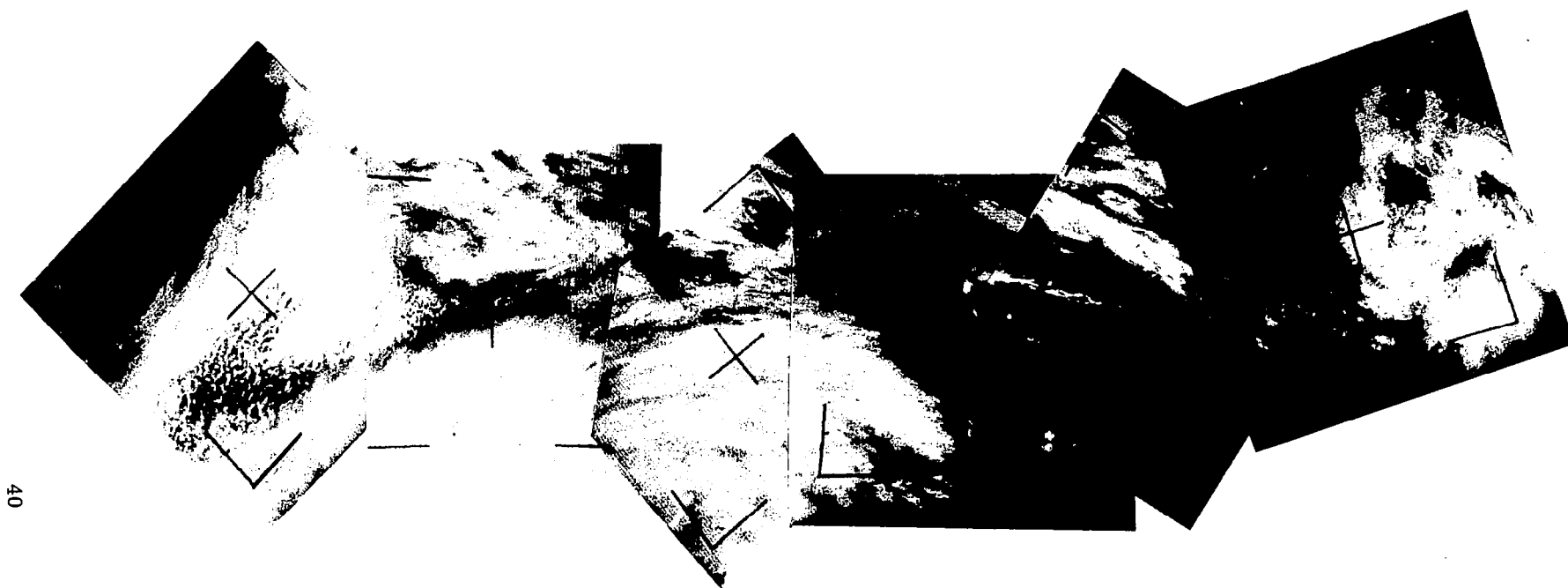1732 UT, 11 September 1964
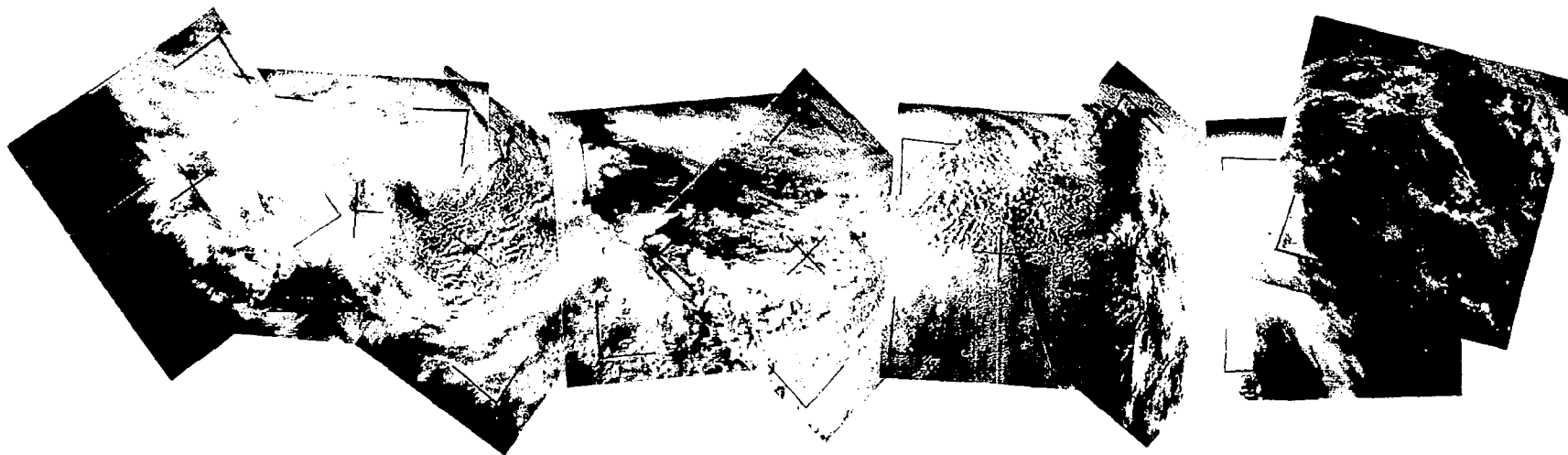
Figure 21a.   TIROS VII Television Picture Mosaic, Orbit 6659/6658,
1907 UT, 11 September 1964

Figure 21b. TIROS VII Operational Nephanalysis, Orbit 6659/6658, 1907 UT, 11 September 1964

T-7 6659/6658
1907Z II SEPT 1964

53

Figure 22. HRIR Data for Orbits 217, 218, 219, 12 September 1964
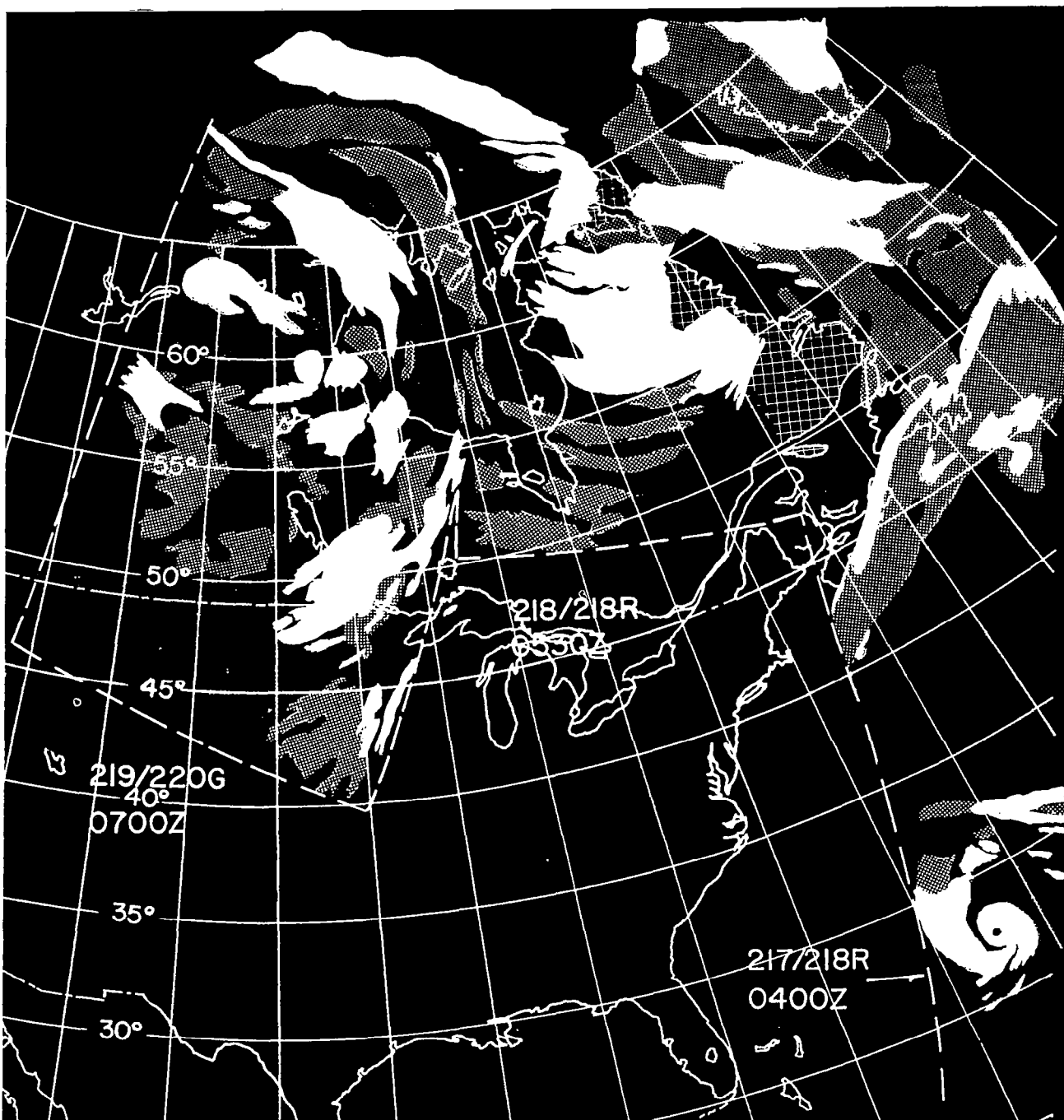
Figure 23. Rectified HRIR Data for 12 September 1964
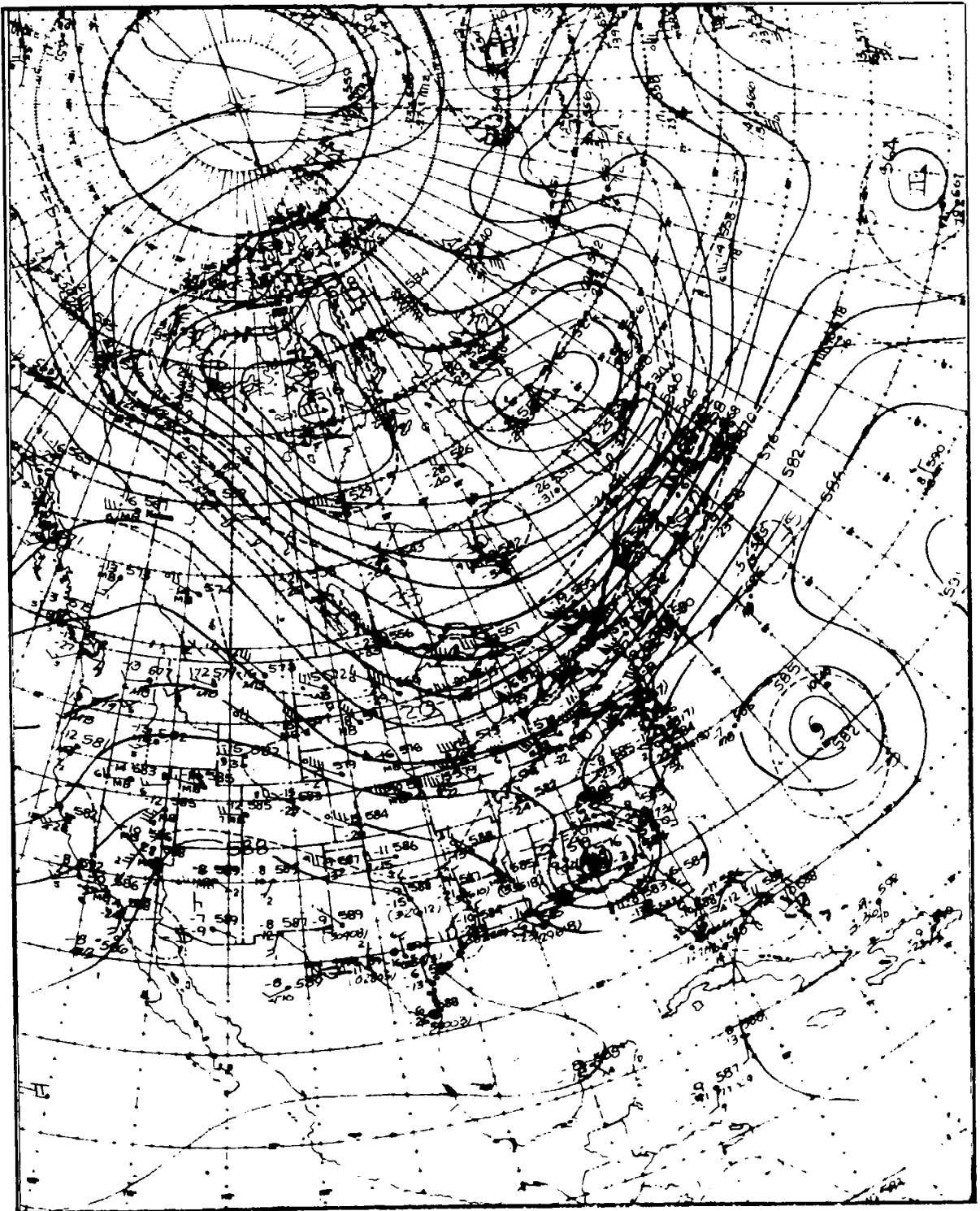
Figure 24. NMC 500 mb Analysis, 1200 UT, 12 September 1964
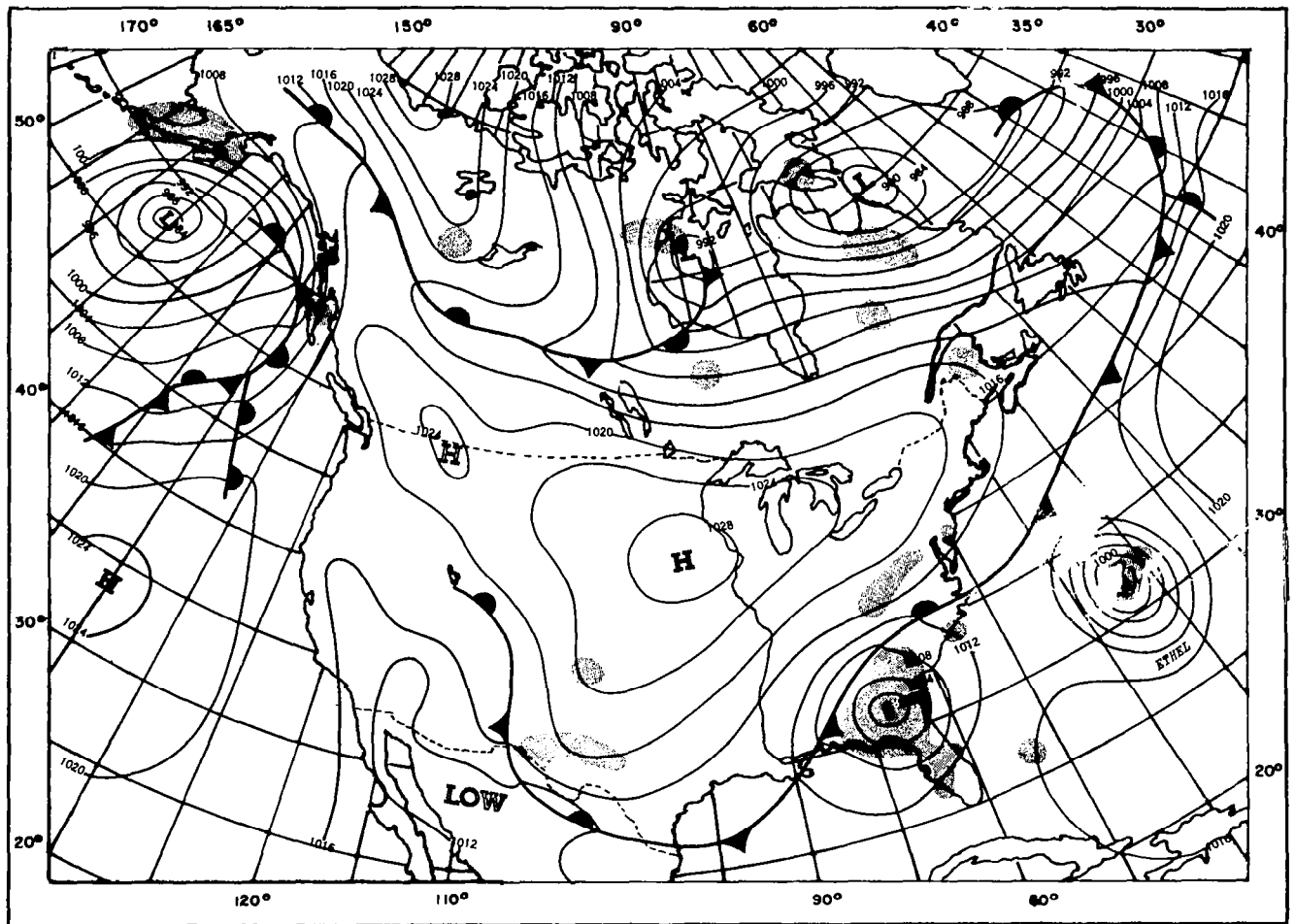
Figure 25.   Surface Analysis, 1800 UT, 12 September 1964

4.1.4.1 The Vortex and Front Over Eastern Canada

The HRIR data place the vortex center near $60°N$, $68°W$, in good agreement with the 500 mb and surface analyses. The two bright (high cloud) areas in the HRIR, east and west of the center, can be associated with short wave troughs moving around the center, which give it a west-northwest - east-southeast elongation. The western bright cloud area can be related to an area of precipitation on the surface chart.

The frontal band extending from the vortex runs southeast through Davis Strait to east of Newfoundland, then southwest across southern Newfoundland and just southeast of Nova Scotia. A slight bulge in the band just east-southeast of Newfoundland is in good agreement with the triple point of the occlusion (Fig. 25).

In Figure 21, the TIROS VII data for orbit 6658 (some ten hours earlier), the frontal band can be seen about the time it was reaching and crossing the coast. It also shows much of the low cloud, well southwest of the vortex center, over and near James Bay, and some heavier cloudiness north of Lake Winnipeg. Since the HRIR data (orbit 217) showed much of the area over Labrador to be clear, at least some of the cellular cloudiness west of the front appears to have dissipated prior to 0400 GMT (about 0000 local time in Labrador). This may very well have been a diurnal effect.

Figure 26 is a mosaic of TIROS VII, orbit 6672, pictures taken about 14 hours after the HRIR data in Figures 22 and 23. It shows the cold frontal band in nearly the same position as in orbit 217 of the HRIR, and various areas of clear to broken cloudiness to its rear. The leading edge of the vortex-related cloudiness which was near the Quebec-Labrador border in the HRIR has moved eastward somewhat faster than those parts of the front at about the same latitude; it now lies slightly east of the northwest coast of the Gulf of Newfoundland. In general, however, the HRIR and TIROS veiws of this situation are entirely compatible.

Landmarks in the general area of the vortex and front that were visible, at least in the working originals of the HRIR data, include most of the Labrador coast, Lake Melville, Anticosti Island, western Newfoundland, the eastern shore of Hudson Bay north of about $58°N$ and parts of Baffin Island. Much of Greenland appears to be visible, but with various degrees of cloudiness; the eastern shore between about $64°$ and $70°N$ was clear.

The cloudiness west of $90°W$ and north of $45°N$ (in HRIR orbit 219) can be explained by a short wave trough near Lake Winnipeg (which was more clearly analyzed in the 0000 GMT 500 mb chart for September 21 than that shown for 1200 GM' and by the closed low and other short wave troughs northwest of Hudson Bay. No

detailed discussion of this system seems appropriate since it was not viewed by the HRIR on the previous day, and since this is the last day of the series.

4.1.4.2 Hurricane Ethel

Hurricane Ethel can be seen in HRIR orbit 217, near 28°N, 68°W. This is somewhat south of the positions in the conventional analyses, even considering the northward movement of the storm at this time. Perhaps the nearness of the storm to the edge of the HRIR data, and the appearance of considerable spacecraft roll on this orbit contributed to the discrepancy.

Figure 27 is a TIROS veiw of Ethel about 15-1/2 hours later. The correspondence to the HRIR view is rather good. Features to note include:

1. The eye, visible in both the HRIR and the TIROS picture.

2. A moat, filled with broken lower clouds, to the west of the storm center. The moat is far more obvious in the HRIR, but without the TIROS picture the low broken cloudiness in it might be overlooked.

3. The high cloud band, starting northeast of the storm and extending east-southeast to about 29°N. The sharp bend in this band in the TIROS neph may be due to the northward movement of the storm center during the 15-1/2 hour interval. It also suggests that the TIROS nephanalyst may not have given adequate consideration to foreshortening when he was entering this band.

4. The faint, narrow cloud bands, just northeast and east of the storm, in the HRIR data. Comparison of the TIROS picture and the HRIR data suggests they represent a mixture of cumuliform bands and cirrus streamers.

4.2 A Western Pacific Vortex Development

This case came to our attention because of the extremely striking vortex which appears chiefly on orbit 252, with the more western parts visible on orbit 253. Further investigation showed that the development of the system could be followed during the two previous days. Because the entire development takes place along or near the Japanese and Kuril Islands, and southern Kamchatka, the 500 mb data are far better than those usually available for studying an oceanic system over several days.

A general analysis based solely on the HRIR data was estimated for each day of the series before consulting the concurrent 500 mb analyses; the Russian surface analyses became available only after part of these discussions had been prepared in draft form.
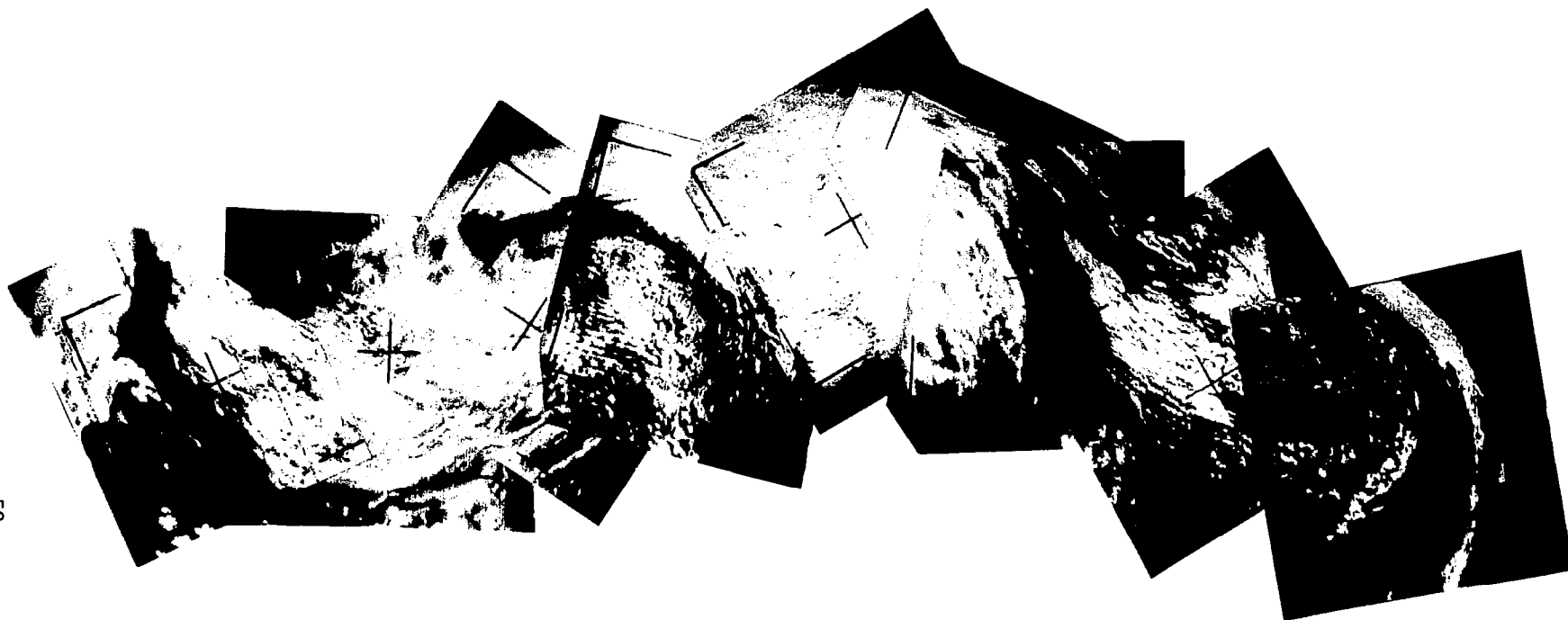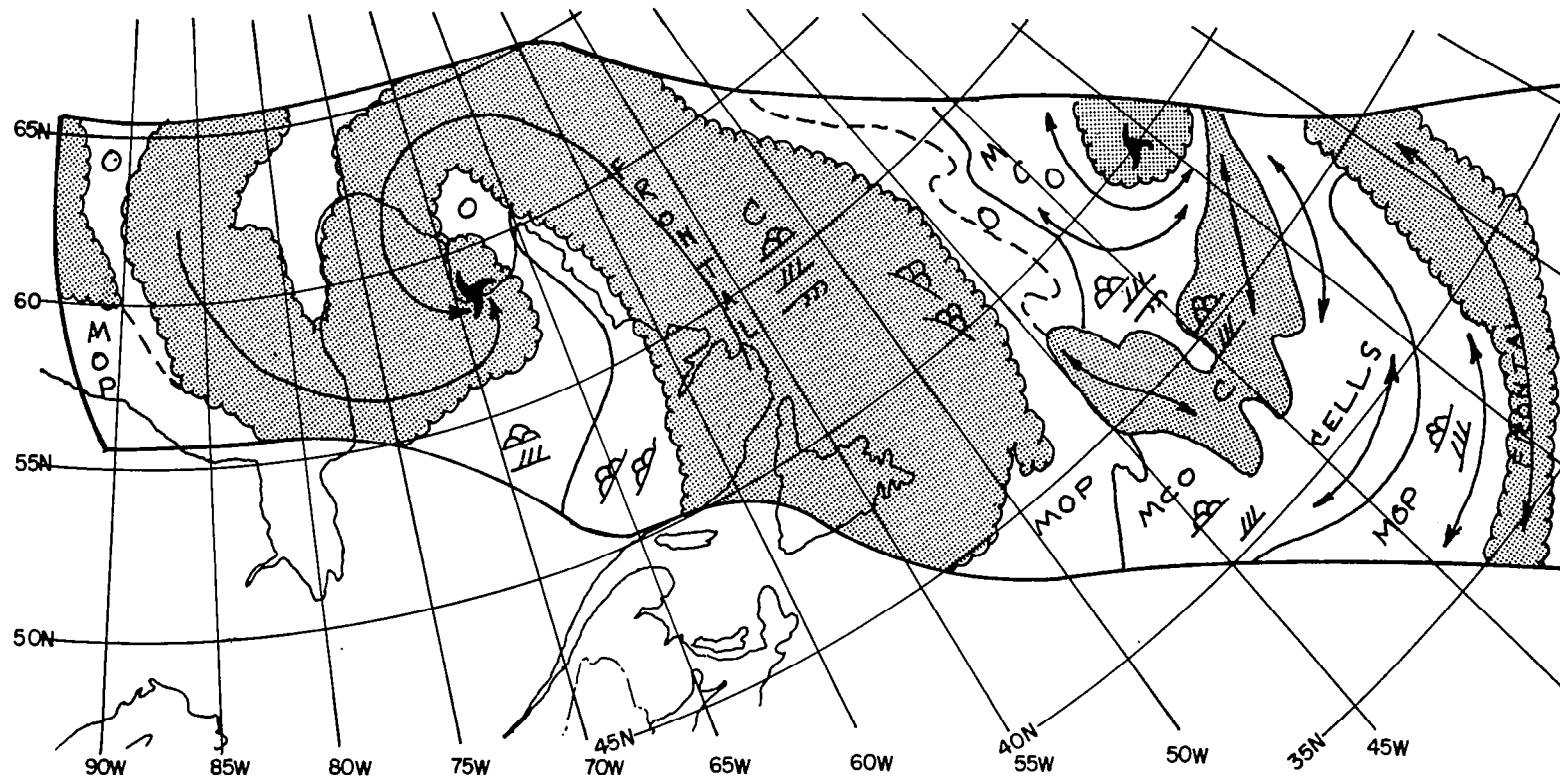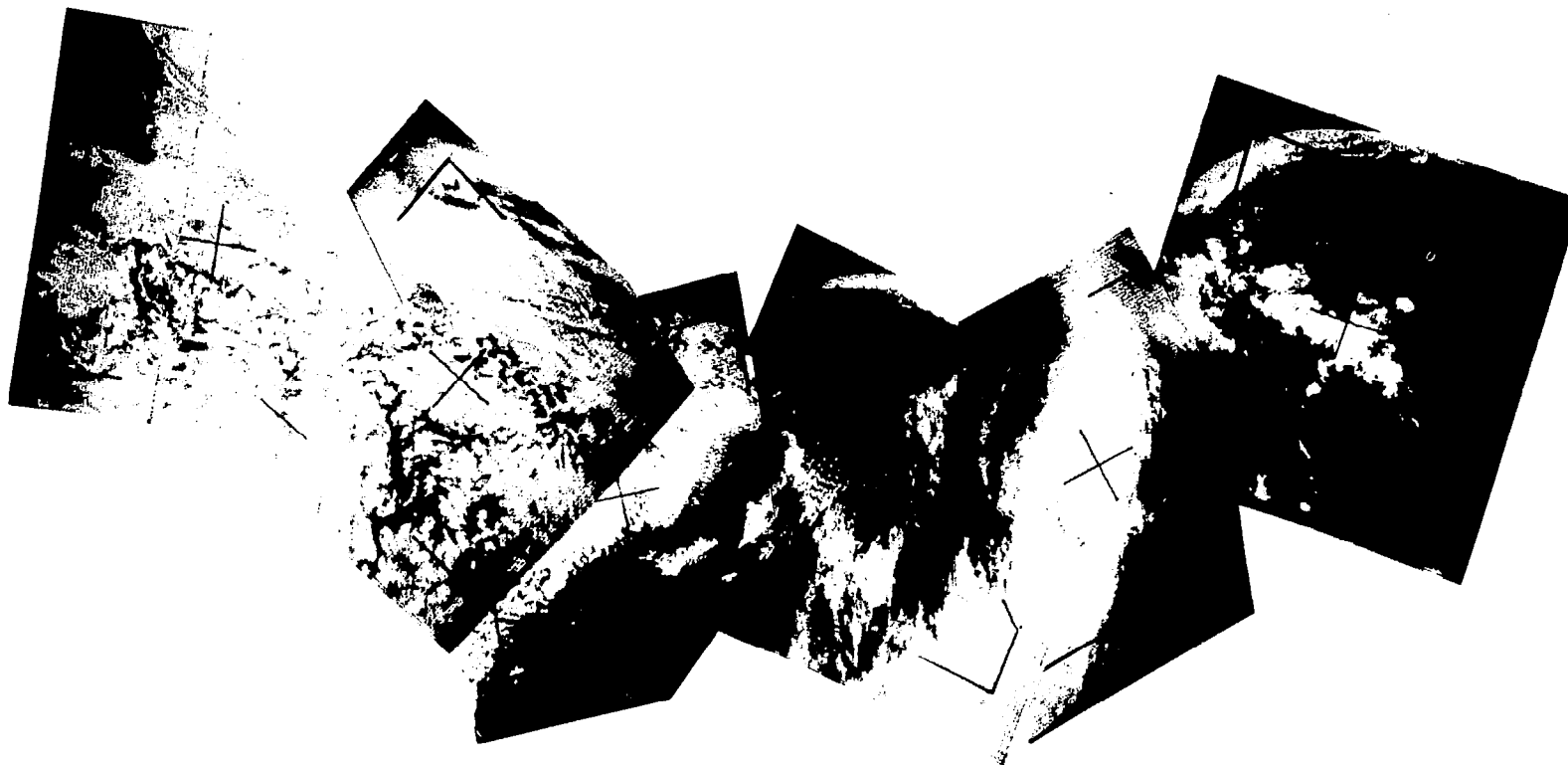
Figure 26a.   TIROS VII Television Picture Mosaic, Orbit 6673/6672,
1755 UT, 12 September 1964

T-VII 6673/6672

1755Z   12 SEPT 1965
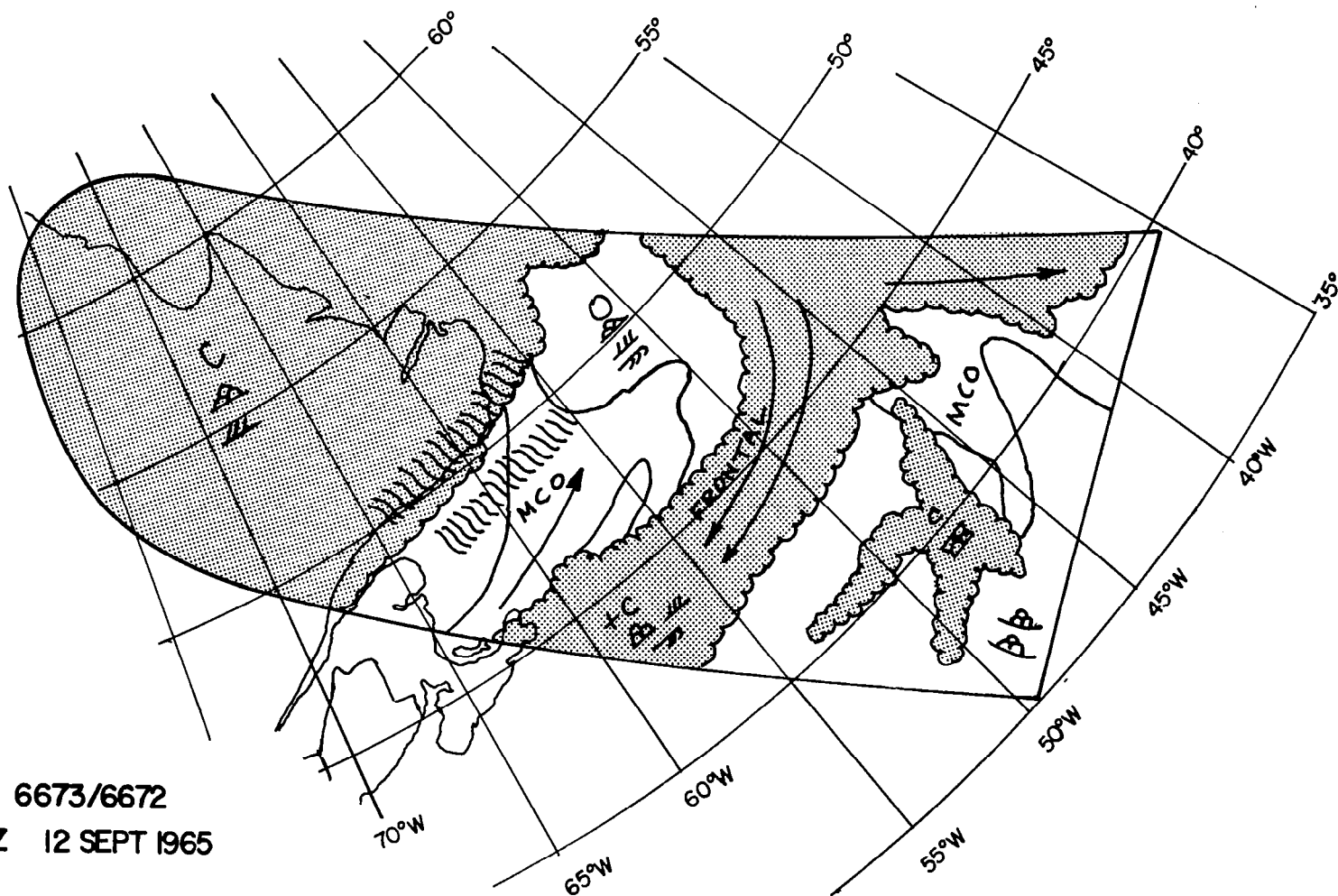
Figure 26b.   TIROS VII Operational Nephanalysis, Orbit 6673/6672,
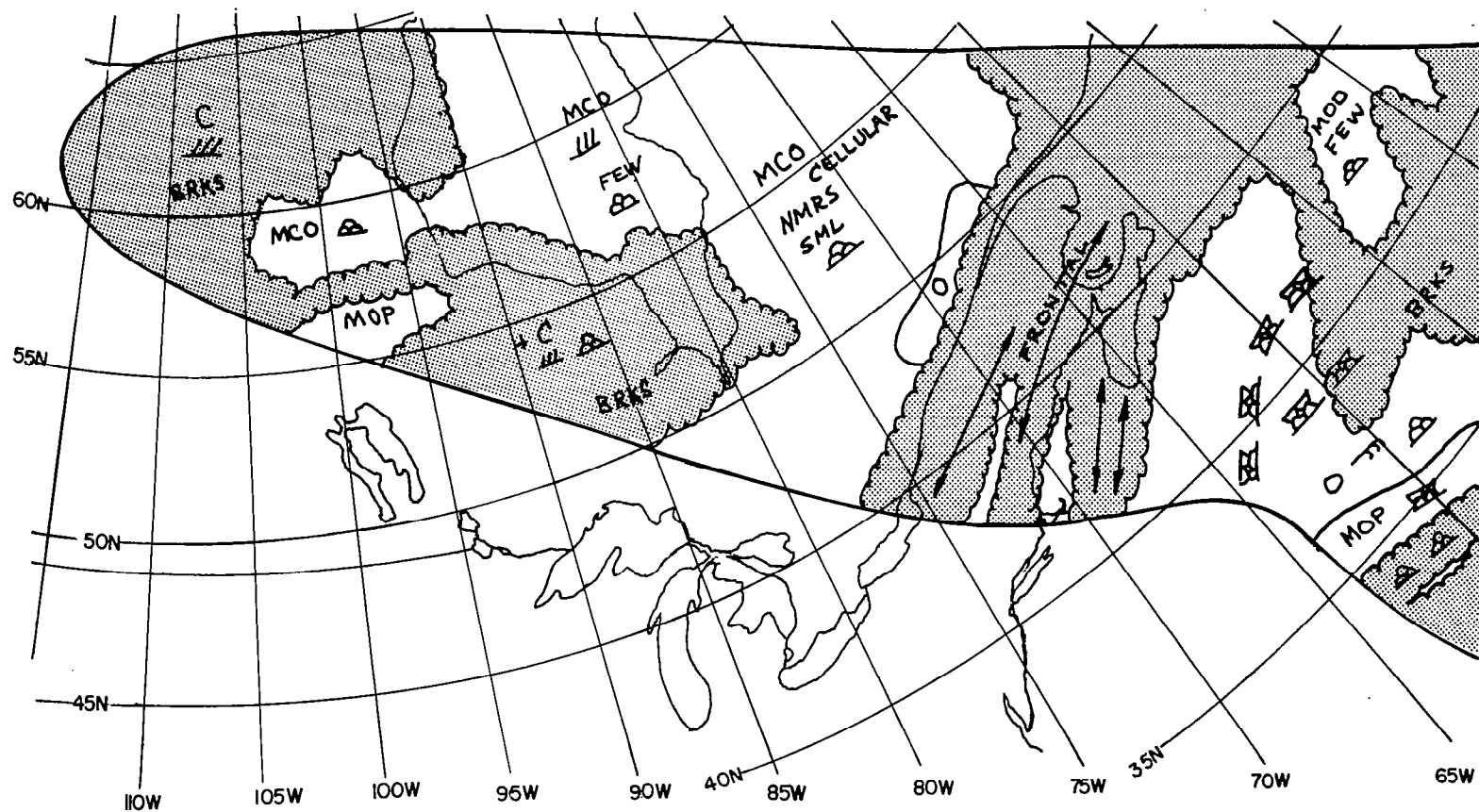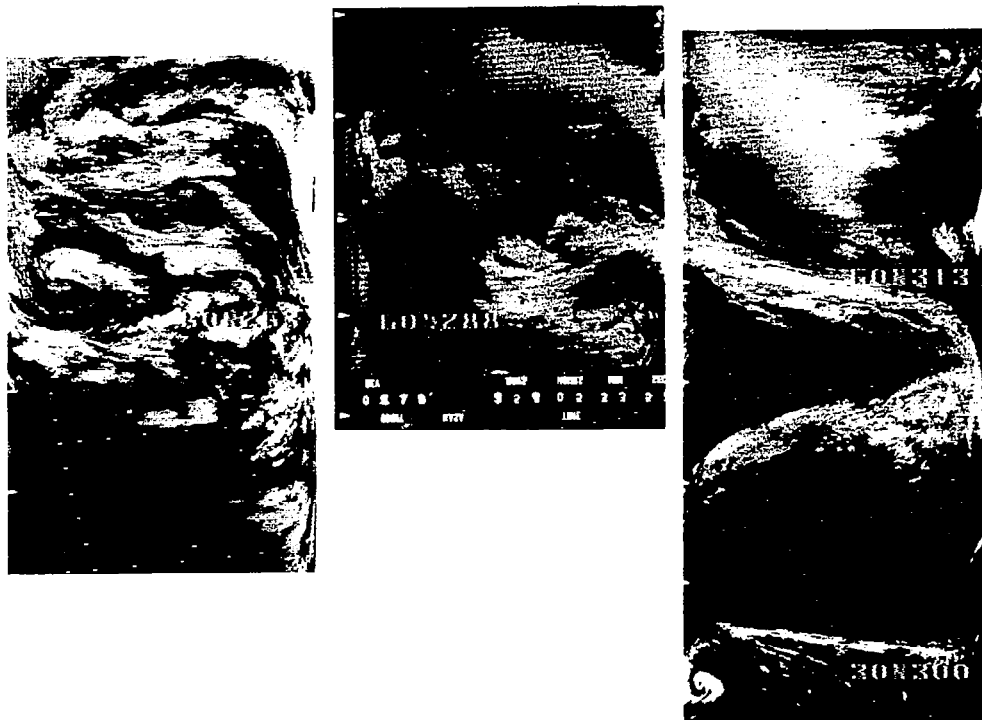1755 UT, 12 September 1964
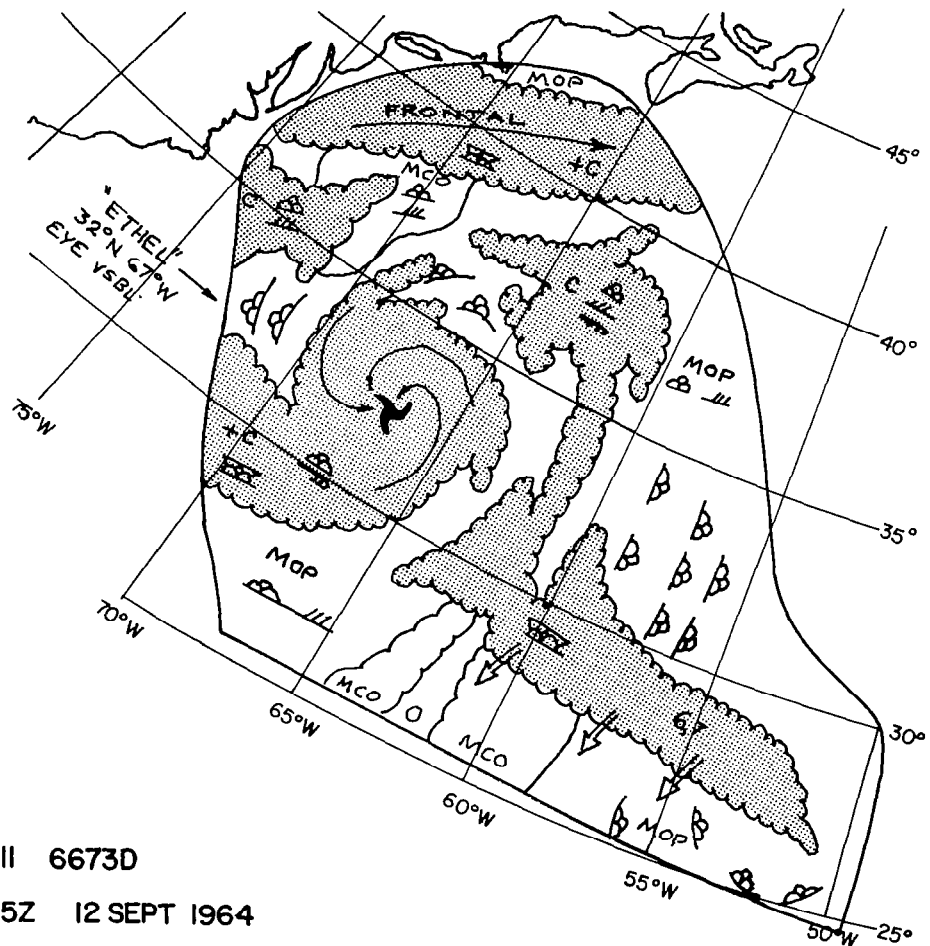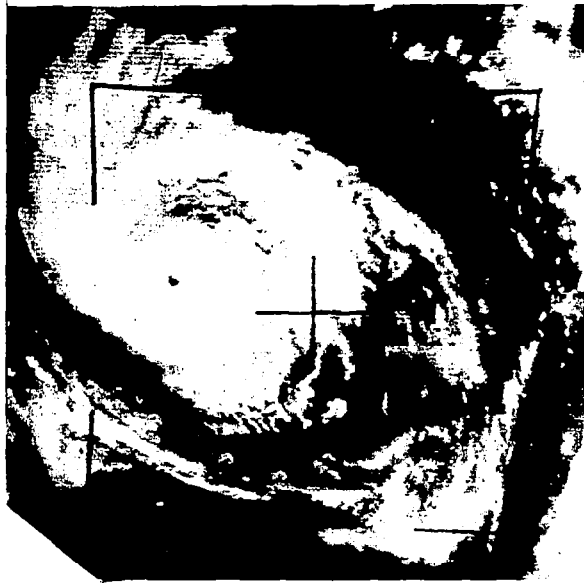
T-VII   6673D

1935Z   12 SEPT 1964

Figure 27.   TIROS VII, Orbit 6673 D, Picture of Hurricane
Ethel, and Operational Nephanalysis, 1935 UT
12 September 1964

4.2.1 The Situation on 12 September 1964

Orbit 224 of the Nimbus I HRIR, taken about 1525 GMT on 12 September 1964, shows a rather broad cloud band extending from Korea northeast along the Sea of Japan, across Hokkaido and Sakhalin, and into the Sea of Okhotsk (Figs. 28 and 29). The general appearance and orientation of the band suggest it coincides with the region of southwesterly flow just east of a significant upper level trough. An active cold front, perhaps with one or more waves along it, would be expected to lie somewhere under the eastern edge of the band. There would appear to be a major disturbed area or cumulonimbus complex over southern Korea, with a relatively large region of cloud tops extending into the upper troposphere. The fine structure of the cloud field as seen in the HRIR suggests some circulation exists, centered more or less near the southwest end of the band. The individual cloud fingers along the southeast edge of the band are very likely related, at least in part, to the topography of the Japanese Islands.

A narrow band, along the northern edge of the eastern part of the major cloud mass, appears to be a jet stream cirrus band. There is no obvious explanation for the two smaller cloud masses, west of the main mass, at about 50°N.

The 500 mb chart for 1200 GMT (Fig. 30), about 3-1/2 hours earlier, shows the expected trough more or less along the east coast of Adia, starting near Korea and extending northward along 128°E. Because of a short wave trough located over Sakhalin, the northern part of the trough appears broadened and expanded in an eastward direction. The latitude of highest winds along 140°E appears to be perhaps 5 degrees south of the position suggested by the narrow cloud band.

The two smaller cloud masses along 50°N can now be seen to lie in the wind shift line along 50°N, which separates westerly flow to the south from southerly flow to the north. Accordingly, these clouds can be attributed to dynamic lifting associated with a region of cyclonic vorticity.

Lower level cloudiness in orbit 224, near 60°N, is apparently associated with the closed low near 65°N, 135°E. Once this association is noted, a weak vortex structure becomes visible in the HRIR data.

The only readily available surface charts for this area were Russian analyses for 0000 GMT of each day (not included). Interpolation between those for the 12th and 13th, places an occluded low near 51°N, 135°E, or just east of the 500 mb low. About the time of the HRIR data, a frontal wave would have been passing over Korea,

Figure 28. HRIR Data for Orbit 224, 1525 UT,

12 September 1964
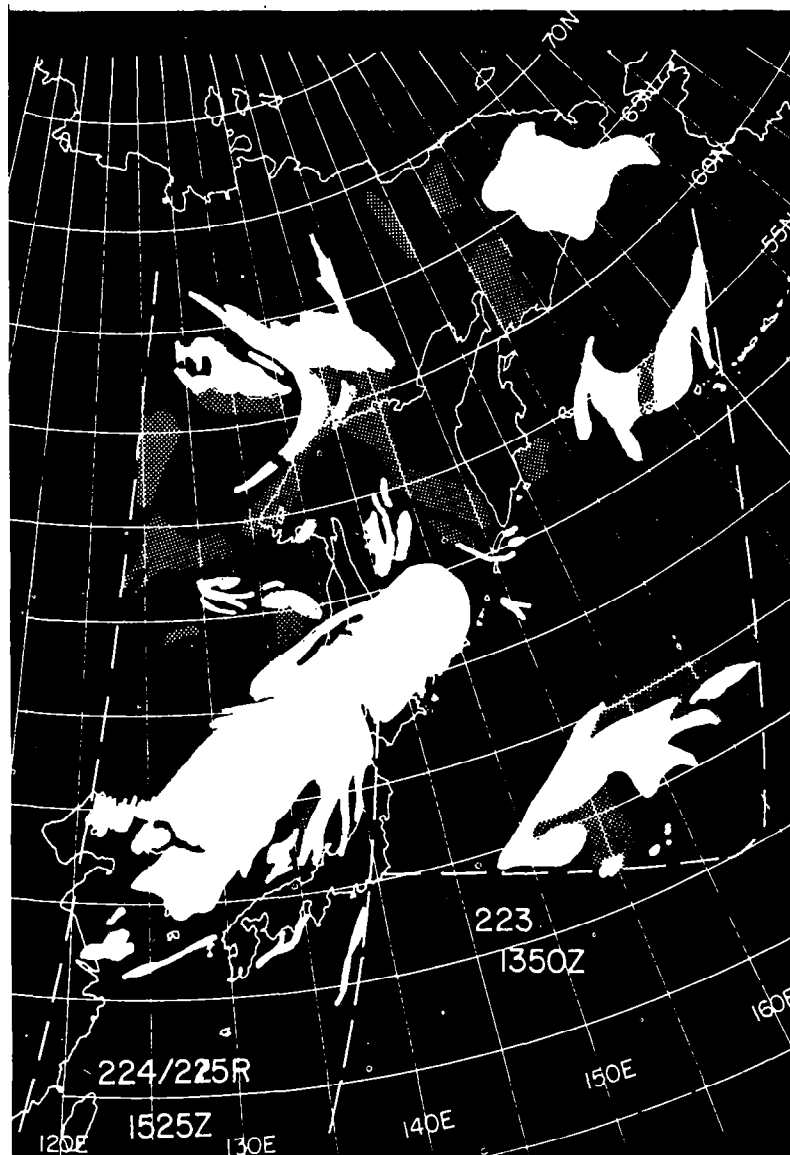
Figure 29. Rectified HRIR Data for Orbits 223 and 224,

12 September 1964
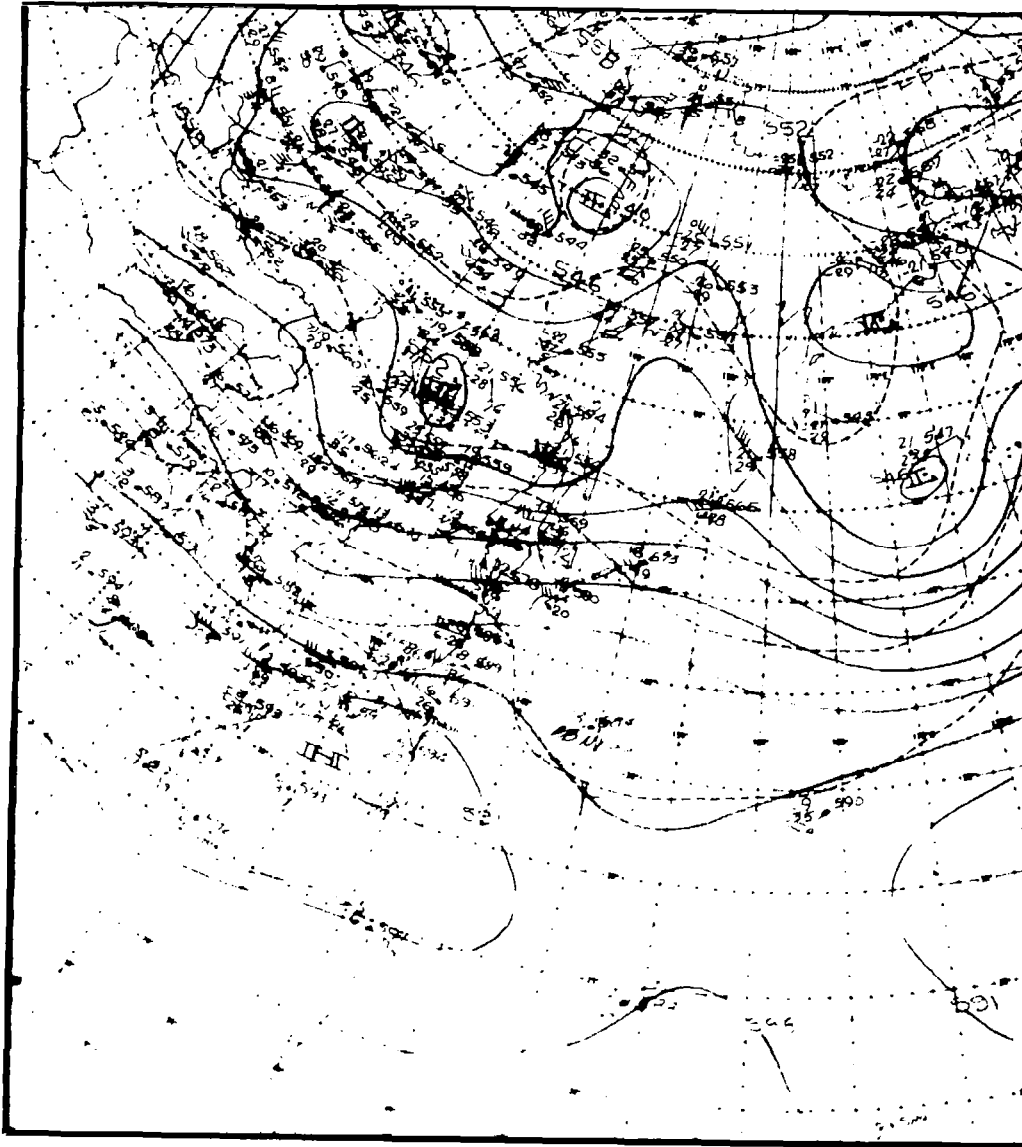
Figure 30.   NMC 500 mb Analysis, 1200 UT, 12 September 1964

accounting for the cumulonimbus complex and the appearance of circulation centered on southern Korea. Although the Russians used a complex, multiple-front analysis at 0000 GMT on September 13, which makes it difficult to use continuity, the overall surface situation is compatible with a cold front in the eastern Sea of Japan at the time of the HRIR data.

Figure 29 also includes a rectification of HRIR orbit 223, which is not illustrated here because of its poor quality and very limited applicability to the main development. Clouds northeast of Kamchatka can be related to the low in the same area. The cloud mass near $37^{O}N$, $155^{O}E$ has the definite appearance of those associated with a frontal wave, and matches the low latitude 500 mb trough near $155^{O}E$. The Russian analyses show a stationary front between $30-35^{O}N$, with an open wave located near $35^{O}N$, $167^{O}E$ at 0000 GMT on September 13.

4.2.2 The Situation on 13 September 1964

Orbit 238, taken about 1420 GMT (Figs. 31 and 32) shows a cloud mass near $45^{O}N$ which has every indication of being associated with a major storm. The southern part of the system, apparently a cold front cloud band, has moved significantly eastward and crossed the Japanese Islands. Less eastward motion has taken place in the northern portions. The total appearance at first suggests that the northern portions are experiencing advection around a closed low. More questionable, however, is whether the center or circulation should be placed near $43^{O}N$ or $45^{O}N$.

The cloud band along $41^{O}N$, between the northern cloud mass and the frontal band, would appear to be the type of band suggested by Merritt[16,25] as indicative of a jet stream. A clear area is definitely present north of the main cloud mass, as verified by the outline (on our working copy) of much of Kamchatka and the northern coast of the Sea of Okhotsk.

The frontal band along approximately $37^{O}N$ extends into the area of coverage of orbit 239 (Figs. 31 and 32). Particularly in orbit 239, it not only includes patches of moderately high clouds, but also definite breaks (very dark areas suggest openings over the Yellow Sea). On the other hand, a TIROS VII, orbit 6680, photograph (not included) of the same area and showing the same frontal band about nine hours earlier shows essentially a solid overcast of uniform reflectivity, except at the very edges of the band. Such features as do show near the centerline of the band are of far smaller scale than those in the HRIR data; furthermore, they are oriented predominantly north-south while those in the HRIR tend principally to east-west. In

both presentations, the band width is approximately 9 degrees of latitude. It is this case, and similar ones like it, that have led us to state that even relative cloud top heights cannot be reliably detected from the TIROS pictures.

Any attempt at quantitative calculations from HRIR data of the quality available to us is fraught with danger. Nevertheless, in this case the quality of our copy of orbit 239 appeared to be particularly good. Just north of the front, Lake Khanka, the Sungari River, and parts of the Yalu River could be identified. All except the highest tropical clouds appeared featured, suggesting the lack of photographic saturation for most clouds. Accordingly, from the range of HRIR brightness visible within this frontal band, it is likely that the cloud top temperature differences are greater than $20^{\circ}C$, which would represent cloud top height differences of at least 10,000 feet. Yet these height differences seem to exist in a cloud band which, in a TIROS photograph, looks comparatively uniform.

Although not directly related to the system of primary concern here, the HRIR data show cloud vortices and suggest cyclonic circulations near $65^{\circ}N$, $170^{\circ}E$, and near $65^{\circ}N$, $145^{\circ}E$; and some form of cyclonic development at about $55^{\circ}N$, west of $120^{\circ}E$.

The 500 mb chart for 1200 GMT (Fig. 33), about three hours earlier than the HRIR data, at first glance suggests that the cloud mass northeast of Japan is associated with the closed low centered near $49^{\circ}N$, $142^{\circ}E$. But this low is too far north to correspond to either of the centers of probable circulation estimated from the cloud pattern, suggesting that while the clouds appear to reach to high levels their effective center of circulation might be at a level below 500 mb, and located somewhat south and east of the 500 mb center. The 0000 GMT, 13 September 500 mb analysis, as well as the 1200 GMT one in Figure 33, makes it very unlikely that a closed circulation at 500 mb existed significantly south of $50^{\circ}N$. Furthermore the HRIR indicates that the clouds near $46^{\circ}N$, $146^{\circ}E$ are higher than those to the east and northeast. This suggests that vertical motion is still making a significant contribution to the western portion of the cloud pattern. This becomes probable when it is noted that this part of the cloud pattern is actually in southwesterly flow southeast of the 500 mb center.

More careful inspection of the 1200 GMT 500 mb chart reveals that:

1. Based on the wind shifts between northern Hokkaido, southern Sakhalin, and eastern Hokkaido, a short wave trough extends across Soya Strait and into eastern Hokkaido, moving around the trough, extending southward from the closed low to the north. The major cloud mass east of Soya Strait should be associated with this short wave trough rather than with the closed low.

Figure 31. HRIR Strips for 13 September 1964
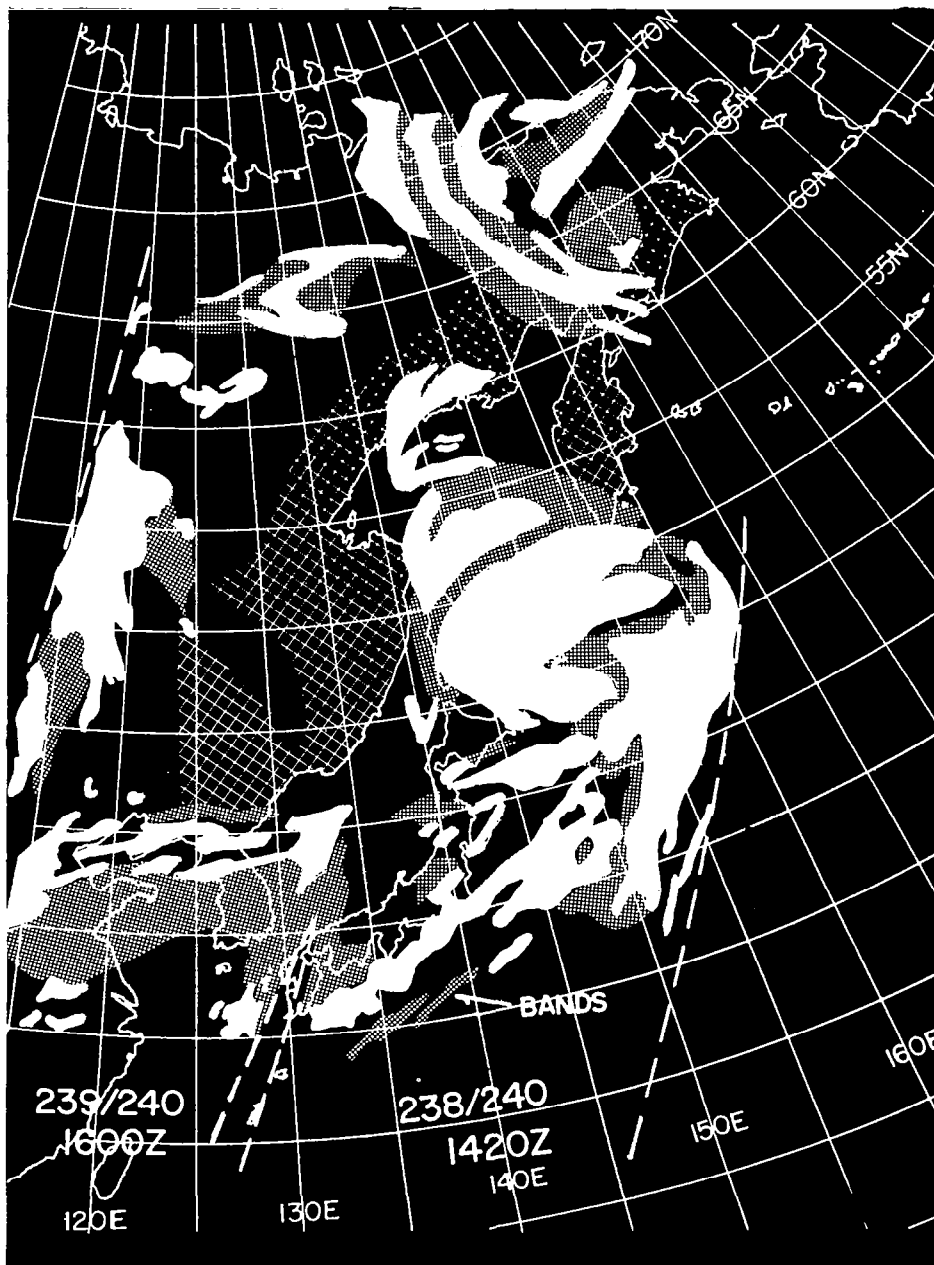
Figure 32. Rectified HRIR Data for 13 September 1964
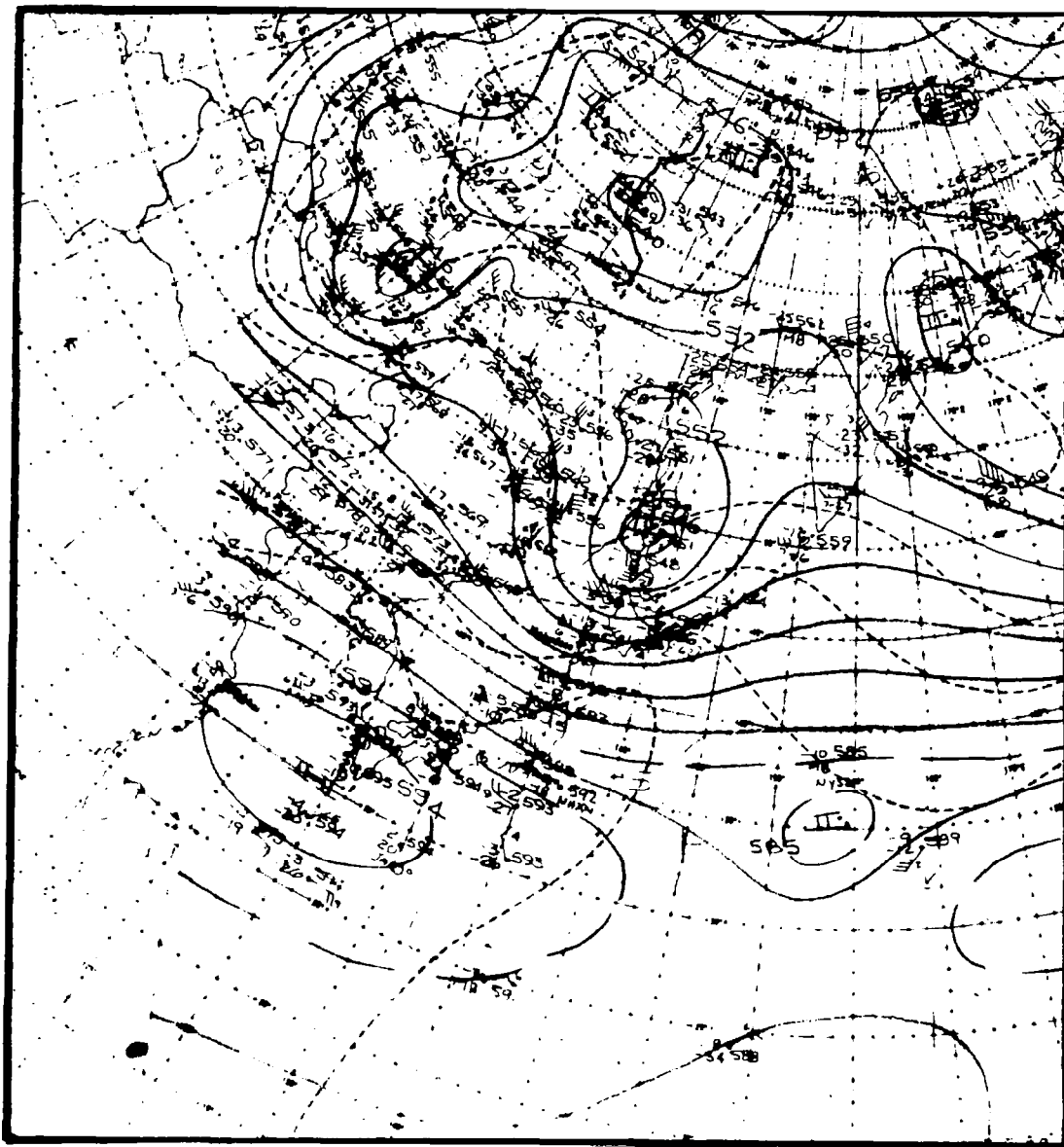
Figure 33. NMC 500 mb Analysis, 1200 UT, 13 September 1964

2. The innermost contour of the closed low may be questionable as to position (it might be moved somewhat northward) and perhaps even as to its existence. It is nowhere supported by an easterly wind. It is based solely on the heights reported by two stations in southern Sakhalin, both of which reports have values higher than that of the analyzed closed contour.

After this inspection, the cloud mass now can be seen to resemble, at the large scale, the pattern considered representative of a short wave trough. The breaks east of 150°E (and especially east of 155°E) can be attributed to the ridge near 155°E.

After this analysis, it is immediately apparent that the cloud band along the northwest coast of the Sea of Okhotsk is associated with the circulation around the northern portion of the closed low over Sakhalin.

From the 1200 GMT 500 mb chart, it can also be noted that:

1. The cloud band southeast of Hokkaido, of the type Merritt[16, 25] associated with a jet stream position, lies along or just slightly north of the zone of highest 500 mb winds (70 knots or greater, over northern Honshu).

2. The clear area over to the west and to the southeast of Kamchatka corresponds to the 500 mb ridge line and the area to its east.

3. The cloud vortex near 65°N, 170°E corresponds well to a closed low over eastern Siberia northeast of Kamchatka. The cloud vortex near 65°N, 145°E lies in a data sparse area northwest of Kamchatka where a col rather than a closed circulation is analyzed but a closed low could as well exist. The cloud mass near 55°N, 120°E can be associated with a trough only some 10 degrees further east.

Interpolation between the Russian surface analyses for 0000 GMT on the 13th and 14th places an occluded low near 50°N, 146°E at the time of the HRIR data. The brighter southwest area in the HRIR cloud mass can be associated, at the surface, with an open wave that at 0000 GMT, September 13 was located near 40°N, 135°E, and which twenty-four hours later had been absorbed into the circulation around the occlusion. As suggested by the HRIR data, the cold front runs east of Japan as far south as about 35°N, crossing the Japanese Islands and continuing westward at about this latitude.

The Russian surface analyses also show a low near 65°N, 145°E on the 13th; and one near 55°N, 120°E on the 14th.

4.2.3 The Situation on 14 September 1964

HRIR orbits 252 and 253 (Figs. 34 and 35) show a striking vortex centered near 47^ON, 155^OE. A two-turn cyclonic spiral of higher clouds is most prominent, overlying a lower overcast. The spiral almost certainly depicts a mature cyclonic storm with a closed circulation extending into the middle and upper troposphere.

A broad band of high clouds extends from north of the center of apparent circulation to the southeast, then south and southwest. Near 45^ON, the band is unduly broadened by aspect ratio considerations. Experience with TIROS data suggests that a cold front should lie along and just east of the western edge of this band.

Clear areas are apparent: 1) between the band and the vortex center (due to advection of descending air from the west); 2) over and near northern Kamchatka (excepting some patches of low cloud east of Kamchatka), suggesting a ridge; and 3) east of Honshu, then northeast across northern Hokkaido and along Sikhota Alin and the western coast of the Sea of Okhotsk, also suggesting a ridge. It is to be noted that many coastal areas near northern Kamchatka, obviously very close to sea level, appear less dark, i.e., colder, than the low clouds near and southeast of the vortex center. This illustrates the effect of latitude on HRIR-observed radiation temperatures.

A somewhat broken cold frontal band, west of the assumed ridge, lies across Japan and the Sea of Japan.

The spiral cloud band near the center of circulation can best be ascribed to advection around a closed low, but it can be noted that its width and brightness are modulated by presumed vertical motion processes, with upward motions concentrated in areas of southerly flow. The broad cloud band east of the spiral would correspond to the major area of dynamically induced upward vertical motions.

Of particular note is that without the HRIR, i.e., with only a TIROS or other TV picture, the narrow spiral cloud band could, at best, be detected only with difficulty against the lower overcast. The general appearance might be somewhat like that of the TIROS picture on page 95 of Reference 25 (although that vortex appears to have a narrower frontal band than this HRIR case).

The 500 mb chart for 1200 GMT (Fig. 36) supports the deductions from the HRIR data. It shows a deep closed low near 50^ON, 153^OE; within the error of analysis and HRIR gridding (especially since the vortex is near the edges of the strips) this is an excellent match. One 500 mb ridge coincides with the clear area near northern Kamchatka and another ridge (or the northerly flow east of it), with the clear areas southwest and west of the vortex.

Interpolation between the appropriate 0000 GMT Russian surface analyses also corresponds to the HRIR data. They place the surface center near 49°N, 156°E. This location is consistent with the southeastward displacement of the low clouds in the HRIR data. The primary surface front at 40°N was at about 160°E, or very close to the western edge of the major cloud bands. A ridge extending over northern Kamchatka and a series of cols near Japan and the eastern portions of the Asian mainland correspond to the clear areas.

The 0000 GMT surface analysis for September 15 places an open frontal wave near 37°N, 143°E. A closer look at the HRIR data suggests either that this wave is too far west, or that another wave was earlier located near 35°N, 155°W. The curving band just north of the major band and extending from about 38°N, 156°E to 40°N, 160°E is suggestive of bands north of a developing frontal wave as first noted by Boucher and Newcomb.[4]

The 500 mb analysis suggests that the broad northwest-southeast cloud band, somewhat north and northwest of Kamchatka, may be associated with a wind shift line (from south-southwest to east-southeast) near 66°N.

4.3   A Second Pacific Vortex Case

This case, for the period 18-20 September 1964, was originally noticed because of the large vortical cloud pattern on the HRIR data for orbit 339. Further investigation suggested that the HRIR and other data available on the previous two days would allow the development of this vortex to be followed in some detail. In analyzing this case, an estimate of the synoptic situation was made from the HRIR data alone, before the 500 mb charts were consulted. The Russian surface charts were not even available until the first draft of the discussion was completed.

4.3.1   The Situation at About 1200 GMT, 18 September 1964

Figure 37 shows the HRIR data for orbits 309, 310 and 311, as taken over the temperature portions of the North Pacific Ocean. These data are for about 1050 GMT, 1230 GMT and 1410 GMT, respectively. In Figure 38, these data have been subjectively rectified and placed in their appropriate geographical locations. The affect of aspect ratios on the unrectified pictures are apparent, particularly for the cloud mass centered near 45°N in orbit 310, and that near 40°N and the Kamchatka Peninsula in orbit 311.
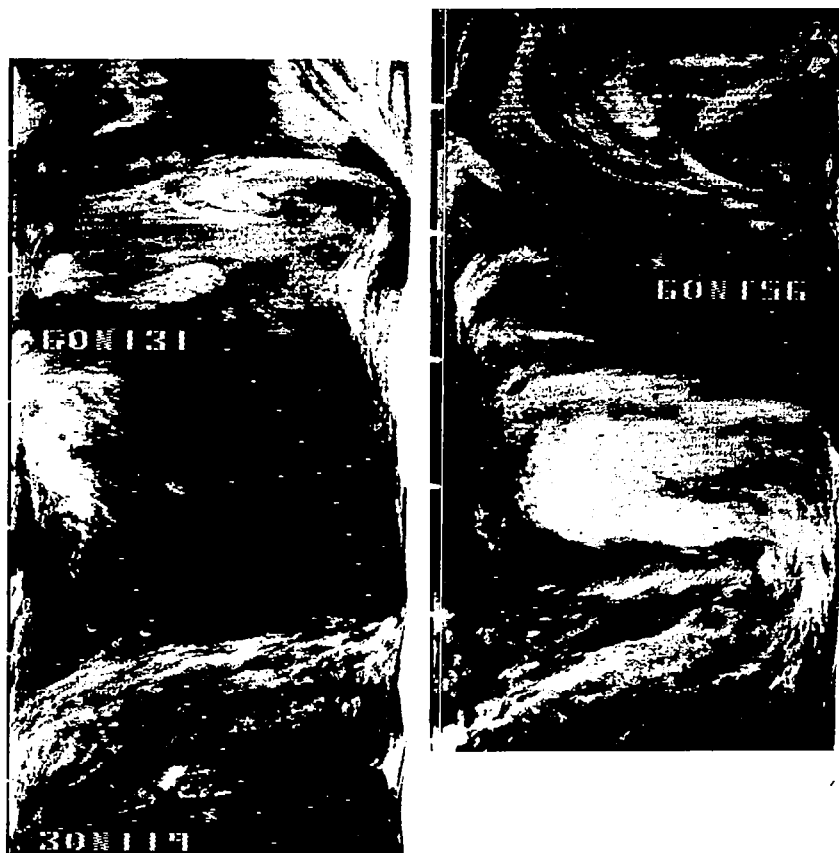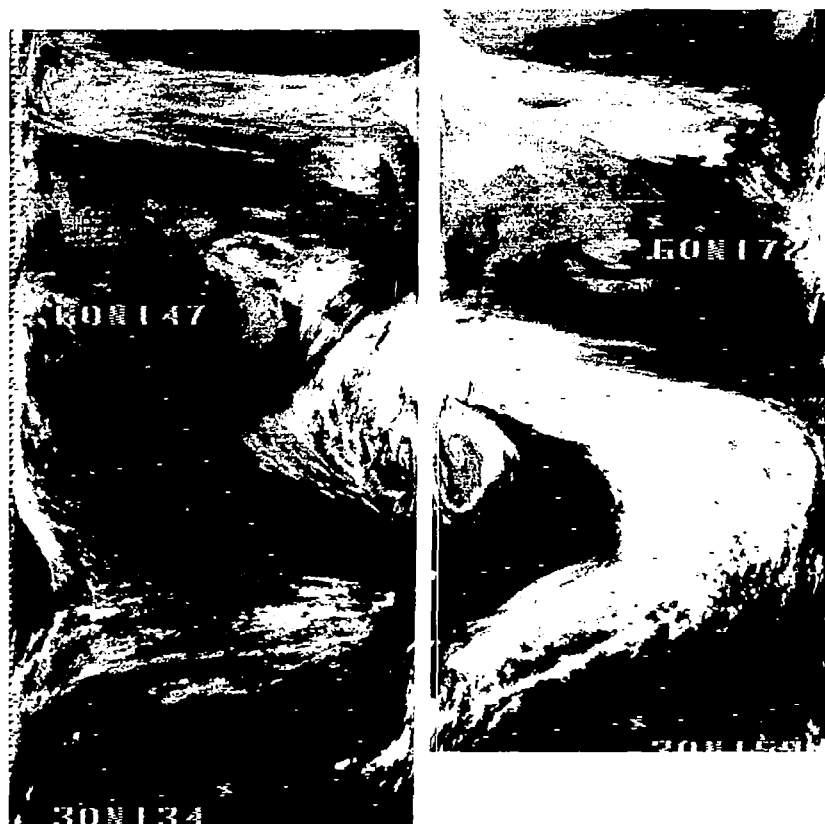
Figure 34. HRIR Strips for 14 September 1964
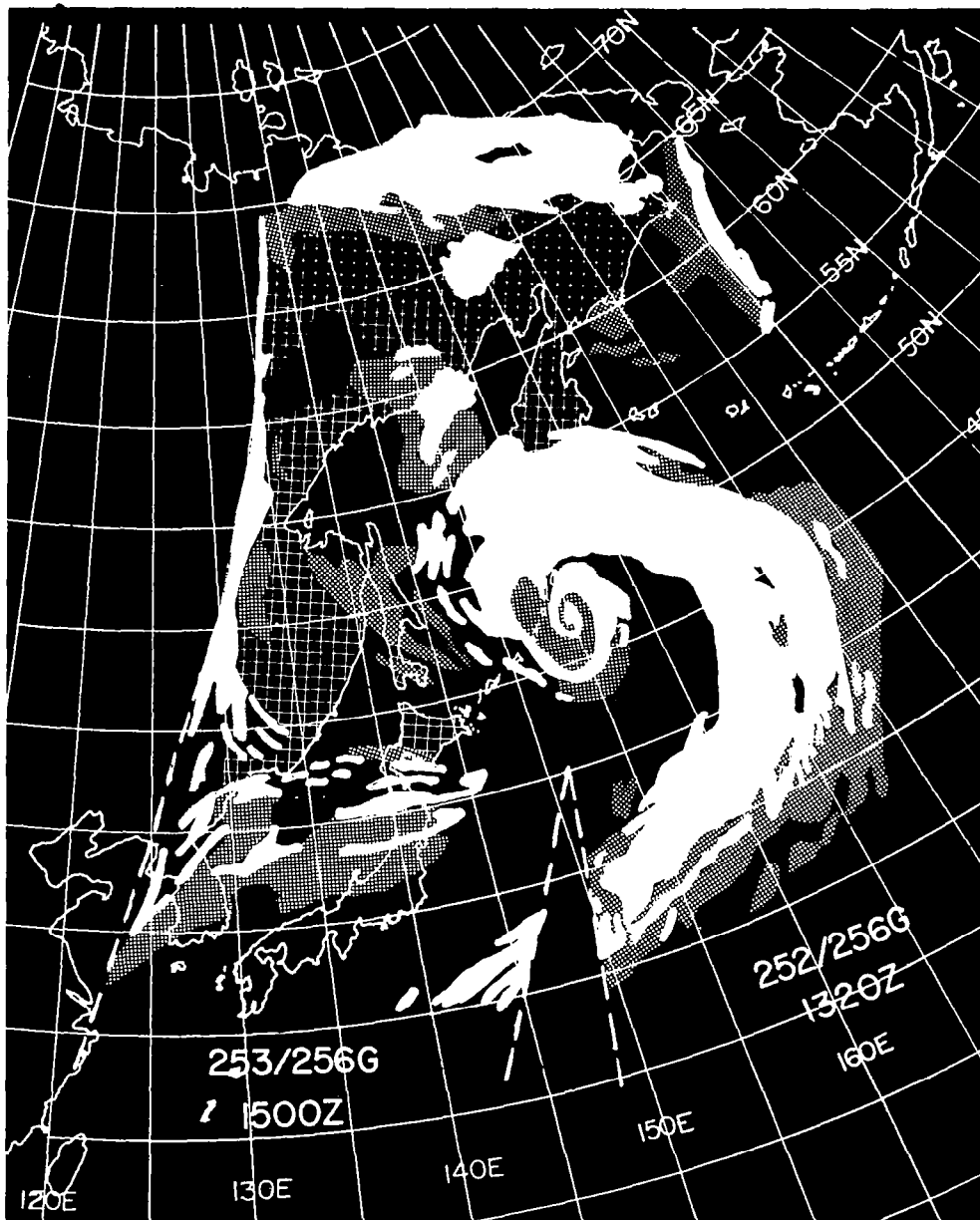
Figure 35.   Rectified HRIR Data for 14 September 1964
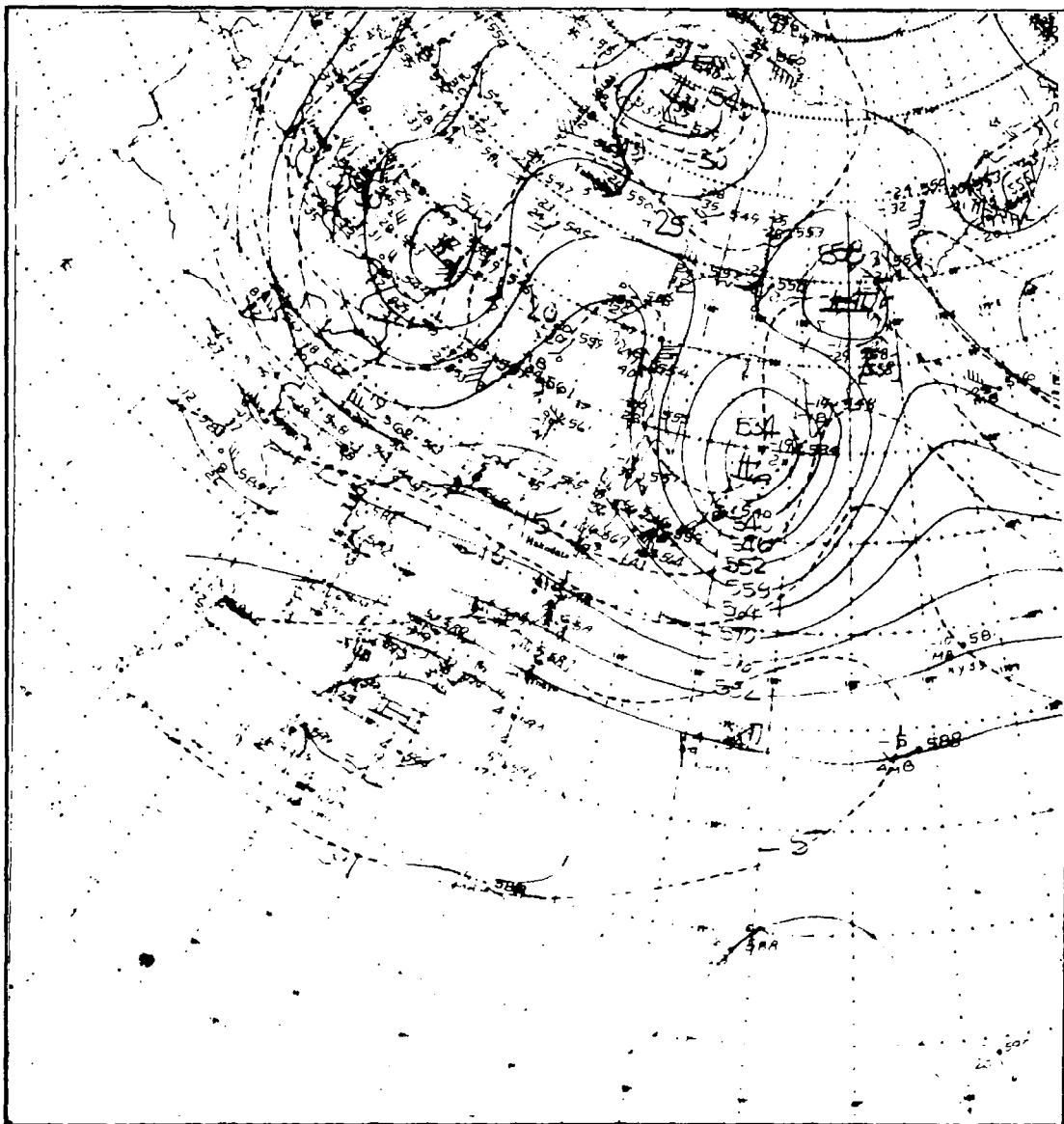
Figure 36.   NMC 500 mb Analysis, 1200 UT 14 September 1964

The most significant feature is the quasi-continuous frontal band which extends across the three swaths at approximately 40°N. The portion of the band which is in the western hemisphere is composed largely of low-level clouds, perhaps broken, with only scattered patches extending to significant altitudes. A distinct, cloud-free break in the band just east of 180° suggests the location of a high or ridge. A very well-developed frontal wave, approaching the occluded stage, is doubtless associated with the cloud mass centered near 46°N, 174°E. There is a second break near 155°E, and a second frontal wave, apparently less well developed, over the Japanese Islands. Lower level cloudiness is present in patches over and on both sides of the Kuril Islands.

The 500 mb chart for 1200 GMT, 18 September 1964 (Fig. 39) tends to confirm this analysis. The front, east of 180°, is under the east side of a weak ridge, with the ridge line corresponding to the break near 180°. The well developed cloud mass centered along 174°E corresponds to a trough along 165°E; and in the absence of conflicting data, suggests that the northern part of the trough may be sharper than indicated. Such a sharpening of the trough exists in the NMC 500 mb chart for 12 hours later (not shown). The second frontal break near 155°E is also just east of a 500 mb ridge line, while the cloud mass over Japan fits the trough line over the Sea of Japan.

The only available surface analyses for this area were Russian charts for 0000 GMT (not included). Interpolating between those for September 18 and 19 shows:

1. The trailing end of a cold front near 45°N, 160°W;

2. A subtropical ridge near and just east of 180°;

3. A frontal wave, just at or very close to occlusion, located near 45°N, 178°E at about the time of the HRIR data;

4. A series of frontal waves, over and near the Japanese Islands, just north of 35°N.

All these features show a very good match to the analysis derivable from the HRIR data.

The low clouds near the Kurils correspond to a low just southeast of Kamchatka, and to the trough and front running from it toward Sakhalin. It is interesting to note that, in a TIROS VII neph (not shown) based on observations about 12 hours earlier, this low cloudiness was stippled to indicate an area of synoptic significance, while in
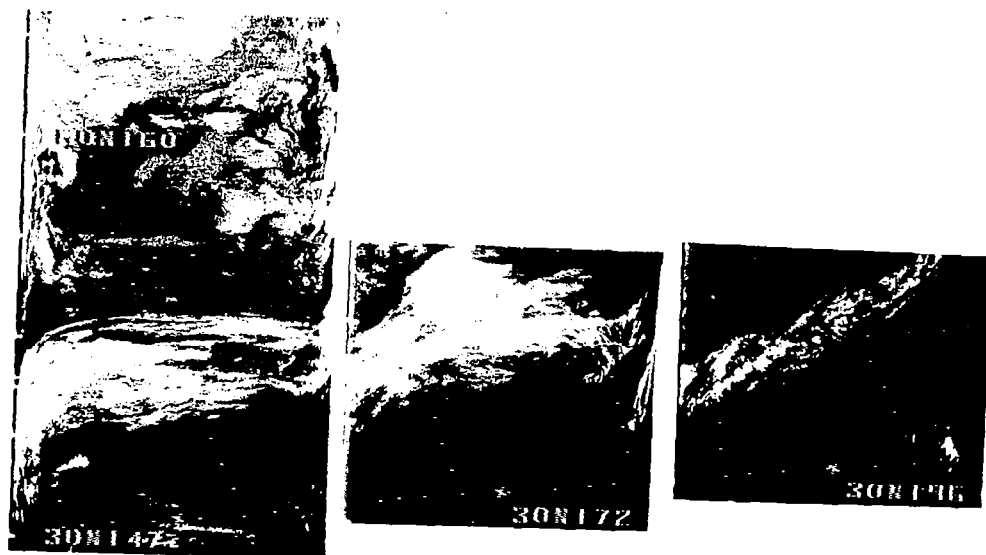
Figure 37. HRIR Strips for 18 September 1964 (Orbit 309, 1050 UT; Orbit 310, 1230 UT; Orbit 311, 1410 UT)
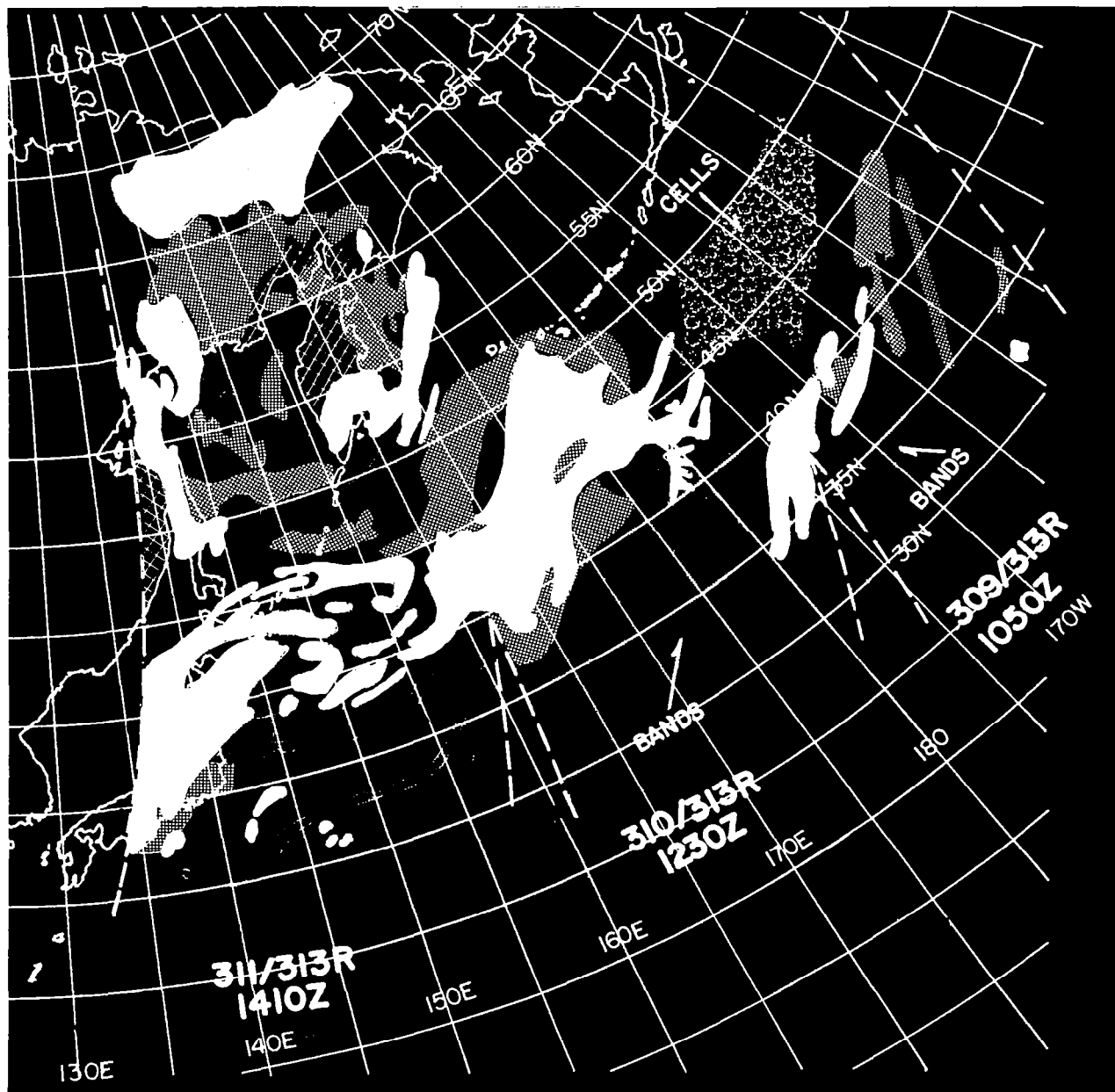
Figure 38. Rectified HRIR Data for 18 September 1964

Figure 39.   NMC 500 mb Analysis, 1200 UT, 18 September 1964
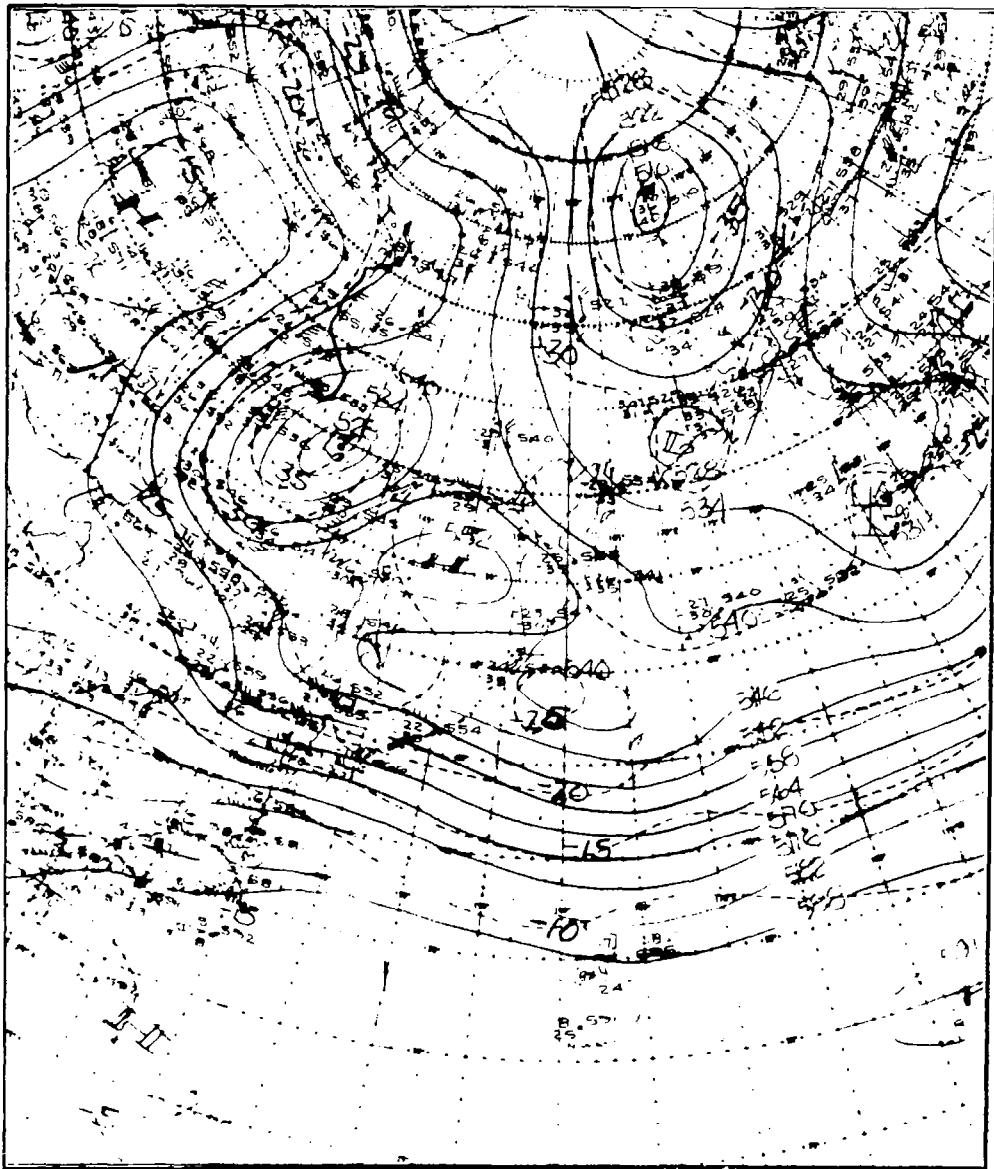
the same neph, the brighter[*] clouds of the west end of the wave near 174°E were merely outlined. Presumably, the analyst was misled by the vortical cloud pattern of the dissipating system, while the part of the wave cloud mass photographed by TIROS was only marginally sufficient for a meaningful analysis. It is unlikely the analyst would have made this misinterpretation if HRIR data, even if only from orbit 311, had been available to him.

The long, narrow high cloud band running through Soya Strait[†] appears to be jet stream cirrus, as confirmed by a northern Hokkaido 500 mb wind observation of 75 knots, with decreasing velocities to the north and south. The second narrow band, just to the south, suggests a double jet but the density of the radiosonde data is insufficient to confirm this conjecture.

The narrow, low level band running south-southwest from about 40°N, 160°E, then turning to the west suggests a very weak cold front, or a weak convergence line, associated with the developing system to its northeast. Its appearance where it crosses one frame of TIROS VII, orbit 6755/6751 (not shown) is not in disagreement with this interpretation. The Russian charts have insufficient data in this area to aid the interpretation.

4.3.2 The Situation at About 1200 GMT, 19 September 1964

The wave development that 24 hours earlier was centered near 46°N, 174°E has now definitely attained the status of an occluded cyclone. In Figures 40 and 41, the southern portion of the associated cloud pattern can be seen near 44°N, 170°W (in orbit 324); clouds associated with the circulation center are near 52°N, 180° (in orbit 325). The positions of these parts of the cloud pattern (near the boundaries of the observed areas) make a full analysis somewhat difficult. Nevertheless, these two parts appear to be interconnected. The very size of the portion near 44°N, 170°W, and its distance from the circulation center, suggest that it may represent a triple-point development. The more southerly cloud lines, running from about 40°N, 170°W to 30°N, 180°, may be some type of warm sector or pre-frontal convergence lines. Various scattered to broken low cloudiness exists between these lines and the frontal band to the northwest.

---

[*] Brighter in the TIROS TV data as well as in the HRIR.

[†] Soya Strait is between Hokkaido and Sakhalin.
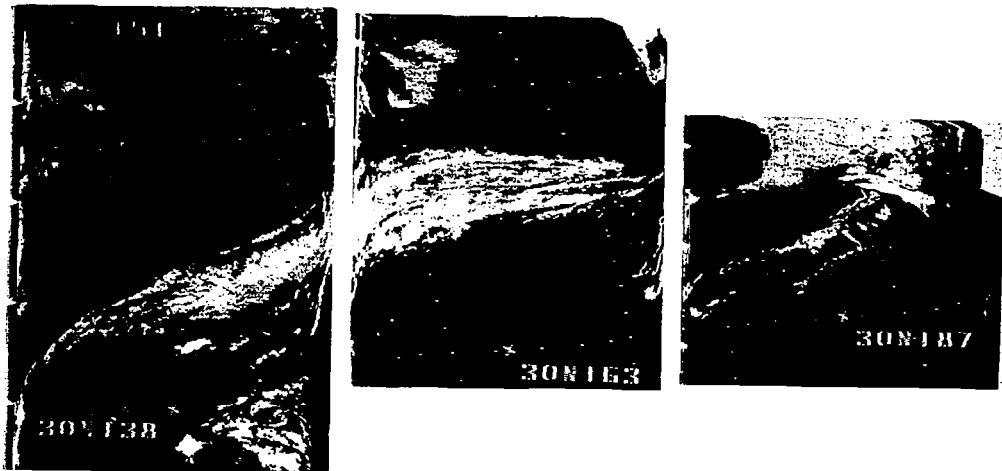
Figure 40. HRIR Strips for 19 September 1964 (Orbits 324, 325, and 326)
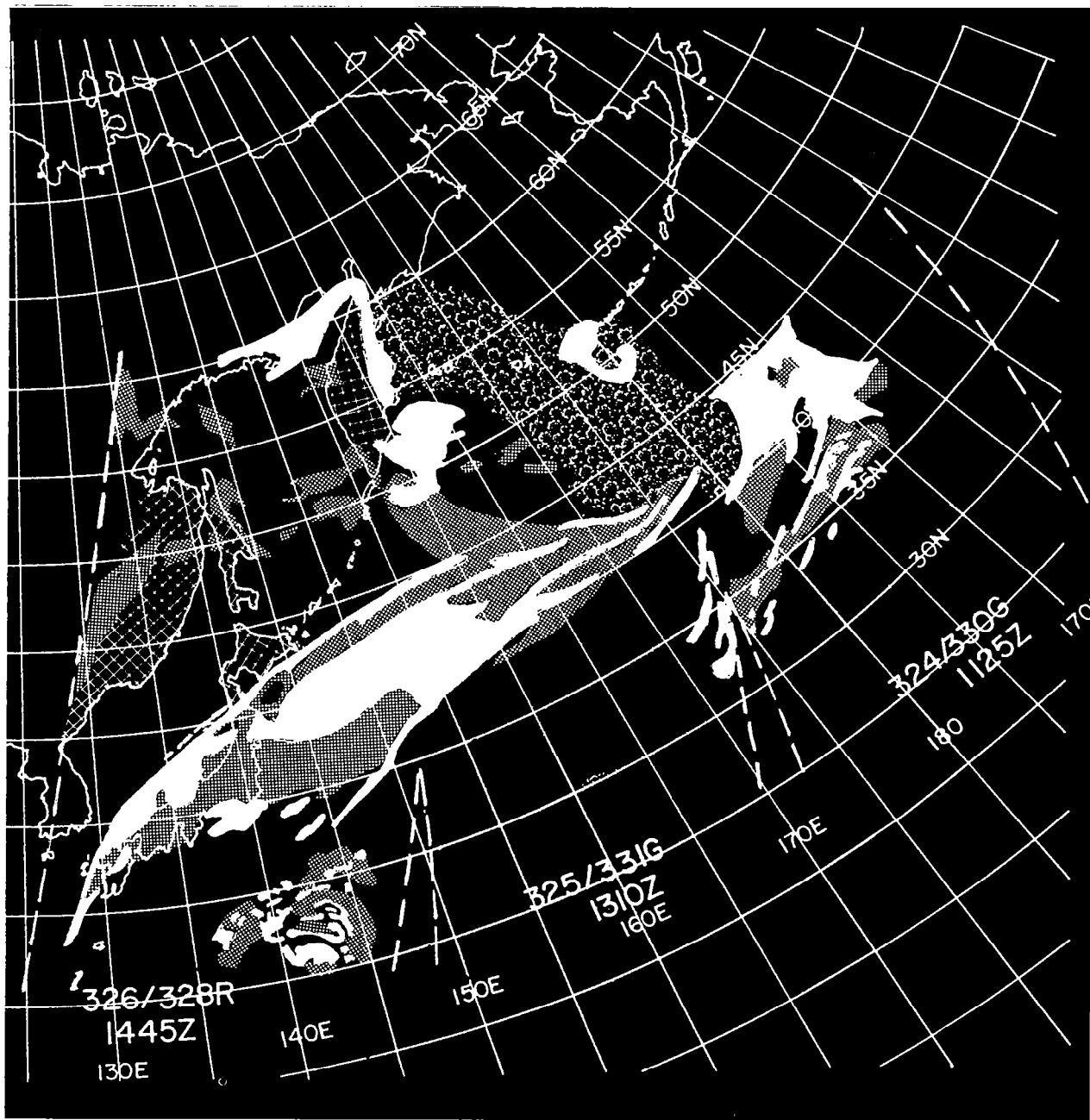
Figure 41.   Rectified HRIR Data for 19 September 1964

Near 52°N, 180°, the distinct hook in the lower to middle clouds indicates a low level closed circulation. The upper clouds evidence the beginning of hooking, suggesting that the upper circulation has recently or is closing off. These patterns can be expected to have resulted from distortive advection, with the major area of upward vertical motion east of the cloud circulations. The clearer tongue of dry air within and to the rear of the vortex is well populated with cellular clouds that do not extend to great altitudes; in this case, the cellular cloud patterns is far more evident than in most other northern hemisphere cases (particularly over North America) so far examined.

South-southwest of the vortex, between 165° - 175°E, the frontal band has a distinct break, suggesting a high pressure area. West of 165°, the breadth of the front suggests that the frontal wave, which a day before was over the Japanese Islands, has moved eastward as an open wave, perhaps now centered near 155°E. Although the frontal band appears weaker and more broken over and just east of Japan, the shape of the band suggests the possibility of a second weak wave there.

Because of the aspect ratios near the strip edges, and perhaps also due in part to a very slight inconsistency in the position from one strip to the next of the 30°N parallel, there is a tendency to insert a break in the front near 150°E when rectifying the data. Careful rectification suggests no such break actually exists in this case.

About 12 hours earlier, TIROS VII photographed the portion of the frontal band from just east of Japan to about 158°E. In the TIROS pictures (not shown) the band was a rather uniform white, giving little or no evidence of the variations in cloud top altitude that can be noticed in the HRIR. There was also no obvious indication in the TIROS data of the narrow cloud band (possibly a broken cirrus jet stream band) which the HRIR shows running along the northern edge of the frontal band.

The 500 mb chart for 1200 GMT, September 19 (Fig. 42) substantiates the previous analysis. North of 43°N, a very sharp trough has now been placed along 180°. Although no closed center is analyzed near 52°N, 180°, this is probably due to a lack of reports for Adak or the area of the trough, and to a northwest wind at Attu (53°N, 174°E). Twelve hours earlier, a north-northeast wind was reported at Attu as the trough line passed that station; twelve hours later (0000 GMT, September 20), a very definite closed 500 mb low (two closed contours) is analyzed at 51°N, 175°W.

Although, again, it is in an area of no data, the 500 mb analysis suggests a short wave trough near 45°N, 175°W; this would correspond to the cloud mass near 44°N, 170°W.
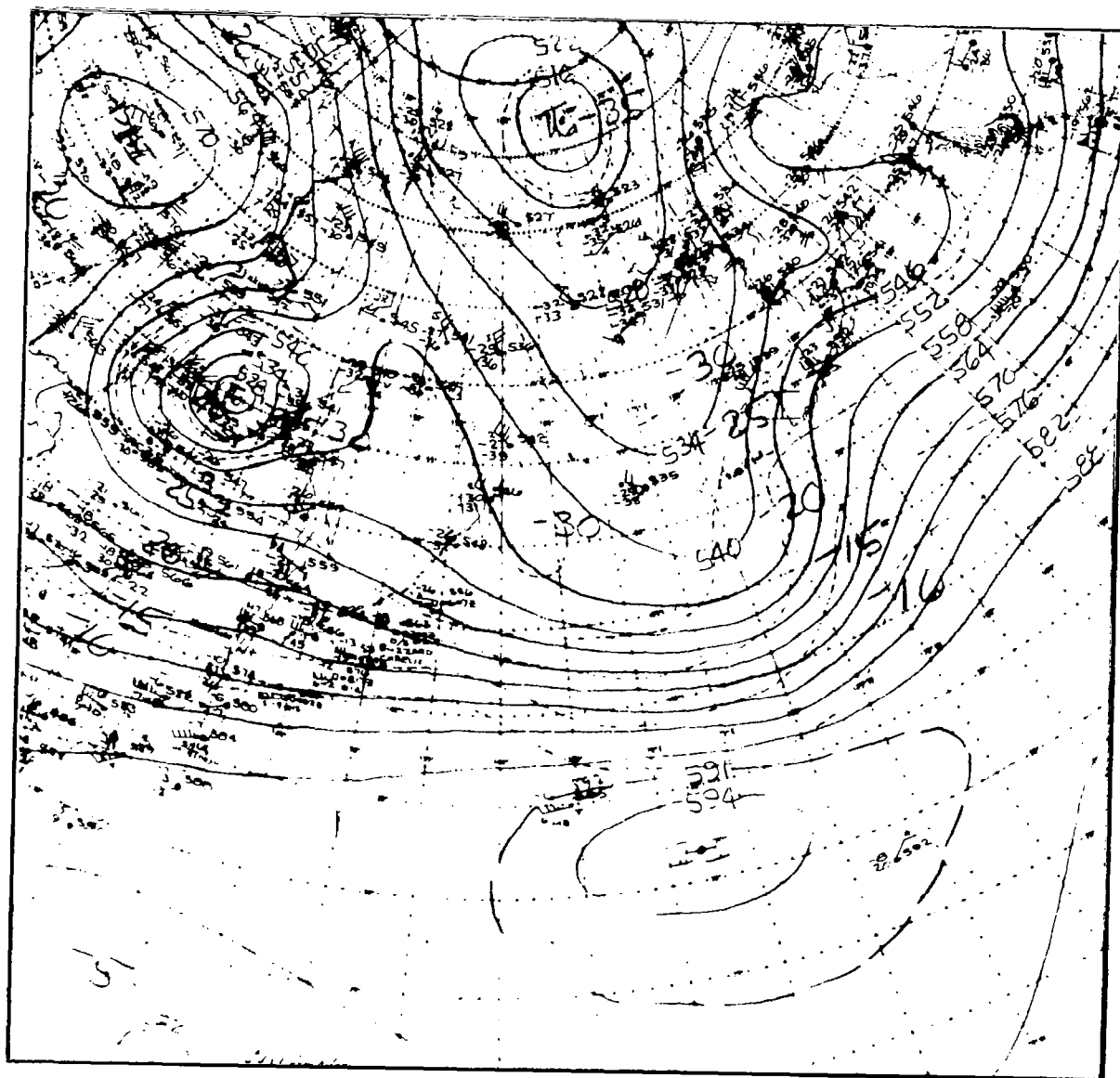
Figure 42.   NMC 500 mb Analysis, 1200 UT, 19 September 1964

West of the trough line the flow (north of 40°N) between it and a very broad and weak ridge near 155°E would account for the break in the front near 170°E. Further south, the frontal band between Japan and 170°E lies under a broad west-east flow, near the latitude of maximum 500 mb wind, and with confluence occurring. This is compatible with the interpretation of a front with open waves running along it; one of these waves is reflected in the 500 mb wind field and in the 570 contour near 42°N, 148°E.

Although the narrow band just along the north side of the frontal cloud band (previously interpreted as a possible, broken jet stream cirrus band) does lie in the general area of maximum winds, it has a definite WSW-ENE orientation while the 500 mb winds over and east of Japan are all due west. Similar discrepancies have been noted by L. F. Whitney of NWSC, and remain to be explained; Whitney's studies suggest that a more meridional flow, nearer the tropospause, is not the explanation.

Interpolating between the Russian 0000 GMT surface analyses for September 19 and 20, we find:

1. A deep occluded cyclone at about 51°N, 175°W, very close to the position of the hooked circulation in orbit 325. Interpolation of the surface data, and edge foreshortening of the HRIR data, may both have contributed to what small discrepancy remains.

2. An occluding wave, breaking away from the primary circulation and located about 5 degrees south and 10 degrees east of its center. This corresponds very well to the estimate of a triple-point development.

3. A double cold front structure slightly east of 180°.

4. A weak ridge just west of 180°.

5. A series of waves, along the zone from 35° - 40°N, and extending from about 160°E westward across the Japanese Islands.

Again, the correspondence between the HRIR interpretation and the Russian analysis is extremely good.

Approximately ten hours later (about 2230 GMT), the Nimbus I AVCS cameras provided data for this area. Because of the film quality and erratic gridding of the copies available to us, they are not reproduced here. They were, however, entirely compatible with the HRIR data just discussed, and with that for orbit 339 (see Fig. 43), to be considered next. The AVCS pictures show (1) an area near 46°N, 172°W of clearer air, south and west of the vortex center, with scattered to broken cellular cumulus; (2) a filamented frontal band to the east and south, approximately in the same

position as the frontal band in HRIR orbit 339; and (3) a mottled overcast to the north, apparently part of the hooked cloud, advected around and to the south of the vortex center. All these features are entirely compatible with the Russian surface analyses for 0000 GMT, September 20. In the AVCS, the cellular clouds are brighter than much of the mottled overcast; in the HRIR, the cellular clouds do not, however, appear to extend as high as the overcast area does. Whether these differences are typical of this case, or merely a sampling problem (note the variations in the whiteness of the hooked cloud in HRIR orbit 339) cannot be determined.

4.3.3 The Situation at 1200 GMT, 20 September 1964

On this day only a single HRIR pass pertinent to the storm system (Fig. 43 and 44) was available, but fortunately it passed nearly directly over the center of the system. This center seems to be at about 52°N, 168°W. The 500 mb analysis (Fig. 45) places the center of the closed circulation in this same location.

The system is now within the limits of the Northern American surface analysis (Fig. 46), which places the storm center at 52.5°N, 165°W. By now, the system is probably vertical, and the difference in the surface and 500 mb analyses is certainly within the probable error of analysis in this area (interpolation of the Russian analyses gives a surface position of 52.5°N, 169°W).

The bright cloud area near 57°N, 160°W can be associated with upward vertical motion due to a disturbance in the flow north-northeast of the closed center, as evidenced by the wind shifts between Unimak Island (55°N, 163°W) and the Pribelof Islands (57°N, 170°W) at both the surface and 500 mb. It is probable that most of the cloud pattern west of about 174°W results, with one exception, principally from advection distortion of cloudiness formed earlier by upward vertical motion. The exception is the high cloud area along 50°N, from about 180° to 174°W. The 500 mb analysis, however, suggests a second disturbance extending just west of the center, which should place an area of upward vertical motion downwind of the disturbance, or near 50°N. The associated distortion of the flow around the west of the center may also explain why the cloud vortex pattern appears to be elongated to the west in this area. In general, with the exception of this high cloud area along 50°N, there is a tendency for the cloud bands to decrease in breadth and height where the flow has a northerly component, and to increase in breadth and height with a southerly component. This suggests that the primarily advective patterns near the storm center are modulated by dynamically induced vertical motions.

Figure 43. HRIR Strip for Orbit 339, 20 September 1964
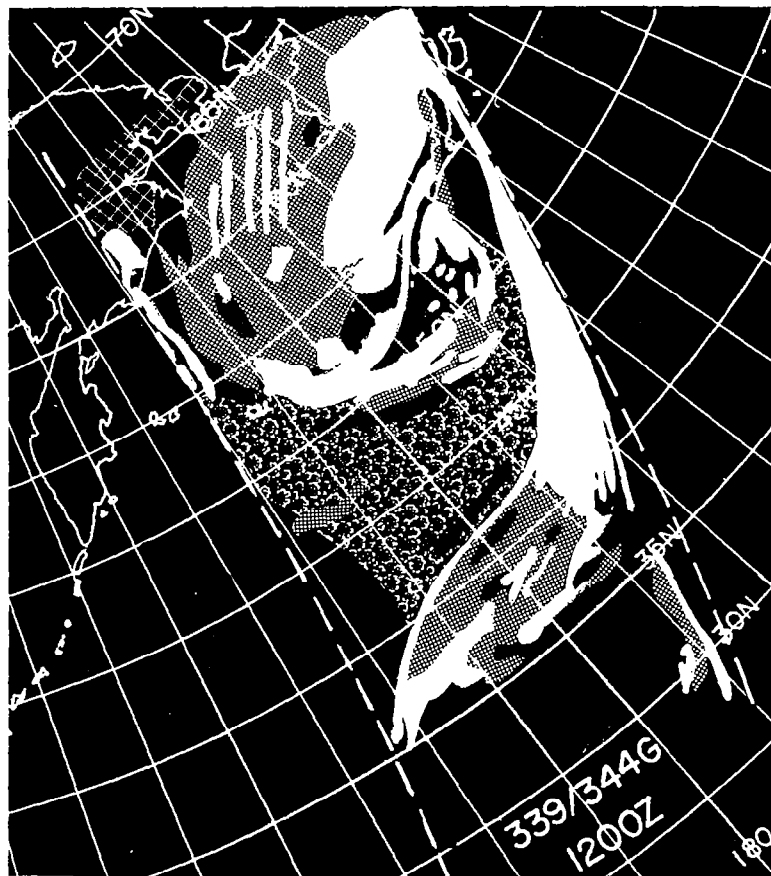
Figure 44. Rectification of Orbit 339 HRIR Data
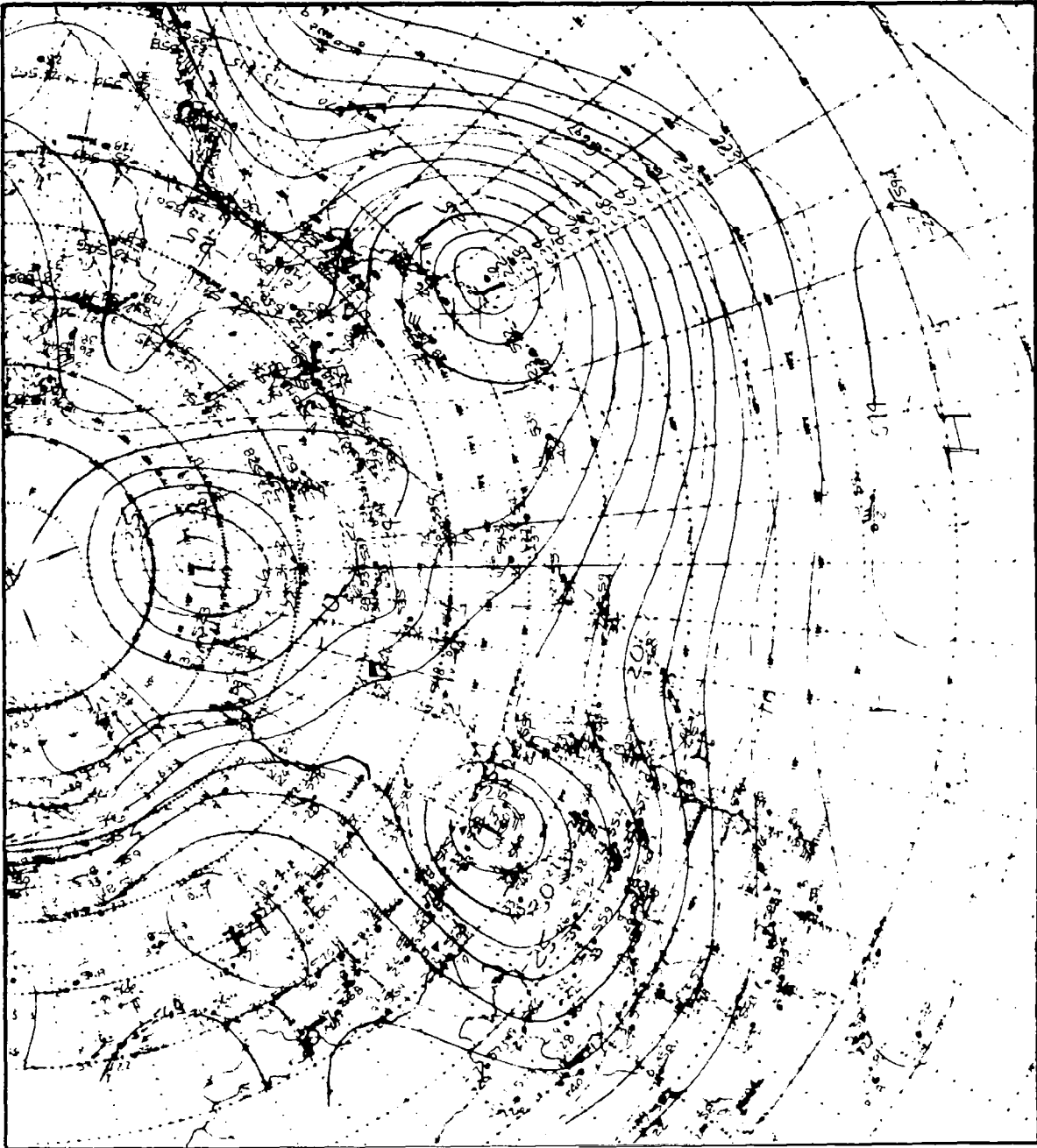
Figure 45. NMC 500 mb Analysis, 1200 UT, 20 September 1964
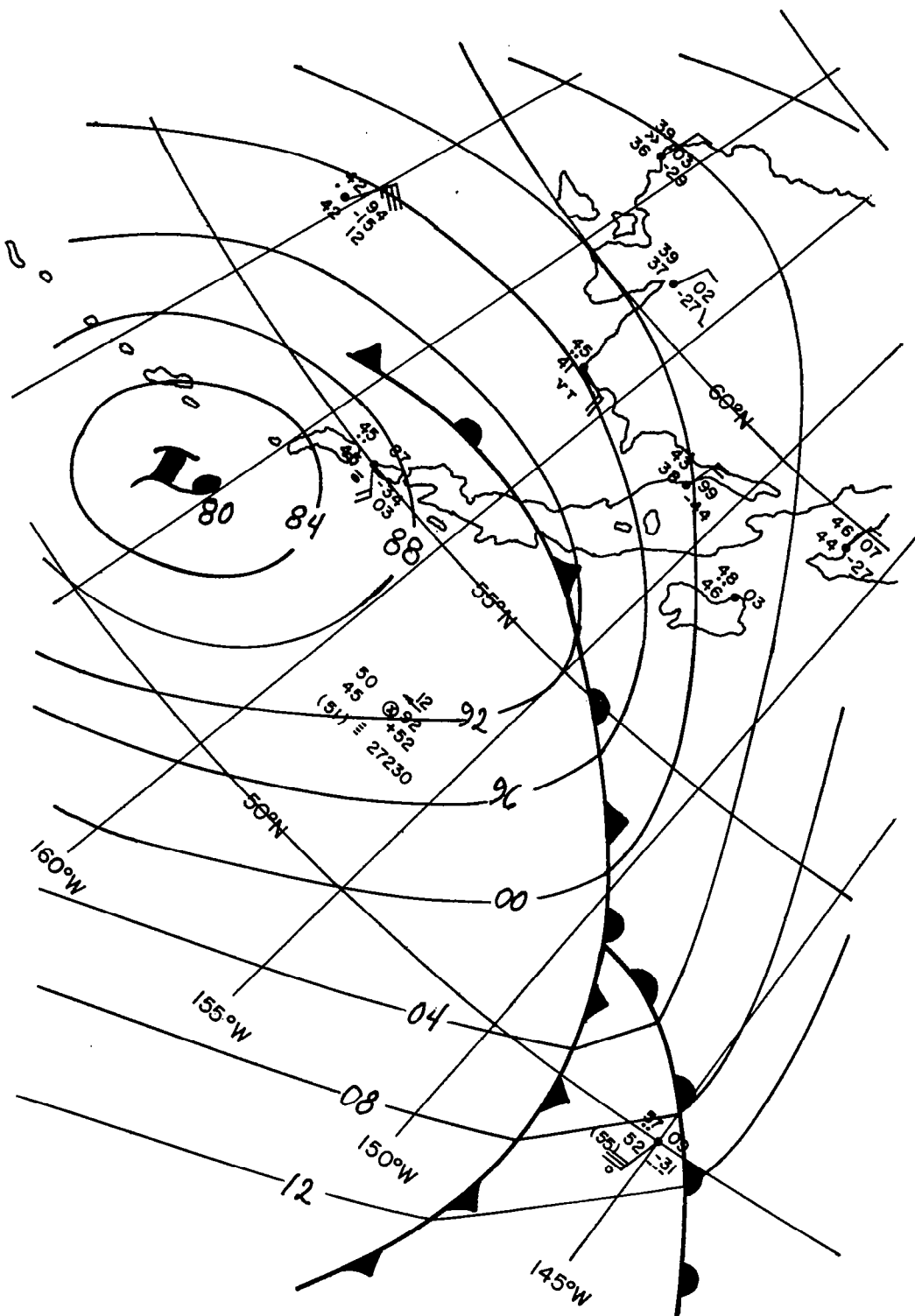
Figure 46.   Northwest Portion of NMC North American Surface
Analysis, 1200 UT, 20 September 1964

The western edge of the bright clouds in the frontal band south of the vortex is near the 500 mb trough line. The broadening of the band near 180° may be indicative of a nascent frontal wave. The Russian analysis for 0000 GMT, September 21, suggests a very early stage of wave development near 42°N, 165°W.

The position of the frontal cloud band suggests that the front may have been placed too far east, near 45°N, in the U.S. surface analysis. (The Russian analysis places the cold front near 45°N, 160°W at 0000 GMT, September 21.) Where surface reports are available, most stations under the higher cloud areas (Unimak Island, 55°N, 163°W; Pribelof Island, 57°N, 170°W; and Cape Newenham, 58.5°N, 163°W) are reporting precipitation.

It is regrettable that the Nimbus I HRIR data does not include similar cases of cyclonic development over the eastern United States where plentiful corroborative data would exist. The best case over North America that we have been able to find developed near the Canadian border and moved into northeast Canada.

4.4   A One Day Case Over Western North America

    4.4.1   Introduction

The HRIR data for orbit 44, over the western United States and central Canada at approximately 0800 GMT, 31 August 1964 (Fig. 47), was selected for study since it contained the following features of meteorological interest:

    1.   The cloud field over the western states appeared to match the frontal wave and low pressure area of the surface map.
    2.   Wave clouds were visible to the east of the Sierra Nevadas.
    3.   A jet stream cloud band was evident over northern Idaho and Montana.
    4.   The curvature of a jet stream band over the Pacific coincided with the upper level trough.
    5.   A patch of cloud and precipitation was evident over southwestern Canada.

Other features of interest on the film included landmarks, such as the western edge of Great Slave Lake, the San Joaquin Valley and other valleys and lakes in California, and the west coast near 45°N, including the mouth of the Columbia River.
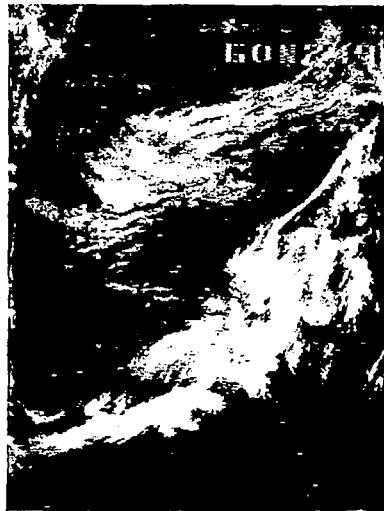
Figure 47. Nimbus I HRIR - A Portion of Orbit 44 Over Western North
America at Approximately 0800 UT, 31 August 1964

Figure 48. A Rectified Map of Cloud Cover as Depicted by HRIR on a
Portion of Orbit 44

4.4.2 Conventional Data and Methods of Analysis

Minute-by-minute positions of the subsatellite track and reports of satellite altitude were available to permit correction of the latitude-longitude grid on Figure 47. Meteorological data readily available included the synoptic teletype reports received at the time in Boston, various synoptic maps, and upper air data. Hourly sequences and pilot reports over the area were unavailable.

Radiosonde ascents at 0000 GMT and 1200 GMT were plotted for stations in and near the areas of interest in order to obtain estimates of cloud heights and lapse rates. Winds aloft at each of the stations in the area were plotted for 0000 GMT 0600 GMT, and 1200 GMT to help delineate the jet stream. Cloud amounts and types from 0600 GMT surface observations were plotted to seek correlations with the HRIR picture and the radiosonde data. Temperatures and wind profiles at stations near the lee wave area were used to compare the observed lee waves and their wave-lengths with theoretical criteria for the formation of lee waves, and with previous empirical findings relating wavelengths to wind velocity.

4.4.3 Results of Analyses and Interpretations

4.4.3.1 HRIR Grid Coordinates

The unambiguous landmark of Gypsum Point in Great Slave Lake permitted comparison of map grid coordinates in the film with known geographical coordinates. The actual coordinates of the point are 61.8°N, 114.6°W, while the HRIR grid coordinates gave 61.0°N, 117.5°W. Therefore, the grid coordinate correction involved shifting the grid 0.8° southward, and 2.9° (1.4° of great circle arc) west-ward relative to features in the data. Approximately the same grid adjustment appear: to apply throughout the area of Figure 47. This amount of error is not important in most of the analyses, and the rectified map of cloud cover as depicted by the HRIR, Figure 48, is based on the data as gridded.

For the lee waves, however, the gridding error was significant, since the lee waves as gridded appeared west of the Sierra Nevadas whereas actually they were almost certainly just east of the Sierras, centered at about 39.5°N, 120.0°W.

4.4.3.2   Synoptic Situation

At the time of HRIR observation the northwestern United States lay in the area of both a surface (Fig. 49) and an upper air (Fig. 50) trough. At 0000 GMT a weak surface low pressure area was centered over southern Idaho, southeast Oregon, and northern Nevada, with a cold low aloft to 300 mb, centered over Washington. The upper air trough extended to at least 200 mb. At 300 mb, a jet stream west and south of the low, ran southward over the eastern Pacific Ocean to northern California, and thence to eastern Montana. At 200 mb, the jet was slightly further south over the United States, and there was a second jet from southern California across southern Nevada to Utah and Colorado and eastward. Frontogenesis was indicated on the 0600 GMT surface map, extending from Montana to California.

At 1200 GMT, the analysis showed two jet streams at 300 mb, the more northerly one oriented SW-NE, somewhat further north over Montana than the 200 mb jet of 12 hours previously, while the southern jet was outside the area of interest. At 200 mb, Figure 50, the northern jet was nearly coincident with that at 300 mb, while the southern jet was also oriented SW-NE, and was displaced somewhat northward over Colorado from its position at 0000 GMT.

Over the Pacific Ocean, a small curved bright jet stream cloud band at about 37°N, 131°W (see Figs. 47 and 48) coincides with approximately the position of the upper level trough, as shown in Figure 50. The jet stream cloud band is just south of the northern jet, and suggests that the trough line was analyzed slightly east of its actual position.

4.4.3.3   Radiosonde Observations

Radiosonde observations from a number of stations in the area for 0000 GMT and 1200 GMT on August 31 (1600 PST, August 30 and 0400 PST, August 31 respectively), were plotted. At 0000 GMT the lapse rates at Great Falls, Spokane, Boise, Winnemucca, Ely and Salt Lake City all approached and even exceeded dry adiabatic in portions of the ascents. Potential temperature increased only 4 to 5°C between the surface and 500 mb. The tropopause was at 200 mb, except at Great Falls, where it was at 250 mb, and at Spokane, where it was between 250 and 300 mb.

The atmosphere over these stations was very dry, with many surface dew points of 5°C, or colder, decreasing to -25°C or colder at 500 mb. The low humidity accounted for the lack of lower clouds despite the unstable air.
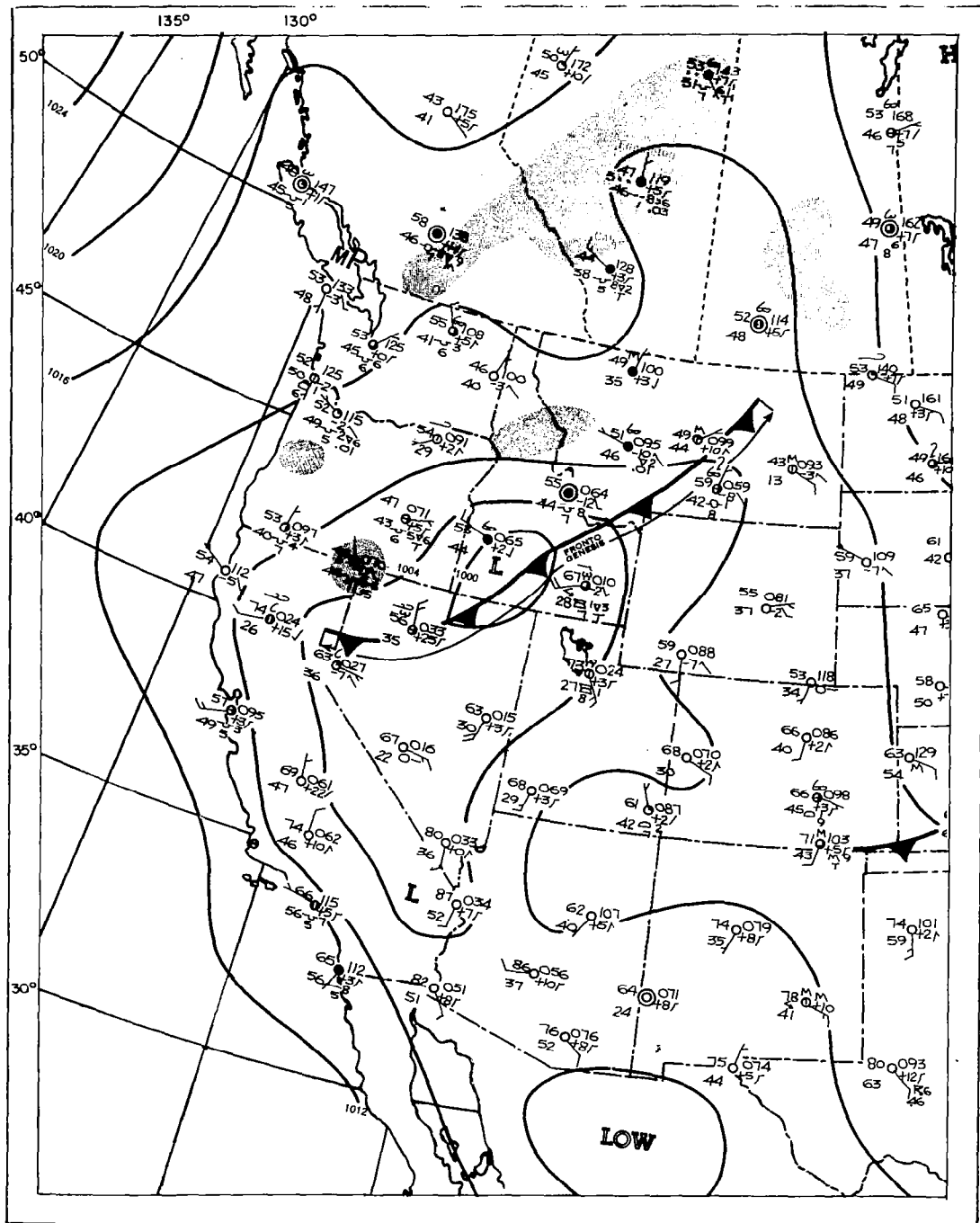
Figure 49.   Surface Weather Map for 0600 UT, 31 August 1964
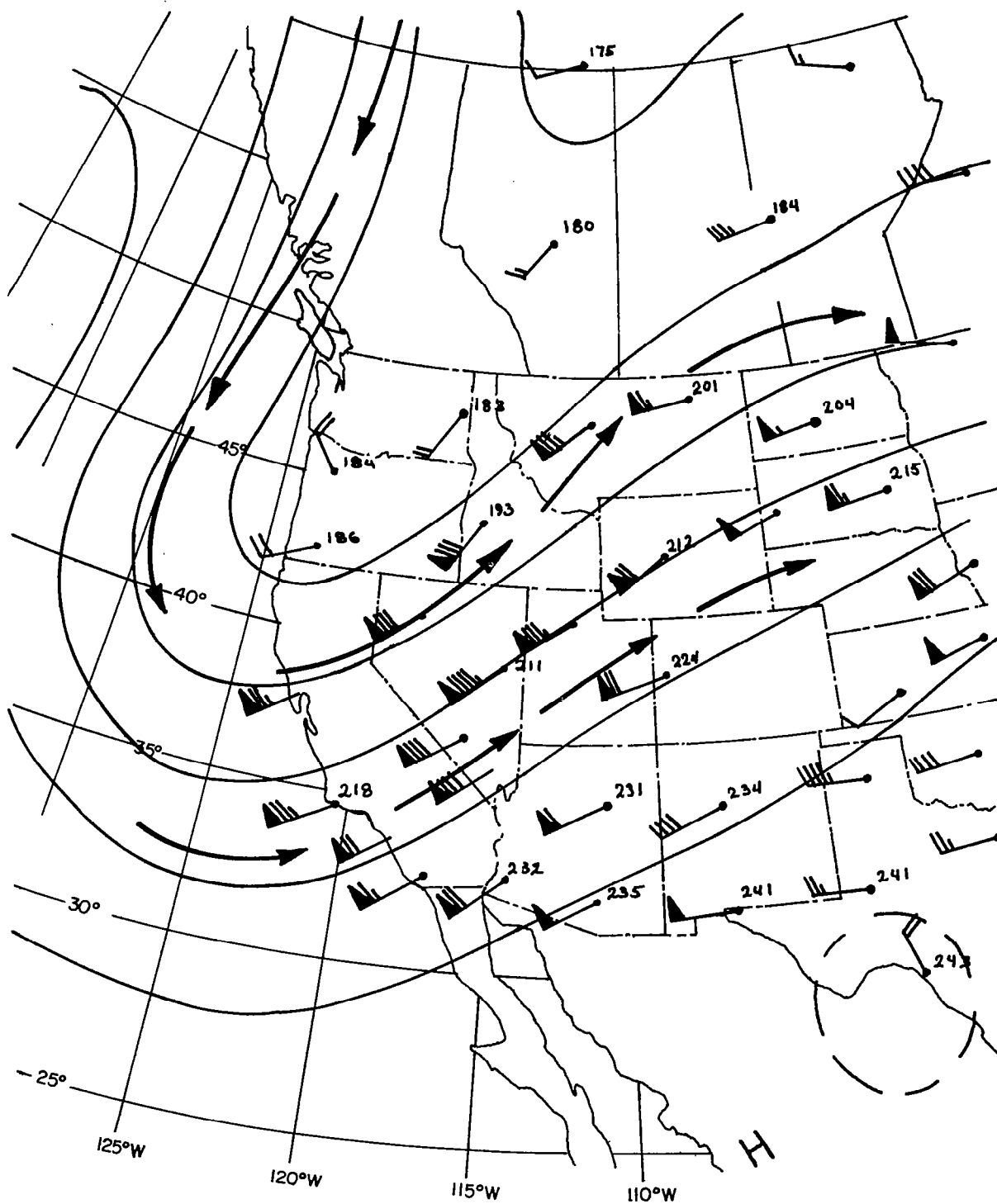
Figure 50.   200 mb Map for 1200 UT, 31 August 1964

At 1200 GMT, the lower atmosphere was colder and more stable than at 0000 GMT, but only minor temperature changes occurred above 500 mb. By and large, twelve-hour dew point changes were small.

At Oakland, the atmosphere was more stable at 0000 GMT than at the other stations discussed above, and at 1200 GMT the stability had increased as the lower atmosphere cooled substantially. The major change at Oakland was the marked increase in humidity from 800 mb to 300 mb, saturation or near-saturation being general throughout this region of the atmosphere near Oakland.

On the basis of these radiosonde ascents, cloud bases and tops were estimated as shown in Table I, which also shows clouds reported at these stations at 0600 GMT, and the relative HRIR temperature at 0800 GMT. The agreement between cloud tops estimated from raob data, and surface observed cloud types is often poor, but is not unexpected, since a lower overcast prevents surface observations of higher clouds. The agreement between the radiosonde observations and the HRIR observations was generally good, especially if the cloud top heights were slightly higher than estimated from the radiosondes.

4.4.3.4 Winds Aloft

Profiles of winds aloft were plotted for 0000 GMT and for 1200 GMT (Fig. 51) from Spokane to Albuquerque on a NW-SE line, and from Oakland to Glasgow on a SW-NE line. These profiles show that at 0000 GMT there was a jet over Grand Junction, Colorado, with 90 knot winds; and another jet over Great Falls, also with 90 knot winds.

By 1200 GMT the maximum winds at these two stations had decreased, but still equaled or exceeded 80 knots. A vertically narrow band of 80 knot winds extended from Oakland to Glasgow at altitudes between 35 and 40,000 feet. At Great Falls they extended down to 30,000 feet, as can be seen in Figure 51. Every station over the western United States with observations to a least 40,000 feet had winds of at least 60 knots; over a broad band from California to Montana they exceeded 80 knots. The winds were mostly from the southwest and west-southwest.

Unfortunately, data for Boise were not received, and the western edge of the jet stream could not be determined accurately. As shown in Figure 51, the eastern edge was near Grand Junction, and the core extended from at least Salt Lake City to Grand Junction. This jet stream may have been associated with the cloud band near the horizon at 38°N (see Fig. 47).

Table I

Clouds at Radiosonde Stations

Station	Time Z	Estimates from raob ascents (mb)			Reports of clouds at 0600 Z			HRIR Observations 0800Z
		Base	Top	Remarks	Total cover eighths	AMT lowest layer, eighths	cloud types	
Boise	0000	500*	350*	No 1200Z data	8	8	AC	Cold or cool
Ely	0000			None	0			
	1200			None				Cool; not wide
Great Falls	1200	545	380*		8	6	SC Ci fib	Cold
Oakland	0000			None	5 [San Francisco]	3	SC;AC	
	1200	730	400*					Cold
Salt Lake City	0000	570	512		1	1	Cb cap AC cum	
	1200			No humidity data above 680 mb				Cool at edge of band
Spokane	0000			None ?	1	1	SC cum	Warm
	1200			None ?				
	0000			None ?				
Winnemucca	1200	500	400-310		5	2	AC Ci sp	Very cold

* These altitudes could not be determined with certainty from the radiosonde observations.

99
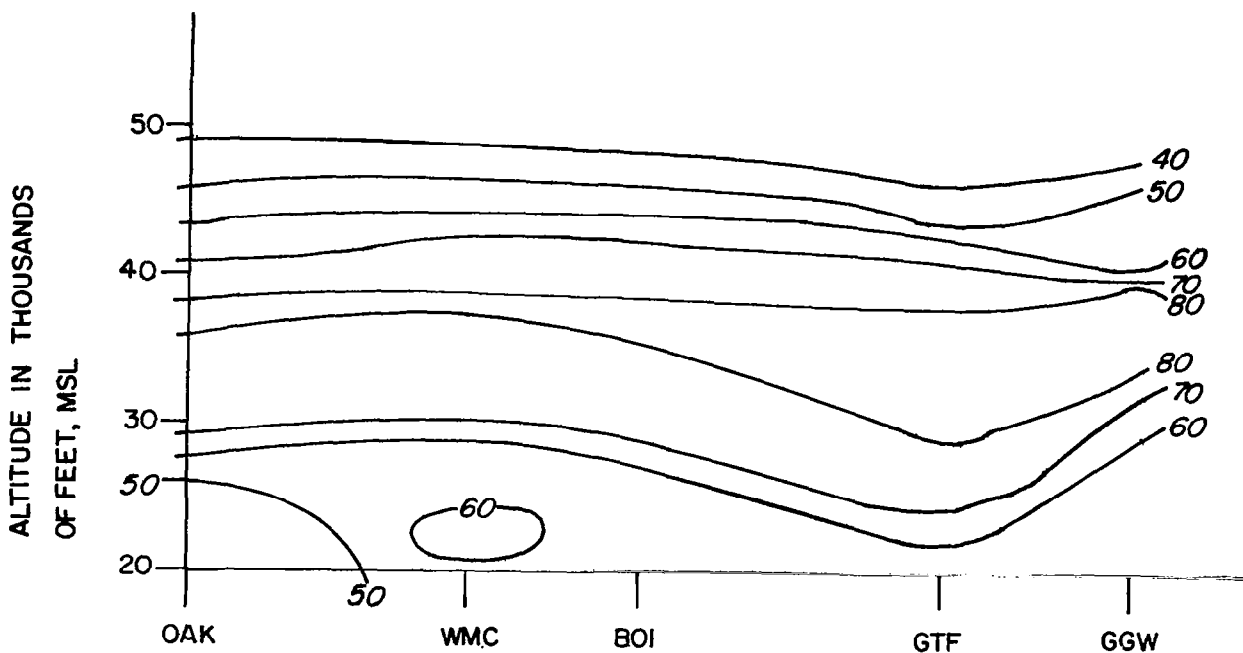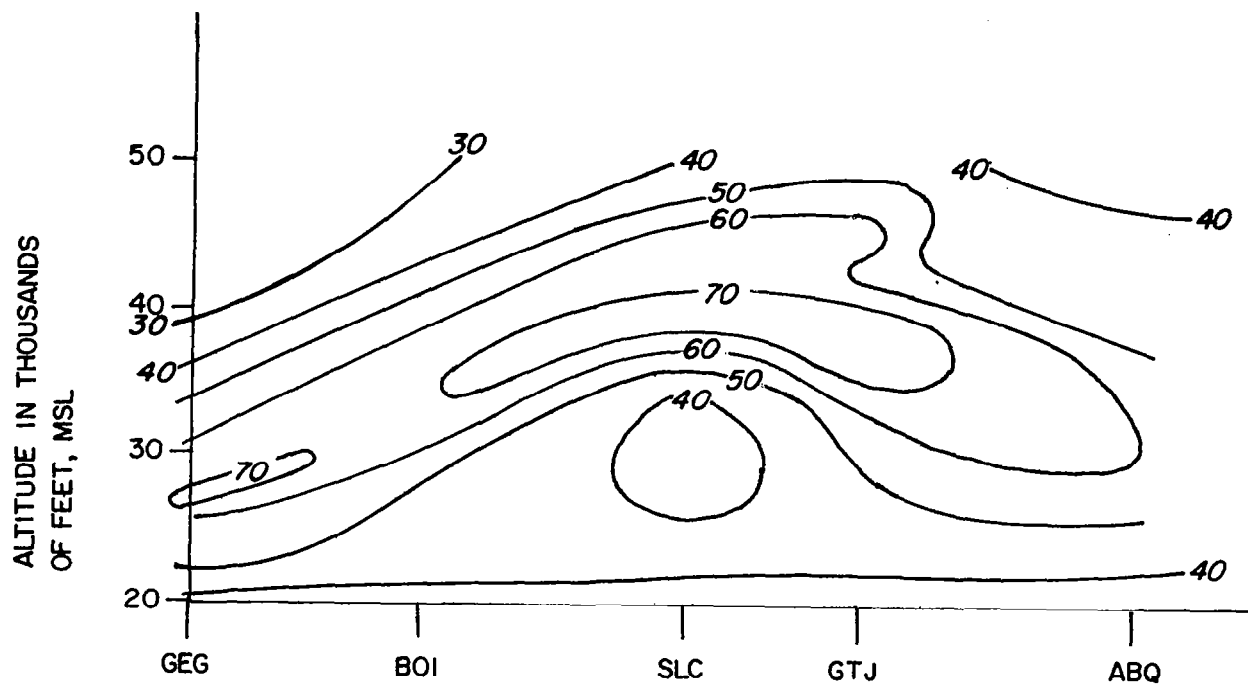
Figure 51. Winds Aloft Over The Western U. S. at 1200 UT, 31 August 1964

Along the axis of the northern jet stream, winds mostly exceeded 50 knots between 20 and 45,000 feet. As expected, the narrow band of upper clouds in the HRIR, extending from about 46°N, 118°W to 53°N, 107°W, is parallel to the northern jet stream, though north of the core. There is no obvious explanation for the absence of this band further southwestward, but westward from the lee wave clouds to 232°E, and also to the northeast of the lee wave cloud area, an irregular band of bright clouds lies nearly along or between the jet stream positions at 200 mb, as shown in Figure 50.

4.4.3.5   Clouds and Precipitation

A map of cloud cover (Fig. 52) for 0600 GMT, two hours before the HRIR observation, was prepared from the station reports and the 0600 GMT surface map. It was, of course, necessary to assume station observations were representative of conditions over the surrounding area, although this assumption was obviously invalid at times (see below). Isolines were drawn for clear, 50% cloud cover (symbol 4 in the synoptic code) and overcast, without reference to the HRIR map. An effort was made to indicate whether cloud cover consisted of high, middle, low, or a combination, recognizing that with an overcast a ground observer would be unable to see any higher clouds present. Areas which had station reports of either current cumulonimbus or precipitation within the past six hours were given an identifying symbol. The resultant cloud map is shown in Figure 52.

A band of cloudiness extended diagonally across the map from the Pacific Coast to nearly Lake Winnipeg, with only two stations therein reporting less than five tenths cloud cover. South of this band, cloudiness decreased to clear skies. North of the band, cloudiness decreased but then increased again over the southern Canadian Rockies and eastward.

Areas of past or present precipitation are scattered about the map, but the two main areas are a narrow belt centered on 112°W between 41° and 48°N, and a large area in Canada between 51° and 56°N from 114° - 118°W.

The cloudy areas include all combinations of cloud cover - exclusively low, middle or high clouds, and combinations of clouds at more than one level.

The correlation between the two cloud cover maps, Figure 48 (the rectified HRIR) and Figure 52 (from conventional data sources), is reasonably good. The area of precipitation and cumulonimbus over the United States corresponds well with the north-south cold HRIR band just east of 248°E (112°W). The precipitation area
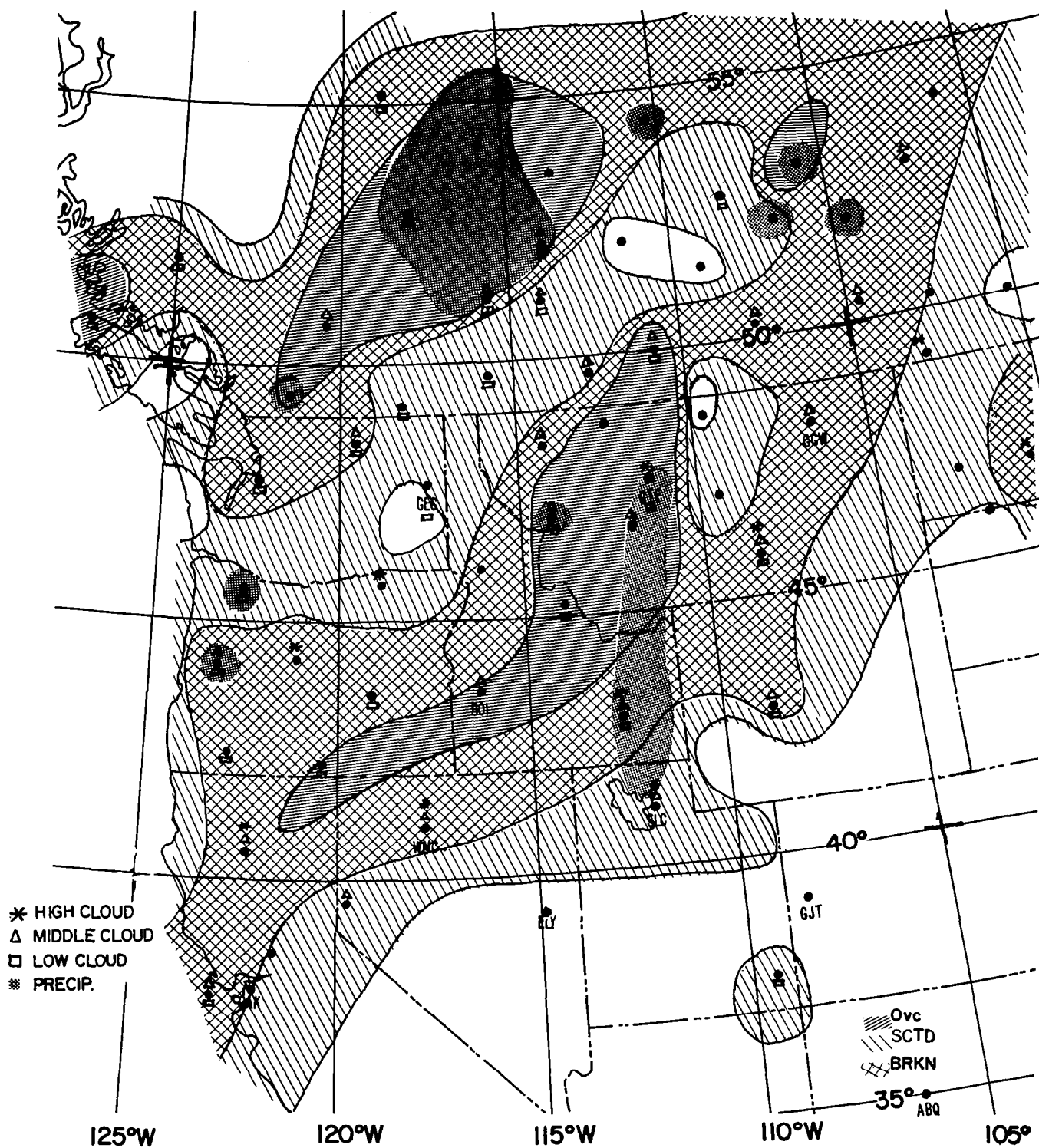
Figure 52. Cloud Cover From Conventional Data at 0600 UT, 31 August 1964

in Canada is larger but warmer (lower cloud tops) in the HRIR picture than the corresponding band in the United States. Since the precipitation at most of the stations was slight, it could be associated with weak low level upslope motion. If so, the clouds producing the precipitation could have comparatively warm tops.

The western edges of the main cloud bands of the map (Fig. 52) and the HRIR data (Figs. 47 and 48) agree closely west of 110°W. Two "past rainy" areas of Oregon have small cool cloud areas northeast of them; another has middle and high clouds near it, though the station reports only low clouds.

Corresponding to the slightly warmer areas just west of 246°E (114°W) in Idaho and Montana are two stations reporting low and middle clouds, and only low clouds, respectively, which thus fit the HRIR. Thunderstorms in Canada at 105°W have their counterparts in the HRIR picture of Figure 48. Other areas of reasonable correlation can be found.

In several areas, Figure 52 could have been analyzed to fit the HRIR map to give nearly perfect agreement between the two without violating the observations. For example, the bright cloud whose southeast corner is at about 240°E (120°W) and 50°N is indicated in Figure 52 by two stations reporting overcast: one with cumulonimbus, the other with altocumulus. The latter station could have cirriform clouds at higher levels, of course, and the analysis could be revised to fit the HRIR data.

Areas of poor correspondence between the two cloud maps not caused by analysis error are also evident. A significant omission from the conventional cloud analysis is the striking jet stream cloud over Idaho, northwestern Montana and southern Alberta and Saskatchewan, not evident from any of the cloud data since stations in this area reported clear or less than five tenths cloud cover. This position for a cirrus cloud band, near the jet stream (see Fig. 50), agrees well with findings of others. The fact that the jet band cloud band does not show in the conventional data is not surprising, however, when it is realized the total field of view from any single station is only about the width of the band near the Canadian border,[25] and the spacing between the stations is far greater than this.

Synoptically, most clouds of Figures 47 and 52 are in the region of the surface low pressure area and slightly downstream from the high level trough, positions which also agree with previous analyses.[19,25] The position of the southwestern portion of the bright cloud band, southwest of the lee wave clouds, agrees well with the 200 mb position of the northern jet stream, as mentioned earlier, so much of it is probably jet stream cirrus. The reason for the ragged appearance of the band is not understood; possibly clouds from several layers contribute to this appearance.

Apparently, upslope motion perhaps in association with the trough over the Rockies, gave enough lift to account for the cloudiness and precipitation over Canada.

4.4.3.6   Lee Wave Clouds

Figures 47 and 48 suggest lee wave clouds in the HRIR data near 38.5°N, 279°E (121°W) though, as indicated above, the map locations are in error. Radiosonde and rawinsonde observations were available from Oakland and Winnemucca, located about 130 miles upwind and downwind of the lee waves, respectively. This permitted comparison of actual conditions with the theory of lee wave formation, and with previous empirical findings relating wavelength to wind velocity. Naturally, possible effects of time and distance on representativeness of the observation must be considered.

Alaka[1] indicates the requirements for lee wave formation as:

"The air mass must be statically stable, and more particularly, there should be marked stability, such as an isothermal layer or an inversion, at levels where the airstream is disturbed by the mountains, i.e., within several hundred metres of their crest level. At higher levels the stability should be less... generally speaking it is necessary for the wind to be within about 30 deg. of the perpendicular to the ridge. The minimum speed at crest level is not particularly critical but values around 7 m/sec appear to be required in the case of small mountains, rising to about 15 m/sec for large mountains such as the Rockies. It is of greater importance that the airstream should comprise a deep current of air in which the direction changes little with height and the speed increases upwards through the troposphere."

Downwind from the lee waves, at Winnemucca, at 0000 GMT there was a stable layer between about 14,600 and 15,700 feet, but this stability was not evident there at 1200 GMT. Oakland did not have a stable layer at these altitudes for either time. The wind criteria were satisfied at both stations. The lee waves occurred under a jet stream at 200 mb.

Theoretically, according to Scorer[18] and as reported by Conover,[5] "...waves are possible only when the parameter, ℓ^2, decreases with height through a fairly thick layer to about one-ninth its value at the bottom of the layer. This parameter is defined by the equation:

$$\ell^2 = \frac{gB}{U^2} - \frac{1}{U} \frac{d^2U}{dZ^2}$$

where:

g = acceleration of gravity

Z = height measured upward

U = horizontal wind component normal to the ridge

B = static stability or $\frac{1}{\theta} \frac{d\theta}{dZ}$, where

θ = potential temperature

Since $\frac{1}{U} \frac{d^2U}{dZ^2}$ is normally small, except occasionally in the lowest layer of the atmosphere, the horizontal wind speed becomes the most important factor in the determination of ℓ^2."

Taking the value of ℓ^2 at 700 mb as more or less representative of the value at the height of the clouds, the values at 200 mb and 300 mb are shown in Table II. At 0000 GMT the criterion was barely met at Oakland and was not met at Winnemucca but at 1200 GMT the criterion was met at both stations at 300 mb and nearly met at 200 mb.

Hanson[13] has expanded on the work of Corby,[6] relating wavelength to mean wind speed from 850 mb to 200 mb. The relationship is:

$$\lambda = (\frac{U}{6} - 2)$$

where

λ = wavelength in nautical miles

U = mean wind speed in knots; $U \geq 12$ knots.

The time and area weighted mean wind speed for the case was approximately 38 knots; according to Corby, this would correspond to a wavelength of about 4.3 nautical miles.

Figure 53 shows an enlargement of the lee wave section of Figure 47. The two dark rectangles to the right are the grid points for 38° and 40°N and 240°E (120°W). The width of the scan lines is clearly apparent. Perpendicular to the scan line direction the data should ideally be sharp-edged but are not. (Fujita and Bandeen[9] present enlargements of HRIR showing similar patterns.)

Table II

Values of the Parameter ℓ^2 at Oakland, California and Winnemucca,
Nevada Near the Time of Lee Waves

$$\ell^2 = \frac{gB}{U^2} - \frac{1}{U} \frac{\partial^2 U}{\partial Z^2} \approx \frac{g}{\theta} \frac{\partial \theta}{\partial Z} \times \frac{1}{U^2}$$

P mb	U m sec^{-1}	θ K deg	$\frac{\partial \theta}{\partial Z}$ K deg m^{-1} x 10^{-3}	ℓ^2 m^{-2} x 10^{-6}	ℓ^2_{700}/ℓ^2_i
			Oakland 0000Z		
700	6.2	312	4.2	3.43	
300	19.4	332	2.8	2.2 x 10^{-1}	16
200	26.2	345	14.3	5.8 x 10^{-1}	6
			Oakland 1200Z		
700	10.3	304	6.2	1.4	
300	40.1	325.5	2.6	4.9 x 10^{-2}	39
200	38.8	351.	16.7	3.1 x 10^{-1}	6
			Winnemucca 0000Z		
700	12.0	312	0.9	2.0 x 10^{-1}	
300	27.8	330	3.2	1.2 x 10^{-1}	1.6
200	30.9	343	8.3	2.5 x 10^{-1}	0.8
			Winnemucca 1200Z		
700	9.0	305	4.5	1.8	
300	34.2	328	2.8	7.2 x 10^{-2}	25
200	40.3	351	14.3	2.5 x 10^{-1}	7.2

Figure 53.   Enlargement of Lee Wave Section of Figure 47

The lee wave clouds are associated with the central white "rectangular" masses. Determination of the lines of the wave crests is complicated by the interaction of these lines and the direction A of the scan lines. Careful inspection suggests the wave crests lie parallel to line B, with a wavelength which is somewhat indeterminate.

The lengths of the dots and the widths of the scan lines in this magnification are probably greater than the sizes of the individual wave clouds. At the satellite altitude of 437 km (the lee waves were scanned near perigee), the width of the nominal instantaneous field of view of the HRIR sensor was 1.9 nautical miles, whereas the corresponding scan line width as reproduced was 5.3 nautical miles.[*] The minimum length of the lee wave clouds in Figure 53 (along the scan) was measured to be 3.3 nautical miles. These values indicate the limiting resolution available in the Nimbus I HRIR data as presented by the facsimile recorder. If the satellite had been at nominal height, the instantaneous field of view over the wave clouds might have been "contaminated" enough by the clear (warm) areas around the wave clouds so that they would have been almost unnoticeable.

Measurement of the wavelengths between crests in Figure 53 was complicated by the indeterminancy of the exact orientation of the lines of crests (line B) and by the difference of scale in the directions parallel to and perpendicular to the horizon. The computed wavelength was about ten nautical miles, which corresponds poorly to Corby's empirical values. Conover[5] has discussed reasons why deviations from Corby's formula may be expected, however, and has indicated he has found a considerable dispersion from it in wave cases he has studied. Fritz[8] reports a case of lee waves in which the atmosphere was less stable than normal and a mean wind speed was less than the Corby normal for the observed wavelength, which is in qualitative agreement with these results.

4.4.3.7   Terrestrial Features

Among terrestrial features that were visible in our working copy of Figure 47 are Gypsum Point on Great Slave Lake, Mount Rainier, the west coast of the United States near $45^{\circ}N$, the mouth of the Columbia River, Crater Lake, Upper Klamath Lake,

---

[*] The satellite moved 5.3 n.m. between successive scans, and the operation of the facsimile recorder causes this to appear as the limiting resolution in the along-track dimension. Because of the aspect ratio near the center of the strip (see Section 2.3) the along-track resolution superficially appears to be better than that along a scan line, but this is not the case as the 1.9 versus 5.3 n.m. figures show.

and in California, the central (San Joaquin) valley, Death Valley, the southern Sierra Nevadas, the White Mountains, Mono Lake and other features.

Identifications must be made with care, however. What at first appears, on the basis of the shape, to be the southern tip of Vancouver Island is in fact a patch of warm water to the north and east.

4.4.4 Summary and Conclusions For This Case

In this case, the clouds associated with a weak surface low pressure area and a deep cold low aloft were seen by HRIR, near local midnight, over the western United States and Canada. Agreement between the HRIR cloud cover, and cloud cover plotted from conventional data was generally very good, including the ability to infer relative cloud top heights from the HRIR data. The HRIR showed several features not evident in the conventional cloud data: a narrow band of jet stream clouds from California to Alberta and Saskatchewan, and a region of wave clouds to the lee of the main range of the Sierra Nevadas, near Lake Tahoe. Over the Pacific Ocean, a small curved jet stream cloud suggested a slight modification to the analyzed position of the upper level trough.

Although the conventional data were too sparse to precisely delineate most cloud boundaries, the conventional observations could usually have been analyzed to fit the HRIR data without violating the conventional observations.

The cloud field over the western states and southern Canada fitted previous concepts of the cloud distribution associated with the observed synoptic situation: an area of high clouds associated with a jet stream and oriented parallel with it; an area of cloudiness and precipitation associated with a weak surface low pressure area; an area of low cloudiness over Canada in association with a shortwave trough northwest of the surface low , where upslope motion is suggested by the low level flow and the topography; and wave clouds in the lee of the Sierra Nevadas under the high level jet stream.

The lee wave clouds occurred under conditions of wind and stability usually found with wave clouds and which theory postulated as necessary for their formation, except that the radiosondes gave little evidence for a stable layer to cap the clouds. Careful analysis was necessary in order to determine the distance between wave crests, since the method of recording results in a pattern which, due to interaction between the scan pattern of the sensor-recorder system and the linear pattern of the waves, could be misinterpreted. The approximate wavelength of 10 nautical miles was substantially greater than Corby's empirical length of 4.3 nautical miles, but a similar degree of dispersion has been noted by other analysts.

Calculations, using the magnified presentation of the recorder scan as shown in Figure 53, suggest a limiting resolution of the Nimbus I HRIR data as presented by the facsimile recorder of about 5.3 nautical miles in the direction of satellite motion and about 3 nautical miles along the HRIR swaths.

4.5   A Stationary Front Over the Eastern United States

4.5.1   Introduction

The data in HRIR orbit 335 (Figs. 54 and 55) were chosen for intensive analysis since, being over the eastern United States and southeastern Canada, good conventional data and adequate radar coverage of several Weather Bureau stations were available for corroboration.   The HRIR observation was made about 0530 GMT, 20 September 1964; TIROS television observations, made about twelve hours earlier and later, were available for much of the area.

Even superficial analysis of the HRIR strip (Fig. 54) shows:

1.   A cloud band, apparently related to a front, extending from the eastern Great Lakes southeast across the middle Atlantic states.   Distinct variations in HRIR brightnesses indicate that the cloud tops within this band extend to widely different levels.

2.   An area of higher clouds, near the horizon, connected to the northwest end of this band.

3.   A second area of higher clouds along the eastern horizon of the strip.

4.   An apparently clear area northeast of the band, over New England and southeastern Canada.   A number of landmarks could be identified within this area.

4.5.2   Available Data and Conventional Analyses

Conventional meteorological data available for comparative analyses included:

Hourly and six hourly surface reports
Twelve-hourly radiosonde reports
Winds aloft
Surface and 500 mb maps

Radar from the following selected stations:

New York City

Washington, D. C.

Buffalo

Cincinnati

Detroit

4.5.2.1 Synoptic Situation

Figure 56 shows the surface weather map at 0600 GMT, half an hour after the HRIR picture. A large high pressure area lay over eastern Canada and the north-eastern United States, with a ridge, extending south-southwest from the high, in-fluencing most of the eastern United States. A stationary front extended from Michigan to Virginia; its stationary characteristics were confirmed by insignificant movement during the twenty-four hour period starting at 1800 GMT, September 19. Over North Carolina and the Atlantic, the stationary front became a cold front; over and north of Michigan, a warm front. While temperature gradients in the immediate vicinity of the front were rather small, temperatures over northern New England were some 30°F colder than those over the southeastern states.

A cold front with a north-south orientation lay just to the west of the warm front, over and north of Lake Superior. The western edge of the low pressure area asso-ciated with Hurricane Gladys can be seen east of Florida.

The 0000 GMT, September 20 500 mb analysis (Fig. 57) showed a ridge over and to the north of New York and New England, with strong northwesterly flow over extreme eastern Canada. A deep trough extended south-southwest from a closed low over Hudson Bay. A short wave trough lay over the Great Lakes and was disturbing the southwesterly flow east of the major trough. Although the winds associated with this short wave trough were generally light, the shear line of the trough could be traced as far southeast as Pennsylvania. It would appear that the weather associated with the stationary and warm fronts over the eastern United States should be dynamically related to the flow pattern of the short wave trough and shear line; the weather associated with the north-south cold front to the west should be related to the region of southwesterly flow east of the deep trough.

The circulation of Hurricane Gladys extended to at least 500 mb, and at this level was centered near 28°N, 69°W.

Figure 54. HRIR Picture of Eastern North America on Orbit 335
at 0530 UT, 20 September 1964
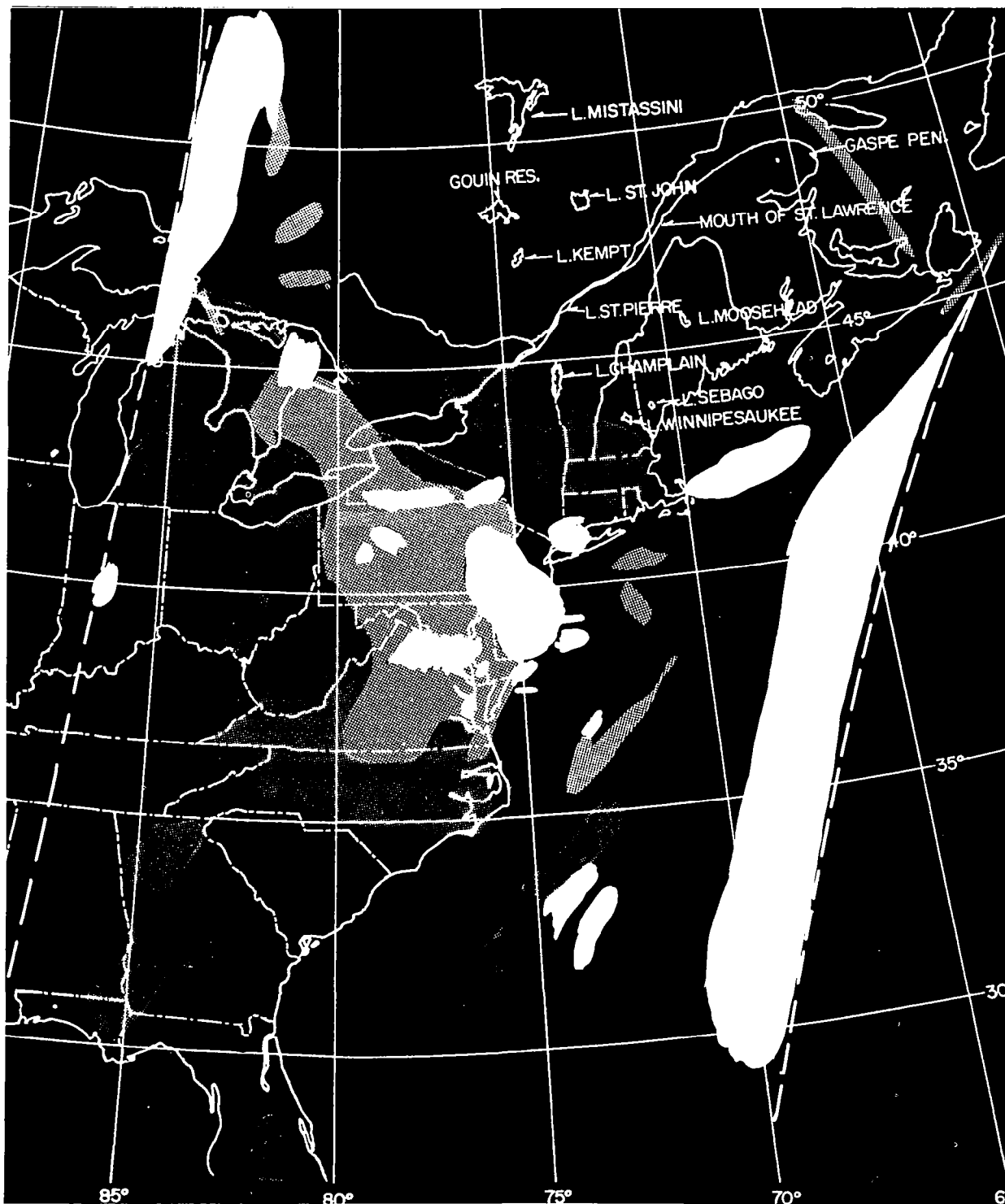
Figure 55. Rectified Map of Cloud Cover as Seen by HRIR on Orbit 335 at 0530 UT, 20 September 1964

113
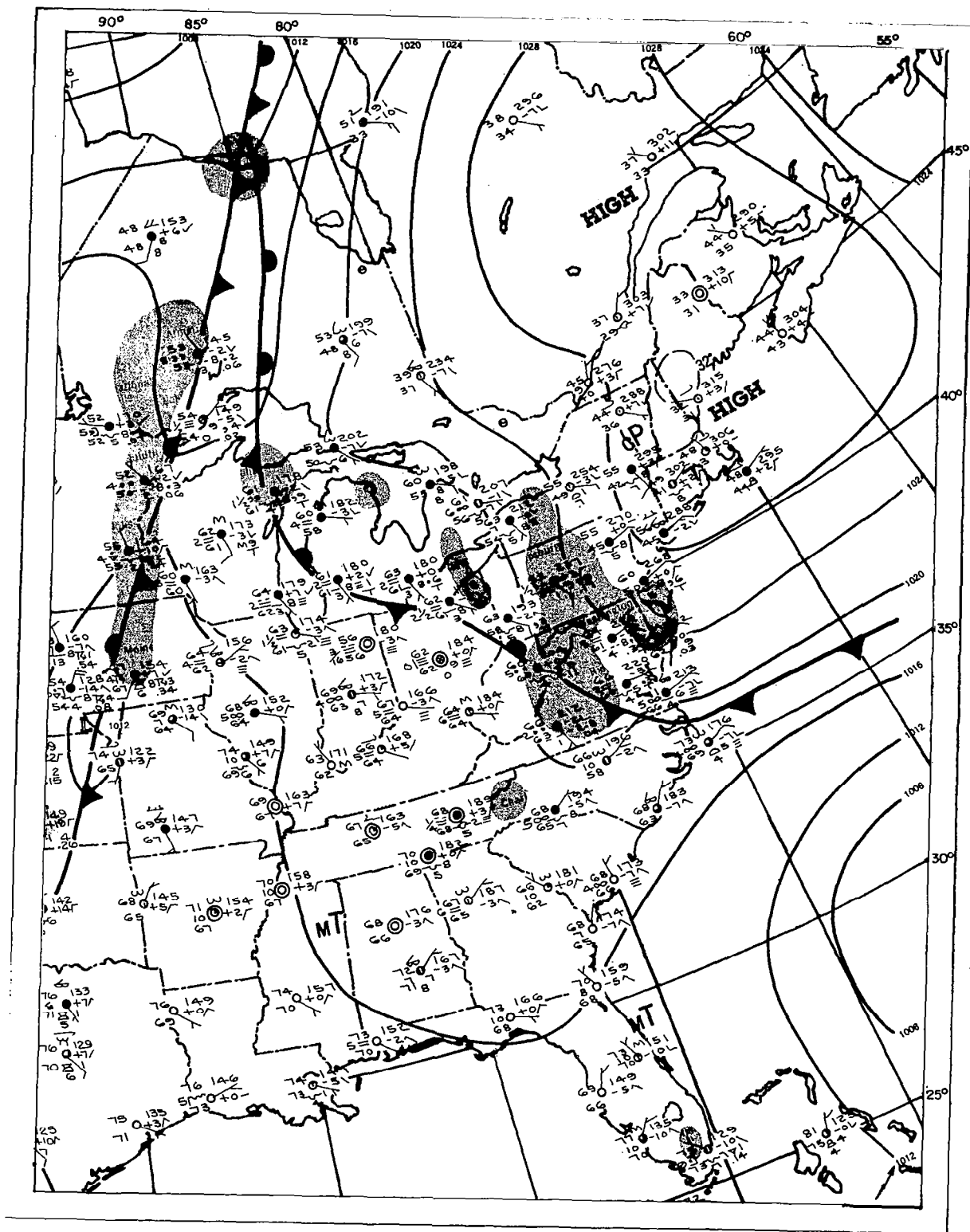
Figure 56.   Surface Weather Map at 0600 UT, 20 September 1964
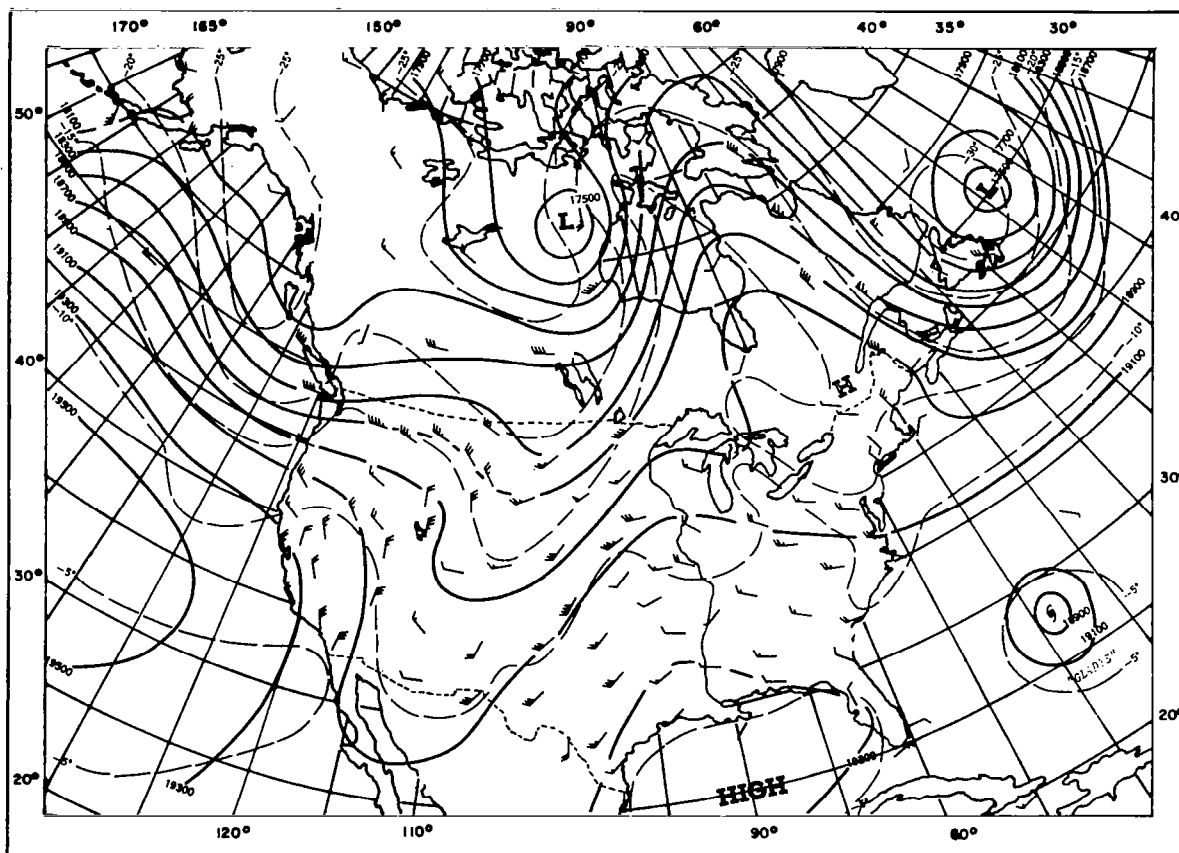
Figure 57.   500 mb Map at 0000 UT, 20 September 1964

4.5.2.2 Raobs

The radiosonde observations for the area of the HRIR data showed little temperature change between 0000 GMT and 1200 GMT, 20 September 1964, except for surface cooling. The dew point curves were more variable but usually not significantly so. Many of the ascents were moist adiabatic through the lower 150-200 mb of the atmosphere.

Several of the ascents will be discussed in greater detail in subsequent sections.

4.5.2.3 Winds Aloft

As mentioned earlier, the winds over the area under discussion were generally light; the average wind speed between the surface and 400 mb was usually less than 20 knots. At most stations the wind veered nearly 180° between the surface and 400 mb. Easterly or southerly surface winds (70° to 200°) shifted to westerly 400 mb winds ($250-310^\circ$). Between 300 and 150 mb, winds from $300^\circ \pm 10^\circ$ of more than 50 knots were found at many stations.

4.5.3 Results of Analyses and Interpretations

4.5.3.1 HRIR Grid Coordinates

Among the many landmarks in the HRIR data (Fig. 54), Lake St. John (about 49°N, 72°W) was useful in comparing actual and HRIR grid coordinates. The HRIR grid was correct as to latitude, but the grid should be shifted westward. The amount of westward shift is variable, depending on both latitude and position with respect to the subsatellite point (or horizon). Near the subsatellite track (which is parallel to the left horizon and 55% of the distance from the eastern to the western horizon), at 40°N, the required shift amounts to about 0.9° of longitude. Near the eastern horizon, it amounts to several degrees of longitude. These corrections were obtained by the ARACON hand-gridding method.[11,12]

Figure 55 is a rectification of Figure 54.

4.5.3.2   Clouds, Fog and Precipitation

4.5.3.2.1   Cloud Cover

In the HRIR data (Figs. 54 and 55), clouds associated with the cold-stationary-warm front may be seen extending across the center of the figures from near the eastern horizon to the western edge of the picture, north of 48°N. Because of fore-shortening at the western edge , it is not clear whether any of the western cold front clouds contribute to the bright area at the western edge of Figure 54.

The fact that the areas of bright cloud associated with the stationary front are mostly small and scattered suggests that whatever active weather may be related to the front (or to the 500 mb short wave trough) is also scattered.

To provide a comparison with the HRIR data, an analysis of surface cloud cover observations is given in Figure 58; the many stations where clouds were ob-scured by fog could not be used for the cloud analysis, but these areas of fog are identified in Figure 58. A large area of overcast stretches more or less continuously from the coast to Michigan, and perhaps to north of Lake Superior.   To the north, including over central New England, the overcast is bounded by patches of broken and scattered clouds, with clear skies further northward coinciding with the surface high pressure area. To the south of the overcast area, skies are mostly clear over South Carolina, Georgia and northern Florida. The western slopes of the Appala-chians have scattered clouds, while large areas of Ohio, Indiana and Michigan have ground fog (see Fig. 59a).

The cloud analysis in Figure 58, since it was made from surface data which are often ambiguous as to cloud top heights, shows only the extent of cloud cover. In spite of this, the patterns are in many ways similar to those in the HRIR data of Figures 54 and 55, which are, of course, functions of cloud top height as well as the extent of cloud cover. Those differences which do exist are often minor and, as we will see, can usually be explained by a more careful and detailed analysis.

A significant problem in the interpretation of HRIR data (or other IR data in an atmospheric window) is the fact that high scattered clouds may provide the same sensor response as lower but more extensive clouds. In our original of Figure 54 (as depicted in the rectification in Figure 55), a faint but uniformly grey band extends across central New England into New York State. It could be either low overcast to broken, or high scattered clouds. Actually, it appears to include both; the surface reports (Fig. 56) show low clouds at and to the south of Hartford, Albany, and Syracuse. On the other hand, Boston, Portland, and Burlington report scattered
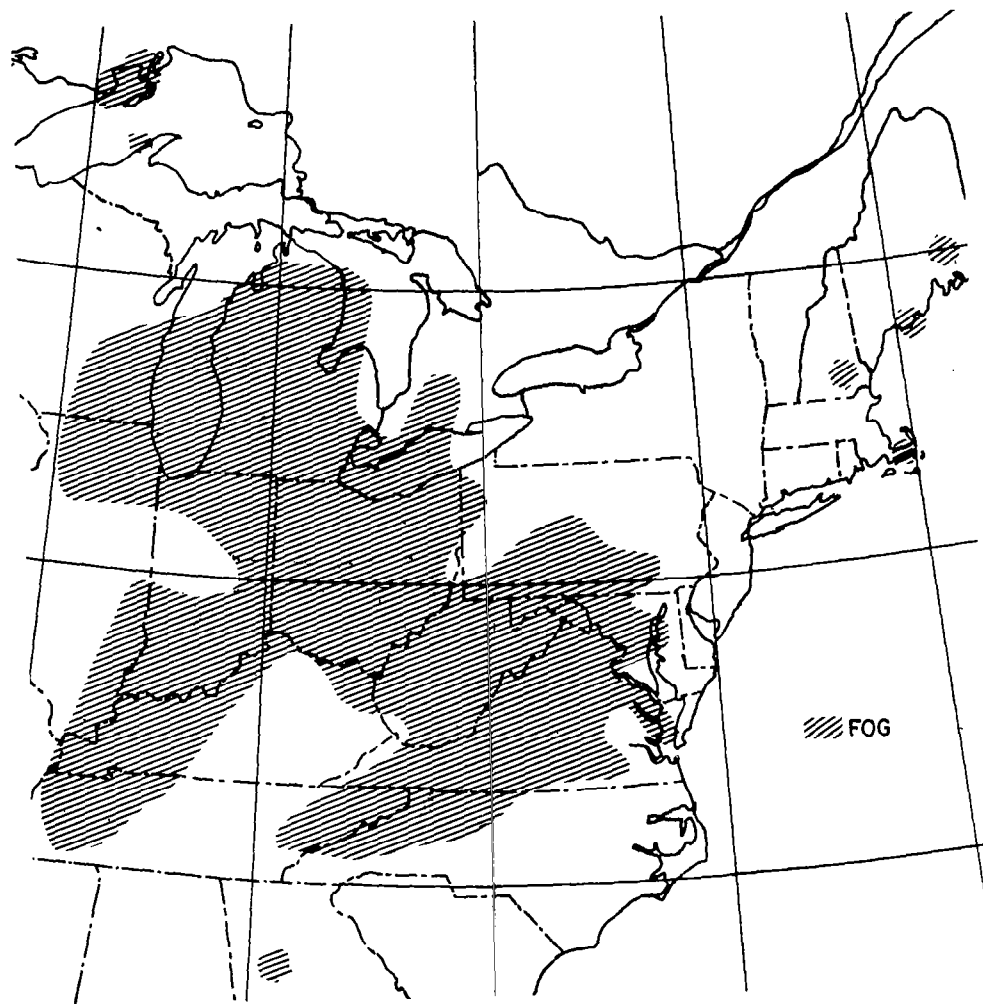
(a) Fog
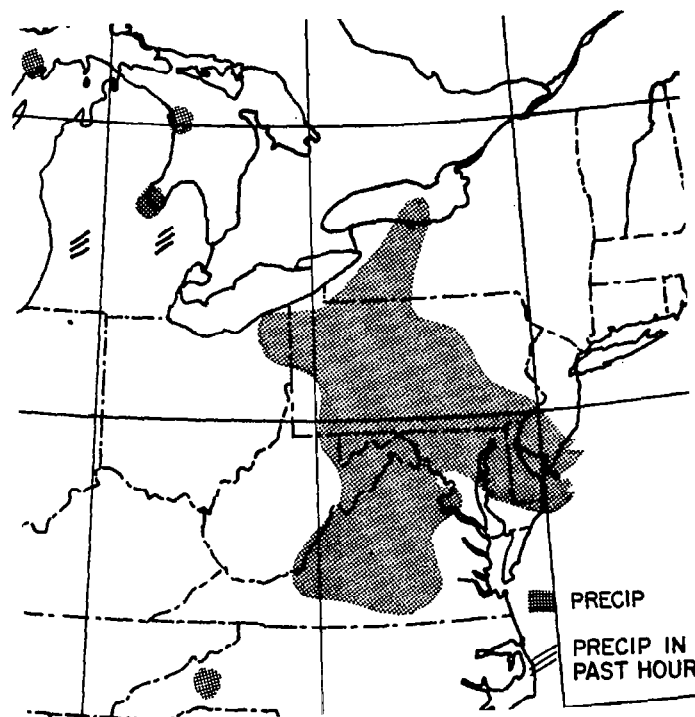
(b) Precipitation

Figure 59.   The Distribution from Ground Station Observations at 0600 UT

This comparison of the fog covered and clear areas in Figures 54 and 55 illustrates two points:

1. The erroneous interpretations that may result if one attempts to relate HRIR brightnesses (or temperatures) to cloud top heights without considering climatological or synoptic factors.

2. The dangers in interpreting any area (regardless of how dark or warm) as necessarily being clear in the absence of visible landmarks.

4.5.3.2.3 Precipitation

The areas of precipitation as reported in surface observations (Figs. 59b and 56) coincide rather well with most of the bright (cold) regions in the HRIR. This is particularly true over the areas away from the edges of the HRIR strip where the data can be rectified and positioned with reasonable accuracy, and where there is also an adequate density of reporting stations. For example, Buffalo radar data (to be discussed in more detail below) show strong echoes which imply precipitation between Pittsburgh and Erie where there are no observing stations. If the surface reports of precipitation in Figure 59b were to be supplemented by radar reports, an even better fit between bright areas in the HRIR and areas of precipitation would exist.

Evidently, most precipitation (at least in this case) falls from thick clouds extending to relatively great heights (as might be anticipated), and accordingly, most of the bright clouds have precipitation associated with them. Other sources of bright (cold) areas (high clouds) in the HRIR include cirrus clouds. Nearly all the bright areas in Figures 54 and 55 which are over land (where confirming surface observations exist) can be associated with concurrent precipitation, precipitation in the recent past, or cirrus clouds.

Radar Observations

Observations from Weather Bureau radars at Buffalo, New York City, and Washington National Airport for 0430, 0530 and 0630 GMT, on 20 September 1964, show precipitation echoes which can be related to the HRIR data. Figure 60 shows the PPI observations for these three stations at 0530 GMT. The Buffalo and New York radars are on the 250 nautical mile range, while the Washington radar is on the 100 nautical mile range.
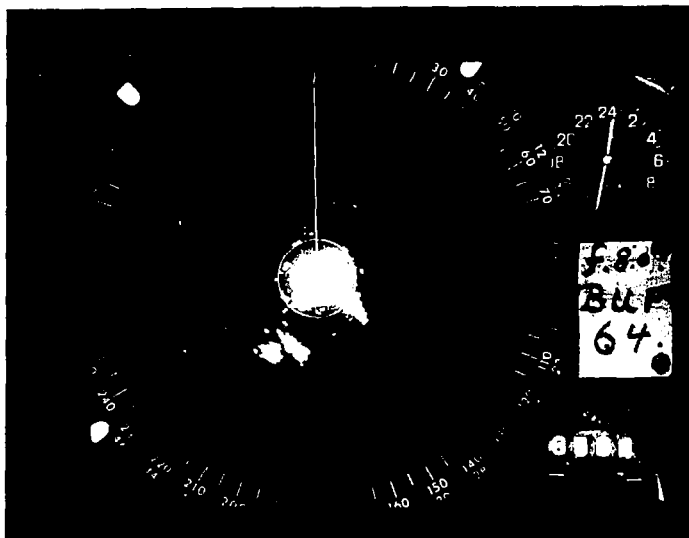
(a) Buffalo,
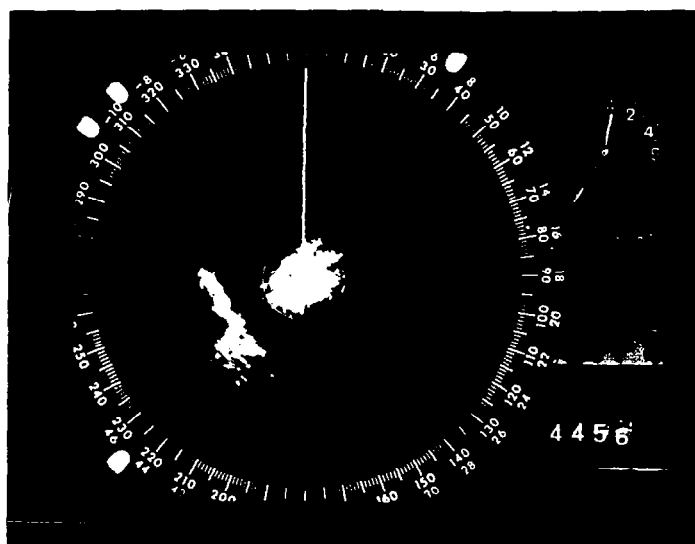
(b) New York City
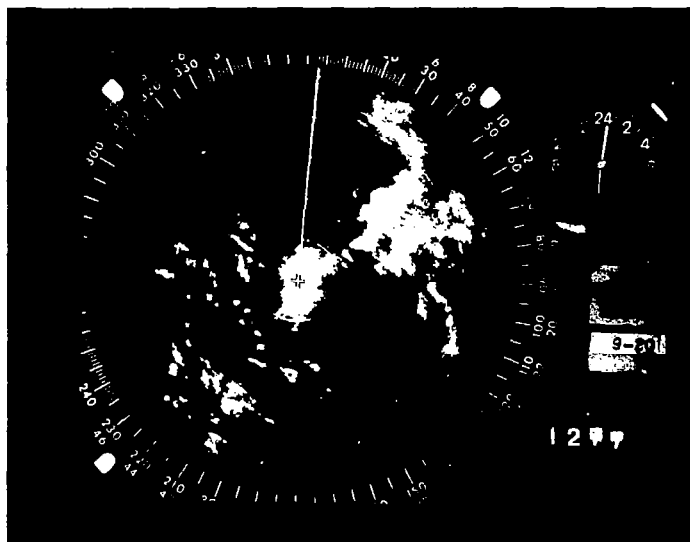
(c) Washington

Figure 60. Radar Observations at 0530 UT, 20 September 1964

The Washington radar data indicated echo tops between 15,000 and 25,000 feet; the New York radar indicated tops to 21,000 feet and Buffalo, to 20,000. These values are in general agreement with the Pittsburgh and Washington radiosondes, which suggested cloud tops near 500 mb. In fact, the correspondence is greater than might be expected, considering the variations in brightness in the HRIR data over this general area. The radar can detect the tops of the higher individual cells, while the probability of a radiosonde ascent coinciding with one of these cells is usually small.

The outstanding features of the Buffalo observation are the two precipitation cells 100 nautical miles to the southwest. The clouds within which the precipitation is embedded are visible in Figure 54 as two cold areas having the same shapes and orientation as the precipitation cells. The sharpness of the precipitation cells marks them as vigorous. The tops may have been at 20,000 feet, a height reported for some of the echoes from Buffalo at this time,but not specifically applied to these two echoes. The echoes were beyond the radar ranges in use at the time at New York and Washington.

The main feature of the radar data from New York and Washington was the large precipitation area lying about midway between the two stations. The precipitation echoes have nearly the same shape at each station, especially when attenuation effects are subjectively considered; apparently, identical precipitation was being viewed. The echoes are less sharp-edged than the echoes seen by Buffalo, indicating a less vigorous and probably an older system. The echoes lie within the large bright area near 40°N, 77°W, in Figure 54, though this bright area is more extensive. This is analogous to the results of Nagle,[17] who found that while bright cloud areas in TIROS pictures often contained areas of precipitation, the precipitating areas covered only parts of bright areas. A spreading out of cirrus and other inactive clouds from the active centers probably accounts for the larger area seen by the HRIR, and would support the conclusion that these precipitation cells are less vigorous than those over western Pennsylvania. The radar observations an hour previously and subsequently (not presented) show only small changes in size or shape.

As mentioned earlier, radar cloud tops, not necessarily applying to this cloud system, were 21,000 feet as seen from New York, and 15,000 to 25,000 feet from Washington.

The Washington radar photograph (Fig. 60c) has other precipitation echoes. Some of these can also be related to features in the HRIR, especially those areas southwest of the bright cloud.

Cincinnati and Detroit reported no precipitation echoes on their radars at this time.

4.5.3.2.4 Lines of Parallel Clouds

In Figure 54, an area of somewhat bright but faint parallel lines, suggestive of wave or billow clouds, can be seen in the vicinity of $39°-40°$N, $78°-80°$W. Although this might only be an area of artificial system noise,[9] its extent in both latitude and longitude, and especially the latitudinal continuity of the lines, suggests it is a cloud pattern.

This area is about over, or just west of, the main range of the Allegheny Mountains, which rise to more than 3,000 feet msl there. Cloud bases observed at 0600 GMT were about 2,400 feet msl at Morgantown, West Virginia, near the center of the area. The Pittsburgh soundings showed moisture up to about 500 mb at both 0000 GMT and 1200 GMT, so it is probable that clouds reached that level, possibly in several layers. The soundings at Huntington, West Virginia, indicated a probable lack of clouds at 0000 GMT, but did indicate clouds, extending to about 660 mb, at 1200 GMT. In Figure 54, this cloud area appears to be colder than the terrain in New England, but warmer than the top of the large cold cloud mass between New York and Washington which is estimated to be about 20,000 feet. Thus, the tops might be at about 15,000-18,000 feet.

Three types of cloud show this pattern when viewed by satellites at a resolution approximately that of the TIROS wide or medium angle cameras, or the Nimbus I HRIR. These are crest clouds,[5,25] lee wave clouds,[5,25] or accentuated cloud rows in billow cloud (Helmholtz wave) conditions.[23,25]

In this case, crest clouds seem unlikely since, although they occur over mountainous terrain, they usually result from convection produced by solar heating, and so are normally only a daytime phenomenon. Furthermore, the lapse rate was moist adiabatic, rather than approaching dry adiabatic, and on the basis of their whiteness in Figure 54 and the radiosonde ascents at Pittsburgh and Huntington, these cloud lines appeared to be thicker than the maximum of 3,000 feet ascribed to crest clouds in Reference 5. (If the cloud tops had been at 7,000 feet, the cloud top temperatures would have been $46°$F, or much warmer than the ground in northern New England.)

Lee wave clouds were also extremely unlikely in this area since the winds were light to well above the presumed level of the clouds, shifting with height, and more nearly parallel then normal to the mountain ranges.

The most reasonable explanation seems to be accentuated rows in billow clouds. In the layers where the clouds appeared to exist, the winds were shifting from about 150° at the surface to about 300° at 400 mb. This would lead to a shear vector which, although weak, was approximately normal to the cloud lines, as required by the theory of Helmholtz waves. Terrain effects may have contributed somewhat to the initiation of the billow cloud waves and to their orientation.

4.5.3.2.5   Other Terrain Related Cloudiness

There is a definite tendency in Figure 54 for the general area of low clouds between gridded coordinates 32°N, 88°W (272°E) and 36°N, 82°W (278°E) to be oriented parallel to the higher terrain of the southern Appalachians. In parts of this area, surface stations are reporting clouds; in others, ground fog. Some of the winds indicate a weak upslope component in the lower levels, possibly enough to induce more cloudiness over higher terrain than elsewhere in the generally humid air. An alternate possibility, that the valleys have fog and that the hills and mountains, although actually cloud-free, are colder and give the appearance of clouds, tends to disagree with TIROS data on the clouds in this region (see Fig. 62).

4.5.3.3   Comparisons with TIROS Pictures

At about 1720 GMT, on both 19 and 20 September 1964, TIROS VII obtained TV photographs of parts of the area seen by the HRIR. Figure 61 shows a mosaic of a portion of the pass on September 19 (orbits 6777/6775) and a copy of the operational nephanalysis prepared at the time. Figure 62 shows analogous data for September 20 (orbits 6792/6790). These TIROS pictures were obtained very close to twelve hours earlier and later, respectively, than the HRIR data.

4.5.3.3.1   The Cloud Band Associated with the Stationary Front

The frontal cloud band extending from the middle Atlantic states northwestward to and across the Great Lakes can be clearly identified in the TIROS data (Figs. 61 and 62) as well as in the HRIR (Figs. 54 and 55). The TIROS data suggest that little change in the local synoptic situation occurred during this twenty-four hour period, except for some eastward drift of the frontal clouds over the Great Lakes. Yet, while

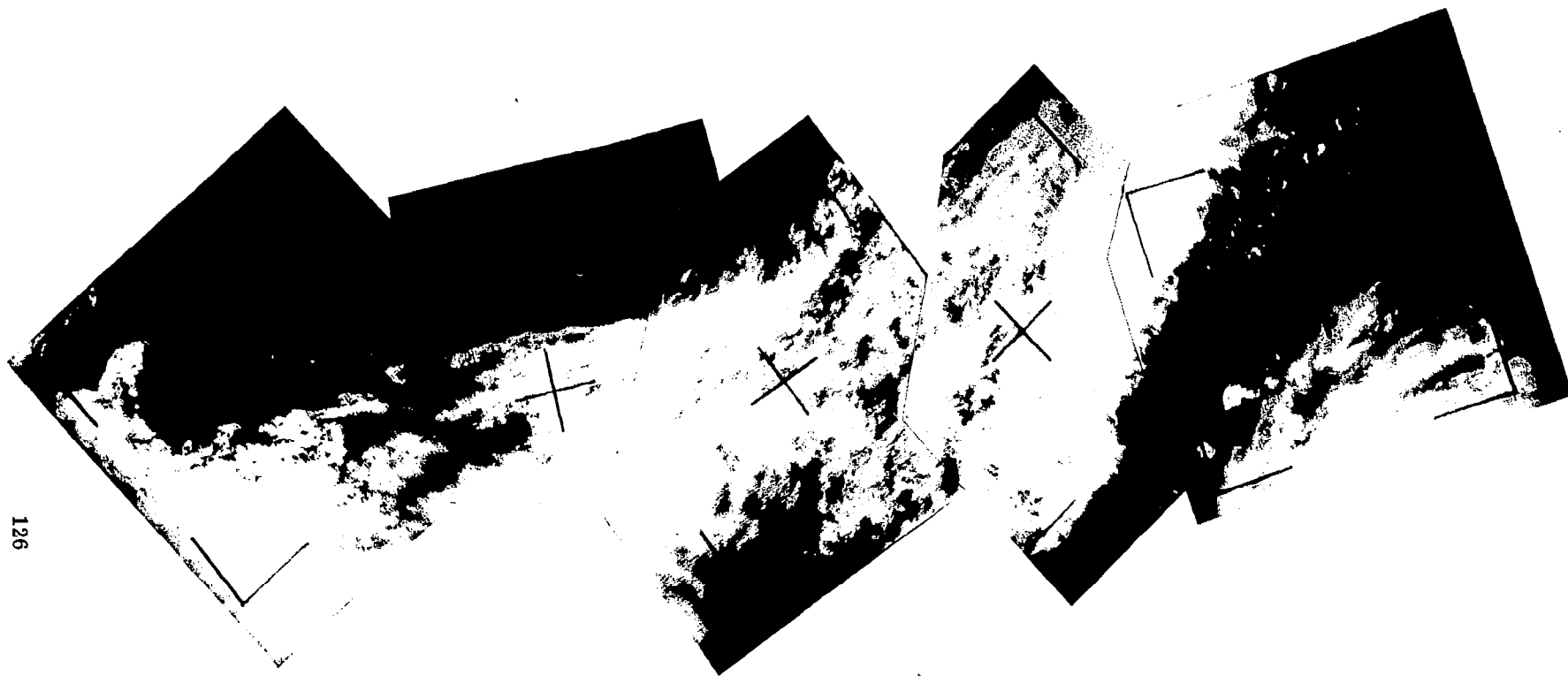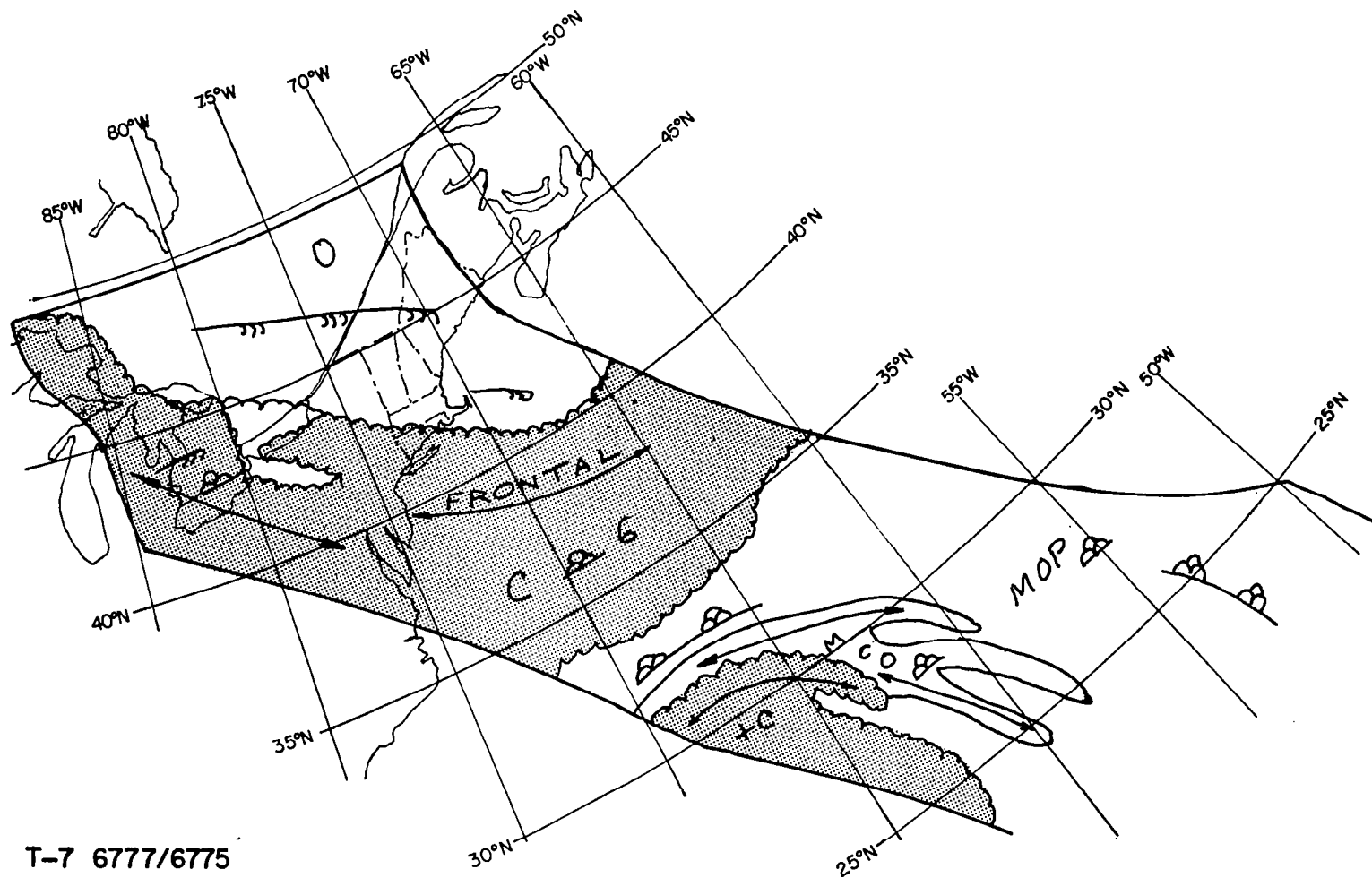Figure 61a. TIROS VII Television Picture Mosaic, Orbit 6777/6775
1710 UT, 19 September 1964

T-7 6777/6775
1712Z 19 SEPT 1964

Figure 61b. TIROS VII Operational Nephanalysis, Orbit 6777/6775,
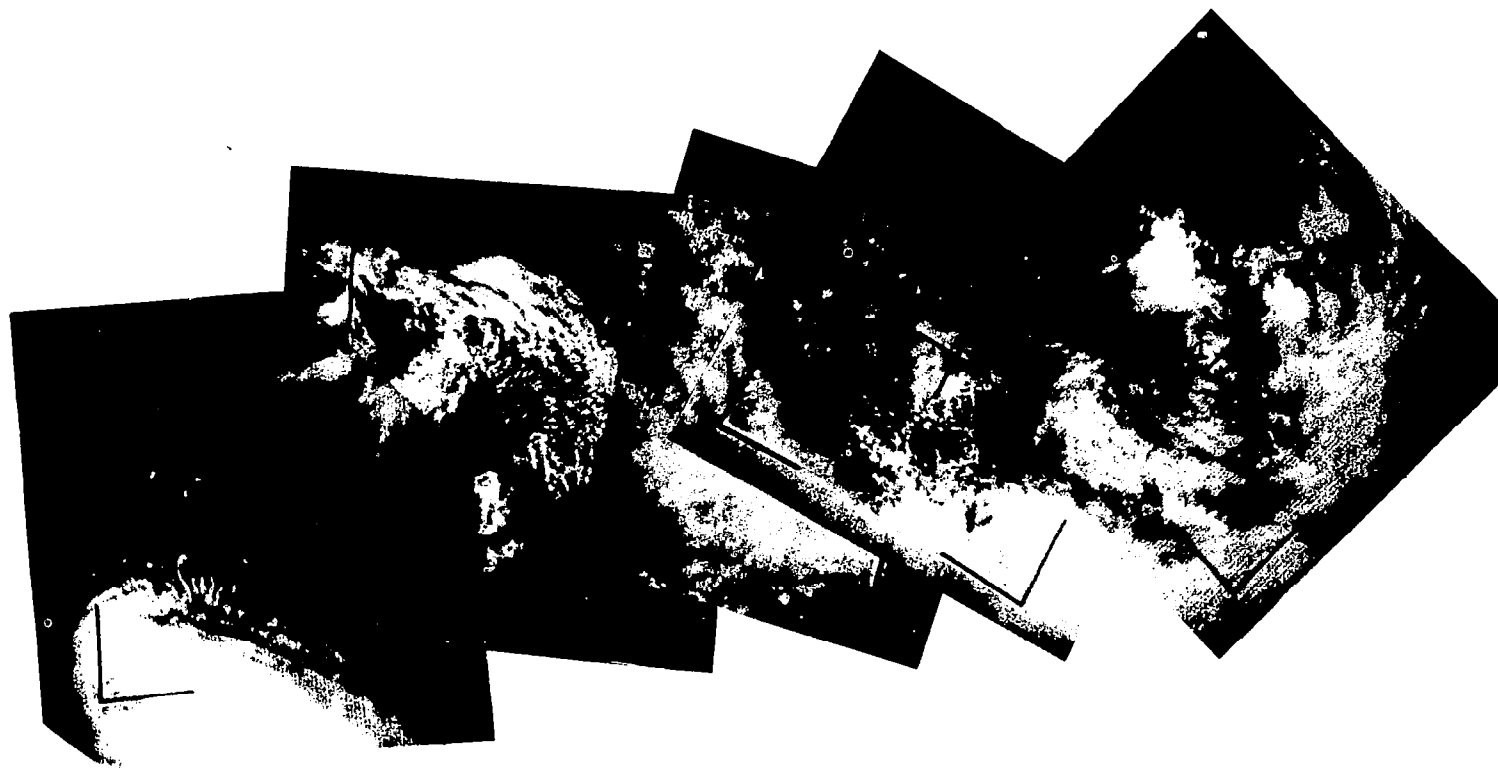1710 UT, 19 September 1964

Figure 62a.   TIROS VII Television Picture Mosaic, Orbit 6792/6790,
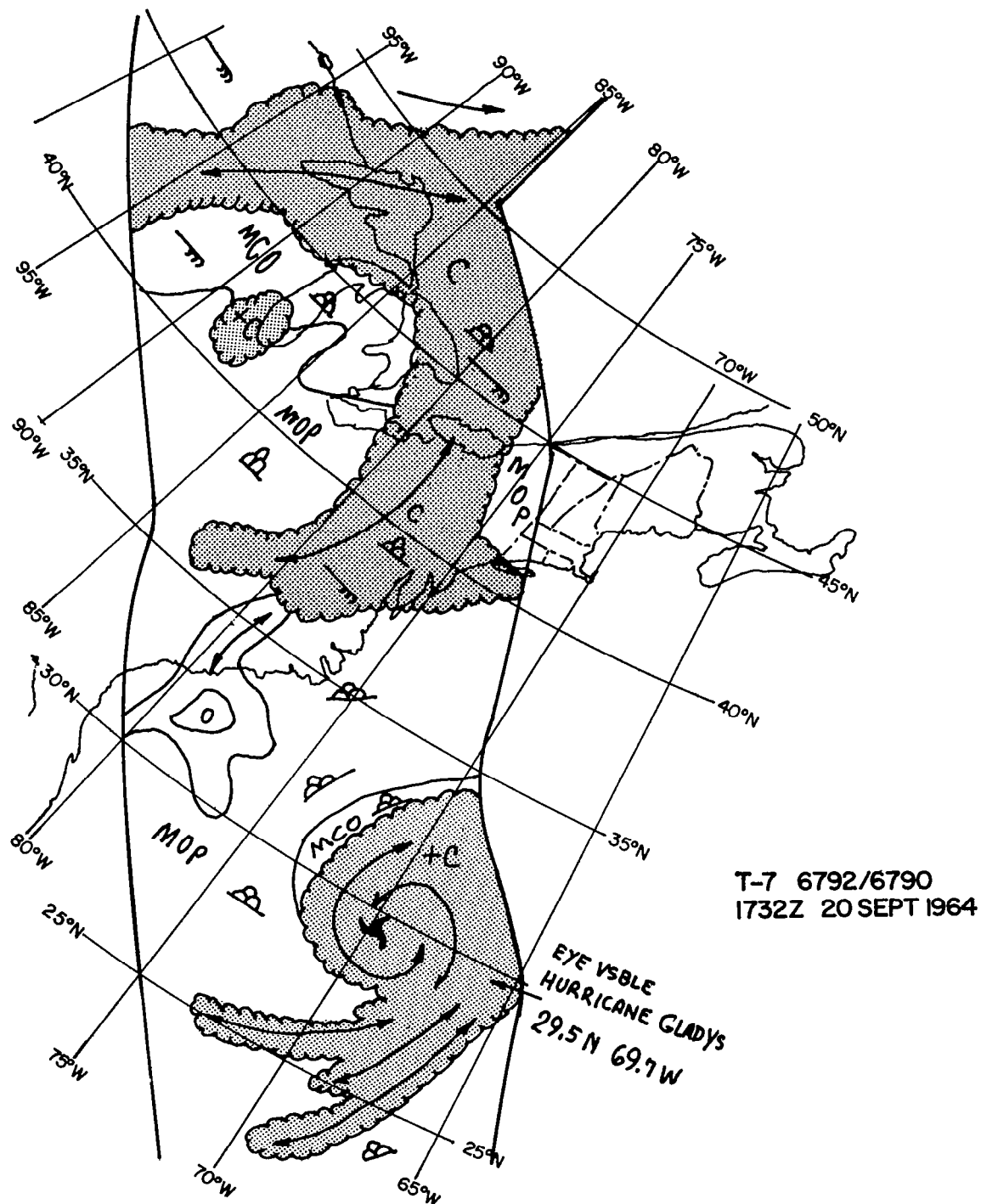1730 UT, 20 September 1964

Figure 62b. TIROS VII Operational Nephanalysis, Orbit 6792/6790
1730 UT, 20 September 1964

129

the TIROS data (Figs. 61 and 62) show a cloud band which is for the most part uniformly bright, the HRIR data (Fig. 54) show that wide variations in cloud top height existed within the frontal band. As discussed earlier, the brighter (higher) areas could be related to areas of precipitation. The correspondence between the two TIROS views twelve hours earlier and later than the HRIR makes it unlikely that the variations seen in the HRIR were due to a general development or dissipation. Rather, it seems likely that if high resolution 10μ IR data had been available at the times of the TIROS pictures, they too would have shown the cloud band to have highly variable cloud top heights, although the locations of the mesoscale cells producing the variations would be expected to change with time. Furthermore, although quantitative cloud top temperatures and heights cannot be inferred from the uncalibrated HRIR data so far available to ARACON, it is obvious that, at least in principle, cloud top heights can be inferred from the HRIR data, while the TIROS pictures permit only very unreliable cloud top estimates. This again emphasizes one of the advantages of the HRIR data, and the desirability of having both types of data available to the analyst.

4.5.3.3.2 Oceanic Observations and Hurricane Gladys

Over the ocean, a remarkable identity in one small cloud pattern is at once evident. In Figure 54, a bright quasi-ring pattern (open to the southwest) is seen at gridded coordinates of 32°N, 76°W (284°E). A very similar pattern (although with the ring closed) is seen in the TIROS mosaic at 78°W. This helps to establish the fact that a very extensive cloud mass visible in the HRIR, eastward of the "ring", can be associated with hurricane Gladys. Further north, the extensive clouds along the eastern edge of the HRIR strip appear to be associated with a trough at 500 mb, extending from the deep low off Newfoundland toward hurricane Gladys (Fig. 57).

At the time of these HRIR data, Nimbus was at a height of about 535 km and at a longitude of 82°W when it scanned Gladys at 30°N. At this altitude, the horizon is about 23° of great circle arc (26° of longitude at 30°N) from the subsatellite point. Thus, at 30°N, the HRIR horizon was at least as far east as 60°W. The nephanalysis of Figure 62 suggests that the eastern edge of Gladys at 30°N lies near 65°W. Assuming the position of Gladys in the HRIR was not greatly different from that twelve hours later in the TIROS pictures, these calculations suggest that the HRIR was able to see completely across Gladys, and indeed, the dark strip (near 30°N) just inside the border of the HRIR strip tends to substantiate the calculation. Because, however,

of the tremendous foreshortening, no detailed analysis of Gladys is feasible from the HRIR data. The clear indentation south of the storm (between the main cloud mass and a major peripheral cloud band, near 27°N, 70°W in Fig. 62) can be identified in the HRIR.

4.5.3.4 Landmarks

Many landmarks were identifiable in the HRIR (Fig. 54), including: Lakes Mistassini, St. John, Kempt, St. Pierre, Champlain, Moosehead, Winnipesaukee and Sebago; Gouin Reservoir; the mouth of the St. Lawrence River; the Gaspe Peninsula; Nova Scotia; the Bay of Fundy; and parts of the coasts of New England, the south Atlantic states, and the Gulf of Mexico.

4.5.4 Summary of This Case Study

A comparative study of (1) the Nimbus I HRIR data for that portion of orbit 335 over eastern Canada and the United States, at about 0530 GMT on 20 September 1964; (2) concurrent conventional weather observations, and (3) TIROS pictures twelve hours earlier and later, has revealed:

1. The heights of cloud tops in a band associated with a stationary front, and with a 500 mb short wave trough and weak wind shear line, were highly variable in the HRIR, although in TIROS pictures, the cloud band was rather uniformly bright.

2. In general, bright areas in the HRIR could be associated with concurrent or recent precipitation. The few exceptions could usually be related to surface observations of cirrus. Concurrent radar observations, although of only a few cases, showed that the shapes of the radar echoes closely matched the shapes of the associated bright clouds in the HRIR when the precipitation was vigorous and precipitation cells were presumably young. The correspondence was less close when precipitation was not vigorous and the cells presumably older. It seems reasonable to ascribe the reduction in correspondence in these latter cases to the spreading of cirrus or other clouds from the tops of the cells.

3. There was no clear distinction in the HRIR between broken-to-overcast lower clouds over New York and New England, and scattered cirrus just to the north of this lower cloud area.

4. An area of fog over the Ohio River Valley appeared dark (warm) in the HRIR and might have been interpreted as a clear area in a superficial analysis. It looked warmer, which it was, than the ground over areas of southeastern Canada and northern New England which identifiable landmarks established as clear. This situation reconfirmed the need to identify landmarks to establish an area as clear, and the importance of climatological and synoptic considerations when interpreting HRIR brightnesses or temperatures.

4.6   Three Daylight HRIR Cases

Three daylight HRIR cases, with corresponding TIROS pictures, have been chosen to illustrate the value and the problems of this type of data.

4.6.1   Clouds Associated with a Short Wave Trough

About 1100 GMT on 11 September 1964, the Nimbus I HRIR, operating under full daylight conditions, made the observations in Figure 63a. The portion of the pass shown extends from North Africa to about $65^{o}N$, and provides good coverage of western Europe. Portions of Spain, France, and the British Isles can easily be identified.

Figure 63b shows the NMC 500 mb analysis for 1200 GMT, only an hour later. In it, we see a complex double closed low, with one center near $70^{o}N$, 0°, and the second center to the east-southeast. West-southwest flow, east of a trough in the Atlantic, covers most of western Europe. Two short wave troughs are perturbing this flow; one is analyzed just west northwest of the British Isles along $10^{o}W$. The second is just to the west of Spain. Most of the clouds in the HRIR strip can be associated with these troughs.

Figure 63c is an unrectified mosaic of TIROS VII pictures, taken about 1239 GMT, which duplicates the coverage of the northern portion of the HRIR data. The TIROS pictures can be geographically located by reference to the copy of the operational nephanalysis in Figure 63d.

Both the general and the detailed correspondence of the features in the HRIR and the TIROS data is extremely good. The following features can be identified and related in both types of data: (1) the major area of vertical motion east of the northern short wave trough, (2) an extensive area of lee wave clouds over and east of much of

Great Britain, (3) the clear area just east of the lee wave clouds, and (4) a some-
what filamented cloud band extending from the Iceland area to northwest of Ireland
(apparently advected around the closed low further north). (The lee wave clouds
here are, however, somewhat less clear than those noted in nighttime orbit 44 over
the Sierra Nevadas, presumably due to the higher altitude and lower resolution of the
daytime portions of Nimbus I orbits.) Closer inspection reveals the correspondence
of far smaller details between TIROS and HRIR data.

The decrease in intensity with cloud top height that complicates interpretation
of the daylight HRIR data (see Section 4.10) can be seen in the major cloud band (over
Scotland and the North Sea) associated with the short wave trough. Note that in the
HRIR the band is less intense than are the lee wave clouds. In the TIROS pictures,
the band is rather bright, and based on other studies, its clouds could be expected to
extend to reasonably high altitudes. Other less bright areas in the HRIR, presumably
also due to high clouds, include the northeastern part of the Iceland-Ireland band
(which, from the TIROS pictures, may very likely be composed in part of cirrus),
and the narrow cloud band, presumably jet stream cirrus, which runs from west
of Brittany across southeast England. Unexplained is the very narrow bright band
just to the north of the presumed jet stream band. Unfortunately, the TIROS pass
did not include this area. In other TIROS pictures of similar situations, taken at
about this orientation relative to the sun, a dark narrow strip of cloud shadow is often
seen. It is not apparent, however, how this could lead to brightening in the daylight
HRIR.

The difficulty of detecting clouds over land in daylight HRIR is apparent in this
strip.

From the viewpoint of meteorological interpretation, the cloud pattern over
the North Sea and its relationship to the 500 mb trough line are typical of a short
wave trough. The organization of the lower, lee wave clouds over and near Scotland
leads one to suspect a closed surface low containing a recently occluded wave. Such
a low and occluded wave were analyzed near 55°N, 10°W on the Russian surface
analysis for 0000 GMT, September 11 (not included).

The lee wave clouds can, of course, be attributed to a moderately strong west-
southwest flow over the hills of northern Great Britain. The winds over this area,
at 500 mb, are 45-50 knots; the Russian surface analysis indicates no significant
change in direction at lower levels. The clouds west and west-northwest of Spain.
too distorted by their proximity to the picture edge to permit shapes to be seen, are
in the area of the southernmost of the two short wave troughs. As would be expected,
the Russian surface analysis places an open wave near 48°N, 13°W, at 0000 GMT.

Figure 63a. Western European Daylight HRIR Data for 1100 UT,
11 September 1964
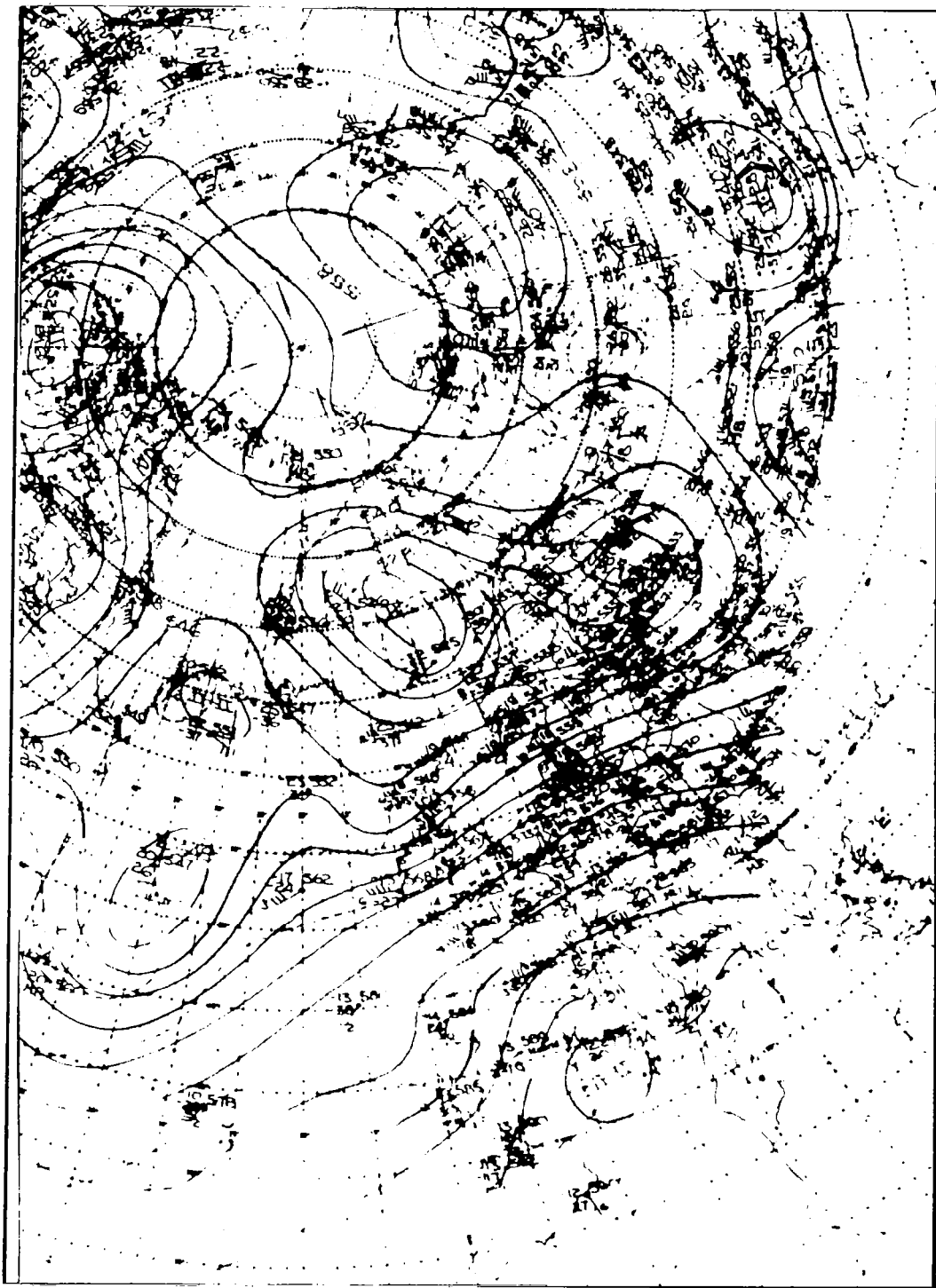
Figure 63b.   1200 UT 500 mb Analysis for 11 September 1964

Figure 63c.   TIROS VII Television Picture Mosaic, Orbit 6656/6654
              1239 UT 11 September 1964

T7— 6656/6654
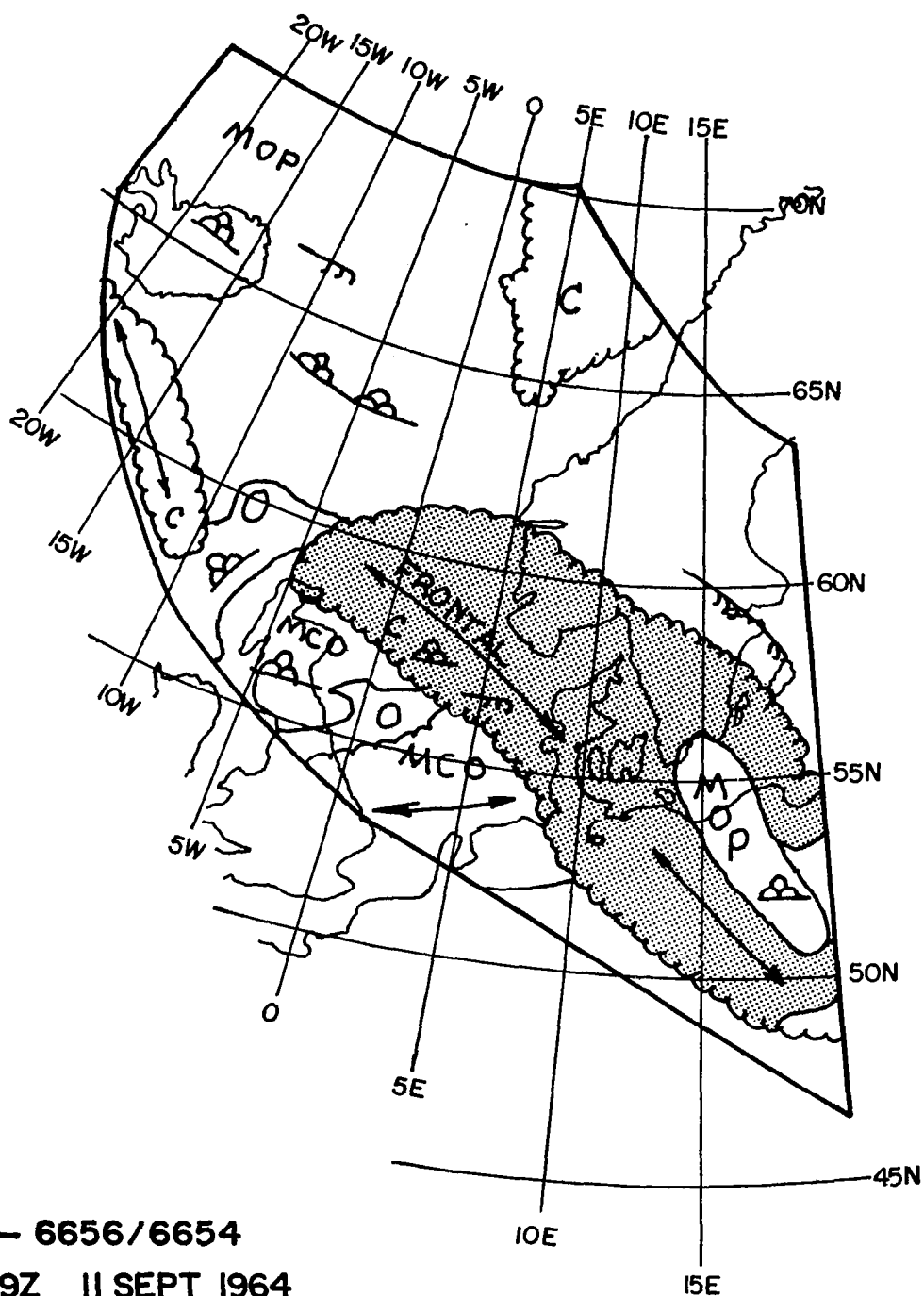
1239Z 11 SEPT 1964

Figure 63d.   TIROS VII Operational Nephanalysis, Orbit 6656/6654
1239 UT 11 September 1964

The jet stream cloud band, mentioned earlier, cuts across the 500 contours (towards low pressure) at an angle of about 30°. Other cases of similar non-parallelism have been found in TIROS data by Mr. L.F. Whitney of the USWB's Meteorological Satellite Laboratory. No explanation is yet apparent.

The clear skies over the Mediterranean make this an excellent case for illustrating several points discussed in Section 2.3 of this report. By reference to Sardinia, Corsica, and the Balearic Islands, the inscribed 40°N and 10°E grid lines are found to be about 1° too far south and too far west, respectively. This magnitude of error is typical of the data used in these studies.

Although the actual distance from Cape Nao (eastern Spain) to Minorca is about the same as that from Minorca to the Algerian coast, the aspect ratio appears to double the Nao-Minorca distance. The shape of Majorca is similarly distorted. The shapes of Corsica, Sardinia, and the Tunisian peninsula are nearly true; they are only slightly to the right of a true aspect ratio strip and so only slightly extended in the north-south direction. The effects of the reverse aspect ratio distortions (or fore-shortening) near the edge of the strip are obvious in the shapes of Italy, the Adriatic, and especially Cirenaica. The problems of rectification near the edge are apparent when it is noted that, while the most eastern grid line is for 10°E, the western tip of Crete (23°E) and parts of Cirenaica east of Derna can be detected. When progressing from the edge of the strip toward the center, the width on the HRIR strip of a given distance in longitude increases (from Cirenaica to Sicily to Sardinia to Majorca) in approximately the ratio 1:2:3:9, respectively.

4.6.2   An Eastern Pacific Ocean Case

Figure 64a shows a portion of a daylight HRIR strip covering the western United States and part of the eastern Pacific Ocean, south to the equator. It was taken about 1845 GMT on 2 September 1964. Figure 64b is from a TIROS pass over much the same area taken about 1500 GMT, or nearly four hours earlier. Figure 64c, the TIROS operational nephanalyses, aids in locating the features in the TIROS pictures.

The TIROS pictures show various cloudiness over the northwestern United States (poorly defined, due to a relatively great nadir angle), stratus to the west of Baja California, two cumulonimbus masses with cirriform tops over and just south of the Gulf of California, various areas of cumuliform cloudiness further south, and a suggestion of a weak cumuliform vortex, at about 15°N, near the western edge of the TIROS coverage.

Figure 64a. Daylight HRIR Data for the Western United States and
Eastern Pacific Ocean, 1845 UT, 2 September 1964
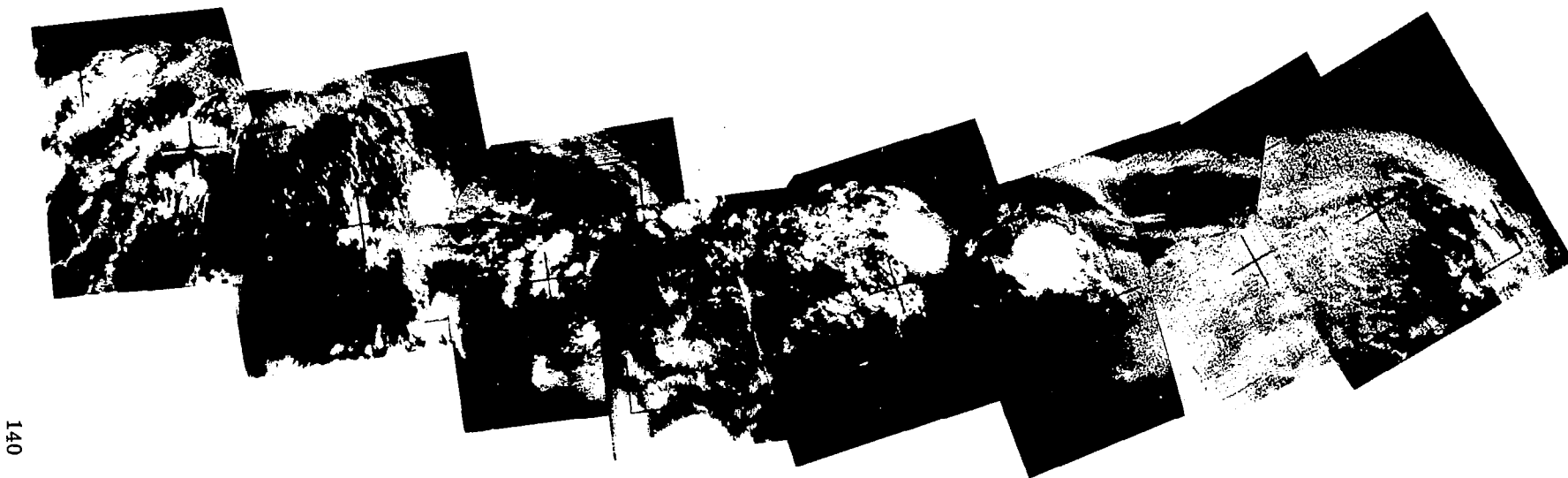
Figure 64b. Tiros VIII Television Picture Mosaic, Orbits 3714 and
3715/3714, 1500 UT, 2 September 1964

Figure 64c.   TIROS VIII Operational Nephanalyses, Orbits 3714 and 3715/3714
1500 UT, 2 September 1964

141

While there is a reasonable match of cloud features between the TIROS and the daylight HRIR, there are several significant differences.

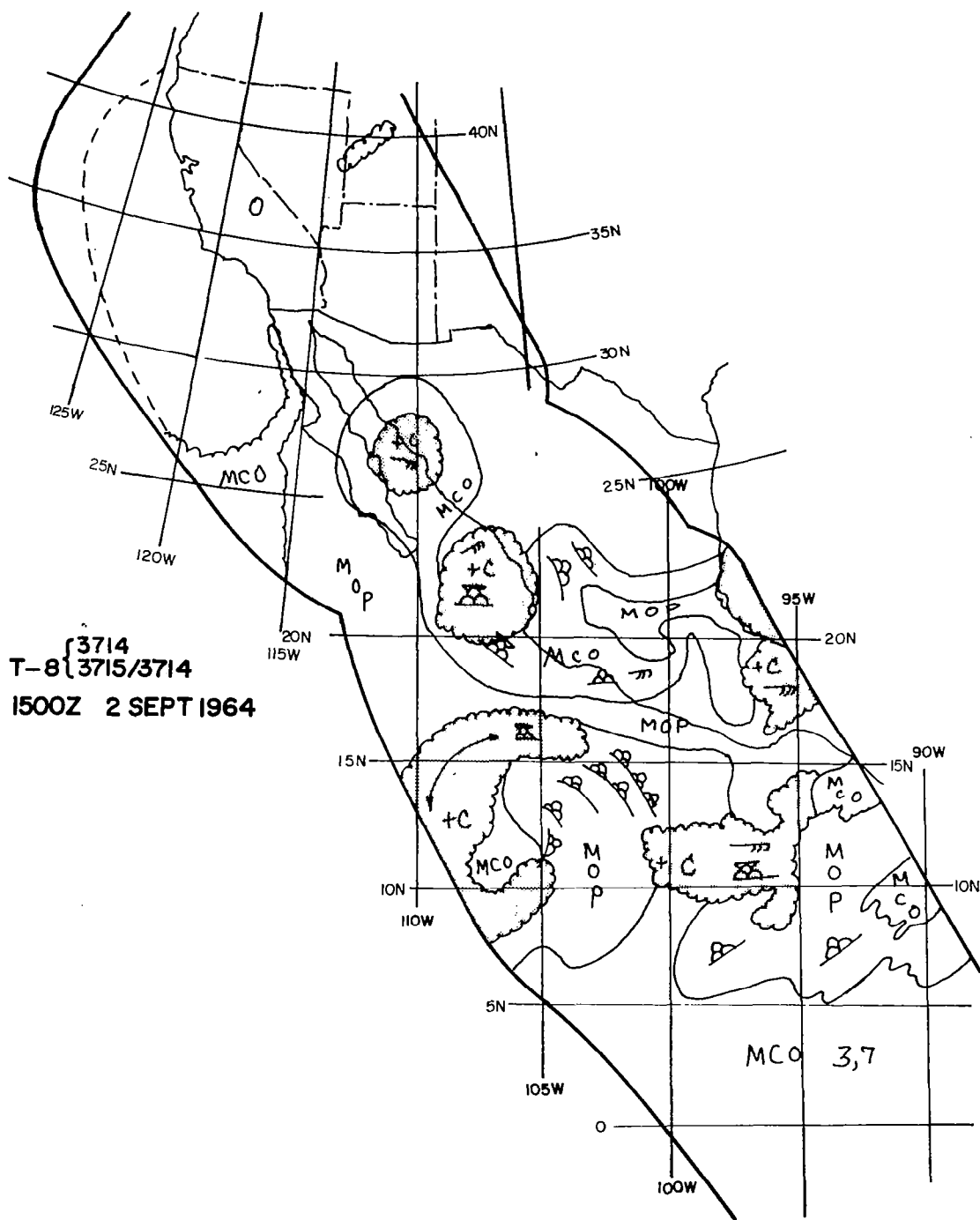In the HRIR data, the stratus west of Baja California is by far the most prominent cloud feature, but this is by no means the case in the TIROS pictures. Some tendency toward dissipation of the stratus during the three hour interval from the TIROS to the HRIR data is apparent near the coast, presumably due to diurnal heating.

Although the HRIR viewed the northwestern United States at a far better perspective than that of TIROS, an analyst would be in doubt as to the presence and extent of the cloud cover which can easily be seen in the TIROS pictures. Most of the North American coastline, and various interior features are, however, far more evident in the HRIR than the TIROS pictures.[*] The Great Salt Lake and various river valleys, such as parts of the Humboldt, are presumably made visible in the HRIR by their low albedo. For mountain ranges, such as the Sierra Nevada and those in eastern Utah and in Colorado (southeast of Great Salt Lake), the reduced temperatures of their higher elevations doubtless play the more significant role. If any of these mountain areas have cloud or snow cover, the temperature reduction has obviously overcome any increase in solar reflectivity in determining the total energy within the HRIR band pass.

The TIROS pictures show significant cumulonimbus masses with cirriform tops near 27°N, 110°W; 22°N, 107°W; 11°N, 98°W; and over the western part of the Gulf of Campeche. In the HRIR, all of these appear far less bright than the stratus. The mass of clouds along the shore of the Gulf of Campeche is hardly noticeable in the HRIR over land; it is seen where it crosses and distorts the shape of the coast line.

The reduced HRIR brightness is especially noticeable in the two cloud masses over and just south of the Gulf of California. The southern one was sufficiently prominent in the TIROS pictures for the operational nephanalyst to have labeled it as a disturbed area; a cirrus plume can be seen extending somewhat to its northeast. Since the TIROS data were taken during the morning hours, while the HRIR were taken about noon (local time), it is unlikely that convective activity was decreasing. The lower thermal emission of high cloud tops is the most reasonable explanation.

The weak vortex near 13°N, 105°W, although near the horizon, is obvious in the TIROS picture, and was called out as such by the analyst. Only with very great difficulty can it even be recognized in the HRIR, and it would probably not have been detected if only the HRIR data were available.

---

[*] In this case, poor nadir angles and low sun angles may have contributed to the poor contrast of many of the geographical features in the TIROS pictures.

In the HRIR, a sun glint seems to exist along the strip center just north of the equator. The cloud mass near $11°N$, $98°W$ in the TIROS picture also suggests partially specular reflection; if this is the case, it could only be due to properly oriented cloud surfaces since both the sun and the satellite were to the southeast of this area at the time.

This example suggests that while daylight HRIR data for situations of this type are very desirable in the absence of TV pictures, they must be analyzed and interpreted with considerable care. Our very small sample suggests more careful analysis is required in tropical and subtropical regions than further poleward.

4.6.3 A Southern Hemisphere Case

Figure 65b is part of a daylight HRIR strip, centered just west of South America. It was taken about 1715 GMT on 11 September 1964. In this case, night HRIR passes for about the same area were available approximately half a day earlier and later. Figure 65a was taken about 0345 GMT on September 11, while Figure 65c is from about 0415 GMT on September 12. A TIROS mosaic, covering the southwest part of the area of Figure 65b, and taken about 1430 GMT on the 11th, is shown as Figure 65d. The operational nephanalysis, Figure 65e, aids in locating the features in the TIROS pictures.

This HRIR sequence, with approximately 12 hour continuity in an area of limited data, will deserve further study provided sufficient conventional data and analyses concurrent with it are available.

Based solely on the HRIR data, the distorted cloud band near $50°S$, $80°W$ (in Fig. 65a) appears to be a wave on a cold front. Particularly because of the western bulge (northwest of $50°S$, $80°W$), this cloud pattern also appears to be associated with a short wave trough in the upper level flow. This development is taking place along and just west of the southern portion of South America. The impeding action of the Andes, which extend nearly to $55°S$, may have aided the development. South of Cape Horn, the front seems to be continuing its eastward movement. There is no unique explanation for the clouds east of the Andes, between $40°$ and $50°S$. They may be due to convergence and/or upslope motion connected with the developing circulation.

Thirteen and one-half hours later (Fig. 65b) the wave system appears to have developed to a closed circulation and to be centered near 52°S, 70°W. Although aspect ratio considerations may be partly responsible, the broadening of the front suggests a further wave development near 40°S, 75°W. A low level cumuliform cloud band, possibly a secondary cold front, runs north-south just east of 90°W. Just west of the South American coast, there would appear to be a convergence line extending north of 40°S.

Eleven hours still later (Fig.65c) the principal development has moved to near the east edge of the HRIR strip, at about 60°S. The mature and perhaps dissipating cyclone centered near 55°S, 90°W, is probably that which a day earlier (^{F}ig. 65a) could be seen near 64°S, 90°W. Some form of wave disturbance (perhaps but not certainly on the secondary front) exists near 57°S, 82°W, and is apparently being drawn into the mature circulation. The primary cold front has crossed the Andes and can be seen near the east edge of the HRIR strip south of about 46°S. A rather broad cirrus band runs from east of Cape Horn, northwest across the Andes and into the Pacific.

Returning now to the daylight HRIR observations (Fig. 65b), Figures 65d and 65e provide essentially duplicate TIROS coverage of the circulation near 52°S, the western low level cumuliform band, and the western portion of the primary frontal band. Again, the general and even the relatively detailed match of the features in the two types of data (about three hours apart) is obvious.

Although the clouds in the closed circulation and in the cumuliform band appear to be of about equal brightness in the TIROS pictures, in the daylight HRIR the closed circulation clouds are darker, presumably due to higher cloud tops. Similar darkening suggests that high cloud tops also exist along the frontal band and along the convergence line to its east.

In the originals of both Figures 6 5a and 65c, extensive low cloud (perhaps stratus) can be seen just off the coast and north of 30°S. Except for a few scattered fragments near the coast, such cloudiness is absent in the daylight HRIR until near and north of 20°S. This could be due either to a diurnal trend, or to the influence of the convergence line.

Parts of the Andes appear as dark, irregular lines in the daylight HRIR, indicating that the cold temperatures near the summits often more than compensate for the reflective snow that probably covers them at this time of year (early southern hemisphere spring). On the other hand, the dark areas in many ways do not match the details of the terrain; for example, the gray strip along 70°W seems to narrow

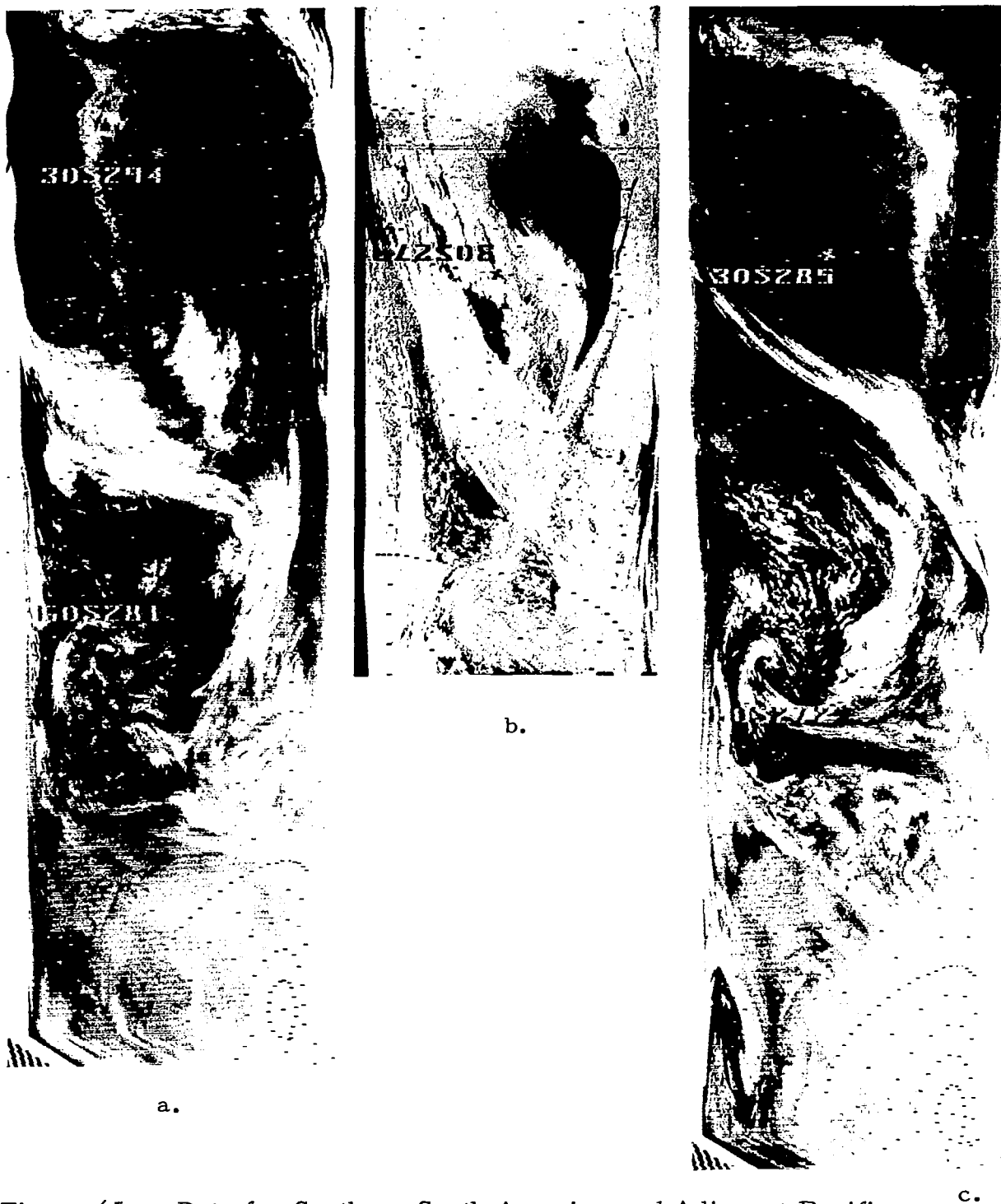Figure 65.   Data for Southern South America and Adjacent Pacific
             Ocean, 11-12 September 1964

             a. Night HRIR Data for About 0345 UT, 11 September
             b. Daylight HRIR Data for About 1715 UT, 11 September
             c. Night HRIR Data for About 0415 UT, 12 September
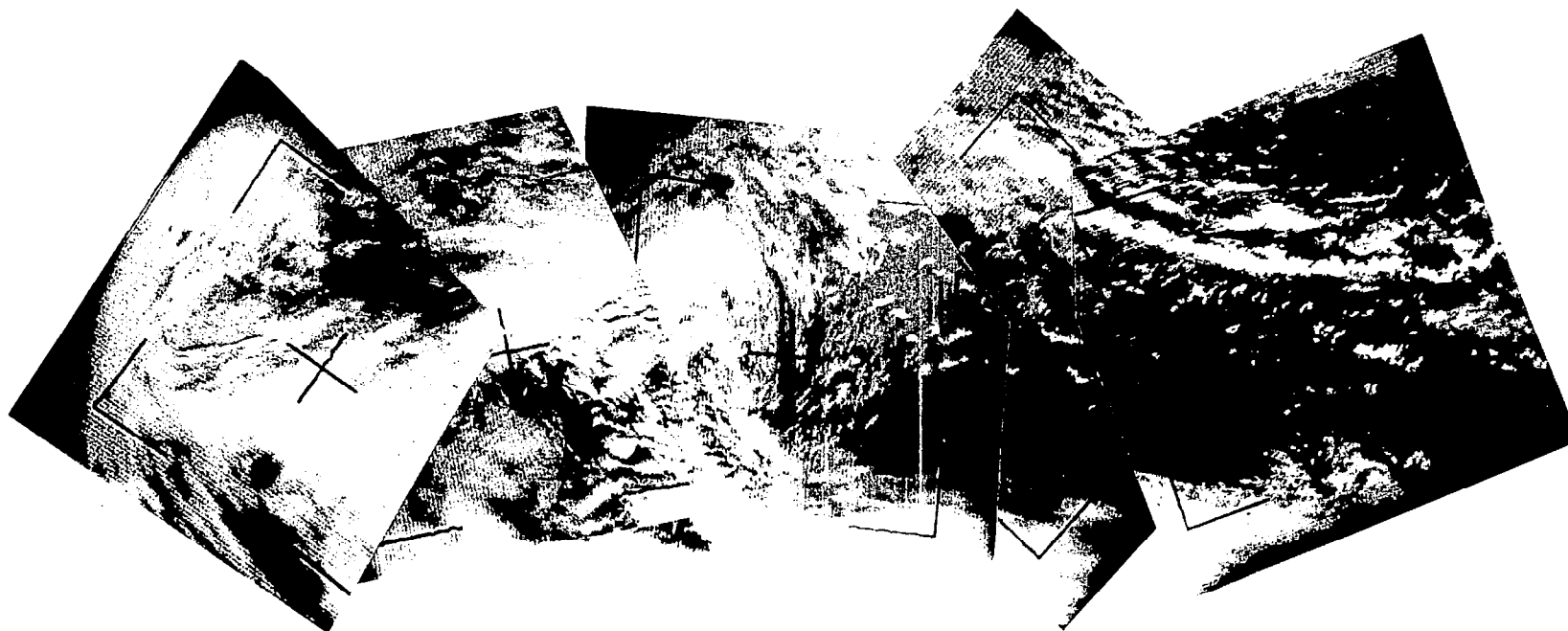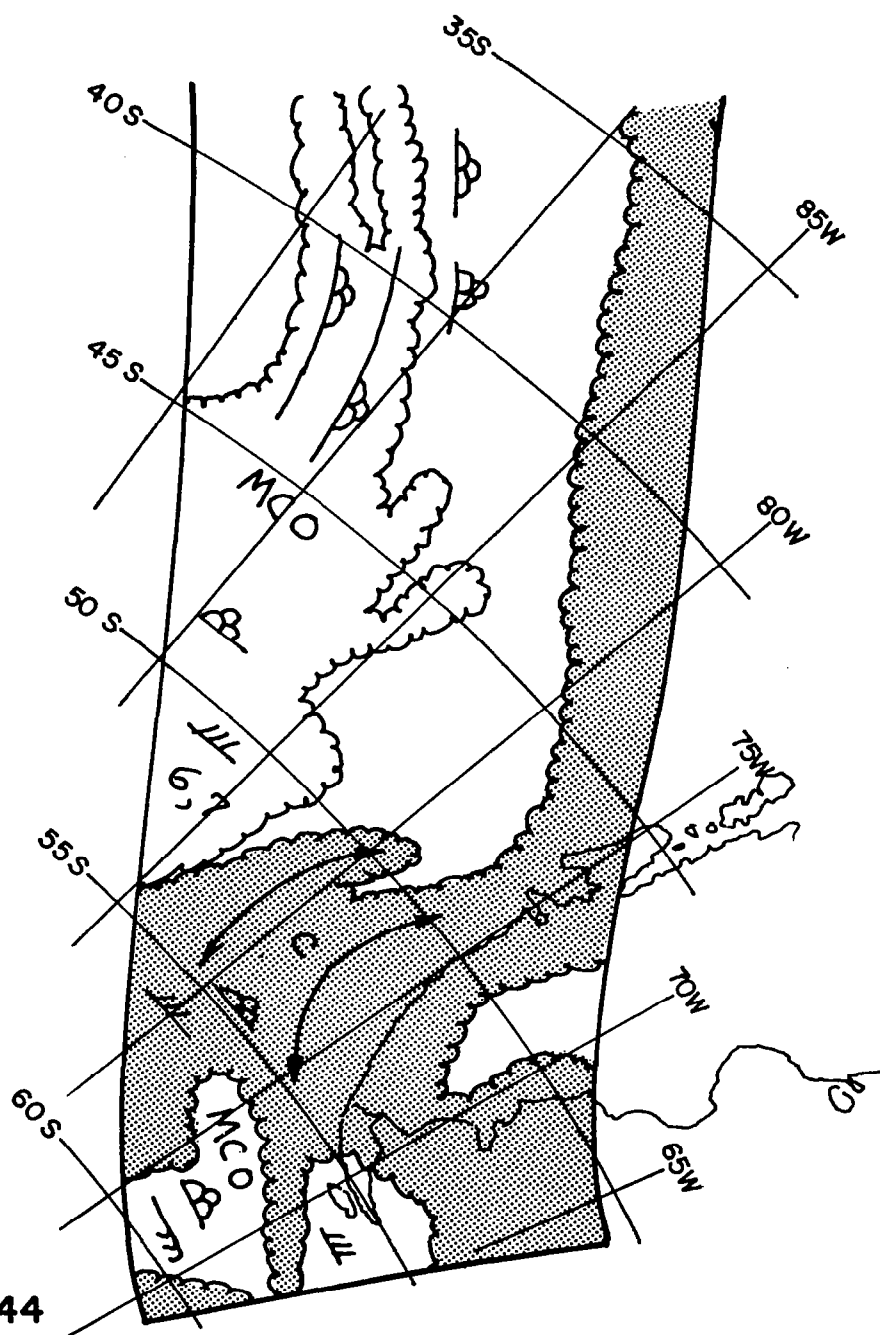
Figure 65d.   TIROS VIII Television Picture Mosaic, Orbit 3852/3844
1432 UT, 11 September 1964

T-8   3852/3844

1432Z   11 SEPT 1964

Figure 65e.   TIROS VIII Operational Nephanalysis, Orbit 3852/3844
1432 UT, 11 September 1964

from 40°S northward to 30°S, while the terrain broadens and increases in average altitude. Dorsey[7] however reports snow reflectivities, over a range that includes the HRIR response, as being only about 45% of those in the visible range. If, as would seem reasonable, snow extends to lower altitudes at increasing latitudes, this broadening could then be explained as a reflectivity rather than an altitude effect.

Even more puzzling is the very narrow strip along 70°W from 20°-30°S, and that north of 20°S. The strip along 70°W might be a very narrow clear area between the coast and a narrow strip of ocean stratus. If, however, the gray blotch just north of 20°S near 70°W is Lake Titicaca, the grid lines would be somewhat north of their proper positions. In this case, the small feature apparently at 28°S, 71°W might be Points Tetas and Angamos, and the coast would be identified as west of the dark strip. In any event, the dark strip to the northeast remains to be explained. It has been suggested that these two strips may represent areas of very steep slope (the southern area to the west of the Andes crest, the northern area to the east) whose very angle reduce upward reflected radiation. In any event, no unambiguous explanation is presently apparent.

The reader may also note, in Figures 65a and 65c, how vividly many of the South American geographical features show up in the night HRIR. In Figure 65a, even features along the east coast can be identified between about 30° and 43°S.

REFERENCES TO APPENDIX C

1. Alaka, M.A. (ed.), 1960: The Airflow Over Mountains, WMO Technical Note No. 34 (WMO No. 98, TP. 43) (Geneva, World Meteorological Organization, 135 pp.

2. Allison, L.J., T.I. Gray, Jr., and G. Warnecke, 1964: A Quasi-Global Presentation of TIROS III Radiation Data, Report No. SP-53, NASA.

3. Bird, J.B., A. Morrison, and M.C. Chown, 1964: World Atlas of Photography from TIROS Satellites I to IV, NASA CR-98.

4. Boucher, R.J.,and R.J. Newcomb, 1962: "Synoptic Interpretation of Some TIROS Vortex Patterns: A Preliminary Cyclone Model," Journal of Applied Meteorology, 1 (2), pp. 127-136.

5. Conover, J.H., 1964: "The Identification and Significance of Orographically Induced Clouds Observed by TIROS Satellites," Journal of Applied Meteorology, 3 (3), pp. 226-234.

6. Corby, G.A., 1957: "A Preliminary Study of Atmospheric Waves Using Radiosonde Data," Quarterly Journal of the Royal Meteorological Society, 83, pp. 49-60.

7. Dorsey, N.E., 1940: Properties of Ordinary Water-Substance, Reinhold, New York.

8. Fritz, S., 1965: "The Significance of Mountain Lee Waves as Seen from Satellite Pictures," Journal of Applied Meteorology, 4 (1), pp 31-37.

9. Fujita, T., and W.Bandeen, 1965: Resolution of the Nimbus High Resolution Infrared Radiometer, Research Paper No. 40, Satellite and Mesometeorology Research Project, The University of Chicago.

10. Goldberg, I.L., 1962: "Nimbus Radiometry," Proceedings of the Nimbus Program Review, NASA, GSFC, Report X-650-62-226

11. Goldshlak, L., and R.B. Smith, 1964: Nimbus I Real Time Scientific Data Operation, Final Report, Contract No. NAS 5-9512, ARACON Geophysics Co.

12. Goldshlak, L., and R.B. Smith, 1964: Nimbus Backup Gridding: AVCS and HRIR, Technical Report No. 1, Contract No. NAS 5-3253.

13. Hanson, D.M., 1963: The Use of Meteorological Satellite Data in Analysis and Forecasting, Technical Note No. 13, Office of Forecast Development, USWB.

14. Kadlec, P.W., 1963: An In-Flight Study of the Relation Between Jet Stream, Cirrus, and Wind Shear Turbulence, Final Report, Contract No. Cwb-10356, Eastern Air Lines, Inc., Miami.

15. Kadlec, P.W., 1964: A Study of Flight Conditions Associated with Jet Stream Cirrus, Atmospheric Temperature Change, and Wind Shear Turbulence, Final Report, Contract No. Cwb-10674, Eastern Air Lines, Inc., Miami.

16. Merritt, E.S., 1963: Fleet Application Meteorological Operational Satellite (Antarctic Area), Final Report, Contract No. N 189(188)-56507A, ARACON Geophysics Company.

17. Nagle, R.E., 1962: Comparison of Time Integrated Radar Detected Precipitation with Satellite Observed Cloud Patterns, Scientific Report No. 1, Contract No. AF 19(628)-284, Stanford Research Institute.

18. Scorer, R.S., 1949: "Theory of Waves in the Lee of Mountains," Quarterly Journal of the Royal Meteorological Society, 75, pp. 41-56.

19. Sherr, P.E., and C.W.C Rogers, 1965: The Identification and Interpretation of Cloud Vortices Using TIROS Infrared Observations, Final Report, Contract No. Cwb 10812, ARACON Geophysics Company.

20. Staff Members, Aeronomy and Meteorology Division, 1965: Nimbus I High Resolution Radiation Data Catalog and User's Manuals, Volume I, Goddard Space Flight Center.

21. Stampfl, R., 1963: The Nimbus Spacecraft and Its Communication System as of September 1961, NASA Technical Note D-1422.

22. Stampfl, R., and H. Press, 1962: "Nimbus Spacecraft System," Aerospace Engineering, 21 (7), pp. 16-28.

23. Whitney, L.F., Jr., 1961: "Another View from TIROS I of a Severe Weather Situation, May 16, 1960," Monthly Weather Review, 89 (11), pp. 447-460.

24. Widger, W.K., and A.H. Glaser, 1963: A Rationale for Geographic Referencing of Meteorological Satellite Data, Technical Report No. 1, Contract No. NAS 5-1204, ARACON Geophysics Co.

25. Widger, W.K., Jr., P.E. Sherr and C.W.C. Rogers, 1964: Practical Interpretation of Meteorological Satellite Data, Final Report, Contract No. AF 19(628)-2471, ARACON Geophysics Company.

"The aeronautical and space activities of the United States shall be conducted so as to contribute . . . to the expansion of human knowledge of phenomena in the atmosphere and space. The Administration shall provide for the widest practicable and appropriate dissemination of information concerning its activities and the results thereof."

—NATIONAL AERONAUTICS AND SPACE ACT OF 1958

NASA SCIENTIFIC AND TECHNICAL PUBLICATIONS

TECHNICAL REPORTS: Scientific and technical information considered important, complete, and a lasting contribution to existing knowledge.

TECHNICAL NOTES: Information less broad in scope but nevertheless of importance as a contribution to existing knowledge.

TECHNICAL MEMORANDUMS: Information receiving limited distribution because of preliminary data, security classification, or other reasons.

CONTRACTOR REPORTS: Technical information generated in connection with a NASA contract or grant and released under NASA auspices.

TECHNICAL TRANSLATIONS: Information published in a foreign language considered to merit NASA distribution in English.

SPECIAL PUBLICATIONS: Information derived from or of value to NASA activities. Publications include conference proceedings, monographs, data compilations, handbooks, sourcebooks, and special bibliographies.

TECHNOLOGY UTILIZATION PUBLICATIONS: Information on technology used by NASA that may be of particular interest in commercial and other nonaerospace applications. Publications include Tech Briefs; Technology Utilization Reports and Notes; and Technology Surveys.

Details on the availability of these publications may be obtained from:

SCIENTIFIC AND TECHNICAL INFORMATION DIVISION

NATIONAL AERONAUTICS AND SPACE ADMINISTRATION

Washington, D.C. 20546